Novel disulfide-bridging conjugation chemistry for antibodies as potential anti-cancer therapeutics

Alkhawaja, Bayan

Award date:
2019

Awarding institution:
University of Bath

Novel disulfide-bridging conjugation chemistry for antibodies as potential anti-cancer therapeutics

Bayan Alkhawaja

A thesis submitted for the degree of Doctor of Philosophy

University of Bath

Department of Pharmacy and Pharmacology

January 2019

Signed: …….. Date: …….

Abstract

This is a multidisciplinary research project in the field of bioconjugation chemistry. Bioconjugation chemistry, in its fundamental aspects, refers to the site specific covalent modification of bio-molecules adding or modulating desired characteristics. The recent advances in bioconjugation approaches have enabled the progressive construction of ground-breaking monoclonal antibodies (mAbs) biotherapies, such as antibody drug conjugates (ADCs) and bispecific antibodies. However, there is still a long list of limitations encountered by the currents approaches such as poor plasma stability, post-modification structural stability and heterogeneity of the produced conjugates, which are usually tackled by expensive and complex biological-based techniques. Therefore, in this study, we aimed to develop novel conjugation chemistry suitable for the construction of antibody-protein conjugates with promising anti-cancer activity.

Production of protein conjugates is usually achieved through targeting thiolate groups of their cysteine residues. We aimed to develop an effective reduction method for activation of thiolates towards conjugation reactions. We developed and evaluated a novel one-pot method by using water soluble azide-derivatised ethylene glycols (PEG-azides) to quench excess trialkylphosphines prior to thiol alkylation reactions. The rates of oxidation of trialkylphosphines with a series of PEG-azides were determined and the applicability of this *in situ* method was evaluated in conjugation reactions.

We have developed a novel rebridging approach of the reduced disulfide bonds of mAbs, based on an aryl bis-haloacetamide scaffold. The proposed scaffold was developed according to our findings related to the impact of a vicinal acetamide group on the reactivity and stability of various electrophiles. Interestingly, rebridging of mAbs with the bis-haloacetamide linkers has revealed a high efficiency in rebridging heavy-light and intra-heavy-heavy disulfide bonds affording half antibody (75 kDa) as a major rebridged product. Rebridging conditions were optimised and utilised to obtain rebridged bi-functional half antibody (75 kDa) modified with bio-orthogonal chemistry. The stability of the rebridged mAbs and the difference in reactivity and selectivity amongst bis-haloacetamide linkers with reduced mAbs have been thoroughly studied.

Moreover, we have developed an elegant bis-rebridging platform based on bis-haloacetamide scaffold. The bis-o-dihaloacetamide PEG linker has been applied in generating mAb conjugates with other proteins, including immunomodulating proteins and antibody fragments in an adaptable procedure with a very good yield. The promising findings imply the applicability of this approach to construct mAb immunoconjugates enabling multi-targets-based intervention in the oncology field.

This thesis is dedicated
to my parents

Acknowledgments

First of all, I want to thank God for bestowing upon me the intellectual ability, courage and strength to successfully accomplish this work.

Foremost, I would like to express my greatest thanking and gratitude to my supervisor, Dr Andrew Watts. It has been a great pleasure to be part of his research group, I could not accomplish this work without all the tremendous support, guidance, and of course patience for the past three years (and a bit). I'm lucky to have had a supervisor who is so enthusiastic, inspiring and supportive, and who give me a chance to master a huge range of research skills throughout this project.
Thanks to my second supervisor Prof. Jean Van Den Elsen and our collaborators in the department of B&B for their great support and help when it comes to biology work.

Thanks to Dr Tim Woodman for his excellent guidance and support in NMR during my PhD and to Dr Shaun Reeksting and Dr Mervyn Lewis for all the mass spectrometry analysis, advice and assistance.

I express my gratitude to my colleague Andreas Michael who helped a lot throughout this project, especially with biology stuff! Thanks to all the members of 3.30 lab, especially Dr Joanna Watt who supported me a lot in my early chemistry days!! And Albert lab members especially Dr Rami Alnajadat. I would also like to thank Dr Zoe Burke for her excellent support and patience to help me starting my cell-culture learning journey. I would like to thank all the people who helped throughout the last three years. Many Thanks to all my friends in P&P, in particular, our lovely office 3.20 whom I share unforgettable memories with.

Most of all, I'm very grateful to my exceptional parents, Dr Abdel-Fattah and Alia to whom this work is dedicated. They have worked tirelessly to ensure my siblings and I received the best education and support. Without their unyielding support, I would not be where I am today. Special thanks to my siblings, Dr Eman, Zaid, Dr Nour and Rashid for their unconditional love and support. I'm lucky to have such incredibly supportive and loving siblings, who are always there for me.

Lastly, I would like to thank all my friends in Jordan who stayed supportive for all that long. Special thanks to Dr Anwar Jaffal and Dr Amani Al Qroom. I'm so fortunate person to come to Bath and meet so special friends from all over the world. Thank you all my dearest Friends Maryam Al Bulushi, Tayba Al Hilali, Marwa Mohamed, Noha Elboghdadly, Nima Ali, Sara Jasem, Aisha Alsheikh Abubaker, Aida Maaz, Sharareh Houshmandyar and Muhammad Kamran for all your support and all of the unforgettable memories that we shared together in Bath.

So thank you all.

Table of Contents

Abstract ..... **ii**

Acknowledgments ..... **v**

Table of Contents ..... **vii**

List of Figures ..... **xv**

List of Tables ..... **xxxiii**

Abbreviations ..... **xxxiv**

1 Introduction **1**

1.1 Bioconjugation chemistry 1

1.2 Applications of protein conjugates 2

1.2.1 Analysis and quantification 3

1.2.2 Detection and imaging of biomolecules 4

1.2.3 Therapeutic conjugates and conjugate vaccines 6

1.3 Antibody drug conjugates 8

1.3.1 Monoclonal antibodies (mAb) 9

1.3.2 Cytotoxic mechanism of ADCs 13

1.3.3 The anatomy of ADCs 14

1.3.4 First generation of approved ADCs 16

1.4 Traditional conjugation chemistries employed in the construction of protein-conjugates 18

1.4.1 Conjugation chemistries targeting amine side chains of lysine 18

1.4.2 Conjugation chemistries targeting thiol side chains of cysteine 21

1.5 The next generation of ADCs: Improved homogeneity and stability 26

1.5.1 THIOMAB drug conjugates 26

1.5.2 Unnatural amino acids 27

1.5.3 Enzymatic techniques 29

1.5.4 Disulfide rebridging strategies 30

1.6 Bioorthogonal cross-coupling reactions using unnatural functional groups 31

1.6.1 Staudinger ligation & traceless Staudinger ligation 32

1.6.2 Azide-Alkyne cycloaddition 'Click' reaction 33

1.7 Aims and objectives 35

2 The use of alkyl azides to quench trialkylphosphine-based reducing agents 37

2.1 Introduction 37

2.2 Synthesis of azide-containing ethylene glycols of increasing molecular mass 41

2.3 Determination of the mass and molar solubilites of PEG-azides and 4-azidobenzoic acid 42

2.4 Rate of consumption of phosphine, TCEP and THPP by using ^{31}P NMR spectroscopy 43

2.5 The application of PEG-azides towards improving protein conjugation yields (experiment carried out by Terrence Kanter)[134,135] 49

2.6 Conclusion 50

3 Evaluation of aryl-sulfonate derivatives as thiolate-reactive alkylating agents 51

3.1 Introduction 51

3.2 Factors affecting the aqueous stability of sulfonate esters 52

3.2.1 Impact of aryl substitution on the aqueous stability of sulfonates 52

3.2.2 Evaluation of the effect of electrophile chain length of sulfonates on hydrolysis rates (propyloxy derivatives) 58

3.2.3 Sulfonate ester acetamide derivatives 59

3.3 Reactivity rates of sulfonates with the thiol containing nucleophile glutathione 62

3.4 Stability of sulfonates in the presence of TCEP 69

3.5 Reactivity of selected sulfonates with proteins 71

3.6 Conclusion 75

4 Bis-haloacetmide derivatives as a novel disulfide rebridging agents 76

4.1 Introduction 76

4.2 *N*,*N*-Di-(chloroacetyl)-amido derivatives as rebridging agent of reduced disulfide bonds 83

4.3 2-chloro-*N*-(2-chloroacetyl)-*N*-phenylacetamide (4.2) as rebridging agent of reduced disulfide bonds 87

4.3.1 Reactivity of 4.3, 4.4 and 4.7 linkers toward with thiophenol 87

4.3.2 Stability of *N*,*N*-di(chloroacetyl)amido derivatives and their reactivity with glutathione 89

4.4 Aryl bis-haloacetamide derivatives as rebridging linkers 95

4.4.1 Synthesis of the aryl bis-haloacetamide derivatives 4.15 and 4.16 96

4.4.2 The aqueous stability of bis-haloacetamide 96

4.4.3 The aqueous stability of aryl bis-haloacetamides in the presence of TCEP 98

4.4.4 Investigation of the reactivity of methyl 3,5-bis(2-chloroacetamido)benzoate (4.15) and methyl 3,4-bis(2-chloroacetamido)benzoate (4.16) towards reduced glutathione 101

4.4.5 Aqueous stability of the glutathione conjugates (4.17-4.19) in buffer.. 103

4.5 The synthesis and evaluation of bis-bromo- and bis-iodo-acetamide derivatives 106

4.5.1 Determination of the reactivity of methyl 3,5-bis(2-haloacetamido)benzoate (4.22 and 4.24) and methyl 3,4-bis(2-haloacetamido)benzoate (4.23 and 4.25) towards glutathione 111

4.5.2 The synthesis and evaluation of *N*-benzyl-2-haloacetamide derivatives 113

4.5.3 The impact of aryl substitution on the aqueous stability and reactivity of bis-haloacetamide linkers towards glutathione 115

4.6 Aryl bis-haloacetamide linkers bearing azide group 117

4.6.1 Synthesis of azide containing aryl bis-haloacetamide linkers 119

4.6.2 Stability and GSH reactivity of azide-bearing bis-haloacetamide linkers 121

5 Rebridging of reduced disulfide bonds of monoclonal antibodies using bis-haloacetamide linkers 126

5.1 Introduction 126

5.1.1 The HER2 receptor 126

5.1.2 Mechanism of action of Trastuzumab 127

5.2 Optimisation of the TCEP reduction of Tmab 129

5.3 Disulfide bond rebridging of fully reduced Trastuzumab 133

5.4 Disulfide bond rebridging of Trastuzumab with azide modified bis-haloacetamide linkers 4.32-4.35 143

5.5 Disulfide bond rebridging of partially reduced Trastuzumab 145

5.6 Selectivity of bis-haloacetamide linkers towards cross-linking heavy-heavy and heavy-light disulfide bonds 150

5.7 Mechanistic understanding the cross-linking of reduced disulfide bonds using bis-haloacetamide linkers 155

5.8 Production of a bi-functional Tmab half antibody: $Tmab_{bis(o\text{-}\mathbf{HL}\text{-}OMe,m\text{-}\mathbf{HH}intra\text{-}N3)}$ 159

5.9 Investigation into the reaction of bis-haloacetamide linkers towards other antibodies: Rituximab 165

5.9.1 Introduction 165

5.9.2 Disulfide bond rebridging of fully reduced Rituximab: Rmab$_{bis\text{-}[(o\text{-}HL,o\text{-}HHintra)\text{-}OMe]}$ 165

5.9.3 Preliminary investigation of the higher order structure of Rmab$_{bis\text{-}[(o\text{-}HL,o\text{-}HHintra)\text{-}OMe]}$ 167

5.10 Stability of rebridged Rmab half antibody: Rmab$_{bis\text{-}[(o\text{-}HL,o\text{-}HHintra)\text{-}OMe]}$ under reducing conditions and after 2 months at 4°C 171

5.11 Cross-linking of human complement protein C3dg 173

5.12 Conclusion 177

6 Synthesis of an immunomodulating antibody conjugate: Trastuzumab–Sbi 178

6.1 Introduction 178

6.1.1 The human complement system 178

6.1.2 Immune evasion mechanisms of *Staphylococcus aureus* 182

6.1.3 The Staphylococcus immunoglobulin-binding (Sbi) protein 185

6.2 Synthesis of bis-dihaloacetamide (PEG)$_3$ 187

6.3 The two employed strategies to produces Tmab-Sbi conjugate 189

6.4 Conjugation of functionalised Tmab with reduced Sbi (Strategy 1) 191

6.4.1 Rebridging of partially reduced Tmab with bis-dihaloacetamide (PEG)$_3$ linker 194

6.4.2 Tmab-Sbi conjugation 196

6.5 Conjugation of functionalised Sbi with partially reduced Tmab (Strategy 2) 197

6.6 Synthesis of bis-o-diiodoacetamide (PEG)$_7$ (6.5) 200

6.7 Application of bis-o-diiodoacetamide $(PEG)_7$ (6.5) in construction of $Tmab_{o\text{-}HL}$-PEG_7-$Sbi_{o\text{-}bis\text{-}Cys}$ conjugate (6.11) 201

6.8 Conclusion and future work 208

7 The chemical synthesis of Fc containing bi-specific antibody using Bis-dihaloacetamide PEG cross-linkers **209**

7.1 Introduction 209

7.1.1 Classes of bi-specific antibodies lacking of Fc region 210

7.1.2 Entire IgG classes: Fc region containing bi-specific antibodies 212

7.2 The rationale for Tmab-IFab bsAb 215

7.3 Construction of the Tmab-IFab bsAb 217

7.3.1 Optimisation of the conjugation method 221

7.4 Conclusion and future work 224

8 Experimental **225**

8.1 General reagents 225

8.2 General methods 225

8.2.1 Chemical synthesis 225

8.2.2 Standard work-up 226

8.2.3 Protein over-expression 226

8.2.4 SDS-PEGE gel electrophoresis 228

8.2.5 Protein LC-MS analysis 230

8.3 Chapter 2 Experimental 231

8.3.1 Chemical synthesis 231

8.3.2 Determination of the mass and molar solubilities of PEG-azide 2.10-2.13 and 4-ABA 2.7 236

8.3.3 Determination of the rate of consumption of TCEP using ^{31}P NMR spectroscopy 236

8.4 Chapter 3 Experimental 237

8.4.1 Chemical synthesis 237

8.4.2 Determination of aqueous stability of sulfonate derivatives using ^{1}H NMR (solvent suppression method) 244

8.4.3 Determination of glutathione reactivity of sulfonates using ^{1}H NMR (solvent suppression method) 245

8.4.4 Conjugation buffer 246

8.4.5 Expression of Sbi IV-Cys 246

8.4.6 Sbi IV-Cys reactivity with sulfonate derivatives 247

8.5 Chapter 4 Experimental 248

8.5.1 Chemical synthesis 248

8.5.2 Evaluation of the aqueous stability of bis-haloacetamides using ^{1}H NMR (solvent suppression method) 277

8.5.3 Determination of bis-haloacetamides reactivity with glutathione of using ^{1}H NMR (solvent suppression method) 278

8.5.4 Determination of the aqueous stability of glutathione conjugates (4.17-4.19) using HPLC 279

8.6 Chapter 5 Experimental 280

8.6.1 TCEP quantification using 5,5'-Dithiobis(2-nitrobenzoic acid) (DNTP) reagent 280

8.6.2 Procedure for TCEP reduction of Tmab 280

8.6.3 Tmab bioconjugates 1-4 280

8.6.4 Rmab bioconjugate 1 284

8.6.5 CD spectrum analysis of Rmab$_{\text{bis-[(o-HL,o-HHintra)-OMe]}}$ 284

8.6.6 DLS analysis of Rmab bioconjugate 1 (Rmab$_{\text{bis-[(o-HL,o-HHintra)-OMe]}}$) 285

8.6.7 Stability of Rmab bioconjugate 1 (Rmab$_{\text{bis-[(o-HL,o-HHintra)-OMe]}}$) in plasma mimicking condition and at 4°C for 2 months 285

8.7 Chapter 6 Experimental 286

8.7.1 Chemical synthesis 286

8.7.2 Expression of Sbi III/IV-2xCys 292

8.7.3 Construction of $Tmab_{o\text{-}HL}$-PEG_7-$Sbi_{o\text{-}bis\text{-}Cys}$ conjugate (6.11) with bis-o-diiodoacetamide $(PEG)_7$ 6.5 295

8.7.4 Sequential purification of $Tmab_{o\text{-}HL}$-PEG_7-$Sbi_{ortho\text{-}bis\text{-}Cys}$ conjugate (6.11) using IMAC followed by size exclusion chromatography (SEC). 295

8.8 Chapter 7 Experimental 296

8.8.1 Construction and purification of the trifunctionalTmab: $Tmab_{o\text{-}HL}$-PEG_7-$IFab_{o\text{-}HL}$ conjugate (7.1) with bis-o-diiodoacetamide $(PEG)_7$ 6.5 linker 296

9 General discussion, conclusion and future implications 298

10 References 307

11 Appendices 342

11.1 Cloning vector 342

11.2 HPLC standard curves of glutathione conjugates 342

11.3 Cell line and toxicity assay 343

11.3.1 Materials and methods 343

11.3.2 *In vitro* cytotoxicity assay 344

11.4 Publications and posters 347

List of Figures

Figure 1.1. Site-specific protein modification of antibodies. **A)** An example of natural post-translation modification of proteins by N-glycosylation of antibodies at C_{H2} domain which is carried out inside the rough endoplasmic reticulum. **B)** An example of bioconjugation chemistry by chemical attachment of a fluorophore to antibodies (fluorescently labelled antibodies) which is widely applied in diagnostic assays. 2

Figure 1.2. ELISA procedure using enzyme-linked antibody to quantify the target analytes (antigens). 3

Figure 1.3. Diels–Alder click reaction of tumor-homing antibody-Trans-cyclooctyne (TCO) conjugate with radiolabelled tetrazine affording radiolabeled antibody accumulated in tumor site in order to be visualized by PET imaging approaches. Picture adapted from reference ([5]). 5

Figure 1.4. The structure of Cimzia® conjugate, which is a humanized Fab′ fragment against TNFα that is chemically conjugated with two PEG chains. Figure adapted from reference ([7]). 7

Figure 1.5. General bilaterally symmetric structure of IgG. Blue stars indicate glycosylation sites of C_{H2} domain of the Heavy chain. 10

Figure 1.6. Interaction of mAbs with cancer cells and their mechanism of causing cell death. **A)** ADCC involves interaction of Fc domain with FcγR on immune effector cells mainly, natural killer cells (NK). NK cells releases perforin and other enzymes to lyse cancer cells in addition to pro-inflammatory mediators, such as IFNγ to activate nearby antigen presentation and adaptive immune responses.[36] **B)** CDC involves complement C1q binding to C_{H2} domain of Fc region, which in turn activate the classical pathway of complement activation. Complement activation result in construction of membrane attack complex (MAC) and cellular lysis.[37] **C)** Signal transduction changes of these receptors on cancer cells which might normalise the malignant symptoms and sensitise cells to cytotoxic drugs.[38] CLTs: cytotoxic lymphocytes. 11

Figure 1.7. Immunoconjugates types between **A**) an antibody and an enzyme (capable of activating a prodrug), **B**) an antibody and a toxin, **C**) an antibody and a radioisotope..... 13

Figure 1.8. Cytotoxic mechanism of ACDs. The process starts when the mAb component recognizes and binds to a specific antigen on cancer cell, followed by rapid internalisation of the antigen-ADC complex. The endosomes are routed to lysosomes where the ADC is degraded leading to the release of the cytotoxic drug, then the drug binds to its target, either DNA or tubulin and cause cellular apoptosis. It may also be released or pumped through the cell membrane which leads to bystander effect. 14

Figure 1.9. The Anatomy of ADCs. ADCs are composed of three main parts: 1) mAb that specifically binds to antigens expressed on cancer cells. 2) Cytotoxic drug that usually binds to tubulin or DNA and leads to cellular apoptosis. 3) Stable linker that ideally attach the cytotoxic drugs at specific sites on mAb and release it through the endosomal-lysosomal pathway. 15

Figure 1.10. The chemical structure of the most widely modified residues in protein conjugation reaction, lysine and cysteine amino acids. 18
Figure 1.11. Reactive amine-based bioconjugation chemistries. **A**) Reaction of isothiocyanates with amine group forming thiourea. **B**) Reaction of NHS activated ester with amine group forming amide linkage. **C**) Reaction of aldehyde group with amine group followed by mild reduction. 19
Figure 1.12. Trastuzumab emtansine conjugation scheme. Firstly, modification of lysine residues on Tmab with NHS activated ester, followed by conjugation of the sulfhydryl of DM1 drug with the activated Tmab. SMCC: succinimidyl 4-(*N*-malemidomethyl) cyclohexane-1-carboxylate (SMCC) linker. DM1: Maytansine, tubulin disrupting cytotoxic drug. Figure adapted from reference ([71]) 21
Figure 1.13. Brentuximab Vedotin conjugation scheme. Firstly, reduction of interchain disulfide bonds on brentuximab, followed by conjugation of the sulfhydryl of brentuximab with maleimide activated MMAE is a microtubule inhibitor derived from auristatins. MMAE: Monomethyl Auristatin E. 23
Figure 1.14. Reversible thiol-maleimide alkylation reaction. Thiosuccinimide ring might undergo retro-Michael addition (undesirable) or hydrolysis and ring opening (desirable). Grey circle refers to the cytotoxic payloads, pink circle refers to proteins of biological system, such as human serum albumin (HAS). 24
Figure 1.15. Cross-linking of cysteine residues of proteins using α-haloacetyl compounds to afford thioether linkage. 25
Figure 1.16. Cross-linking of cysteine residues of proteins using vinyl sulfone compounds through Micheal addition reaction to afford thioether linkage. 25
Figure 1.17. Site-specific conjugation approach using oxime ligation, which attaches alkoxyamine linked with payloads ( ) to *p*-acetylphenylalanine-tagged mAb. 28
Figure 1.18. Site-specific enzymatic conjugation approach using Sortase A enzyme, which attaches poly-glycine-linked payloads ( ) to LPETG-tagged mAb. 30
Figure 1.19. Rebridging approach of the reduced disulfide bonds of mAb using functionalised bis-sulfone reagent to form three carbon bridges between the two reduced cysteine of mAbs. 31
Figure 1.20. **A**) Non-traceless Staudinger ligation and **B**) Traceless Staudinger ligation generating amide linkage. 32
Figure 1.21. Cycloaddition reaction of azides and alkynes groups (copper-free 'Click'reaction). **A**) Azide-alkyne cycloaddition reaction. **B**) Strain-induced azide-cyclooctyne cycloaddition reaction. **C**) Mechanism of Cycloaddition reaction of azides-labelled biomolecule and probe-bearing dibenzocyclooctyne group affording triazole ring. Figure adapted from reference ([112]). 34
Figure 1.22. Rebridging approach of the reduced disulfide bonds of mAb using functionalised bis-haloacetamide reagents 36
Figure 2.1. General conjugation strategy of protein labeling by reduction of disulfide bonds prior to alkylation of the obtained thiols using Michael acceptors. 37

Figure 2.2. A) Mechanism of reversible reduction of disulfide bonds using DTT (**2.1**). **B**) Mechanism of irreversible reduction of disulfide bonds using TCEP (**2.2**). 38
Figure 2.3. The reaction between TCEP (**2.2**) and THPP (**2.3**) with the Michael acceptor, N-ethylmaleimide (**2.4**) forming the ylene adduct (**2.5**) and N-ethylsuccinimide (**2.6**), respectively..... 40
Figure 2.4. The mechanism of Staudinger reaction between TCEP (**2.2**) with 4-azidobenzoic acid (**2.7**). 41
Figure 2.5. Chemical synthesis of the PEG-azides **2.10**-**2.13**. **a**) (**i**) 4-Toluenesulphonyl chloride, pyridine, DCM, room tempreture, 3h, (**ii**) NaN_3, acetone/water (3:1), room temperature overnight. 42
Figure 2.6. ^{31}P NMR spectrum of TCEP control reaction analysed at times **A)** 3 minutes and **B)** 63 minutes. No peak corresponding to phosphine oxide (57 ppm) was observed..... 44
Figure 2.7. ^{31}P NMR spectrum of TCEP reaction with penta-PEG azide (**2.13**) analysed every 10 minutes. Phosphine oxide peak was observed at 57 ppm. 45
Figure 2.8. Oxidation rates of TCEP in the presence of the PEG-azides (250 mM) in Tris.HCl buffer (100 mM, pH 7) and 4-ABA (**2.7**, 26 mM) in Tris.HCl buffer (100 mM, pH 8). 46
Figure 2.9. ^{31}P NMR spectrum of TCEP reaction with 4-ABA (**2.7**) analysed every 10 minutes. Phosphine oxide peak was observed at 57 ppm. 47
Figure 2.10. ^{31}P NMR spectrum of THPP reaction with **A**) penta-PEG azide (**2.13**) and **B**) di-PEG azide (**2.10**) analysed after 3 minutes. Phosphine oxide peak was observed at 60.45 ppm. 48
Figure 2.11. SDS-PAGE analysis of application of PEG-azides in labelling of yeast enolase with fluorescein-maleimide. Yeast enolase (11 mM) in Tris.HCL buffer (500 mM, pH = 7.2, 5 mM EDTA) was reduced with TCEP or THPP (1, 5 or 10 equiv.) for 45 minutes at room temperature then reacted with N-(5-fluorescinyl)maleimide (1 mM) for 18 h at 37 °C. In a parallel experiment, reduced yeast enolase was treated with PEG-azide **2.12** for 1 hr at 37 °C prior to addition of N-(5-fluorescinyl)maleimide (1 mM) for 18 h at 37 °C. 49
Figure 3.1. A) General Mechanism of nucleophilic substitution reactions (S_N2). **B**) Thiolate alkylation with sulfonyl ester (tosylate) affording thioether linkage with liberation of sulfonic acid anion (k_1). Sulfonyl ester (tosylate) hydrolysis (k_2). 52
Figure 3.2. Chemical synthesis of ethoxy-sulfonate derivatives **3.1**-**3.5**. (**a**) Anhydrous DCM, anhydrous pyridine. 54
Figure 3.3. ^{1}H NMR spectra of 2-methoxyethyl 4-nitrobenzenesulfonate (**3.5**) over 4 days at **A**) pH 7 and **B**) 8.5. Arrows indicate the aromatic peaks that were followed to calculate hydrolysis rates using Equation 3.1, maroon arrows correspond to aromatic protons of sulfonate group of 2-methoxyethyl 4-nitrobenzenesulfonate (2 x NO_2CCH), while green arrows correspond to aromatic protons of sulfonate group of sulfonic acid (2 x NO_2CCH). 55
Figure 3.4. Percentage remaining sulfonates (**3.1**-**3.5**) over 4 days. Stability was appraised in phosphate buffer (100 mM, pH 7, 8 or 8.5) using solvent suppression method. 56
Figure 3.5. The correlation between log hydrolysis rates (h^{-1}) and Hammett sigma σ values. 58

Figure 3.6. Chemical synthesis of propyloxy-sulfonate derivatives **3.6**-**3.8**. **a**) Anhydrous DCM, anhydrous pyridine. 59
Figure 3.7. Percentage remaining of sulfonates (**3.1, 3.4**-**3.8**) in aqueous buffer over 4 days. Stability was appraised in phosphate buffer (100 mM, pH 7, 8 or 8.5) using solvent suppression method. 60
Figure 3.8. Chemical synthesis of acetamide sulfonate derivatives **3.9 and 3.10**. **a**) Anhydrous DCM, anhydrous pyridine, 2 h. 61
Figure 3.9. Percentage remaining of sulfonates (**3.1**, **3.4**-**3.8**, and **3.9**) in aqueous buffer over 4 days. Stability was appraised in phosphate buffer (100 mM, pH 8) using solvent suppression method. 61
Figure 3.10. Reaction of glutathione (**3.23**, 3 equiv.) with sulfonate derivatives in aqueous in phosphate buffer (100 mM, pH 7.5). 62
Figure 3.11. **A**) Percentage remaining of sulfonates **3.4**, **3.7**, and **3.8** in absence of glutathione in aqueous phosphate buffer (100 mM, pH 7.5). **B**) Percent of remaining of sulfonates **3.4**, **3.7**, and **3.8** in presence of glutathione (**3.23**, 3 equiv.) in aqueous phosphate buffer (100 mM, pH 7.5). Data presented as mean ±SD of 3 independent experiments. 63
Figure 3.12. A) ^{1}H NMR spectrum of tosyl acetamide (**3.9**) in the absence of glutathione. **B)** ^{1}H NMR spectrum of tosyl acetamide (**3.9**) in the presence of glutathione (3 equiv.). Arrows indicate the aromatic peaks that have been followed to calculate reactivity rates using Equation 3.1. Red arrows correspond to the aromatic protons of sulfonate group of tosyl acetamide (**3.9**) (2 x SO_2CCH) while green arrows correspond to the aromatic protons of sulfonate group of sulfonic acid (2 x SO_2CCH). 65
Figure 3.13. A) Percentage remaining of sulfonates (**3.1**, **3.6**, and **3.9)** over 2 days at pH 7.5. Stability was appraised in phosphate buffer (100 mM, pH 7.5) using solvent suppression method. **B**) Percentage remaining of sulfonates (**3.1**, **3.6**, and **3.9)** in the presence of glutathione (**3.23**, 3 equiv.) in aqueous phosphate buffer (100 mM, pH 7.5). Data are represented as mean ±SD of n=3. 66
Figure 3.14. A) ^{1}H NMR spectrum of mesyl acetamide (**3.10**) in the absence of glutathione. **B**) ^{1}H NMR spectrum of mesyl acetamide (**3.10**) in the presence of glutathione (**3.23**, 3 equiv.), arrows indicate the peaks that were followed to obtain the reactivity rates (substitution of mesylic acid anion). 68
Figure 3.15. Percentage remaining of sulfonates (**3.9**, **3.10**) in the presence of glutathione (**3.23**, 3 equiv.) in phosphate buffer (100 mM, pH 7.5). Data are represented as mean ±SD of n=3. 69
Figure 3.16. Stability of 3-methoxypropyl3-chlorobenzene sulfonate (**3.7**) in the presence of TCEP (**2.2,** 3 equiv.). ^{1}H NMR spectra of 3-methoxypropyl-3-chlorobenzene sulfonate (**3.7**) in the absence and presence of TCEP. Arrows in the expanded region indicate the aromatic peaks of sulfonic acid (hydrolysis) that obtained in the absence and presence of TCEP after 24 h. 70
Figure 3.17. Stability of tosyl acetamide (**3.9**) in the presence of TCEP (**2.2,** 3 equiv.). **A**) ^{1}H NMR spectrum of tosyl acetamide (**3.9**) in the presence of TCEP. Arrows in the expanded region indicate the aromatic peaks that were followed to calculate reactivity rates using Equation 3.1. **B**) Percentage remaining of tosyl acetamide (**3.9**) in presence of TCEP (3 equiv.) in aqueous phosphate buffer (100 mM, pH 7.5). 71

Figure 3.18. Deconvoluted protein MS spectra of Sbi IV-Cys (2 mg/mL, 0.187 mM) reacted with sulfonates **3.6** and **3.8** (1.87mM, 10 equiv.) at pH 7.5. **A**) Sbi IV-Cys control. **B**) Sbi IV-Cys reaction with 3-methoxypropyl-4-methylbenzene sulfonate (**3.6**) at pH 7.5 with no detection of product peak. **C)** Sbi IV-Cys reaction with 3-methoxypropyl-4-nitrobenzene sulfonate (**3.8**) at pH 7.5, yielding a mass of 10801 Da. with difference of 71.85 Da. 73

Figure 3.19. Deconvoluted protein MS spectra of Sbi IV-Cys (2 mg/mL, 0.187 mM) reacted with sulfonates **3.9** and **3.10** (1.87mM, 10 equiv.) at pH 7.5. **A**) Sbi IV-Cys reaction with tosyl acetamide (**3.9**) at pH 7.5, yielding a mass of 10844.25 Da. with difference of 115.35 Da. **B**) Sbi IV-Cys reaction mesyl acetamide (**3.10**) at pH 7.5, yielding a mass of 10844.23 Da. with difference of 115.09 Da. 74

Figure 4.1. Addition-elimination mechanism of a bis-sulfone linker (ThioBridge®) coupled with cytotoxic drug ( ) in cross-linking the reduced inter-chain disulfide bonds of mAbs affording 3-carbon bridges. 77

Figure 4.2. A) Mono-labeling of thiol group with dibromomaleimide (**4b**) reagent. **B**) Cross-linking of the disulfide bond of somatostatin by dibromomaleimide (**4b**) reagent forming bisthiomaleimide 2-carbon bridge. 79

Figure 4.3. A) Di-TECP-substituted dithiophenolpyridazinedione (**4g**) with dual reduction and rebridging activities of mAb disulfide bonds. **B**) Dibromopyridazinediones (**4h**) with two different reactive, clickable handles for dual chlick reactions. 81

Figure 4.4. Cross-linking mechanism of a nitrogen mustard (Mechlorethamine) with N-7 of guanine base of DNA which leads to cell cytotoxicity. 83

Figure 4.5. The proposed mechanism of rebridging of the reduced disulfide bonds using 2-chloro-*N*-(2-chloroacetyl)-*N*-(2-methoxyethyl)acetamide (**4.1**) linker. 84

Figure 4.6. Our attempts to synthesise 2-chloro-N-(2-chloroacetyl)-N-(2-methoxyethyl)acetamide (**4.1**) through acetylation of 2-chloro-N-(2-methoxyethyl)acetamide (**4.3**) in absence or presence of a base, such as pyridine or TEA. 84

Figure 4.7. The previously described procedures to synthesise *N*,*N*-di-chloroacetyl amido derivative. **A**) (a) 2-chloroacetyl chloride, pyridine, DCM, 15 h.[158] **B**) (b) 2-chloroacetyl chloride, reflux, 3 h.[159] 85

Figure 4.8. A) ^{1}H NMR spectrum of one of the unidentified separated product of 2-chloro-*N*-(2-methoxyethyl)acetamide (**4.2**) synthesis trail using TEA as a base. **B)** MS spectra of the reaction crude of the base- free trail showing the mass of the starting material (**4.3**) and a product of methoxy group elimination. 86

Figure 4.9. Chemical synthesis of 2-chloro-*N*-(2-chloroacetyl)-*N*-phenylacetamide (**4.2**). **a**) Dry toluene, 48 h and reflux. 87

Figure 4.10. Chemical reaction of 2-chloro-*N*-(2-chloroacetyl)-*N*-(3,4,5-trimethoxyphenyl)acetamide (**4.9**) with thiophenol (**4.6**). **a**) Mixture of MeCN (1 mL) and Tris.HCl buffer (100 mM, pH 7.5, 1 mL) at room temperature 6 h. 89

Figure 4.11. Stability of ethyl 4-(2-chloroacetamido)benzoate (**4.12**) linker in aqueous buffer. ^{1}H NMR spectra of ethyl 4-(2-chloroacetamido)benzoate **4.12** (1.00 mg/ml, 4.15 mM) in phosphate buffer (100 mM, pH 7.5) over 4 days. Arrow indicates the signals of α-methylene protons that were followed at δ 4.38 ppm ($ClCH_2CONH$) over 4 days. 91

Figure 4.12. A) Hydrolysis of ethyl 4-(2-chloro-*N*-(2-chloroacetyl)acetamido)benzoate (**4.11**) in aqueous buffer. (a) Tris.HCl buffer (100 mM, pH 7.5, 30 % DMF) at room temperature overnight. **B**) ^{1}H NMR spectrum of ethyl 4-(2-chloro-*N*-(2-chloroacetyl)acetamido)benzoate (**4.11**) held in aqueous buffer overnight showing only spectrum of ethyl 4-(2-chloroacetamido)benzoate (**4.12**) with its assigned peaks. **C**) MS spectra of Ethyl 4-(2-chloro-*N*-(2-chloroacetyl)acetamido)benzoate (**4.11**) held in aqueous buffer overnight showing only *m/z* 264 of ethyl 4-(2-chloroacetamido)benzoate (**4.12**). 92

Figure 4.13. The mechanism of alkaline hydrolysis of *N*-(o-carboxyphenyl)-phthalimide.[161] 93

Figure 4.14. The proposed mechanisms of hydrolysis of compound **4.11** in the presence of glutathione under aqueous conditions to afford the mono-glutathione conjugate **4.13** 94

Figure 4.15. The mechanism of cross-linking reaction between complementary oligodeoxynucleotides strands using *N*,*N*'-bis-bromoacetyl-1,2-diaminebenzene (**4.29**), which was selective for the complementary N7 of 2-deoxyguanosine. 95

Figure 4.16. Our proposed approach of rebridging of reduced inter-chain disulfide bonds of mAb using bis-haloacetamide linkers. 96

Figure 4.17. Stability of bis-chloroacetamide linkers in aqueous buffer. **A**) ^{1}H NMR spectrum of methyl 3,5-bis(2-chloroacetamido)benzoate **4.15** (1.00 mg/ml, 3.14 mM) and **B**) methyl 3,4-bis(2-chloroacetamido)benzoate **4.16** (1.00 mg/ml, 3.14 mM) in aqueous phosphate buffer over 4 days. Arrows indicate the followed peaks at at δ 4.43 ppm for α-methylene protons (2 x $ClCH_2CONH$). 97

Figure 4.18. Percentage remaining of haloacetamide **4.12** (1.00 mg/ml, 4.15 mM), **4.15** (1.00 mg/ml, 3.14 mM) and **4.16** (1 mg/ml, 3.14 mM) over 4 days. Stability was determined in phosphate buffer (100 mM, pH 7.5) containing 10-30% DMF-d_7. % of remaining was calculated by measuring the change in the integration of α-methylene using ^{1}H NMR solvent suppression method. 98

Figure 4.19. Stability of methyl 3,5-bis(2-chloroacetamido)benzoate (**4.15**) in presence of TCEP (**2.2**). **A**) ^{1}H NMR spectrum of methyl 3,5-bis(2-chloroacetamido)benzoate (**4.15**) in presence of TC2P (**2.2**, 3 equiv.) in aqueous phosphate buffer, arrows indicate the followed disappearance of signal peak at δ 4.21 ppm of α-methylene protons and appearance of signal peaks at δ 2.5 ppm to obtain the reactivity rate. **B**) Percentage remaining of methyl 3,5-bis(2-chloroacetamido)benzoate (**4.15**) (1.00 mg/ml, 3.14 mM) in TEA the presence of TCEP (2.36 mg/ml, 9.42 mM, 3 equiv.) in phosphate buffer (100 mM, pH 7.5). 99

Figure 4.20. A) acetamide-TCEP adduct. **B**) IR spectrum of acetamide-TCEP adduct confirming the absence of distinctive peak of C=P (usual range of 1180−1230 cm^{-1}). 100

Figure 4.21. Percentage remaining of methyl 3,5-bis(2-chloroacetamido)benzoate **4.15** (1.00 mg/ml, 3.14 mM) and methyl 3,4-bis(2- chloroacetamido) benzoate **4.16** (1.00 mg/ml, 3.14 mM) in presence of GSH (5.79, 18.8 mM, 6 equiv.) in phosphate buffer (100 mM, pH 7.5). 102

Figure 4.22. A) 3D structure of methyl 3,5-bis(2-chloroacetamido)benzoate (**4.15**) showing its planner conformation. **B**) 3D structure of methyl 3,4-bis(2-chloroacetamido)benzoate (**4.16**) showing its non-planner conformation allowing better backside attack of thiolate anion at the α-methylene carbon (2 x $ClCH_2CONH$) attached to halogen (green)..... 103

Figure 4.23. A) Percent remaining of glutathione-conjugates (1.0 mg/ml, 1.2 mM) in the presence and absence of DTT (50 mM) over 4 weeks in aqueous phosphate buffer (100 mM, pH 7). Data presented as mean± SD of three independent samples. **B)** ^{1}H NMR spectrum analysing the stability of Mal-glutathione (1.0 mg/ml, 2.3 mM) in the presence of DTT over the four weeks (28 days). Arrows indicated the followed signals to calculate the percentage of remaining of Mal-glutathione **4.19.**..... 105

Figure 4.24. Chemical synthesis of ethyl 4-(2-bromoacetamido)benzoate (**4.20**) and ethyl 4-(2-iodoacetamido)benzoate (**4.21**). **a**) TEA, DCM, 2 h. **b**) KI, dry acetone, reflux, 3h..... 106

Figure 4.25. Stability of haloacetamide **4.20** and **4.21** in aqueous buffer. **A**) ^{1}H NMR spectrum of ethyl 4-(2-bromoacetamido)benzoate **4.20** (1.00 mg/ml, 3.51 mM) in phosphate buffer over 4 days. Arrow indicates the signals that were followed at δ 4.10 ppm for acetamide proton ($BrCH_2CONH$) over 4 days. **B**) ^{1}H NMR spectrum of ethyl 4-(2-iodoacetamido)benzoate (**4.21**) (1 mg/ml, 3 mM) in phosphate buffer over 4 days, arrow indicates the signals that were followed at δ 3.99 ppm for acetamide protons (ICH_2CONH) over 4 days..... 108

Figure 4.27. Study of reactivity of ethyl 4-(2-bromoacetamido)benzoate (**4.19**) and ethyl 4-(2-iodoacetamido)benzoate (**4.20**) towards glutathione. ^{1}H NMR spectrum of **A**) ethyl 4-(2-bromoacetamido)benzoate **4.19** (1.00 mg/ml, 3.51 mM) and **B**) ethyl 4-(2-iodoacetamido)benzoate (**4.20**) (1 mg/ml, 3 mM) in the presence of glutathione (1.1 equiv.) in aqueous phosphate. Arrow indicates the followed acetamide peaks at δ 4.02 ppm for bromo-acetamide or at 3.86 ppm for iodo-acetamide and at 3.46 ppm for acetamide-glutathione adduct to obtain the reactivity rates..... 112

Figure 4.28. Percentage remaining of ethyl 4-(2-chloroacetamido)benzoate (**4.12**) (1.00 mg/ml, 4.15 mM) in the presence of glutathione (3 equiv.); ethyl 4-(2-bromoacetamido)benzoate **4.20** (1.00 mg/ml, 3.51 mM) and ethyl 4-(2-iodoacetamido)benzoate **4.21** (1 mg/ml, 3 mM) in presence of glutathione (1.1 equiv.) in phosphate buffer (100 mM, pH 7.5). 113

Figure 4.29. Percentage remaining of ethyl 4-(2-chloroacetamido)benzoate **4.12** (1.00 mg/ml, 4.15 mM) and N-benzyl-2-chloroacetamide **4.26** (1.00 mg/ml, 5.47 mM) in presence of glutathione (3 equiv.); ethyl 4-(2-bromoacetamido)benzoate **4.20** (1.00 mg/ml, 3.51 mM) and N-benzyl-2-bromoacetamide **4.27** (1.0 mg/ml, 4.4 mM) in presence of glutathione (1.1 equiv.) in aqueous phosphate buffer (100 mM, pH 7.5). The employed lower equivalent of glutathione (1.1 equiv.) precludes the completion of the reaction observed with **4.27** linker..... 115

Figure 4.31. Synthesis of 2-(2-(2-(2-azidoethoxy)ethoxy)ethoxy)ethan-1-amine (**4.46**). **a**) 4-toluenesulphonyl chloride, pyridine, DMC, **b**) NaN_3, acetone/water (3:1), 37°C, o/n, **c**) Ph_3P, 5% HCl. .. 119

Figure 4.32. Synthesis of *N*,*N*'-(4-((2-(2-(2-(2-azidoethoxy)ethoxy)ethoxy)ethyl)carbamoyl)-1,2-phenylene)bis(2-iodoacetamide) (**4.35**). **a**) $ClCOCH_2Cl$, THF, **b**) NHS, EDC.HCl, THF, **c**) 2-(2-(2-(2-azidoethoxy)ethoxy)ethoxy)ethan-1-amine, THF, **d**) KI, dry acetone, reflux, 3 h. 120

Figure 4.33. Synthesis of *N*,*N*'-(4-((2-(2-(2-(2-azidoethoxy)ethoxy)ethoxy)ethyl)carbamoyl)-1,2-phenylene)bis(2-bromoacetamide) (**4.34**). **a**) KBr, dry acetone, reflux, 4 days. 121

Figure 4.34. Comparison of the aqueous stability of aryl bis-haloacetamide linkers. Percentage remaining of the bis-haloacetamide derivatives (**4.22-4.25** and **4.32-4.35**) over 4 days. Stability was appraised in phosphate buffer (100 mM, pH 7.5) with final concentration of 10% DMF-d7 using solvent suppression method. 122

Figure 4.35. Percentage remaining of the bis-haloacetamide derivatives **4.32** and **4.43** (1.0 mg/ml, 1.7 mM), **4.33** and **4.35** (1.00 mg/ml, 1.45 mM) in the presence of glutathione (1.1 equiv.) in aqueous phosphate buffer (100 mM, pH 7.5). 123

Figure 5.1. HER2 signaling pathways in breast cells and the site of action of the currently available anti-HER2 receptors drugs**.** Trastuzumab mAb binds and blocks the extracellular domain of HER2, in particular domain IV, while Pertuzumab inhibits dimerization of HER2 receptor by binding to domain II of the extracellular domain of the receptor. Lapatinib is small drug molecule that inhibits tyrosine kinase.[176] 127

Figure 5.2. The possible products species of mAbs reduced with 1, 2 or 4 equivalents of TCEP with the masses of the observed bands under non-reducing conditions (dark gray represents the major products). 130

Figure 5.3. SDS-PAGE analysis of optimisation of Tmab reduction using TCEP (**2.2**) varying concentration of Tmab and reduction time. L: protein ladder. Lane 1-4: Tmab (1.0 mg/mL, 6.9 µM), Lane 5-8: Tmab (10 mg/mL, 69 µM) in Tris.HCl buffer (100 mM, 150 mM NaCl, 5 mM EDTA, pH 7.5). Lane 1: Tmab reduced with 2.2 equiv. of TCEP (1.52 µM) for 1 h, lane 2: Tmab reduced with 2.2 equiv. of TCEP (1.52 µM) for 2 h, lane 3: Tmab reduced with 2.5 equiv. of TCEP (1.72 µM) for 1 h, lane 4: Tmab reduced with 2.5 equiv. of TCEP (1.72 µM) for 2 h, lane 5: Tmab reduced with 2.2 equiv. of TCEP (15.2 µM) for 1 h, lane 6: Tmab reduced with 2.2 equiv. of TCEP (15.2 µM) for 2 h, lane 7: Tmab reduced with 2.5 equiv. of TCEP (17.2 µM) for 1 h, lane 8: Tmab reduced with 2.5 equiv. of TCEP (1.72 µM) for 2 h, at 4 °C. lane 9: Tmab control (non-reducing dye). HC: heavy chain, LC: light chain. Protein samples were resolved by non-reducing SDS-Page (10% gel). 131

Figure 5.4. SDS-PAGE analysis of optimisation of Tmab reduction using TCEP (**2.2**) varying the reduction time. L: protein ladder. Tmab (5 mg/mL, 34 µM), in Tris.HCl buffer (100 mM, 150 mM NaCl, 5 mM EDTA, pH 7.5). L: protein ladder, lane 1: Tmab control (non -reducing dye), lane 2: Tmab reduced with 2 equiv. of TCEP (6.8 µM) for 1 h at 4°C, lane 3: Tmab reduced with 2 equiv. of TCEP (6.8 µM) for 2 h at 4°C, lane 4: Tmab reduced with 2.2 equiv. of TCEP (7.5 µM) for 1 h at 4°C, lane 5: Tmab reduced with 2.2 equiv. of TCEP (7.5 µM) for 2 h at 4°C, lane 6: Tmab reduced with 5 equiv. of TCEP (17 µM) for 2 h at room temperature. Protein samples were resolved by non-reducing SDS-Page (10% gel). 132

Figure 5.5. SDS-PAGE analysis of optimisation of Tmab reduction using TCEP (**2.2**). Lane 1-4: Tmab (5.0 mg/mL, 34 µM) in Tris.HCl buffer (100 mM, 150 mM NaCl, 5 mM EDTA, pH 7.5). L: protein ladder, lane 1: Tmab control (non -reducing dye), lane 2: Tmab reduced with 2.2 equiv. of TCEP (7.5 µM) for 2 h at 4°C, lane 3: Tmab reduced with 5 equiv. of TCEP (17 µM) for 2 h at room temperature, lane 4: Tmab reduced with 10 equiv. of TCEP (34 µM) for 2 h at 37 °C. Protein samples were resolved by non-reducing SDS-Page (10% gel). 133

Figure 5.6. SDS-PAGE analysis of cross-linking of fully reduced Tmab (5.0 mg/ml, 34 µM) in Tris.HCl buffer (100 mM, pH 7.5) containing 150 mM NaCl, and 5 mM EDTA ,with bis-bromoacetamide linkers. Tmab was reduced with 5 equiv. of TCEP **2.2** (170 µM) for 2 h at room temperature and incubated with 5 (17 µM) or 8 equiv. (27.2 µM) of each linker. L: protein ladder, lane 1: Tmab incubated with 5 equiv. of methyl 3,4-bis(2-bromoacetamido)benzoate (**4.23**), lane 2: Tmab incubated with 8 equiv. of methyl 3,4-bis(2-bromoacetamido)benzoate (**4.23**), lane 3: Tmab incubated with 5 equiv. of methyl 3,5-bis(2-bromoacetamido)benzoate (**4.22**), lane 4: Tmab incubated with 8 equiv. of methyl 3,5-bis(2-bromoacetamido)benzoate (**4.22**), lane 5: Tmab incubated with 5 equiv. of *N*,*N*'-(1,2-phenylene)bis(2-bromoacetamide) (**4.29**), lane 6: Tmab incubated with 8 equiv. of *N*,*N*'-(1,2-phenylene)bis(2-bromoacetamide) (**4.29**), lane 7: Tmab incubated with 5 equiv. of *N*,*N*'-(1,3-phenylene)bis(2-bromoacetamide) (**4.28**), lane 8: Tmab incubated with 8 equiv. of *N*,*N*'-(1,3-phenylene)bis(2-bromoacetamide) (**4.28**). HC: heavy chain, LC: light chain, LC-LC: light chain homodimers, HC-HC: heavy chain homodimers. Protein samples were resolved by reducing SDS-PAGE (4-12% gel). Bands annotation is based on the protein MS results. 135

Figure 5.8. A) Schematic representation of the produced half antibody with two rebridged disulfide bonds, intra-chain heavy-heavy and heavy-light chains. **B)** Deconvoluted spectrum protein MS of Tmab. Full spectrum of Tmab cross-linked with 4 equiv. of methyl 3,4-bis(2-bromoacetamido) benzoate (**4.23**) showing a major peak at 74,528.03 Da. **C**) Expansion of the spectrum at 74 kDa region showing major peaks at 74,528.03 Da and 74,689.24 Da. 137

Figure 5.9. Deconvoluted spectrum protein MS of cross-linked Tmab with *N*,*N*'-(1,2-phenylene)bis(2-bromoacetamide) (**4.29**). **A**) Full view MS spectrum of cross-linked Tmab showing a major peak at 74,572.57 Da. **B**) Expansion of the spectrum at 74 kDa region showing major peaks at 74,572.57 Da and 74,410.91 Da. 138

Figure 5.10. SDS-PAGE analysis of cross-linking of fully reduced Tmab (5.0 mg/ml, 34 µM) in Tris.HCl buffer (100 mM, 150 mM NaCl, 5mM EDTA, pH 6, 7.5, or 8) incubated with bis-haloacetamide linkers. Tmab (34 µM) was reduced with 5 equiv. of TCEP (170 µM) for 2 h at room temperature and incubated with (17 µM, 5 equiv.) of each linker. Lane 1, 5 and 9: Tmab incubated with 5 equiv. of methyl 3,4-bis(2-bromoacetamido)benzoate (**4.23**), Lane 2, 6 and 10: Tmab incubated with 5 equiv. of methyl 3,5-bis(2-bromoacetamido)benzoate (**4.22**), Lane 3, 7 and 11: Tmab incubated with 5 equiv. of *N*,*N*'-(1,2-phenylene)bis(2-bromoacetamide) (**4.29**), Lane 4, 8 and 12: Tmab incubated with 5 equiv. of *N*,*N*'-(1,3-phenylene)bis(2-bromoacetamide) (**4.28**). HC: heavy chain, LC: light chain, LC-LC: light chain

homodimers, HC-HC: heavy chain homodimers. Protein samples were resolved by reducing SDS-PAGE (10% gel). 141

Figure 5.11. SDS-PAGE of cross-linking of fully reduced Tmab (5 mg/ml, 34 µM) in Tris.HCl buffer (100 mM, pH 7.5) containing 150 mM NaCl, and 5 mM EDTA, with bis-iodoacetamide linkers. Tmab was reduced with 5 equiv. of TCEP **2.2** (170 µM) for 2 h at room temperature and incubated with (17 µM, 5 equiv.) of each linker. L: protein ladder, lane 1: Tmab control (Non-reducing dye), lane 2: Tmab control (reducing dye), lane 3: Tmab incubated with 5 equiv. of methyl 3,4-bis(2-iodooacetamido)benzoate (**4.25**), Lane 4: Tmab incubated with 5 equiv. of methyl 3,5-bis(2-iodoacetamido)benzoate (**4.24**), Lane 5: Tmab incubated with 5 equiv. of N,N'-(1,2-phenylene)bis(2-iodoacetamide) (**4.31**), Lane 6: Tmab incubated with 5 equiv. of N,N'-(1,3-phenylene)bis(2-bromoacetamide) (**4.30**). HC: heavy chain, LC: light chain, LC-LC: light chain homodimers, HC-HC: heavy chain homodimers. Protein samples were resolved by reducing SDS-PAGE (10% gel). 142

Figure 5.12. A) SDS-PAGE analysis of cross-linking of reduced Tmab (5 mg/ml, 34 µM) in Tris.HCl buffer (100 mM, pH 7.5) containing 150 mM NaCl, and 5 mM EDTA with 5 equiv. of TCEP (150 µM) for 2 h at room temperature and incubated with (17 µM, 5 equiv.) of each linker overnight. L: ladder, lane 1: Tmab incubated with 5 equiv. of **4.34**, lane 2: Tmab incubated with 5 equiv. of **4.32**, lane 3: Tmab incubated with 5 equiv. of **4.35**, lane 4: Tmab incubated with 5 equiv. of **4.33** at room temperature overnight. **B**) Deconvoluted spectrum protein MS of rebridged Tmab with **4.35** linker showing a major peak at 75,059.82 Da. 145

Figure 5.13. The two methods investigated to attain rebridged heavy-light chains of Tmab (cross-linked heavy-light disulfide bonds). 146

Figure 5.14. SDS-PAGE of analysis of partially reduced Tmab (5 mg/mL, 34 µM) cross-linking in Tris.HCl buffer (100 mM, 150 mM NaCl, 5 mM EDTA, pH 6, 7.5, or 8) with bis-bromoacetamide linkers (7.5 µM) using direct method. Tmab (34 µM) was reduced with 2.2 equiv. of TCEP (75 µM) for 2 h and incubated with (7.5 µM) of each linker at room temperature overnight. L: ladder, lane 1, 5 and 9: Tmab incubated with 2.2 equiv. of methyl 3,4-bis(2-bromoacetamido)benzoate (**4.23**), lane 2, 6 and 10: Tmab incubated with 2.2 equiv. of methyl 3,5-bis(2-bromoacetamido)benzoate (**4.22**), lane 3, 7 and 11: Tmab incubated with 2.2 equiv. of *N*,*N*'-(1,2-phenylene)bis(2-bromoacetamide) (**4.29**), lane 4, 8 and 12: Tmab incubated with 2.2 equiv. of *N*,*N*'-(1,3-phenylene)bis(2-bromoacetamide) (**4.28**). Protein samples were resolved by reducing SDS-PAGE (10% gel). 147

Figure 5.15. SDS-PAGE of partially reduced Tmab (5 mg/mL, 34 µM) cross-linking in Tris.HCl buffer (100 mM, pH 7.5) containing 150 mM NaCl, and 5 mM EDTA, with bis-bromoacetamide linkers using portion-wise method. Tmab (5 mg/mL, 34 µM) was reduced with 1 equiv. of TCEP (34 µM) for 2 h and incubated with 1 equiv. of bis-bromoacetamide linkers (3.4 µM) at room temperature overnight (Lane 1-4). Lane 1: Tmab incubated with 1 equiv. of methyl 3,4-bis(2-bromoacetamido)benzoate (**4.23**), Lane 2: Tmab incubated with 1 equiv. of methyl 3,5-bis(2-bromoacetamido)benzoate (**4.22**), Lane 3: Tmab incubated with 1 equiv. of *N*,*N*'-(1,2-phenylene)bis(2-bromoacetamide) (**4.29**), Lane 4: Tmab incubated

with 1 equiv. of *N*,*N*'-(1,3-phenylene)bis(2-bromoacetamide) (**4.28**). Tmab was further reduced with 1 equiv. of TCEP (34 µM) for 2 h and incubated with 1 equiv. of bis-bromoacetamide linkers (3.4 µM) at room temperature overnight (Lane 5-8) in same order of lane 1-4. Lane (9-12): same samples as in lane 5-8 under non-reducing conditions. 149

Figure 5.16. Deconvoluted spectrum protein MS of cross-linked Tmab with 2.2 equiv. methyl 3,5-bis(2-bromoacetamido)benzoate (**4.22**). Full view MS spectrum of cross-linked Tmab showing a peak at 74,277.53 Da corresponds to rebridged heavy-light chains of Tmab. 150

Figure 5.17. A) SDS-PAGE analysis representing the selectivity of bis-bromoacetamide linkers in cross-linking Tmab (5 mg/mL, 34 µM) in Tris.HCl buffer reduced with 4 equiv. of TCEP (136 µM) and incubated with (6.8 µM, 2 equiv.) of each bis-bromoacetamide linker at room temperature overnight. L: protein ladder, lane 1: Tmab control (non-reducing dye), Lane 2: Tmab control (reducing dye), Lane 3: Tmab incubated with 2 equiv. of methyl 3,4-bis(2-bromoacetamido)benzoate (**4.23**), Lane 4: Tmab incubated with 2 equiv. of methyl 3,5-bis(2-bromoacetamido)benzoate (**4.22**), Lane 5: Tmab incubated with 2 equiv. of *N*,*N*'-(1,2-phenylene)bis(2-bromoacetamide) (**4.29**), Lane 6: Tmab incubated with 2 equiv. of *N*,*N*'-(1,3-phenylene)bis(2-bromoacetamide) (**4.28**). Protein samples were resolved by reducing SDS-Page (10% gel). **B**) Percent conversion of Tmab into various cross-linked products analysed using Gel Image studio 5.2. 152

Figure 5.18. SDS-PAGE gel evaluating selectivity of bis-iodoacetamide linkers in cross-linking Tmab (5 mg/mL, 34 µM) in Tris.HCl buffer (100 mM, pH 7.5) containing 150 mM NaCl, and 5 mM EDTA, reduced with 4 equiv. of TCEP (136 µM) and incubated with (6.8 µM, 2 equiv.) of each bis-iodooacetamide linker at room temperature overnight. L: protein ladder, lane 1: Tmab incubated with 2 equiv. of methyl 3,4-bis(2-iodoacetamido)benzoate (**4.25**), lane 2: Tmab incubated with 2 equiv. of methyl 3,5-bis(2-iodoacetamido)benzoate (**4.24**), lane 3: Tmab incubated with 2 equiv. of *N*,*N*'-(1,2-phenylene)bis(2-iodoacetamide) (**4.31**), lane 4: Tmab incubated with 2 equiv. of *N*,*N*'-(1,3-phenylene)bis(2-iodoacetamide) (**4.30**). lane 5: Tmab incubated with 2 equiv. of *N*,*N*'-(4-((2-(2-(2-(2-azidoethoxy)ethoxy)ethoxy)ethyl)carbamoyl)-1,3-phenylene)bis(2-iodoacetamide) (**4.33**). lane 6: Tmab incubated with 2 equiv. of *N*,*N*'-(4-((2-(2-(2-(2-azidoethoxy)ethoxy)ethoxy)ethyl)carbamoyl)-1,2-phenylene)bis(2-iodoacetamide) (**4.35**). Protein samples were resolved by reducing SDS-Page (10% gel). 153

Figure 5.19. Deconvoluted protein MS spectra of Tmab cross-linked with 2 equiv. of **A**) *N*,*N*'-(4-((2-(2-(2-(2-azidoethoxy)ethoxy)ethoxy)ethyl)carbamoyl)-1,2-phenylene)bis(2-iodoacetamide) (**4.35**) showing major peak at 50,594.97 Da and 50,756.09 Da (unfunctionalised heavy chain), **B**) *N*,*N*'-(4-((2-(2-(2-(2-azidoethoxy)ethoxy)ethoxy)ethyl)carbamoyl)-1,3-phenylene)bis(2-iodoacetamide) (**4.33**) showing major peaks at 51,026.31 Da and 51,189.24 Da [cross-linked Tmab (Tmab-N_3)]. 155

Figure 5.20. SDS-PAGE gel evaluating the selectivity of linkers in cross-linking Tmab (5 mg/mL, 34 µM) in Tris.HCl buffer (100 mM, pH 7.5) which has reduced with 4 equiv. of TCEP (136 µM). L: protein ladder, lane 1: Tmab incubated with 2 equiv. of methyl 3,4-bis(2-bromoacetamido)benzoate (**4.23**), lane 2:

Tmab incubated with 2 equiv. of *N*,*N*'-(4-((2-(2-(2-(2-azidoethoxy)ethoxy)ethoxy)ethyl)carbamoyl)-1,3-phenylene)bis(2-iodoacetamide) (**4.33**), lane 3: Tmab incubated with 2 equiv. of **4.23** in the presence of 2% SDS, lane 4: Tmab incubated with 2 equiv. of **4.33** in the presence of 2% SDS, lane 5: Tmab incubated with 2 equiv. of **4.23** in the presence of 4% SDS, lane 6: Tmab incubated with 2 equiv. of **4.33** in the presence of 4% SDS. Protein samples were resolved by reducing SDS-Page (10% gel). 156

Figure 5.21. SDS-PAGE of Tmab (5 mg/mL, 34 µM) conjugation with methyl 3,4-bis(2-bromoacetamido)benzoate (**4.23**) and DiBr-Mal (**4b**) linkers in the absence and presence of SDS (2%) in Tris.HCl buffer (100 mM, 150 mM NaCl, 5 mM EDTA, pH 7.5). Tmab was reduced with 4 equiv. of TCEP (170 µM) for 2 h at room temperature and then incubated with (17 µM, 5 equiv.) of each linker at room temperature. L: protein ladder, lane 1 and 5: Tmab incubated with 5 equiv. of methyl 3,4-bis(2-bromoacetamido) benzoate (**4.23**) linker, lane 2 and 6: Tmab incubated with 5 equiv. of DiBr-Mal (**4b**), lane 3 and 7: Tmab incubated with 5 equiv. of methyl 3,4-bis(2-bromoacetamido) benzoate (**4.23**) linker in the presence of SDS (2%), lane 4 and 8: Tmab incubated with 5 equiv. of DiBr-Mal (**4b)** in the presence of SDS (2%). Protein samples were resolved by reducing SDS-Page (10% gel). 158

Figure 5.22. Deconvoluted protein MS spectra of cross-linking intra-chain disulfide bond of the light chain of Tmab with methyl 3,4-bis(2-bromoacetamido)benzoate (**4.23**) in the presence of 2% SDS showing a major peak at 23,685.78 Da. 159

Figure 5.23. SDS-PAGE of bifunctional cross-linking of Tmab (5 mg/ml) in Tris.HCl buffer (100 mM, pH 7.5) containing 150 mM NaCl, and 5 mM EDTA, using sequential method. Tmab was reduced with 2.2 equiv. of TCEP for 2 h and incubated with 2.2 equiv. of methyl 3,4-bis(2-bromoacetamido)benzoate (**4.23**) at room temperature overnight (lane 1). Functionalised $Tmab_{bis\text{-}(o\text{-}\mathbf{HL}\text{-}OMe)}$ was further reduced with 2.2 equiv. of TCEP for 2 h and incubated with 4 equiv. of *N*,*N*'-(4-((2-(2-(2-(2-azidoethoxy)ethoxy)ethoxy)ethyl)carbamoyl)-1,3-phenylene)bis(2-iodoacetamide) (**4.33**) at room temperature overnight (lane 2). Protein samples were resolved by reducing SDS-Page (10% gel). 161

Figure 5.24. Deconvoluted protein MS spectra of bi-functional cross-linking of Tmab with methyl 3,4-bis(2-bromoacetamido)benzoate (**4.23**) and *N*,*N*'-(4-((2-(2-(2-(2-azidoethoxy)ethoxy)ethoxy)ethyl)carbamoyl)-1,3-phenylene)bis(2-iodoacetamide) (**4.33**) using sequential method. **A**) Full view MS spectrum of cross-linked Tmab showing major peak at 74,711.99 Da. **B**) Expansion of the spectrum at 74 kDa region. Showing major peaks at 74,711.99 Da and 74,874.13 Da. 162

Figure 5.25. The production of bifunctional Tmab with **4.23** linker ( ) followed by **4.33** linker ( ) with the proposed reduction order of disulfide bonds with TCEP. 164

Figure 5.26. SDS-PAGE analysis of cross-linking of fully reduced Rmab (5 mg/mL, 35 µM) in Tris.HCl buffer with bis-bromoacetamide linkers. Rmab was reduced with 5 equiv. of TCEP **2.2** (175 µM) for 2 h at room temperature and then incubated with (17.5 µM, 5 equiv.) of each linker overnight. L: protein ladder, lane 1: Rmab incubated with 5 equiv. of methyl 3,4-bis(2-bromoacetamido)benzoate (**4.23**), lane 2: Rmab incubated with 5 equiv. of methyl 3,5-bis(2-bromoacetamido)benzoate (**4.22**), lane 3: Rmab incubated with 5 equiv. of *N*,*N*'-(1,2-phenylene)bis(2-bromoacetamide) (**4.29**), lane 4: Tmab incubated

with 5 equiv. of *N*,*N*'-(1,3-phenylene)bis(2-bromoacetamide) (**4.28**). HC: heavy chain, LC: light chain, LC-LC: light chain homodimers, HC-HC: heavy chain homodimers. Protein samples were resolved by reducing SDS-PAGE (10% gel). 166

Figure 5.27. Deconvoluted protein MS spectra of Rmab control showing major peaks 23036.26 and 50521.24 Da at and cross-linked Rmab with 5 equiv. of methyl 3,4-bis(2-bromoacetamido)benzoate (**4.23**) showing a major peak at 74,036.03 Da. 167

Figure 5.28. CD spectrum of Rmab samples over range of 205-260 nm wavelength at 25 ℃ showing different spectrum of the cross-linked Rmab comparing to the control Rmab. 168

Table 5.1. Deconvoluted CD data Rmab samples (acquired at 25℃) over the range of 205-260 nm. Data obtained using CDNN software. 169

Figure 5.29. Variable temperature CD data for Rmab samples showing structural abundance of α-helix, and β-sheet as a percentage of the total protein. Measured over a temperature range of 25-90℃. 170

Figure 5.30. Hydrodynamic radius distribution by intensity for Rmab and cross-linked Rmab at 2 mg/mL, indicating that there is a major peak for Rmab and cross-linked Rmab-OMe with methyl 3,4-bis(2-bromoacetamido) benzoate (**4.23**) at 14.92 nm and 12.00 nm, respectively 171

Figure 5.31. Stability of fully rebridged half antibody ($Rmab_{bis\text{-}[(o\text{-}\mathbf{HL},o\text{-}\mathbf{HH}intra)\text{-}OMe]}$) in plasma mimicking condition. SDS–PAGE analysis of cross-linked Rmab following incubation in plasma mimicking conditions for 0, 1, 3, 5 and 7 days (lanes 2-6, respectively). Protein samples were resolved by reducing SDS-PAGE (10% gel). 172

Figure 5.32. Stability of fully rebridged half antibody ($Rmab_{bis\text{-}[(o\text{-}\mathbf{HL},o\text{-}\mathbf{HH}intra)\text{-}OMe]}$) after storage at 4℃. SDS–PAGE analysis of rebridged Rmab following incubation in fresh buffer at 4℃ after 0, 1, 2, 4, 6 and 8 weeks (lanes 1-6, respectively). Protein samples were resolved by reducing SDS-PAGE (10% gel). ... 173

Figure 5.33. Cross-linking of C3dg (2 mg/ml, 5 µM) with linkers bis-haloacetamide linkers (**4.22, 4.23, 4.24, 4.25**). L: protein ladder, lane 1: control (non-reducing dye), lane 2: C3dg incubated with 5 kDa PEG-maleimide (10 equiv.), lanes 3: C3dg incubated with 0.75 equiv. methyl 3,4-bis(2-bromoacetamido) benzoate (**4.23**), lane 4: C3dg incubated with 0.75 equiv. methyl 3,5-bis(2-bromoacetamido) benzoate (**4.22**), lanes 5: C3dg incubated with 0.75 equiv. methyl 3,4-bis(2-iodoacetamido) benzoate (**4.25**), lane 6: C3dg incubated with 0.75 equiv. methyl 3,5-bis(2-iodoacetamido) benzoate (**4.24**) at room temperature overnight. Protein samples were resolved by reducing SDS-Page (10% gel). 174

Figure 5.34. Cross-linking of C3dg (2 mg/ml, 5 µM) with methyl 3,4-bis(2-bromoacetamido) benzoate (**4.23**) linker. L: protein ladder, lane 1: control (non-reducing dye), lanes 2: C3dg incubated with 0.5 equiv. methyl 3,4-bis(2-bromoacetamido) benzoate (**4.23**), lane 3: C3dg incubated with 0.75 equiv. methyl 3,4-bis(2-bromoacetamido) benzoate (**4.23**), lane 4: C3dg incubated with 1.5 equiv. methyl 3,4-bis(2-bromoacetamido) benzoate (**4.23**) at room temperature overnight. Protein samples were resolved by reducing SDS-Page (15% gel). 175

Figure 5.35. Deconvoluted spectrum protein MS of Cross-linking of C3dg with bis-haloacetamide linkers. **A**) Native C3dg showing a peak at 34,742.28. **B**) Cross-linked C3dg with 0.5 equiv. of methyl

3,4-bis(2-bromoacetamido) benzoate (**4.23**) showing a cross-linked monomer peak at 34,988.40 Da and homo-dimer peak at 69,730.48 Da. 176

Figure 6.1. Complement activation pathways. Regardless of the initiators of each pathway, all three pathways aim to form C3 convertase which activates the central component of the complement system C3. C5 convertase will then be constructed to cleave C5 and form C5b-C9 membrane attack complex (MAC). C3a and C5a are well-known chemotactic agents..... 179

Figure 6.2. Full domains structure of Sbi protein. It comprises four extracellular globular domains (I-IV), the cell wall spanning domain (Wr) and the tyrosine rich region (Y). 185

Figure 6.3. Our proposed mechanism of the immunoconjugates of Trastuzumab-Sbi III/IV which activate the C3 component of complement system to selectively opsonize HER-2 positive cancer cells with C3b and ultimately causing cellular lysis. 187

Figure 6.4. Schematic representation of the conjugation format used to attain conjugation of Tmab and Sbi ( ). 188

Figure 6.7. SDS-PAGE analysis of cross-linking of partially reduced Tmab in Tris.HCl buffer (100 mM, 150 mM NaCl, 5 mM EDTA, pH 7.5) with bis-bromoacetamide linkers. Tmab was reduced with 1.1 equiv. of TCEP for 2 h at 4°C and incubated with 1.1 equiv. each linker at room temperature overnight. Lane 1, 9 and 17: Tmab incubated with 1.1 equiv. of methyl 3,4-bis(2-bromoacetamido)benzoate (**4.23**), Lane 2, 10 and 18: Tmab incubated with 1.1 equiv. of methyl 3,5-bis(2-bromoacetamido)benzoate (**4.22**), Lane 3, 11 and 19: Tmab incubated with 1.1 equiv. of *N*,*N*'-(1,2-phenylene)bis(2-bromoacetamide) (**4.29**), Lane 4, 12 and 20: Tmab incubated with 1.1 equiv. of *N*,*N*'-(1,3-phenylene)bis(2-bromoacetamide) (**4.28**). Lane 5-8, 13-16, and 21-24 represent the same reactions in the same described order but run under non-reducing conditions (non-reducing dye)..... 192

Figure 6.8. A) Deconvoluted protein MS spectrum of cross-linked Tmab with 1.1 equiv. of methyl 3,4-bis(2-bromoacetamido) benzoate (**4.23**) showing major peak at half antibody at 74,384.17 Da and a peak at 50,765.12 Da (unfunctionalised heavy chain). **B**) Deconvoluted protein MS spectrum of cross-linked Tmab with 1.1 equiv. *N*,*N*'-(1,2-phenylene)bis(2-bromoacetamide) (**4.27**) showing two major peaks at 50,756.23 Da (unfunctionalised heavy chain) and half-antibody at 74,442.24 Da. Both spectra showed light chain peak at 23,439.7 Da (unfunctionalised light chain). 193

Figure 6.9. SDS-PAGE of cross-linking of partially reduced Tmab (5.0 mg/ml, 34 µM) in Tris.HCl buffer (100 mM, pH 7.5) containing 150 mM NaCl, and 5 mM EDTA, with bis-o-diiodoacetamide $(PEG)_3$ linker (**6.2**). Tmab was reduced with 1.1 equiv. of TCEP (37 µM) for 2 h at 4°C and incubated with the linker at room temperature overnight. Lane 1: Tmab incubated with 1 equiv. of bis-o-diiodoacetamide $(PEG)_3$ linker (**6.2**), Lane 2: Tmab incubated with 2 equiv. of bis-o-diiodoacetamide $(PEG)_3$ linker (**6.2**), Lane 3: Tmab incubated with 1.1 equiv. of methyl 3,4-bis(2-bromoacetamido)benzoate (**4.23**) at room temperature overnight. 194

Figure 6.10. SDS-PAGE of cross-linking of partially reduced Tmab (5.0 mg/ml, 34 µM) in Tris.HCl buffer (100 mM, pH 7.5) containing 150 mM NaCl, and 5 mM EDTA, with bis-o-dihaloacetamide $(PEG)_3$

linkers. Tmab was reduced with 1.1 equiv. of TCEP (37 µM) for 2 h at 4 °C and incubated with the linkers at room temperature overnight. Lane 1: Tmab control non-reducing dye, lane 2: Tmab control reducing dye, lane 3: Tmab incubated with 1.1 equiv. of methyl 3,4-bis(2-bromoacetamido)benzoate (**4.23**), lane 4: Tmab incubated with 5 equiv. of bis-dibromoacetamide $(PEG)_3$ linker (**6.1**), lane 5: Tmab incubated with 5 equiv. of bis-o-diiodoacetamide $(PEG)_3$ linker (**6.2**). 195

Figure 6.11. SDS-PAGE representing conjugation of partially reduced Tmab and Sbi III/IV-2xCys in Tris.HCl buffer using bis-dihaloacetamide $(PEG)_3$ linkers **6.1** and **6.2**. Tmab was reduced with 1.1 equiv. of TCEP for 2 h at 4°C. Sbi III/IV-2xCys was reduced with 2 equiv. of TCEP for 1 h followed by quenching step with hexa-diazide (10 equiv..) for 1 h. lane 1: Tmab control (non-reducing dye). lane 2: Tmab control (reducing dye), lane 3: Tmab was incubated with 1.1 equiv. of methyl 3,4-bis(2-bromoacetamido)benzoate (**4.23**) linker at room temperature for 3 h, lane 4: Tmab incubated with 5 equiv. of bis-o-diiodoacetamide $(PEG)_3$ linker (**6.2**) at room temperature for 3 h, lane 5: Tmab incubated with 5 equiv. of bis-dibromoacetamide $(PEG)_3$ linker (**6.1**) at room temperature for 3 h, lane 6: Tmab was incubated with 1.1 equiv. of methyl 3,4-bis(2-bromoacetamido)benzoate (**4.23**) at room temperature overnight, lane 7: conjugation reaction of functionalised Tmab-diiodoacetamide with Sbi III/IV-2xCys (4 equiv.) at room temperature overnight, lane 8: conjugation reaction of functionalised Tmab-dibromoacetamide with Sbi III/IV-2xCys (4 equiv.) at room temperature overnight. Protein samples were resolved by reducing SDS-Page (10% gel). 197

Figure 6.12. A) Affinity chromatography purification of Tmab-Sbi conjugation reaction to separate unfunctionalised Tmab **3** from Tmab-Sbi conjugate **5**. **B**) SDS-PAGE analysis of conjugation of partially reduced Tmab and Sbi III/IV-2xCys in Tris.HCl buffer (100 mM, pH 7.5) using bis-o-diiodoacetamide $(PEG)_3$ linker (**6.2**). Lane 1: Tmab incubated with 1.1 equiv. of methyl 3,4-bis(2-bromoacetamido)benzoate (**4.23**), lane 2: Tmab conjugation with Sbi III/IV-2xCys at room temperature overnight before performing affinity chromatography purification, lane 3: collected early fractions (F1-4) of affinity chromatography purification, lane 4: collected eluted fractions (F16-23), lane 5: collected eluted fractions (F24-25), lane 6: collected eluted fractions (F26-33). Arrow indicates the expected band of Tmab-Sbi conjugate around 90 kDa. Protein samples were resolved by reducing SDS-Page (10% gel). 199

Figure 6.13. Synthesis of di-amino$(PEG)_7$ (**6.6**). **a**) *p*-TsCl, pyridine, DMC, **b**) NaN_3, DMF, 80°C, reflux, **c**) Ph_3P, dry THF overnight, then H_2O overnight. 200

Figure 6.14. Synthesis of bis-o-diiodoacetamide $(PEG)_7$ **(6.5**). **a**) di-amine$(PEG)_7$ (**6.6**) THF, **b**) KI, dry acetone, reflux 3 h. 201

Figure 6.15. SDS-PAGE analysis of conjugation of partially reduced Tmab and Sbi III/IV-2xCys in Tris.HCl buffer (100 mM, pH 7.5) containing 150 mM NaCl, and 5 mM EDTA, using bis-o-diiodoacetamide $(PEG)_7$ linker (**6.5**). Lane 1: Tmab control (non-reducing), lane 2: Tmab control (reduced dye), lane 3: Tmab incubated with 1 equiv. of methyl 3,4-bis(2-bromoacetamido)benzoate (**4.23**), lane 4: Tmab incubated with 3 equiv. of bis-o-diiodoacetamide $(PEG)_7$ linker (**6.5**), lane 5: Sbi III/IV-2xCys

Incubated with 5 equiv. of bis-o-diiodoacetamide $(PEG)_7$ linker (**6.5**), lane 6: Tmab conjugation with Sbi III/IV-Cys at room temperature overnight before affinity chromatography purification showing the correct estimated mass of the conjugate around 90 kDa, lane 7: combined early fractions of affinity chromatography purification, lane 8: combined eluted fractions of affinity chromatography with His-B buffer (1 mM imidazole) using Ni^{2+} column (1 mL HisTrap, FF). Protein samples were resolved by reducing SDS-Page (10% gel). 202

Figure 6.16. A) Deconvoluted protein MS spectrum of Sbi III/IV-2xCys control showing major peak at 15,671.98 Da. **B**) Deconvoluted spectrum protein MS of functionalised Sbi III/IV-2xCys with bis-o-diiodoacetamide $(PEG)_7$ linker (**6.5**) showing major peak at 16,272.07 Da. 203

Figure 6.17. A) SDS-PAGE analysis of conjugation of partially reduced Tmab and Sbi III/IV-2xCys in Tris.HCl buffer (100 mM, pH 7.5) containing 150 mM NaCl, and 5 mM EDTA, using bis-o-diiodoacetamide $(PEG)_7$ linker (**6.5**). Lane 1: Tmab control (non-reducing), lane 2: Tmab control (reduced dye), lane 3: Tmab incubated with 1.1 equiv. of methyl 3,4-bis(2-bromoacetamido)benzoate (**4.23**), lane 4: Tmab conjugation with Sbi III/IV-2xCys at room temperature overnight before affinity chromatography purification step showing the correct estimated mass of the conjugate around 90 kDa, lane 5: collected early fractions (F1-5), lane 6: collected eluted fractions (F19-25), lane 7: collected eluted fractions (F27-29). Lane 8: Tmab conjugation reaction with Sbi III/IV-2xCys at room temperature overnight using bis-o-diiodoacetamide $(PEG)_7$ linker (**6.5**) without the quick in between purification step (see Figure 6.15). Lane 9: Tmab conjugation reaction with Sbi III/IV-2xCys at room temperature overnight using bis-o-diiodoacetamide $(PEG)_3$ linker (**6.2**) (see Figure 6.12). Protein samples were resolved by reducing SDS-PAGE (4-12% gel). **B)** Affinity chromatography purification of unconjugated Tmab (lane 5) from Tmab-Sbi conjugate (lane 6 and 7) using Ni^{2+} column (1 mL HisTrap, FF). 205

Figure 6.18. A) SDS-PAGE analysis of conjugation of partially reduced Tmab and Sbi III/IV-2xCys in Tris.HCl buffer (100 mM, pH 7.5) containing 150 mM NaCl, and 5 mM EDTA, using bis-o-diiodoacetamide $(PEG)_7$ linker (**6.5**). Lane 1: Tmab incubated with 1.1 equiv. of methyl 3,4-bis(2-bromoacetamido)benzoate (**4.23**), lane 2: Tmab conjugation with Sbi III/IV-2xCys at room temperature overnight before affinity chromatography, lane 4: collected pure fractions (F19-25) before performing SEC, lane 5: size exclusion chromatography purification (F10-G5). **B)** Size exclusion chromatography purification of Sbi-Tmab conjugation reaction to separate unconjugated Sbi III/IV-2xCys from Tmab-Sbi conjugate (lane 5). Protein samples were resolved by reducing SDS-Page (10% gel). 206

Figure 6.19. Deconvoluted protein MS spectrum of Tmab-Sbi III/IV conjugate, showing a mass around 156,990.64 Da of the degraded product (Tmab-Sbi IV). 207

Figure 7.1. Schematic representation of the two well-known bispecific antibody classes lacking of the Fc region. Orange and green indicate different specificities (binds to different antigens). scFv: single-chain variable domain fragment, TaFvs: Tandem single chain variable fragments, Dbs: diabodies. 211

Figure 7.2. Schematic representation of some of the Fc-containing bsAbs classes. Orange and green indicate different specificities (binds to different antigens). DVD: dual variable-domain. 213

Figure 7.3. Schematic representation of anti-HER2/anti-CTLA-4 bsAb antibody (Trifunctional antibody) with mAb-Fab format that will be further constructed in this work. Orange represents mAb (anti-HER2) and green represents Fab (anti-CTLA-4). 216

Figure 7.4. A) SDS-PAGE analysis of conjugation of partially reduced Tmab and IFab in Tris.HCl buffer (100 mM, 150 mM NaCl, 5 mM EDTA, pH 7.5) using bis-o-diiodoacetamide $(PEG)_3$ linker (**6.2**). Lane 1: crossed-linked Ipilimumab-fab using bis-o-diiodoacetamide $(PEG)_3$ linker (**6.2,** 4 equiv.), lane 2: Tmab incubated with 1.1 equiv. of methyl 3,4-bis(2-bromoacetamido)benzoate (**4.23**), Lane 3: Tmab conjugation with crossed-linked IFab at room temperature overnight before size exclusion chromatography purification, lane 4: size exclusion column purification collected fractions (FA7-A14), lane 5: size exclusion column purification collected fractions (FE7-F1), lane 6: size exclusion column purification collected fractions (FF9-G1). **B)** Size exclusion chromatography of Tmab-Fab conjugation reaction to separate functionalised IFab (lane 6) from Tmab-IFab conjugate (lane 5). 219

Figure 7.5. SDS-PAGE analysis of conjugation of partially reduced Tmab and IFab in Tris.HCl buffer (100 mM, pH 7.5) containing 150 mM NaCl, and 5 mM EDTA, using bis-o-diiodoacetamide $(PEG)_7$ linker (**6.5**). Lane 1: Tmab control (non-reducing), lane 2: Tmab control (reduced dye), lane 3: Tmab incubated with 1.1 equiv. of methyl 3,4-bis(2-bromoacetamido)benzoate (**4.23**), lane 4: Tmab incubated with 3 equiv. of bis-o-diiodoacetamide $(PEG)_7$ linker (6.5), lane 5: IFab incubated with 5 equiv. of bis-o-diiodoacetamide $(PEG)_7$ linker (6.5), lane 6: Tmab conjugation with IFab at room temperature overnight showing the correct estimated mass of the conjugate around 125 kDa. 220

Figure 7.6. A) Schematic representation of functionalisation of IFab with bis-o-diiodoacetamide $(PEG)_7$ (**6.5**) linker. **B**) Deconvoluted protein MS spectrum of IFab control (non-reduced) showing major peaks at 47,636.32 Da. **C**) Deconvoluted protein MS spectrum of functionalised IFab with bis-o-diiodoacetamide $(PEG)_7$ linker (**6.5**) showing major peaks at 48,690.90 Da. 221

Figure 7.7. A) SDS-PAGE analysis of conjugation of partially reduced Tmab with Ipilimumab-fab in Tris.HCl buffer (100 mM, pH 7.5) containing 150 mM NaCl, and 5 mM EDTA, using bis-o-diiodoacetamide $(PEG)_7$ linker (6.5). Lane 1: Tmab incubated with 1.1 equiv. of methyl 3,4-bis(2-bromoacetamido)benzoate (**4.23**), lane 2: Tmab conjugation with IFab at room temperature overnight showing the correct estimated mass of the conjugate around 125 kDa with significant reduction of the 75 kDa band (half-antibody) before performing size exclusion chromatography, lane 4: size exclusion column purification collected fractions (F6-G2), lane 5: size exclusion column purification collected fractions (G4-G13), lane 6: : size exclusion column purification collected fractions (H1-H7). **B)** Size exclusion chromatography of Tmab-Fab conjugation reaction to separate cross-linked IFab (lane 6) from Tmab-Fab conjugate (lane 4). 223

Figure 8.1. Standard curve of BSA standards (2000, 1500, 1000, 750, 500, 250, 125, 25 and 0 µg/mL) used in the BCA protein assay. 228

Figure 8.2. Protein band profile of the prestained PageRuler™ ladder. **A**) Images are from 15% and 10% tris-glycine gel, **B**) Images are from a 4-12% Bis-Tris gel (Thermo Scientific). 230

Figure 8.3. A) Chromatogram of immobilized metal affinity purification of the lysate containing Sbi IV-Cys protein using nickel column. **B**) SDS-PAGE (15%) analysis of the eluted F6-13. 247
Figure 8.4. A) AKTA purification of the lysate using HisTrap column. **B**) SDS-PAGE gel 15%. P (Pellet), S (supernatant), FT (flow through). 294
Figure 11.1. Standard curve of Mal-glutathione conjugate (4.19) 342
Figure 11.2. Standard curve of 3.5 DAB-glutathione conjugate (**4.17**) 343
Figure 11.3. Standard curve of 3.4 DAB-glutathione conjugate (**4.18**) 343
Figure 11.4. Inhibition of the survival in BT 474-cancer cell line by using different concentration levels of Tmab and Tmab-Sbi. HCS: human complement serum. 346

List of Tables

Table 2.1. Aqueous mass and molar solubilites of 4-azidobenzoic acid (**2.7**) and PEG-azides (**2.10**-**2.13**) in H_2O and aqueous Tris.HCl buffer (100 mM, pH 7). 43

Table 3.1. The predicted pK_a values of the chosen sulfonic acid derivatives. [a] values obtained from Scifinder. [b] values were obtained from literature ([140,141]). 53

Table 3.2. Calculated hydrolysis rates (h^{-1}) of sulfonate derivatives **3.1**-**3.5**. 57

Table 4.1. Summary of the reactivity rates of aryl and alkyl haloacetamide linkers with glutathione. 115

Table 4.2. Summary of the aqueous stability and glutathione reactivity of aryl bis-haloacetamide linkers. [a] % of remaining are stated regarding to the least stable linker. 125

Table 8.1. Composition of SDS-PAGE gel, stacking and resolving gels, running buffer, Coomassie blue stain and destain solution. 229

Table 8.2. Tmab-bioconjugates prepared in this project. 281

Table 8.3. The details regarding the buffer used in SEC and the run specifications. 296

Abbreviations

^{18}F-FDG	2-deoxy-2-^{18}F-fluoro-β-D glucose
ADCC	Antibody dependent cell-mediated cytotoxicity
ADCs	Antibody Drug Conjugates
aHUS	atypical hemolytic uremic syndrome
AMD	Age-related macular degeneration
AML	Acute Myeloid Leukemia
AP	Alternative pathways
APS	Ammonium persulfate
BiTE	T-cell engagers
BsAbs	Bispecific antibodies
BT-474	Breast tumour 474
CD	Circular dichroism
CDC	Complement-dependent cytotoxicity
CHIPS	Chemotaxis inhibitory protein of *S. aureus*
ClfA	Clumping factor A
CP	Classical pathway
DAF	Decay accelerating factor
DAR	Drug antibody ratio
DCM	Dichloromethane
DLS	Dynamic light scattering
DMF	Dimethylformamide
DMSO	Dimethyl sulfoxide
DTT	Dithiothreitol
Efb	Extracellular fibrinogen-binding protein
ELISA	Enzyme-linked immunosorbant assay
Fab	Antigen-binding fragment
fB	Factor B
fD	Factor D
fH	Factor H
fI	Factor I
GAGs	Glycosaminoglycans
GSH	Glutathione
HAMA	Human Anti-Mouse Antibody
HAS	Human serum albumin
HCl	Hydrochloric acid
HER-2	Human epidermal growth factor receptor-2

Hib	*Haemophilus influenzae* type b
HRMS	High resolution mass spectrometry
HSAB	Hard-soft acid base model
HSC	Human serum complement
IFab	Ipilimumab-Fab
Imab	Ipilimumab
IMAC	Immobilized metal affinity chromatography
LP	Lectin pathway
mAb	Monoclonal antibody
MCP	Membrane cofactor protein
MDR1	Multidrug resistance protein 1
MMAE	Monomethyl Auristatin E
MMAF	Monomethyl Auristatin F
MW	Molecular weight
NHL	Non-Hodgkin's B-cell lymphomas
NK	Natural Killer
PAGE	Polyacrylamide gel electrophoresis
PBS	Phosphate buffer saline
PD	Pharmacodynamic
PEG	Polyethylene glycol
PET	Positron emission tomography
Ph_3P	Triphenylphosphine
PK	Pharmacokinetic
ppm	Parts per million
PSGL-1	P-selectin glycoprotein ligand
PTM	Post-translational modification
p-TsCl	p-Toluenesulphonyl chloride
RA	Rheumatoid arthritis
Rmab	Rituximab
S. aureus	*Staphylococcus aureus*
Sbi	Staphylococcus immunoglobulin-binding protein
SDS-PAGE	Sodium dodecyl sulphate polyacrylamide gel electrophoresis
SEC	Size exclusion chromatography
SpA	Staphylococcal cell wall anchored protein A
SPAAC	Strain-promoted azide−alkyne cycloaddition
SSL-7	Staphylococcal superantigen-like protein 7
TCEP	Tris(2-carboxyethy)phosphine
TCR	T cell receptors
TDCs	THIOMAB drug conjugates
TEA	Triethylamine
TEMED	Tetramethylethylenediamine

THPP	Tris(3-hydroxypropyl)phosphine
TLC	Thin layer chromatography
TNFα	Human tumor necrosis factor alpha
UV	Ultraviolet

1 Introduction

1.1 Bioconjugation chemistry

Over billions of years, nature has developed post-ribosomal protein modification processes, which are known as post-translational modifications (PTMs). PTMs are covalent modification events of proteins that take place either by hydrolytic break down of proteins or by attachment of specific functionalities to one or more amino acids of proteins.[1] These events take part after ribosomal protein synthesis, in order to amend the physicochemical characteristics of proteins, modulate their activity, and control the process of protein–protein interaction.[2] For instance, the glycosylation process of proteins or the attachment of carbohydrates to proteins is one of the most adopted biological tools to improve the solubility of proteins, and more importantly to modulate protein–receptor interactions (Figure 1.1 A).[3] Other natural PTMs include phosphorylation, ubiquitination, methylation, nitrosylation, acetylation, lipidation and proteolysis.[4] In attempts to mimic these natural PTMs, scientists have made significant efforts to covalently amend proteins with various functionalities.[5]

In its most central aspect, bioconjugation chemistry is a multidisciplinary field, which refers to site specific chemical manipulation of biomolecules of interest, thus covalently adding unique functionalities in order to fulfil the requirements in demand. The process of synthesis of bioconjugates mainly aims to create new complexes which possess properties of each constituent taking part. One of the obvious examples of the application of bioconjugation chemistry is the fluorescently-labelled antibodies. Fluorescently-labelled antibodies bind specifically to a desired antigen and with the added fluorescent properties, they can be visually detected unlike unlabelled antibodies (Figure 1.1 B).[6,7]

Amongst the variety of biomolecules, proteins are the central to what bioconjugation chemistry is all about. A great deal of efforts has been devoted to develop specialized site-specific reagents and procedures to selectively modify proteins for unending number of biological and therapeutic applications. Commercially, a huge number of reagents are available at present, to fulfil the aforementioned applications and other

purposes.[8] One example of biological applications is to provide a means to specifically track intracellular proteins which ultimately could afford a better understanding of biological processes and help in developing opportunistic targets for therapeutic interventions. Moreover, bioconjugation chemistry has played a chief role in the development of vast ground-breaking bio-therapeutics with promising targeted approaches particularly in cancer treatment.[5]

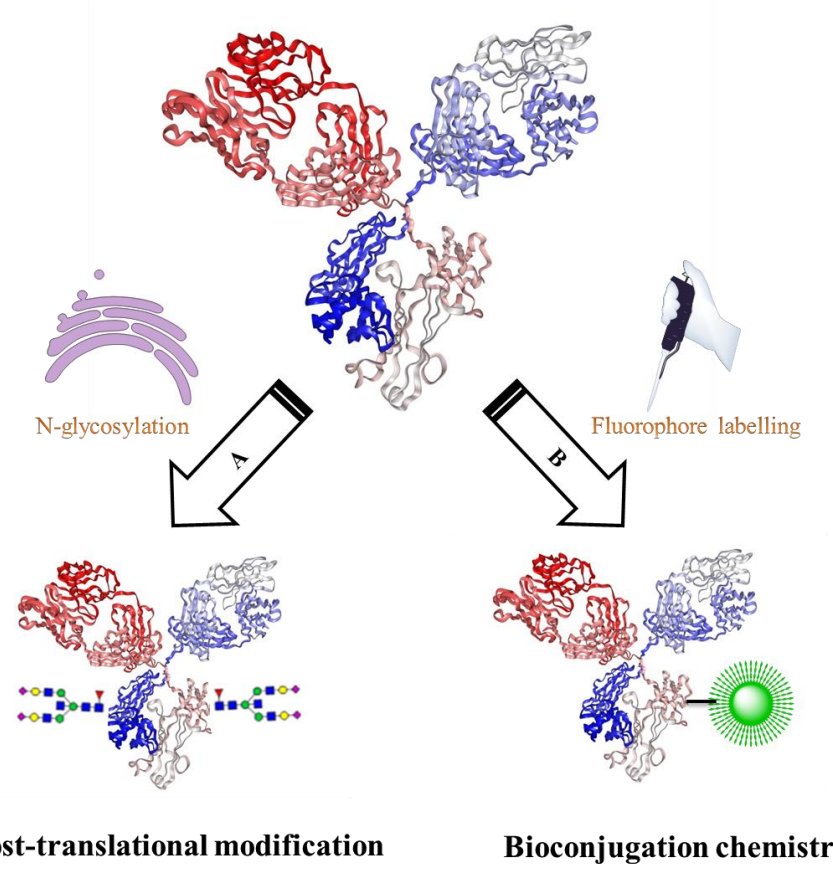

Figure 1.1. Site-specific protein modification of antibodies. **A)** An example of natural post-translation modification of proteins by N-glycosylation of antibodies at C_{H2} domain which is carried out inside the rough endoplasmic reticulum. **B)** An example of bioconjugation chemistry by chemical attachment of a fluorophore to antibodies (fluorescently labelled antibodies) which is widely applied in diagnostic assays.

1.2 Applications of protein conjugates

Recently, the applications of bioconjugation chemistry products have been hugely expanded in different fields, but they can be concisely grouped into three major applications:

1) Analysis and quantification;
2) Detection and imaging of bio-targets;
3) Therapeutics, vaccines and immune modulation.

These applications will be further describe in the following Sections (1.2.1-1.2.3). There are ever-increasing number of applications of bioconjugation chemistry including capture, purification, catalysis and chemical modification of specific biomolecules.

1.2.1 Analysis and quantification

Assay of targeted analyte, in complex mixture of other analytes, is one of the most prevalent direct applications of bioconjugation chemistry. This can be mainly achieved via employing a chemically modified antibody (fluorescently labelled antibody, enzyme-linked antibody, or biotinylated antibody) possessing high affinity toward the analyte of interest.

Enzyme-linked immunosorbant assay (ELISA) system is the most well-known sensitive bioassays that used to quantify a specific antigen through using enzyme-linked antibody.[9] This assay is performed through subsequent steps starting by adding samples of analytes to the wells with captured specific antibody, and allowing the target analyte (antigen) to bind to the captured antibodies. Then, a primary antibody is added which binds to a different epitope on the antigen. A secondary enzyme-linked antibody is added which binds to the primary antibody. Finally, specific substrate which is catalysed by the enzyme generating detectable product will be added (Figure 1.2). An essential washing step is required between the above mentioned procedural steps.

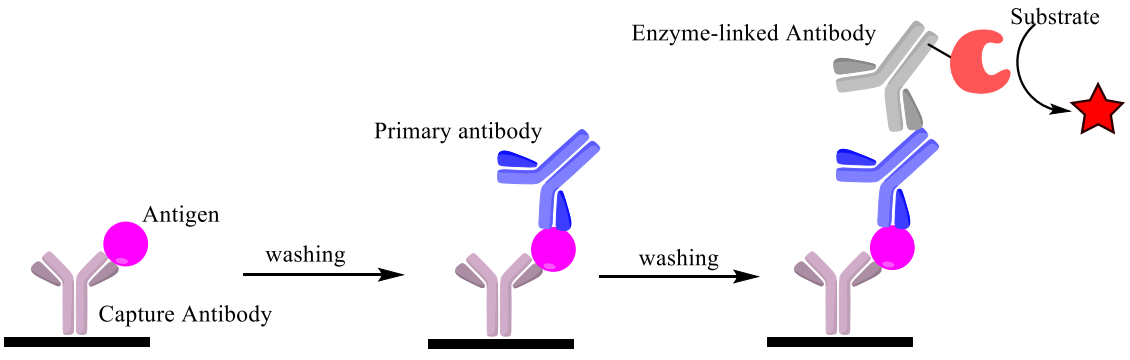

Figure 1.2. ELISA procedure using enzyme-linked antibody to quantify the target analytes (antigens).

1.2.2 Detection and imaging of biomolecules

Conjugated proteins with a fluorophores or radiolabel are usually employed in detection and imaging techniques. Labelled proteins can be either followed *in vitro* (for instance, immunofluorescence) or *in vivo* (for instance, molecular imaging techniques).

Western blots are considered the golden standard used for the *in vitro* detection of certain biomolecules. This techniques is based on employing secondary antibody–enzyme conjugates and streptavidin–enzyme conjugates for the recognition of certain proteins. The procedure involves separation of protein sample based on their molecular weight using SDS polyacrylamide gel electrophoresis (PAGE), followed by transferring the separated proteins to nitrocellulose membrane for immunochemical detection. Then, a binding step of the primary antibodies or biotinylated primary antibodies to the target protein is followed by a secondary binding step through using secondary antibody–enzyme conjugate or streptavidin–enzyme conjugates, respectively. In either of the aforementioned procedures, a subsequent detection step through using specific substrate is followed to develop a detectable signal of at the site of binding.[10]

In vivo imaging tools, such as positron emission tomography (PET) continues to grow mainly in clinical diagnosis, staging, and prognosis of cancer disease, certain brain diseases and dementias. In this technique, gamma rays are indirectly generated and detected to obtain internal organs images. Positron-emitting radionuclide, in particular ^{18}F (fluoro group) is linked to certain compounds, such as deoxyglucose to create the radiopharmaceutical agent, 2-deoxy-2-^{18}F-fluoro-β-D glucose (^{18}F-FDG). ^{18}F-FDG is the most widely used radioactive drug in the detection of malignancies. After injection to the patient, ^{18}F-FDG is circulated inside the target cells by glucose transporters and trapped within those cells.[11] However, FDG are nonspecific for cancer tissue and can also be up taken by inflamed or infected lesions and, of course, by normal tissues/organs. Thus, the interpretation of obtained imaging results might not be accurate.

Recently, immuno-positron emission tomography, imparts selectively through attachment of the radiolabel to monoclonal antibody (mAb) or mAb fragments.

Radiolabelled mAbs bind to specific antigens that is expressed differently on tumour cells, therefore, the imaging procedure will address questions regarding the presence, location, and size of the malignant neoplasm.[12,13] Zeglis *et al.* introduced radiolabeled antibodies to attain pre-targeted PET imaging tool. They used tumor homing antibodies that attached to trans-cyclooctene (TCO) group in a mouse xenograft tumor model. TOC-mAb could selectively and rapidly react with a radiolabeled tetrazine ring through Diels–Alder click chemistry, thus affording a visible antibody to be detected by PET scanner (Figure 1.3).[14] Rashidian *et al.* on the other hand, have used ^{18}F-labelled antibody fragments for PET imaging. The ^{18}F-labelled antibody fragments were constructed through sortase-mediated installing of TCO into the protein of interest, followed by selectively reacting it with a tetrazine-labeled FDG.

The previously described approaches provide an efficient and selective method of imaging through utilising ^{18}F-labeled antibodies and their fragments with improved level of specificity over the conventional FDG-based imaging.[15]

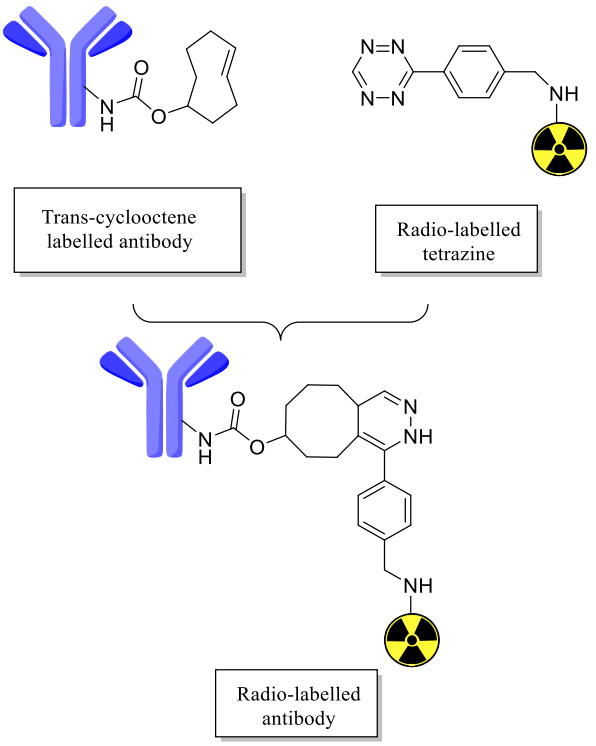

Figure 1.3. Diels–Alder click reaction of tumor-homing antibody-Trans-cyclooctyne (TCO) conjugate with radiolabelled tetrazine affording radiolabeled antibody accumulated in tumor site in order to be visualized by PET imaging approaches. Picture adapted from reference ([5]).

1.2.3 Therapeutic conjugates and conjugate vaccines

Therapeutic proteins are hugely disseminated class of drugs with wide range of therapeutic indications. More than 200 normal and modified therapeutic proteins have been approved by the European Union and the USA for clinical use.[16] Unfavourable drawbacks of employing native proteins have been encountered, ranging from pharmacokinetics properties and short half-life to immunogenicity and allergic reactions. One of the well-recognised adopted chemical modifications of therapeutic proteins is the covalently attachment of PEG - a process known as PEGylation. PEGylation is usually performed to address the limitations of using native bio-therapeutics, including instability, short half-life, and immunogenicity. PEGs are non-toxic, hydrophilic, nonimunogenic and uncharged polymer. PEGylated proteins have displayed enhanced pharmacokinetic properties *in vivo*.[17]

Perhaps the best known example of PEGylated protein is Cimzia® (certolizumab pegol). Cimzia® is a humanized monoclonal Fab′ fragment against human tumor necrosis factor alpha (TNFα) which covalently bound to an approximately 40-kDa PEG molecule through alkylation of the cysteine residues in the hinge region using a branched maleimide-PEG affording a defined conjugate of approximately 91 kDa (Figure 1.4). The conjugate binds to TNFα and neutralize its activity, which is well-known inflammatory mediator and indicated mainly for the treatment of Crohn's disease and severely active cases of rheumatoid arthritis.[18]

Conjugate vaccines are another growing class of medical compounds which typically are consisting of a polysaccharide antigen (weak antigen) bound to a carrier molecule such as bovine serum albumin (BSA), keyhole limpet hemocyanin (KLH), tetanus toxoid, diphtheria toxoid, and tuberculin purified protein derivative (PPD) through various chemical conjugation methods. Conjugate vaccines are constructed to improve the stability and more importantly the efficacy of the vaccine.[19]

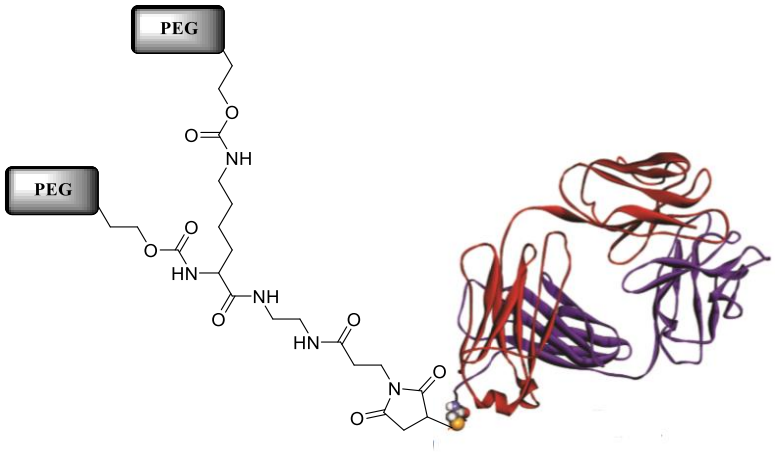

Figure 1.4. The structure of Cimzia® conjugate, which is a humanized Fab′ fragment against TNFα that is chemically conjugated with two PEG chains. Figure adapted from reference ([7]).

Many of the invasive infection-causing bacteria (such as *Salmonella typhi*, *Haemophilus influenzae* type b (Hib), *Streptococcus pneumoniae* and *Neisseria meningitidis*) have outer polysaccharide capsule as virulence mechanism, providing protection against complement system and phagocytosis. Purified capsular polysaccharides are unsatisfactory and insufficient immunogenic agents when administrated as vaccines to protect against invasive infections. Hib plain polysaccharide alone has been evaluated as a vaccine, however, it has induced relatively low titers of serum antibodies that are insufficient to protect against invasive infectious disease. The limited immunogenicity of polysaccharides is due to the lack of T-cells recognition (only recognized by B-cells). Therefore, induction of T-independent response which prevents the proper development of B-cells i.e. class-switched antibody production and avidity maturation.[19]

Hib conjugate was the first approved conjugate vaccine in clinical practice. It was approved in the USA in 1987, and shortly it has been licensed in infant immunisation schedule. Hib conjugate vaccine has found to be effective in reducing the incidence of Hib infectious diseases in childhood.[20,21]

Recently, one of the most vital applications of bioconjugation chemistry in human therapeutics is the chemical conjugation of mAb with cytotoxic drugs, which known as Antibody Drug Conjugates (ADCs). ADCs are modern targeted approaches in cancer therapy in which the mAb leads the cytotoxic drug to malignant cells, whereupon the

cytotoxic payload performs certain cellular killing mechanism. Four ADCs have been approved by the FDA for treatment of various refractory and metastatic malignancies and around 60 are under investigation in clinical trials.[22]

1.3 Antibody drug conjugates

The basis of traditional cancer therapy is to remove and kill cancer cells either by surgery, radiation or the non-selective conventional chemotherapy drugs. Surgery and radiation therapy could be effective in solid and localised tumor, while non-selective conventional chemotherapy drugs are mainly used in metastatic cancer types. Conventional chemotherapeutic drugs are generally directed toward rapidly proliferating cancerous cells, but can also kill other normal dividing cells. Adopting non-selective conventional chemotherapy drugs - as the name implies - is associated with non-avoidable severe side effects.[23]

Traditional chemotherapeutic agents can be classified into three major families based on their mode of action:

- Antimetabolites family, such as purine analogues (6-mercaptopurine and 6-thioquanine), folate analogues (methotrexate), and fluoropyrimidine (5-FU) which still remains the cornerstone for treatment of colorectal cancer.[24,25]
- Antimicrotubule (mitotic inhibitor) family, such as vinca alkaloids (vinblastine and vincristine) which mainly interacts with tubulin protein and disrupt microtubule function, and eventually causing metaphase arrest.[26]
- The third major family is DNA damaging agents, such as alkylating agent (nitrogen mustard) which are one of the oldest class of anticancer drugs and DNA intercalating agents (anthracyclines).[27,28]

Tyrosine kinases inhibitors (Imatinib) are recently introduced group of anti-cancer agents that interfere with the signaling cascade mediated by tyrosine kinases. Tyrosine kinases can be either activated in response to external or internal stimuli, subsequently they convey the stimuli intracellular, and eventually govern different biological processes such as growth, differentiation, metabolism, and apoptosis.[29]

A great number of research has been conducted to obtain in depth mechanistic understanding of cancer at the cellular level. These efforts have facilitated the discovery of differentially expressed antigens that could be selectively targeted in cancer therapy using mAbs. Shortly thereafter, mAb has been hugely disseminated in treatment of various inflammatory diseases and cancer. Perhaps the most crucial feature of mAbs is their high specificity to target antigens that are either overexpressed, mutated or selectively expressed on cancer tissue.[30]

Over the last two decades, mAbs have been considered as a well-deserved mainstream branch in treatment of various types of cancer. As of October 2017, there are 61 mAbs in clinical use after been approved by FDA and/or EMA, approximately 40% of the approved mAbs are used for the treatment of cancer.[31]

1.3.1 **Monoclonal antibodies (mAb)**

Antibodies (Immunoglobulins, Igs) are 150 kDa heterodimeric glycoproteins comprise of four polypeptide chains: two identical heavy chains and two identical light chains (Figure 1.5). Each heavy chain is comprised of one variable (V_H) and three constant domains (C_{H1}, C_{H2}, C_{H3}), while each light chain is composed of only a single variable (V_L) and a constant (C_L) domain. Variable domain is responsible for antigen binding and therefore, this region displays high level of variation in amino acid composition. Each variable domain is composed of three regions of high sequence variability, (complementarity determining regions, or CDRs) and four regions of relatively high sequence consistency (framework regions, or FRs). Each heavy and light polypeptites chains are held together through non-covalent interactions and covalent inter-chain disulfide bonds to construct a bilaterally symmetric structure of antibody.[32]

Light chain can be either κ or γ chain type. Igs are divided into five main classes according to the type of constant domains of the heavy chain: IgM, IgG, IgA, IgD, and IgE. IgG is the major class found in human body with the longest serum half-life in comparison with all other Igs classes. Moreover, amongst the five classes of Igs, IgG is the most extensively studied and used in therapeutic application. Four IgG subclasses

(IgG_1, IgG_2, IgG_3 and IgG_4) were identified based on structural, antigenic and functional differences in the constant domain of the heavy chain (mainly C_{H1} and C_{H3}).[33]

In order to facilitate the early study of the structure of antibody, digestion enzymes, such as papain, were used. Papain digests IgG into two Fab fragments, and a single Fc fragment. The Fab consists of a variable fragment (Fv: V_H and V_L domains), and a constant fragment (Fc: C_L and C_{H1} domains). Fc fragments specify effector functions of antibody, including activation of complement system through binding to C1q and phagocytosis via binding to Fc receptors (FcγR). In addition to be responsible for the effector function, C_{H2}-C_{H3} domains of Fc region determine the serum level of IgGs through binding to the Fc neonatal receptor (FcRn).[34]

It worthwhile mentioning that IgG_1 has 4 solvent exposed inter-chain disulfide bonds holding heavy-light and heavy-heavy chains along with another 12 intra-chain disulfide bonds that are not solvent accessible and buried within each domain of the 12 domains (Figure 1.5).[35]

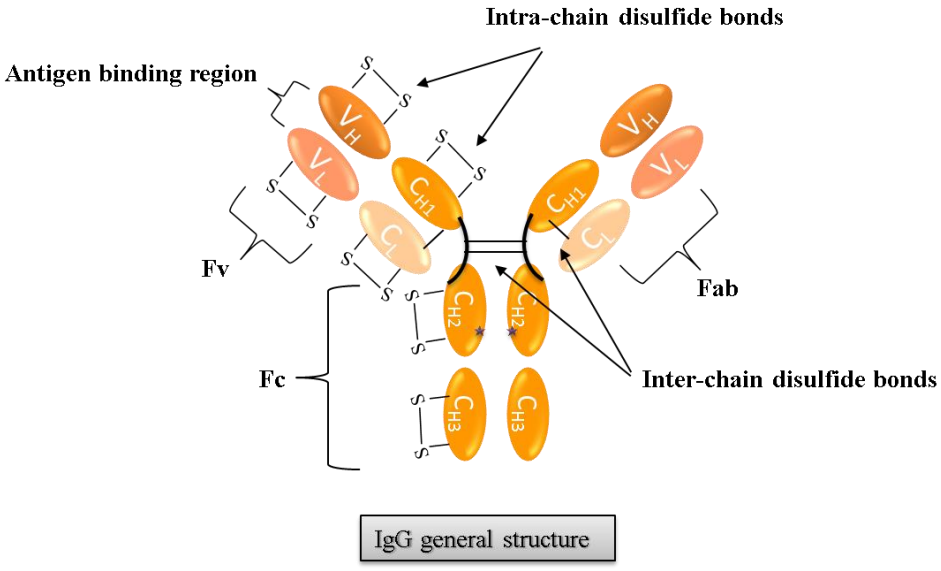

Figure 1.5. General bilaterally symmetric structure of IgG. Blue stars indicate glycosylation sites of C_{H2} domain of the Heavy chain.

Once mAbs bound to their specific receptors, mAbs initiate cell death through different pathways, including complement-dependent cytotoxicity (CDC) or antibody dependent

cell-mediated cytotoxicity (ADCC). Moreover, mAbs interfere with downstream signaling events associated with these receptors, such as growth and regulation of differentiation of cells (Figure 1.6).[30]

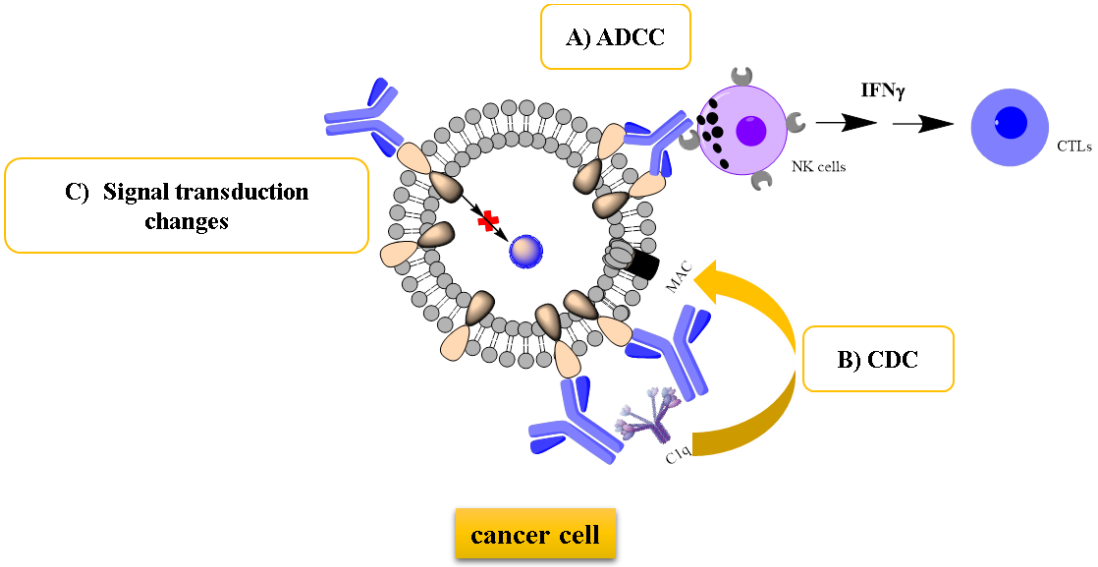

Figure 1.6. Interaction of mAbs with cancer cells and their mechanism of causing cell death. **A)** ADCC involves interaction of Fc domain with FcγR on immune effector cells mainly, natural killer cells (NK). NK cells releases perforin and other enzymes to lyse cancer cells in addition to pro-inflammatory mediators, such as IFNγ to activate nearby antigen presentation and adaptive immune responses.[36] **B)** CDC involves complement C1q binding to C_{H2} domain of Fc region, which in turn activate the classical pathway of complement activation. Complement activation result in construction of membrane attack complex (MAC) and cellular lysis.[37] **C)** Signal transduction changes of these receptors on cancer cells which might normalise the malignant symptoms and sensitise cells to cytotoxic drugs.[38] CLTs: cytotoxic lymphocytes.

Early used mAbs were of murine origin and therefore immunogenicity and triggering Human Anti-Mouse Antibody (HAMA) response were the major problems encountered with using mAbs in the clinical practice. In attempt to overcome the immunogenicity problem, genetically engineered types of mAb were employed in clinical practice: Chimeric mAb (where the constant regions of human antibody are combined with a murine variable region) or humanization (where only the murine CDR regions used and sewn onto a human antibody). The current state of the art immunogenicity mitigation is the so-called fully human mAbs, which was made possible by two widely employed techniques: phage display, and genetically modified mice expressing a human antibody repertoire.[39–41]

In 1997, a major breakthrough occurred in clinical oncology when rituximab (Rmab) was approved as a first mAb in the treatment of cancer. Rituximab, the largest-selling biologic drug in clinical oncology, is a chimeric monoclonal antibody that binds to CD20 antigen on both normal B cells, and on most low-grade and some higher grade B-cell lymphomas. It is primarily used in combination with standard chemotherapies in the treatment of patients with non-Hodgkin's B-cell lymphomas and chronic lymphocytic leukemia.[42]

The second monoclonal antibody that has proven high efficacy in clinical oncology is Trastuzumab (Tmab), a humanised mAb anti-HER2 (human epidermal growth factor receptor 2) receptor. It is primarily used in conjunction with chemotherapy for patients with human HER2 positive breast cancer.[42]

There are 12 mAbs that have received FDA approval for the treatment of different solid tumors and hematological malignancies, in addition to numerous therapeutic antibodies in their early- and late-stage clinical trials.[30] Nonetheless, studies have shown that most of the available mAbs have demonstrated suboptimal clinical activity and as a result, they are used in conjunction with chemotherapy.[38,43] Thereby, researchers are focused on empowering the activity of mAb through different approaches to take advantage of their specificity that has amended most of the unavoidable side effects associated with conventional anticancer therapeutics.

Accordingly, immunoconjugates between mAb and an effector molecule have been produced, either between an antibody and an enzyme (to activate a prodrug), a cytotoxic drug, or a radioisotope (Figure 1.7).

As mentioned earlier, mAbs have been employed in ADCs as a vehicle for targeting a cytotoxic drug toward cancer cells. By fulfilling the theory of magic bullet of Paul Ehrlich, ADCs provide a selective mean of delivery of cytotoxic payloads to cancer cells. This approach is currently receiving remarkable attention in cancer therapy.

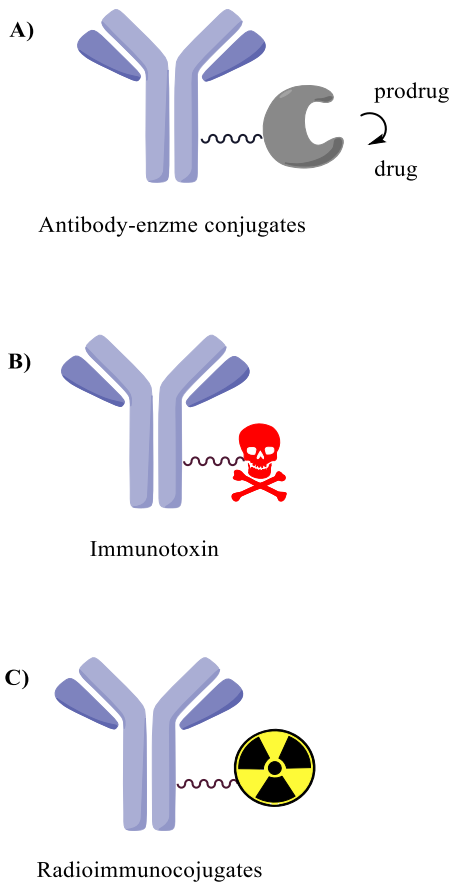

Figure 1.7. Immunoconjugates types between **A**) an antibody and an enzyme (capable of activating a prodrug), **B**) an antibody and a toxin, **C**) an antibody and a radioisotope.

1.3.2 Cytotoxic mechanism of ADCs

ADCs exert their cytotoxicity through internalisation into cancer cells with the process of receptor-mediated endocytosis after selectively recognizing specific receptors on cancer cells. Normally, cells continuously internalise their surface receptors through receptor-mediated endocytosis. Clathrin-dependent endocytosis is the chief mechanism for the internalisation of cell surface receptors. Briefly, endocytosis generally starts when a ligand binds a cell-surface receptor, which initiates an array of subsequent steps, starting from selection of receptors by adaptor proteins for internalisation, to the movement of clathrin from the cytoplasm to adaptor protein-enriched regions of the membrane. Then polymerization of clathrin takes place, followed by inward budding of the plasma membrane and formation of early endosomes, which either recycle the receptor back to plasma membrane or routed to lysosomes. Lysosomes have acidic and proteolytic-rich

environment, therefore the cytotoxic drugs are degraded from ADCs and released into the cell to exert certain killing mechanism. It might kill neighbor cells through bystander effect (Figure 1.8).[44,45]

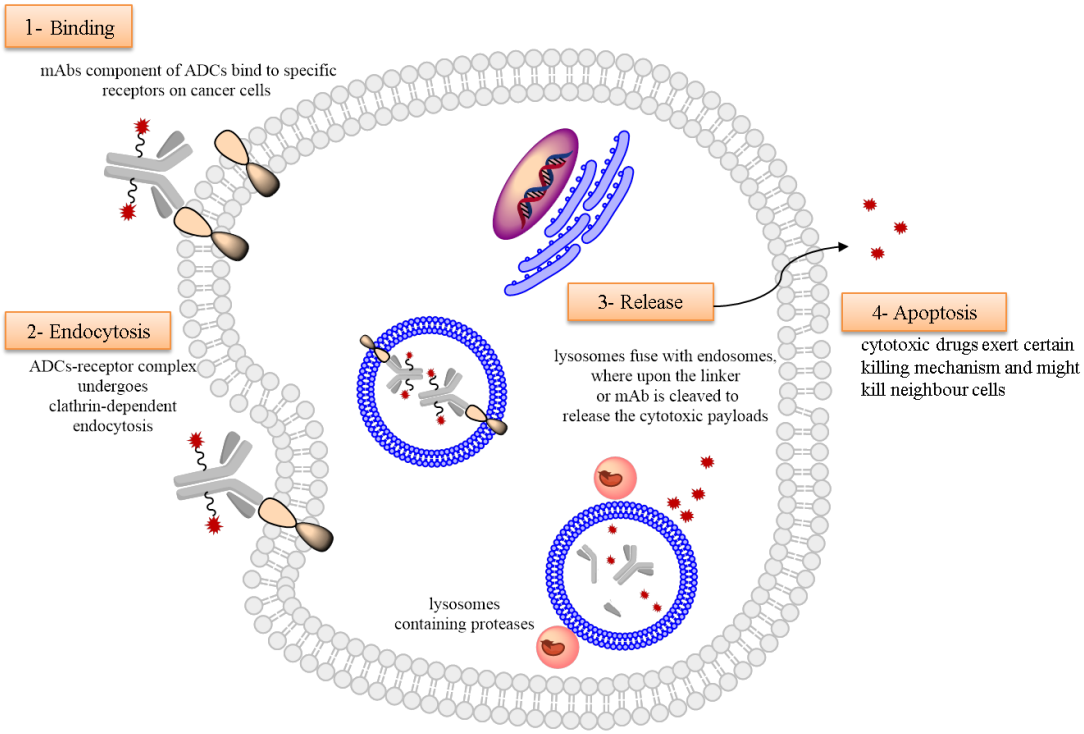

Figure 1.8. Cytotoxic mechanism of ACDs. The process starts when the mAb component recognizes and binds to a specific antigen on cancer cell, followed by rapid internalisation of the antigen-ADC complex. The endosomes are routed to lysosomes where the ADC is degraded leading to the release of the cytotoxic drug, then the drug binds to its target, either DNA or tubulin and cause cellular apoptosis. It may also be released or pumped through the cell membrane which leads to bystander effect.

1.3.3 The anatomy of ADCs

ADCs are composed of three major components as shown in Figure 1.9:

1) An antibody targeting a receptor that expressed differently on cancer cell.
2) A cytotoxic payload that is considered too toxic to be utilized as stand-alone therapy.
3) A linker connecting the mAb to the cytotoxic drug.

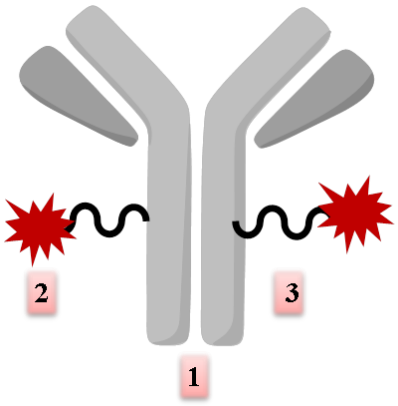

Figure 1.9. The Anatomy of ADCs. ADCs are composed of three main parts: 1) mAb that specifically binds to antigens expressed on cancer cells. 2) Cytotoxic drug that usually binds to tubulin or DNA and leads to cellular apoptosis. 3) Stable linker that ideally attach the cytotoxic drugs at specific sites on mAb and release it through the endosomal-lysosomal pathway.

Choosing the tumor antigen is the first step in the assembly process of ADCs. Antigens must be found on the cell surface and expressed differently on cancer cells i.e. highly or specifically expressed on cancer cells. In addition, ideally, targeted antigen must undergo endocytosis to internalize the ACDs inside the cell to be able to release the cytotoxic payload. Antibodies, should display high binding affinity to the target antigen (K_d<10 nM) and preferably it should not be immunogenic.[46]

Once the antigen and the mAb selected, the next essential step is to develop the conjugation method (linkers) to construct the ACD. Innovations in linker development are centered on plasma stability and cellular release of the cytotoxic drug. Ideally, the linker should have maximum plasma stability, yet should allow rapid release of the cytotoxic drug inside the cancer cell. The linkers have three sub-components: a functional group to attach to a specific site on mAb, a spacer which mostly deemed as hydrophilic moiety of the linker, and a trigger that specifically release the cytotoxic drug once ADC reached intended cancer cells.[47] Linkers can be divided into two major types: cleavable and non-cleavable linkers. As lysosome has an acidic environment and filled with lysosomal enzymes, cleavable linkers have been designed based on the encountered lysosomal conditions: acid-labile linkers and proteases cleavable linkers, respectively. A third type of the cleavable linker is the disulfide linkers which release the cytotoxic payloads based on the high cellular level of reduced glutathione. The release of cytotoxic

drugs with non-cleavable linker depends on the degradation of the ADC complex inside the cell to release the cytotoxic agents with attached amino acids. Non-cleavable linkers afford higher plasma stability over the cleavable linkers.[48,49]

The cytotoxic drug, the third component of the ADC, must meet certain criteria of potency and stability in order to be selected as cytotoxic payload of ADCs. The cytotoxic payload should display high potency and normally the selected cytotoxic drug can't be used as such. Additionally, it should be resistant to multidrug resistance protein 1 (MDR1), which is well-known resistance mechanism mediating drug efflux. And lastly, it should be amendable to chemical modification to be attached to the linker.[45]

Currently, there are two major categories of cytotoxic drugs fulfilling the required aforementioned criteria: microtubule inhibitors and DNA-damaging agents. Commonly used microtubule inhibitors are derived from auristatins, and maytansinoids. Microtubule inhibitors binds to tubulin, inhibits their polymerization, and eventually cause cell cycle arrest and apoptosis.[50] DNA-damaging cytotoxic agents, include duocarmycin and calicheamicin analogous, bind to DNA in the double-helix minor groove, initiate double-strand breaks in DNA and ultimately leading to cellular death.[43]

1.3.4 First generation of approved ADCs

1.3.4.1 Gemtuzumab ozogamicin (Mylotarg®)

Gemtuzumab ozogamicin (Mylotarg®) was approved by FDA in 2000 for the treatment of CD33 positive Acute Myeloid Leukemia (AML) patients. It comprises of Anti-CD33 antibody that is chemically linked through its lysine residues to calicheamicin cytotoxic payload. It was voluntarily withdrawn from the market in 2010 after post-approval confirmatory trials. It has been found that the risks outweighed the benefits of using Mylotarg® in treatment of AML patients. Nevertheless, it was reintroduced in 2017 with a new dosing regimen.[51]

The construction of ADC gemtuzumab ozogamicin was achieved through random acetylation of lysine residues of gemtuzumab humanized mAb (IgG_4) using a cleavable

hydrazone linkers. Drug antibody ratio (DAR) is around 2–3 calicheamicin moieties per antibody and approximately 50% of ADCs are unconjugated mAb (naked).[52]

Conjugation through lysine residues produces random and complex of ADCs species, therefore the stability of these conjugates, their pharmacokinetic (PK) properties and their associated biological responses will vary among the patients.[53]

1.3.4.2 Brentuximab vedotin (Adcetris®)

Brentuximab vedotin was approved in 2011 for the treatment of Hodgkin's lymphoma and anaplastic large cell lymphoma.[54] It composed of Anti-CD30 chimeric mAb that is chemically linked through its cysteine residues to auristatin derivative drug, Monomethyl Auristatin E (MMAE). CD30 is a tumor necrosis factor receptor considered as a primary diagnostic marker in Hodgkin's lymphoma with no noticeable expression on healthy tissue and non-activated lymphocytes.[55] Chemical conjugation of Anti-CD30 mAb with MMAE was achieved using enzymatic cleavable linker (maleimidocaproyl-valine-citrulline-para-aminobenzyl). A maleimide functionality mediates binding to the reduced Anti-CD30 mAb cysteine residues, and the stable peptide is the trigger sub-component of the linker which remains stable in plasma and releases MMAE via proteolysis at the active site.[55] DAR ratio is around 2–8 MMAE moieties per antibody with a small amount of naked antibody.[56]

1.3.4.3 Ado-trastuzumab emtansine (Kadcyla®)

Ado-trastuzumab emtansine (Kadcyla®) was approved in 2013 by FDA for the treatment of HER2-positive metastatic breast cancer patient. It comprises Anti-HER2 mAb (Trastuzumab) that is chemically linked through its solvent accessible lysine residues to the tubulin disrupting cytotoxic drug, maytansine (DM1). HER2 overexpression has been found in approximately 20–30% of breast cancers, which is referred to as HER2-positive subtype.[57]

Trastuzumab is chemically conjugated to DM1 through non-cleavable linker, succinimidyl 4-(*N*-maleimidomethyl)-cyclohexane-1-carboxylate (SMCC) forming amide bonds with a DM1 average of 3.5 per antibody.[58]

1.4 Traditional conjugation chemistries employed in the construction of protein-conjugates

Amongst the available biomolecules including proteins, carbohydrates, and nucleic acids, proteins are indeed at the centre of what bioconjugation chemistry is all about and ADCs are considered as one of the most essential applications of protein bioconjugates. Traditional protein modification has been widely achieved through targeting functionalities found in the side chains of the natural amino acids. Among these amino acids, two main amino acids namely lysine and cysteine, are the most widely targeted residues.

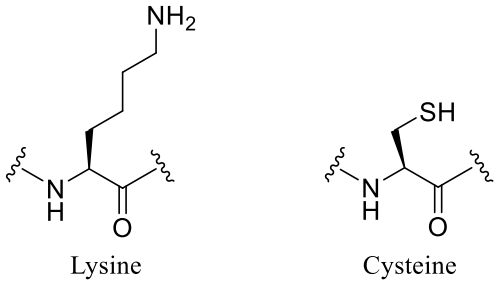

Figure 1.10. The chemical structure of the most widely modified residues in protein conjugation reaction, lysine and cysteine amino acids.

1.4.1 Conjugation chemistries targeting amine side chains of lysine

Coupling to amine group-containing amino acids, such as lysine and amino group in the N-terminus are considered one of the oldest and most common functional group targeted in cross-linking reaction of biomolecules. The ε-amine group of lysine has pK_a value of about 10, thus most of lysine amino groups are protonated at physiological pH and are located on the surface of the protein. Given that protonation significantly decreases their reactivity, basic buffers of high pH are required to deprotonate amino groups. ε-amine group of lysine has been modified by increasing number of chemical reagents, such as activated esters (*N*-hydroxysuccinimides (NHS), sulfo-NHS, acyl azides), isothiocyanates, isocyanates, and aldehydes. Among these reagents, NHS esters and the water soluble sulfo-NHS are the most widely applied ones.[59,60]

Given that proteins have other different reactive nucleophiles, such as sulfhydryl group of cysteine, and hydroxyl group of tyrosine, the selectivity of aforementioned electrophilic groups is not only limited to amine group of lysine, particularly, when these nucleophiles are solvent-reachable groups and found on the surface of the protein.

1.4.1.1 Isocyanates and Isothiocyanates

Amine groups readily react with isocyanates and isothiocyanates to form stable ureas and thioureas, respectively (Figure 1.11 A). Isothiocyanate-based reagents are commercially more accessible and stable analogues of isocyanates.

Fluorescein isothiocyanate (FITC), which is more stable analogue of isocyanates, has been introduced for fluorescent labelling of antibodies by Riggs and co-workers in 1958. Shortly thereafter, these labelling reagents have been widely disseminated in diverse bioconjugation fields and proved to be effective for specifically labelling of proteins.[61–64]

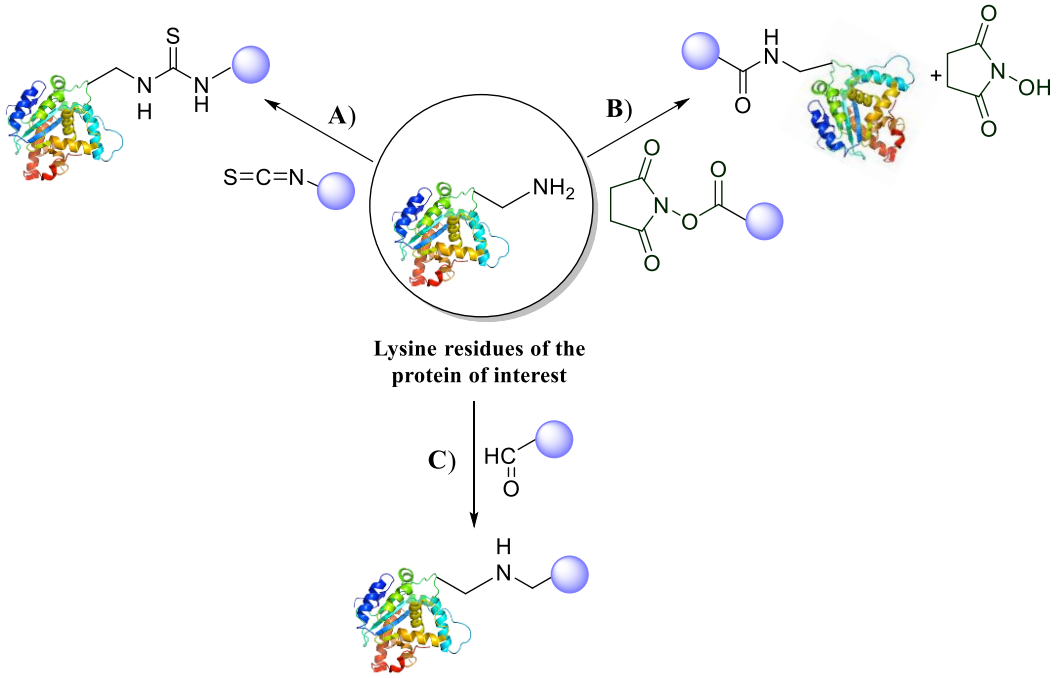

Figure 1.11. Reactive amine-based bioconjugation chemistries. **A**) Reaction of isothiocyanates with amine group forming thiourea. **B**) Reaction of NHS activated ester with amine group forming amide linkage. **C**) Reaction of aldehyde group with amine group followed by mild reduction.

1.4.1.2 NHS and sulfo-NHS activated esters

N-Hydroxysuccinimide (NHS) activated esters were introduced by Anderson and co-workers as a new approach in construction of the peptide bonds.[60] NHS esters were among the first reagents employed in diverse bioconjugation applications. Nowadays, NHS esters are the most disseminated reagents used in covalent protein modification. In comparison with isothiocyanates, NHS esters are more selective for amine group labelling, and can be pursued at faster rates and lower buffer pHs to afford more stable conjugate products.[65–68]

NHS ester and the water soluble sulfo-NHS react with amino group, forming an acylated product (Figure 1.11 B). Sulfhydryl and hydroxyl groups can also react with NHS activated esters, but the conjugated products of these reactions are unstable in aqueous environments especially in the presence of amine nucleophiles. The optimum pH for reactions of NHS-esters in aqueous buffers was found to be between pH 7 to 8. Given the abundance of solvent-reachable surface lysine on most proteins, the reaction unfavourably results in a mixture of labelled products at multiple protein positions.[69]

One of the well-known examples of employing NHS-activated ester in covalent protein modification is the commercially available Ado-trastuzumab emtansine (Kadcyla®). The construction of the ADCs was achieved through functionalization of lysine residues on Tmab with NHS activated ester bearing maleimide function group to be further conjugated to the sulfhydryl group of DM1 drug (Figure 1.12).[70]

1.4.1.3 Aldehydes

Amine groups undergo nucleophilic addition reaction with aldehyde groups forming imine functionality (Schiff base) which then can be selectively reduced using a mild reducing agent, such as sodium cyanoborohydride, to give a stable alkyl amine bond (Figure 1.11 C). This approach is not as popular in protein conjugations as activated ester or isothiocyanate-based approaches.[6]

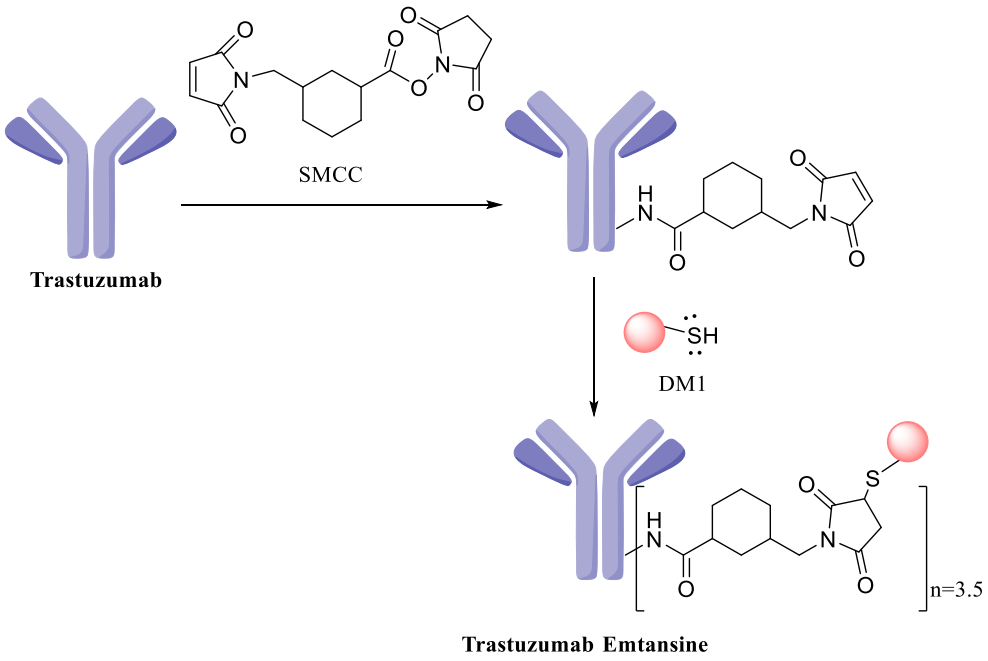

Figure 1.12. Trastuzumab emtansine conjugation scheme. Firstly, modification of lysine residues on Tmab with NHS activated ester, followed by conjugation of the sulfhydryl of DM1 drug with the activated Tmab. SMCC: succinimidyl 4-(*N*-malemidomethyl) cyclohexane-1-carboxylate (SMCC) linker. DM1: Maytansine, tubulin disrupting cytotoxic drug. Figure adapted from reference ([71]).

However, reductive amination is widely applied approaches in carbohydrate–protein conjugates construction.[72] Glycoprotein conjugate vaccines, such as Menactra (meningococcal diseases), HIBTiter (Haemophilus influenzae type b associated diseases), and Prevnar (pneumococcal diseases) are FDA approved conjugate vaccines that are routinely used for the prevention of invasive bacterial infections. The carrier protein, Cross-Reactive-Material-197 (CRM197), is a mutant non-toxic version of the diphtheria toxin is cross-linked to bacterial polysaccharide through reductive amination at lysine moieties and N-terminus.[73,74]

1.4.2 Conjugation chemistries targeting thiol side chains of cysteine

Sulfhydryl group has been deemed as the most disseminated functionality employed for biomolecules conjugation owing to two main reasons. Firstly, the high nucleophilicity of cysteine's thiolate group (pK_a of thiolate group≈8.3). Secondly, the relative rare abundance of cysteine amino acid in proteins (1–2%) which provide site-specific modification of proteins.[75,76] Given that most cysteine amino acids are tied up in

disulfide bridges, free thiols can be generated by selectively reducing cystine disulfides with reducing agent or can be introduced through site specific mutagenesis in the sequence of the protein of interest providing a single reactive site.[77,78]

1.4.2.1 Maleimide derivatives

The double bond of maleimides ring undergoes alkylation reaction with thiolate group of cysteine forming stable thioether bonds. Maleimide coupling chemistry is highly specific for thiols functional group at pH range between 6.5 -7.5.[79]

Owing to the very fast kinetics and high selectivity toward protein cysteine residues, coupling of maleimide to cysteine of proteins is considered the most widely disseminated applied strategy for bioconjugation application.[80–82]

Currently, the FDA-approved ADCs: Brentuximab vedotin (Adcetris®) (Figure 1.13) and PEGylated conjugate Cimzia®, are the examples of modified protein therapeutics which have been constructed based on thioether linkage between maleimide group and thiolate group of either Brentuximab or TNFα, respectively.[83]

Nonetheless, it becomes widely known that maleimide−thiol conjugates formed through Michael addition, are not stable and might slowly undergo retro-Michael addition to reform maleimide and in the presence of free thiols, as in most biological environment, a new thiol conjugate will be assembled. In case of ADCs, retro-Michael reaction is associated with mitigation of the efficacy, and most importantly, undesired off-target toxicity due to the de-attachment of the cytotoxic payloads.[84]

In addition to retro-addition, thiosuccinimide ring might undergo irreversible hydrolysis and ring opening to provide succinamic acids derivatives. However, it has been proposed that intentionally hydrolysing succinimide ring will stabilise the conjugates and prevent thiol exchange (Figure 1.14).[85]

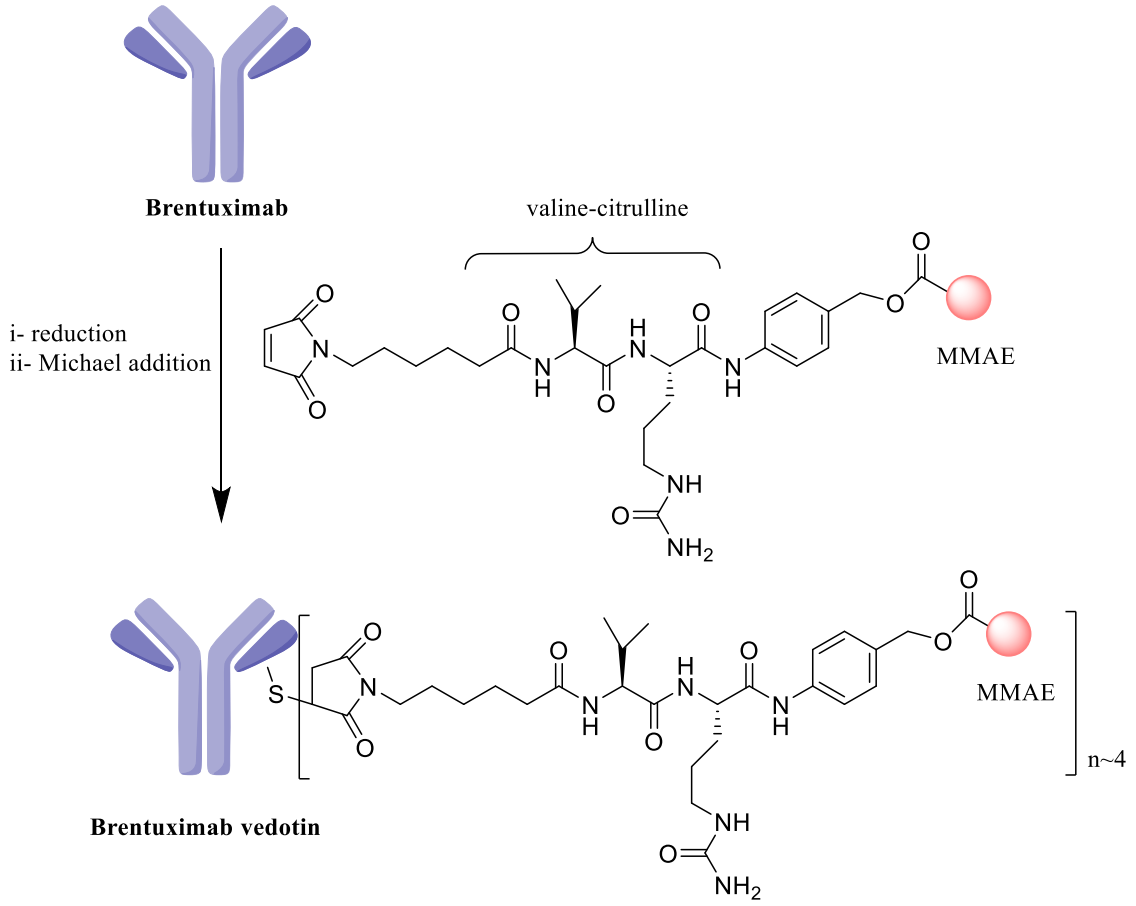

Figure 1.13. Brentuximab Vedotin conjugation scheme. Firstly, reduction of interchain disulfide bonds on brentuximab, followed by conjugation of the sulfhydryl of brentuximab with maleimide activated MMAE is a microtubule inhibitor derived from auristatins. MMAE: Monomethyl Auristatin E.

Lyon *et al.* reported a method for intentional hydrolysis of succinimide ring and ring-opening in order to stabilise thiol-maleimide conjugates and prevent thiol exchange in plasma through incorporation of a primary amine in close proximity to the succinimide ring. They proposed a mechanism involving intramolecular base catalysis by the amine group.[86]

On the other hand, Fontaine *et al.* argued that intentionally hydrolysing succinimide ring by the closely positioned amine is due to the electron withdrawing inductive effect. Given that amine groups are largely protonated at physiological pH, thus they are unable to act as a general base. To confirm their hypothesis, they found that incorporation of other electron withdrawing groups in close proximity to succinimide ring has increased the observed hydrolysis rates of the ring.[83]

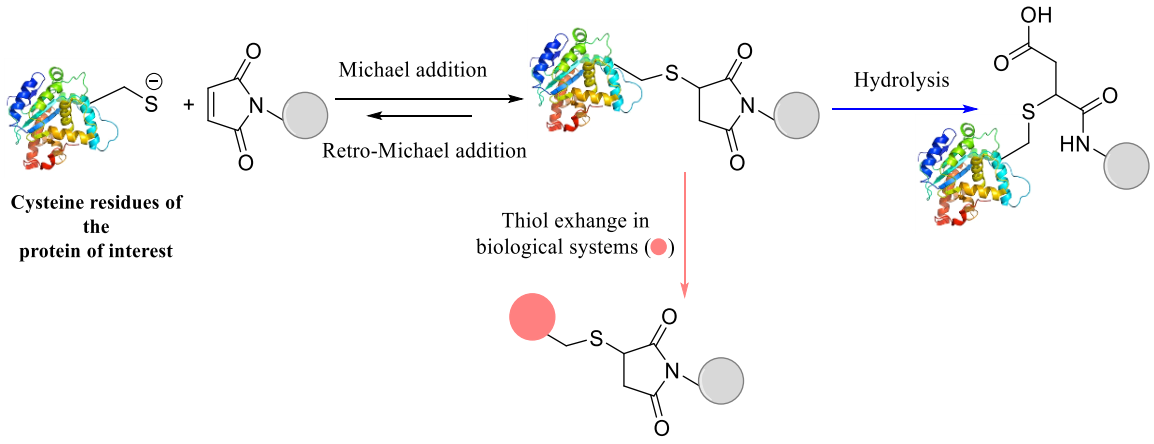

Figure 1.14. Reversible thiol-maleimide alkylation reaction. Thiosuccinimide ring might undergo retro-Michael addition (undesirable) or hydrolysis and ring opening (desirable). Grey circle refers to the cytotoxic payloads, pink circle refers to proteins of biological system, such as human serum albumin (HAS).

1.4.2.2 α-Haloacetyl derivatives

Since the introduction of iodoacetamide in 1935, α-haloacetyl compounds have been widely used in the crosslinking, bioconjugation, and immobilization of cysteine-containing proteins and peptides.[87,88]

The reactivity of this group is attributed the electrophilic characteristics of the central carbon which come from the direct attachment to electron-withdrawing group, the carbonyl group, and to the electronegative halogen atom. Nucleophiles, such as thiols undergo nucleophilic substitution reaction of the halogen with simultaneous formation of a thioether bond. Among α-haloacetate, the order of reactivity toward sulfhydryl group of cysteine is I > Br > Cl > F, fluorine displays almost negligible reactivity (Figure 1.15).

Although maleimide-based chemistry is more prevalent because of their higher kinetics, α-haloacetyl-based bioconjugation chemistry is usually preferred in certain applications where the stability and size of the conjugates are fundamental aspects. α-Iodoacetyl-based chemistry is commercially available and widely applied, including cross-linkers, biotinylation reagents and immobilisation kits.[89]

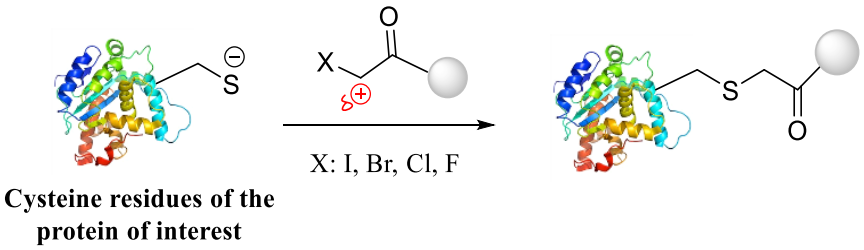

Figure 1.15. Cross-linking of cysteine residues of proteins using α-haloacetyl compounds to afford thioether linkage.

The reactions of thiolate group with haloacetamides are performed under physiological and alkaline conditions (pH≈7.2– 9.0). It is important to perform iodoacetamides reaction under dark conditions in order to prevent free iodine generation, which might react with other amino acid such as tyrosine, histidine and tryptophan residues. It is worthwhile to mention that iodoacetyl groups might react with amine groups, particularly at basic conditions and when all cysteine residues have been consumed.[89]

1.4.2.3 Vinyl sulfone derivatives

Vinyl sulfone undergoes Michael addition reaction with thiolate group of cysteine forming a stable thioether linkage. These reactions require slight basic conditions to be performed. Perhaps the most important advantage of using vinyl sulfone chemistry is their superior stability compared with maleimide-based bioconjugation (Figure1.16).[90–92]

Vinyl sulfone-mediated cross-linking have been used mainly for PEGylation of proteins with functionalised PEG derivatives.[93]

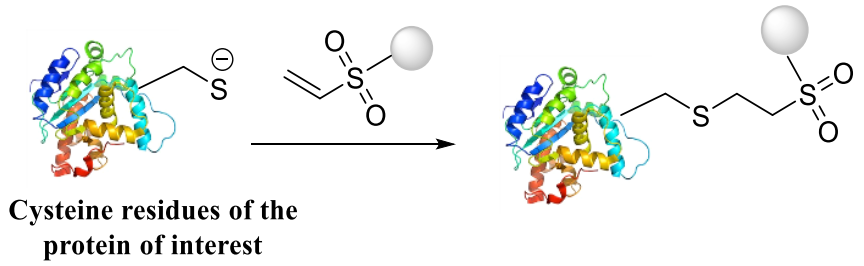

Figure 1.16. Cross-linking of cysteine residues of proteins using vinyl sulfone compounds through Micheal addition reaction to afford thioether linkage.

In summary, despite the large number of conjugation chemistries targeting lysine and cysteine amino acids, each mentioned strategy has drawbacks ranging from specificity toward certain side chains to the stability of the constructed conjugates.

Given that ADCs are deemed as promising therapeutic approach in the field of oncology, significant efforts have been made to modify the conjugation strategies to attain homogeneous, well-defined and stable antibodies conjugates.

1.5 The next generation of ADCs: Improved homogeneity and stability

The first generation ADCs' conjugation methods were predominantly achieved on solvent reachable reactive amino acid residues with nucleophilic properties, in particular lysine and cysteine. Lysine and reduced cysteine based-conjugation result in a range of 0-8 conjugated drugs per antibody. Indeed, use of conventional conjugation methods produces heterogeneous mixture of ADC species and their pharmacokinetic (PK) and pharmacodynamic (PD) properties are likewise heterogeneous. Heterogeneity of ADCs species has a number of drawbacks, such as competitive inhibition of conjugated mAbs by unconjugated mAbs, and increment of clearance of ADCs species with high DAR ratio. In contrast, homogeneous mixture of ADC species would have more predicted batch-to-batch consistency, predicted PK properties and more importantly, improved therapeutic index.[94,95]

Due to the earlier mentioned drawbacks associated with first generation of ADCs, improved, sites-specific, and stable conjugation approaches have been optimised to attain the next generation of homogeneous ADCs with preferable safety characteristics and superior therapeutic window properties.[96] Most of the recent reports suggested DAR of four as a preferable target in ADC construction.[97]

1.5.1 THIOMAB drug conjugates

Cysteine is the most disseminated target for bioconjugation owing to two main reasons. Firstly, the high nucleophilicity of thiolate group of cysteine. Secondly, the relative rare abundance of cysteine amino acid in proteins (1–2%).[75,76]

Reduction of the disulfide bonds to produce free thiolate have many drawbacks that should be considered, most importantly, the structural stability of the reduced antibody.[95] One of the earliest approaches to tackle these issues is genetically modifying mAbs with engineered cysteine residues, also known as THIOMABs. Genentech pioneered THIOMABs for site-specific and defined conjugation with cytotoxic payloads. THIOMABs allow production of a homogeneous mixture of ADC species with defined number of loaded cytotoxic drugs. Nonetheless, choosing site of introduction of cysteine is essential and difficult step as it affect the structure and function of antibody.[98]

Anti-MUC16 antibodies with engineered reactive cysteine residues (HC-A114C), were conjugated with monomethyl auristatin E (MMAE) to construct THIOMAB drug conjugates (TDCs). It was directly compared *in vitro* and *in vivo* with the traditional anti-MUC16 ADCs. Anti-MUC16 ADCs and TDCs displayed comparable *in vitro* cytotoxicity and similar efficiency *in vivo* against a transplant xenograft model of ovarian cancer. However, the latter showed wider therapeutic window and superior safety properties in animal models with lower liver and bone marrow toxicity. The improved safety profile can be attributed to the absence of high-drug loaded ADC species and the greater stability of the TDC in circulation.[95]

Choosing the engineering site of cysteine has an essential impact on the stability and the efficacy of ADCs. Ben-Quan Shen *et al.* argued that conjugation to buried engineered cysteine residues (less solvent accessible) affords more stable conjugates. Moreover, the environment surrounding the conjugation site displayed a profound effect on the stability of ADCs, where conjugation in positively charged environment accelerates the hydrolysis of succinimide to succinic acid, and the later has superior plasma stability toward retro-addition reaction and drug release.[85]

1.5.2 Unnatural amino acids

In addition to the engineered cysteine amino acid, antibodies with engineered selenocysteine and noncanonical amino acids, such as acetylphenylanaline have been employed as alternative approaches for construction of homogeneous ADC species. Selenium or selenocysteine (^{34}Se, 79 Da), the twenty-first amino acid, has selenolate

group which has lower pKa (5.2) than thiolate group (8.3), which renders it a stronger nucleophile.[99] Anti-HER2 (selenomab) with a C-terminal selenium residue was produced and conjugated with MMAF derivative peptides using iodoacetamide. Their stability and efficacy were tested both *in vitro* and *in vivo*, using selenocysteine as a reactive target offered highly stable selenomab-drug conjugates and demonstrated improved potency and selectivity (mouse models of breast cancer).[96]

Acetylphenylanaline, on the other hand, contains a keto group which can be conjugated to auristatin derivative bearing alkoxy-amine to attain an oxime ligation. *p*-acetylphenylalanine was site-specifically incorporated into an anti-HER2 antibody in two sites on antibody constant region (Figure 1.17). The mutant antibody was conjugated to an auristatin derivative in 4 days through a stable oxime linkage. The resulting conjugates displayed similar pharmacokinetics to unconjugated antibodies, more potent *in vitro* cytotoxic activity against HER2 positive cancer cells, and complete tumor regression in 14 days in rodent xenograft models.[100]

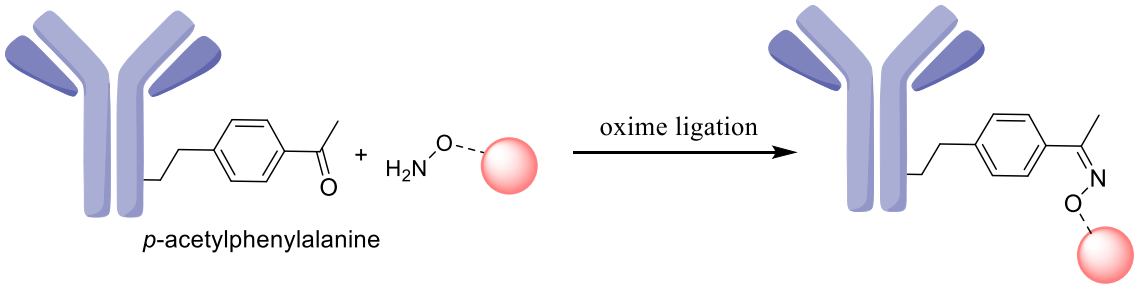

Figure 1.17. Site-specific conjugation approach using oxime ligation, which attaches alkoxyamine linked with payloads ( ) to *p*-acetylphenylalanine-tagged mAb.

Zimmerman and his group used a different unnatural amino acid, namely *p*-azidomethyl-L-phenylalanine providing the antibody with azide functionality. They demonstrated that site-specific incorporation of *p*-azidomethyl-L-phenylalanine enabled the conjugation of two MMAF drug per antibody using strain-promoted azide−alkyne cycloaddition (SPAAC). The constructed ADC of trastuzumab exhibited potent cytotoxicity against HER2 positive cancer cells.[101]

1.5.3 Enzymatic techniques

Enzymatic techniques were also utilized as another strategy to attain site specific antibody drug conjugation. Mainly, two enzymes were used in homogeneous ADCs construction, glycotransferases and transglutaminases.[102]

Mutated glycotranferases used to link a modified sugar moiety to the oligosaccharide attached to Asn-279 of the Fc fragment of human IgG antibodies. A mutated glycotranferase has been produced to transfer a modified galactose having a chemical group at the C2 position, such as ketone or azide to degalactosylaed G0 form antibodies.[103]

Transglutaminase from *Streptoverticillium mobaraense*, catalyzes the formation of a covalent bond between a glutamine side chain and a primary amine, but it does not recognize naturally occurring glutamines in the Fc constant regions of antibodies, so engineered glutamine tag into antibody were produced. Anti-M1S1-vc-MMDA conjugate were produced using transglutaminase enzyme into engineered glutamine. Both *in vitro* and *in vivo* activities were evaluated, and the results demonstrated that conjugation through this strategy does not affect activity and affinity of antibody.[104]

NEB Therapeutics established another enzymatic method using Sortase A enzyme. Sortase A is *Staphylococcus aureus* enzyme that catalyzes transpeptidation reactions. It cleaves between threonine and glycine of LPETG sequence forming LPET-enzyme adduct. Then, it forms a bond between poly-glycine residues and threonine of LPET. The developed technology is termed SMAC technology (Sortase Mediated Antibody Conjugation), was established to produces a stable and homogeneous ADC species. The strategy involve engineering the antibody with incorporation of LPETG peptide, and subsequently the conjugation via addition of Sortase A and a poly-glycine linked-payload (Figure 1.18).[105]

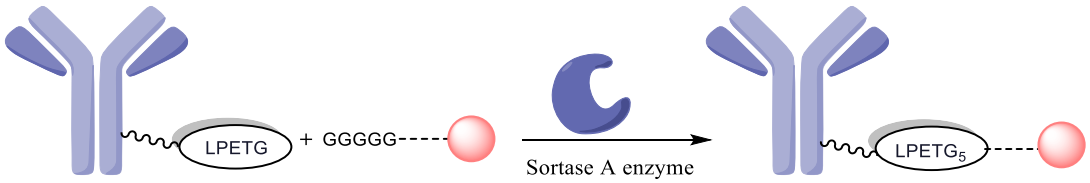

Figure 1.18. Site-specific enzymatic conjugation approach using Sortase A enzyme, which attaches poly-glycine-linked payloads ( ) to LPETG-tagged mAb.

1.5.4 Disulfide rebridging strategies

Most proteins do not have free cysteine, and cysteine can either be introduced through mutagenesis or via reduction of disulfide bond using reducing agents.[106–108]

Although, genetic-based and enzymatic-based methods have been increasingly developed, these methods are expensive, require complex expression and purification tactics, and none of them has found its way to the market yet. On the other hand, according to many studies, the currently adopted monoalkylation of the reduced disulfide bonds using maleimide-based approaches also have major limitations. Primarily, the stability of the conjugates in plasma in the presence of competing glutathione and albumin which would eventually release free cytotoxic drug in plasma.[109]

Recently, an elegant approach has been proposed to covalently rebridge the free thiolate anions derived from the reduced disulfide bonds to attain stable and defined antibodies-conjugates with maintained post-reduction structure of antibodies. One of the earliest examples of rebridging reagents that have been suggested in construction of ADCs is bis-sulfone cross-linker (Figure 1.19). The mechanisms of bis-alkylate disulfide bonds using bis-sulfone reagents and the other developed rebridging agents are further elaborated in chapter 4.

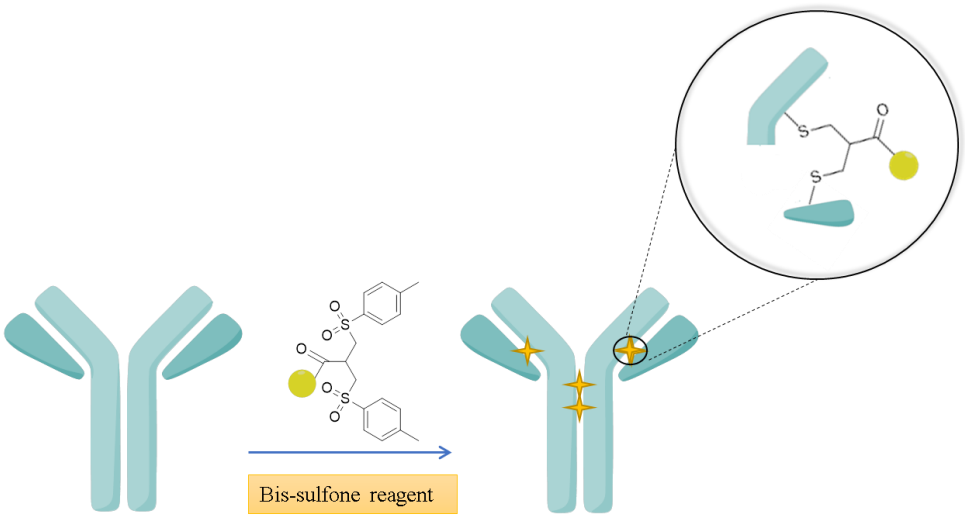

Figure 1.19. Rebridging approach of the reduced disulfide bonds of mAb using functionalised bis-sulfone reagent to form three carbon bridges between the two reduced cysteine of mAbs.

1.6 Bioorthogonal cross-coupling reactions using unnatural functional groups

The previously mentioned bioconjugation reactions are mainly devoted to covalently attach fluorescent label, PEGs, isotope, affinity tags, or cytotoxic payloads to certain amino acids of proteins *in vitro*. Another intended application of conjugation chemistry is to cross-couple individual proteins to attain chemically-linked protein-protein entities.[110,111]

Moreover, in the coming years, scientific applications of bioconjugation chemistry are increasingly moving toward bioorthogonal cross-linking of proteins and biomolecules with tracking probe inside living cells and animals providing vivid, functional and dynamic sensors to measure diverse intracellular physiological interactions (*in vivo*). Thus, for the sake of *in vivo* labeling applications, bioconjugation approaches have to obey certain necessities, including being specific, of high yield, non-toxic, of good kinetics and most importantly, to be biocompatible with normal biological processes (bioorthogonal).[112] In simplified terms, biomolecules in cells can be tagged with benign functionalities, such as azide group by incubating the cells with metabolic precursor bearing azide group. Then, the tagged biomolecule is reacted with a tracking probe carrying a complementary functional group.[113]

Azides are small, unnatural group, stable toward most reaction conditions and only decompose and release nitrogen at high temperature. Moreover, they do not interfere or react with nucleophiles present in biomolecules. For these mentioned reasons, azides are considered outstanding group and widely applied in bioconjugation cross-coupling reactions.[114]

1.6.1 Staudinger ligation & traceless Staudinger ligation

The Staudinger ligation, developed by Bertozzi and co-workers in 2000, was the first reaction developed for *in vivo* bioconjugation applications. In this reaction, azides react with phosphines to form aza-ylide intermediate. In the presence of water, this intermediate hydrolyses readily to a primary amine and phosphine oxide. However, in the presence of ester group within the phosphine structure and in close proximity of aza-ylide intermediate, it reacts with the intermediate forming amide bond rather than hydrolysis (Figure 1.20 A).[115]

Traceless Staudinger ligation, on the other hand, has the same reaction principle but affords an advantage over the normal Staudinger ligation. The phosphine moiety is removed from the final conjugated product (during hydrolysis) and thereby allowing the formation of a native amide bond linkage without residual, unnatural moieties (Figure 1.20 B).[116]

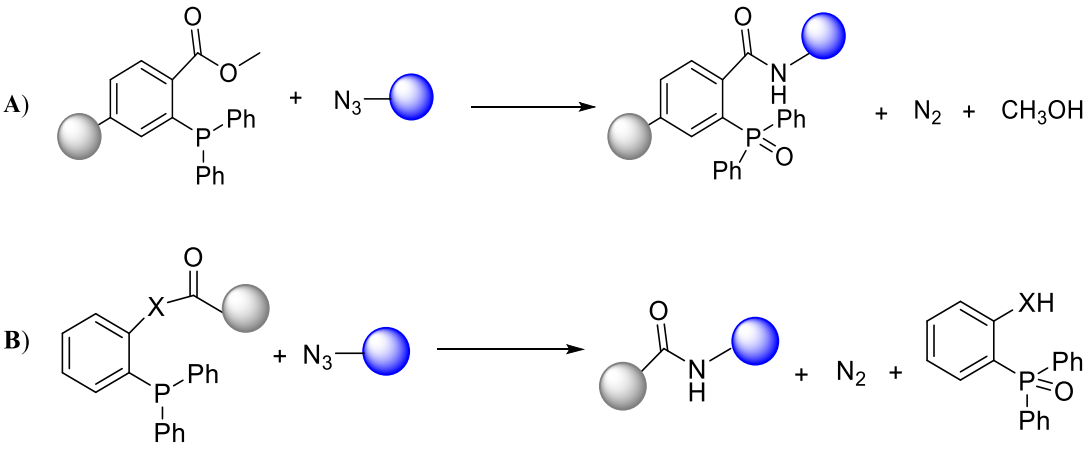

Figure 1.20. **A**) Non-traceless Staudinger ligation and **B**) Traceless Staudinger ligation generating amide linkage.

1.6.2 Azide-Alkyne cycloaddition 'Click' reaction

The relatively slow kinetics of Staudinger ligation is one of the main drawback limiting the wide applicability of this ligation in biological systems. To this end, researchers aimed to find a substitute bioorthogonal reaction replacing Staudinger ligation.

Cycloaddition reactions were viewed as promising alternative to Staudinger ligation. Huisgen developed the [3+2] cycloaddition between an azide and an acyclic alkyne groups in 1963.[117] However, this reaction required high heat in order to overcome the activation energy to perturb the alkyne's linear bond angle (180º) forming triazole ring with bond angle of 120º (Figure 1.21 A). In order to decrease the required heat to perform cycloaddition reactions, Cu(I) was employed as a catalyst, but it is associated with cellular toxicity which halt its applicability in bioorthogonal bioconjugation chemistry.[118]

However, azide-alkyne cycloaddition reaction found the way back to popularity in bioconjugation chemistry when stained-induced cycloaddition was introduced. The use of cyclooctyne (**1.1**) (the bond angle is ~ 160°) will reduce the required heat for the reaction and thus it can be performed at room temperature with significant acceleration of reaction rate (Figure 1.21 B). Furthermore, the addition of flouro and di-flouro (**1.2**) increases the rate of the cycloaddition reaction 60 times. Nowadays, the most widely used activated-cyclooctyne are dibenzocyclooctyne-based derivatives (**1.3**) which showed similar rate of cycloaddition reaction to di-flourocyclooctyne (**1.2**), these stained system are easy to prepare and with more room to be modified and functionalised.[112]

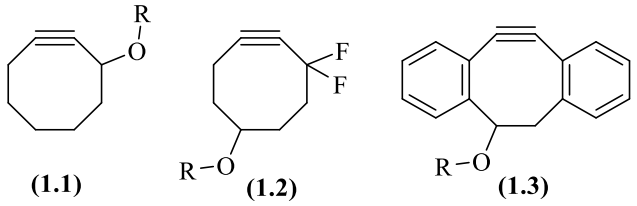

(1.1) **(1.2)** **(1.3)**

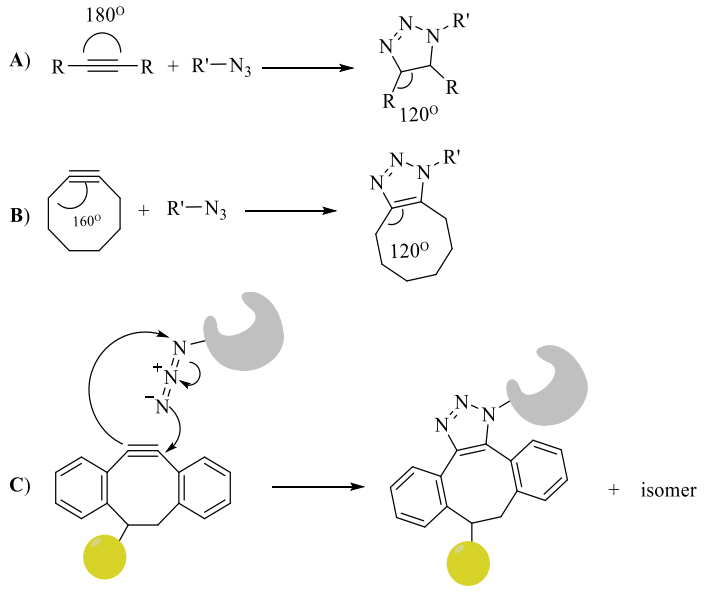

Figure 1.21. Cycloaddition reaction of azides and alkynes groups (copper-free 'Click'reaction). **A**) Azide-alkyne cycloaddition reaction. **B**) Strain-induced azide-cyclooctyne cycloaddition reaction. **C**) Mechanism of Cycloaddition reaction of azides-labelled biomolecule and probe-bearing dibenzocyclooctyne group affording triazole ring. Figure adapted from reference ([112]).

In Summary, bioconjugation chemistry is receiving huge attention with increasing number of applications enabling the recent growth of bio-therapeutics, ADCs, bispecific antibodies, and chemical biology methods. Protein conjugates (mainly mAbs conjugates) are usually achieved through conventional chemistries to label cysteine and lysine amino acids, with noticeable growing in the genetic engineering-based approaches. However, recent advances in bioconjugation methods have shed light on the limitations of the current approaches, including:

- the poor plasma stability of conjugates, mainly maleimide-based conjugates,
- the lack of specificity of the available reagents and the heterogeneity of the constructed products,
- and the limited versatility of chemical-based methods to construct new bio-therapeutics, such as bispecific antibodies provided that most of well-applied methods are based on genetics and biological methods.
- the complexity of the genetics and biological methods, which require complex and expensive expressing and purification methods with questionable reduced bioactivity of fusion protein.

1.7 Aims and objectives

In this project we aimed to develop of a novel and improved conjugation chemistry to construct stable and well-defined antibody-protein conjugates.

Our first objective in this study is to develop effective reduction method for activation of thiols towards conjugation. Chapter 2 describes the development and evaluation of PEG-azides as water soluble reagents for quenching of excess TCEP prior to thiol alkylation reactions.

The next objective of our study is to develop new and improved rebridging chemistry to maintain the post reduction structure of mAbs and construct antibody-protein conjugates. Chapter 3 describes the evaluation of using sulfonates as electrophilic scaffold and the factors affecting their aqueous stability and reactivity, most importantly the nature of acceptor groups.

Then, we aimed to evaluate a novel bis-haloacetamide scaffold to be employed as rebridging approach. Chapter 4 describes the development and evaluation of aqueous stability and reactivity of various bis-haloacetamide linkers. In addition, the synthesis, aqueous stability and reactivity aryl bis-haloacetamide linkers bearing azide group were described in Chapter 4.

Then, in Chapter 5 we thoroughly evaluated the biological application of various aryl bis-haloacetamide linkers to rebridge reduced mAbs, their selectivity toward reduced disulfide bonds. In addition, we reported the comprehensive evaluation of the stability and characterisation the rebridged mAbs. We also developed a novel approach to obtain bi-functional mAbs (Figure 1.22). The described work offers a novel and promising bis-haloacetamide-based rebridging linkers that could be hugely applied in the construction of stable and well-defined ADCs.

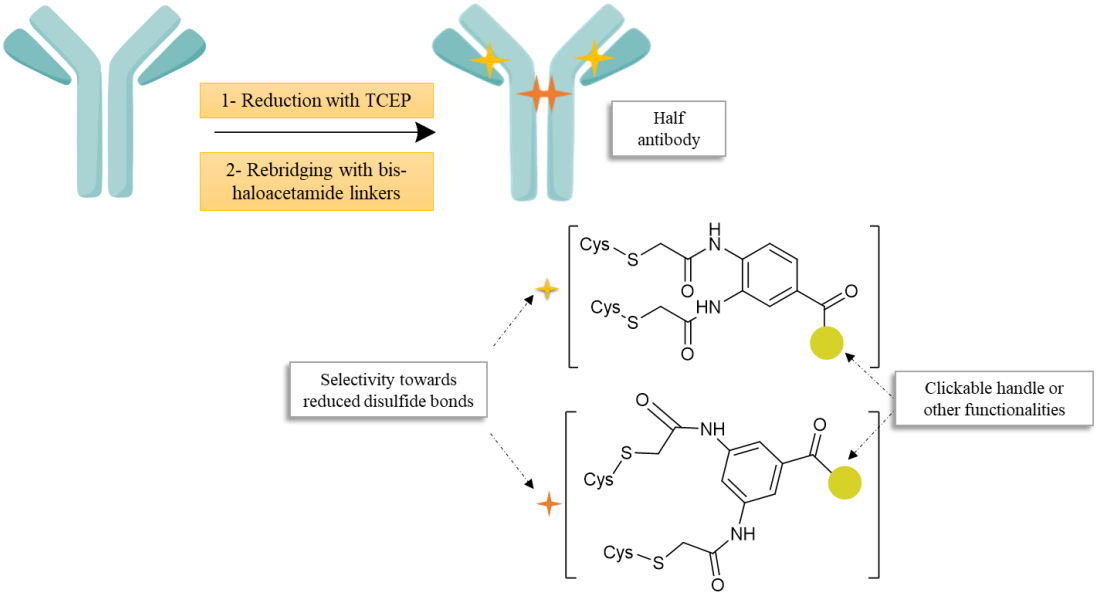

Figure 1.22. Rebridging approach of the reduced disulfide bonds of mAb using functionalised bis-haloacetamide reagents.

Our last objective of this study is to develop bis-rebridging agent that can be employed in the construction mAb-protein conjugates (immunoconjuagtes). In Chapter 6 we described the development of bis-dihaloacetamide PEG linker and evaluation of the factors affecting the construction of immunoconjugates of a unique microbial immune evasion protein (staphylococcal binder of immunoglobulin (Sbi)). The described chemical platform in chapter 6 offers a novel conjugation method based to generate site-specific, homogeneous, antibodies conjugates in applicable procedure and good yield which can be widely applied in the development of bio-therapeutics.

The suitability of our developed bis-dihaloacetamide PEG approach in the construction of anti-HER2/anti-CTLA-4 (Tmab-IFab) trifunctional antibody is described in chapter 7.

2 The use of alkyl azides to quench trialkylphosphine-based reducing agents

2.1 Introduction

The labelling of proteins via their nucleophilic amino acids, in particular cysteine residues is one of most disseminated approach in bioconjugation chemistry. Provided that most cysteine amino acids are tied up in disulfide bonds, free cysteine (thiol) can be generated by reducing cystine disulfide bonds with reducing agents prior to alkylation with Michael acceptors, such as maleimides (Figure 2.1).[77,78,119]

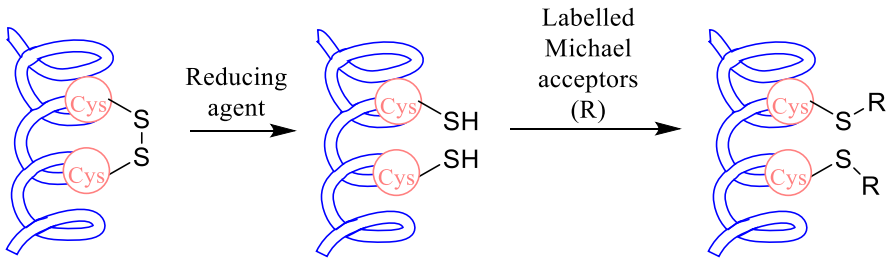

Figure 2.1. General conjugation strategy of protein labeling by reduction of disulfide bonds prior to alkylation of the obtained thiols using Michael acceptors.

Disulfide reducing agents employed in protein conjugation can be divided into two main groups: thiol reductants, such as dithiothreitol (DTT, **2.1**) and phosphine reductants, such as the water soluble tris(2-carboxyethy)phosphines (TCEP, **2.2**) and tris(3-hydroxypropyl)phosphine (THPP, **2.3**).

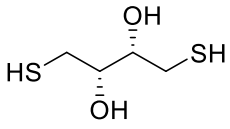

2.1

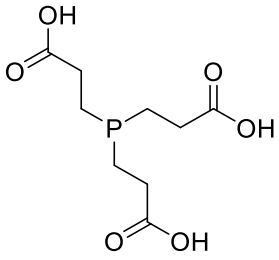

2.2

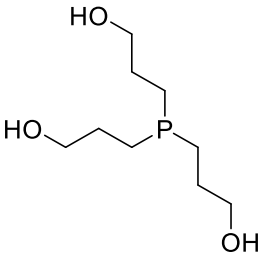

2.3

DTT (**2.1**), water soluble thiol reductants, has been used widely in protein conjugation chemistry. The mechanism of disulfide bonds reduction by thiol agents takes place via thiolate exchange where DTT nucleophilic agent attacks on the disulfide bond of the

protein to reduce the first sulfur atom of the protein and generate reductant-protein disulfide intermediate with the second sulfur atom. Then, the second free thiol of DTT attacks intermediate disulfide bond to afford two reduced thiols groups with DTT being converted into disulfide-containing 6-membered ring (Figure 2.2 A).[120] Thiol reductants should be removed before performing thiol-alkylation reactions as they compete directly with thiol-alkylating agents, thus significantly reduce the yield of protein conjugates products. In addition, thiol reductants have a number of drawbacks that have derived researchers to consider the alternative phosphine-based reducing agents.

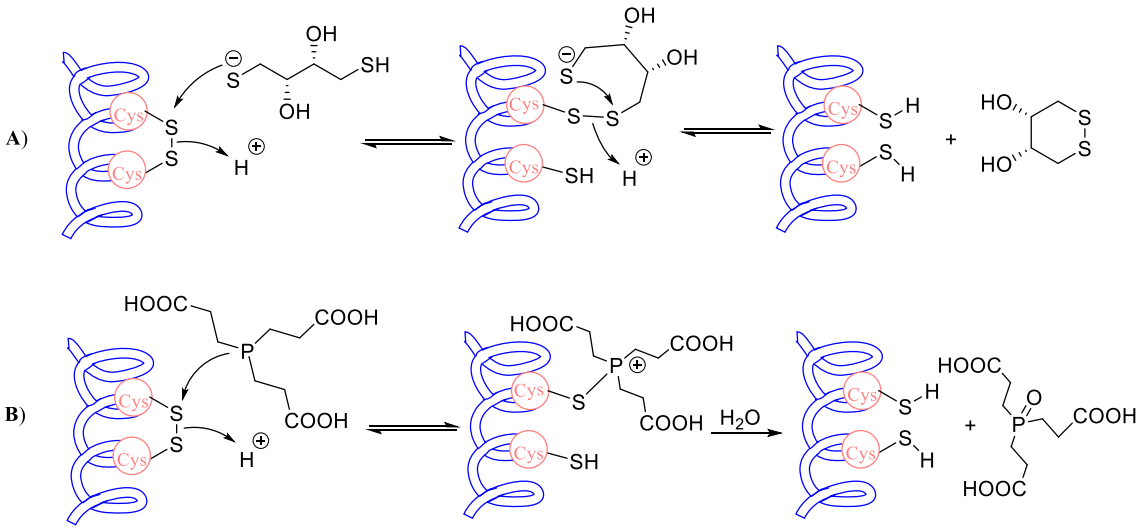

Figure 2.2. A) Mechanism of reversible reduction of disulfide bonds using DTT (**2.1**). **B**) Mechanism of irreversible reduction of disulfide bonds using TCEP (**2.2**).

Historically, phosphine reductants such as TCEP (**2.2**) have been practically overlooked for long time before a convenient method for their synthesis was published, and they became commercially available.[121] In aqueous solutions, TCEP's phosphine atom attacks on the first target sulfur atom to generate the first thiol fragment with thiophosphonium salt being generated on the first target sulfur atom. Subsequently, a rapid hydrolysis step releases the second thiol and phosphine oxide (Figure 2.2 B). The reduction of disulfide bonds with TCEP is stoichiometric and irreversible due to the generated strong phosphine oxide bond.[119]

Adopting reduction using TCEP offers a number of advantages over thiol-based reducing agents. Generally, TCEP is odorless and more stable toward aerial oxidation. Thiol reductants showed reversible reduction of disulfide bonds and their activity is questioned at acidic pH. TCEP is a more efficient reducing agent than DTT with superior redox potential as it irreversibly reduces disulfide bonds. Metals, such as Ni^{2+} can catalyze oxidation of DTT, but not TCEP. In protein purification, Ni^{2+} columns are employed to purify His-tag linked protein, thus free Ni^{2+} will be eluted with protein which in turn will reduce the efficiency of the reduction of protein using DTT. Moreover, TCEP has poor metal ion-chelation properties compared to DTT, so therefore has lower potential to interfere in biochemical studies.[122–124]

Tris(3-hydroxypropyl)phosphine (THPP, **2.3**) is another water soluble alkyl phosphine that has similar properties to TCEP and has been used in bioconjugation chemistry.[125]

TCEP (**2.2**) is widely reported to be compatible with Michael acceptors, such as maleimide, therefore a purification prior to conjugation is not required.[126,127] However, there are many indications from literature that this might not be the case. This raised fundamental questions regarding the compatibility of trialkylphosphine with Michael acceptors and whether the yield of maleimide-protein labelling would be significantly reduced in the presence of trialkylphosphines.

Visser *et al.* used TCEP to stabilise thiolate groups and found that it did not interfere significantly with the maleimide-base thiol alkylation. However, they have used up to 17.5-fold excess of maleimide to perform the coupling reaction.[128] On the other hand, when lower equivalents of maleimide were utilised in the fluorescent labelling of myosin, Getz *et al.* found that the level of labelling significantly decreased in the presence of TCEP.[120] These reports suggested the need to further investigate the stability of maleimide linkers in the presence of TCEP.

This debate was recently resolved as it has been shown that both TCEP and THPP react with N-ethylmaleimide (**2.4**) under typical bioconjugation conditions to form the ylene adduct (**2.5**) and N-ethylsuccinimide (**2.6**), respectively (Figure 2.3).[129]

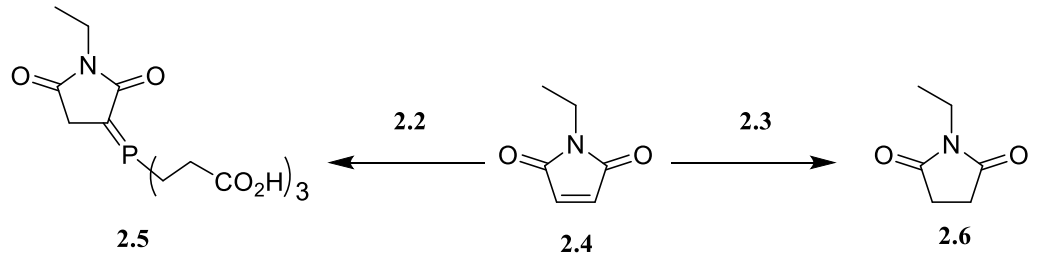

Figure 2.3. The reaction between TCEP (**2.2**) and THPP (**2.3**) with the Michael acceptor, N-ethylmaleimide (**2.4**) forming the ylene adduct (**2.5**) and N-ethylsuccinimide (**2.6**), respectively.

Therefore, it was shown to be essential to remove trialkylphosphines prior addition of Michael acceptors. There are a number of available methods for the removal of phosphines from proteins; however, each has drawbacks that should be considered.

Dialysis and gel filtration are commonly employed procedure before performing protein conjugation. However, adopting such protocols is associated with loss of protein and potential for re-oxidisation of the protein through long exposure to oxidizing condition.[130] Alternatively, agarose gel-immobilized TCEP is commercially available and can be used to reduce the interested protein followed by filtration of the solid support. However, some reports claimed the low yield of recovery and the possibility of cationic protein loss due to electrostatic interaction with TCEP carboxylate moieties.[131]

Recently, Henkel *et al.* have reported an elegant *in situ* approach utilizing 4-azidobenzoic acid (4-ABA, **2.7**) to quench excess TCEP through a Staudinger reaction (Figure 2.4). Thus, excess trialkylphosphine will be oxidise to phosphine oxide without the need for a purification step prior to thiol alkylation using Michael acceptor.[132,133] Nevertheless, the poor solubility of 4-azidobenzoic acid (**2.7**) limits the practical usefulness of this reagent in typical bioconjugation conditions (aqueous buffer).

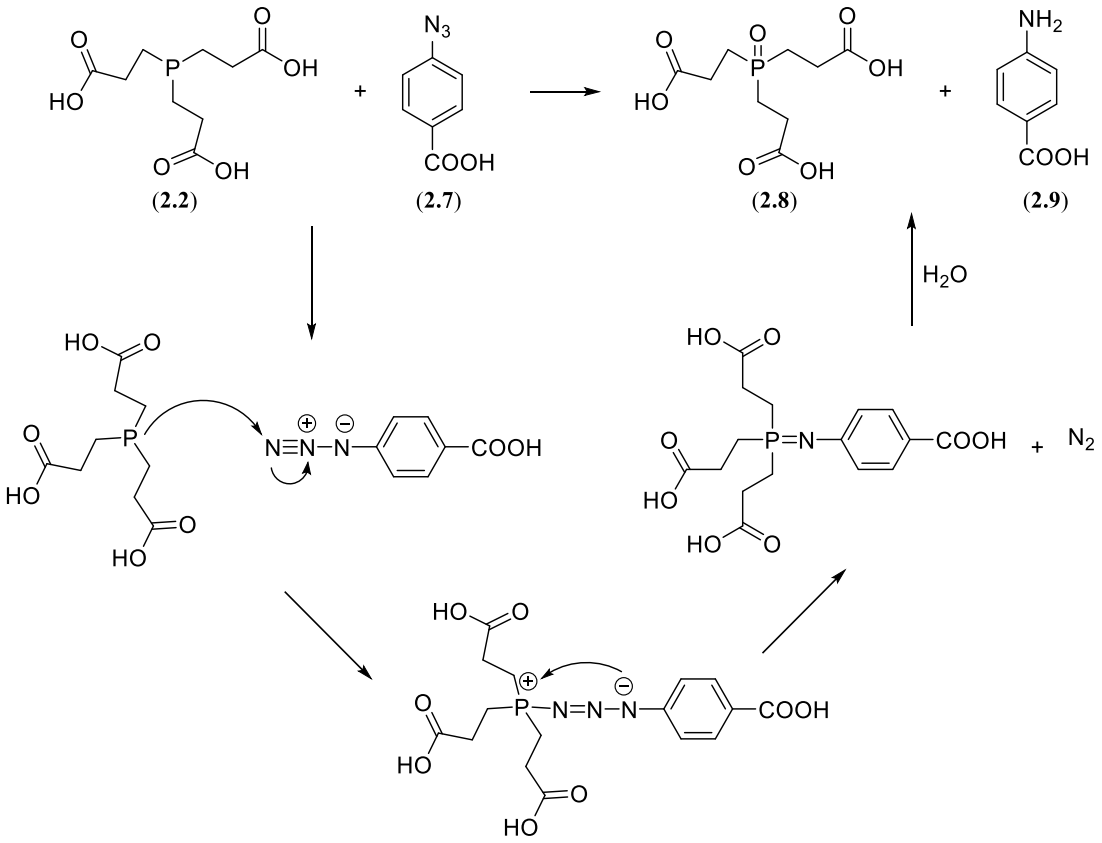

Figure 2.4. The mechanism of Staudinger reaction between TCEP (**2.2**) with 4-azidobenzoic acid (**2.7**)

Given the importance of effective phosphine removal prior to addition of Michael acceptors and the elegance of using alkyl azide to achieve this, we sought here to evaluate and optimise one-pot method of using water-soluble azide-bearing ethylene glycols to quench excess trialkylphosphines.

2.2 Synthesis of azide-containing ethylene glycols of increasing molecular mass

We set out to investigate the use of more water soluble alkyl azides to promote the oxidation of phosphines. Polyethylene glycols are known to be water soluble derivatives of hydrocarbons. As such, we set out to synthesise a series of azide-containing ethylene glycols to evaluate the impact of the polymer length on their aqueous solubities. The diazide derivatives **2.10-2.13** were synthesised in a good yields accoding to previously reported methods as shown in Figure 2.5.

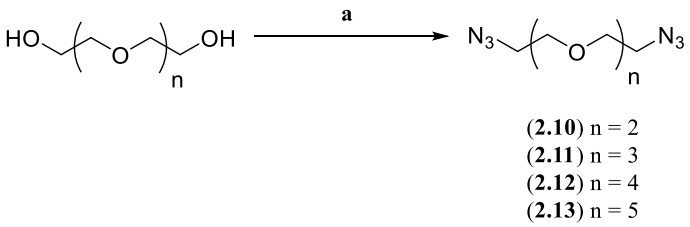

(**2.10**) n = 2
(**2.11**) n = 3
(**2.12**) n = 4
(**2.13**) n = 5

Figure 2.5. Chemical synthesis of the PEG-azides **2.10**-**2.13**. **a**) (**i**) 4-Toluenesulphonyl chloride, pyridine, DCM, room tempreture, 3h, (**ii**) NaN_3, acetone/water (3:1), room temperature overnight.

2.3 Determination of the mass and molar solubilites of PEG-azides and 4-azidobenzoic acid

The aqueous solubilites of 4-azidobenzoic acid (**2.7**) and the synthesised PEG-azides (**2.10**-**2.13**) were measured in water and in aqueous buffer Tris.HCl (100 mM, pH 7) Table 2.1. All PEG-azides were found to be readily soluble in water and aqueous buffer Tris.HCl. The compounds displayed increasing aqueous solubility with increasing molecular weight, ranging from 20 mg/mL for di-PEG azide (**2.10**) up to 100 mg/mL for penta-PEG azide (**2.13**). It is worth mentioning that PEG-azides showed higher solubility values in Tris.HCl buffer.

On the other hand, 4-azidobenzoic acid (**2.7**) has a dramatically lower solubility of 0.5 mg/mL under typical bioconjugation conditions. Thus, in order to improve its solubility, different solvent systems were used including Tris.HCl (100 mM) at pH 8 and 50% MeOH/water, the value of mass solubility were found 4.4 and 1.5 mg/mL, respectively.

Table 2.1. Aqueous mass and molar solubilites of 4-azidobenzoic acid (**2.7**) and PEG-azides (**2.10**-**2.13**) in H_2O and aqueous Tris.HCl buffer (100 mM, pH 7).

Azide	**Aqueous Solubility (H_2O)**		**Solubility in buffer (Tris.HCl, 100 mM, pH 7)**	
	Mass (mg/mL)	Molar (mM)	Mass (mg/mL)	Molar (mM)
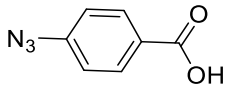 (**2.7**)	0.42	2.6	0.5	3
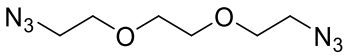 (**2.10**)	20	100	25	125
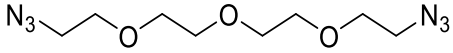 (**2.11**)	50	205	60	246
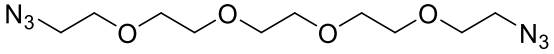 (**2.12**)	70	240	88	304
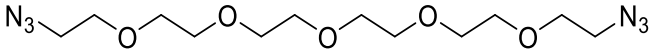 (**2.13**)	100	300	130	356

2.4 Rate of consumption of phosphine, TCEP and THPP by using ^{31}P NMR spectroscopy

Given the aqueous solubility of PEG-azides were measured at typical conjugation conditions; we set out to evaluate the impact of the polymer length on TCEP oxidation rate. As such, we aimed to measure the rate of oxidation of TCEP and THPP by following the disappearance of phosphine signal and appearance of phosphine oxide signal using ^{31}P NMR.

Firstly, the rate of aerial oxidation of TCEP was evaluated. A solution of TCEP (100 mM) in Tris.HCl buffer (100 mM, pH 7) was held at 37°C and the mixture analysed at zero time (3 minutes) and after 63 minutes using ^{31}P NMR spectroscopy.

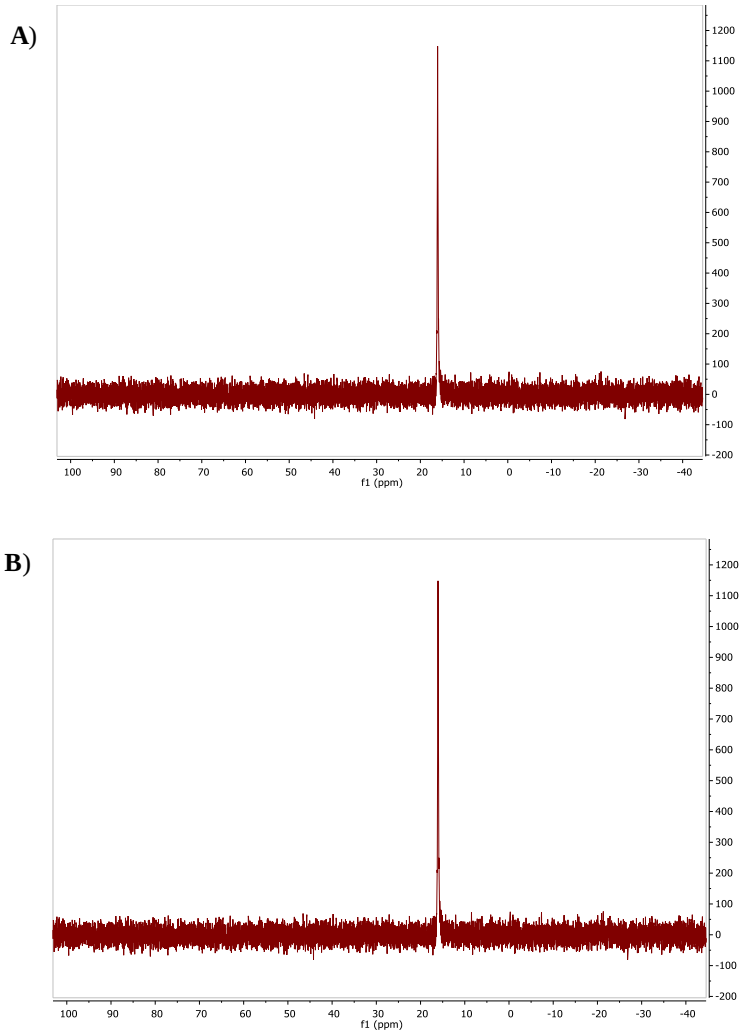

Figure 2.6. ^{31}P NMR spectrum of TCEP control reaction analysed at times **A)** 3 minutes and **B)** 63 minutes. No peak corresponding to phosphine oxide (57 ppm) was observed.

No oxidation of TCEP was observed under these conditions, indicating that spontaneous oxidation does not contribute to TCEP oxidation under the studied conditions (Figure 2.6). Having demonstrated that TCEP is stable under the studied conditions, we next tend to measure the rates of TCEP oxidation. A solution of TCEP and each azide-PEG (10 equiv.) in 100 mM Tris.HCl buffer was held at 37°C and analysed by ^{31}P NMR spectroscopy every 10 minutes over 60 minutes.

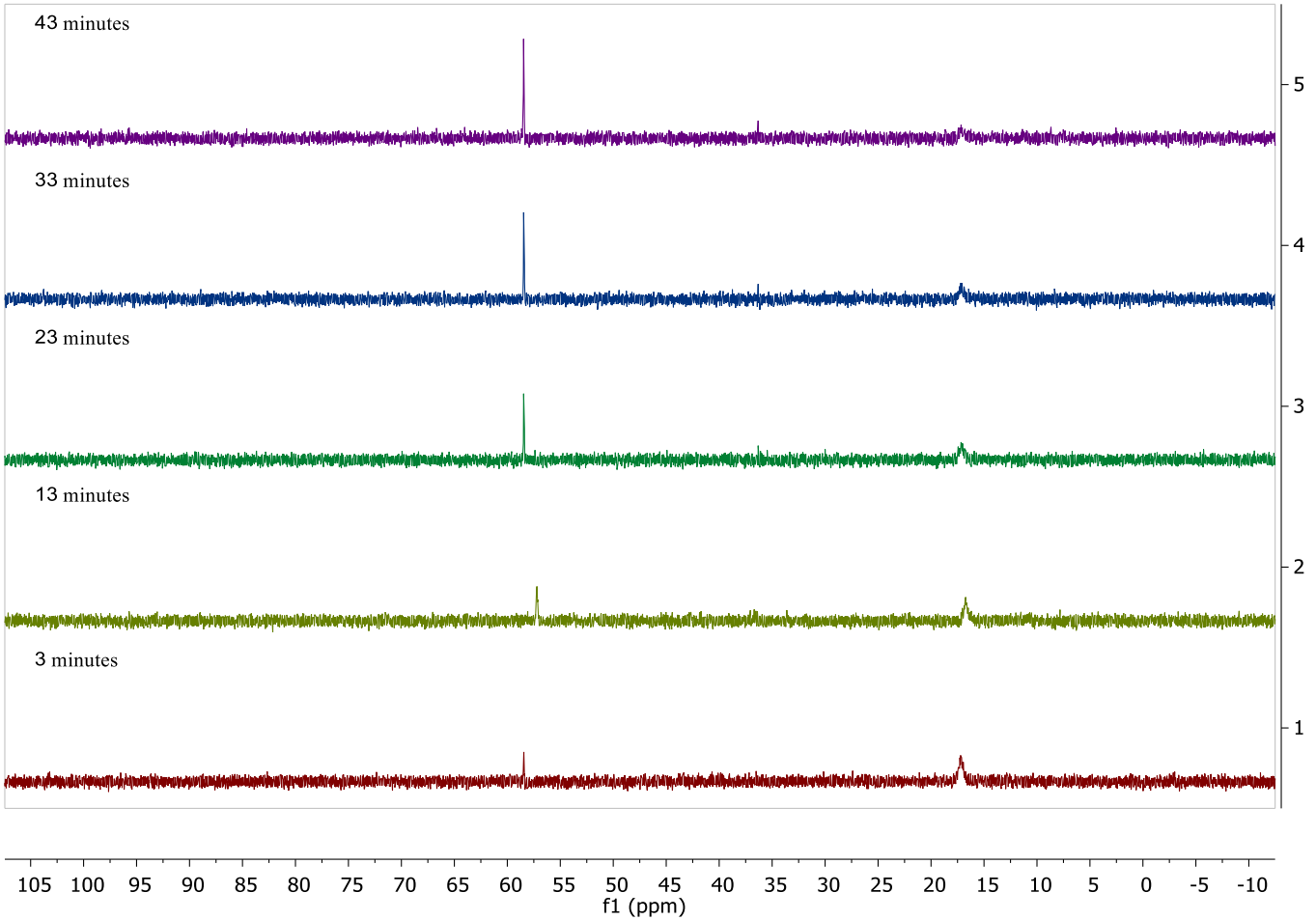

Figure 2.7. ^{31}P NMR spectrum of TCEP reaction with penta-PEG azide (**2.13**) analysed every 10 minutes. Phosphine oxide peak was observed at 57 ppm.

The level of TCEP oxidation was calculated by comparison of integrals corresponding to the phosphine (15 ppm) and phosphine oxide (57 ppm). Penta-PEG azide (**2.13**) showed higher rates of reaction with TCEP with almost complete oxidization within 40 minutes (Figure 2.7). All the PEG-azides (**2.10-2.13**) showed complete TCEP oxidation within 60 minutes.

The percent of remaining TCEP was calculated using Equation 2.1. PEG-azides reactivity rates with TECP reflect and correlated positively with their solubility profile with di-PEG azide (**2.10**) was found to be the least reactive one, possibly due to its lower aqueous solubility (Figure 2.8).

$$\textbf{\textit{Percentage of remaining TCEP}} = \frac{I_p}{(I_p + I_{po})} * 100 \qquad \textbf{(Equation 2.1)}$$

Where;

I_p= Integration of phosphine peak at δ 16 ppm.
I_{po}= integration of phosphine oxide peak at δ 57 ppm.

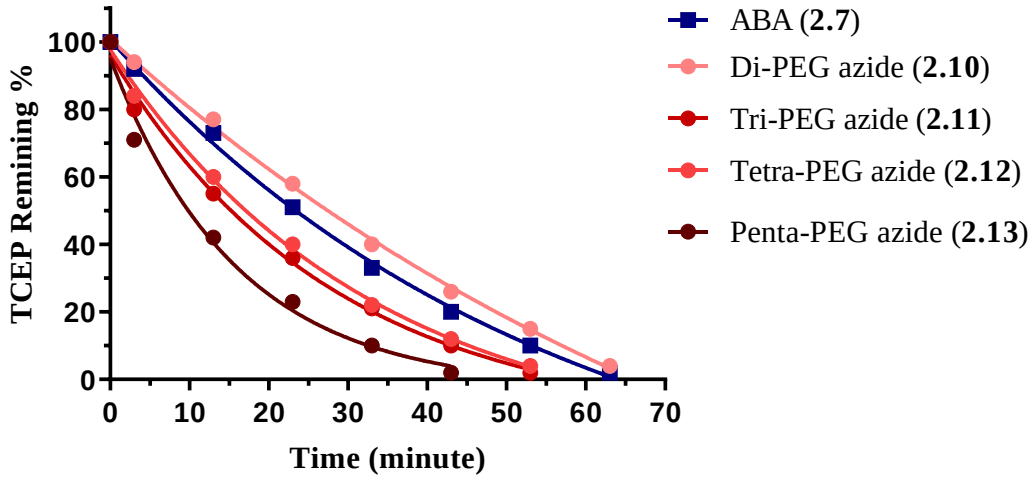

Figure 2.8. Oxidation rates of TCEP in the presence of the PEG-azides (250 mM) in Tris.HCl buffer (100 mM, pH 7) and 4-ABA (**2.7**, 26 mM) in Tris.HCl buffer (100 mM, pH 8).

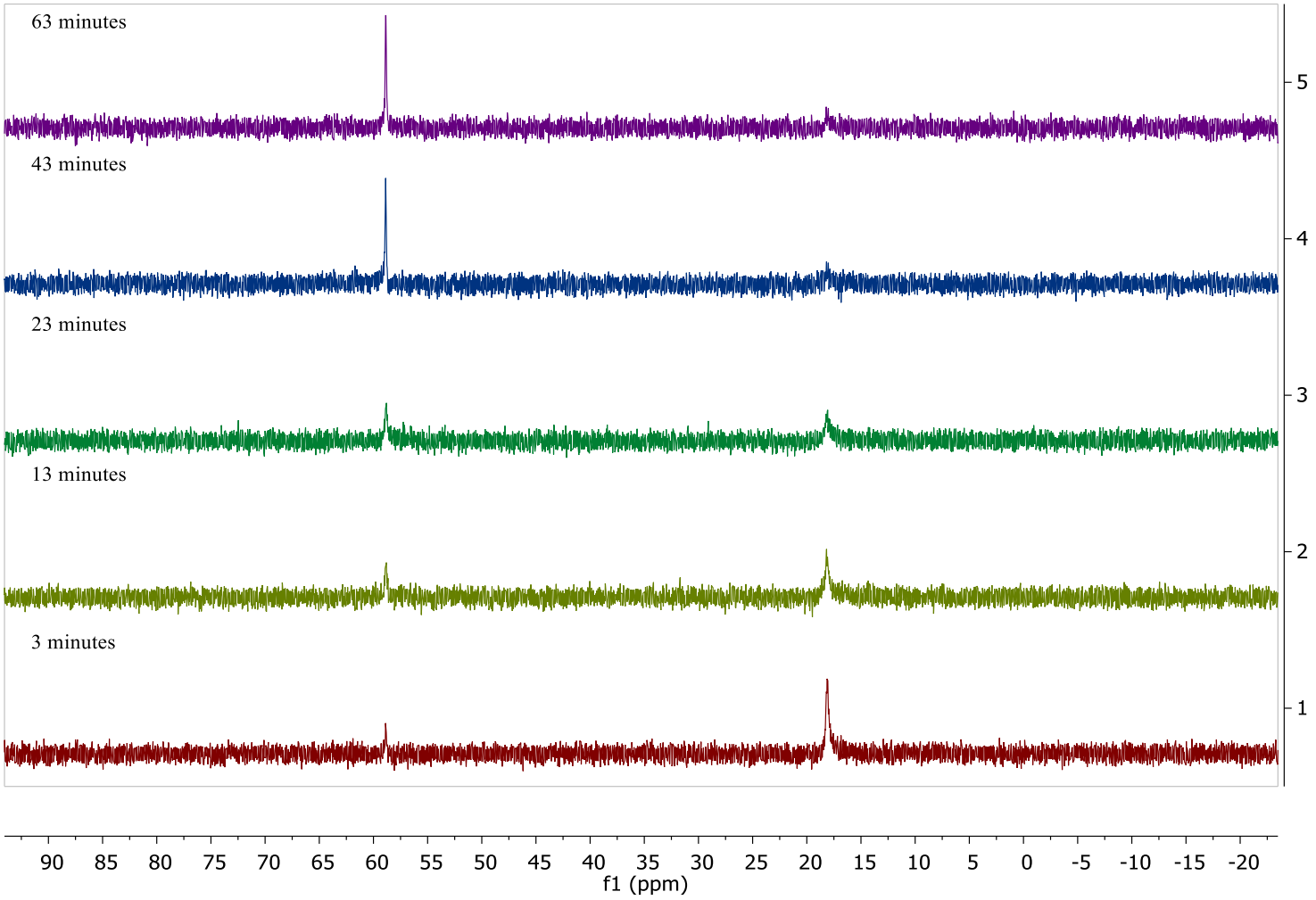

Figure 2.9. ^{31}P NMR spectrum of TCEP reaction with 4-ABA (**2.7**) analysed every 10 minutes. Phosphine oxide peak was observed at 57 ppm.

Unfortunately, direct comparison between TCEP oxidizing rate between 4-ABA (**2.7**) and the PEG-azides (**2.10**-**2.13**) was not possible owing to the limited solubility of the former. Therefore, the rate of TCEP oxidation was determined using only 3 equivalents of 4-ABA (**2.7**) in Tris-HCl buffer (pH 8) (Figure 2.7). Under these conditions, 4-ABA (**2.7**) oxidised TCEP at a comparable rate to di-PEG azide (**2.10**), with complete consumption of THPP observed after 60 minutes (Figure 2.9).

Lastly, all the PEG-azides (**2.10**-**2.13**) were effective in oxidation of THPP under similar conditions previously used to study the oxidation of TCEP, however oxidation occurred at much higher rates and complete oxidation of THPP was observed in less than 5 minutes (Figure 2.10).

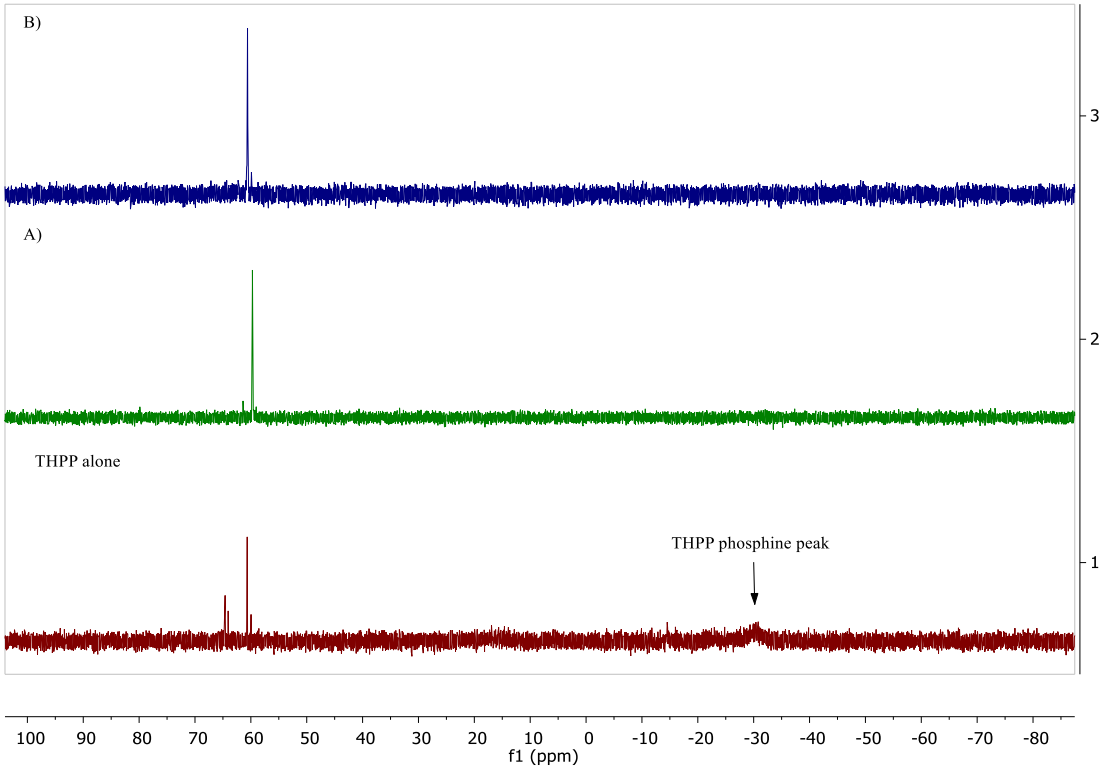

Figure 2.10. ^{31}P NMR spectrum of THPP reaction with **A**) penta-PEG azide (**2.13**) and **B**) di-PEG azide (**2.10**) analysed after 3 minutes. Phosphine oxide peak was observed at 60.45 ppm.

2.5 The application of PEG-azides towards improving protein conjugation yields (experiment carried out by Terrence Kanter)[134,135]

Given that solubility and reactivity rates of PEG-azides (**2.10-2.13**) with TCEP (**2.2**) were now known, the applicability of using PEG-azide approach in a protein conjugation was then evaluated. Fluorescent labelling of yeast enolase using the commercially available N-(5-fluorescinyl)maleimide was evaluated in the presence or absence of the tetra-PEG azide (**2.12**).

As such, denatured yeast enolase was reduced with TCEP **2.2** (1, 5 or 10 equiv.) and then incubated directly with N-(5-fluorescinyl)maleimide. In parallel experiment, denatured yeast enolase was reduced with TCEP **2.2** (1, 5 or 10 equiv.) and then incubated with the tetra-PEG azide **2.12** for 1 h before being incubated with N-(5-fluorescinyl)maleimide. From the results obtained, it was demonstrated that the degree of fluorescent labelling of yeast enolase was decreased with increasing the equivalents of TCEP in the absence of PEG-azide **2.12** (Figure 2.11 A). On the other hand, when PEG-azide **2.12** was used to quench excess TCEP prior to commencing protein labelling, significant levels of fluorescence were obtained (Figure 2.11 A) for all the tested equivalents of TCEP. Similar results were obtained when THPP (**2.3**) was used as the reducing agent, as level of labelling of yeast enolase was significantly increased in the presence of PEG-azide **2.12** regardless of the used concentration of THPP (Figure 2.11 B).

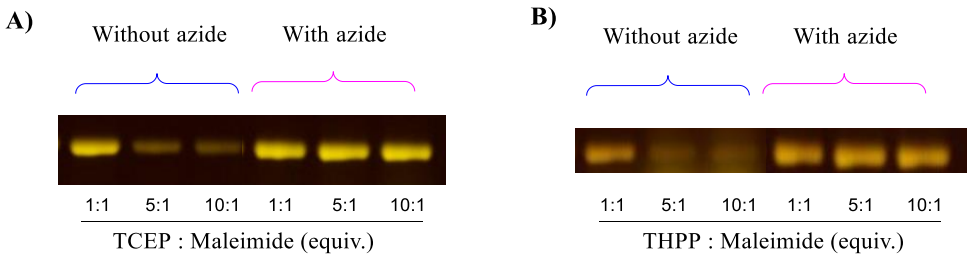

Figure 2.11. SDS-PAGE analysis of application of PEG-azides in labelling of yeast enolase with fluorescein-maleimide. Yeast enolase (11 mM) in Tris.HCL buffer (500 mM, pH = 7.2, 5 mM EDTA) was reduced with TCEP or THPP (1, 5 or 10 equiv.) for 45 minutes at room temperature then reacted with N-(5-fluorescinyl)maleimide (1 mM) for 18 h at 37 °C. In a parallel experiment, reduced yeast enolase was treated with PEG-azide **2.12** for 1 hr at 37 °C prior to addition of N-(5-fluorescinyl)maleimide (1 mM) for 18 h at 37 °C.

2.6 Conclusion

In conclusion, a series of water soluble PEG-azides were synthesised and their rate of reactivity with trialkylphosphines were investigated under the commonly used protein conjugation conditions with Michael acceptors, such as maleimide. It was shown that the increased aqueous solubility of the PEG-azides (**2.10-2.13**) correlated positively with their increased abilities to oxidise TCEP within one hour of incubation. Moreover, the provided soluble PEG-azides approach to quench excess TCEP offers practical advantages over the previously reported 4-ABA-based approach, particularly the poor aqueous solubility issues.

Furthermore, it has been found that the incubation of reduced protein with PEG-azides, such as **2.12** prior to the addition of the maleimide label, permits the use of higher TCEP equivalents and improves the yields of protein conjugates.

3 Evaluation of aryl-sulfonate derivatives as thiolate-reactive alkylating agents

3.1 Introduction

Cysteine targeted bioconjugation using the maleimide-based approaches have certain drawbacks, most importantly, the poor plasma stability of the attained protein conjugates. Therefore, we set out to evaluate sulfonate-based cysteine conjugation approach as alternative method for monoalkylation of cysteine as these products would exhibit improved plasma stability.

Successful development of a cysteine targeted alkylating agent for bioconjugation depends in part on understanding the factors affecting electrophile reactivity. Although sulfonate chemistry has been known for a long time, it has been largely overlooked and underutilised in the area of bioconjugation chemistry. The primary objective of this work was to study the aqueous stability (hydrolysis rates) and reactivity of sulfonate derivatives twords cysteine (thiolate). The main emphasis is to evaluate various parameters affecting compound reactivity including pK_a of the corresponding sulfonic acid, chain length and the nature of electrophilic group (acceptor group), as well as the pH of the reaction.

Sulfonyl ester derivatives are reactive species owing to the low pK_a of the corresponding sulphonic acid. They are susceptible to nucleophilic substitution (S_N1 or S_N2) reactions. Generally, the nucleophilic reagent (Nu) attacks the substrate at the electrophilic atom which is accompanied by liberation of the leaving group (X) (Figure 3.1 A). The thiolate group (RS^-) of cysteine (nucleophile) attacks the carbocation attached to sulfonate group (k_1) with the latter being liberated and stabilised by resonance (Figure 3.1 B). However, as bioconjugation reactions are carried out in aqueous solvent systems, hydroxyl groups (OH^-) will compete with thiolates and result in hydrolysis of sulfonate groups (k_2).[79,136–138] Therefore, it is essential to evaluate the aqueous stability (hydrolysis rates) of sulfonate derivatives under the typical conjugation conditions to determine whether these compounds could be considered effective thiol alkylating agents.

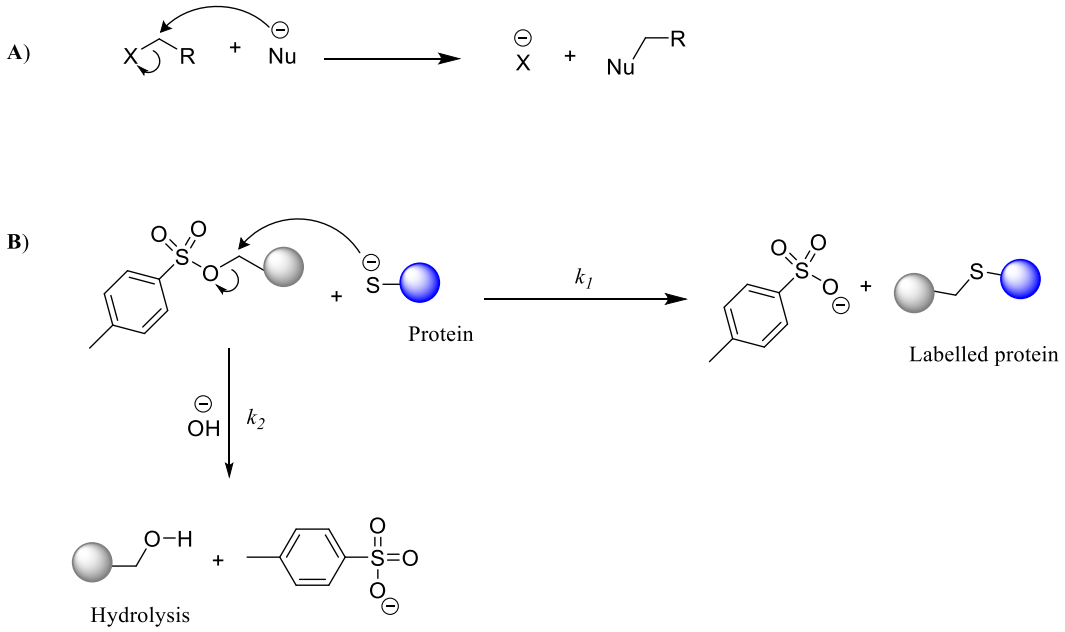

Figure 3.1. A) General Mechanism of nucleophilic substitution reactions (S_N2). **B**) Thiolate alkylation with sulfonyl ester (tosylate) affording thioether linkage with liberation of sulfonic acid anion (k_1). Sulfonyl ester (tosylate) hydrolysis (k_2).

3.2 Factors affecting the aqueous stability of sulfonate esters

3.2.1 Impact of aryl substitution on the aqueous stability of sulfonates

In order to evaluate the aqueous stability of sulfonates under a range of conditions, a series of arylsulfonates independently substituted at meta-, and para-positions with a range of groups were chosen based on the pK_a values of the corresponding sulfonic acid. The substituted sulfonates chosen in this study are shown in Table 3.1, along with the pK_a values of their corresponding sulfonic acid. Hammett σ values (also known as substituent constant) of the chosen substituents are also listed in Table 3.1. The substituent constant relates to the electronic (inductive and resonance) impact of a substituent. Electron-withdrawing groups, such as nitro group have positive σ value, while electron-donating substituents, such as methyl group have a negative σ value. Each substituent will exert different effects related to its regiochemistry relative to the reaction center (meta- or para-positions).[139]

Table 3.1. The predicted pK_a values of the chosen sulfonic acid derivatives. [a] values obtained from Scifinder. [b] values were obtained from literature ([140,141]).

Entry	Sulfonic acid	Predicted pK_a of sulfonic acid[a]	Hammett[b] σ_m or σ_p
1	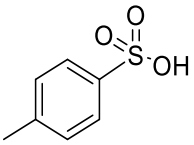	-0.43±0.50	-0.17
2	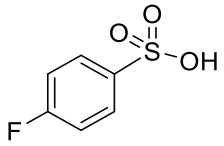	-0.66±0.50	-0.03
3	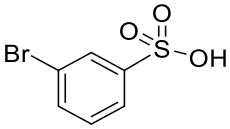	-0.83±0.50	0.391
4	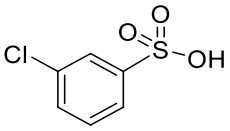	-0.83±0.50	0.373
5	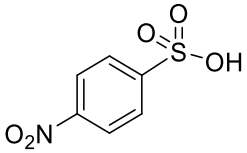	-1.38±0.50	1.27

The synthesis of each of the sulfonate esters was accomplished in anhydrous DCM to prevent hydrolysis of the respective acid chloride, with pyridine employed as base to neutralise the generated HCl. The reactions were left overnight at room temperature, except for the 2-methoxyethyl 4-nitrobenzenesulfonate (**3.5**) which was carried out over 2 h. The reactions were then subjected to standard work-up (EtOAc) and the products were purified by silica gel chromatography. The yields obtained of sulfonate products (**3.1**-**3.5**) ranged from 59-91% (Figure 3.2).

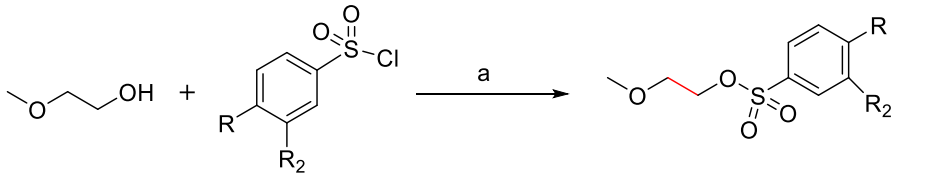

		Yield (%)
(2.22) R= CH_3, R_2= H	**(3.1)** R= CH_3, R_2= H	90
(3.13) R= F, R_2=H	**(3.2)** R= F, R_2=H	91
(3.15) R= H, R_2=Br	**(3.3)** R= H, R_2=Br	71
(3.16) R= H, R_2=Cl	**(3.4)** R= H, R_2=Cl	91
(3.17) R= NO_2, R_2=H	**(3.5)** R= NO_2, R_2=H	59

Figure 3.2. Chemical synthesis of ethoxy-sulfonate derivatives **3.1**-**3.5**. (**a**) Anhydrous DCM, anhydrous pyridine.

The aqueous stability of sulfonate derivatives (**3.1**-**3.5**) was determined at pH 7, this pH is typically used in conjugation reactions. Stability was also determined at more basic pH's (8 and 8.5) which is close to the pK_a of the cysteine thiol group and would be expected to result in higher rates of alkyltion by the sulfonate derivatives.

^{1}H-NMR (solvent suppression experiment at 4.7 ppm) analysis was performed over 4 days to test the stability and to calculate the hydrolysis rates (Figure 3.3). The percentage (%) remaining of 2-methoxyethyl 4-nitrobenzenesulfonate (**3.5**) was calculated using Equation 3.1. The percentage remaining of each sulfonate derivative (**3.1**-**3.4**) was calculated accordingly.

$$\boldsymbol{Percent\ (\%)\ remaining\ of\ sulfonate} = \frac{I_s}{(I_s + I_{sa})} * \mathbf{100} \qquad \textbf{(Equation 3.1)}$$

Where;

I_s= Integration of the aromatic sulfonate peak at δ 8.45 ppm which corresponds to the aromatic protons of sulfonate group of **3.5** (2 x $NO_2CC\underline{H}$).
I_{sa}= Integration of the aromatic sulfonic acid peak at δ 8.35 ppm which corresponds to the aromatic protons of sulfonate group of sulfonic acid (2 x $NO_2CC\underline{H}$).

The remaining percentage of sulfonate derivatives (**3.1**-**3.5**) over 4 days at pH 7, 8 and 8.5 were calculated using Equation 3.1 and compared as shown in (Figure 3.4). The hydrolysis rates of ethyloxy-sulfonate derivatives were obtained and found to be independent of the solution pH (Table 3.2). Moreover, the rates of hydrolysis showed a

direct correlation with the pK_a values, so the lower the pK_a, the greater the hydrolysis rate (Table 3.2).

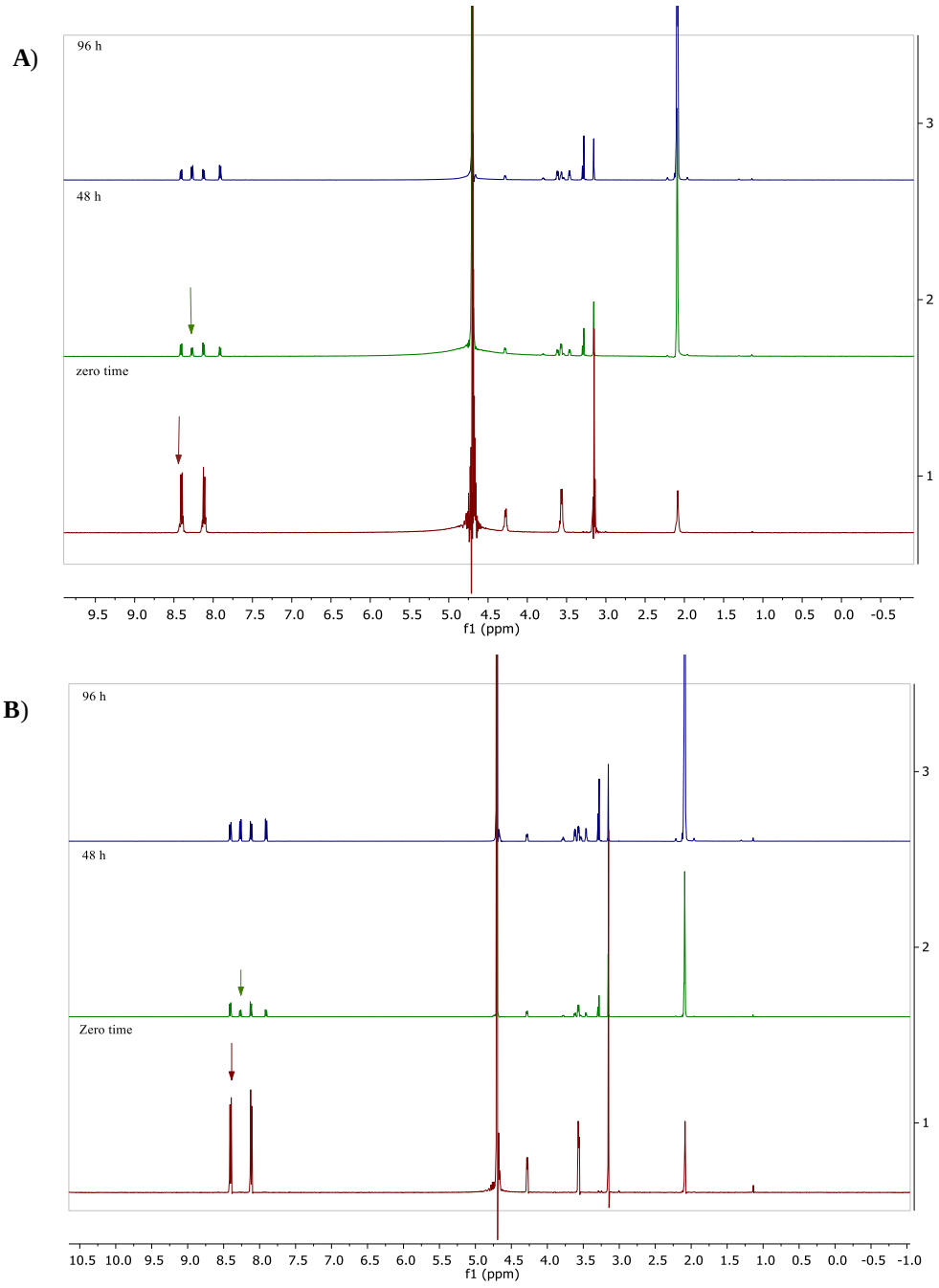

Figure 3.3. ^{1}H NMR spectra of 2-methoxyethyl 4-nitrobenzenesulfonate (**3.5**) over 4 days at **A**) pH 7 and **B**) 8.5. Arrows indicate the aromatic peaks that were followed to calculate hydrolysis rates using Equation 3.1, maroon arrows correspond to aromatic protons of sulfonate group of 2-methoxyethyl 4-nitrobenzenesulfonate (2 x $NO_2CC\underline{H}$), while green arrows correspond to aromatic protons of sulfonate group of sulfonic acid (2 x $NO_2CC\underline{H}$).

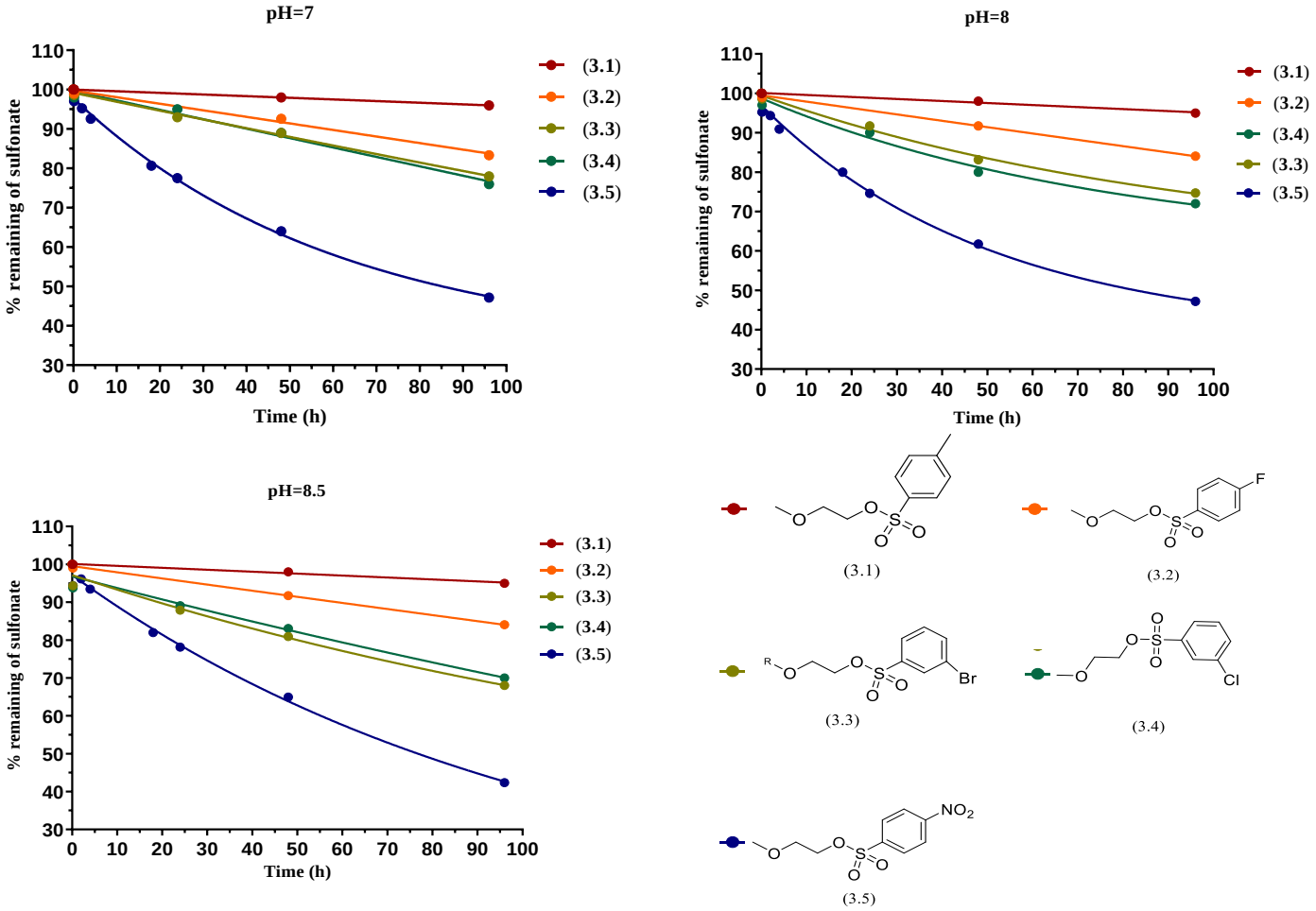

Figure 3.4. Percentage remaining sulfonates (**3.1**-**3.5**) over 4 days. Stability was appraised in phosphate buffer (100 mM, pH 7, 8 or 8.5) using solvent suppression method.

Electron-rich methyl-substituted arylsulfonate displayed higher aqueous stability (lower hydrolysis rates) compared to the electron-withdrawing halogen-substituted arylsulphonate derivatives. The presence of a strong electron withdrawing group (resonance effect) at the para-position (**3.5**) significantly increases the hydrolysis rates (decreases the hydrolytic stability) (Table 3.2). Lastly, it is worth noting that both the 3-Br (**3.3**) and 3-Cl (**3.4**) substituted arylsulfonates which have the same predicted pK_a's, showed comparable hydrolysis rates.

Table 3.2. Calculated hydrolysis rates (h^{-1}) of sulfonate derivatives **3.1**-**3.5**.

Entry	Sulfonic acid	pH	Hydrolysis rates k (h^{-1})
1	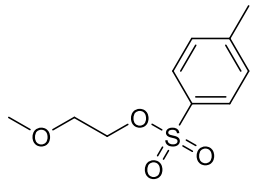 (**3.1**)	7	0.002
		8	0.002
		8.5	0.002
2	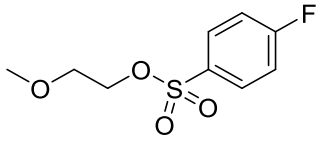 (**3.2**)	7	0.004
		8	0.004
		8.5	0.004
3	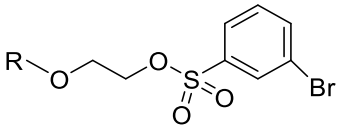 (**3.3**)	7	0.006
		8	0.007
		8.5	0.008
4	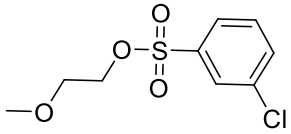 (**3.4**)	7	0.007
		8	0.007
		8.5	0.008
5	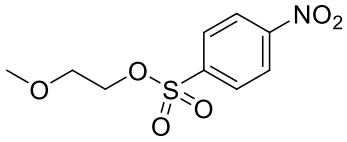 (**3.5**)	7	0.018
		8	0.018
		8.5	0.020

Further evaluation of the impact of each substituent on hydrolysis rates was then done by fitting the hydrolysis rates to the Hammett equation (Equation 3.2) against Hammett σ values which provided reasonable correlation, but non-linear correlation (R^2 = 0.86). The non-linearity can be attributed to different factors, such as the regiochemistry of the substituents (meta- and para-positions), and experimental errors,[142] which can be possibly improved by increasing the number of the experimental trails (Figure 3.5).

From the equation, the reaction constant ρ was 0.5786 ($\rho > 0$), which indicate that the hydrolysis of sulfonates is favoured by electron withdrawing group to stabilise the negative charge of the generated sulfonic acid anion.

$$\boldsymbol{Log\ K = \sigma\rho + log\ K°} \qquad \textbf{(Equation 3.2)}$$

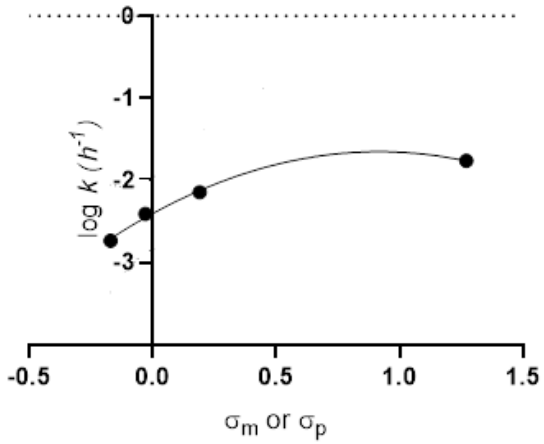

Figure 3.5. The correlation between log hydrolysis rates (h^{-1}) and Hammett sigma σ values.

3.2.2 Evaluation of the effect of electrophile chain length of sulfonates on hydrolysis rates (propyloxy derivatives)

Next, we sought to evaluate the impact of the length of the electrophile carbon chain on the aqueous stability of sulfonates. Based upon the previously determined hydrolysis results for ethyloxy-sulfonate derivatives, we selected the most, intermediate, and least stable sulfonate derivatives, 4-methyl (**3.6**), 3-chloro (**3.7**), and 4-nitro (**3.8**) propyloxy sulfonates, respectively, to be further evaluated in this Section. The synthesis procedure was again accomplished in anhydrous DCM, with pyridine being employed as base. The reactions were left overnight at room temperature, except for 3-methoxypropyl 4-

nitrobenzenesulfonate derivative (**3.8**) which was only left for 2 h. The reactions were then subjected to standard work-up (EtOAc) and the products were purified by silica gel chromatography, to give the sulfonates **3.6-3.8** in very good yields which ranged from 82-96% (Figure 3.6).

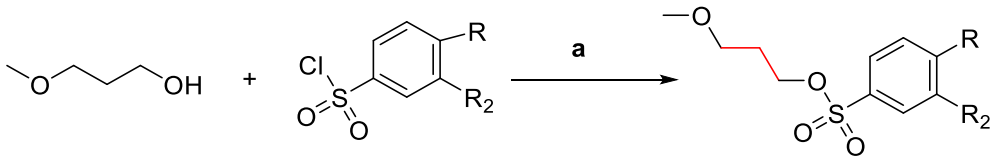

		Yield (%)
(2.22) R= H, R_2=Br	**(3.6)** R= CH_3, R_2=H	96
(3.16) R= H, R_2=Cl	**(3.7)** R= H, R_2=Cl	93
(3.17) R= NO_2, R_2=H	**(3.8)** R= NO_2, R_2=H	82

Figure 3.6. Chemical synthesis of propyloxy-sulfonate derivatives **3.6-3.8**. **a**) Anhydrous DCM, anhydrous pyridine.

The stability of the propyloxy sulfonate derivatives **3.6-3.8** was then evaluated using a similar ^{1}H-NMR method that was employed earlier to determine the stability of ethyloxy sulfonate derivatives. Stability of propyloxy sulfonate derivatives was directly compared to the ethyloxy analogues. The Propyloxy sulfonates derivatives **3.6-3.8** showed lower aqueous stability in comparison to the relative ethyloxy sulfonate analogues. Moreover, the percentages of remaining of sulfonate derivatives 3.6-3.8 reflect inherent substituent effects which directly correlate with their pK_a values. (Figure. 3.7).

3.2.3 Sulfonate ester acetamide derivatives

α-Halocacetamide electrophiles are amongst the earliest alkylating reagents used for the modification of the cysteines in keratin back in 1935. Since then, protein alkylation with these electrophiles has been extensively disseminated in a range of applications, such as protein mass spectroscopy and peptide mapping.[143] In an attempt to mimic α-halocacetamide electrophiles, we set out to appraise the influence of amide group as a component of the electrophile on the aqueous stability and reactivity of sulfonate derivatives.

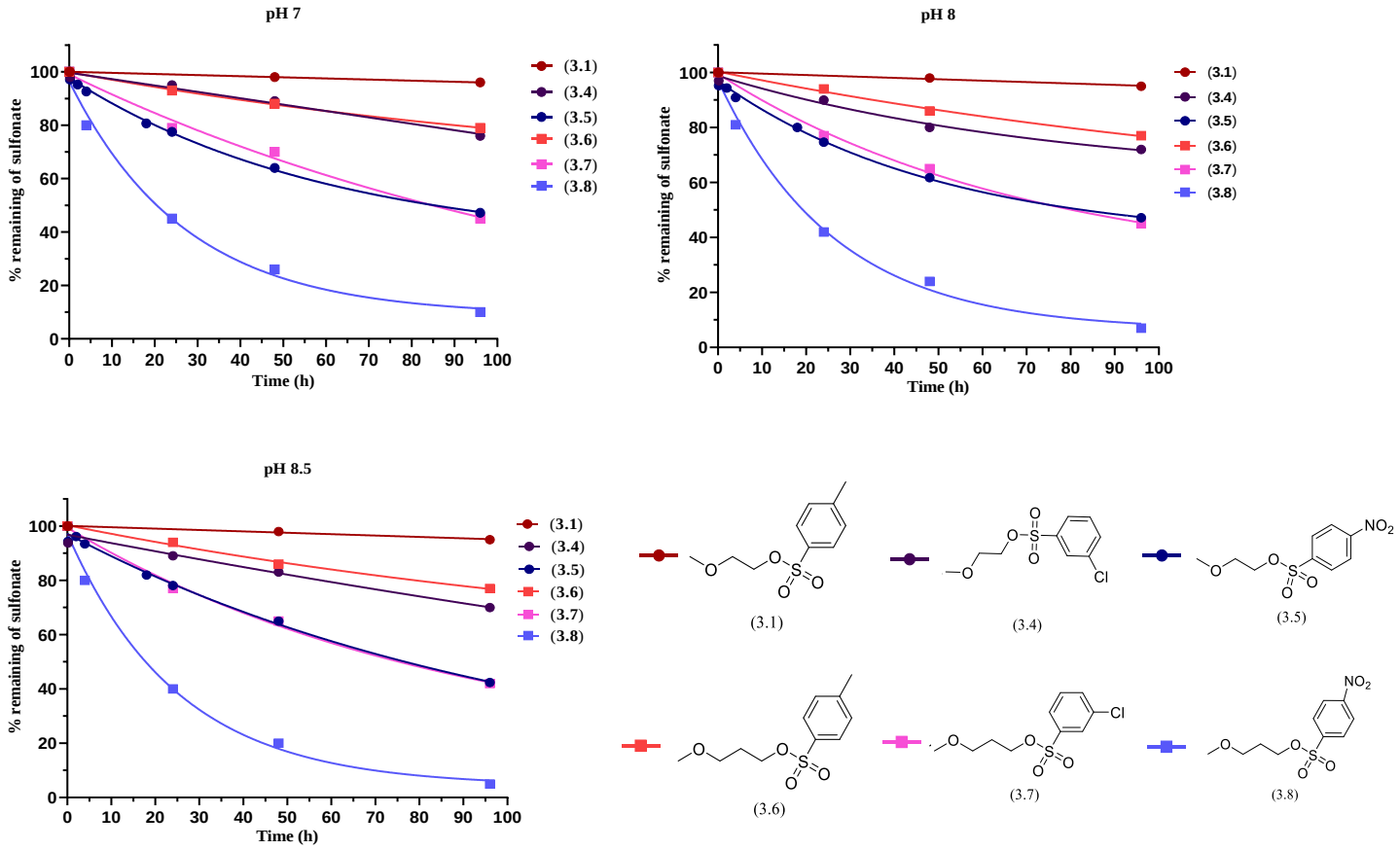

Figure 3.7. Percentage remaining of sulfonates (**3.1, 3.4-3.8**) in aqueous buffer over 4 days. Stability was appraised in phosphate buffer (100 mM, pH 7, 8 or 8.5) using solvent suppression method.

The synthesis of sulfonyl ester acetamide derivatives **3.9** and **3.10** was carried out according to the previously followed synthesis procedure. The reactions were left only for 2 h. Then, the reactions were subjected to standard work-up (EtOAc) and the products were purified by silica gel chromatography (Figure 3.8).

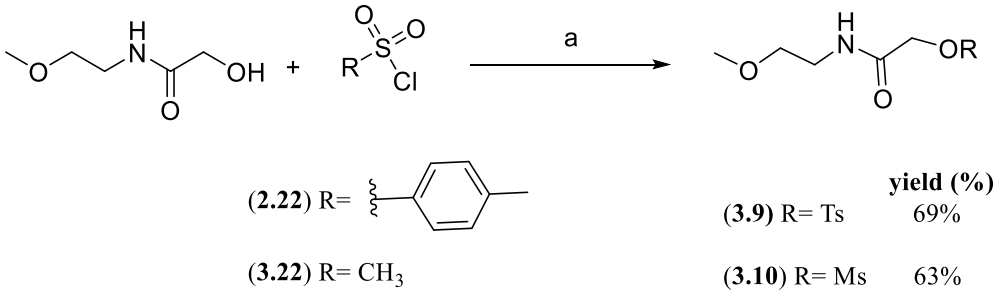

Figure 3.8. Chemical synthesis of acetamide sulfonate derivatives **3.9 and 3.10**. **a**) Anhydrous DCM, anhydrous pyridine, 2 h.

The stability of tosyl acetamide (**3.9)** was evaluated at a single pH (pH 8) using the previously mentioned ^{1}H-NMR method. The aqueous stability was conducted at only one pH, given that the conducted hydrolysis rates of ethyloxy and propyloxy solufonate derivatives **3.1-3.8** were found to be pH independent. As shown in Figure 3.9, the presence of α-amide group as part of the electrophile stabilises the tosyl acetamide (**3.9**) toward hydrolysis in comparison to the 3-methoxypropyl 4-methylbenzene sulfonate (**3.6**).

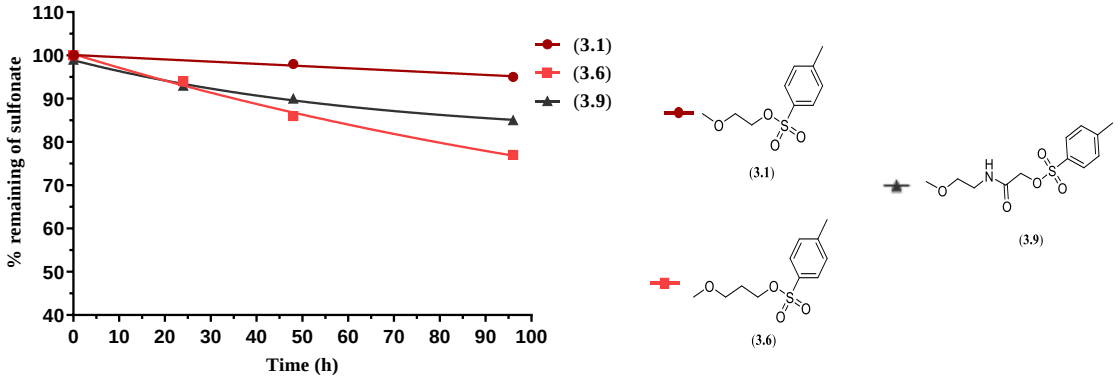

Figure 3.9. Percentage remaining of sulfonates (**3.1**, **3.4-3.8**, and **3.9**) in aqueous buffer over 4 days. Stability was appraised in phosphate buffer (100 mM, pH 8) using solvent suppression method.

In summary, the hydrolysis profile of the synthesised sulfonate derivatives has been appraised. Propyloxy sulfonate derivatives displayed lower aqueous stability than ethyloxy sulfonate analogues, while the tosyl acetamide sulfonate **3.9** displayed higher stability than **3.6** under the evaluated conditions. It can be concluded that the presence of alkyl group next to the electrophilic center (carbocation) increases the reactivity of sulfonate derivative towards hydroxide group (hard nucleophile), whereas the presence of α-amide group reduces the reactivity of sulfonate derivative towards the hydroxide group.

3.3 Reactivity rates of sulfonates with the thiol containing nucleophile glutathione

Next, we sought to test the reactivity of sulfonate derivatives **3.4**, **3.7**, and **3.8** towards a thiol nucleophile and subsequently compare rates of hydrolysis to rates of thiol alkylation.

Reduced glutathione **3.23** (3 equiv.), cysteine containing tripeptide, was incubated with each sulfonate derivative at room temperature in phosphate buffer (100 mM, pH 7.5) (Figure 3.10). Excess equivalents of glutathione were employed to account for areal-oxidation of the reduced glutathione. In a parallel experiment, each sulfonate derivative was held in phosphate buffer (100 mM, pH 7.5). In the absence of glutathione, to evaluate hydrolysis.

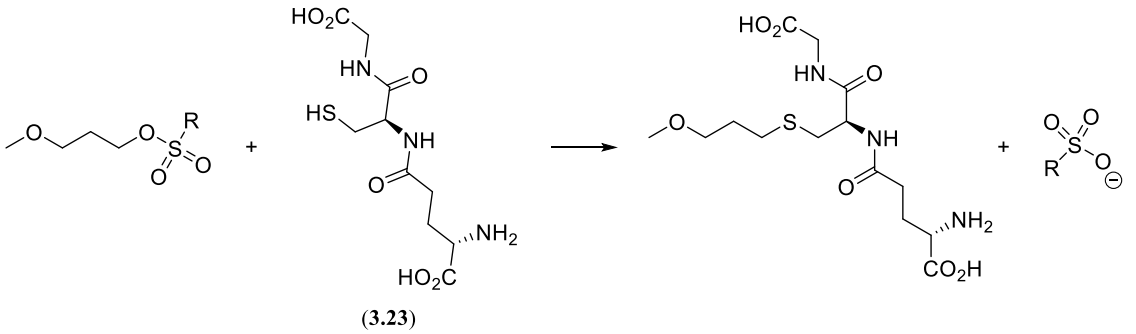

Figure 3.10. Reaction of glutathione (**3.23**, 3 equiv.) with sulfonate derivatives in aqueous in phosphate buffer (100 mM, pH 7.5).

The percentage of remaining sulfonates in the presence and absence of glutathione over 2 days was calculated using a ^{1}H-NMR method similar to those used previously to determine the aqueous stability of sulfonate derivatives. As such, the rate of hydrolysis of 3-methoxypropyl 4-nitrobenzene sulfonate (**3.8**) was calculated to be 0.063 h^{-1} (half-life = 27.5 h), whereas the rate of reaction with glutathione was calculated by subtracting the % of remaing sulfonates in the presence of glutathione, from the % of remaining sulfonates in the absence of glutathione and found to be 0.004 h^{-1} (Figure 3.11 A and B). These results suggest that higher equivalent of sulfonate ester linkers is required in bioconjugation reactions to compensate the hydrolytic instability of them and achieve higher labelling yields.

The reaction rates of 2-methoxyethyl 3-chlorobenzene sulfonate (**3.4**) and 3-methoxypropyl 3-chlorobenzene sulfonate (**3.7**) with glutathione (3 equiv.) were found to be 0.002 and 0.003 h^{-1}, respectively (Figure 3.11 A and B).

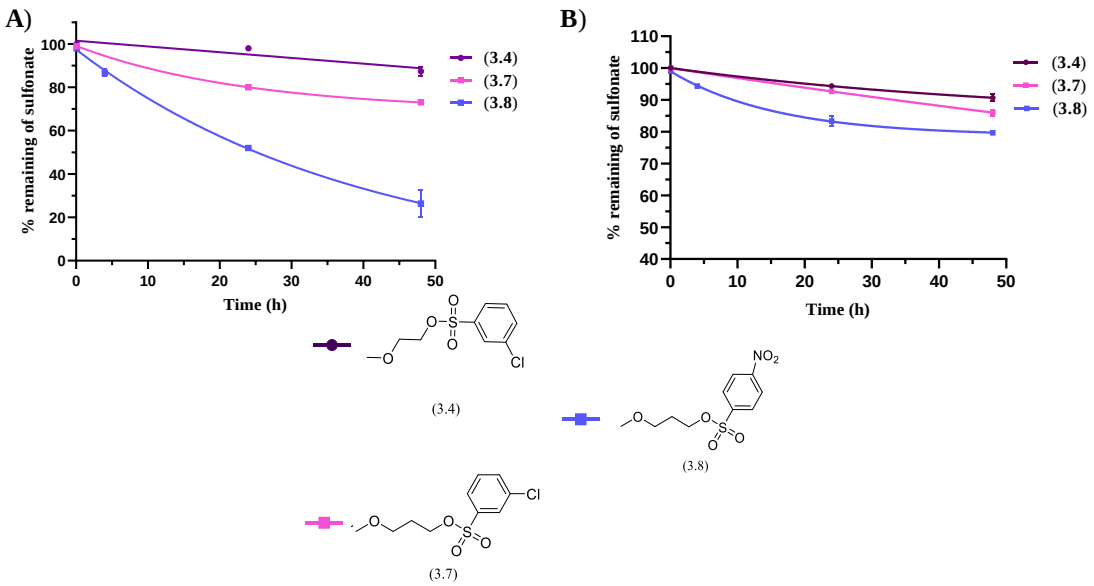

Figure 3.11. **A**) Percentage remaining of sulfonates **3.4**, **3.7**, and **3.8** in absence of glutathione in aqueous phosphate buffer (100 mM, pH 7.5). **B**) Percent of remaining of sulfonates **3.4**, **3.7**, and **3.8** in presence of glutathione (**3.23**, 3 equiv.) in aqueous phosphate buffer (100 mM, pH 7.5). Data presented as mean ±SD of 3 independent experiments.

Consistent with previous results the presence of the α-amide group reduced the rate of hydrolysis of the tosylate group, as less than 6% hydrolysis was observed over 2 days at pH 7.5 (Figure 3.12 A). As such, the rate of reactivity with glutathione can be obtained

by assuming that rate the of hydrolysis is negligible. Glutathione (3 equiv.) was held with tosyl acetamide (**3.9**) in phosphate buffer (100 mM, pH 7.5) and analysed using ^{1}H NMR (Figure 3.12 B). Surprisingly, tosyl acetamide (**3.9**) reacted completely with glutathione in less than 10 h and the rate of reactivity was found to be 0.161 h^{-1} (Figure 3.13).

Our obtained results are consistant with the previously established reactivity of alkyl halides with thiolate group of cysteine.[144] Dahl and Mckinley-Mckee (1981) have reported the parameters affecting the reaction rates of alkyl halides with the thiolate of cysteine. A range of different α-substituents were chosen and the rates of their reactivity were determined. They proved that the nature of α-substituents has crucial impact on the reactivity of the electrophile when the same leaving group was compared.[144] It has been shown that α-haloacetamides are more reactive than α-haloacids, and both are far more reactive than α-halo-alkyl derivatives towards the thiolate anion. The order of reactivity of thiolate group towards electrophiles is as follows:

$R\text{-}CH(X)\text{-}CONH_2$ > $R\text{-}CH(X)\text{-}COOH$ > $R\text{-}CH_2(X)$ > $R\text{-}CH(X)\text{-}CH_2OH$. Where X is the same halogen.[144]

Therefore, in comparison to the alkyl tosylates **3.1** and **3.6,** the reactivity rate of tosylate derivative with appended α-amide functionality **3.9** towards glutathione has been dramatically increased (Figure 3.13 A and B).

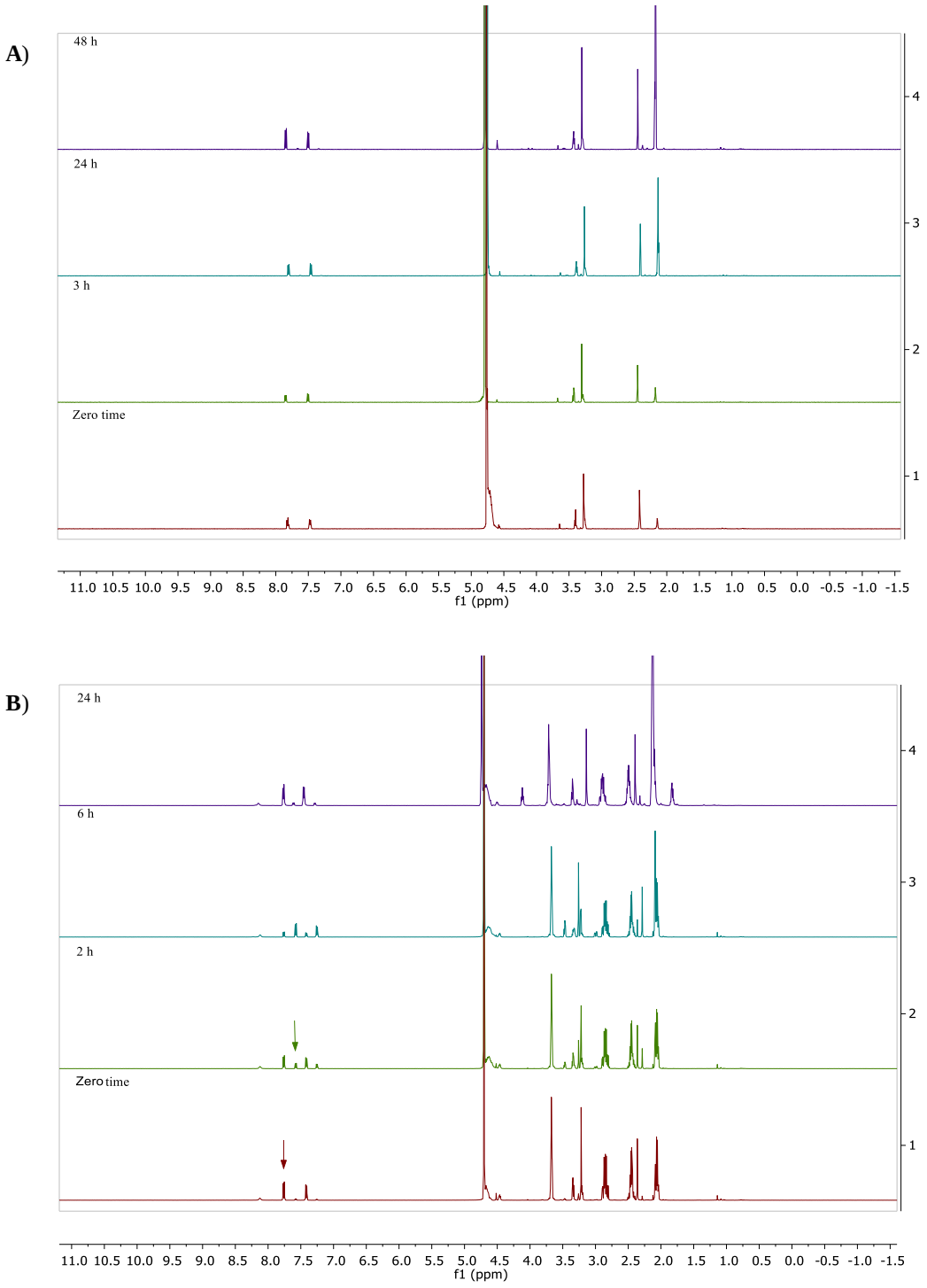

Figure 3.12. A) ^{1}H NMR spectrum of tosyl acetamide (**3.9**) in the absence of glutathione. **B)** ^{1}H NMR spectrum of tosyl acetamide (**3.9**) in the presence of glutathione (3 equiv.). Arrows indicate the aromatic peaks that have been followed to calculate reactivity rates using Equation 3.1. Red arrows correspond to the aromatic protons of sulfonate group of tosyl acetamide (**3.9**) (2 x $SO_2CC\underline{H}$) while green arrows correspond to the aromatic protons of sulfonate group of sulfonic acid (2 x $SO_2CC\underline{H}$).

The significant increase observed in the reactivity rates of tosyl acetamide (**3.9**) in comparison to alkyl tosylates **3.1** and **3.6** can be explained by considering the hard-soft acid base model (HSAB). A hard nucleophile, such as a hydroxide group will primarily react with a hard electrophile, while a soft nucleophile (lower electronegativity) such as thiolate group predominantly reacts faster with a soft electrophile. The presence of vicinal amide group renders the partial positive charge on the carbocation less dense, and therefore, more reactive towards thiolate nucleophile.[145]

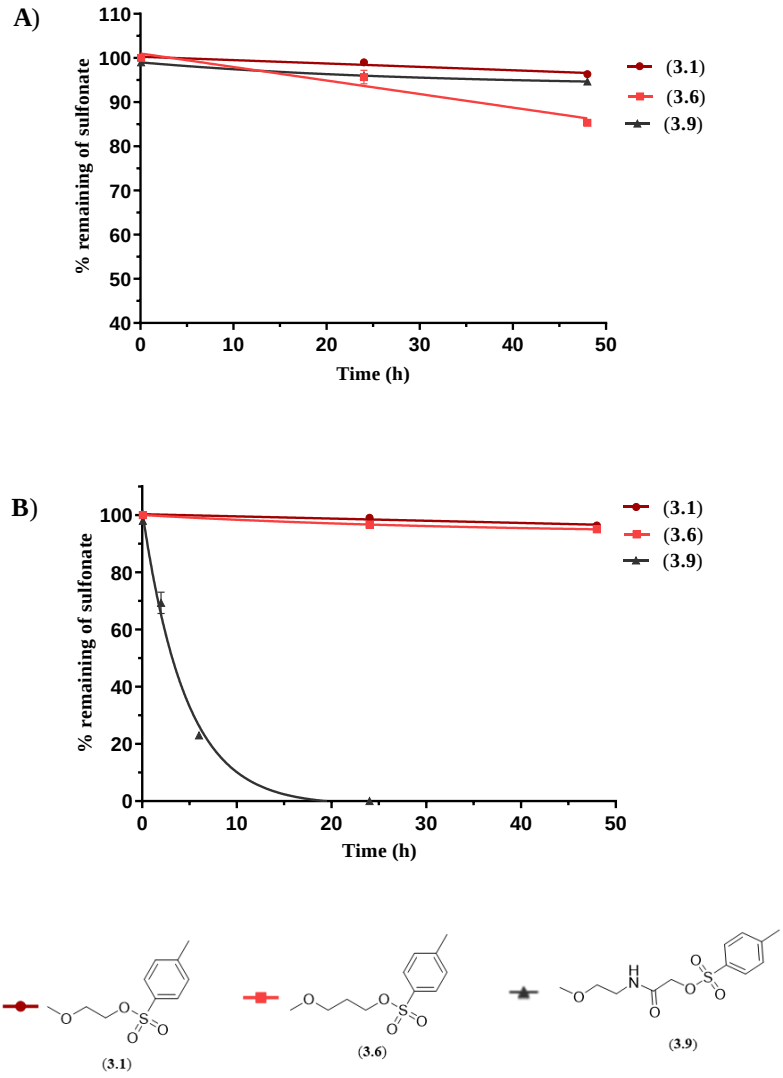

Figure 3.13. A) Percentage remaining of sulfonates (**3.1**, **3.6**, and **3.9)** over 2 days at pH 7.5. Stability was appraised in phosphate buffer (100 mM, pH 7.5) using solvent suppression method. **B**) Percentage remaining of sulfonates (**3.1**, **3.6**, and **3.9)** in the presence of glutathione (**3.23**, 3 equiv.) in aqueous phosphate buffer (100 mM, pH 7.5). Data are represented as mean ±SD of n=3.

The introduction of acetamide group had a significant effect on reaction rates of the tosylate (**3.9**) with glutathione. Thus, we next aimed to study the impact of steric hindrance of the bulky leaving group on their reactivity rate.

Accordingly, mesyl acetamide (**3.10**) was synthesised according to the previously mentioned method (Figure 3.8) and its stability and reactivity rate with reduced glutathione (**3.23,** 3 equiv.) were determined. Over a period of 48 h, mesyl acetamide (**3.10**) was stable in water with no detected peaks of hydrolysis (Figure 3.14 A).

Again, the reaction rates with glutathione can be calculated assuming that the hydrolysis rate is neglibable. ^{1}H-NMR (solvent suppression experiment at 4.7 ppm) analysis over 2 days was used to calculate the reaction rates of **3.10** with glutathione (Figure 3.14 B). The percent (%) of remaining mesyl acetamide (**3.10**) was calculated using Equation 3.3.

$$\%\ \boldsymbol{of\ remaining\ mesyl\ acetamide\ (3.10)} = \frac{I_s}{(I_s + I_{sa})} * 100 \qquad \textbf{(Equation 3.3)}$$

Where;

I_s= Integration of the peak at δ 3.2 ppm which corresponds to the methyl protons of mesylate group of **3.10** ($CH_2OSO_2C\underline{H_3}$).

I_{sa}= Integration of the sulfonic acid peak at δ 2.65 ppm which corresponds to the methyl protons of mesylate group of mesylic acid ($HOSO_2C\underline{H_3}$).

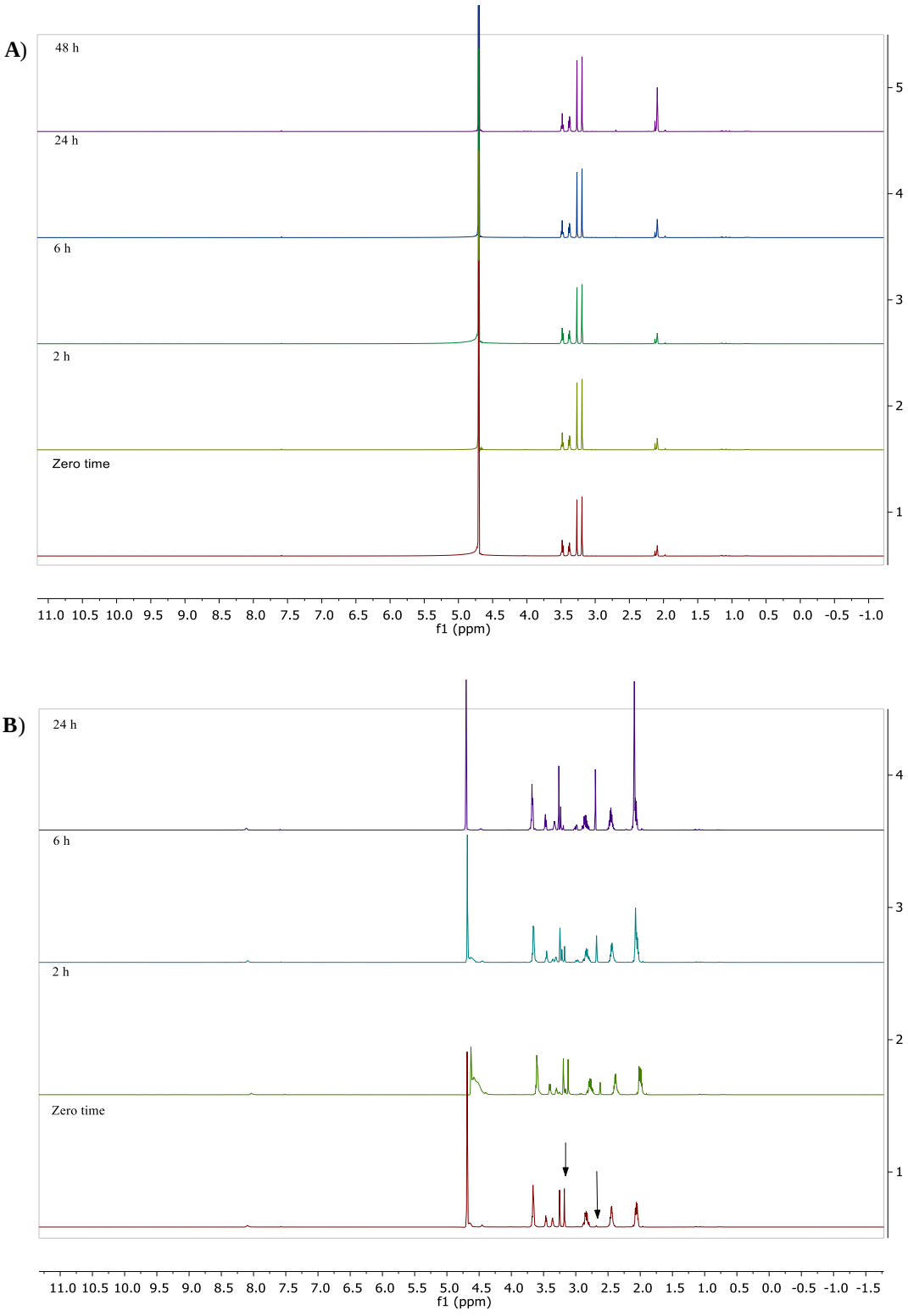

Figure 3.14. A) ^{1}H NMR spectrum of mesyl acetamide (**3.10**) in the absence of glutathione. **B**) ^{1}H NMR spectrum of mesyl acetamide (**3.10**) in the presence of glutathione (**3.23**, 3 equiv.), arrows indicate the peaks that were followed to obtain the reactivity rates (substitution of mesylic acid anion).

Surprisingly, both tosyl acetamide (**3.9**) and mesyl acetamide (**3.10**) showed comparable reactivity rates with glutathione **3.23** (3 equiv.) which are 0.161 and 0.159 h^{-1}, respectively (Figure 3.15). According to the predicted pK_a of 4-toluenesulfonic acid (-0.43±0.50) and methanesulfonic acid (1.75±0.50), tosyl acetamide (**3.9**) is expected to be more reactive than mesyl acetamide (**3.10**). However, the comparable reactivity results obtained could be attributable to the bulky tosylate leaving group in comparison to the mesylate group to account for the similar reaction rates observed with glutathione.

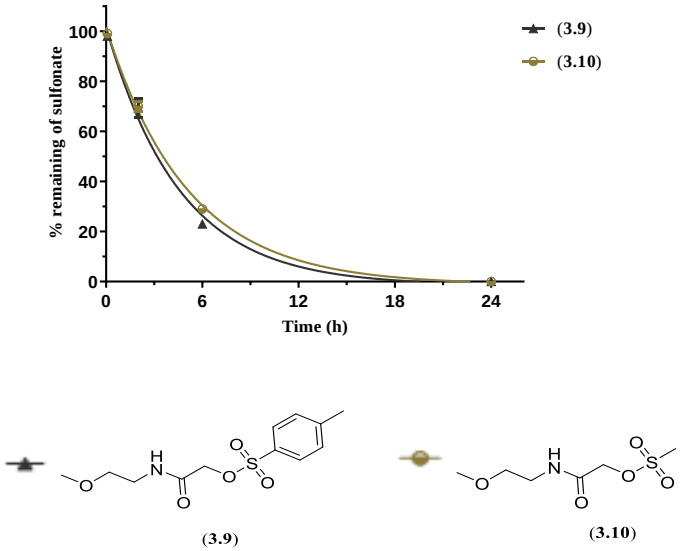

Figure 3.15. Percentage remaining of sulfonates (**3.9**, **3.10**) in the presence of glutathione (**3.23**, 3 equiv.) in phosphate buffer (100 mM, pH 7.5). Data are represented as mean ±SD of n=3.

3.4 Stability of sulfonates in the presence of TCEP

Considering that most cysteine residues in proteins are paired in disulfide bonds, a reduction step is typically required before commencing thiol alkylation. Phosphines reductants, such as the water soluble TCEP (**2.2**), which were investigated in Chapter 2, are widely used reducing agents in protein conjugation. It is essential to evaluate the compatibility of sulfonate derivatives with TCEP to determine whether a quenching step in between is necessary during the conjugation reaction.

Thus, we set out to evaluate the stability of sulfonate derivatives in the presence of TCEP. The 3-methoxypropyl-3-chlorobenzene sulfonate (**3.7**), and tosyl acetamide (**3.9**) were held with TCEP **2.2** (3 equiv.) and analysed by ^{1}H NMR over 2 days. In a parallel

experiment, 3-methoxypropyl-3-chlorobenzene sulfonate (**3.7**) was held in phosphate buffer (100mM, pH 7.5) without TCEP. As only hydrolysis peaks were observed by ^{1}H NMR (Figure 3.16), 3-methoxypropyl-3-chlorobenzene sulfonate (**3.7**) was found to be stable in the presence TCEP.

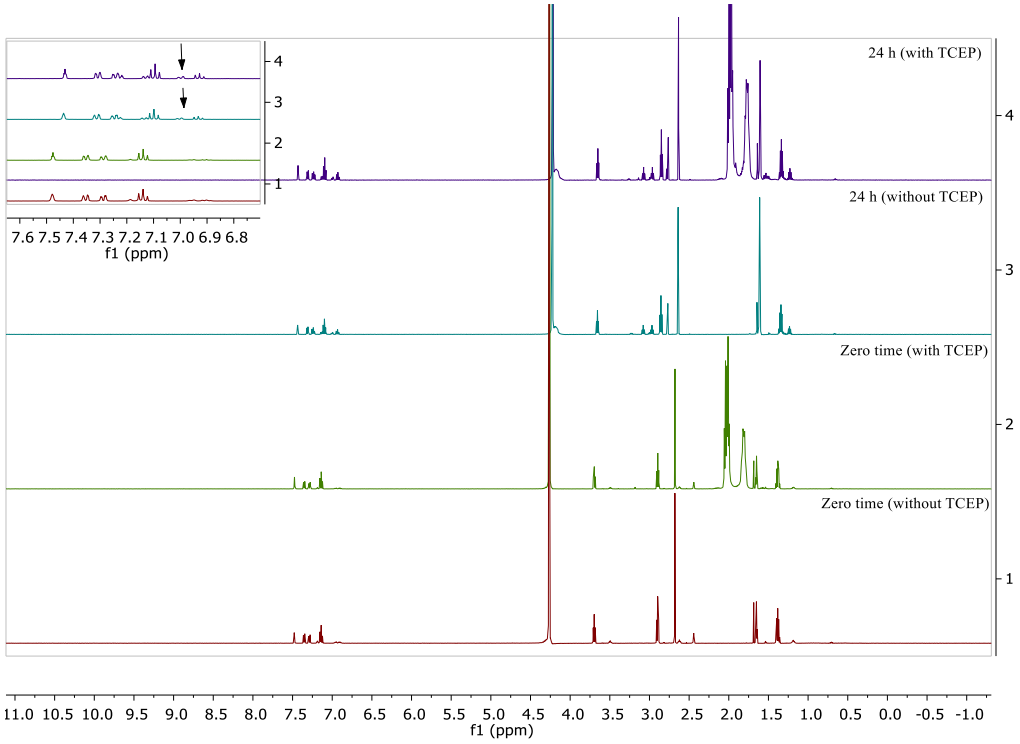

Figure 3.16. Stability of 3-methoxypropyl3-chlorobenzene sulfonate (**3.7**) in the presence of TCEP (**2.2,** 3 equiv.). ^{1}H NMR spectra of 3-methoxypropyl-3-chlorobenzene sulfonate (**3.7**) in the absence and presence of TCEP. Arrows in the expanded region indicate the aromatic peaks of sulfonic acid (hydrolysis) that obtained in the absence and presence of TCEP after 24 h.

Again, ^{1}H NMR experiment was used to determine the reaction rate of tosyl acetamide (**3.9**) with TCEP (Figure 3.17 A). In contrast to 3-methoxypropyl-3-chlorobenzene sulfonate (**3.7**), the tosyl acetamide (**3.9**) was found to react with TCEP, possibility through nucleophilic substitution of tosylate anion to afford an ylide or ylene product.

The rate of reactivity of tosyl acetamide (**3.9**) with TCEP was found to be 0.096 h^{-1} (Figure 3.17 B). Therefore, since tosyl acetamide is not stable in the presence of TCEP, it is necessary to use our previously mentioned quenching method in Chapter two to oxidize excess TCEP prior to the addition of sulfonate ester linkers in bioconjugation reactions.

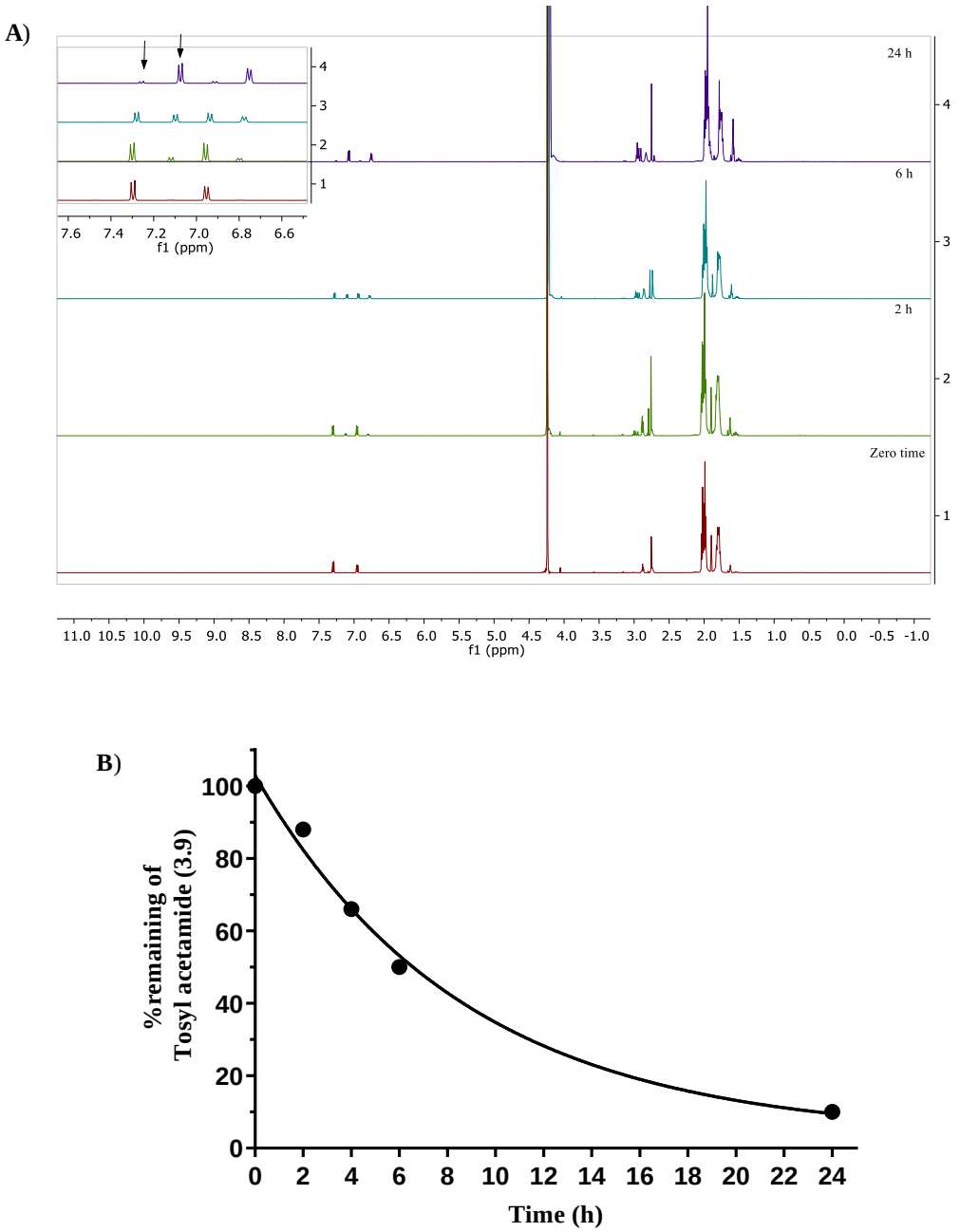

Figure 3.17. Stability of tosyl acetamide (**3.9**) in the presence of TCEP (**2.2,** 3 equiv.). **A**) ^{1}H NMR spectrum of tosyl acetamide (**3.9**) in the presence of TCEP. Arrows in the expanded region indicate the aromatic peaks that were followed to calculate reactivity rates using Equation 3.1. **B**) Percentage remaining of tosyl acetamide (**3.9**) in presence of TCEP (3 equiv.) in aqueous phosphate buffer (100 mM, pH 7.5).

3.5 Reactivity of selected sulfonates with proteins

Finally, as the aqueous stability and reactivity rates have been evaluated, we sought to investigate the reaction of several sulfonates with Sbi IV-Cys at pH 7.5. Sbi IV-Cys

was selected as a model protein as it is small (10 kDa) and has only one cysteine residue at its N-terminus. Thiol alkylation of the cysteine group of Sbi IV-Cys was investigated using protein mass spectroscopy. This mass spectrometric analysis was performed on an Agilent 6520 CHIPCube Q-TOF LC/MS.

Sbi IV-Cys (2 mg/mL) in Tris.HCl buffer (100 mM, 150 mM NaCl, 5mM EDTA, pH 7.5) was reduced using TCEP **2.2** (2 equiv.) for 1 h at room temperature, then the reduced Sbi IV-Cys was held with the penta-PEG azide **2.13** (5 equiv.) for 1 h at room temperature to quench excess TCEP before incubation with sulfonate derivatives (10 equiv.) at room temperature overnight. Excess linkers were then removed by buffer exchange [3 times, using Amicon® Ultra-0.5mL (3 kDa) centrifugal filter] and analysed by mass spectroscopy.

From the MS analysis obtained, one can identify that approximately less than 10 % of Sbi IV-Cys labelling was observed when 3-methoxypropyl-4-nitrobenzene sulfonate (**3.8**) was employed. These results suggest that higher equivalents should be used to compensate the higher hydrolysis rate of 3-methoxypropyl-4-nitrobenzene sulfonate (**3.8**) (Figure 3.18 C). 3-methoxypropyl-4-methylbenzene sulfonate (**3.6**) showed no detectable labelling of Sbi IV-Cys (Figure 3.18 B).

Conversely, the acetamide sulfonate derivatives showed a higher level of protein labelling compared to alkyl sulfonate derivatives. Tosyl acetamide (**3.9**) showed highest labelling level with almost complete thiol alkylation of the protein. These results are in line with the previously determined reaction rates using glutathione (Figure 3.19 A). Surprisingly, the mesyl acetamide (**3.10**) showed a lower efficiency of labelling of Sbi IV-Cys (Figure 3.19 B).

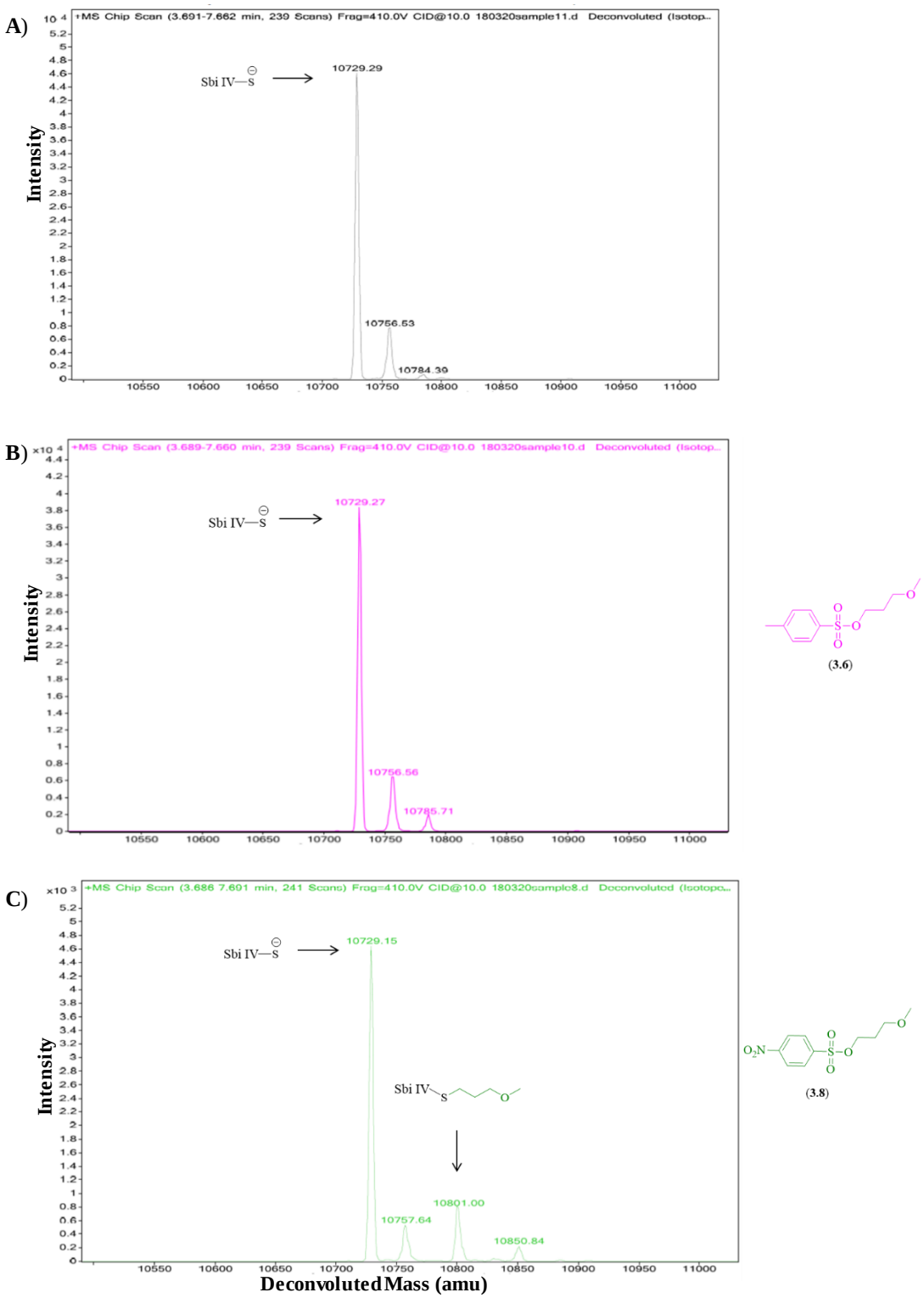

Figure 3.18. Deconvoluted protein MS spectra of Sbi IV-Cys (2 mg/mL, 0.187 mM) reacted with sulfonates **3.6** and **3.8** (1.87mM, 10 equiv.) at pH 7.5. **A**) Sbi IV-Cys control. **B**) Sbi IV-Cys reaction with 3-methoxypropyl-4-methylbenzene sulfonate (**3.6**) at pH 7.5 with no detection of product peak. **C)** Sbi IV-Cys reaction with 3-methoxypropyl-4-nitrobenzene sulfonate (**3.8**) at pH 7.5, yielding a mass of 10801 Da. with difference of 71.85 Da.

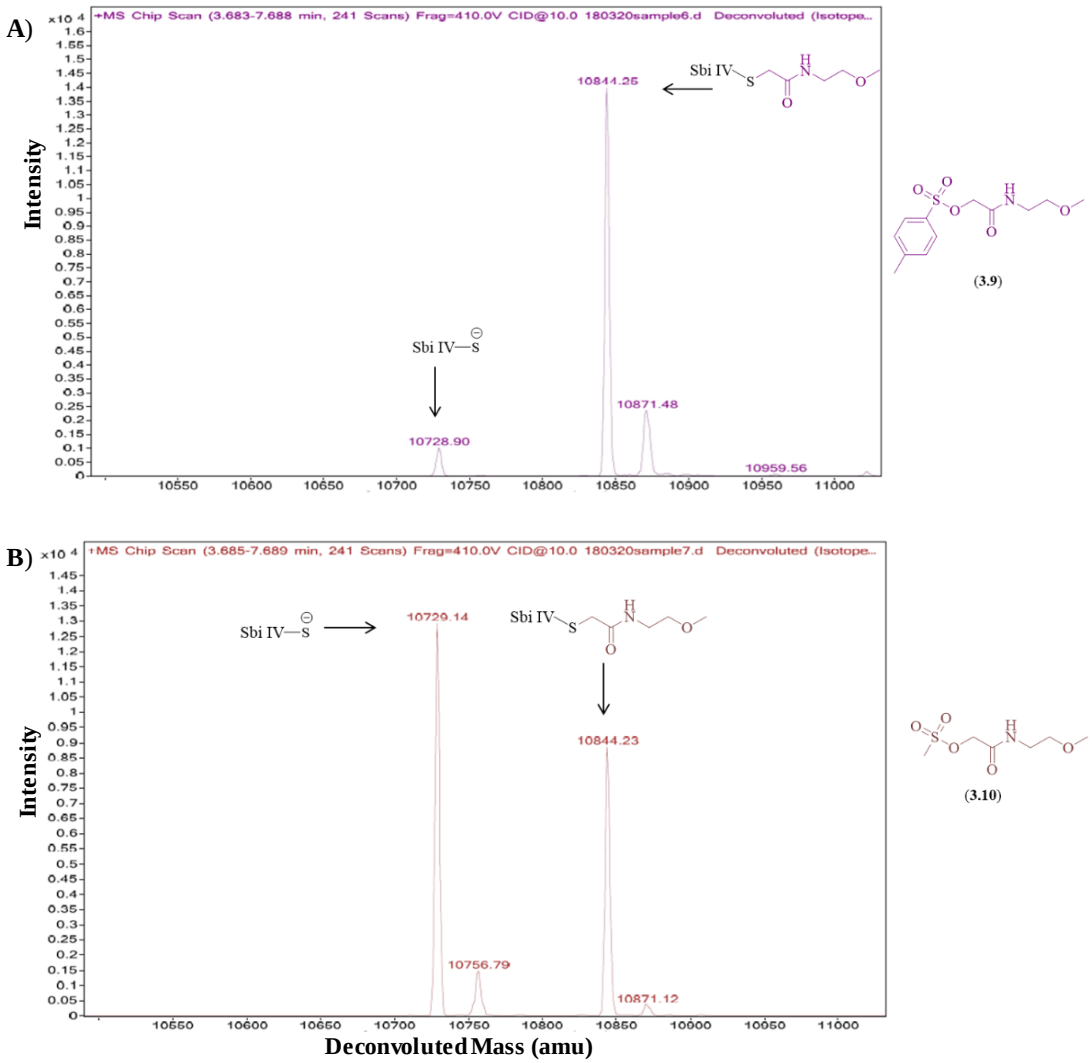

Figure 3.19. Deconvoluted protein MS spectra of Sbi IV-Cys (2 mg/mL, 0.187 mM) reacted with sulfonates **3.9** and **3.10** (1.87mM, 10 equiv.) at pH 7.5. **A**) Sbi IV-Cys reaction with tosyl acetamide (**3.9**) at pH 7.5, yielding a mass of 10844.25 Da. with difference of 115.35 Da. **B**) Sbi IV-Cys reaction mesyl acetamide (**3.10**) at pH 7.5, yielding a mass of 10844.23 Da. with difference of 115.09 Da.

3.6 Conclusion

In this Chapter we aimed to find alternative thiolate alkylating method in order to tackle the drawbacks of the currently wide-applied approaches, mainly maleimide-based conjugation methods. Maleimide-based approaches has been widely used due to their specificity and outstanding reaction kinetics;[146] therefore, it has been employed in cross-linking, fluorescent labeling and in PEGylation reactions. As mentioned earlier (see Section 1.4.2.1), the major drawback of this approach is the instability of the constructed conjugates through retro-Michael addition mechanism to reform maleimide, which leads to the assembly of a new thiol conjugate in the presence of free thiols.[84]

We evaluated the potential use sulfonate derivatives as cysteine alkylating agents through understanding the factors affecting their electrophilic reactivity. The nature of the α-substituent groups was found the most essential factor affecting both the aqueous stability and the reactivity of sulfonate derivatives. The α-amide group was the best identified acceptor group amongst the studied ethyloxy and propyloxy sulfonate derivative. Based on the evaluated hydrolysis rates, reactivity rates and protein functionalisation of the synthesised range of sulfonates (**3.1**-**3.10**), tosyl acetamide (**3.9**) provided the most promising results. This included low hydrolysis rate, high reaction rates with glutathione, and almost complete protein labelling.

However, due to the relatively slow kinetics obtained with tosyl acetamide (**3.9**) in compared to the known maleimide-based approaches,[146,147] we can conclude that the presence of the α-amide group renders sulfonate derivatives better electrophilic groups, but still not enough to be suitable for protein labelling.

4 Bis-haloacetmide derivatives as a novel disulfide rebridging agents

4.1 Introduction

Antibody drug conjugates (ADCs) are one of the cutting-edge antibody-based therapeutic approaches, which have attracted substantial attention over the last two decades. ADCs comprise a mAb which is employed as a vehicle to direct a cytotoxic drug to a specific malignant cell or tissue. The construction of ADCs requires specific linker characteristics in order to attain plasma-stable antibody drug conjugates.

The construction of the first-generation of ADCs utilised the inherent nucleophilic functionality of the amino acid residues within the antibody, mainly cysteine and lysine amino acids. In order to generate cysteine-based conjugates, a pre-reduction step of inter-chain disulfide bonds is required. The IgG_1 subclass of IgGs is the most abundant one in human serum and most common type employed in mAb-based therapeutics.[148] IgG_1 has a total of four inter-chain disulfide bonds, two inter-chain disulfide bonds are between heavy/light chains and two inter-chain between heavy/heavy chains in the hinge region.[148] A great number of studies have shown the importance of the 4 inter-chain disulfide bonds, not only to maintain the structure of mAbs and optimal antigen binding, but also to preserve the effecter function of mAbs. A reduction in CDC and ADCC were observed for a chimeric mouse/human IgG when a mutated IgG lacking of inter heavy chain disulfide bonds was tested. It has been found that even partial reduction of the four inter-chain disulfide bonds of IgG resulted in a dramatic reduction in their complement fixation function and CDC.[149–151]

Given that disulfide bonds are essential to maintain the proper folding, structure and more importantly, the function of mAbs, it is essential to maintain the post-reduction structure of recombinant antibodies prior to the construction of mAb conjugates. In attempts to avoid the complex and expensive genetic re-engineering of mAbs to maintain the post-reduction structure of mAbs and retain a defined conjugation approach, Abzena has pioneered a novel approach of producing homogenous and stable ADCs based on rebridging of the reduced inter-chain disulfide bonds. ThioBridge®

technology is a bis-sulfone-based reagent which re-anneals the reduced inter-chain disulfide bonds of mAbs forming a 3-carbon bridge, and by doing so, ThioBridge® maintains the post-reduced disulfide structure of the antibody. The accessible reduced disulfide bonds are cross-linked through sequential addition-elimination mechanism, first starting by Michael addition of a thiolate group of the reduced disulfide bond, followed by elimination of p-toluene sulfinic acid generating the second Michael acceptor (α-β unsaturated carbonyl) as shown in Figure 4.1. The vicinal thiolate group then reacts through a second Michael addition to form a 3-carbon linkage between the two cysteine thiols.[152,153]

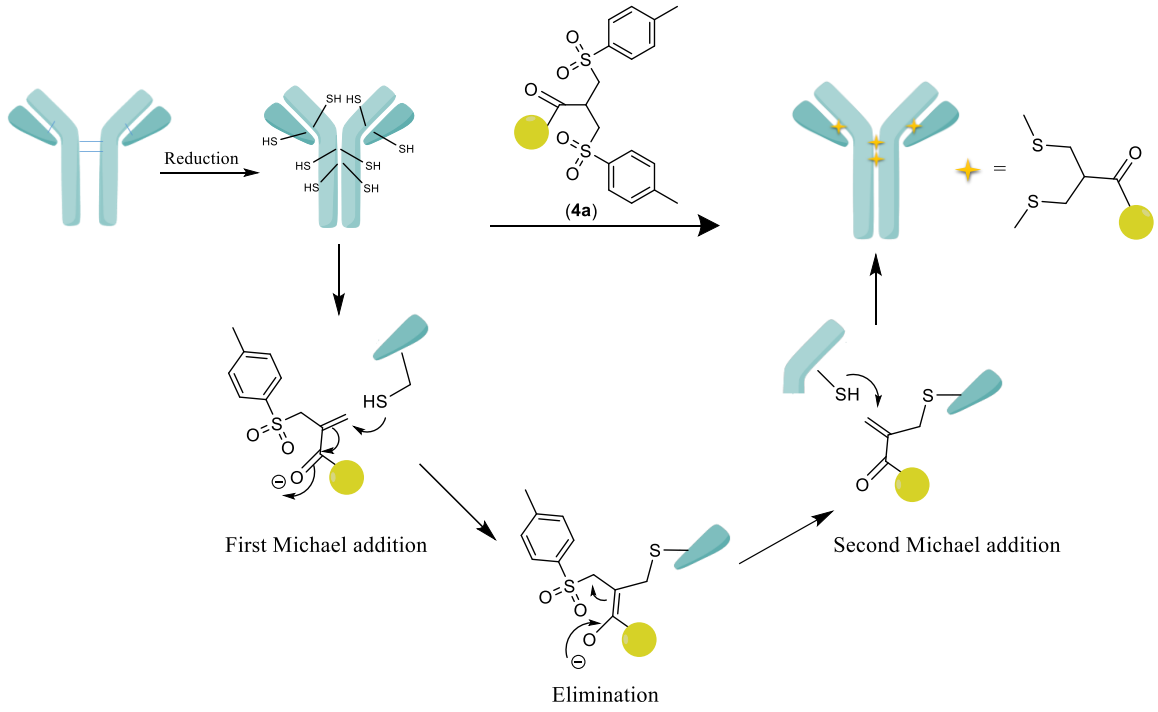

Figure 4.1. Addition-elimination mechanism of a bis-sulfone linker (ThioBridge®) coupled with cytotoxic drug (●) in cross-linking the reduced inter-chain disulfide bonds of mAbs affording 3-carbon bridges.

Given that the primary aim of using bis-sulfone linkers is to attain better plasma stability of the ADCs, the increased plasma stability has been appraised by comparing fluorescently-labeled trastuzumab using a maleimide linkage, with fluorescently-labeled bis-alkylated trastuzumab.[152] The latter displayed significant serum stability over 5 days in the presence of high concentrations of albumin.[152] Moreover, it has been confirmed

that using bis-sulfone reagent bearing MMAE in the construction of ADCs of trastuzumab, fully retained binding activity of trastuzumab to the HER2 receptor, and displayed potent antiproliferative activity in HER2 positive cell lines.[152]

Shortly following the development of ThioBridge® technology, a number of different rebridging reagents have been developed to tackle the drawbacks of bis-sulfone reagents, including the slightly basic pH requirement to commence the rebridging, poor solubility of the reagents and the slow reaction kinetics and time taken between reduction of the disulfide and completion of re-annealing process which has potential to affect the structure of the protein.

As such, more reactive re-annealing reagents were developed utilizing the inherent reactivity of maleimide derivatives towards thiolates to attain what is known as bis-reactive maleimide linkers or next-generation maleimide, such as dibromomaleimide (**4b**). Bis-reactive maleimide linkers were developed as disulfide rebridging agent through 2-carbon bridge to attain bis-thiomaleimide linkage.[154] The fast reaction kinetics of bis-reactive maleimide derivatives offers higher protein structure integrity and broader reaction pH range (6-8) compared to bis-sulfone derivatives.

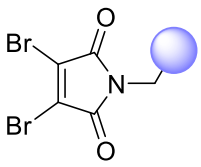

(**4b**)

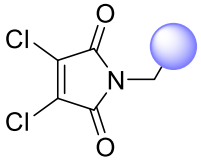

(**4c**)

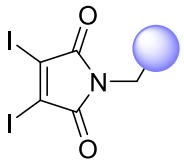

(**4d**)

Other 3,4-dihalosubstituted maleimide derivatives, such as dichloro (**4c**) and diiodomaleimide (**4d**) have been also evaluated and the latter has showed superior reactivity rates towards thiolates. 3,4-Dithiomaleimide reagents were also assessed as rebridging agents and among them, dithiophenolmaleimide (**4e**) showed comparable reactivity rate to dibromomaleimide (**4b**) and due to the higher stability of dithiophenolmaleimide toward TCEP in comparison to dihalomaleimides, **4e** was considered the most efficient bis-reactive maleimide derivative for *in situ* disulfide rebridging.[154]

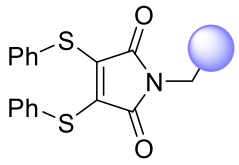

(**4e**)

Bis-sulfone reagents and dibromomaeimide derivatives are deemed as the earliest and most established rebridging reagents for reduced disulfides. Nonetheless, each has associated drawbacks. For example, poor water solubility of these reagents and lack of selectivity between reduced disulfides bonds and unpaired cysteine residues under reducing conditions. This has been demonstrated by Smith *et al.* where they used the dibromomaleimide (**4b**) reagent to mono-alkylate a single cysteine residue (in high yield) in a mutated protein followed by second thiol-alkylation of different thiol-containing peptides, such as glutathione (Figure 4.2 A). However, they also demonstrate the usefulness of dibromomaleimide (**4b**) in cross-linking a disulfide bond of peptide hormone Somatostatin generating a bisthiomaleimide with a 2-carbon bridge (Figure 4.2 B).[155]

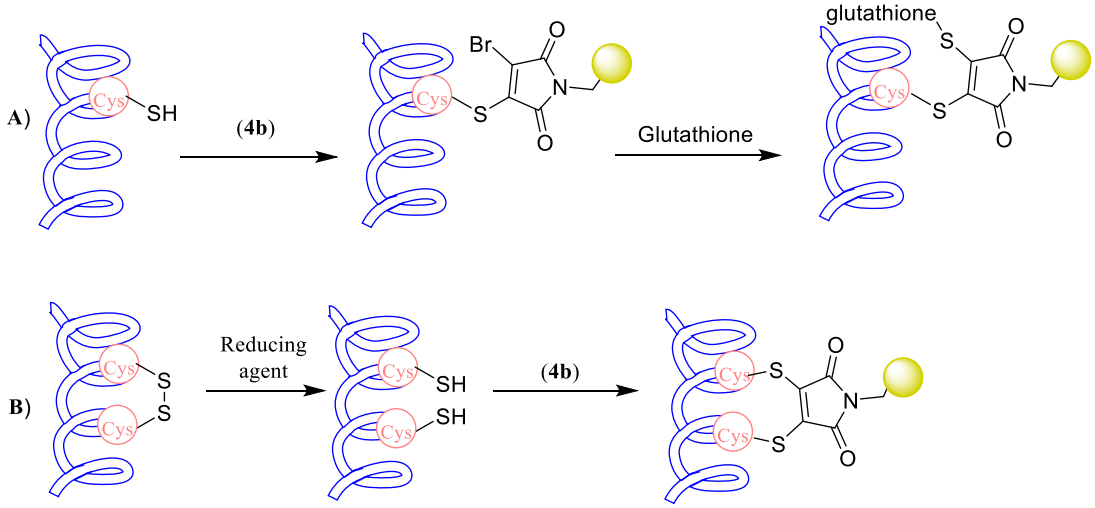

Figure 4.2. A) Mono-labeling of thiol group with dibromomaleimide (**4b**) reagent. **B**) Cross-linking of the disulfide bond of somatostatin by dibromomaleimide (**4b**) reagent forming bisthiomaleimide 2-carbon bridge.

Therefore, many researchers seek to find alternative rebridging agents with different molecular scaffolds to overcome the limitations of the aforementioned rebridging agents.

One example of other scaffolds are the pyridazinedione-based compounds, such as dibromopyridazinedione (**4f**), which cross-links disulfide bonds through a 2-carbon bridges.[153]

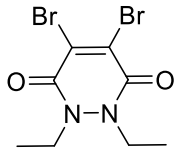

(**4f**)

Taking advantage of the stability of dithiophenolmaleimide in the presence of TCEP, di-TECP-substituted dithiophenolpyridazinedione (**4g**) has been synthesized as both reducing agent and stable cross-linker at the same time (Figure 4.3 A). Lee *et al.* used di-TCEP-substituted dithiophenolpyridazinedione as dual agent in the cross-linking of a Fab from trastuzumab.[156] Moreover, they attempted to minimize disulfide scrambling (intra-disulfide cross-linking) through using **4g**, which was incubated with full mAb, trastuzumab, to fully cross-link the four disulfide bond and reduce the scrambling of them (intra-chain cross-linking of heavy/heavy disulfide bonds).[156]

Maruani *et al.* went a step further by developing pyridazinedione-based linkers with two functionalities can be introduced on each N atom of the pyridazinedione ring. They produced dibromopyridazinediones (**4h**) bearing two reactive, clickable handles: alkyne and strained alkyne handles for sequential copper catalysed 'Click'reaction and stain-promoted 'Click'reactions, respectively (Figure 4.3 B).[153]

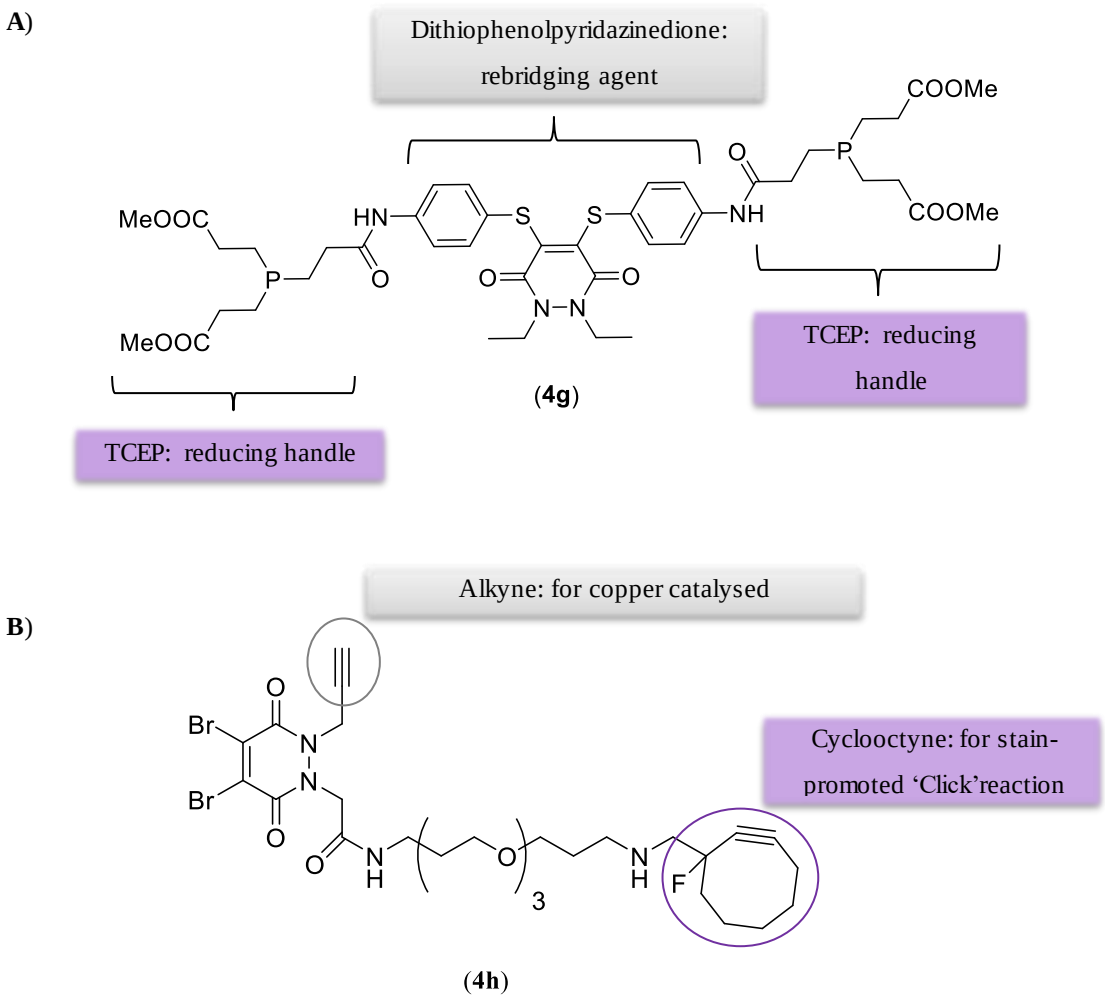

Figure 4.3. A) Di-TECP-substituted dithiophenolpyridazinedione (**4g**) with dual reduction and rebridging activities of mAb disulfide bonds. **B**) Dibromopyridazinediones (**4h**) with two different reactive, clickable handles for dual chlick reactions.

Rebridging strategies are considered elegant approaches that enable the introduction of reactive functional groups to the reduced mAbs while maintaining the well-define post-reduction structure of them. Despite the recent advances and considerable research efforts in this area, the aforementioned rebridging approaches either through forming 2- and 3-carbon bridges still have practical limitations that needed to be further addressed. With all major emphasis being on fully cross-linking the heavy-light and heavy-heavy inter-chain disulfide bonds to attain a fully cross-linked antibody (150 kDa), the previously described re-bridging methods have overlooked the potential advantages of construction of a half-antibody (75 kDa) as an intended product. In addition, to the best of our knowledge, the previous rebridging approaches have shown no significant

selectivity between heavy-heavy and heavy-light disulfide bonds. Therefore, site-selective protein labelling to attain a hetero-bifunctioanal mAb is still an unresolved challenge.

Therefore, this work set out to evaluate haloacetamide derivatives as next-generation rebridging agents with emphasis on the hetero rebridging of full mAbs.

As described previously in Chapter 3, tosylate derivatives with α-amido group, such as (**3.9**), displayed superior reactivity rates with the thiolate anion of cysteine, as well as being relatively stable towards hydrolysis. Given that electrophiles with an α-amido group and bearing halogens as the leaving group (which is a better leaving group than tosylate anion) are ideal to attain fast reaction kinetics towards thiolates group of proteins. As such, we postulated that α-halo-acetamide derivatives would be more suitable for cross-linking of a protein. Therefore, in this Chapter we sought to evaluate the use of aryl bis-haloacetamides as rebridging agents of reduced disulfide bonds.

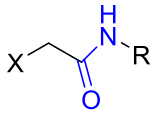

X = Ts (**3.9**)
X = Cl (**4.1**, **4.4**, **4.15**, **4.16**)

The concept of cross-linking biomolecules using alkyl-halides is well-established and has been used since the discovery of nitrogen mustard (Mechlorethamine) as an alkylating agent in 1942. These compounds exert their biological activity by alkylation of DNA, cross-linking two helical strands, thus preventing DNA replication which ultimately leads to cellular death (Figure 4.4).[157]

The two distinct reactive alkyl-chloride functionalities of these alkylating agents permits cross-linking of DNA, RNA and proteins and by doing so, disturbs the normal structure and function of biological molecules. [201]

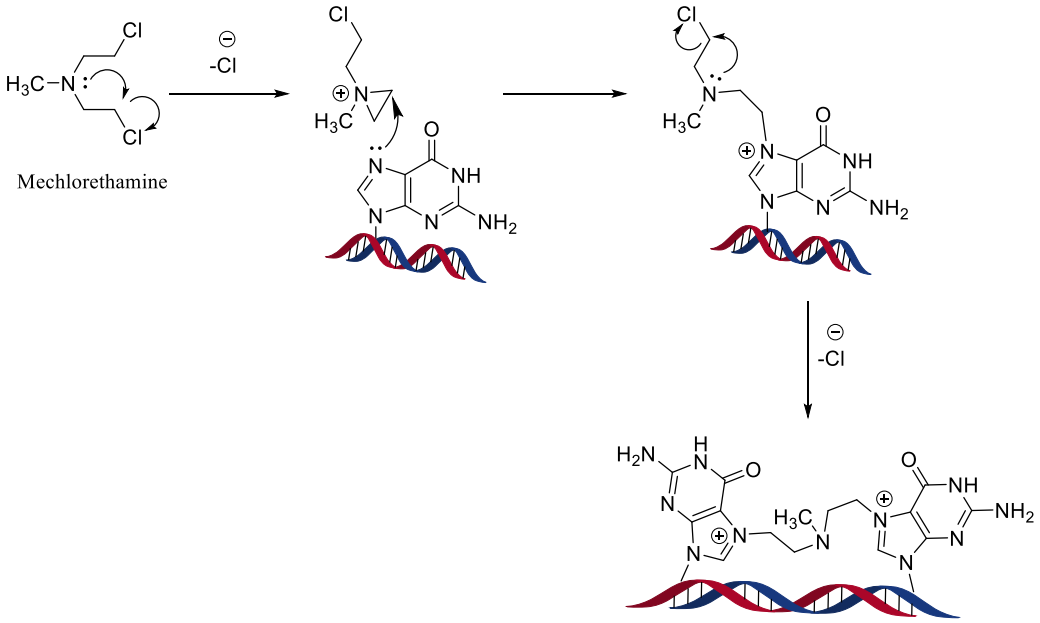

Figure 4.4. Cross-linking mechanism of a nitrogen mustard (Mechlorethamine) with N-7 of guanine base of DNA which leads to cell cytotoxicity.

Inspired by nitrogen mustard agents, herein we first aimed to evaluate two different scaffolds, namely *N*,*N*-di-chloroacetyl amido derivatives ($(ClCH_2CO)_2NR$) (**4.1** and **4.2**) as agents for rebridging reduced disulfide bonds of mAbs, in order to maintain their structural integrity, optimal antigen binding and normal effector functions.

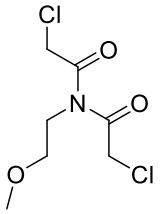

(**4.1**)

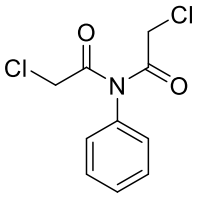

(**4.2**)

4.2 *N*,*N*-Di-(chloroacetyl)-amido derivatives as rebridging agent of reduced disulfide bonds

Herein, 2-chloro-*N*-(2-chloroacetyl)-*N*-(2-methoxyethyl)acetamide (**4.1**) was postulated as a bis-alkylating linker which permit bis-alkylation of reduced disulfide cysteine anions, therefore rebridging the reduced inter-chain disulfide bonds (Figure 4.5).

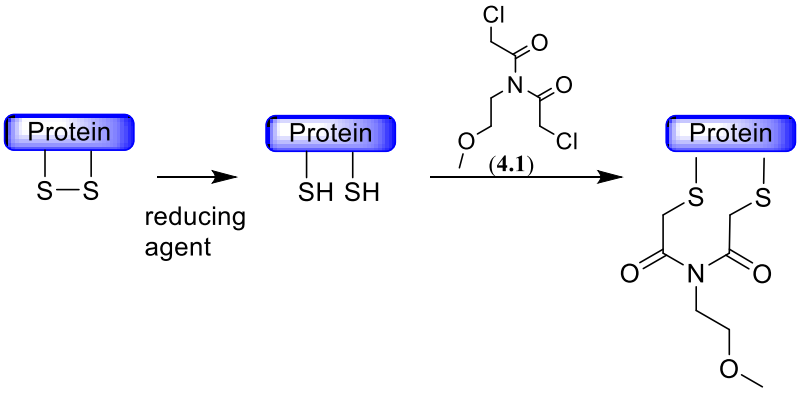

Figure 4.5. The proposed mechanism of rebridging of the reduced disulfide bonds using 2-chloro-*N*-(2-chloroacetyl)-*N*-(2-methoxyethyl)acetamide (**4.1**) linker.

Accordingly, several synthesis methods were followed in order to synthesise 2-chloro-*N*-(2-chloroacetyl)-*N*-(2-methoxyethyl)acetamide (**4.1**) (Figure 4.6).

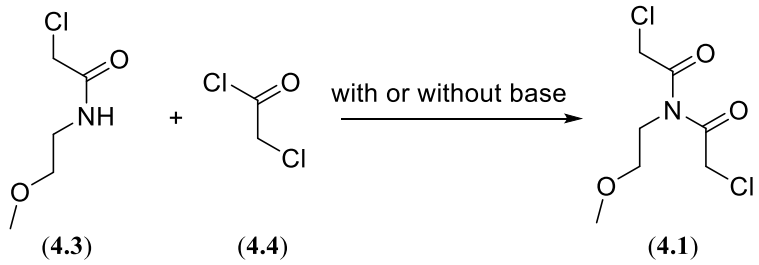

Figure 4.6. Our attempts to synthesise 2-chloro-N-(2-chloroacetyl)-N-(2-methoxyethyl)acetamide (**4.1**) through acetylation of 2-chloro-N-(2-methoxyethyl)acetamide (**4.3**) in absence or presence of a base, such as pyridine or TEA.

As such, pyridine (2.5 equiv.) was used as a base and added to a reaction mixture of 2-chloro-*N*-(2-methoxyethyl)acetamide (**4.3**) and 2-chloroacetyl chloride in DCM. The reaction left stirring for 24 h, however, a complex mixture of products was obtained and none of the products obtained could be defined. However, according to Shatsauskas *et al.* they reported that they used pyridine as a base in acylation reaction of their amine starting material, 3-aminopyridin-2(1H)-one (**4i**) with 2-chloroacetyl chloride resulted in the imide derivative (**4j**) in 75% yield (Figure 4.7 A).[158]

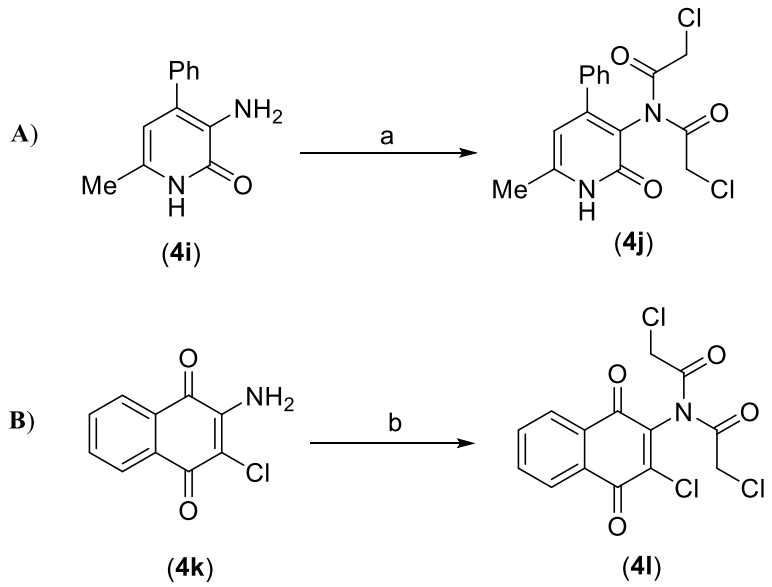

Figure 4.7. The previously described procedures to synthesise *N*,*N*-di-chloroacetyl amido derivative. **A)** (a) 2-chloroacetyl chloride, pyridine, DCM, 15 h.[158] **B)** (b) 2-chloroacetyl chloride, reflux, 3 h.[159]

Next, in attempt to follow the procedure similar to that described by Chan *et al.*, TEA (2.5 equiv.) was added over a period of 4 h to a reflux of reaction 2-chloro-*N*-(2-methoxyethyl)acetamide (**4.3**) and 2-chloroacetyl chloride mixture in DCM.[160] Following work-up and purification, a mixture of undefined products was obtained, though the desired product could not be confirmed by ^{1}H NMR. An example of the purified unknown product is shown in Figure 4.8 A, which has a ^{1}H NMR spectrum similar to the desired product.

Lastly, a base-free reaction was performed as follows. A mixture of 2-chloro-*N*-(2-methoxyethyl)acetamide (**4.3**) was refluxed with excess 2-chloroacetyl chloride in dry toluene for 24 h. After 24 h of reflux, the reaction mixture was subjected to standard work up (DCM) and analysed using MS. Only the starting material (**4.3**) was identified in addition to the product of elimination of the methoxy group, with expected mass ($M+H^{+}$) = m/z 120.0216 and found = m/z 120.0228 (Figure 4.8 B).

However, according to Khraiwesh *et al.* they described synthesis procedure of *N*,*N*-bis-(chloroacetyl)-derivative (**4l**) by refluxing their amine starting material, 2-amino-3-chloro-1,4-naphthoquinone (**4k**) in excess 2-chloroacetyl chloride at high temperatures (Figure 4.7 B).[159] Notably, this reaction was performed on an aryl amine derivative.

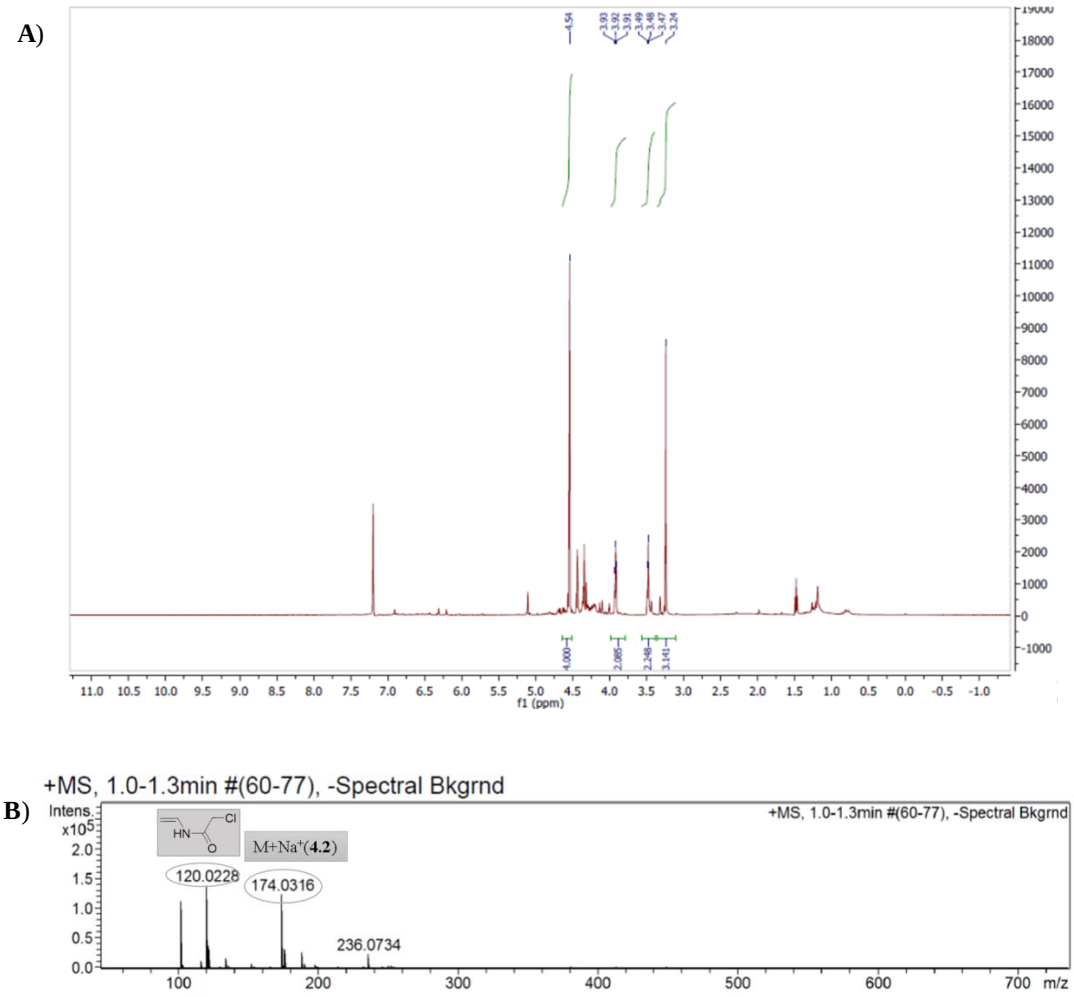

Figure 4.8. A) ^{1}H NMR spectrum of one of the unidentified separated product of 2-chloro-*N*-(2-methoxyethyl)acetamide (**4.2**) synthesis trail using TEA as a base. **B)** MS spectra of the reaction crude of the base- free trail showing the mass of the starting material (**4.3**) and a product of methoxy group elimination.

As it was not possible to prepare 2-chloro-*N*-(2-chloroacetyl)-N-(2-methoxyethyl)acetamide (**4.1**) linker, in part due to the presence of the methoxy group which was susceptible to both basic and acidic elimination. We decided to attempt synthesis of more stable aryl *N*,*N*-di-(chloroacetyl)amido derivative (**4.2**) based on the observation of Khraiwesh *et al.* As all these methods were attempted on aromatic amines (aniline derivatives), we moved towards synthesis of aniline bearing *N*,*N*-bis-(chloroacetyl) group as an alternative scaffold, which also imparts the advantage of possessing additional functionalisation sites for the subsequent development of bi-functional linkers.

4.3 2-chloro-*N*-(2-chloroacetyl)-*N*-phenylacetamide (4.2) as rebridging agent of reduced disulfide bonds

We next attempted to synthesise 2-chloro-N-(2-chloroacetyl)-*N*-phenylacetamide (**4.2**) as a more stable *N*,*N*-di-(chloroacetyl)-amido derivative.

Synthesis of 2-chloro-*N*-(2-chloroacetyl)-*N*-phenylacetamide (**4.2**) was attempted by refluxing 2-chloro-N-phenylacetamide (**4.5**) with 5 equivalents of 2-chloroacetyl chloride in dry toluene for 24 h according to the procedure described by Khraiwesh *et al.*[159] Following standard work-up, 2-chloro-*N*-(2-chloroacetyl)-*N*-phenylacetamide (**4.2**) was obtained in 50% yield as confirmed by NMR (^{1}H and ^{13}C) and MS.

In attempt to improve the yield, the reaction was repeated using higher equivalents of 2-chloroacetyl chloride and longer refluxing time (for 48 h), the yield of the reaction significantly increased (75%), indicating that 2-chloroacetyl chloride might be evaporating while refluxing in toluene (Figure 4.9).

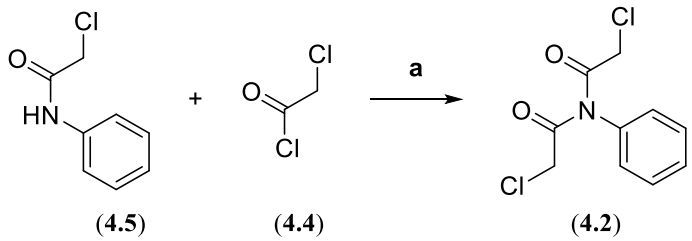

Figure 4.9. Chemical synthesis of 2-chloro-*N*-(2-chloroacetyl)-*N*-phenylacetamide (**4.2**). **a**) Dry toluene, 48 h and reflux.

Next, we aimed to evaluate the reactivity of the prepared **4.5** and **4.2** linkers, along with the commercially available linker towards strong nucleophiles, such as thiophenol.

4.3.1 Reactivity of 4.3, 4.4 and 4.7 linkers toward with thiophenol

Thiophenol (**4.6**) was chosen as a strong thiol-nucleophile to initially evaluate the reactivity with the previously prepared *N*,*N*-di(chloroacetyl)amino derivatives **4.2** and **4.5**.

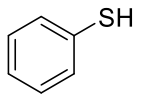

(**4.6**)

As such, thiophenol initially reacted with 2-chloro-*N*-phenylacetamide (**4.5**) to evaluate the tested condition. Thiophenol (6 equiv.) was added to a solution of 2-chloro-*N*-phenylacetamide (**4.5**) in a mixture of MeCN (1 mL) and Tris.HCl buffer (100 mM, pH 7.5, 1 mL). The reaction was evaluated by MS after 6 h, and the product of alkylation **4.7** was confirmed by HRMS (*m/z* 266.0583 ($M+Na^+$)).

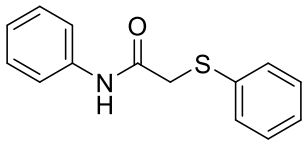

(**4.7**)

Satisfied that the product of thiophenol and chloro-acetamide reaction can be confirmed under the evaluated conditions [MeCN and Tris.HCl buffer pH 7.5 (1:1)], thiophenol was then reacted with 2-chloro-*N*-(2-chloroacetyl)-*N*-phenylacetamide (**4.2**). The reaction was monitored by HRMS and the product of alkylation **4.8** was confirmed by HRMS (*m/z* 416.0708 ($M+Na^+$)).

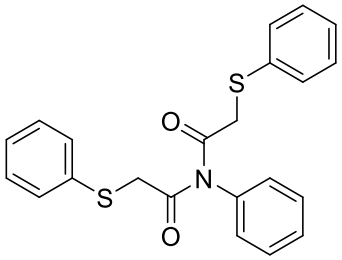

(**4.8**)

Lastly, the commercially available 2-chloro-*N*-(2-chloroacetyl)-*N*-(3,4,5-trimethoxyphenyl)acetamide (**4.9**) was also reacted with thiophenol under the described conditions (Figure 4.10). The product **4.10** was confirmed by HRMS (*m/z* 506.1078 ($M+Na^+$)).

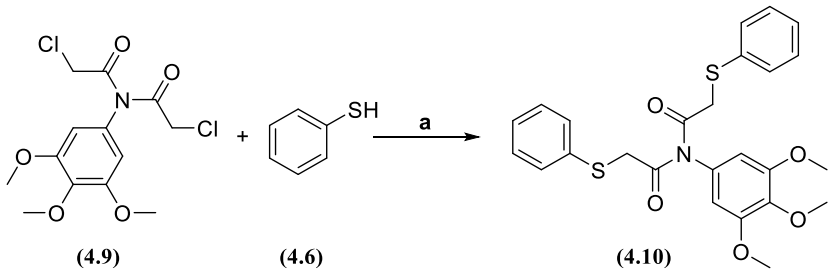

Figure 4.10. Chemical reaction of 2-chloro-*N*-(2-chloroacetyl)-*N*-(3,4,5-trimethoxyphenyl)acetamide (**4.9**) with thiophenol (**4.6**). **a**) Mixture of MeCN (1 mL) and Tris.HCl buffer (100 mM, pH 7.5, 1 mL) at room temperature 6 h.

With this initial reactivity test, we concluded that *N*,*N*-di(chloroacetyl)amino derivatives are reactive towards thiolate group of the strong nucleophile thiophenol, thus we sought to evaluate the stability and glutathione reactivity of these *N*,*N*-di(chloroacetyl)amino derivatives in the following Sections.

4.3.2 Stability of *N*,*N*-di(chloroacetyl)amido derivatives and their reactivity with glutathione

As mentioned previously, one advantage of employing aromatic amines (aniline derivatives) is that they possess additional functionalisation sites to attain bi-functional linkers. Thus, we sought also to synthesise another *N*,*N*-bis-(chloroacetyl)-amido derivative possessing an ester functionality in order to evaluate the impact of the presence of this functionality on the stability and reactivity of this class of compounds toward thiol nucleophiles. Carrying out these experiments by using functionalised *N*,*N*-bis-(chloroacetyl)-amido derivatives would enable us to gather more practical results towards the applicability of these linkers in rebridging of reduced disulfide bonds of mAbs.

As such, ethyl 4-(2-chloro-*N*-(2-chloroacetyl)acetamido)benzoate (**4.11**) was synthesized following similar method to the previously mentioned method to attain **4.2** linker. Ethyl 4-(2-chloro-*N*-(2-chloroacetyl)acetamido)benzoate (**4.11**) was obtained in good yield (76%).

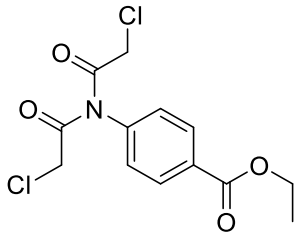

(**4.11**)

Having successfully synthesised **4.11**, we next sought to evaluate its usefulness as a rebridging agent by evaluating its stability and reactivity towards thiol nucleophiles. Ester functionalised derivative, ethyl 4-(2-chloro-*N*-(2-chloroacetyl)acetamido)benzoate (**4.11**) was deemed as a better linker to be further evaluated as rebridging agents. Particularly, because of the presence of ester group, which could give preliminary indications regarding the development of bi-functional rebridging agents.

As protein labelling conjugation reactions are carried out under aqueous conditions, it was important to evaluate the aqueous stability of these linkers. As shown earlier in Chapter 3, sulfonate-bearing α-amide groups (**3.9** and **3.10**) exhibited high aqueous stability, thus we postulated that α-halo-acetamide derivatives are stable under the typical conjugation conditions.

Before evaluating the aqueous stability of ethyl 4-(2-chloro-*N*-(2-chloroacetyl)acetamido)benzoate (**4.11**), the aqueous stability of α-haloacetamide derivatives **4.12** was initially evaluated, as we considered starting with the simple structure of ethyl 4-(2-chloroacetamido)benzoate (**4.12**) would enable us to assign the required peaks needed to be followed in order to attain the hydrolysis rates of **4.11**.

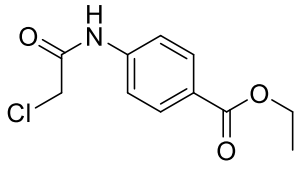

(**4.12**)

The stability of ethyl 4-(2-chloroacetamido)benzoate **4.12** was studied by ^{1}H NMR (solvent suppression experiment at 4.7 ppm). Compound **4.12** (1 mg/mL) was held in phosphate buffer (100 mM, pH 7.5) containing 10% DMF-d_7. ^{1}H-NMR spectra were

acquired at time 0, 24, 48 and 96 h. The stability of ethyl 4-(2-chloroacetamido)benzoate (**4.12**) was assessed by following the change in the integration of α-methylene protons at δ 4.38 ppm. The high aqueous stability of **4.12** over 4 days was confirmed as no change in the integration of α-methylene protons could be observed along with no clear hydrolysis peak being observed (Figure 4.11).

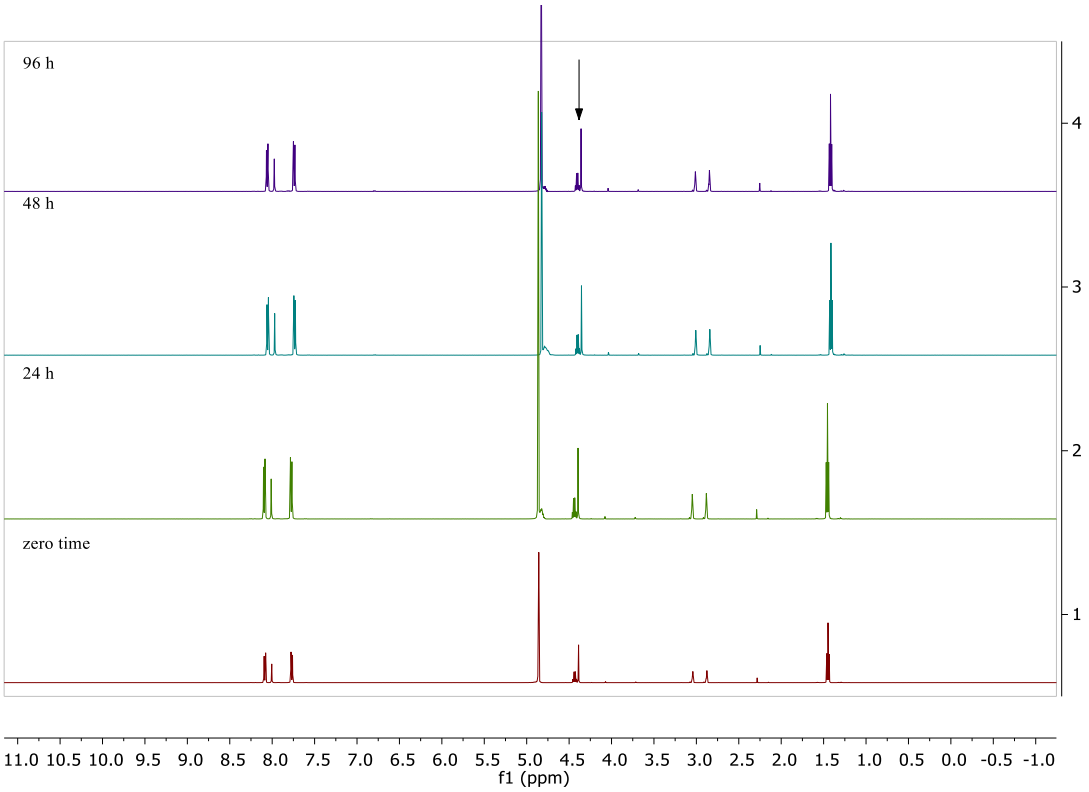

Figure 4.11. Stability of ethyl 4-(2-chloroacetamido)benzoate (**4.12**) linker in aqueous buffer. ^{1}H NMR spectra of ethyl 4-(2-chloroacetamido)benzoate **4.12** (1.00 mg/ml, 4.15 mM) in phosphate buffer (100 mM, pH 7.5) over 4 days. Arrow indicates the signals of α-methylene protons that were followed at δ 4.38 ppm (ClC$\underline{H_2}$CONH) over 4 days.

Then, the stability of Ethyl 4-(2-chloro-*N*-(2-chloroacetyl)acetamido)benzoate (**4.11**) under similar aqueous conditions was evaluated. Ethyl 4-(2-chloro-*N*-(2-chloroacetyl)acetamido)benzoate **4.11** (1 mg/mL) was dissolved in phosphate buffer (100 mM, pH 7.5) containing 30% DMF-d_7 and held at room temperature overnight.

The hydrolysis of one acetamide arm of ethyl 4-(2-chloro-N-(2-chloroacetyl)acetamido)benzoate (**4.11**) to afford ethyl 4-(2-chloroacetamido)benzoate

(**4.12**) was confirmed by both ^{1}H NMR and MS, which indicated that **4.11** is not stable in aqueous buffer (Figure 4.11).

A)

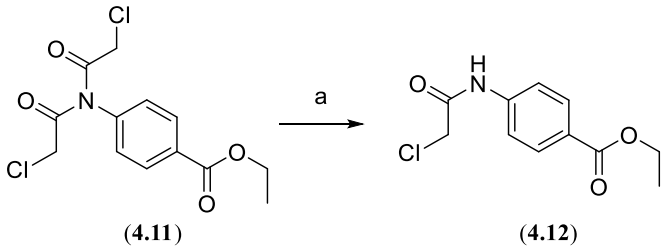

(**4.11**) (**4.12**)

B)

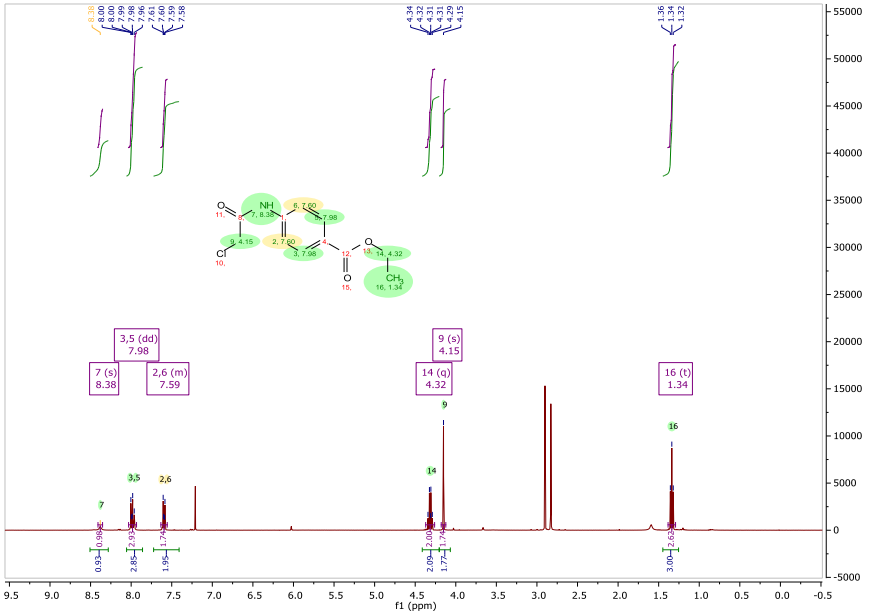

C)

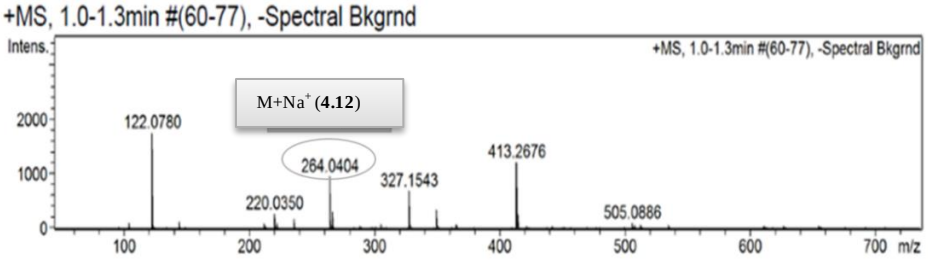

Figure 4.12. A) Hydrolysis of ethyl 4-(2-chloro-*N*-(2-chloroacetyl)acetamido)benzoate (**4.11**) in aqueous buffer. (a) Tris.HCl buffer (100 mM, pH 7.5, 30 % DMF) at room temperature overnight. **B)** ^{1}H NMR spectrum of ethyl 4-(2-chloro-*N*-(2-chloroacetyl)acetamido)benzoate (**4.11**) held in aqueous buffer overnight showing only spectrum of ethyl 4-(2-chloroacetamido)benzoate (**4.12**) with its assigned peaks. **C)** MS spectra of Ethyl 4-(2-chloro-*N*-(2-chloroacetyl)acetamido)benzoate (**4.11**) held in aqueous buffer overnight showing only *m/z* 264 of ethyl 4-(2-chloroacetamido)benzoate (**4.12**).

The poor stability of *N*,*N*-di(chloroacetyl)amido derivatives under aqueous conditions has been observed previously where imide derivatives displayed slow hydrolysis rates below pH 7 and faster rates at pH above 7.[161] Donskikh *et al.* studied the hydrolysis of *N*-(o-carboxyphenyl)-phthalimide over a range of pHs to attain *N*-phthalanthranilic acid. They proposed the mechanism of hydrolysis starting by rate limiting step of attacking of hydroxyl ion towards the carbon atom of the carbonyl group. In addition, they confirm the high stability of the obtained *N*-phthalanthranilic acid as it required high temperature and alkaline conditions to be completely hydrolysed (Figure 4.13).[161]

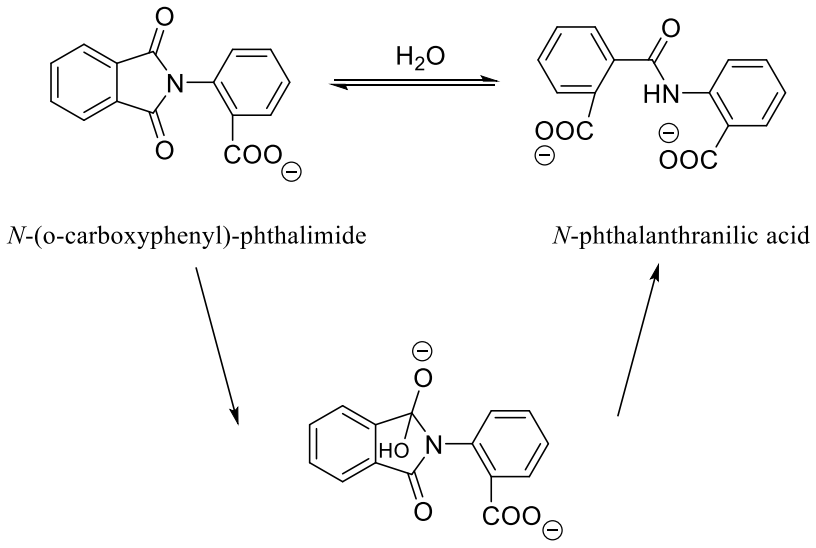

Figure 4.13. The mechanism of alkaline hydrolysis of *N*-(o-carboxyphenyl)-phthalimide.[161]

Given the poor hydrolytic stability of ethyl 4-(2-chloro-*N*-(2-chloroacetyl)acetamido)benzoate (**4.11**), we tend to evaluate if the rate of hydrolysis of the imide derivative **4.11** is faster than the rate of reactivity with thiolates and whether *N*,*N*-di(chloroacetyl)amino derivatives are still possible rebridging candidates. Thus, ethyl 4-(2-chloro-*N*-(2-chloroacetyl)acetamido)benzoate (**4.11**) was reacted with reduced glutathione.

Ethyl 4-(2-chloro-*N*-(2-chloroacetyl)acetamido)benzoate (**4.11**) was dissolved in THF and added gradually to glutathione aqueous solution. The reaction was held overnight at room temperature. Acetamide-glutathione adducts were purified using C-18 column. Only mono glutathione-adduct (hydrolysis of the second chloroacetamide arm) was the

obtained product (**4.13**). We proposed that the rate of thiol alkylation (k_2) is faster than the rate of hydrolysis (k_1). However, we were not able to identify the order of these reactions. Moreover, the final separated product **4.13** could be possibly formed as a result of the hydrolysis of the **4.14** conjugate (Figure 4.14).

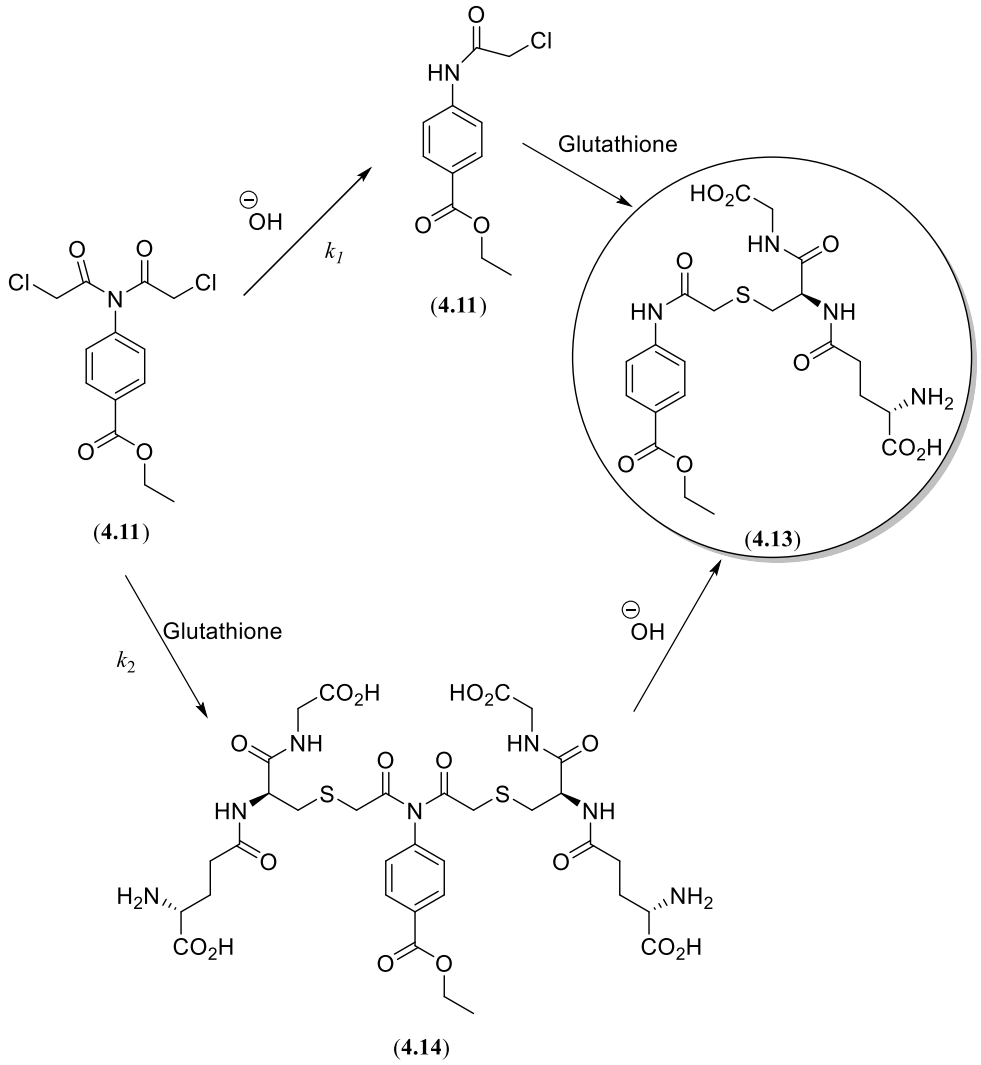

Figure 4.14. The proposed mechanisms of hydrolysis of compound **4.11** in the presence of glutathione under aqueous conditions to afford the mono-glutathione conjugate **4.13**.

Given the instability of ethyl 4-(2-chloro-*N*-(2-chloroacetyl)acetamido)benzoate (**4.11**) and possibly its alkylated products in aqueous buffer, it was concluded that these reagents cannot be employed in rebridging reactions of reduced disulfide bonds.

4.4 Aryl bis-haloacetamide derivatives as rebridging linkers

As it is not possible to utilise *N*,*N*-di-(chloroacetyl)-amido derivatives as disulfide rebridging agents, and considering the observed aqueous stability of the α-haloacetamide derivative **4.12,** we next sought to investigate aryl bis-haloacetamides as an alternative scaffold for rebridging of the reduced inter-chain disulfide bonds of mAbs.

α-Haloacetamide derivatives have previously been reported as DNA-cross-linkers. Tabone *et al.* have evaluated oligodeoxynucleotides-bearing an α-haloacetamide as DNA-cross-linkers. Various factors addressing the extent of DNA cross-linked by the haloacetamide-bearing oligodeoxynucleotides have been addressed, including the reactivity of the halogen. They found that the best cross-linking yields were associated with α-bromoacetamide derivatives.[162] Later, a series of bis-bromoacetyldiamines were evaluated as electrophiles, which cross-link DNA complementary strands *via* alkylation of deoxyguanosine bases (Figure 4.15). Of these electrophiles, the *N*,*N*'-bis-bromoacetyl-1,2-diaminebenzene (**4.29**) displayed higher yields of cross-linking of complementary DNA strands, the proposed mechanism of cross-linking oligodeoxynucleotides strands using *N*,*N*'-bis-bromoacetyl-1,2-diaminebenzene (**4.29**) is shown in Figure 4.15.[163]

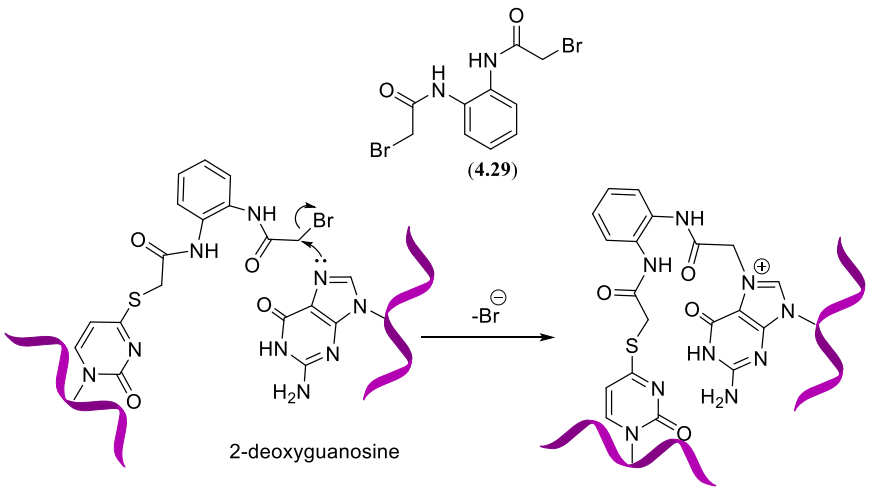

Figure 4.15. The mechanism of cross-linking reaction between complementary oligodeoxynucleotides strands using *N*,*N*'-bis-bromoacetyl-1,2-diaminebenzene (**4.29**), which was selective for the complementary N7 of 2-deoxyguanosine.

Herein, we sought to evaluate aryl bis-haloacetamide derivatives as disulfide bond rebridging linkers that may operate according to the method shown in Figure 4.16.

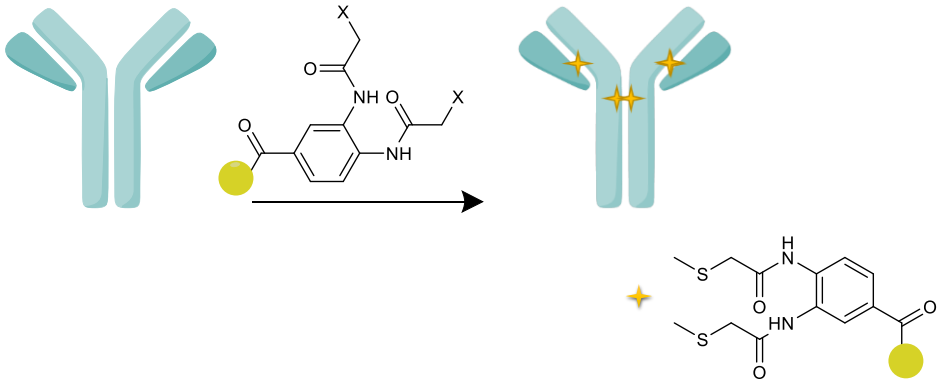

Figure 4.16. Our proposed approach of rebridging of reduced inter-chain disulfide bonds of mAb using bis-haloacetamide linkers.

4.4.1 Synthesis of the aryl bis-haloacetamide derivatives 4.15 and 4.16

Bis-haloacetamide derivatives **4.15** and **4.16** were synthesised by N-acetylation of the corresponding di-amines using 2-chloroacetyl chloride at room temperature for 2 h to give the products **4.15** and **4.16** in yields of 89% and 79%, respectively.

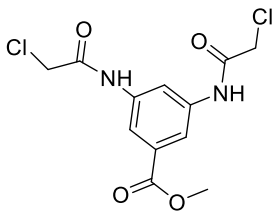

4.15

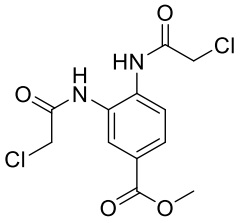

4.16

4.4.2 The aqueous stability of bis-haloacetamide

With both bis-haloacetamide derivatives **4.15** and **4.16** in hand, it was necessary to evaluate their stability under the typical conjugation conditions (aqueous buffer) and in the presence of reducing agents (such as TCEP). As shown previously, stability of ethyl 4-(2-chloroacetamido)benzoate **(4.12)** in aqueous buffer was studied using ^{1}H NMR over 4 days and found to be stable (Figure 4.11).

Following the ^{1}H NMR solvent suppression method used for compound **4.12**, the aqueous stability of both methyl 3,5-bis(2-chloroacetamido)benzoate (**4.15**) and methyl 3,4-bis(2-chloroacetamido)benzoate (**4.16**) aqueous stability was appraised in phosphate buffer (100 mM, pH 7.5) containing 30% DMF-d_7. The stability of **4.15** and **4.16** were assessed by following the change in integrals of α-methylene protons at δ 4.43 ppm (2 x ClC<u>H₂</u>CONH) (Figure 4.17 A and B).

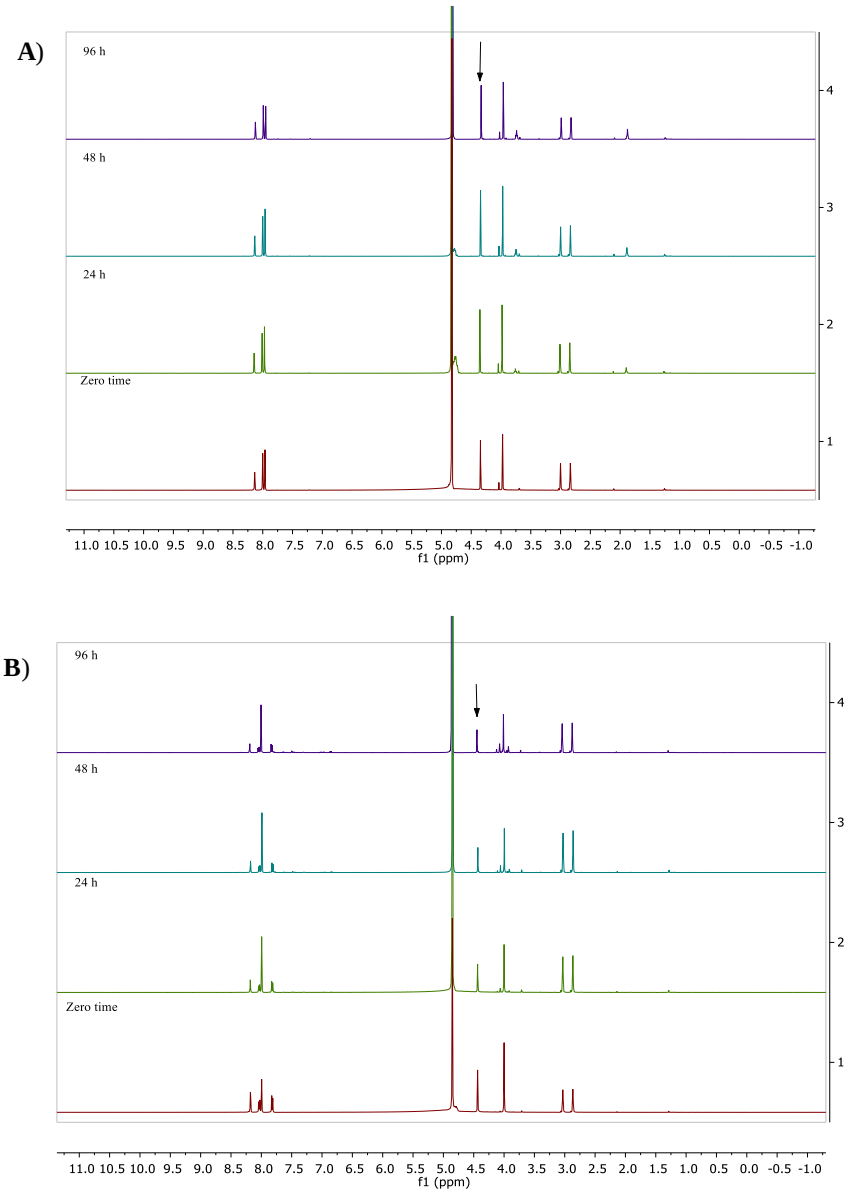

Figure 4.17. Stability of bis-chloroacetamide linkers in aqueous buffer. **A**) ^{1}H NMR spectrum of methyl 3,5-bis(2-chloroacetamido)benzoate **4.15** (1.00 mg/ml, 3.14 mM) and **B**) methyl 3,4-bis(2-chloroacetamido)benzoate **4.16** (1.00 mg/ml, 3.14 mM) in aqueous phosphate buffer over 4 days. Arrows indicate the followed peaks at at δ 4.43 ppm for α-methylene protons (2 x ClC<u>H₂</u>CONH).

Both methyl 3,5-bis(2-chloroacetamido)benzoate (**4.15**) and methyl 3,4-bis(2-chloroacetamido)benzoate (**4.16**) were found to be relatively stable in aqueous buffer, with less than 20% hydrolysis observed within 24 h. Methyl 3,5-bis(2-chloroacetamido)benzoate (**4.15**) showed superior aqueous stability over methyl 3,4 -bis(2-chloroacetamido)benzoate (**4.16**) with the results plotted in (Figure 4.18).

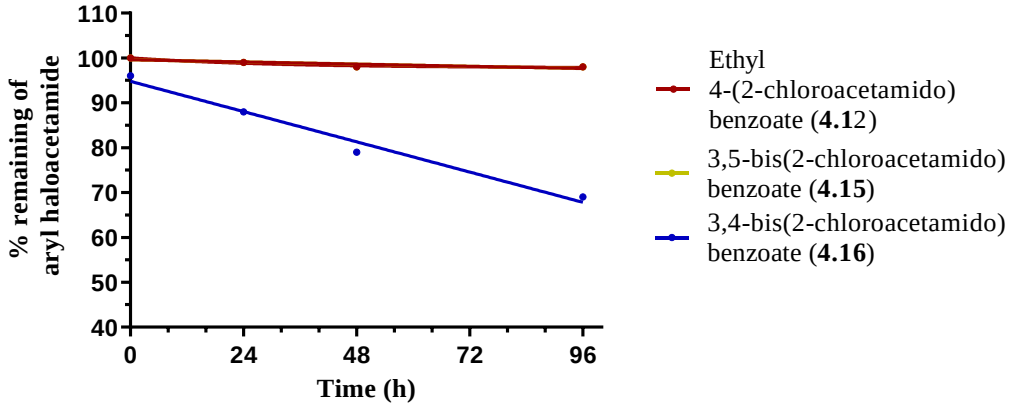

Figure 4.18. Percentage remaining of haloacetamide **4.12** (1.00 mg/ml, 4.15 mM), **4.15** (1.00 mg/ml, 3.14 mM) and **4.16** (1 mg/ml, 3.14 mM) over 4 days. Stability was determined in phosphate buffer (100 mM, pH 7.5) containing 10-30% DMF-d_7. % of remaining was calculated by measuring the change in the integration of α-methylene using ^{1}H NMR solvent suppression method.

4.4.3 The aqueous stability of aryl bis-haloacetamides in the presence of TCEP

As the primary sought-after use of these bis-haloacetamide linkers is the rebridging of reduced cysteine residues that were paired up in disulfide bonds and as phosphines reductants, such as the water soluble TCEP (**2.2**) are broadly used as reductants in protein conjugation, we set out to evaluate the stability of Methyl 3,5-bis(2-chloroacetamido)benzoate (**4.15**) in presence of TCEP (**2.2**).

As such, methyl 3,5-bis(2-chloroacetamido)benzoate (**4.15**) was incubated with 3 equiv. of TCEP in Tris.HCl buffer and held at room temperature. ^{1}H-NMR spectra were acquired after 12 and 24 h and it was observed that methyl 3,5-bis(2-chloroacetamido)benzoate (**4.15**) reacted with TCEP (**2.2**), as the signal at δ 4.21 ppm corresponding to α-methylene protons (2 x ClC$\underline{H_2}$CONH) had disappeared over time.

In order to follow the rate of the reaction, next both TCEP (**2.2**) and Methyl 3,5-bis(2-chloroacetamido)benzoate (**4.15**) were held together and in phosphate buffer (pH 7.5). ^{1}H-NMR spectra were acquired every 30 minutes (Figure 4.19 A). The half-life of 3,5-bis(2-chloroacetamido)benzoate (**4.15**) in presence of TCEP (**2.2**) was found to be 108.3 minutes (Figure 4.19 B).

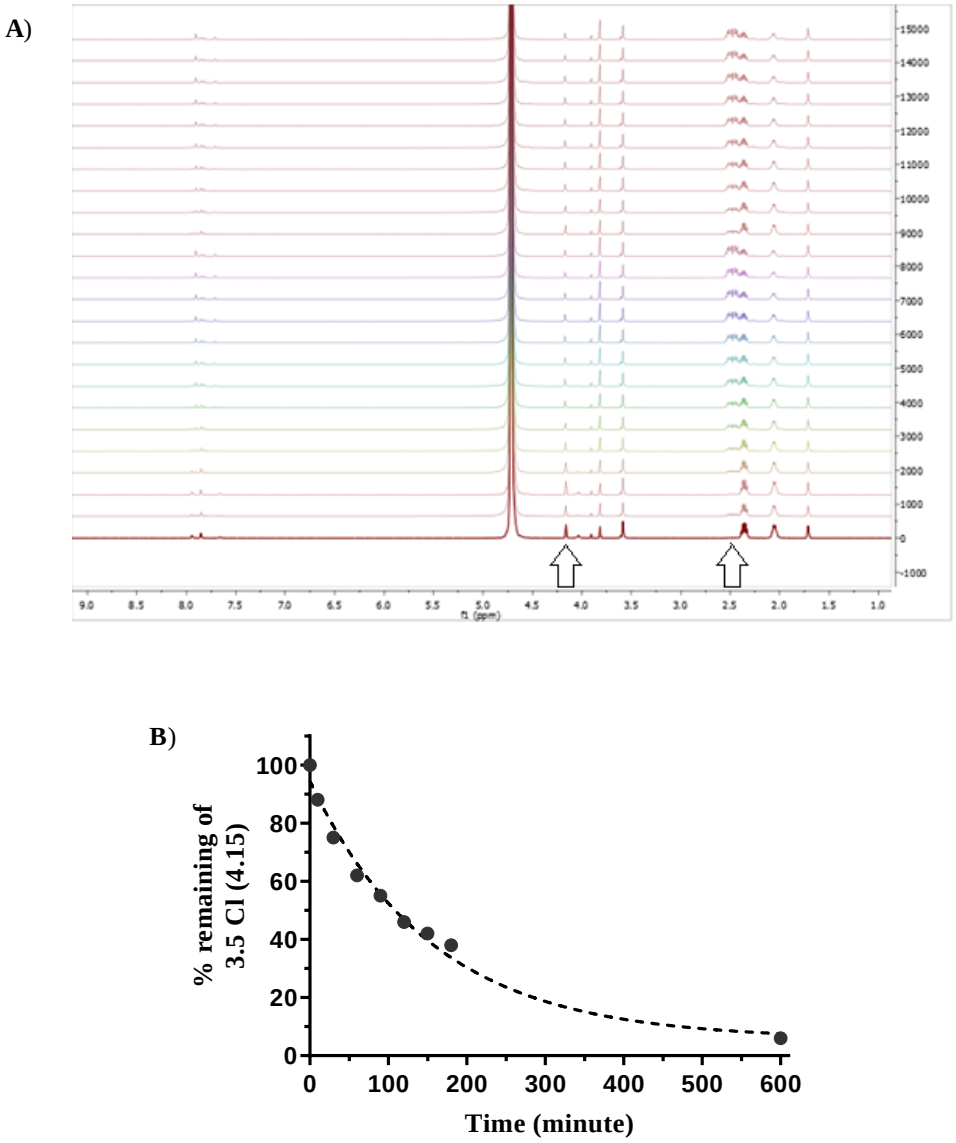

Figure 4.19. Stability of methyl 3,5-bis(2-chloroacetamido)benzoate (**4.15**) in presence of TCEP (**2.2**). **A**) ^{1}H NMR spectrum of methyl 3,5-bis(2-chloroacetamido)benzoate (**4.15**) in presence of TC2P (**2.2**, 3 equiv.) in aqueous phosphate buffer, arrows indicate the followed disappearance of signal peak at δ 4.21 ppm of α-methylene protons and appearance of signal peaks at δ 2.5 ppm to obtain the reactivity rate. **B**) Percentage remaining of methyl 3,5-bis(2-chloroacetamido)benzoate (**4.15**) (1.00 mg/ml, 3.14 mM) in TEA the presence of TCEP (2.36 mg/ml, 9.42 mM, 3 equiv.) in phosphate buffer (100 mM, pH 7.5).

A preparative scale reaction was then performed to characterise the product of the reaction between TCEP (**2.2**) and methyl 3,5-bis(2-chloroacetamido)benzoate (**4.15**). Methyl 3,5-bis(2-chloroacetamido)benzoate in THF was added gradually to a solution of TCEP in phosphate buffer (pH 7.5) and held overnight (room temperature). The reaction was purified using a C-18 reverse column to give the TCEP adduct (Figure 4.20 A), which was characterised using NMR (^{1}H, ^{13}C, MS and IR (absence of distinctive peak of C=P, usual range of 1180−1230 cm^{-1}) (Figure 4.20 B).

A)

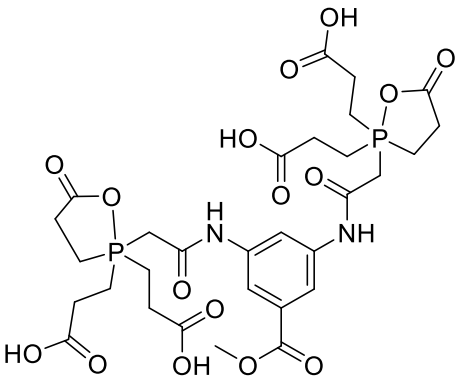

B)

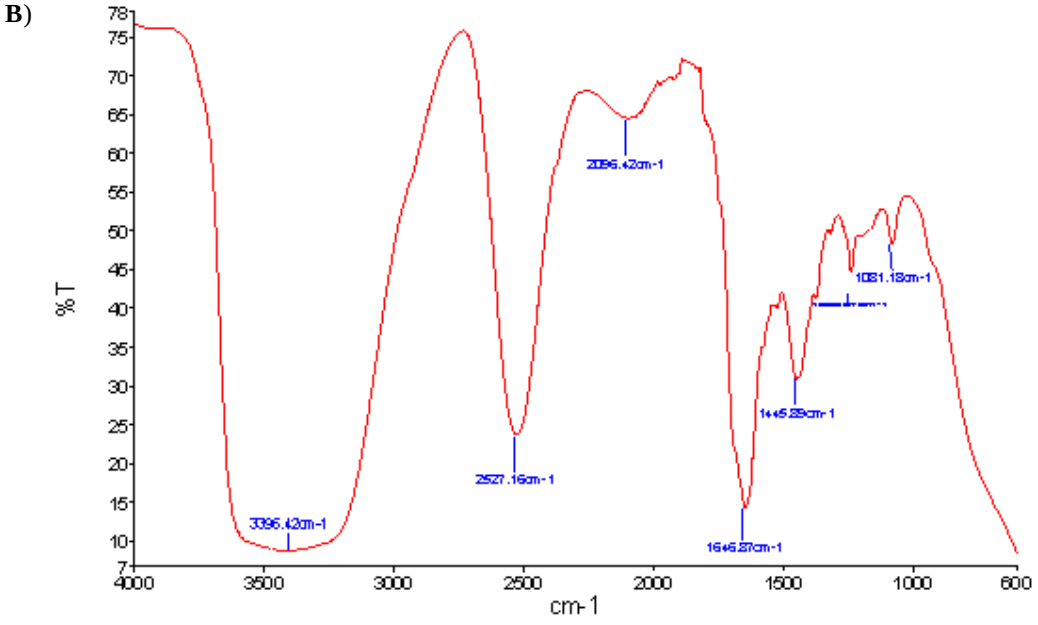

Figure 4.20. A) acetamide-TCEP adduct. **B**) IR spectrum of acetamide-TCEP adduct confirming the absence of distinctive peak of C=P (usual range of 1180−1230 cm^{-1}).

The confirmed instability of the bis-chloroaceatmide **4.15** in the presence of TCEP demonstrates the necessity of employing our azide quenching method developed in Chapter 2.

4.4.4 Investigation of the reactivity of methyl 3,5-bis(2-chloroacetamido)benzoate (4.15) and methyl 3,4-bis(2-chloroacetamido)benzoate (4.16) towards reduced glutathione

Having determined previously that the bis-chloroaceatmides **4.15** and **4.16** were both relatively stable under aqueous conditions, we next sought to determine their reactivity towards glutathione.

As such, methyl 3,5-bis(2-chloroacetamido) benzoate (**4.15**) and methyl 3,4-bis(2-chloroacetamido) benzoate (**4.16**) were treated with GSH (6 equiv.) in phosphate buffer at pH 7.5 containing 10% DMF-d_7 and the rates of reaction were calculated using ^{1}H NMR spectroscopy (solvent suppression method) based on the disappearance from the signal of acetamide protons (2 x ClC$\underline{H_2}$CONH) at δ 4.3 ppm and the appearance of a signal at δ 3.46 ppm which corresponds to the acetamide-glutathione product. The percentage remaining of each linker was determined using ratio of integration of the peak at δ 4.3 ppm to the sum of integration of the peaks at δ 4.3 and 3.46 ppm. Reaction rates of acetamide linkers with GSH were calculated by fitting to a first-order kinetic equation to natural log transformed percent remaining data (Equation 4.1). The half-life of the bis-acetamide linkers in the presence of glutathione was calculated using Equation 4.2.[140]

$$\boldsymbol{ln}([\boldsymbol{acetamide}]) = -\boldsymbol{Kt} + \boldsymbol{ln}([\boldsymbol{acetamide_0}]) \qquad \textbf{(Equation 4.1)}$$

$$\boldsymbol{t_{1/2}} = \boldsymbol{0.693/K} \qquad \textbf{(Equation 4.2)}$$

The rates of reaction of methyl 3,5-bis(2-chloroacetamido)benzoate (**4.15**) and methyl 3,4-bis(2-chloroacetamido)benzoate (**4.16**) with GSH were calculated to be 0.009 and 0.04 min^{-1}, respectively (Figure 4.21). The calculated half-lives of reaction of methyl

3,5-bis(2-chloroacetamido)benzoate (**4.15**) and methyl 3,4-bis(2- chloroacetamido) benzoate (**4.16**) were 50 and 23 minutes, respectively.

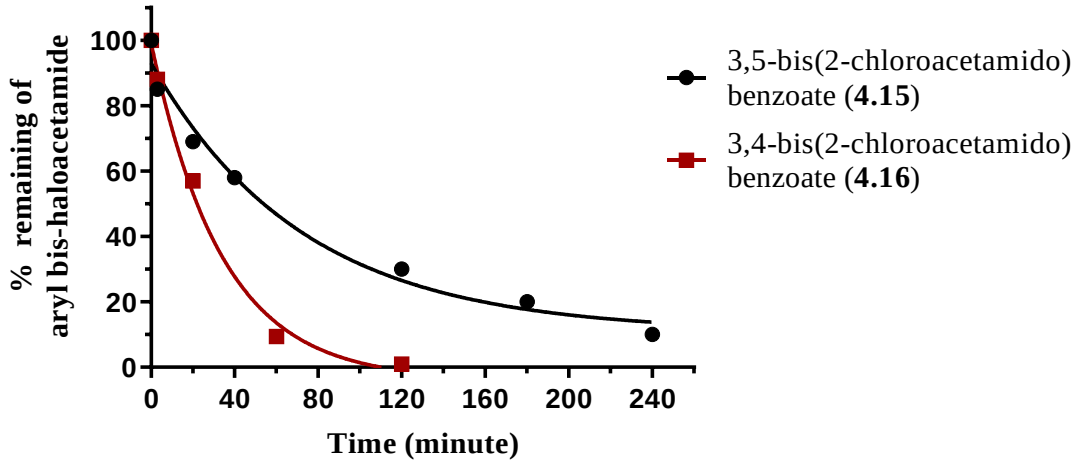

Figure 4.21. Percentage remaining of methyl 3,5-bis(2-chloroacetamido)benzoate **4.15** (1.00 mg/ml, 3.14 mM) and methyl 3,4-bis(2- chloroacetamido) benzoate **4.16** (1.00 mg/ml, 3.14 mM) in presence of GSH (5.79, 18.8 mM, 6 equiv.) in phosphate buffer (100 mM, pH 7.5).

Interestingly, the differences in regiochemistry of the acetamide groups relative to each other on the benzene ring (ortho- and meta-positions) showed a significant difference in both aqueous stability and reaction rates with glutathione. One possible explanation for such differences is the 3D structures of each compound. Methyl 3,5-bis(2-chloroacetamido)benzoate (**4.15**) is predicted to have a planar conformation (Figure 4.22 A). Thus, steric hindrance could slow the backside attack of thiolate at the carbon attached to halogen (through an SN2 mechanism) mainly in methyl 3,5-bis(2-chloroacetamido)benzoate (**4.15**) compound. This might explain the greater reactivity of methyl 3,4-bis(2-chloroacetamido)benzoate (**4.16**) which is not planar and might afford a more accessible carbon for backside attack (Figure 4.22 B).

A)

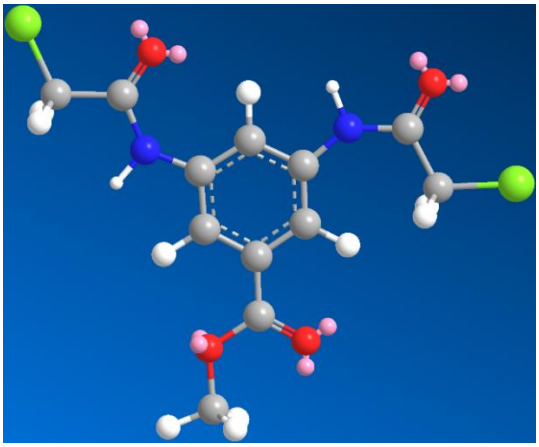

B)

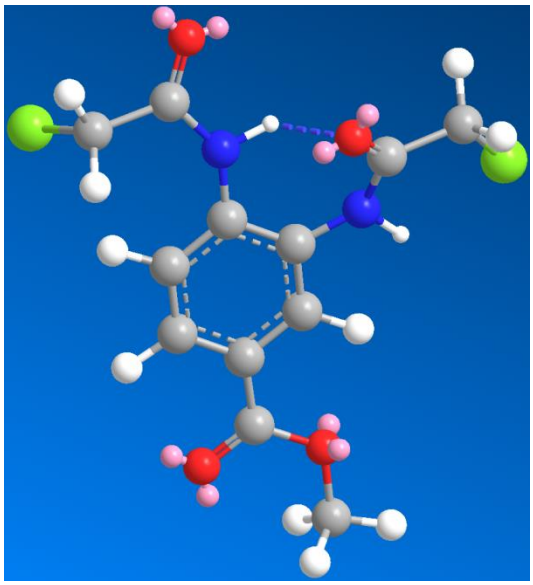

Figure 4.22. A) 3D structure of methyl 3,5-bis(2-chloroacetamido)benzoate (**4.15**) showing its planner conformation. **B**) 3D structure of methyl 3,4-bis(2-chloroacetamido)benzoate (**4.16**) showing its non-planner conformation allowing better backside attack of thiolate anion at the α-methylene carbon (2 x $ClCH_2CONH$) attached to halogen (green).

4.4.5 Aqueous stability of the glutathione conjugates (4.17-4.19) in buffer

As a major drawback of the well-known maleimide-based conjugation approach is the susceptibility of the reaction products to retro-Michael reactions and their associated poor plasma stability, we sought to determine the aqueous stability of our glutathione-acetamide conjugates. To this end, both bis-glutathione conjugates **4.17** and **4.18** were prepared on a larger scale, purified using a C-18 reverse column and fully characterised using NMR and MS.

The stability of these glutathione-conjugates was then evaluated in 100 mM phosphate buffer at pH 7.4 using HPLC-UV over 4 weeks and compared against the glutathione-Mal conjugate **4.19**. Both of the conjugates were found to be more stable at room temperature over 4 weeks compared to glutathione-Mal conjugate (77% remain after 4 weeks).

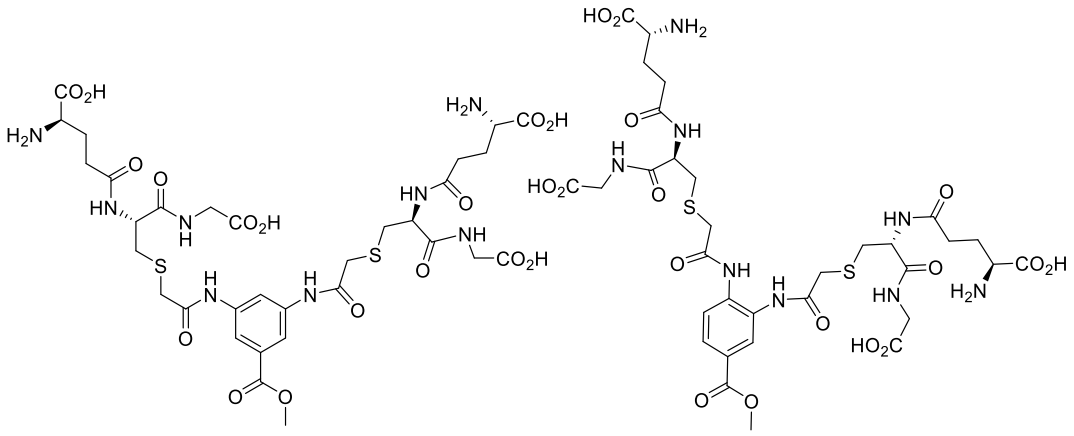

(**4.17**)
3,5-bis-glutathione conjugate

(**4.18**)
3,4-bis-glutathione conjugate

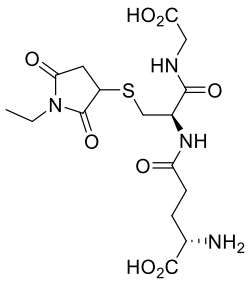

(**4.19**)
glutathione-Mal conjugate

A further stability test was then carried out under similar conditions (pH 7, 4 weeks) in the presence of DTT (50 mM) to imitate nucleophiles found under plasma conditions. The overall stability of glutathione-conjugates were slightly reduced in the presence of DTT. Furthermore, Mal-glutathione was found to be the least stable conjugate (Figure 4.21 A). Unfortunately, a direct comparison of Mal-glutathione with the bis-acetamide-glutathione conjugates was not possible due to the presumed formation of a DTT-maliemide adduct interfering with HPLC analysis. Therefore, the stability of Mal-glutathione in the presence of DTT was further analysed using ^{1}H NMR which showed approximately more than 50 % loss over the four weeks (Figure 4.23 B).

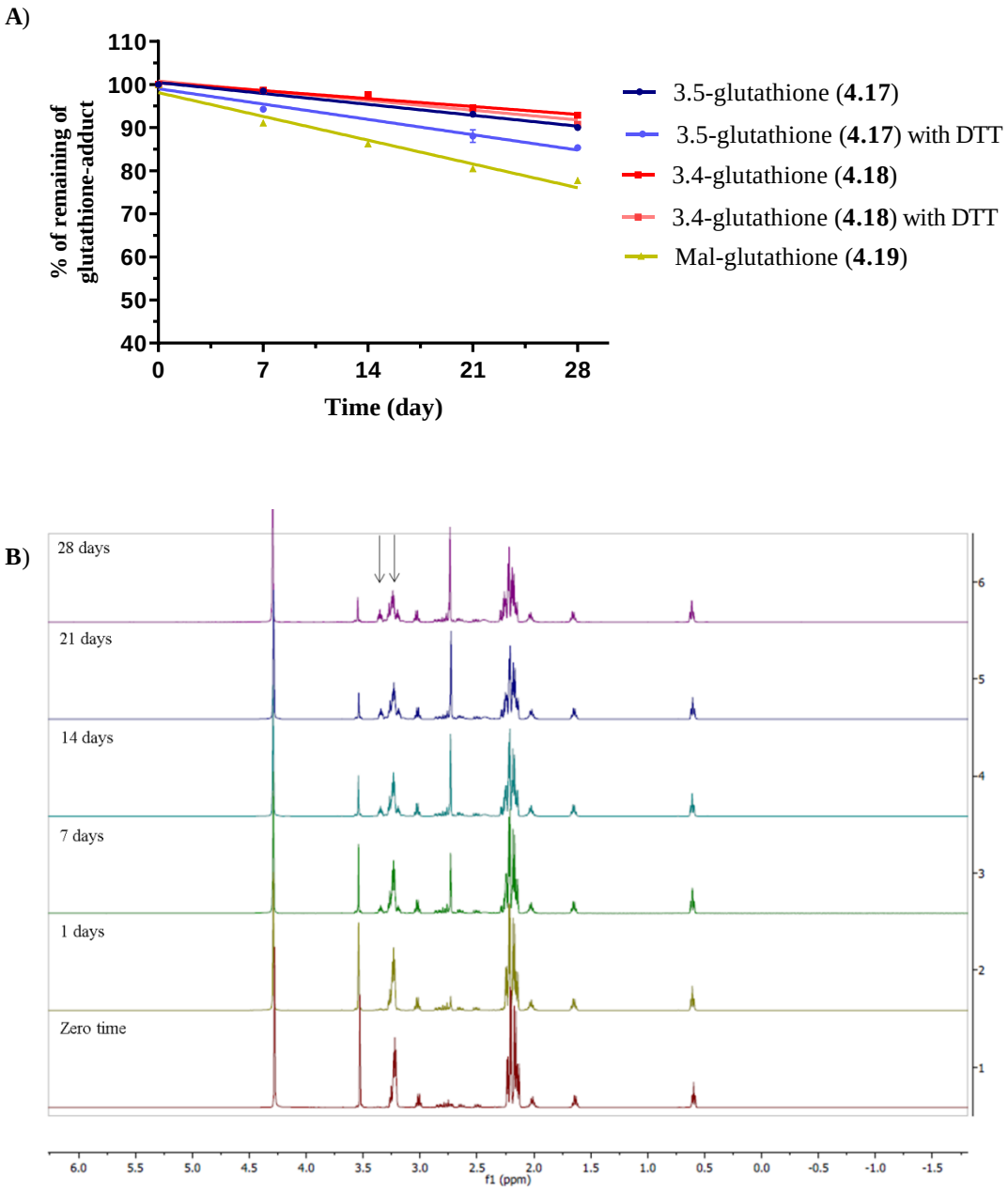

Figure 4.23. A) Percent remaining of glutathione-conjugates (1.0 mg/ml, 1.2 mM) in the presence and absence of DTT (50 mM) over 4 weeks in aqueous phosphate buffer (100 mM, pH 7). Data presented as mean± SD of three independent samples. **B)** ^{1}H NMR spectrum analysing the stability of Mal-glutathione (1.0 mg/ml, 2.3 mM) in the presence of DTT over the four weeks (28 days). Arrows indicated the followed signals to calculate the percentage of remaining of Mal-glutathione **4.19.**

4.5 The synthesis and evaluation of bis-bromo- and bis-iodo-acetamide derivatives

Bromides and iodides are known to be better leaving groups than chlorides, therefore, bromo- and iodo-acetamide derivatives undergo faster substitution reactions. As such, we next set out to synthesise bromo- and iodo-acetamide derivatives and to evaluate their aqueous stability and reactivity with reduced glutathione and compare these compounds to the corresponding chloride derivatives.

Ethyl 4-(2-bromoacetamido)benzoate (**4.20**) was synthesised by N-acetylation of benzocaine with 2-bromoacetyl bromide (2.2 equiv.) at room temperature for 2 h (69% yield). Ethyl 4-(2-iodoacetamido)benzoate (**4.21**) was synthesised by refluxing Ethyl 4-(2-chloroacetamido)benzoate (**4.12**) with KI in dry acetone for 3 h (90% yield) (Figure 4.24).

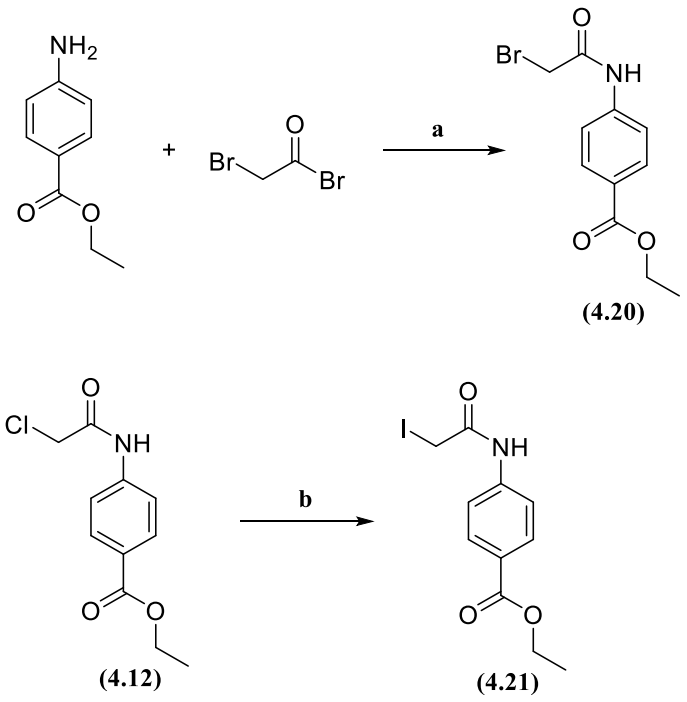

Figure 4.24. Chemical synthesis of ethyl 4-(2-bromoacetamido)benzoate (**4.20**) and ethyl 4-(2-iodoacetamido)benzoate (**4.21**). **a**) TEA, DCM, 2 h. **b**) KI, dry acetone, reflux, 3h.

The aqueous stability of ethyl 4-(2-bromoacetamido)benzoate (**4.20**) and ethyl 4-(2-iodoacetamido)benzoate (**4.21**) were then determined in phosphate buffer (pH 7.5)

containing 30% DMF-d_7 using a similar ^{1}H-NMR solvent suppression method as described earlier.

The stability of 4-(2-bromoacetamido)benzoate (**4.20**) and ethyl 4-(2-iodoacetamido)benzoate (**4.21**) were assessed by following the change in integration of α-methylene protons at δ 4.10 ppm (BrC$\underline{H_2}$CONH) and at δ 3.99 ppm (IC$\underline{H_2}$CONH), respectively. Both ethyl 4-(2-bromoacetamido)benzoate (**4.20**) and ethyl 4-(2-iodoacetamido)benzoate (**4.21**) found to be stable as no change in the integration of α-methylene protons was displayed after 4 days, along with no clear hydrolysis peak being observed (Figure 4.25 A and B). The observed aqueous stability results are comparable to the earlier observed aqueous stability of ethyl 4-(2-chloroacetamido)benzoate **(4.12**) (Figure 4.11).

To investigate the impact of regiochemistry, methyl 3,5-bis(2-haloacetamido)benzoate and methyl 3,4-bis(2-haloacetamido)benzoate derivatives **4.22-4.25** were synthesised using similar methods to those described earlier for the synthesis of the mono-haloacetamide derivatives **4.20** and **4.21**. The aqueous stability of compounds **4.22-4.25** were then determined using a similar ^{1}H NMR method used for the mono-haloacetamide derivatives **4.20-4.21** under the same conditions (4 days, room temperature, pH 7.5).

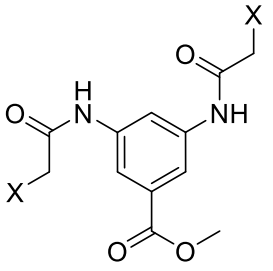

X= Br (4.22)
X= I (4.24)

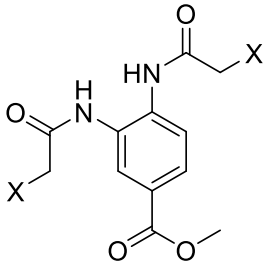

X= Br (4.23)
X= I (4.25)

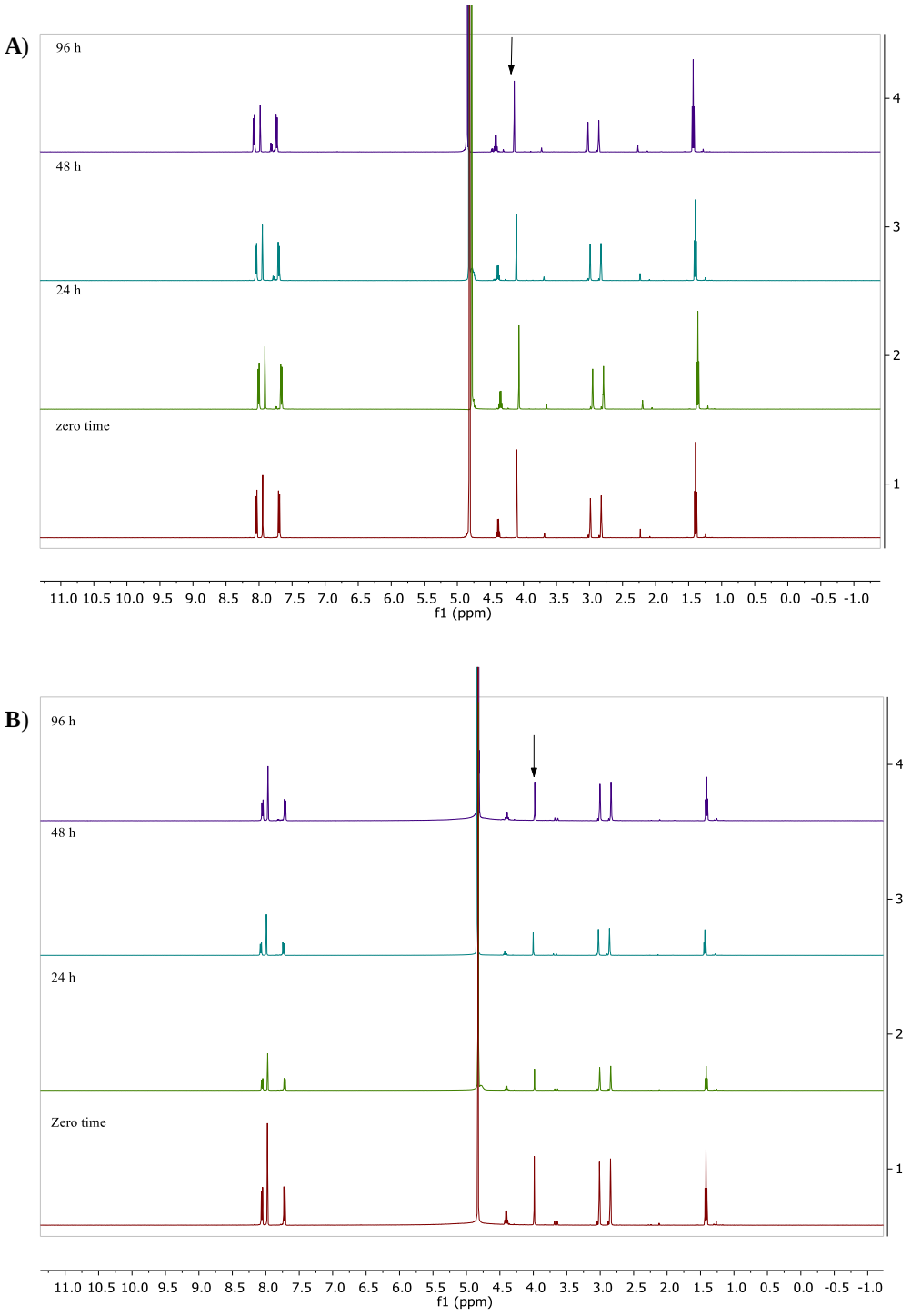

Figure 4.25. Stability of haloacetamide **4.20** and **4.21** in aqueous buffer. **A**) ^{1}H NMR spectrum of ethyl 4-(2-bromoacetamido)benzoate **4.20** (1.00 mg/ml, 3.51 mM) in phosphate buffer over 4 days. Arrow indicates the signals that were followed at δ 4.10 ppm for acetamide proton (BrC$\underline{H_2}$CONH) over 4 days. **B**) ^{1}H NMR spectrum of ethyl 4-(2-iodoacetamido)benzoate (**4.21**) (1 mg/ml, 3 mM) in phosphate buffer over 4 days, arrow indicates the signals that were followed at δ 3.99 ppm for acetamide protons (IC$\underline{H_2}$CONH) over 4 days.

Both of the meta-substituted linkers, methyl 3,5-bis(2-bromoacetamido)benzoate (**4.22**) and methyl 3,5-bis(2-iodoacetamido)benzoate (**4.24**), were found to be very stable over 4 days as no hydrolysis peaks were observed. On the other hand, the ortho substituted derivatives methyl 3,4-bis(2-bromoacetamido)benzoate (**4.23**) and methyl 3,4-bis(2-iodoacetamido)benzoate (**4.25**) were found to be less stable under the same conditions. The percent (%) of remaining of methyl 3,5-bis(2-haloacetamido)benzoate and methyl 3,4-bis(2-haloacetamido)benzoate derivatives **4.22-4.25** were determined by following the change in the integration of acetamide protons at δ 4.27 ppm ($BrC\underline{H_2}CONH$) for bromo-acetamide derivatives and at δ 3.95 ppm ($IC\underline{H_2}CONH$) for iodo-acetamide derivatives (Figure 4.26).

Ethyl 4-(2-haloacetamido)benzoate derivatives were very stable over time in aqueous phosphate buffer. The meta-substituted methyl 3,5-bis(2-haloacetamido)benzoate derivatives **4.15**, **4.22** and **4.24** showed high aqueous stability in phosphate buffer with only a slight decrease in the stability of bromo-and iodo-derivatives in comparison to the chloro-derivative. The percentage remaining of **4.15**, **4.22** and **4.24** after 4 days was found to be 98%, 80% and 90%, respectively. On the other hand, the ortho-substituted methyl 3,4-bis(2-haloacetamido)benzoate derivatives **4.16**, **4.23** and **4.15** showed reduced aqueous stability in phosphate buffer with a considerable decrease in the stability of the bromo-and iodo-derivatives in comparison to the chloro-derivative. The percentage remaining of **4.16**, **4.23** and **4.25** after 4 days were found to be 70%, 25% and 20%, respectively (Figure 4.26).

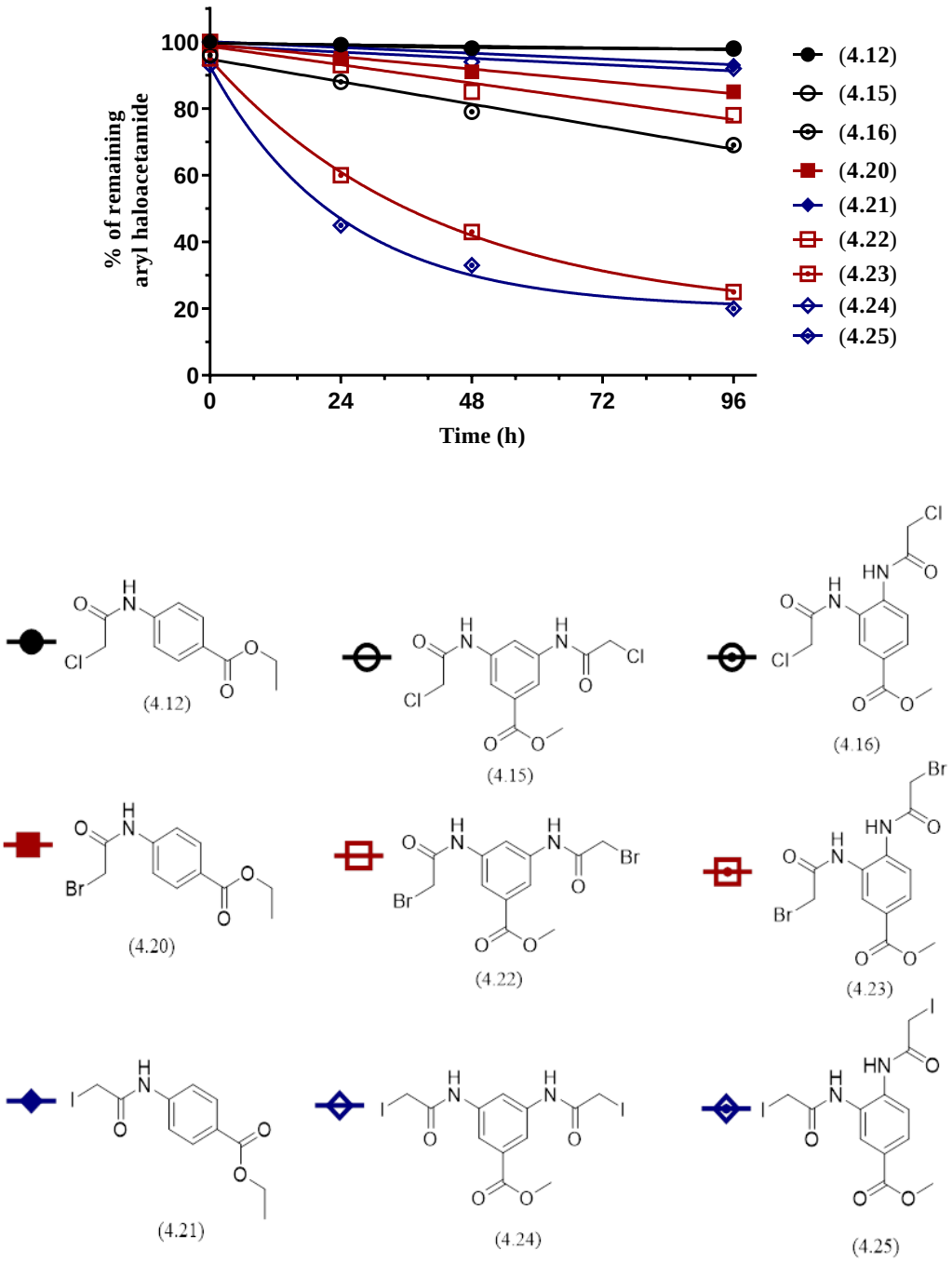

Figure 4.26. Comparison of the aqueous stability of haloacetamide derivatives **4.12**, **4.15**, **4.16**, and **4.20**-**4.25** over 4 days. Stability was determined in phosphate buffer (100 mM, pH 7.5) in the presence of 10% DMF-d_7 using ^{1}HNMR solvent suppression method.

4.5.1 Determination of the reactivity of methyl 3,5-bis(2-haloacetamido)benzoate (4.22 and 4.24) and methyl 3,4-bis(2-haloacetamido)benzoate (4.23 and 4.25) towards glutathione

Next, we sought to measure the reaction rates of ethyl 4-(2-bromoacetamido)benzoate (**4.19**) and ethyl 4-(2-iodoacetamido)benzoate (**4.20**) towards glutathione in phosphate buffer (pH 7.5) containing 10% DMF-d_7 using the ^{1}H NMR method employed previously. In both cases, the glutathione alkylation reactions were found to be completed within 3 minute when 3 equiv. of glutathione was employed. Therefore, direct comparison with ethyl 4-(2-chloroacetamido)benzoate (**4.9**) using 3 equiv. of GSH was not possible as the reaction rates could not be measured.

As such, lower equivalent of glutathione (1.1 equiv.) was then employed to measure the reaction rates of **4.19** and **4.20**. The reaction rates were calculated based on the disappearance of the peak from acetamide protons (XC$\underline{H_2}$CONH) and the appearance of a peak at δ 3.43 ppm which corresponds to the formed acetamide-glutathione adduct (Figure 4.27 A and B). The percentage remaining of each linker was determined using ratio of integral of the acetamide peak to the sum of integral of acetamide peaks and the peak at 4.01 or 3.8 ppm. Reaction rates of acetamide linkers **4.19** and **4.20** with glutathione were calculated by fitting to a first-order kinetic equation to natural log transformed percent remaining data (Equation 4.1). The half-life of acetamide linkers **4.19** and **4.20** in the presence of glutathione was then calculated using Equation 4.2.

Both ethyl 4-(2-bromoacetamido)benzoate (**4.20**) and ethyl 4-(2-iodoacetamido)benzoate (**4.21**) showed similar rates of reaction with glutathione and their half-lives in the presence of glutathione (1.1 equiv.) were both 0.75 minutes. By comparison, the half-life of ethyl 4-(2-chloroacetamido)benzoate (**4.9**) in the presence of glutathione (3 equiv.) was 33 minute (Figure 4.28).

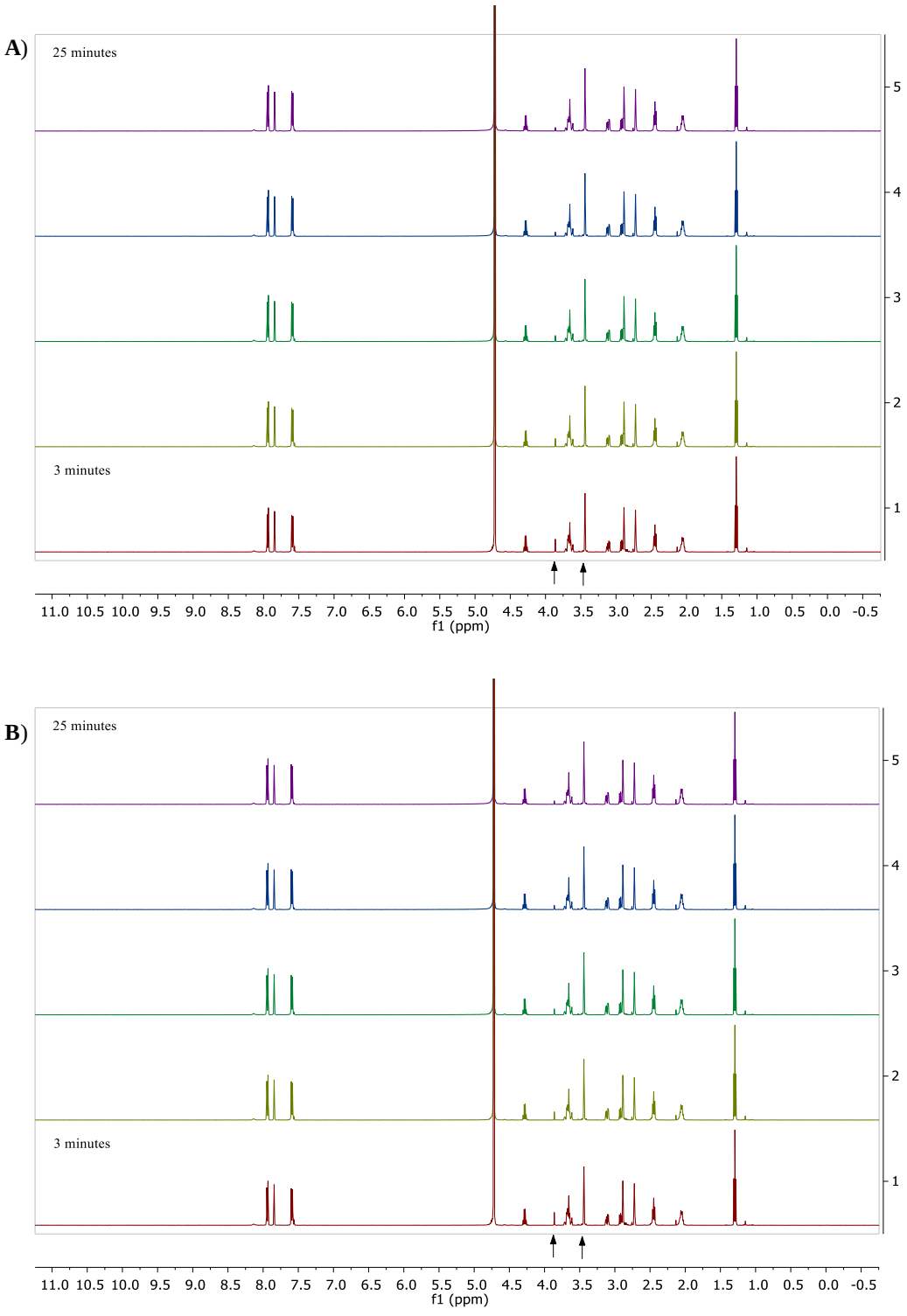

Figure 4.27. Study of reactivity of ethyl 4-(2-bromoacetamido)benzoate (**4.19**) and ethyl 4-(2-iodoacetamido)benzoate (**4.20**) towards glutathione. ^{1}H NMR spectrum of **A**) ethyl 4-(2-bromoacetamido)benzoate **4.19** (1.00 mg/ml, 3.51 mM) and **B**) ethyl 4-(2-iodoacetamido)benzoate (**4.20**) (1 mg/ml, 3 mM) in the presence of glutathione (1.1 equiv.) in aqueous phosphate. Arrow indicates the followed acetamide peaks at δ 4.02 ppm for bromo-acetamide or at 3.86 ppm for iodo-acetamide and at 3.46 ppm for acetamide-glutathione adduct to obtain the reactivity rates.

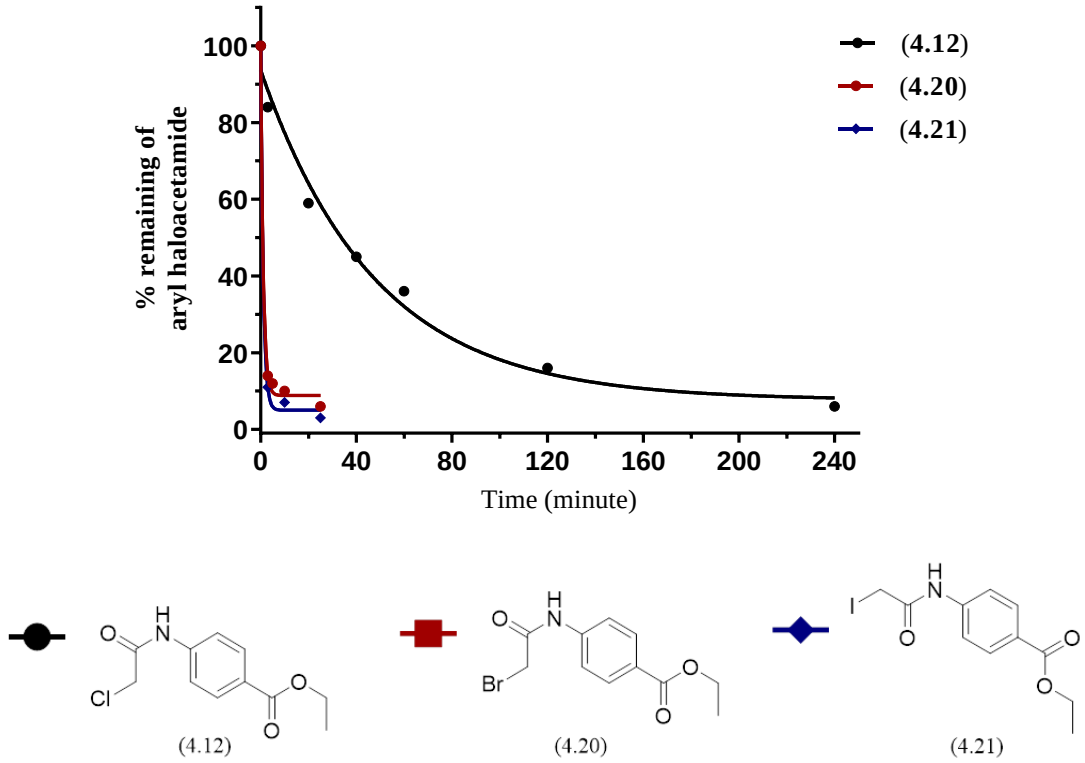

Figure 4.28. Percentage remaining of ethyl 4-(2-chloroacetamido)benzoate (**4.12**) (1.00 mg/ml, 4.15 mM) in the presence of glutathione (3 equiv.); ethyl 4-(2-bromoacetamido)benzoate **4.20** (1.00 mg/ml, 3.51 mM) and ethyl 4-(2-iodoacetamido)benzoate **4.21** (1 mg/ml, 3 mM) in presence of glutathione (1.1 equiv.) in phosphate buffer (100 mM, pH 7.5).

The rates of reaction of methyl 3,5-bis(2-bromoacetamido)benzoate (**4.22**), methyl 3,5-bis(2-iodoacetamido)benzoate (**4.24**), methyl 3,4-bis(2-bromoacetamido)benzoate (**4.23**) and methyl 3,4-bis(2-iodoacetamido)benzoate (**4.25**) with glutathione (2.2 equiv.) were not measurable using the ^{1}H NMR method, as complete thiol alkylation occurred within the first 3 minutes of the addition of these linkers to the aqueous solution of glutathione.

With the aqueous stability and glutathione reactivity of our linkers in hand, the following Sections set out to evaluate the impact of other chemical factors on their reactivity.

4.5.2 The synthesis and evaluation of *N*-benzyl-2-haloacetamide derivatives

Next, we aimed to study the importance of direct attachment of the acetamide to the conjugated system (aryl amides), and evaluate if benzyl amides (alkyl amides) share

similar stability and reactivity characteristics. To this end, the stability and glutathione reactivity of benzyl derivatives, *N*-benzyl-2-chloroacetamide (**4.26**) and *N*-benzyl-2-bromoacetamide (**4.27**) were appraised using a similar ^{1}H NMR method described previously and the rates of reaction of those linkers with glutathione (and half-lives) were calculated using Equation 4.1 and 4.2.

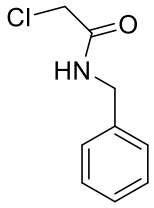

4.26

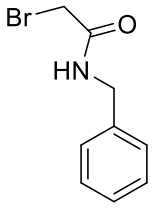

4.27

It was found that *N*-benzyl-2-chloroacetamide (**4.26**) and *N*-benzyl-2-bromoacetamide (**4.27**) demonstrated good aqueous stability under the same evaluated conditions (4 days, room temperature, pH 7.5). However, **4.26** and **4.27** were found to be significantly less reactive with glutathione in comparison to ethyl 4-(2-chloroacetamido)benzoate (**4.14**) and ethyl 4-(2-bromoacetamido)benzoate (**4.20**) (Figure 4.29 and Table 4.1).

One can conclude from these results that aryl amides are more reactive towards glutathione (thiolate group) than alkyl amide derivatives. Therefore, we intended to carry on our further investigation of haloacetamide linkers focusing on aryl amides derivatives.

The difference in the reaction rates of the haloacetamide group between the aryl amides and alkyl amides towards glutathione have been studied by Jöst *et al.*, where they investigated the impact of 11 moieties attached to different electrophiles (α-haloacetamide being amongst them) and how the substituents affected their reactivity towards glutathione and inhibitory activity towards certain enzymes. Both aromatic and benzylic amides were among the moieties tested. The aryl amides showed superior reactivity rate with glutathione while benzylic amides were not reactive under the tested conditions.[164] Therefore, the observations of Jöst *et al.* are consistent with the results generated here.

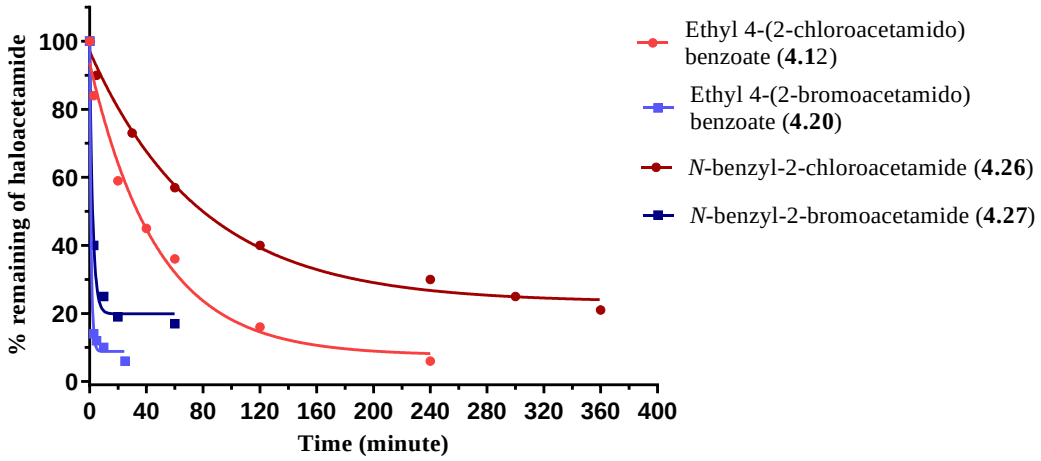

Figure 4.29. Percentage remaining of ethyl 4-(2-chloroacetamido)benzoate **4.12** (1.00 mg/ml, 4.15 mM) and N-benzyl-2-chloroacetamide **4.26** (1.00 mg/ml, 5.47 mM) in presence of glutathione (3 equiv.); ethyl 4-(2-bromoacetamido)benzoate **4.20** (1.00 mg/ml, 3.51 mM) and N-benzyl-2-bromoacetamide **4.27** (1.0 mg/ml, 4.4 mM) in presence of glutathione (1.1 equiv.) in aqueous phosphate buffer (100 mM, pH 7.5). The employed lower equivalent of glutathione (1.1 equiv.) precludes the completion of the reaction observed with **4.27** linker.

Table 4.1. Summary of the reactivity rates of aryl and alkyl haloacetamide linkers with glutathione.

	compound (4.12)	**compound (4.20)**	**compound (4.21)**	**compound (4.26)**	**compound (4.27)**
***K* (min $^{-1}$)**	0.01	0.1	0.1	0.004	0.02
Half Life (minutes)	33.01	0.7537	0.7538	54.43	1.54
glutathione (equivalent)	3	1.1	1.1	3	1.1

4.5.3 The impact of aryl substitution on the aqueous stability and reactivity of bis-haloacetamide linkers towards glutathione

Given that aryl acetamide derivatives are more reactive linkers, next we set out to further investigate the impact of aryl substitution on the stability and reactivity of bis-haloacetamide linkers (aryl amides).

As shown in previous Sections of this Chapter, aryl bis-haloacetamide linkers bearing an ester substituent were proposed as rebridging cross-linkers of reduced disulfide bonds. In this Section, we wanted to appraise the impact of aryl substitution (ester group) on the stability and reactivity of bis-haloacetamide linkers by directly comparing them to the non-substituted aryl bis-haloacetamide linkers **4.28**-**4.31**.

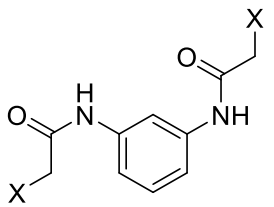

X= Cl (4.38)
X= Br (4.28)
X= I (4.30)

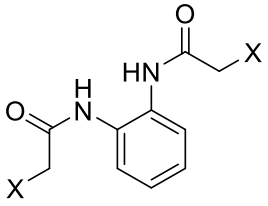

X=Cl (4.39)
X= Br (4.29)
X= I (4.31)

As such, *N*,*N*'-(1,3-phenylene)bis(2-haloacetamide) (**4.28** and **4.30**) and *N*,*N*'-(1,2-phenylene)bis(2-haloacetamide) (**4.29** and **4.31)** linkers were synthesised using similar methods to the methods described earlier to synthesis analogous ester derivatives **4.22**-**4.25**. Both aqueous stability and reactivity of *N*,*N*'-(1,3-phenylene)bis(2-haloacetamide) and *N*,*N*'-(1,2-phenylene)bis(2-haloacetamide) derivatives towards glutathione were carried out using similar ^{1}H NMR methods as described earlier.

N,*N*'-(1,3-phenylene)bis(2-chloroacetamide) **4.38** and *N*,*N*'-(1,2-phenylene)bis(2-chlorocetamide) **4.39** showed a greater aqueous stability in comparison to the bromo- and iodo-analogues. The *N*,*N*'-(1,3-phenylene)bis(2-haloacetamide) and *N*,*N*'-(1,2-phenylene)bis(2-haloacetamide) derivatives **4.28**-**4.31** were found to be more reactive towards glutathione compared to chloro-analogues. Similar to the results for **4.22**-**4.25** (aryl bis-haloacetamide linkers bearing an ester substituent), meta-substituted acetamide linkers **4.28** and **4.30** showed higher hydrolytic stability and lower reactivity rates with glutathione in comparison to ortho-substituted acetamide linkers **4.29** and **4.31** (Figure 30 A and B).

One can conclude that the rates of hydrolysis and rates of reaction of ester-substituted bis-haloacetamide linkers (both ortho- and meta-substituted haloacetamide) **4.22**-**4.25** towards glutathione have slightly increased in comparison to the non-substituted bis-

haloacetamide linkers **4.28-4.31**. The observed results can be attributed to the impact of the electron withdrawing effect of the carbonyl group (CO) directly linked to the aromatic ring. Nevertheless, this negligible impact of the presence of ester functionality on reactivity of aryl bis-haloacetamide linkers permits the attachment of a 'clickable' handle to them, such as an azide group (see Section 4.6) or other required functionality, with no impairment of the aqueous stability or reaction rates with thiolates (such as glutathione).

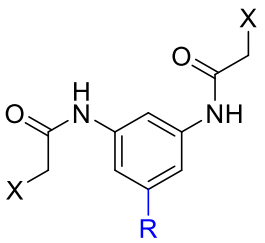

R= COOMe (**4.22**,**4.24**)
R = H (**4.28**, **4.30**)

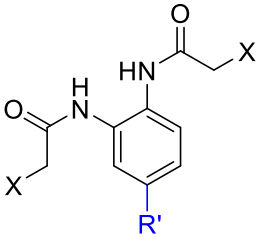

R'= COOMe (**4.23**,**4.25**)
R'= H (**4.29**, **4.31**)

4.6 Aryl bis-haloacetamide linkers bearing azide group

Having studied the aqueous stability and reactivity of bis-haloacetamide linkers towards glutathione, we next set out to investigate a bis-haloacetamide based rebridging approach and expand its application. Given that the chief use of bis-haloacetamide rebridging chemistry is to construct ADCs (as discussed earlier in Section 4.1), we set out to synthesise and evaluate bis-haloacetamides bearing an azide group, which can be subsequently used in a cross-coupling reaction with alkyne group ('Click' reaction, see Section 1.6.2). There are a huge number of therapeutics and imaging applications which could be made available through the use 'Click' chemistry to selectively link a cytotoxic drug, radiolabel or fluorescent probe.[165,166]

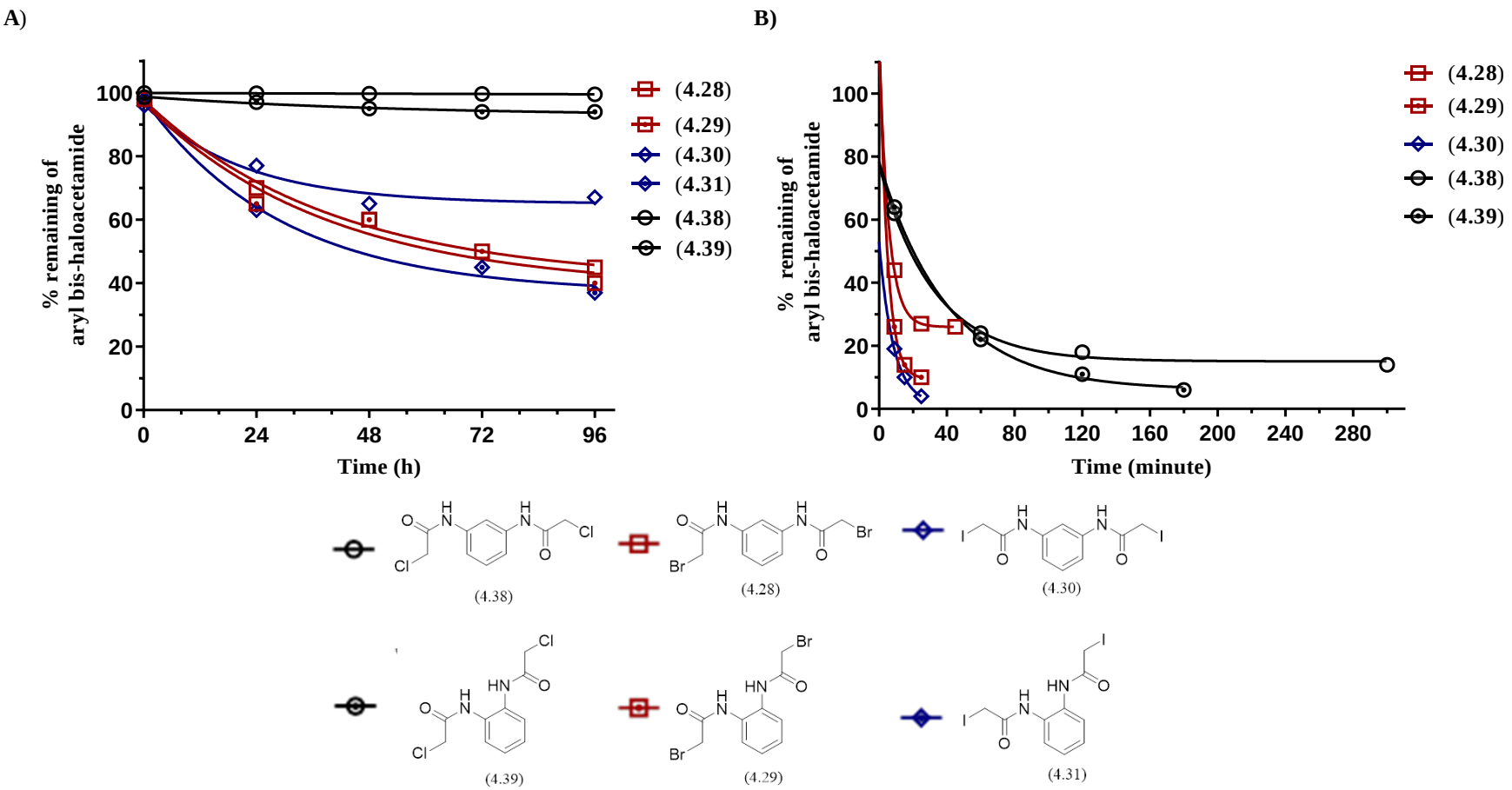

Figure 4.30. A) Percentage remaining of the *N*,*N*'-(1,3-phenylene)bis(2-haloacetamide) and *N*,*N*'-(1,2-phenylene)bis(2-haloacetamide) derivatives over 4 days. Stability was determined in phosphate buffer (100 mM, pH 7.5) containing 10% DMF-d_7 using ^{1}H NMR solvent suppression method. **B**) Percentage remaining of the *N*,*N*'-(1,3-phenylene)bis(2-haloacetamide) and *N*,*N*'-(1,2-phenylene)bis(2-haloacetamide) derivatives in the presence of glutathione (1.1 equiv.) in aqueous phosphate buffer (100 mM, pH 7.5). We were unable to be measured the rates of **4.31** using the ^{1}H NMR method as complete thiol alkylation occurred within the first 3 minutes of the addition of these linkers to the aqueous solution of glutathione.

4.6.1 Synthesis of azide containing aryl bis-haloacetamide linkers

In order to introduce an azide functionality to our bis-haloacetamide linkers, an azide-containing spacer of polyethylene glycol was initially synthesised as these are known to be water soluble derivatives of hydrocarbons. As such, Synthesis of 2-(2-(2-(2-azidoethoxy)ethoxy)ethoxy)ethan-1-amine (**4.46**) was achieved over 3 steps with 40% yield starting from tetraethyleneglycol (**2.19**) (Figure 4.31).

Firstly, tosylation reaction of tetraethyleneglycol (**2.19**) was achieved using 4-toluenesulphonyl chloride, overnight (85% yield). Then, 1,11-diazido-3,6,9-trioxaundecane (**2.11**) was synthsised through a substitution reaction with NaN_3 (82% yield). Lastly, a selective reduction to the mono-amine using triphenylphosphine (Ph_3P) was performed to obtain 2-(2-(2-(2-azidoethoxy)ethoxy)ethoxy)ethan-1-amine **4.46** (56% yield) (Figure 4.31).

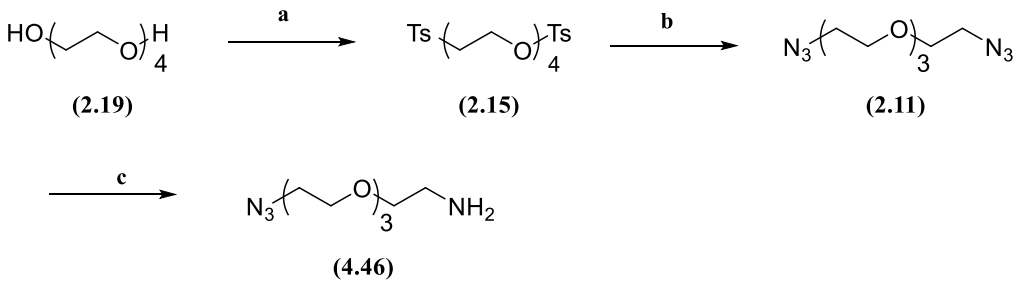

(2.19) (2.15) (2.11) (4.46)

Figure 4.31. Synthesis of 2-(2-(2-(2-azidoethoxy)ethoxy)ethoxy)ethan-1-amine (**4.46**). **a**) 4-toluenesulphonyl chloride, pyridine, DMC, **b**) NaN_3, acetone/water (3:1),37°C, o/n, **c**) Ph_3P, 5% HCl.

Then, synthesis of *N*,*N*'-(4-((2-(2-(2-(2-azidoethoxy)ethoxy)ethoxy)ethyl)carbamoyl)-1,2-phenylene)bis(2-iodoacetamide) (**4.35**) was achieved over 4 steps. Starting with acetylation of 3,4-diaminobenzoic acid using 2-chloroacetyl chloride (90% yield), followed by synthesis of activated ester using *N*-hydroxysuccinimide (45% yield). In the following step the activated ester (**4.45**) was reacted with 2-(2-(2-(2-azidoethoxy)ethoxy)ethoxy)ethan-1-amine (**4.46**) for 1 h (40% yield) to attain *N*,*N*'-(4-((2-(2-(2-(2-azidoethoxy)ethoxy)ethoxy)ethyl)carbamoyl)-1,2-phenylene)bis(2-iodoacetamide) (**4.37**), and finally it was converted to iodo-derivatives by reflux with KI for 3 h (73% yield) (Figure 4.32).

Synthesis of *N*,*N*'-(4-((2-(2-(2-(2-azidoethoxy)ethoxy)ethoxy)ethyl)carbamoyl)-1,3-phenylene)bis(2-iodoacetamide) (**4.33**) was achieved using the same 4 steps described with 28% overall yield.

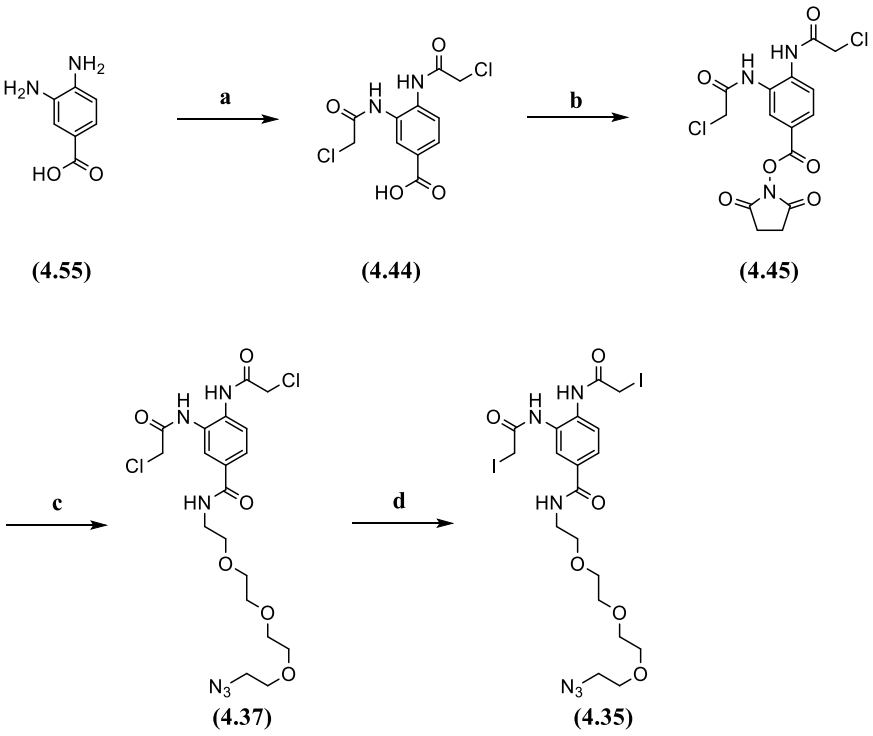

Figure 4.32. Synthesis of *N*,*N*'-(4-((2-(2-(2-(2-azidoethoxy)ethoxy)ethoxy)ethyl)carbamoyl)-1,2-phenylene)bis(2-iodoacetamide) (**4.35**). **a**) $ClCOCH_2Cl$, THF, **b**) NHS, EDC.HCl, THF, **c**) 2-(2-(2-(2-azidoethoxy)ethoxy)ethoxy)ethan-1-amine, THF, **d**) KI, dry acetone, reflux, 3 h.

In order to synthesise the bromo-derivative *N*,*N*'-(4-((2-(2-(2-(2-azidoethoxy)ethoxy)ethoxy)ethyl)carbamoyl)-1,2-phenylene)bis(2-bromoacetamide) (**4.34**), an analogous pathway was followed from *N*,*N*'-(4-((2-(2-(2-(2-azidoethoxy)ethoxy)ethoxy)ethyl)carbamoyl)-1,2-phenylene)bis(2-chloroacetamide) (**4.37**) using KBr. However, the rate of the reaction was lower, with only 75% of chloro-derivative (**4.37**) converted to the bromo-derivative (**4.34**) after refluxing for 2 days (confirmed by ^{1}H NMR). Therefore, for complete conversion of the chloro-derivative (**4.37**) to the desired bromo-derivative (**4.34**), reflux of the reaction with KBr was held for 4 days (43% yield) (Figure 4.33).

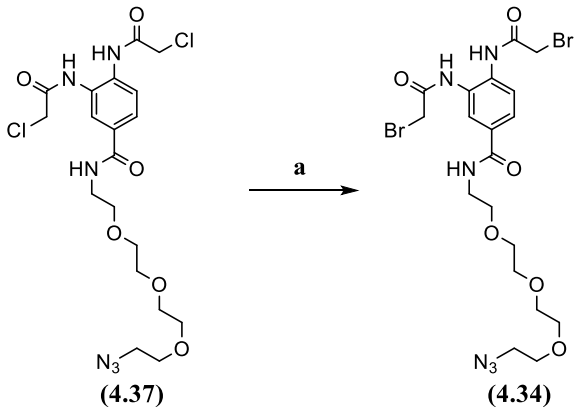

Figure 4.33. Synthesis of *N*,*N*'-(4-((2-(2-(2-(2-azidoethoxy)ethoxy)ethoxy)ethyl)carbamoyl)-1,2-phenylene)bis(2-bromoacetamide) (**4.34**). **a**) KBr, dry acetone, reflux, 4 days.

N,*N*'-(4-((2-(2-(2-(2-azidoethoxy)ethoxy)ethoxy)ethyl)carbamoyl)-1,3-phenylene)bis(2-bromoacetamide) (**4.32**) was synthesised using the same KBr reflux method for 4 days with 51% yield.

4.6.2 Stability and GSH reactivity of azide-bearing bis-haloacetamide linkers

N,*N*'-(4-((2-(2-(2-(2-azidoethoxy)ethoxy)ethoxy)ethyl)carbamoyl)-1,2-phenylene)bis(2-haloacetamide) and *N*,*N*'-(4-((2-(2-(2-(2-azidoethoxy)ethoxy)ethoxy)ethyl)carbamoyl)-1,3-phenylene)bis(2-haloacetamide) derivatives **4.32-4.35** stability was determined in phosphate buffer at pH 7.5 containing 10% DMF-d_7 using a similar ^{1}H-NMR solvent suppression method the described previously. ^{1}H-NMR spectra were acquired at time 0, 24, 48 and 96 h. Over four days, all azide-bearing linkers were stable with less than 15 % overall hydrolysis (Figure 4.34). Overall, amide-based linkers (**4.32-4.35**) displayed excellent aqueous stability to compared to the ester-substituted bis-haloacetamide linkers (**4.22-4.25**) (Figure 4.34). It is worthwhile mentioning that the presence of $(PEG)_3$ also significantly increased the aqueous solubility of **4.32-4.35** linkers as only 10% DMF-d_7 was required to solubilise them.

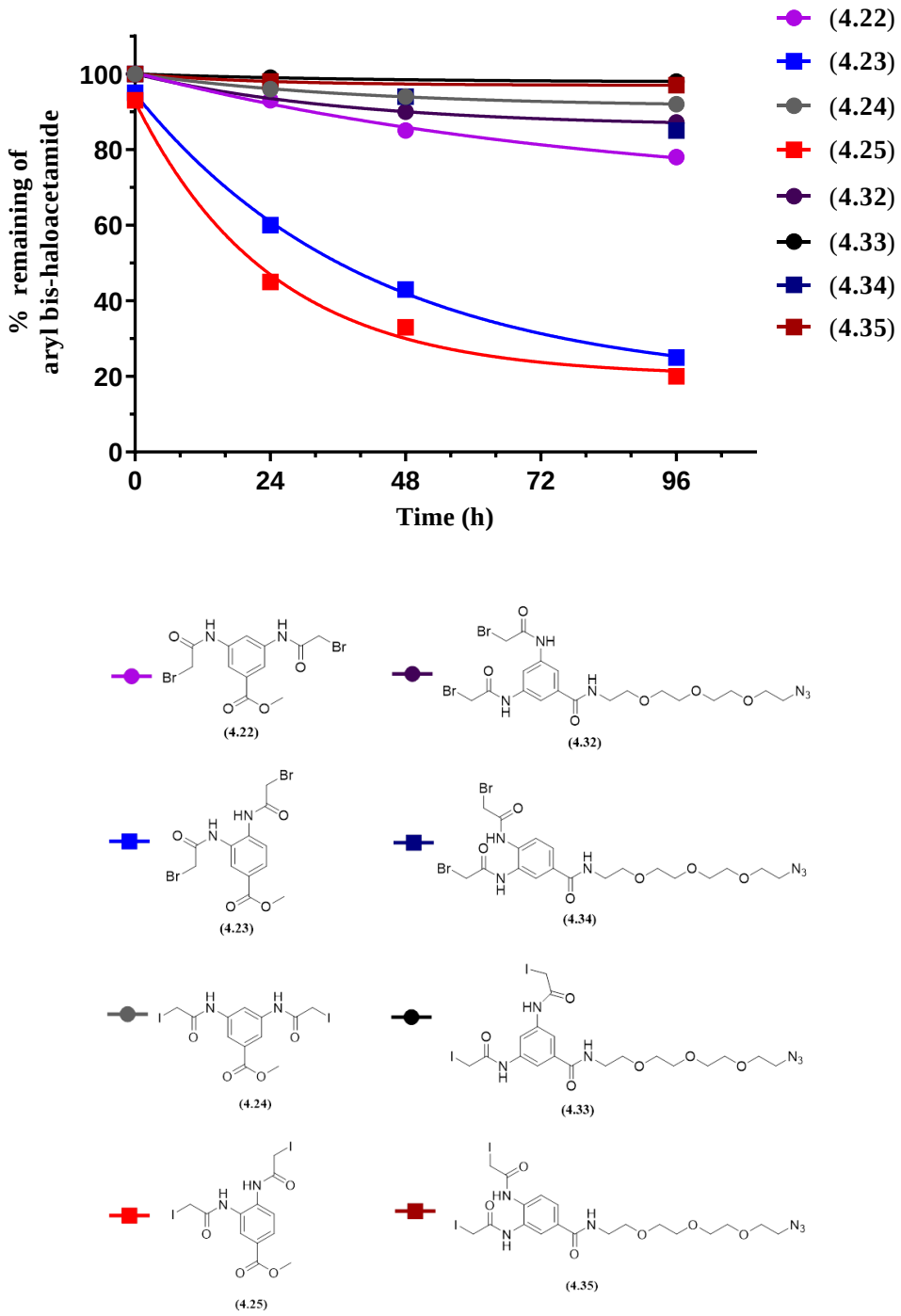

Figure 4.34. Comparison of the aqueous stability of aryl bis-haloacetamide linkers. Percentage remaining of the bis-haloacetamide derivatives (**4.22-4.25** and **4.32-4.35**) over 4 days. Stability was appraised in phosphate buffer (100 mM, pH 7.5) with final concentration of 10% DMF-d7 using solvent suppression method.

Next, we sought to study reaction rates of *N*,*N*'-(4-((2-(2-(2-(2-azidoethoxy)ethoxy)ethoxy)ethyl)carbamoyl)-1,2-phenylene)bis(2-haloacetamide) and

N,*N*'-(4-((2-(2-(2-(2-azidoethoxy)ethoxy)ethoxy)ethyl)carbamoyl)-1,3-phenylene)bis(2-haloacetamide) linkers **4.32-4.35** with glutathione (2.2 equiv.) in phosphate buffer (pH 7.5) containing 10% DMF-d_7. All bis-haloacetamide bearing azide group **4.32-4.35** reacted readily with glutathione within less than 10 min (Figure 4.35).

Similar to **4.22-4.25** (aryl bis-haloacetamide linkers bearing an ester substituent), meta-acetamide linkers **4.32** and **4.33** showed higher aqueous stability and lower reactivity rates with glutathione in comparison to ortho-acetamide linkers **4.34** and **4.35.**

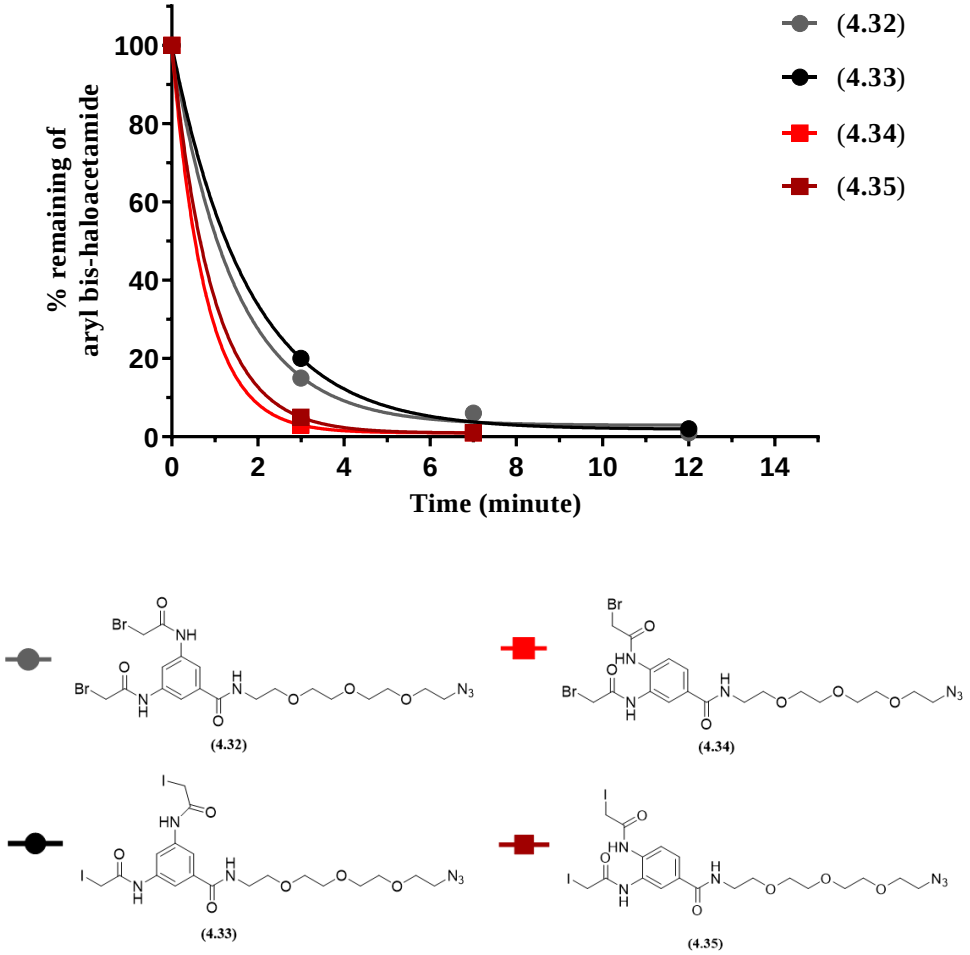

Figure 4.35. Percentage remaining of the bis-haloacetamide derivatives **4.32** and **4.43** (1.0 mg/ml, 1.7 mM), **4.33** and **4.35** (1.00 mg/ml, 1.45 mM) in the presence of glutathione (1.1 equiv.) in aqueous phosphate buffer (100 mM, pH 7.5).

All the aryl bis-haloacetimide derivatives tested showed very rapid thiolate alkylation reaction rates with glutathione [less than 20 minutes for the slowest non-substiteted bis-haloacetamide derivatives (**4.28**-**4.31**)]. The aryl bis-haloacetimides bearing ester group found to be very reactive and we were unable to measure the reaction rates with glutathione using the ^{1}H NMR method. On the other hand, aryl bis-haloacetimides bearing an amide group were found to be slightly less reactive, which can be partly attributed to the smaller inductive effect of the N atom (CONH), while the steric influence of the bulky $(PEG)_3$ group could also attribute to the slower reaction rates with glutathione (Table 4.2).

In conclusion, in this Chapter, we were able to synthesise and evaluate the stability and glutathione reactivity of alkyl and aryl bis-haloacetamide linkers. We found that aryl bis-haloacetamide linkers are the most reactive towards thiolate alkylation. Different parameters were addressed in this Chapter, including the regiochemistry of the haloacetamide groups relative to each other and aryl substitution. Both meta- and ortho-aryl bis-haloacetamide linkers are reactive towards glutathione and relatively stable in aqueous buffer. Both bis bromo-and iodo-acetamide linkers have similar aqueous stability and reactivity profile towards thiolate alkylation of glutathione. Aryl substitution has not significantly affected the reactivity rates, which enabled us to synthesise and evaluate aryl bis-haloacetamide linkers bearing azide group.

Lastly, we synthesised glutathione conjugates of aryl bis-haloacetamide derivatives, and studied the stability of bis-glutathione conjugates in aqueous buffer and in the presence of DTT over 4 weeks. We found that the constructed conjugates are very stable in the presence and the absence of DTT, we can conclude that the various aryl bis-haloacetamide linkers provided in this Chapter hold promising advantages over the available conjugation approaches. Therefore, these linkers, summarised in Table 4.2, will be subsequently applied towards rebridging of reduced mAb disulfide bonds (Chapter 5).

Table 4.2. Summary of the aqueous stability and glutathione reactivity of aryl bis-haloacetamide linkers. [a] % of remaining are stated regarding to the least stable linker.

	Linkers	Glutathione reactivity	Stability
Unsubstituted linkers	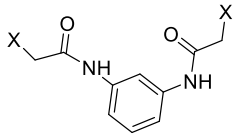 **X= Br (4.28)** **X= I (4.30)**	Thiol alkylation reaction require 20-40 minutes	45% remains unhydrolysed after 4 days[a]
	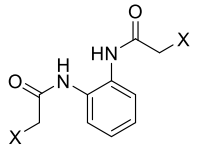 **X= Br (4.29)** **X= I (4.31)**	Thiol alkylation reaction require less than 20 minutes	37% remains unhydrolysed after 4 days[a]
Ester derivatised linkers	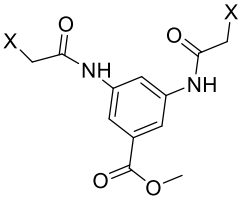 **X= Br (4.22)** **X= I (4.24)**	Complete thiol alkylation reaction within 3 minutes	78% remains unhydrolysed after 4 days[a]
	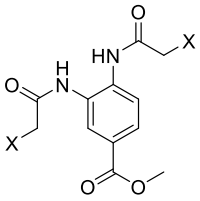 **X= Br (4.23)** **X= I (4.25)**	Complete thiol alkylation reaction within Less than 3 minutes	20% remains unhydrolysed after 4 days[a]
Azide derivatised linkers	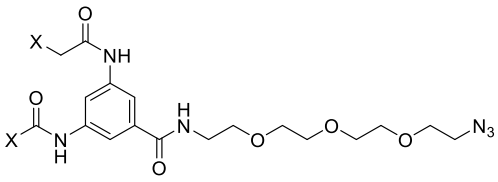 **X=Br (4.32)** **X=I (4.33)**	Complete thiol alkylation reaction within less than 10 minutes	87% remains unhydrolysed after 4 days[a]
	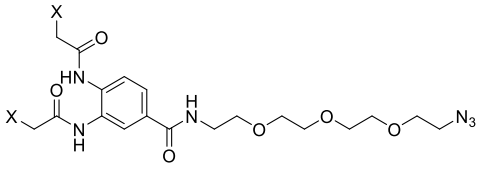 **X=Br (4.34)** **X=I (4.35)**	Complete thiol alkylation reaction within less than 10 minutes	85% remains unhydrolysed after 4 days[a]

5 Rebridging of reduced disulfide bonds of monoclonal antibodies using bis-haloacetamide linkers

5.1 Introduction

The monoclonal antibody therapeutic Trastuzumab (Tmab) was approved by FDA in 1998 for HER2 positive breast cancer patients.[167] HER2 overexpression or gene amplification has been found in approximately 20–30% of breast cancer patients, which is referred to as the HER2 positive subtype.[57]

Trastuzumab is a recombinant humanized mAb which binds with high affinity to the extracellular domain of the HER2 receptor. It was the first approved biological therapeutic drug for the treatment of the HER2 positive subtype. It is widely acknowledged that using trastuzumab, either as a single agent therapy or in combination with conventional chemotherapy, has produced remarkable clinical benefits as it has significantly improved the prognosis and increased the survival of HER2 subset of breast cancer patients.[168,169]

5.1.1 The HER2 receptor

HER2 is a 185-kDa receptor that belongs to the HER family (HER-1-4). HER family of receptors are transmembrane receptors with embedded tyrosine kinases. These receptors have 3 main domains: extracellular ligand binding domain, a transmembrane domain and (apart from HER-3) an intracellular tyrosine kinase domain that interacts with multiple intracellular signaling molecules. The intracellular tyrosine kinase domains are triggered by both homo- and hetero-dimerization, which is mainly induced by specific ligands binding to the extracellular domain.[170–172]

HER2 is unique among HER family receptors and is known as an ‘orphan receptor’, because it has no known endogenous ligand. HER2 can adopt the active conformation without ligand binding when it homo- or hetero-dimerises with another HER2 or one of the other HER family receptors, leading to autophosphorylation of tyrosine residues within their intracellular domain. Active HER2 receptors modulate a number of signaling pathways, in particular PI3K/AKT and RAS/MEK/MAPK pathways that are

involved in cell proliferation, differentiation and survival of both normal and malignant breast cells (Figure 5.1).[173]

Clinically, cancer drug therapy for the HER2 positive subtype of breast cancer patients can be classified into two major groups: Humanized monoclonal antibodies directed against the HER2 extracellular domain (Trastuzumab), or against HER2 dimerization (Pertuzumab); and or a drug molecule against the tyrosine kinase domain (Lapatinib).[174,175]

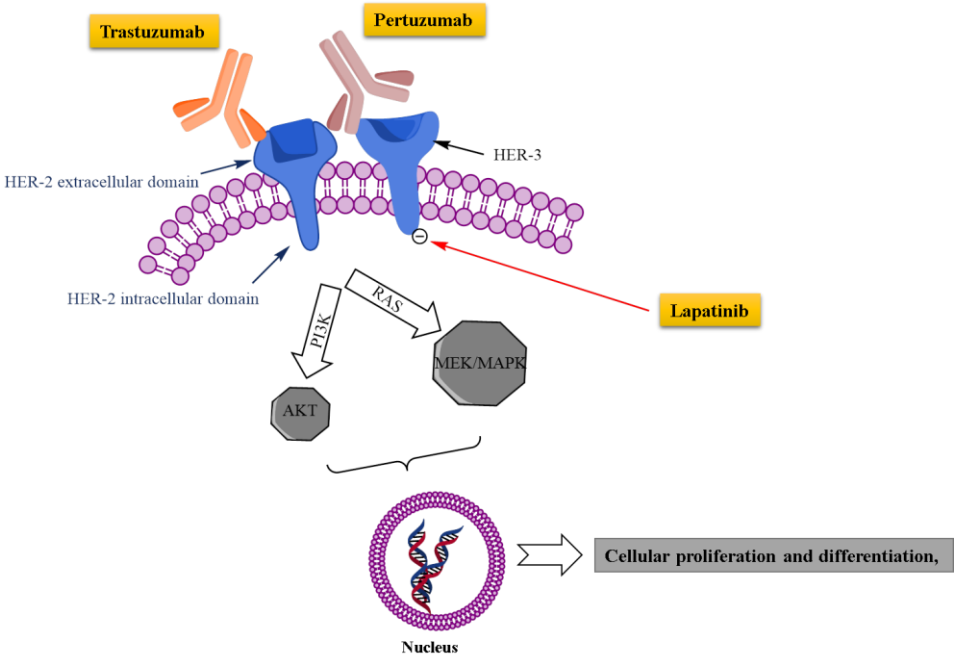

Figure 5.1. HER2 signaling pathways in breast cells and the site of action of the currently available anti-HER2 receptors drugs. Trastuzumab mAb binds and blocks the extracellular domain of HER2, in particular domain IV, while Pertuzumab inhibits dimerization of HER2 receptor by binding to domain II of the extracellular domain of the receptor. Lapatinib is small drug molecule that inhibits tyrosine kinase.[176]

5.1.2 Mechanism of action of Trastuzumab

Interaction of Trastuzumab with the HER2 receptor prevents HER2-receptor dimerization, which increases endocytotic destruction of the receptor and eventually interferes with downstream signaling pathways, (mainly the PI3K/ AKT pathway) therefore promoting cellular apoptosis.[177]

In addition to the aforementioned impacts of Trastuzumab interactions with the HER2 receptors on cancer cells, studies have proved that it also activates antibody-dependent cellular cytotoxicity (ADCC). Several preclinical studies suggested that trastuzumab activates immune effector cells, mostly NK cells where animals with deficiency of FcγR expression on effector cells displayed significant loss of therapeutic response to Trastuzumab treatment.[177] Given that overexpression of HER2 has been directly linked with the increased angiogenesis process, one of the proposed mechanism of action of Trastuzumab is inhibition of angiogenesis and induction of normalization and regression of the vasculature.[178,179]

Since it has introduced in 1998, Trastuzumab has significantly improved the outcomes of HER2 positive patients' treatment. It is worthwhile mentioning that resistance to trastuzumab, however, has reduced the beneficial response to this therapy. Approximately, 70% of the patients who initially responded to trastuzumab therapy, developed resistance within one year of starting their therapy, while about 65% of HER2 positive patients did not benefit from the treatment.[180]

Different mechanisms of resistance to Trastuzumab have been reported. Notably, the increase in insulin-like growth factor-I receptor (IGF-IR) signaling. IGF-IR is a tyrosine kinase receptor that is over-expressed and activated in breast cancer cells. Nhta *et al.* have demonstrated that HER2 interacts, and forms hetero-dimers, with IGF-IR in Trastuzumab resistant cells. By IGF-I stimulation, the level of phosphorylation of the HER2 receptor in resistant cells is enhanced. Moreover, they found that by inhibition of IGF-IR, the sensitivity of resistant cells to trastuzumab increased.[181] Steric hindrance was also postulated as another resistance mechanism of cancer cells where the level of expression of the membrane-associated glycoprotein MUC4 was found to be increased to sterically hinder Trastuzumab accessibility to HER2.[182,183]

Trastuzumab is a well-established biological drug, which has been approved since 1998, however, with the limited advantages of Tmab as a mono therapy and its associated resistance, researchers have focused on enhancing the activity through conjugation to cytotoxic drugs as discussed earlier in Section 1.3.4.3. Given that the activity of Tmab

has been extensively studied *in vitro* and *in vivo* and it has been already widely applied in maleimide-based chemical conjugation, we chose it as a good model to evaluate our newly developed rebridging strategy.

With all the aqueous stability and glutathione reactivity results from aryl bis-haloacetamide linkers in hand (Chapter 4), the disulfide rebridging activity of bis-haloacetamide linkers in cross-linking reduced proteins will be investigated in this Chapter.

5.2 Optimisation of the TCEP reduction of Tmab

Prior to evaluating cross-linking of Tmab using bis-haloacetamides, we set out to optimise the reduction conditions of Tmab to obtain either fully or partially reduced Tmab with reducing agents, such as TCEP (**2.2**).

Reduction of Tmab inter-chain disulfide bonds with TCEP will produce multiple possible products, the nature of which depend mainly on the equivalents of TCEP employed. It has been found that the reduction of disulfide bonds of the IgG_1 subclass of IgGs will proceed in the following order: heavy-light disulfide bonds, upper-heavy-heavy and then lower-heavy-heavy disulfide bonds.[148] A heterogeneous mixture of reduced fragments was observed with the non-specific reduction of antibodies using TCEP, even when lower equivalents were employed.[122]

To this end, we first sought to evaluate the impact of different reduction parameters, such as concentration of protein, time and incubation temperature, in order to obtain optimum reduction conditions. Reduction of mAbs is essential step to be optimised and evaluated, thus, enabling consistent rebridging of the inter-chain disulfide bonds of Tmab. Figure 5.2 represents the expected reduced species based on the employed equivalents of TCEP and the molecular mass of the bands that would be observed by SDS-PAGE under non-reducing conditions.

As described earlier, it has been demonstrated in the literature that heavy-light disulfide bonds are more susceptible towards reduction and therefore reduced first. Evaluation of the products of reduction by using SDS-PAGE (non-reducing) is not straight forward as

heavy-heavy chains are still associated together by non-covalent interactions and we are not able to separate them under non-reducing conditions (50 and 25 kDa). As a result, in order to interpret the level of the reduction, the disappearance of the 150 and 125 kDa bands (reduction of heavy-light chains) will be followed.

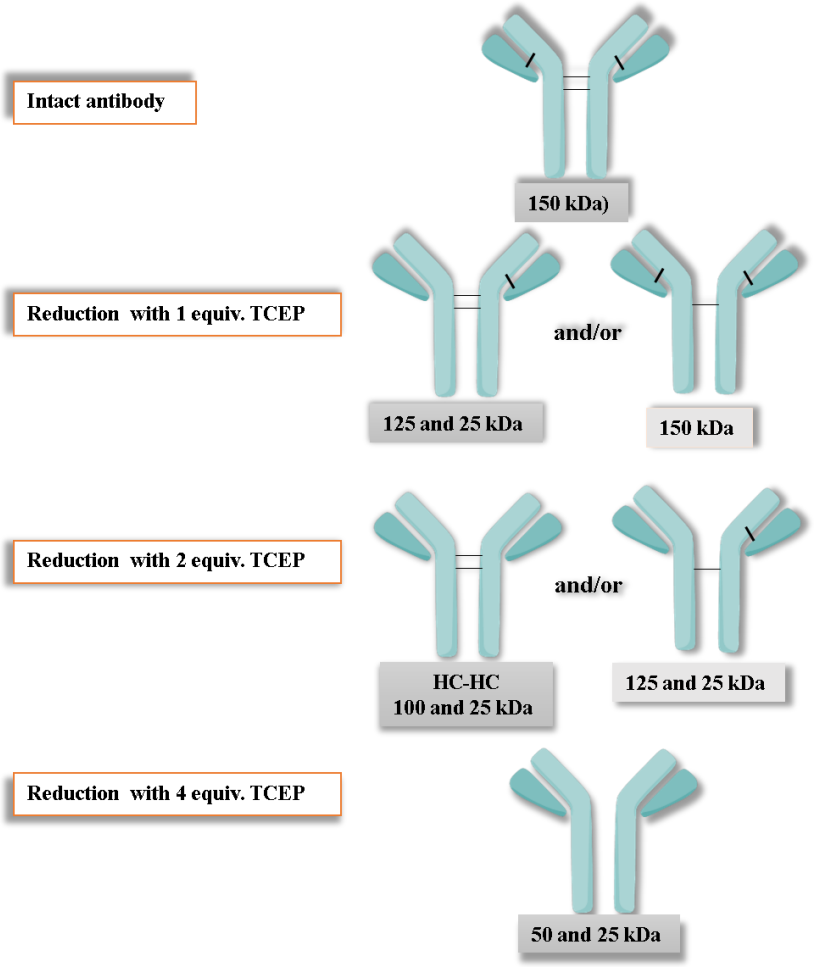

Figure 5.2. The possible products species of mAbs reduced with 1, 2 or 4 equivalents of TCEP with the masses of the observed bands under non-reducing conditions (dark gray represents the major products).

Firstly, in order to optimise the partial reduction of Tmab (only heavy-light disulfide bonds), the impact of Tmab concentration of on the rate of reduction was evaluated. By selectively reducing heavy and light disulfide bonds, a band at around 100 kDa would be observed under non-reducing condition. However, as the samples were resolved by SDS-PAGE under non-reducing conditions and without heating (still folded), they might run at different molecular weight and do not match perfectly with the ladder.

Moreover, intact non-reduced sample of Tmab was run under the same tested conditions (non-reducing gels, unheated sample) to confirm that what we would observe is due to the performed reduction process.

Two sets of concentrations were appraised: 1 mg/mL and 10 mg/mL. Tmab was reduced with either 2.2 or 2.5 equivalents of TCEP (**2.2**) at 4°C. At 10 mg/mL concentration of Tmab (concentrated solution), a superior reduction rate was obtained as observed with a 115 kDa band (corresponds to heavy-heavy chains) obtained as the major product (Figure 5.3, lane 5-8). In contrast, at 1 mg/mL concentration of Tmab, slower reduction rates were observed as most of Tmab remains as intact antibody as observed at 185 kDa. Moreover, one can note that longer incubation of Tmab with TCEP (reduction time increased to 2 h), the selectivity of the heavy-light disulfide bonds was reduced as more of the 80 kDa band (corresponding to HC-LC fragment) was observed which implies that the a proportion of heavy-heavy disulfide bonds have been reduced (Figure 5.3, lane 6 and 8).

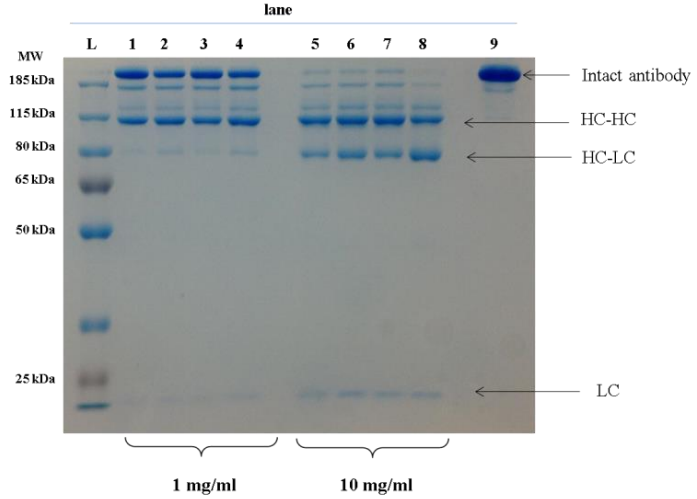

Figure 5.3. SDS-PAGE analysis of optimisation of Tmab reduction using TCEP (**2.2**) varying concentration of Tmab and reduction time. L: protein ladder. Lane 1-4: Tmab (1.0 mg/mL, 6.9 µM), Lane 5-8: Tmab (10 mg/mL, 69 µM) in Tris.HCl buffer (100 mM, 150 mM NaCl, 5 mM EDTA, pH 7.5). Lane 1: Tmab reduced with 2.2 equiv. of TCEP (1.52 µM) for 1 h, lane 2: Tmab reduced with 2.2 equiv. of TCEP (1.52 µM) for 2 h, lane 3: Tmab reduced with 2.5 equiv. of TCEP (1.72 µM) for 1 h, lane 4: Tmab reduced with 2.5 equiv. of TCEP (1.72 µM) for 2 h, lane 5: Tmab reduced with 2.2 equiv. of TCEP (15.2 µM) for 1 h, lane 6: Tmab reduced with 2.2 equiv. of TCEP (15.2 µM) for 2 h, lane 7: Tmab reduced with 2.5 equiv. of TCEP (17.2 µM) for 1 h, lane 8: Tmab reduced with 2.5 equiv. of TCEP (1.72 µM) for 2 h, at 4 °C. lane 9: Tmab control (non-reducing dye). HC: heavy chain, LC: light chain. Protein samples were resolved by non-reducing SDS-Page (10% gel).

Next, as the rate of reduction has significantly affected by the concentration of Tmab, a 5 mg/mL concentration was chosen to be evaluated in order to optimise the reduction conditions and minimise the non-specific reduction of heavy-heavy inter-chain disulfide bonds. One can note that the rate of TCEP reduction of heavy-heavy inter-chain disulfide bonds was reduced at 5 mg/mL concentration as more intact antibody was observed at 185 kDa MW. In addition, 2 hours of reduction is required to obtain greater proportion of reduced heavy-light disulfide bonds (115 kDa band). In conclusion, TCEP preferably reduces heavy-light inter-chain disulfide bonds but also reduces a fraction of heavy-heavy inert-chain disulfide bonds which explains the presence of a distinct band at 80 kDa (HC-LC) (Figure 5.4, lane 1-5).

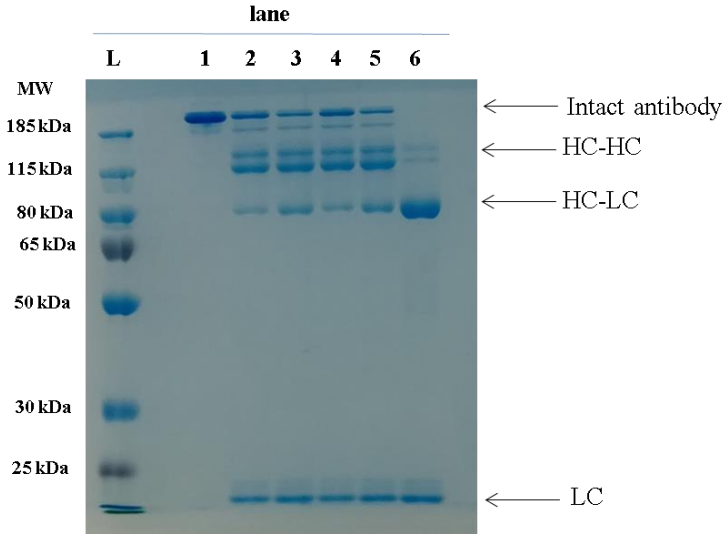

Figure 5.4. SDS-PAGE analysis of optimisation of Tmab reduction using TCEP (**2.2**) varying the reduction time. L: protein ladder. Tmab (5 mg/mL, 34 µM), in Tris.HCl buffer (100 mM, 150 mM NaCl, 5 mM EDTA, pH 7.5). L: protein ladder, lane 1: Tmab control (non -reducing dye), lane 2: Tmab reduced with 2 equiv. of TCEP (6.8 µM) for 1 h at 4°C, lane 3: Tmab reduced with 2 equiv. of TCEP (6.8 µM) for 2 h at 4°C, lane 4: Tmab reduced with 2.2 equiv. of TCEP (7.5 µM) for 1 h at 4°C, lane 5: Tmab reduced with 2.2 equiv. of TCEP (7.5 µM) for 2 h at 4°C, lane 6: Tmab reduced with 5 equiv. of TCEP (17 µM) for 2 h at room temperature. Protein samples were resolved by non-reducing SDS-Page (10% gel).

Next, we sought to fully reduce Tmab (the 4 inter-chain disulfide bonds) at both room temperature and 37°C. Analysis of the reduction condition by SDS-PAGE showed Tmab reduction with 5 equivalent of TCEP at room temperature for 2 h was sufficient to fully reduce the heavy-heavy and heavy-light disulfide bonds, as demonstrated by the disappearance of the 150 and 125 kDa bands in Figure 5.5, lane 3. However, in order

to reduce only heavy-light disulfide bonds, a lower temperature (4°C) is required to selectively reduce these disulfide bonds without minimum reduction of heavy-heavy disulfide bonds (Figure 5.5, lane 2).

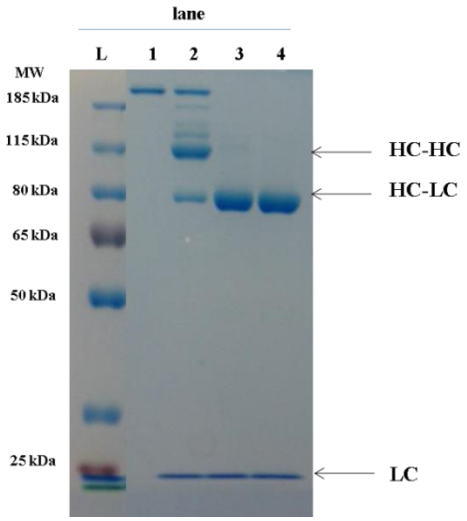

Figure 5.5. SDS-PAGE analysis of optimisation of Tmab reduction using TCEP (**2.2**). Lane 1-4: Tmab (5.0 mg/mL, 34 µM) in Tris.HCl buffer (100 mM, 150 mM NaCl, 5 mM EDTA, pH 7.5). L: protein ladder, lane 1: Tmab control (non -reducing dye), lane 2: Tmab reduced with 2.2 equiv. of TCEP (7.5 µM) for 2 h at 4°C, lane 3: Tmab reduced with 5 equiv. of TCEP (17 µM) for 2 h at room temperature, lane 4: Tmab reduced with 10 equiv. of TCEP (34 µM) for 2 h at 37 °C. Protein samples were resolved by non-reducing SDS-Page (10% gel).

5.3 Disulfide bond rebridging of fully reduced Trastuzumab

Having optimised the reduction conditions required to obtain fully reduced Tmab (5 equiv. for 2 h at room temperature) we next sought to determine the efficiency of bis-haloacetamide linkers to rebridge the fully reduced Tmab and characterise the obtained product.

Initially, we attempted to cross-link fully reduced Tmab using the bromo-linkers, methyl 3,5-bis(2-bromoacetamido)benzoate (**4.22**), methyl 3,4-bis(2-bromoacetamido)benzoate (**4.23**), *N*,*N*'-(1,3-phenylene)bis(2-bromoacetamide) (**4.28**), and *N*,*N*'-(1,2-phenylene)bis(2-bromoacetamide) (**4.29**). As such, Tmab (5 mg/mL) in Tris.HCl (100 mM, pH 7.5) containing 150 mM NaCl and 5 mM EDTA, was reduced by incubation with TCEP **2.2** (5 equiv.) for 2 h at room temperature. The reduced Tmab was incubated with 5 or 8 equiv. of each bis-bromoacetamide linker (**4.22**, **4.23**, **4.28** and **4.29**) and

held at room temperature overnight. Excess linkers were used to account for the remaining TCEP.

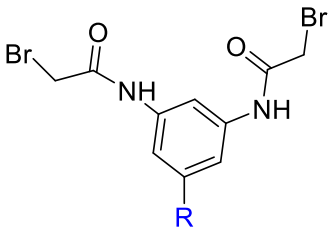

R = COOMe (**4.22**)
R = H (**4.28**)

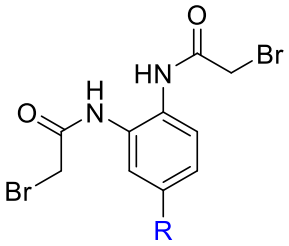

R = COOMe (**4.23**)
R = H (**4.29**)

The products of reaction were then resolved and analysed by using SDS-PAGE under reducing conditions. Unexpectedly, the major product of cross-linking was half-antibody observed at (75 kDa) for all bis-bromoacetamide linkers (**4.22**, **4.23**, **4.28** and **4.29**) (Figure 5.6). These results suggest that these bis-haloacetamide linkers react differently to the existing rebridging linkers (**4a-4f**) by rebridging HC-LC disulfide but not inter-chain HC-HC disulfide bonds.

Given that sufficient equivalents of reducing agents were used to fully reduce Tmab along with excess linkers were employed to quench excess TCEP and rebridge the four disulfide bonds, it is expected to obtain fully bridged Tmab (150 kDa), therefore we next sought to investigate the reason behind these results.

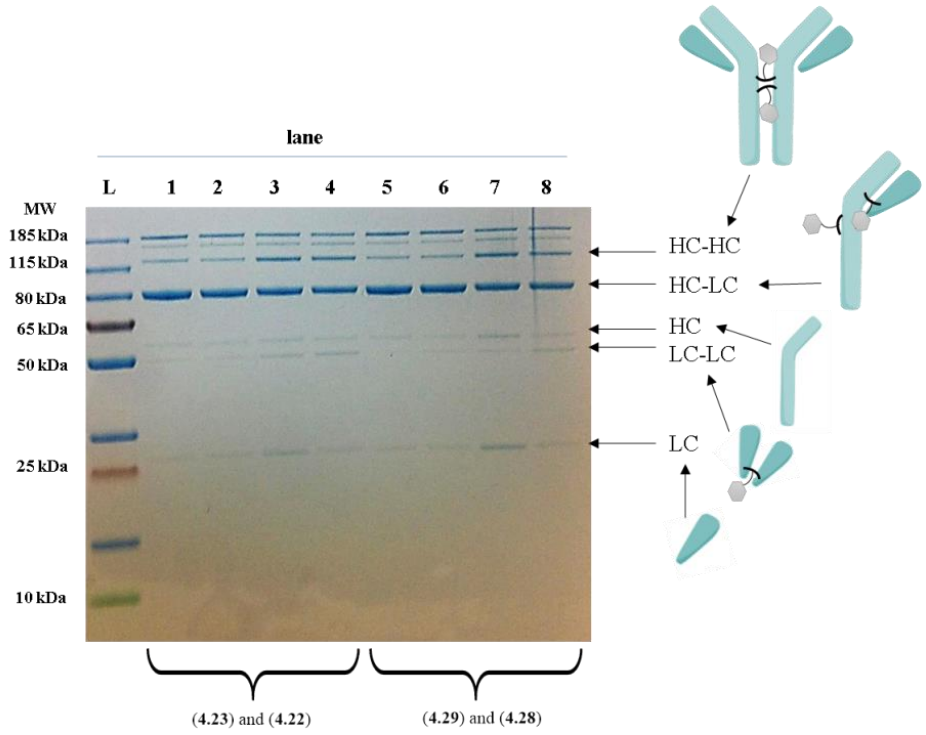

Figure 5.6. SDS-PAGE analysis of cross-linking of fully reduced Tmab (5.0 mg/ml, 34 µM) in Tris.HCl buffer (100 mM, pH 7.5) containing 150 mM NaCl, and 5 mM EDTA ,with bis-bromoacetamide linkers. Tmab was reduced with 5 equiv. of TCEP **2.2** (170 µM) for 2 h at room temperature and incubated with 5 (17 µM) or 8 equiv. (27.2 µM) of each linker. L: protein ladder, lane 1: Tmab incubated with 5 equiv. of methyl 3,4-bis(2-bromoacetamido)benzoate (**4.23**), lane 2: Tmab incubated with 8 equiv. of methyl 3,4-bis(2-bromoacetamido)benzoate (**4.23**), lane 3: Tmab incubated with 5 equiv. of methyl 3,5-bis(2-bromoacetamido)benzoate (**4.22**), lane 4: Tmab incubated with 8 equiv. of methyl 3,5-bis(2-bromoacetamido)benzoate (**4.22**), lane 5: Tmab incubated with 5 equiv. of *N*,*N*'-(1,2-phenylene)bis(2-bromoacetamide) (**4.29**), lane 6: Tmab incubated with 8 equiv. of *N*,*N*'-(1,2-phenylene)bis(2-bromoacetamide) (**4.29**), lane 7: Tmab incubated with 5 equiv. of *N*,*N*'-(1,3-phenylene)bis(2-bromoacetamide) (**4.28**), lane 8: Tmab incubated with 8 equiv. of *N*,*N*'-(1,3-phenylene)bis(2-bromoacetamide) (**4.28**). HC: heavy chain, LC: light chain, LC-LC: light chain homodimers, HC-HC: heavy chain homodimers. Protein samples were resolved by reducing SDS-PAGE (4-12% gel). Bands annotation is based on the protein MS results.

In order to have more thorough characterisation of the product obtained from Tmab cross-linking, reactions of methyl 3,4-bis(2-haloacetamido) benzoate (**4.23**) with Tmab was further analysed by protein MS.

MS of control Tmab (reduced) was first obtained, which showed the LC peak with a mass of 23,439.18 Da (Figure 5.7 A) and two peaks corresponds to the two main glycoforms of the HC with masses of 50,590.03 and 50,754.90 Da (Figure 5.7 B) with a difference of 161.87 Da, which represents N-glycosylation difference (extra galactose

sugar moiety). Tmab is IgG_1 mAb, which is glycosylated at C_{H2} domain of Fc region at Asn297 amino acid residues.[184]

According to MS results of rebridging reaction with **4.23** linker, the major cross-linked product of Tmab is a half-antibody with 2 linkers attached. The only possible explanation for the observed molecular weight is that the linker has rebridged both the inter-chain heavy-light disulfide and intra-chain heavy-heavy disulfide bonds (Figure 5.8 A). The expected mass of two cross-linked disulfide is calculated as 74,524.49 Da, and was observed at 74,528.03 Da (Figure 5.8).

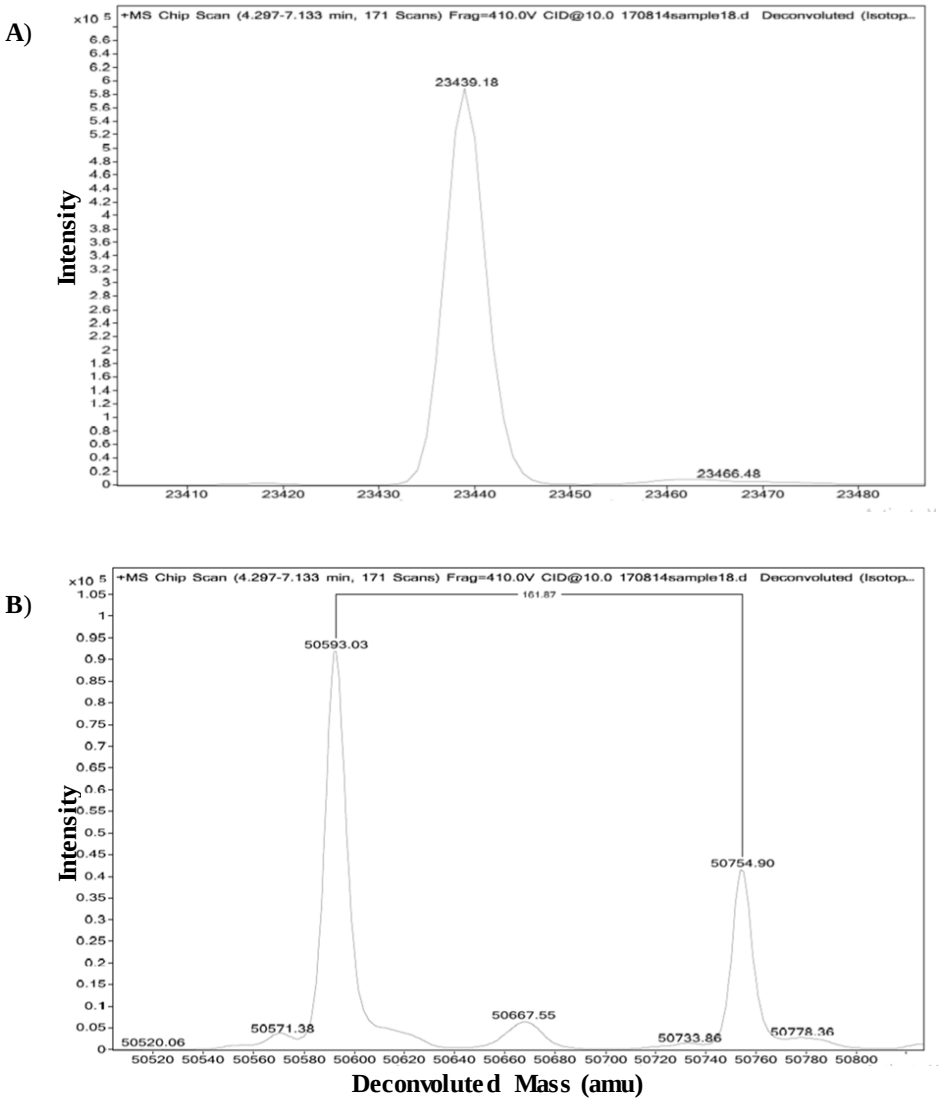

Figure 5.7. Deconvoluted protein MS spectra of Tmab. **A**) Control MS spectrum of Tmab light chain. Showing a peak at 23,439.18. **B**) Control MS spectrum of Tmab heavy chain showing two peaks at 50,593.03 and 50754.90 Da.

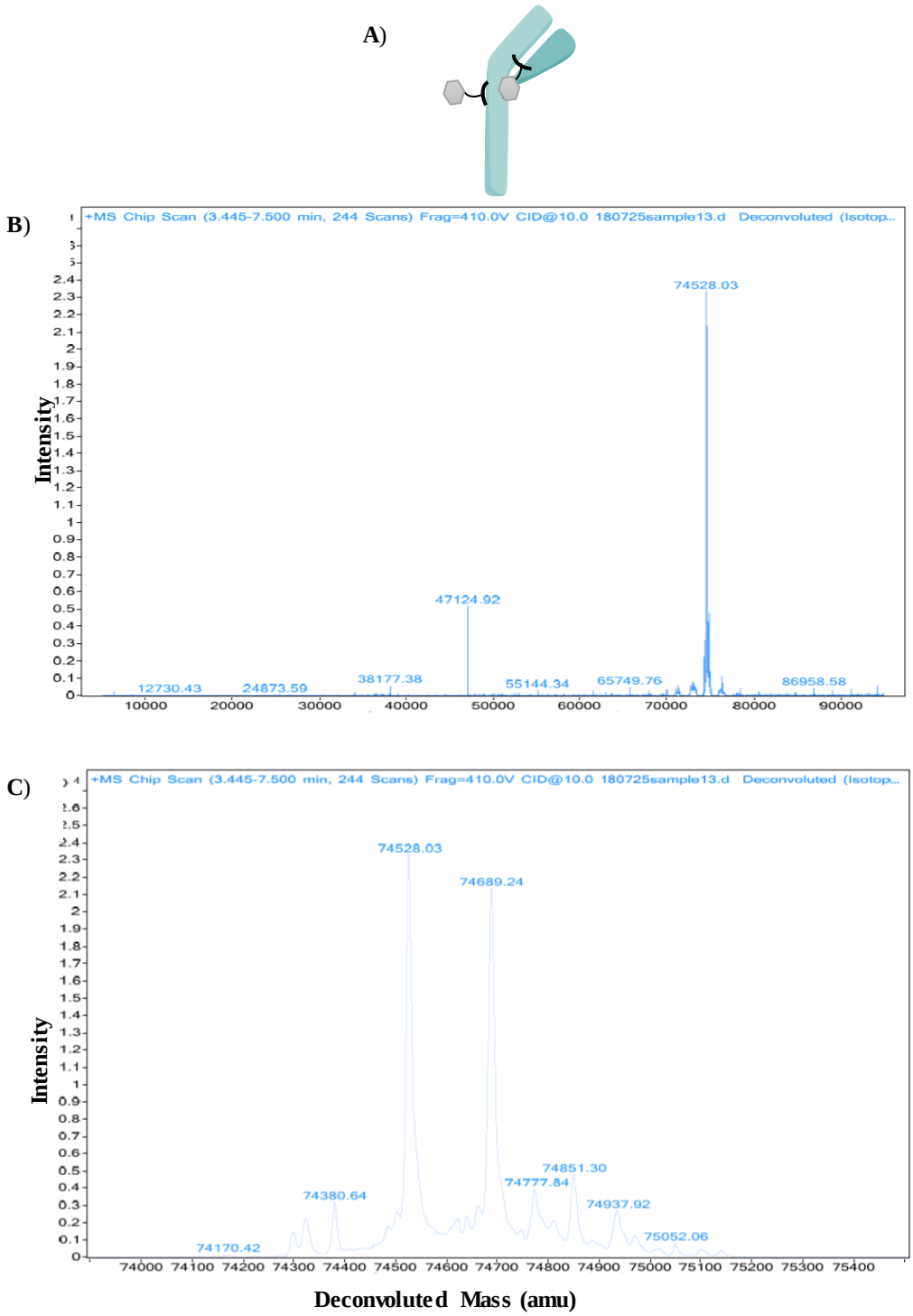

Figure 5.8. A) Schematic representation of the produced half antibody with two rebridged disulfide bonds, intra-chain heavy-heavy and heavy-light chains. **B)** Deconvoluted spectrum protein MS of Tmab. Full spectrum of Tmab cross-linked with 4 equiv. of methyl 3,4-bis(2-bromoacetamido) benzoate (**4.23**) showing a major peak at 74,528.03 Da. **C**) Expansion of the spectrum at 74 kDa region showing major peaks at 74,528.03 Da and 74,689.24 Da.

According to MS results of rebridging reaction with **4.29** linker, the major cross-linked product of Tmab is a half-antibody with 2 linkers attached, which again implies that the linker **4.29** has rebridged both the inter-chain heavy-light disulfide and intra-chain heavy-heavy disulfide bonds. Thus, similar cross-linking results were obtained and half-antibody (75 kDa) is the major product. The expected mass of two cross-linked disulfide is calculated as 74,572.81 Da, and was observed at 74,572.57 Da (Figure 5.9).

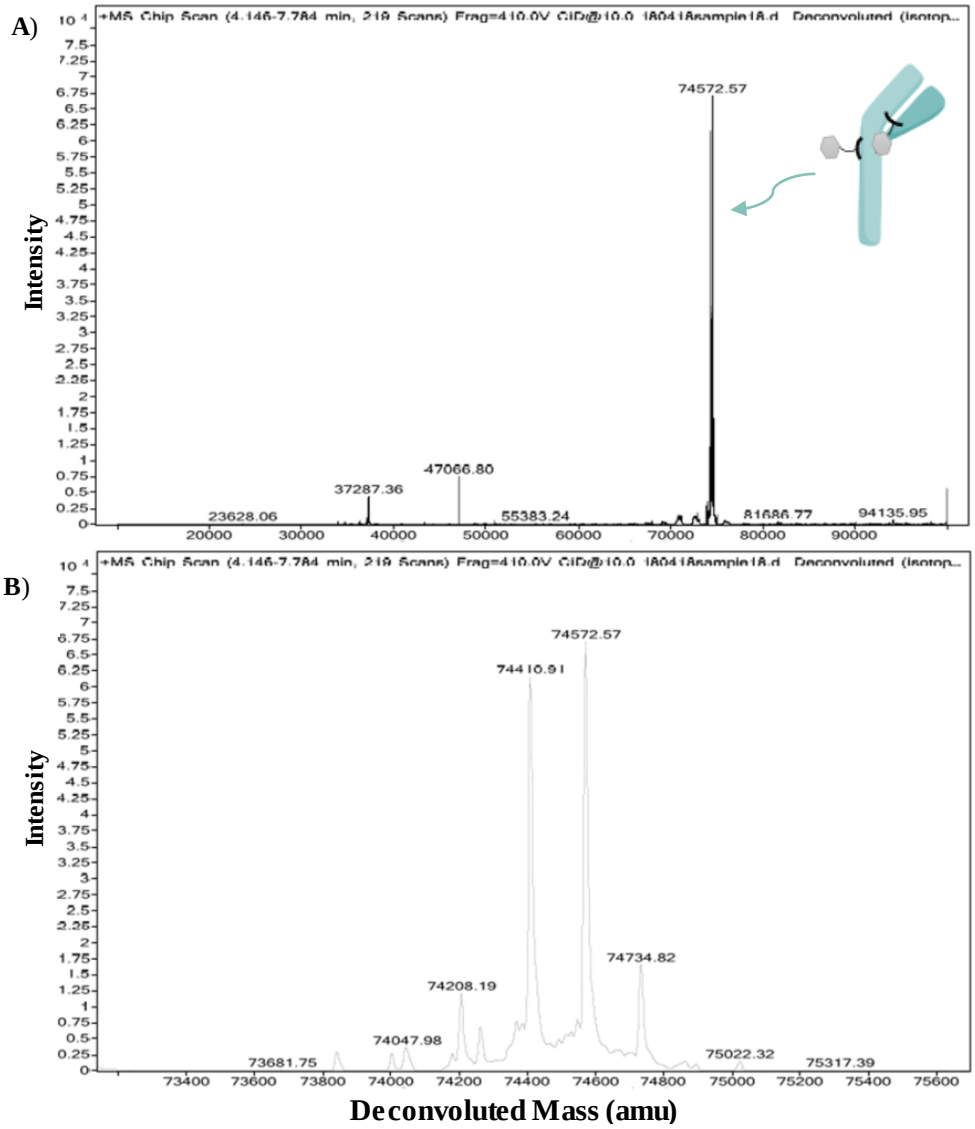

Figure 5.9. Deconvoluted spectrum protein MS of cross-linked Tmab with *N*,*N*'-(1,2-phenylene)bis(2-bromoacetamide) (**4.29**). **A**) Full view MS spectrum of cross-linked Tmab showing a major peak at 74,572.57 Da. **B**) Expansion of the spectrum at 74 kDa region showing major peaks at 74,572.57 Da and 74,410.91 Da.

Rebridging of fully reduced Tmab can result either in fully cross-linked Tmab (inter-chain bridges between heavy chains) or half-antibody (intra-chain bridges between heavy chains). Construction of half-antibody species (75 kDa) with bis-haloacetamide linkers is due to the preference of formation of intra-chain bridges.

To the best of our knowledge, bis-haloacetamide linkers react differently with fully reduced mAb (the four disulfide bonds) in comparison to next generation maleimide linkers mainly, dibromomaleimide (**4b**). Nevertheless, **4b** reagent produced fully bridged mAb (150 kDa) as a major product, but it has also produced minor proportion of half-antibody, the so-called disulfide bond shuffling as described by Schumacher *et al.* They proposed *in situ* protocol of conjugation to avoid disulfide bond shuffling.[185] Also, Lee *et al.* proposed using di-TCEP-substituted dithiophenolpyridazinedione compound (**4e**) to minimize disulfide shuffling (intra-disulfide cross linking).[156]

For detailed comparison between different linkers in this discussion, we are using both ortho- and meta-substituted linkers acronyms to refer to the regiochemistry of the two α-haloacetamide groups relative to each other, regardless of the aryl substituent.

Compared to ortho-substituted linker, both meta-substituted linkers, methyl 3,5-bis(2-bromoacetamido)benzoate (**4.22**) (Figure 5.6, lane 3-4) and *N*,*N*'-(1,3-phenylene)bis(2-bromoacetamide) (**4.28**) (Figure 5.6, lane 7-8) displayed higher proportion of cross-linked light- light chains and heavy-heavy chains as displayed as distinct bands around 100 kDa and 50 kDa revealed under reducing conditions. While ortho-substituted linkers, methyl 3,4-bis(2-bromoacetamido)benzoate (**4.23**) and *N*,*N*'-(1,2-phenylene)bis(2-bromoacetamide) (**4.29**) showed more selective rebridging of heavy-light and intra-heavy heavy disulfide bonds with very minor proportion of cross-linked light-light chains and heavy-heavy chains. As observed by both the SDS-PAGE analysis and protein MS.

At this stage we sought to evaluate whether the reaction pH is influencing the observed preference of the bis-haloacetamide linkers to form intra-chain heavy-heavy cross-linking. As such, Tmab (5 mg/mL) in conjugation Tris.HCl buffer (100 mM, 150 mM NaCl, 5 mM EDTA, pH 6, 7.5, or 8) was reduced by incubation with TCEP **2.2** (5

equiv.). Tmab was incubated with 5 equiv. of each bis-bromoacetamide linkers (**4.22**, **4.23**, **4.28** and **4.29**) and held at room temperature overnight.

Resolving of the reaction products by SDS-PAGE revealed that changing the pH has showed similar reaction products to those previously observed at pH 7.5. The cross-linked half-antibody product at pH 6 and 8 was the major observed product (Figure 5.10).

However, as the percentage of conversion to half-antibody product (HC-LC) at pH 7.5 was the highest with lower proportion of unreacted heavy and light chains compared with the other pHs, this pH was considered the optimum to carry rebridging experiments at (Figure 5.10, lane 5-8).

It is expected to have higher availability of thiolate anion at more basic pH (pKa of thiolate is 8.3), however, the possible explanation of the reduced the efficiency of the cross-linking (higher proportion of unreacted HC and LC were observed under reducing conditions) is the reduced aqueous stability of the bis-haloacetamide linkers at alkaline conditions (Figure 5.10, lane 9-12). On the other hand, working under relative acidic conditions, have shown less optimum results, which can be attributed to the lower availability of thiolate anion at this pH (pKa of thiolate is 8.3)[186] (Figure 5.10, lane 1-4).

It is worth pointing out that the observed preference of the reactivity of meta-substituted and ortho-substituted likers have not changed at more acidic or basic conditions. Ortho-substituted likers gave lower fraction of the cross-linked inter-heavy-heavy and light-light chains (Figure 5.10, lanes 1, 3, 5, 7, 9 and 11).

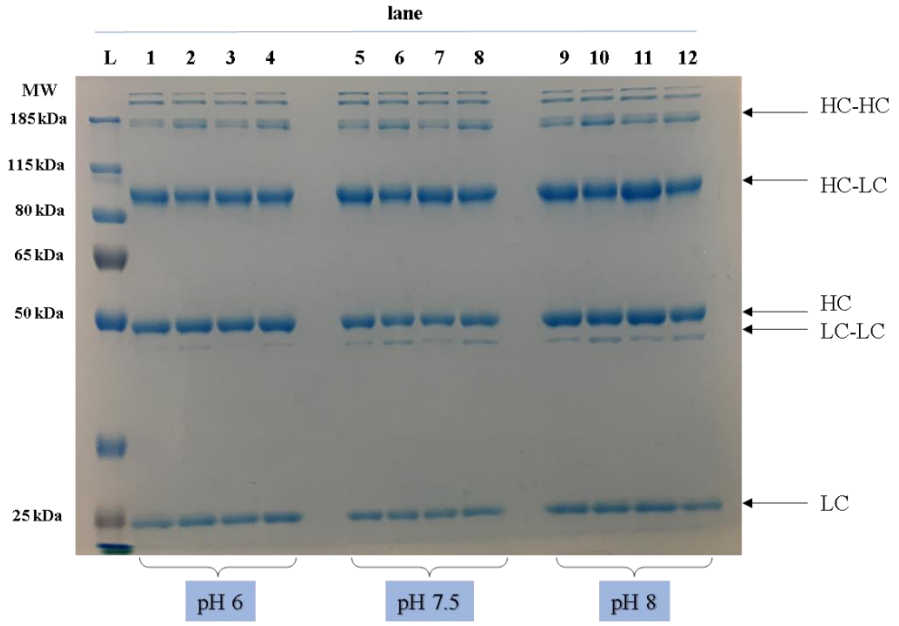

Figure 5.10. SDS-PAGE analysis of cross-linking of fully reduced Tmab (5.0 mg/ml, 34 µM) in Tris.HCl buffer (100 mM, 150 mM NaCl, 5mM EDTA, pH 6, 7.5, or 8) incubated with bis-haloacetamide linkers. Tmab (34 µM) was reduced with 5 equiv. of TCEP (170 µM) for 2 h at room temperature and incubated with (17 µM, 5 equiv.) of each linker. Lane 1, 5 and 9: Tmab incubated with 5 equiv. of methyl 3,4-bis(2-bromoacetamido)benzoate (**4.23**), Lane 2, 6 and 10: Tmab incubated with 5 equiv. of methyl 3,5-bis(2-bromoacetamido)benzoate (**4.22**), Lane 3, 7 and 11: Tmab incubated with 5 equiv. of *N*,*N*'-(1,2-phenylene)bis(2-bromoacetamide) (**4.29**), Lane 4, 8 and 12: Tmab incubated with 5 equiv. of *N*,*N*'-(1,3-phenylene)bis(2-bromoacetamide) (**4.28**). HC: heavy chain, LC: light chain, LC-LC: light chain homodimers, HC-HC: heavy chain homodimers. Protein samples were resolved by reducing SDS-PAGE (10% gel).

With optimized reduction and cross-linking conditions (5 equiv. TCEP for 2 h, 5 equiv. of bis-bomoacetamide linkers overnight at pH 7.5), we intended to compare the efficiency of bis-iodoacetamide linkers in the rebridging of reduced disulfide bonds of Tmab and investigate whether they would display different products of reaction.

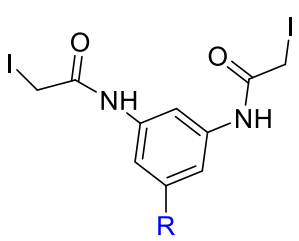

R = COOMe (**4.24**)
R = H (**4.30**)

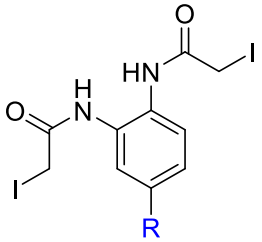

R = COOMe (**4.25**)
R = H (**4.31**)

As such, Tmab (5 mg/mL) in Tris.HCl (100 mM, 150 mM NaCl, 5 mM EDTA, pH 7.5) was reduced by incubation with TCEP **2.2** (5 equiv.) for 2 h at room temperature. The reduced Tmab was incubated with 5 equivalents of each bis-iodoacetamide linker (**4.24**, **4.25**, **4.30** and **4.31**) and held at room temperature overnight. The reaction products were then revealed by SDS-PAGE.

Similar results were observed with the iodo-acetamide linkers to those observed with their bromo analogues. The major product of cross-linking of Tmab with bis-iodoacetamide linkers is half-antibody (Figure 5.11). In similar manner to the corresponding bis-bromoacetamides, meta-substituted linkers, methyl 3,5-bis(2-iodoacetamido)benzoate (**4.24**) (Figure 5.11, lane 4) and *N*,*N*'-(1,3-phenylene)bis(2-iodooacetamide) (**4.30**) (Figure 5.11, lane 6), displayed higher proportion of light-light chain and heavy-heavy chain homodimers when compared with the ortho-substituted linkers **4.25** and **4.31** (Figure 5.11, lane 3 and 5).

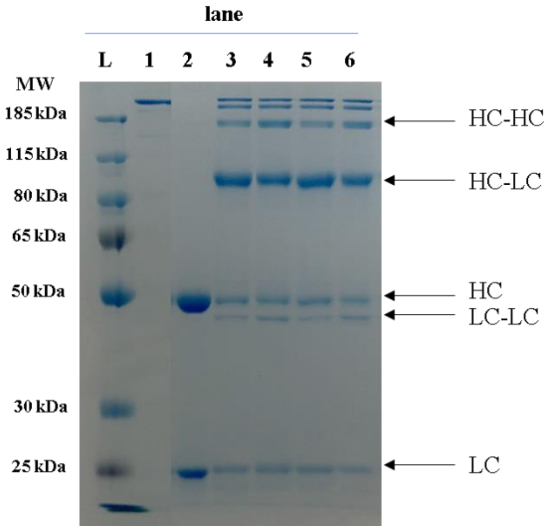

Figure 5.11. SDS-PAGE of cross-linking of fully reduced Tmab (5 mg/ml, 34 µM) in Tris.HCl buffer (100 mM, pH 7.5) containing 150 mM NaCl, and 5 mM EDTA, with bis-iodoacetamide linkers. Tmab was reduced with 5 equiv. of TCEP **2.2** (170 µM) for 2 h at room temperature and incubated with (17 µM, 5 equiv.) of each linker. L: protein ladder, lane 1: Tmab control (Non-reducing dye), lane 2: Tmab control (reducing dye), lane 3: Tmab incubated with 5 equiv. of methyl 3,4-bis(2-iodooacetamido)benzoate (**4.25**), Lane 4: Tmab incubated with 5 equiv. of methyl 3,5-bis(2-iodoacetamido)benzoate (**4.24**), Lane 5: Tmab incubated with 5 equiv. of N,N'-(1,2-phenylene)bis(2-iodoacetamide) (**4.31**), Lane 6: Tmab incubated with 5 equiv. of N,N'-(1,3-phenylene)bis(2-bromoacetamide) (**4.30**). HC: heavy chain, LC: light chain, LC-LC: light chain homodimers, HC-HC: heavy chain homodimers. Protein samples were resolved by reducing SDS-PAGE (10% gel).

With the encouraging and consistent rebridging results observed with the tested bis-haloacetamide linkers, the produced fully rebridged half antibody (75 kDa) offers a number of advantages over intact antibody, most importantly the smaller size and better tissue penetration, which could find interesting new applications in the oncology field (see Chapter 9). Moreover, the reproducibility and good rebridging capabilities of aryl bis-haloacetamide linkers have promoted us to evaluate them as a promising rebridging approach (the following Sections).

5.4 Disulfide bond rebridging of Trastuzumab with azide modified bis-haloacetamide linkers 4.32-4.35

Having established suitable conditions for the disulfide rebridging of Tmab using model bis-haloacetamide linkers, we now wanted to investigate the reactivity of bis-haloacetamide linkers functionalised with bio-orthogonal chemistries, which are suitable for cross-coupling reactions, such as the 'Click' reaction.

As such, we sought to appraise the efficiency of the azide derivatised bis-haloacetamide linkers **4.32-4.35** in rebridging reduced disulfide bonds. First, Tmab (5 mg/mL) in conjugation buffer Tris.HCl (100 mM, pH 7.5) containing 150 mM NaCl, and 5 mM EDTA, was reduced by incubation with TCEP **2.2** (5 equiv.) for 2 h at room temperature. The reduced Tmab was incubated with 5 equiv. of each of the azide derivatised bis-haloacetamide linkers **4.32-4.35** and held at room temperature overnight. The reaction products were then resolved separately using SDS-PAGE (Figure 5.12 A), as described previously.

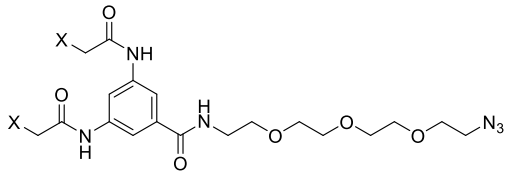

X = Br (4.32)
X = I (4.33)

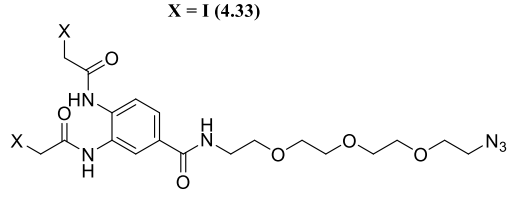

X = Br (4.34)
X = I (4.35)

One can note that the major product of cross-linking is again the half-antibody (HC-LC) (Figure 5.12 A). Moreover, in a similar manner to the corresponding bis-bromoacetamides (**4.22**, **4.23**, **4.28** and **4.29**), ortho-substituted linkers *N*,*N*'-(4-((2-(2-(2-(2-azidoethoxy)ethoxy)ethoxy)ethyl)carbamoyl)-1,2-phenylene)bis(2-haloacetamide) (**4.34-4.35**) showed superior rebridging of inter-chain heavy-light disulfide bonds (half-antibody) with only minor light-light chain and heavy-heavy chain homodimer formation (Figure 5.12 A, lane 1 and 3).

In order to further characterise the products obtained from Tmab cross-linking with *N*,*N*'-(4-((2-(2-(2-(2-azidoethoxy)ethoxy)ethoxy)ethyl)carbamoyl)-1,2-phenylene)bis(2-iodoacetamide) (**4.35**) linker, the reaction was analysed by protein MS. The expected mass of two rebridged disulfide bonds (intra heavy-heavy and inter heavy-light disulfide bonds) is calculated as 75,060.46 Da and was observed as 75,059.82 Da (Figure 5.12 B).

The obtained results suggested a high efficiency for our azide derivatised bis-haloacetamide linkers in rebridging the reduced disulfide bonds of Tmab. Therefore, these linkers provide azide-functionalised Tmab (Tmab-azide) that could be applied in 'Click' reactions (azide-octyne cycloaddition reactions).

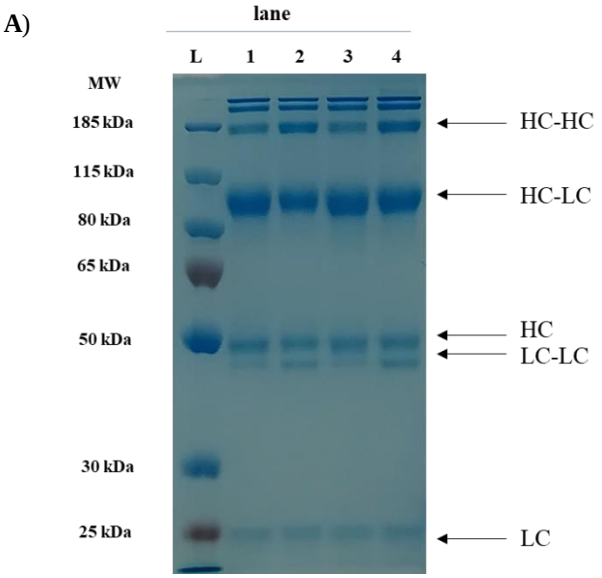

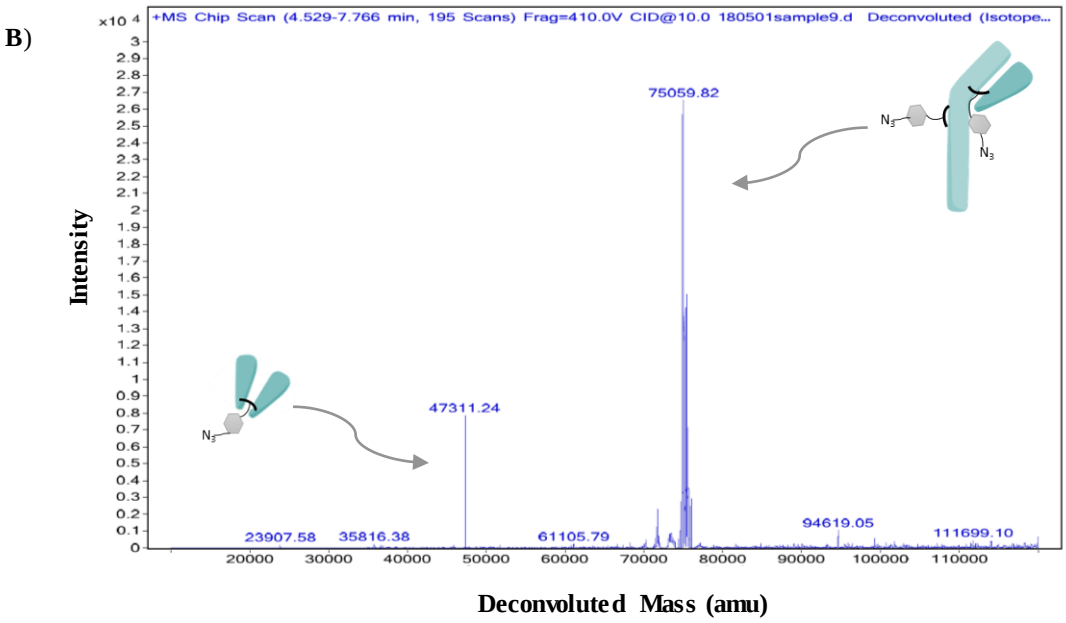

Figure 5.12. A) SDS-PAGE analysis of cross-linking of reduced Tmab (5 mg/ml, 34 µM) in Tris.HCl buffer (100 mM, pH 7.5) containing 150 mM NaCl, and 5 mM EDTA with 5 equiv. of TCEP (150 µM) for 2 h at room temperature and incubated with (17 µM, 5 equiv.) of each linker overnight. L: ladder, lane 1: Tmab incubated with 5 equiv. of **4.34**, lane 2: Tmab incubated with 5 equiv. of **4.32**, lane 3: Tmab incubated with 5 equiv. of **4.35**, lane 4: Tmab incubated with 5 equiv. of **4.33** at room temperature overnight. **B**) Deconvoluted spectrum protein MS of rebridged Tmab with **4.35** linker showing a major peak at 75,059.82 Da.

5.5 Disulfide bond rebridging of partially reduced Trastuzumab

Having established the efficiency of bis-haloacetamide linkers in rebridging fully reduced Tmab to produce a new class of rebridged half antibody, we sought next to

evaluate the utility of employing our bis-haloacetamide linkers in selectively cross-linking only heavy-light disulfide bonds. By capping only heavy-light disulfide bonds initially, we might be subsequently able to introduce a different functionality through rebridging heavy-heavy disulfide bonds using a different bis-haloacetamide linker (this will be further discussed in Section 5.8).

As discussed earlier in Section 5.2, we established the necessary reduction conditions for TCEP to selectively reduce heavy-light disulfide bonds with minimum reduction of heavy-heavy disulfide binds (lower equivalents of TCEP, 2h at 4°C).

As such, two protocols were evaluated to construct the rebridged heavy-light chains of Tmab: A direct *in situ* reduction method and a portion-wise reduction method (Figure 5.13).

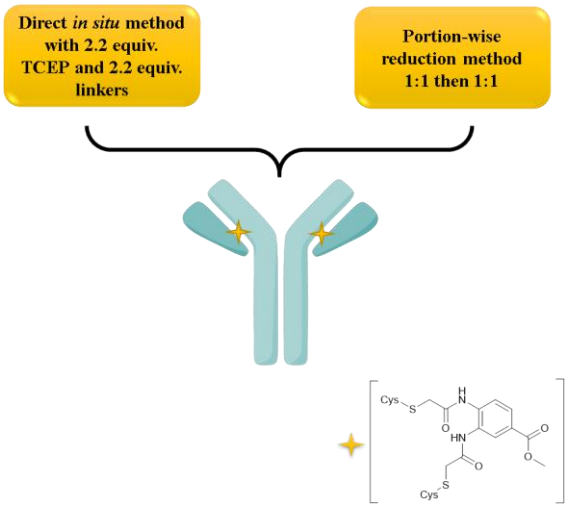

Figure 5.13. The two methods investigated to attain rebridged heavy-light chains of Tmab (cross-linked heavy-light disulfide bonds).

Initially we sought to evaluate the direct reduction method. As such, Tmab (5 mg/mL, 0.034 µmol) in Tris.HCl buffer (100 mM, pH 7.5) containing 150 mM NaCl, and 5 mM EDTA, was reduced with TCEP **2.2** (2.2 equiv.) for 2 h at 4°C. The reduced protein was then incubated with 2.2 equiv. of bis-bromoacetamide linkers (**4.22**, **4.23**, **4.28** and **4.29**). The reaction products were resolved by using SDS-PAGE analysis.

None of the linkers evaluated showed complete rebridging of heavy-light disulfide bonds, as confirmed by the presence of unreacted heavy and light chains (under reducing gel conditions). The ortho-substituted linkers methyl 3,4-bis(2-bromoacetamido)benzoate (**4.23**) (Figure 5.14, lane 5) and *N*,*N*'-(1,2-phenylene)bis(2-bromoacetamide) (**4.29**) (Figure 5.14, lane 7) displayed higher conjugation yields in comparison to the meta-substituted linkers **4.22** and **4.28**. These latter linkers (meta-linkers) displayed higher amount of light-light chain and inter-heavy-heavy chain cross-linking in line with what was observed earlier.

The incomplete rebridging of the reduced heavy-light disulfide bonds we observed with bis-bromoacetamide linkers could possibly be attributed to the incomplete reduction of heavy-light disulfide bonds as observed before with TCEP reduction of Tmab (see Figure 5.4).

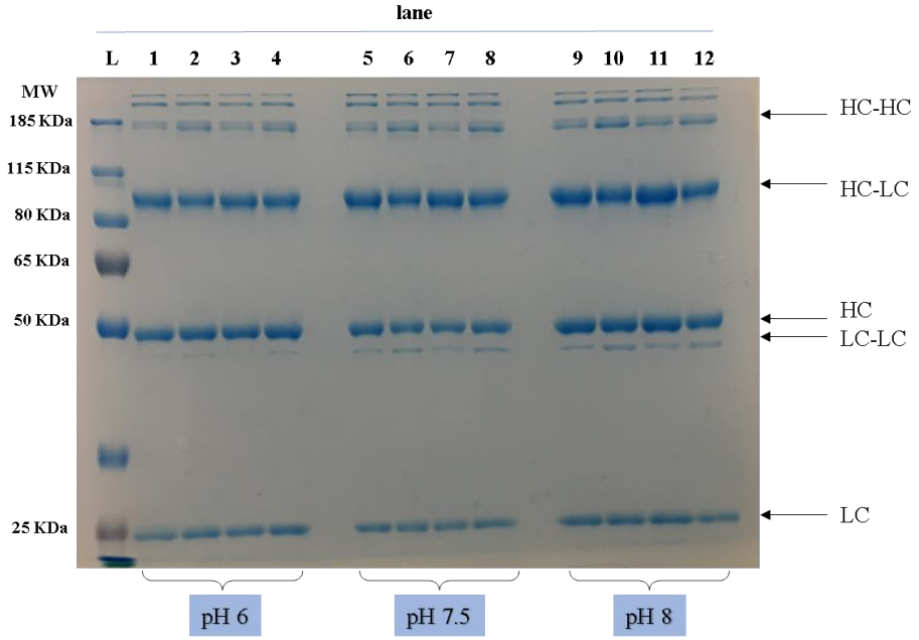

Figure 5.14. SDS-PAGE of analysis of partially reduced Tmab (5 mg/mL, 34 µM) cross-linking in Tris.HCl buffer (100 mM, 150 mM NaCl, 5 mM EDTA, pH 6, 7.5, or 8) with bis-bromoacetamide linkers (7.5 µM) using direct method. Tmab (34 µM) was reduced with 2.2 equiv. of TCEP (75 µM) for 2 h and incubated with (7.5 µM) of each linker at room temperature overnight. L: ladder, lane 1, 5 and 9: Tmab incubated with 2.2 equiv. of methyl 3,4-bis(2-bromoacetamido)benzoate (**4.23**), lane 2, 6 and 10: Tmab incubated with 2.2 equiv. of methyl 3,5-bis(2-bromoacetamido)benzoate (**4.22**), lane 3, 7 and 11: Tmab incubated with 2.2 equiv. of *N*,*N*'-(1,2-phenylene)bis(2-bromoacetamide) (**4.29**), lane 4, 8 and 12: Tmab incubated with 2.2 equiv. of *N*,*N*'-(1,3-phenylene)bis(2-bromoacetamide) (**4.28**). Protein samples were resolved by reducing SDS-PAGE (10% gel).

In an attempt to evaluate if the pH of the reaction might influence the reaction products, the protocol was evaluated at two other pHs, 6 and 8. Neither of the these pHs resulted in improved rebridging, as pH 7.5 was optimum for rebridging heavy-light disulfide bonds as the cross-linked HC-LC band was observed as the major product (Figure 5.14, lane 5-8). Consistent with what we observed earlier, a higher degree of unreacted (non-linked) heavy and light chains were still observed at pH 6 and 8) (Figure 5.14, lane 1-4 and 9-12).

Next, in order to improve the yield of the rebridged heavy-light chains product, we rationalised that using portion-wise reduction followed by the sequential cross-linking would mitigate the non-selective reduction of heavy-heavy disulfide bonds and afford higher conjugation yield of heavy-light disulfide bonds, through a reduction in the number of unpaired inter-chain disulfide bonds present at any given time.

As such, Tmab (5 mg/mL, 0.033 μmol) in Tris.HCl buffer (100 mM, pH 7.5) containing NaCl (150 mM), and EDTA (5 mM), was initially reduced by incubation with TCEP **2.2** (1 equiv.) for 2 h at 4°C. 1 equiv. of bis-bromoacetamide linkers was added then to the reduced protein and held at room temperature overnight. Then, a second reduction step with TCEP (1 equiv.) for 2 h at 4°C was performed prior to incubation with the bis-bromoacetamide linkers (1 equiv.) at room temperature overnight. The reaction products following both the first and second rebridging steps were the resolved using SDS-PAGE.

To our delight, optimum rebridging results of first heavy-light inter chain disulfide bonds of Tmab were obtained (Figure 5.15, lane 1-4), as almost equal band intensity of HC and HC-LC was observed, mainly with ortho-substituted linkers (Figure 5.15, lane 1 and 4).

However, the second reduction and rebridging step has not displayed as optimum results as the first reduction and rebridging step as non-reacted HC and LC bands were observed (Figure 5.15, lane 5-8), which possibly reflects the minor non-selective reduction of heavy-heavy disulfide bonds followed by rebridging of intra and inter-chain disulfide bonds of heavy chain.

To confirm this suggestion, the sample were resolving under non-reducing gel conditions, where the presence of half-antibody (HC-LC) and heavy-heavy (HC-HC) bands represent the rebridging of intra- and inter-chains heavy-heavy disulfide bonds, respectively (Figure 5.15, lane 9-12), therefore confirming our assumption regarding the minor and non-selective reduction of heavy-heavy disulfide bonds.

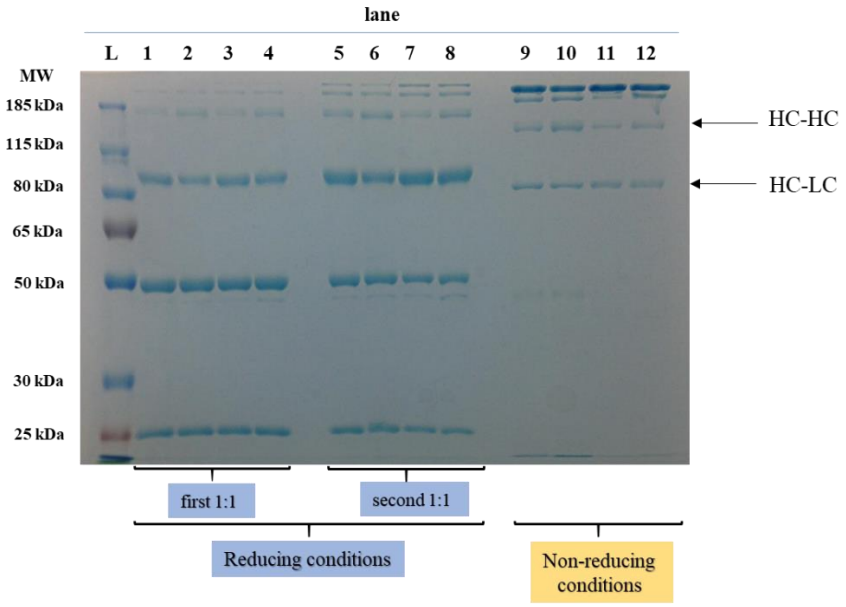

Figure 5.15. SDS-PAGE of partially reduced Tmab (5 mg/mL, 34 µM) cross-linking in Tris.HCl buffer (100 mM, pH 7.5) containing 150 mM NaCl, and 5 mM EDTA, with bis-bromoacetamide linkers using portion-wise method. Tmab (5 mg/mL, 34 µM) was reduced with 1 equiv. of TCEP (34 µM) for 2 h and incubated with 1 equiv. of bis-bromoacetamide linkers (3.4 µM) at room temperature overnight (Lane 1-4). Lane 1: Tmab incubated with 1 equiv. of methyl 3,4-bis(2-bromoacetamido)benzoate (**4.23**), Lane 2: Tmab incubated with 1 equiv. of methyl 3,5-bis(2-bromoacetamido)benzoate (**4.22**), Lane 3: Tmab incubated with 1 equiv. of *N*,*N*'-(1,2-phenylene)bis(2-bromoacetamide) (**4.29**), Lane 4: Tmab incubated with 1 equiv. of *N*,*N*'-(1,3-phenylene)bis(2-bromoacetamide) (**4.28**). Tmab was further reduced with 1 equiv. of TCEP (34 µM) for 2 h and incubated with 1 equiv. of bis-bromoacetamide linkers (3.4 µM) at room temperature overnight (Lane 5-8) in same order of lane 1-4. Lane (9-12): same samples as in lane 5-8 under non-reducing conditions.

In order to more thoroughly characterise the product obtained from the cross-linking, reaction of methyl 3,5-bis(2-bromoacetamido)benzoate **4.22** (2.2 equiv.) using the direct method was further analysed by protein MS. According to MS results, the major cross-linked product of Tmab is the half-antibody with one linker rebridging the inter-chain heavy-light disulfide bond. The expected mass of Tmab with a rebridged heavy-light disulfide bonds is calculated as 74,277.60 Da and was observed at 74,277.53 Da (Figure 5.16).

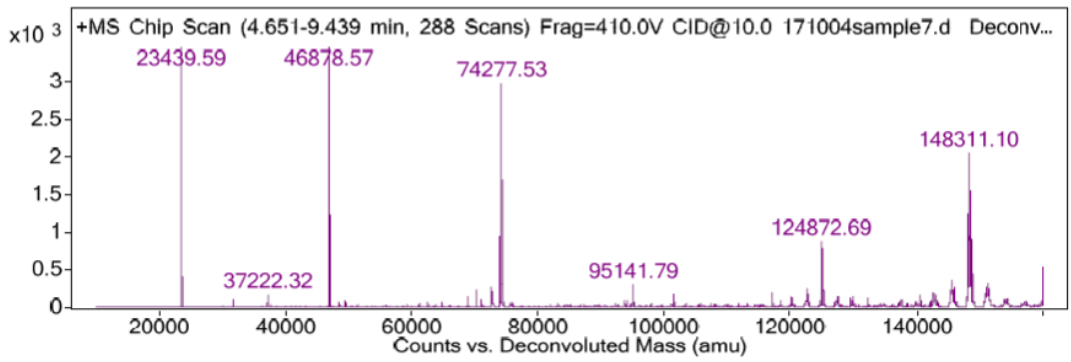

Figure 5.16. Deconvoluted spectrum protein MS of cross-linked Tmab with 2.2 equiv. methyl 3,5-bis(2-bromoacetamido)benzoate (**4.22**). Full view MS spectrum of cross-linked Tmab showing a peak at 74,277.53 Da corresponds to rebridged heavy-light chains of Tmab.

In conclusion, provided that both methods evaluated showed comparable rebridging of the heavy-light disulfide bonds, the first direct *in situ* protocol is more manageable and easier to follow. The cross-linked heavy-light disulfide bonds of Tmab can be further used to produce bifunctional azide-linked Tmab (Section 5.8).

5.6 Selectivity of bis-haloacetamide linkers towards cross-linking heavy-heavy and heavy-light disulfide bonds

From the previously observed rebridging results of fully and partially reduced Tmab using bis-haloacetamide linkers, a different rebridging manner was observed especially with meta-substituted linkers where they tend to cross-link the inter-chain heavy–heavy disulfide bonds and light-light chains forming homo-dimers as a minor reaction products.

To evaluate the selectivity difference of reaction towards the reduced inter-chain disulfide bonds between ortho- and meta-substituted bis-haloacetamides linkers, all of the four inter-chain disulfide bonds of Tmab were reduced prior to incubation with limited equivalents of bis-haloacetamide each linker (2 equivalents).

As such, Tmab (5 mg/mL) in Tris.HCl buffer (100 mM, pH 7.5) containing 150 mM NaCl, and 5 mM EDTA, was reduced by incubation with TCEP (4 equiv.) for 2 h at room temperature. The reduced Tmab was then incubated

with 2 equiv. of each bis-bromoacetamide linker and held at room temperature overnight. The reaction products were resolved using SDS-PAGE analysis.

The ortho-substituted methyl 3,4-bis(2-bromoacetamido)benzoate (**4.23**), and *N*,*N*'-(1,2-phenylene)bis(2-bromoacetamide) (**4.29**) were observed to display a higher selectivity towards rebridging heavy-light disulfide bonds (Figure 5.17 A, lane 3 and 5). On the other hand, the meta-substituted methyl 3,5-bis(2-bromoacetamido)benzoate (**4.22**) and *N*,*N*'-(1,3-phenylene)bis(2-bromoacetamide) (**4.28**) have showed less selectivity towards cross-linking heavy-light disulfide bonds, and higher proportion of rebridged heavy-heavy disulfide bonds (Figure 5.17 A, lane 4 and 6).

Percent conversion to each product was calculated using Gel Image studio 5.2 to estimate the percent conversion of Tmab into each product [inter-chain heavy-heavy (100 kDa), or inter-chain heavy-light (75 kDa)]. Clearly, the ester derivatised methyl 3,4-bis(2-bromoacetamido)benzoate (**4.23**) had higher percentage of half antibody (20%) in comparison to methyl 3,5-bis(2-bromoacetamido)benzoate (**4.22**) (10%) (Figure 5.17 B). On the other hand, unsubstituted bromo-linkers **4.28** and **4.29** did not display a clear selectivity manner towards the reduced disulfide bonds (Figure 5.17 B).

Similar experiment was repeated with bis-iodoacetamide linkers to evaluate their selectivity towards rebridging the reduced disulfide bonds of Tmab. Fully reduced Tmab was incubated with only 2 equivalents of each bis-iodoacetamide linker (**4.24**, **4.25**, **4.30**, **4.31, 4.33 and 4.35**) and held at room temperature overnight. The reaction products were resolved using SDS-PAGE analysis. Bis-iodoacetamide linkers (**4.24**, **4.25**, **4.30**, and **4.31**) did not, however, display analogous pattern of selectivity toward the reduced disulfide bonds (Figure 5.18, lane 1-4).

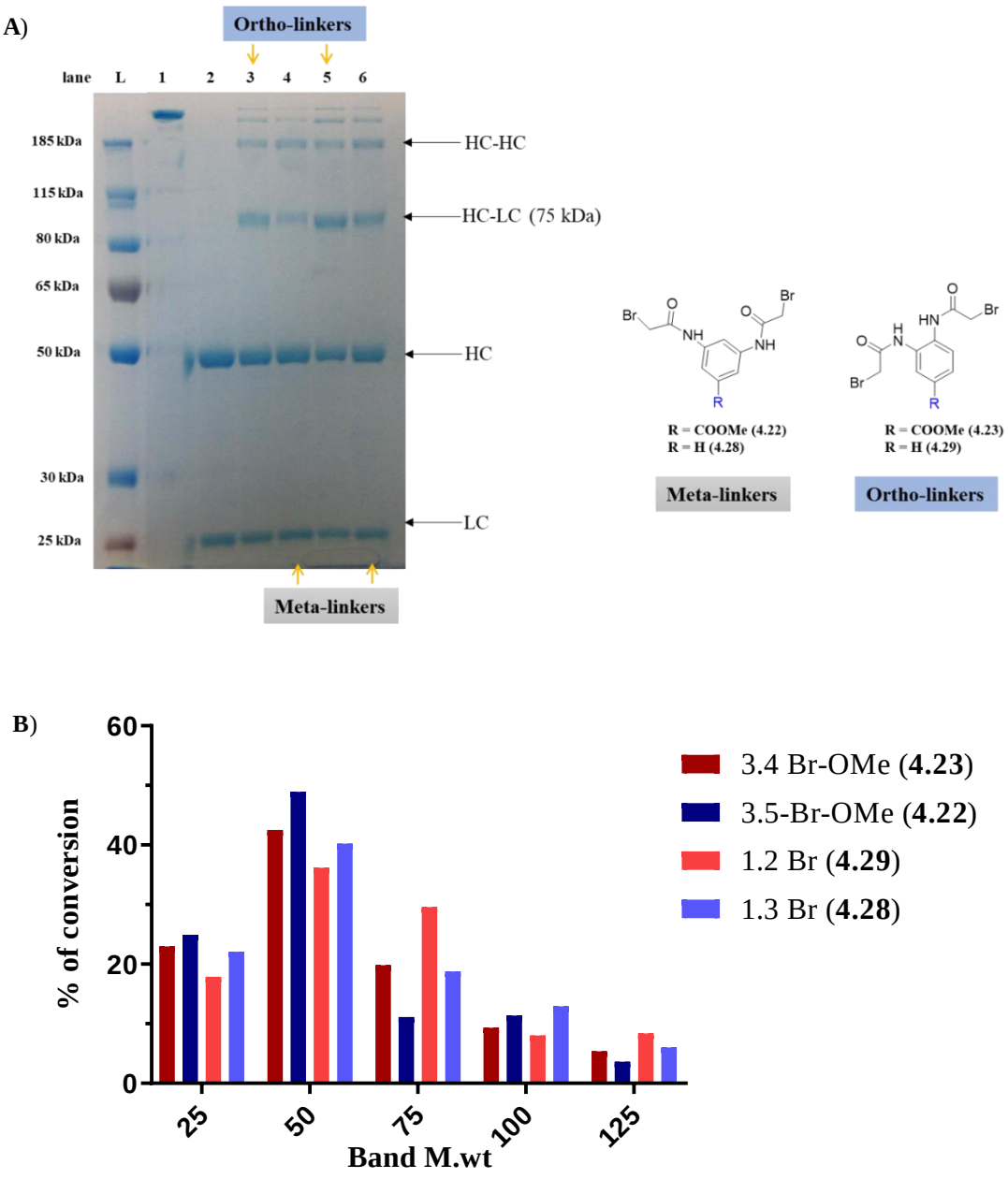

Figure 5.17. A) SDS-PAGE analysis representing the selectivity of bis-bromoacetamide linkers in cross-linking Tmab (5 mg/mL, 34 µM) in Tris.HCl buffer reduced with 4 equiv. of TCEP (136 µM) and incubated with (6.8 µM, 2 equiv.) of each bis-bromoacetamide linker at room temperature overnight. L: protein ladder, lane 1: Tmab control (non-reducing dye), Lane 2: Tmab control (reducing dye), Lane 3: Tmab incubated with 2 equiv. of methyl 3,4-bis(2-bromoacetamido)benzoate (**4.23**), Lane 4: Tmab incubated with 2 equiv. of methyl 3,5-bis(2-bromoacetamido)benzoate (**4.22**), Lane 5: Tmab incubated with 2 equiv. of *N*,*N*'-(1,2-phenylene)bis(2-bromoacetamide) (**4.29**), Lane 6: Tmab incubated with 2 equiv. of *N*,*N*'-(1,3-phenylene)bis(2-bromoacetamide) (**4.28**). Protein samples were resolved by reducing SDS-Page (10% gel). **B**) Percent conversion of Tmab into various cross-linked products analysed using Gel Image studio 5.2.

On the other hand, azide modified bis-iodoacetamide linkers (**4.33** and **4.35**) displayed an interesting manner of selectivity, as meta-substituted linker **4.33** (Figure 5.18, lane 5), displayed less fraction of rebridged heavy-light disulfide bonds in comparison with ortho-substituted linker **4.35** (Figure 5.18, lane 6), which prompted us to further analyse the reaction by MS to investigate the possibility for rebridging intra-chain heavy-heavy disulfide bonds.

As shown in Figure 5.19, expansion at the heavy chain region revealed that the major obtained product is cross-linked heavy chain with one linkers attached. The only possible explanation for the observed molecular weight is that the linker has rebridged the intra-chain heavy-heavy disulfide bonds, the expected masses of cross-linked heavy chain with one azide linker is calculated as 51,027.16 Da and 51,188.28 Da (glycoforms) and they were observed at 51,026.31 Da and 51,189.24 Da (Figure 5.19 B). In contrast, ortho- substituted linker **4.35** displayed lower ability in rebridging of the intra-chain heavy-heavy disulfide bonds (Figure 5.18, lane 6 and Figure 5.19 A).

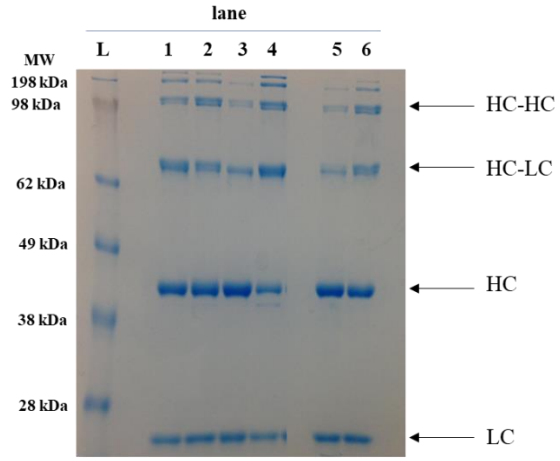

Figure 5.18. SDS-PAGE gel evaluating selectivity of bis-iodoacetamide linkers in cross-linking Tmab (5 mg/mL, 34 µM) in Tris.HCl buffer (100 mM, pH 7.5) containing 150 mM NaCl, and 5 mM EDTA, reduced with 4 equiv. of TCEP (136 µM) and incubated with (6.8 µM, 2 equiv.) of each bis-iodooacetamide linker at room temperature overnight. L: protein ladder, lane 1: Tmab incubated with 2 equiv. of methyl 3,4-bis(2-iodoacetamido)benzoate (**4.25**), lane 2: Tmab incubated with 2 equiv. of methyl 3,5-bis(2-iodoacetamido)benzoate (**4.24**), lane 3: Tmab incubated with 2 equiv. of *N*,*N*'-(1,2-phenylene)bis(2-iodoacetamide) (**4.31**), lane 4: Tmab incubated with 2 equiv. of *N*,*N*'-(1,3-phenylene)bis(2-iodoacetamide) (**4.30**). lane 5: Tmab incubated with 2 equiv. of *N*,*N*'-(4-((2-(2-(2-(2-azidoethoxy)ethoxy)ethoxy)ethyl)carbamoyl)-1,3-phenylene)bis(2-iodoacetamide) (**4.33**). lane 6: Tmab incubated with 2 equiv. of *N*,*N*'-(4-((2-(2-(2-(2-azidoethoxy)ethoxy)ethoxy)ethyl)carbamoyl)-1,2-phenylene)bis(2-iodoacetamide) (**4.35**). Protein samples were resolved by reducing SDS-Page (10% gel).

According to the observed pattern of reactivity of different bis-haloacetamide linkers, we concluded that the parameters affecting the selectivity of bis-haloacetamide linkers toward cross-linking the different reduced disulfide bonds of mAbs are: Firstly, the regiochemistry of the α-haloacetamide group related to each other (ortho or meta), secondly, the size of the halogen group and thirdly, the size of the aryl substituent, either the azide-$(PEG)_3$ or the small ester group.

The factors have contributed to the observed preference of *N*,*N*'-(4-((2-(2-(2-(2-azidoethoxy)ethoxy)ethoxy)ethyl)carbamoyl)-1,3-phenylene)bis(2-iodoacetamide) (**4.33**) towards cross-linking intra-chain heavy-heavy disulfide bonds are the bigger size of the halogen (iodo vs. bromo), and the presence of bulk azide-$(PEG)_3$ through amide linkage, which significantly reduced its reactivity towards heavy-light disulfide bonds. This mainly explains why methyl 3,4-bis(2-bromoacetamido)benzoate (**4.23**) with small halogen (Br) and small ester functionality (COOMe) displayed higher selectivity toward inter-chain heavy-light disulfide bonds.

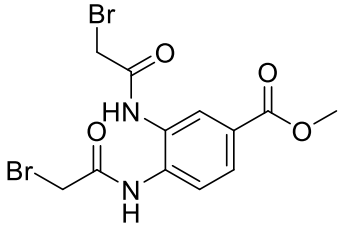

(**4.23**)

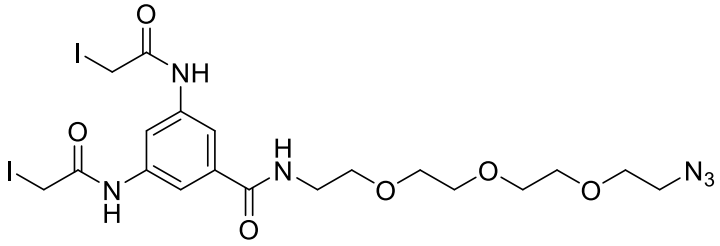

(**4.33**)

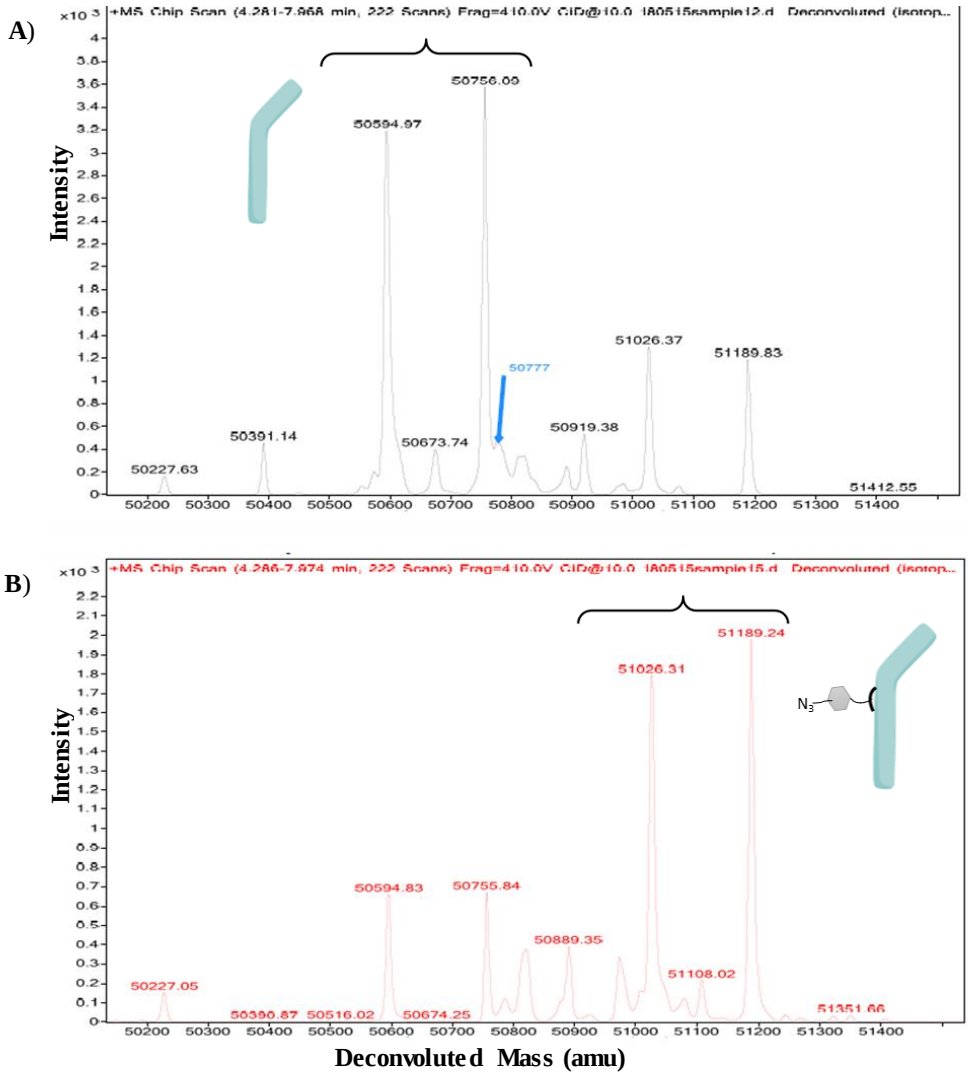

Figure 5.19. Deconvoluted protein MS spectra of Tmab cross-linked with 2 equiv. of **A**) *N*,*N*'-(4-((2-(2-(2-(2-azidoethoxy)ethoxy)ethoxy)ethyl)carbamoyl)-1,2-phenylene)bis(2-iodoacetamide) (**4.35**) showing major peak at 50,594.97 Da and 50,756.09 Da (unfunctionalised heavy chain), **B**) *N*,*N*'-(4-((2-(2-(2-(2-(2-azidoethoxy)ethoxy)ethoxy)ethyl)carbamoyl)-1,3-phenylene)bis(2-iodoacetamide) (**4.33**) showing major peaks at 51,026.31 Da and 51,189.24 Da [cross-linked Tmab (Tmab-N_3)].

5.7 Mechanistic understanding the cross-linking of reduced disulfide bonds using bis-haloacetamide linkers

Interestingly, with all the performed MS analysis on Tmab reaction products with bis-haloacetamide linkers, we did not see any mono-labelling of light chain or heavy chain, which lead us to propose that cross-linking of the reduced disulfide using bis-haloacetamide linkers proceeds in two reaction steps, the first thiol alkylation is the rate-

limiting step and both thiolates groups should be in close proximity or associated together in order to be cross-linked with bis-haloacetamide linkers.

As such, in order to investigate our hypothesis if both thiolate groups should be in close proximity or associated to be cross-linked with bis-haloacetamide linkers, we incubated Tmab with 4 equiv. of TCEP prior to incubation with 2 equiv. of bis-haloacetamide linkers in the presence of 2% or 4% SDS. SDS (2%) is mainly used to denature the proteins and negatively charge them prior to SDS-PAGE analysis.

Two linkers were evaluated, methyl 3,4-bis(2-bromoacetamido)benzoate (**4.23**) which found to be more selective towards cross-linking of inter-chain heavy-light disulfide bonds and *N*,*N*'-(4-((2-(2-(2-(2-azidoethoxy)ethoxy)ethoxy)ethyl)carbamoyl)-1,3-phenylene)bis(2-iodoacetamide) (**4.33**) which found to be more selective towards cross-linking of intra-chain heavy-heavy disulfide bonds.

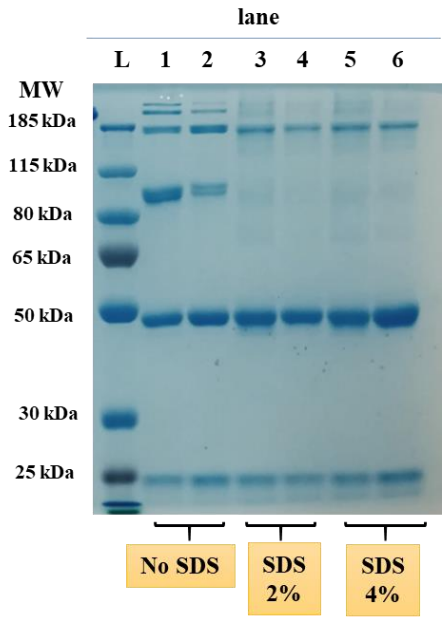

Figure 5.20. SDS-PAGE gel evaluating the selectivity of linkers in cross-linking Tmab (5 mg/mL, 34 µM) in Tris.HCl buffer (100 mM, pH 7.5) which has reduced with 4 equiv. of TCEP (136 µM). L: protein ladder, lane 1: Tmab incubated with 2 equiv. of methyl 3,4-bis(2-bromoacetamido)benzoate (**4.23**), lane 2: Tmab incubated with 2 equiv. of *N*,*N*'-(4-((2-(2-(2-(2-azidoethoxy)ethoxy)ethoxy)ethyl)carbamoyl)-1,3-phenylene)bis(2-iodoacetamide) (**4.33**), lane 3: Tmab incubated with 2 equiv. of **4.23** in the presence of 2% SDS, lane 4: Tmab incubated with 2 equiv. of **4.33** in the presence of 2% SDS, lane 5: Tmab incubated with 2 equiv. of **4.23** in the presence of 4% SDS, lane 6: Tmab incubated with 2 equiv. of **4.33** in the presence of 4% SDS. Protein samples were resolved by reducing SDS-Page (10% gel).

Performing the cross-linking of heavy and light chains in the presence of SDS (2% and 4%) denature Tmab heavy and light chains and separate them and therefore exposes intra-chain disulfide bonds. As expected, the presence of SDS (2% and 4%) resulted in loss of the cross-linking of heavy-light chain capabilities of bis-haloacetamide linkers (**4.23** and **4.33**) as indicated by the absence of half antibody band (Figure 5.2, lane 8-11). Therefore, the presence of cysteine amino acids in close proximity (associated) is a prerequisite in order for the cross-linking by bis-haloacetamide linkers to take place, which can be related to the several factors, including the pK_a value of the thiolate groups.[187]

Next, we wanted to evaluate the cross-linking of fully reduced Tmab in the presence of SDS (2%) in comparison to the control rebridging agent DiBr-Mal (**4b**). To this end, Tmab was reduced with 5 equivalent of TCEP followed by cross-linking with 5 equivalent of methyl 3,4-bis(2-bromoacetamido)benzoate (**4.23**) linker and the control rebridging agent DiBr-Mal (**4b**). Samples were taken after 3 h and after 16 h (overnight). In parallel experiment, SDS (2%) was added to the conjugation buffer, and Tmab was reduced with 5 equivalent of TCEP followed by cross-linking with 5 equivalent of methyl 3,4-bis(2-bromoacetamido)benzoate (**4.23**) or DiBr-Mal (**4b**).

Using SDS (2%) leads to denaturate the tertiary structure of Tmab, which resulted in loss of the cross linking of heavy-light chains and reduced significantly heavy-heavy cross-linking with both methyl 3,4-bis(2-bromoacetamido)benzoate (**4.23**) and the control rebridging agent DiBr-Mal (**4b**) (Figure 5.21, lane 3-4 and 7-8). These results demonstrate that the reduced thiolates should be in close proximity in order to be cross-linked, similar to what was observed previously.

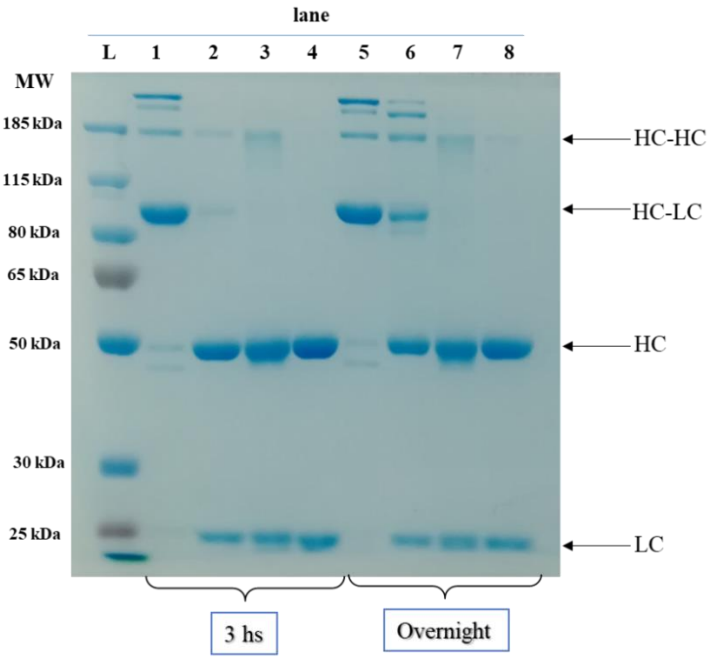

Figure 5.21. SDS-PAGE of Tmab (5 mg/mL, 34 µM) conjugation with methyl 3,4-bis(2-bromoacetamido)benzoate (**4.23**) and DiBr-Mal (**4b**) linkers in the absence and presence of SDS (2%) in Tris.HCl buffer (100 mM, 150 mM NaCl, 5 mM EDTA, pH 7.5). Tmab was reduced with 4 equiv. of TCEP (170 µM) for 2 h at room temperature and then incubated with (17 µM, 5 equiv.) of each linker at room temperature. L: protein ladder, lane 1 and 5: Tmab incubated with 5 equiv. of methyl 3,4-bis(2-bromoacetamido) benzoate (**4.23**) linker, lane 2 and 6: Tmab incubated with 5 equiv. of DiBr-Mal (**4b**), lane 3 and 7: Tmab incubated with 5 equiv. of methyl 3,4-bis(2-bromoacetamido) benzoate (**4.23**) linker in the presence of SDS (2%), lane 4 and 8: Tmab incubated with 5 equiv. of DiBr-Mal (**4b)** in the presence of SDS (2%). Protein samples were resolved by reducing SDS-Page (10% gel).

Analysis of Tmab reaction with methyl 3,4-bis(2-bromoacetamido)benzoate (**4.23**) linker in the presence of (SDS, 2%) using protein MS revealed the absence of half-antibody product (75 kDa) consistent with the SDS-PAGE analysis (Figure 5.22). However, interestingly, despite that there was no detected mono-labelling product of light chain (expected mass 23,765.02 Da), only intra-chain disulfide bond cross-linking was observed. The only possible explanation for this behaviour is through rebridging of the intra-chain disulfide bond of the light chain, which is not accessible to reduction under native conditions and only susceptible to reduction and cross-linking when Tmab has been denatured (the expected mass of cross-linked intra chain disulfide bond of light chain is calculated as 23,685.12, and was observed at 23,685.78 Da) (Figure 5.22).

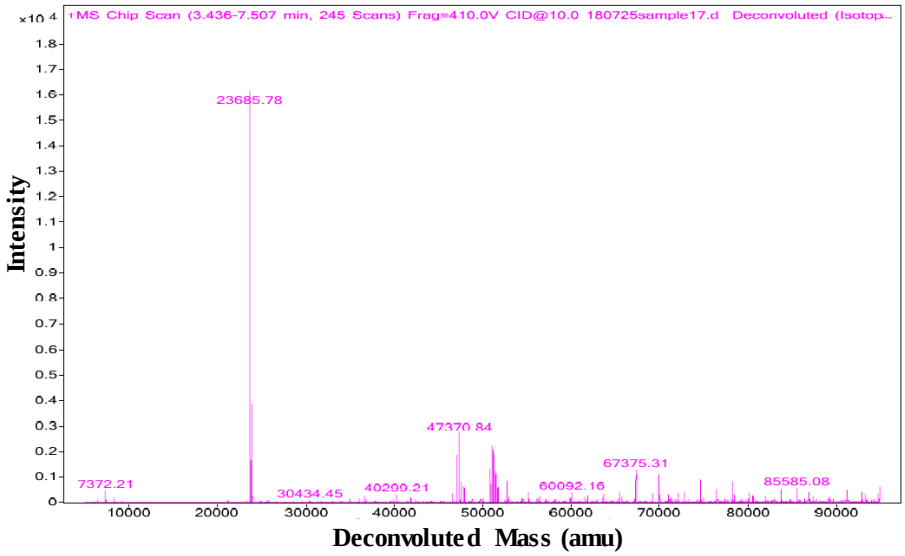

Figure 5.22. Deconvoluted protein MS spectra of cross-linking intra-chain disulfide bond of the light chain of Tmab with methyl 3,4-bis(2-bromoacetamido)benzoate (**4.23**) in the presence of 2% SDS showing a major peak at 23,685.78 Da.

To sum up, disulfide rebridging with bis-haloacetamides occurs mainly if the reduced disulfide bonds are in close proximity and the absence of mono-labelling of the heavy and light chains as shown by MS implies that the second vicinal thiolate group is increasing the reactivity of the first thiolate and the second alkylation is very rapid step. Also, as the denaturation step of Tmab exposes the buried intra-chain disulfide bonds and thus, the available linkers will either react with the reduced intra-chain disulfide bonds or with the already exposed reduced thiolate (reduced inter-chain heavy-light or heavy-heavy disulfide bonds). Based on the MS results obtained, which shows that bis-haloacetamide linkers selectively reacted with the reduced intra-chain disulfide bonds, thus it demonstrate the validity of our proposed cross-linking mechanism.

5.8 Production of a bi-functional Tmab half antibody: $Tmab_{bis(o\text{-}\mathbf{HL}\text{-}OMe,m\text{-}\mathbf{HH}intra\text{-}N_3)}$

Firstly, in order to more thoroughly describe the conjugation reaction products, we sought to use annotation system describing the constructed products of Tmab, which refers to the regiochemistry of the linkers (o: ortho, m: meta), the position of the rebridged disulfide bond (HL: heavy-light, HH_{inta}: inta-chain heavy-heavy disulfide bonds) and the aryl substituent (OMe: ester-derivatised linkers, N_3: azide-derivatised).

Herein, we propose a dual labelling approach to develop a bi-functional mAb which can afford a possible wide range of applicable opportunities in developing diagnostic and therapeutic tools. Previously, we demonstrated the usefulness of bis-haloacetamide linkers in rebridging the reduced disulfide bonds of Tmab in high yields and the selectivity manner of various linkers towards either heavy-heavy or heavy-light disulfide bonds has been discussed. Therefore, we next sought to produce bi-functional Tmab functionalised with a bio-orthogonal group (an azide group), which is suitable for 'Click' reaction with a cyclooctyne derivatised cytotoxic drug, fluorescent probe or radiolabel.

We rationalised that using portion-wise (sequential) reduction followed by the cross-linking would mitigate the non-selective reduction of inter-chain heavy-heavy disulfide bonds and afford higher conjugation yield of heavy-light disulfide bonds.

As such, Tmab (5 mg/mL, 0.033 μmol) in conjugation buffer Tris.HCl (100 mM, pH 7.5) containing 150 mM NaCl, and 5 mM EDTA, was initially reduced by incubation with TCEP **2.2** (2.2 equiv.) for 2 h at 4°C. Then, 2.2 equiv. of methyl 3,4-bis(2-bromoacetamido)benzoate (**4.23**) was then incubated with the reduced protein and held at room temperature overnight. Subsequently, a second reduction step using TCEP (2.2 equiv.) for 2 h at 4°C was performed, prior to incubation with *N*,*N*'-(4-((2-(2-(2-(2-azidoethoxy)ethoxy)ethoxy)ethyl)carbamoyl)-1,3-phenylene)bis(2-iodoacetamide) (**4.33**) (4 equiv.) at room temperature overnight (Figure 5.23).

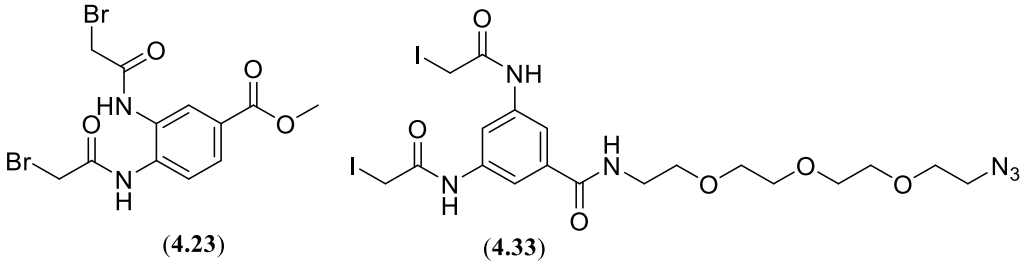

(**4.23**) (**4.33**)

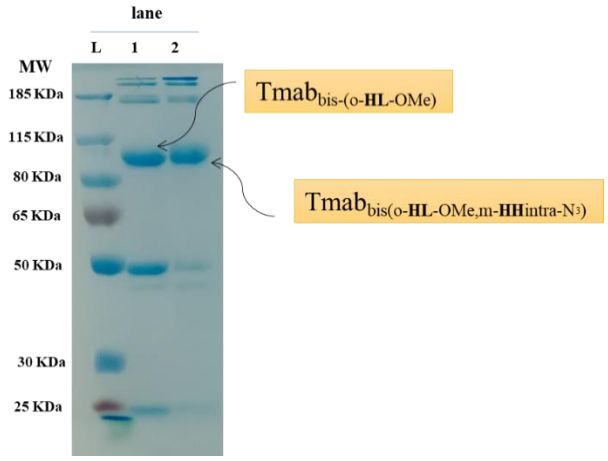

Figure 5.23. SDS-PAGE of bifunctional cross-linking of Tmab (5 mg/ml) in Tris.HCl buffer (100 mM, pH 7.5) containing 150 mM NaCl, and 5 mM EDTA, using sequential method. Tmab was reduced with 2.2 equiv. of TCEP for 2 h and incubated with 2.2 equiv. of methyl 3,4-bis(2-bromoacetamido)benzoate (**4.23**) at room temperature overnight (lane 1). Functionalised $Tmab_{bis\text{-}(o\text{-}\mathbf{HL}\text{-}OMe)}$ was further reduced with 2.2 equiv. of TCEP for 2 h and incubated with 4 equiv. of *N*,*N*'-(4-((2-(2-(2-(2-azidoethoxy)ethoxy)ethoxy)ethyl)carbamoyl)-1,3-phenylene)bis(2-iodoacetamide) (**4.33**) at room temperature overnight (lane 2). Protein samples were resolved by reducing SDS-Page (10% gel).

The cross-linked Tmab was analysed by protein MS. To our delight, we were successful to obtain the bi-functional Tmab product as a major product with expected mass of 74,712.60 Da, and was observed at 74,711.99 Da (Figure 5.24 A).

Expansion around 74 kDa region, revealed two major peaks at 74,711.99 Da and 74,874.13 Da (Figure 5.24 B) with a difference of 162.14 Da, which represents N-glycosylation difference (extra galactose sugar moiety).

Peaks correspond to rebridged Tmab half antibody (heavy-light disulfide bond and inta-chain heavy-heavy disulfide bond) with either two methyl 3,4-bis(2-bromoacetamido)benzoate (**4.23**) or two *N*,*N*'-(4-((2-(2-(2-(2-azidoethoxy)ethoxy)ethoxy)ethyl)carbamoyl)-1,3-phenylene)bis(2-iodoacetamide) (**4.33**) were also detected, the masses were observed at 74,524 Da and 74,898 Da, respectively (Figure 5.24 B).

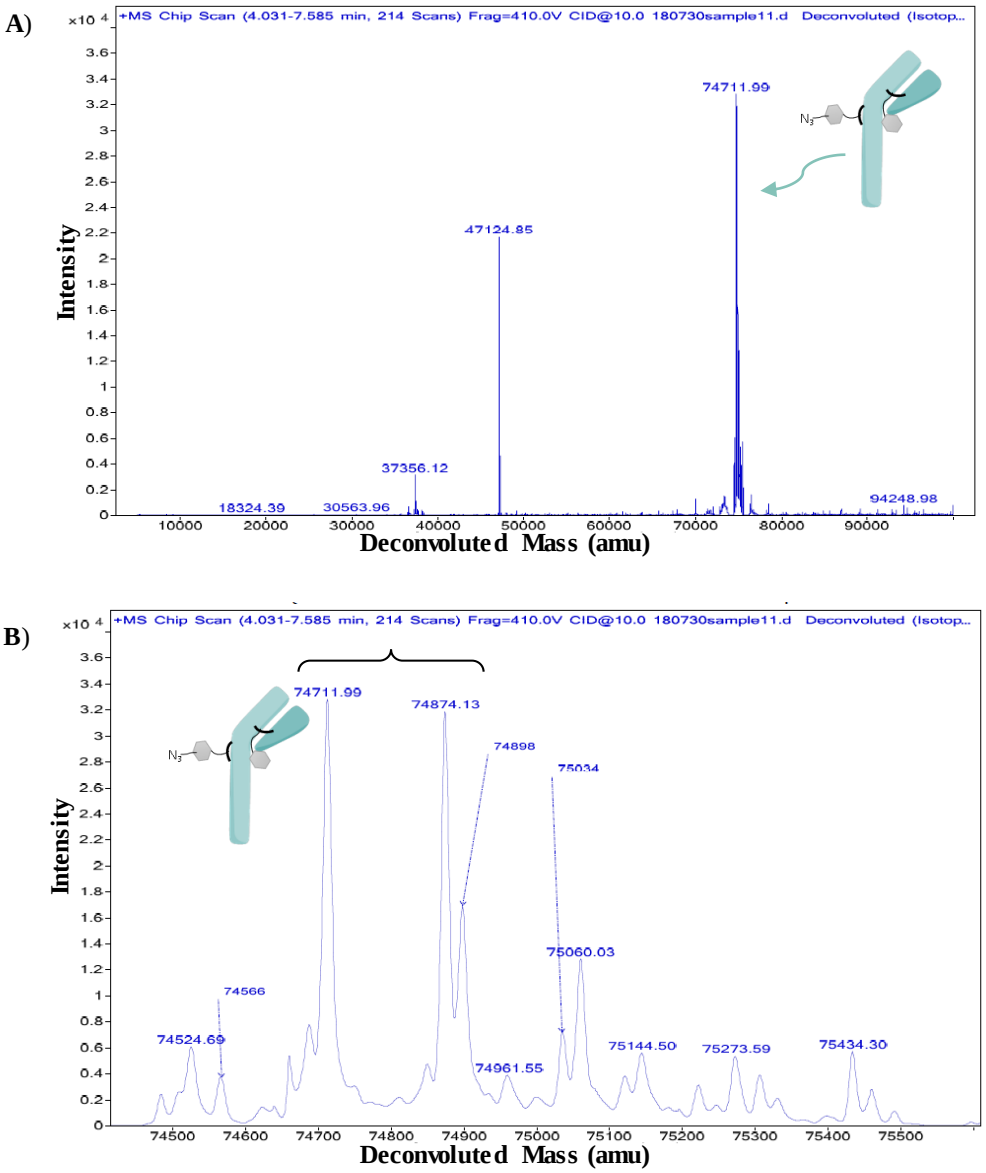

Figure 5.24. Deconvoluted protein MS spectra of bi-functional cross-linking of Tmab with methyl 3,4-bis(2-bromoacetamido)benzoate (**4.23**) and *N*,*N*'-(4-((2-(2-(2-(2-azidoethoxy)ethoxy)ethoxy)ethyl)carbamoyl)-1,3-phenylene)bis(2-iodoacetamide) (**4.33**) using sequential method. **A**) Full view MS spectrum of cross-linked Tmab showing major peak at 74,711.99 Da. **B**) Expansion of the spectrum at 74 kDa region. Showing major peaks at 74,711.99 Da and 74,874.13 Da.

The earlier observed reduction optimisation results using TCEP, suggests that selective reduction of inter-chain heavy-light disulfide bonds was not possible even if the reduction was performed at lower temperature in order to slow down the reaction and increase the selectively, which raise a fundamental question of ranking order of disulfide bond susceptibility to reduction.

It has been found that the inter-chain heavy-light disulfide bonds were more susceptible to reduction than the inter-chain heavy-heavy disulfide bonds, and the upper disulfide bond of the two inter chain heavy-heavy disulfide bonds was more susceptible than the lower one.[148]

When two different linkers were used in sequential reduction and cross-linking reactions, as described in above. The production of fully rebridged half antibody with two different linkers as a major product, suggests the consistency with our previous finding regarding the selective reduction of heavy-light disulfide bonds when lower TCEP equivalents were employed (Figure 5.25 a).

However, the presence of Tmab half antibody fully labelled with two methyl 3,4-bis(2-bromoacetamido)benzoate (**4.23**) suggested that a small fraction of Tmab upper bond of the two inter chain disulfide bond has reduced with TCEP which might followed by disulfide bond rearrangement (Figure 5.25 b) to obtain fully rebridged half antibody with the same linker. Given that Tmab has light chain of κ type, the observed results can be explained by what Hongcheng Liu *et al.* have found. They subjected mAbs to different reduction concentration of DTT and found that $IgG_1\kappa$ displayed smaller susceptibility difference between heavy-light and heavy-heavy disulfide bonds compared with $IgG_1\gamma$.[148]

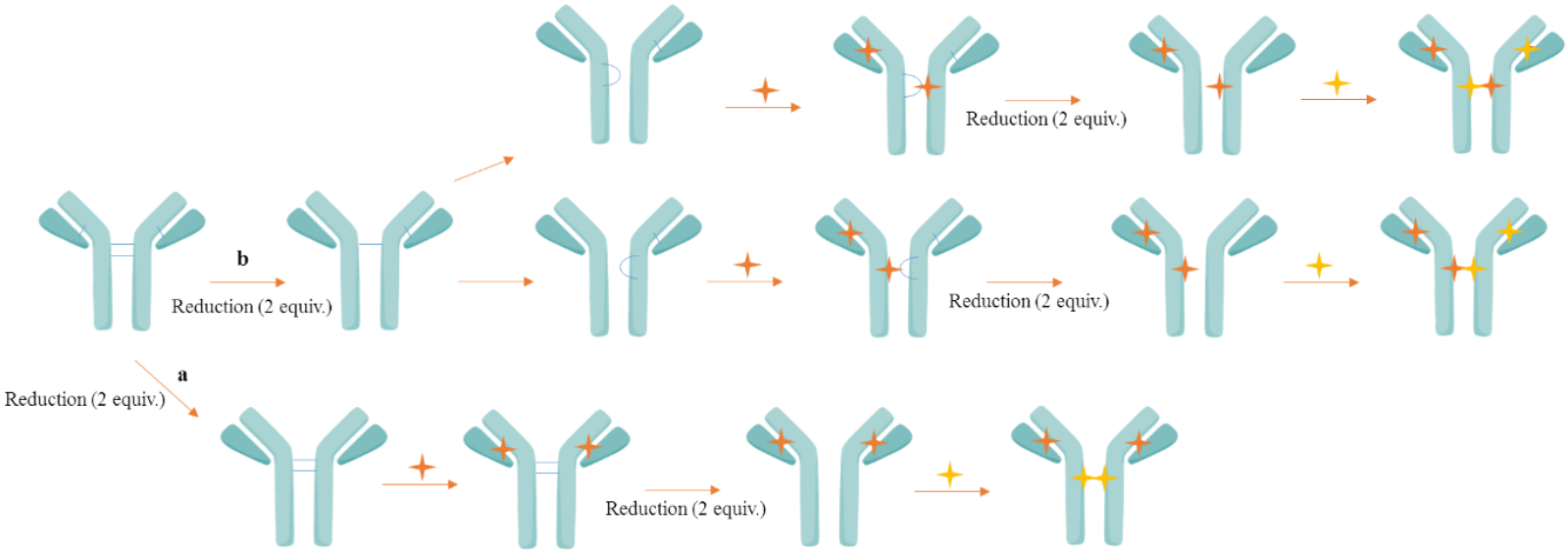

Figure 5.25. The production of bifunctional Tmab with **4.23** linker (✦) followed by **4.33** linker (✦) with the proposed reduction order of disulfide bonds with TCEP.

5.9 Investigation into the reaction of bis-haloacetamide linkers towards other antibodies: Rituximab

5.9.1 Introduction

With optimised reduction and rebridging conditions of Tmab in hand, we set out to evaluate the versatile applicability of our bis-haloacetamide linkers on different mAb. As such, Rituximab (Rmab) mAb was chosen as another model of well-established and widely used mAb in hemato-malignancies since it has been approved in 1997.

Rmab was the first approved mAb in cancer clinical practice. It was approved initially for the treatment of relapsed or refractory, CD20-positive, low-grade non-Hodgkin's B-cell lymphomas (NHL).[188] Later, Rmab was approved in 2006 for the treatment of rheumatoid arthritis (RA).[189] Rituximab is a chimeric anti-CD20 mAb engineered via expressing murine variable regions against the CD20 antigen (anti-CD20) with human constant regions of IgG antibody.[190]

NHL is the most common hematological malignancy in adults and approximately 85% of all NHLs cases are B-cell lymphomas. Fortunately, B-cell lymphomas are characterized by high level of expressed surface proteins, such as CD19, CD20, and CD22, which afford vital targets of potential therapeutic approches.[191] CD20 is overexpressed in majority of B-cells malignancies with more than 90% of all NHLs cases are CD20 positive.[192] CD20 is a 33-37 kDa, non-glycosylated phosphoprotein which is expressed selectively on the surface of almost all B-cells, including non-malignant cells.[193] CD20 is a transmembrane receptor that is selectively expressed on B-cells but not on either the precursor lymphoid cells nor on plasma cells. CD20 plays role in the development and differentiation of B-cells.[194]

5.9.2 Disulfide bond rebridging of fully reduced Rituximab: Rmab$_{\text{bis-[(o-}\mathbf{HL}\text{,o-}\mathbf{HH}\text{intra)-OMe]}}$

Initially we sought to evaluate the capability of the bis-bromoacetamide linkers to cross-link fully reduced Rmab.

As such, Rmab (5 mg/mL, 0.035 µmol) in Tris.HCl (100 mM, pH 7.5), was initially reduced with TCEP **2.2** (5 equiv.) for 2 h at room temperature. The reduced Tmab was incubated with 5 equivalent of each bis-bromoacetamide linkers (**4.22**, **4.23**, **4.28** and **4.29**) and held at room temperature overnight. The reaction products were resolved using SDS-PAGE (Figure 5.26).

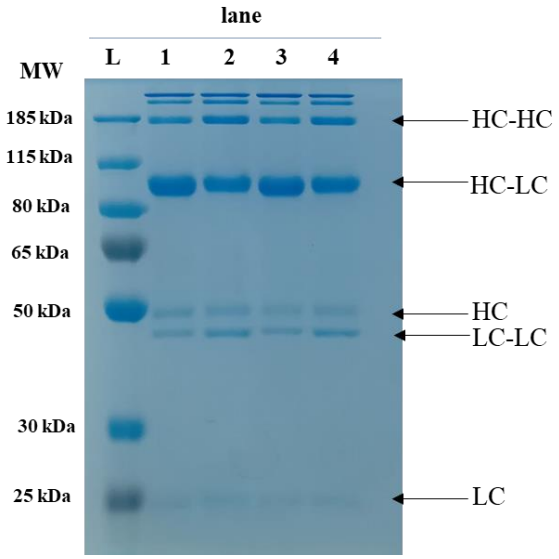

Figure 5.26. SDS-PAGE analysis of cross-linking of fully reduced Rmab (5 mg/mL, 35 µM) in Tris.HCl buffer with bis-bromoacetamide linkers. Rmab was reduced with 5 equiv. of TCEP **2.2** (175 µM) for 2 h at room temperature and then incubated with (17.5 µM, 5 equiv.) of each linker overnight. L: protein ladder, lane 1: Rmab incubated with 5 equiv. of methyl 3,4-bis(2-bromoacetamido)benzoate (**4.23**), lane 2: Rmab incubated with 5 equiv. of methyl 3,5-bis(2-bromoacetamido)benzoate (**4.22**), lane 3: Rmab incubated with 5 equiv. of *N*,*N*'-(1,2-phenylene)bis(2-bromoacetamide) (**4.29**), lane 4: Tmab incubated with 5 equiv. of *N*,*N*'-(1,3-phenylene)bis(2-bromoacetamide) (**4.28**). HC: heavy chain, LC: light chain, LC-LC: light chain homodimers, HC-HC: heavy chain homodimers. Protein samples were resolved by reducing SDS-PAGE (10% gel).

Interestingly, the major product of cross-linking was again half-antibody observed at (75 kDa) for all bis-bromoacetamide linkers (**4.22**, **4.23**, **4.28** and **4.29**) (Figure 5.26). Moreover, in similar observed manner, both meta-substituted linkers, methyl 3,5-bis(2-bromoacetamido)benzoate (**4.22**) (Figure 5.26, lane 2) and *N*,*N*'-(1,3-phenylene)bis(2-bromoacetamide) (**4.28**) (Figure 5.26, lane 4) displayed higher proportion of cross-linked light-light chains and heavy-heavy chains as displayed as distinct bands around 50 kDa and 100 kDa revealed under reducing conditions. While ortho-substituted linkers methyl 3,4-bis(2-bromoacetamido)benzoate (**4.23**) and *N*,*N*'-(1,2-phenylene)bis(2-bromoacetamide) (**4.29**) showed more selective rebridging of heavy-light disulfide bonds

with only a very minor proportion of cross-linked light-light chains and inter-chain heavy-heavy disulfide bonds (Figure 5.26, lane 1 and 3).

Protein MS was performed next to confirm the rebridging consistency of bis-haloacetamides linkers. The MS showed a major peak at 74,036.03 Da corresponding to bridged Rmab half-antibody with two linkers (rebridging both intra-chain heavy-heavy disulfide bonds and inter-chain heavy-light disulfide bonds) (Figure 5.27).

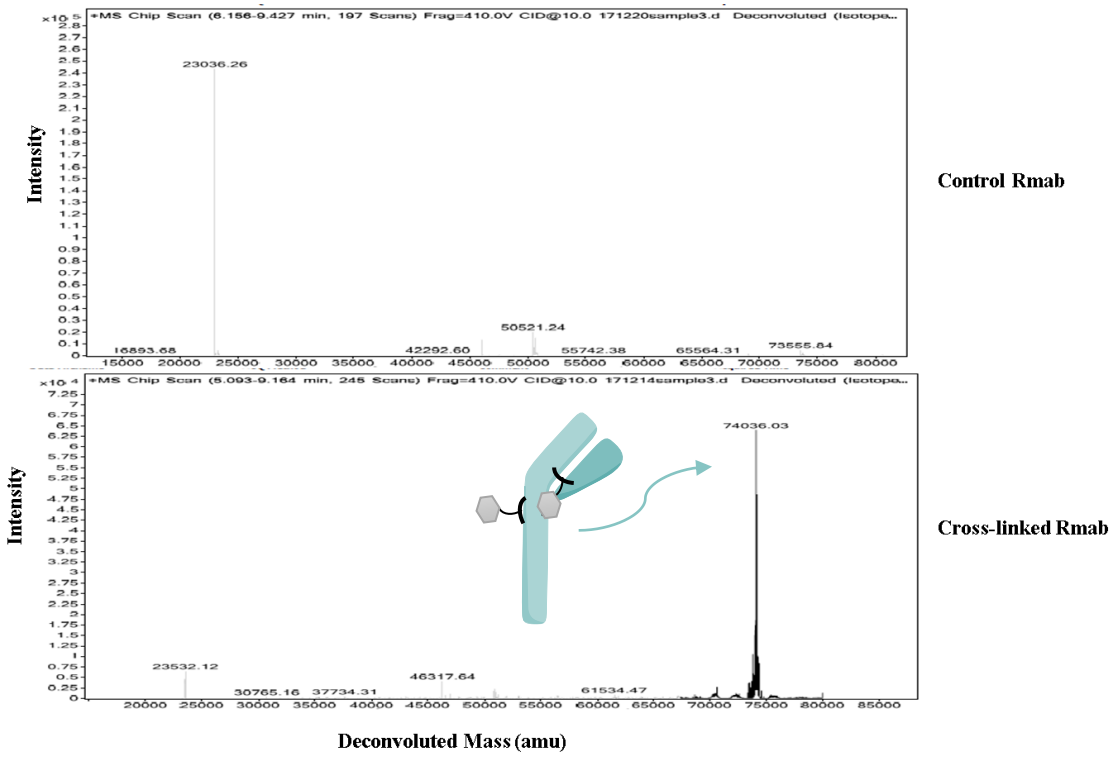

Figure 5.27. Deconvoluted protein MS spectra of Rmab control showing major peaks 23036.26 and 50521.24 Da at and cross-linked Rmab with 5 equiv. of methyl 3,4-bis(2-bromoacetamido)benzoate (**4.23**) showing a major peak at 74,036.03 Da.

5.9.3 Preliminary investigation of the higher order structure of Rmab$_{\text{bis-[(o-}\mathbf{HL}\text{,o-}\mathbf{HH}\text{intra)-OMe]}}$

With the rebridged half antibody characterised in Figure 5.27, we next sought to determine the secondary structure of the constructed Rmab conjugate (Rmab$_{\text{bis-[(o-}\mathbf{HL}\text{,o-}\mathbf{HH}\text{intra)-OMe]}}$) using CD analysis. Circular dichroism (CD) spectroscopy is a commonly used method for evaluating high order structure of proteins. CD spectrum using a

Chirascan spectrophotometer was used analyse the secondary structure difference between native Rmab and the cross-linked Rmab-OMe ($Rmab_{bis\text{-}[(o\text{-}\mathbf{HL},o\text{-}\mathbf{HH}intra)\text{-}OMe]}$).

In addition, another cross-linked Rmab was prepared using a similar method as described above to obtain fully rebridged half antibody with the azide derivatised linker (**4.35**) to construct the cross-linked Rmab-N_3 ($Rmab_{bis\text{-}[(o\text{-}\mathbf{HL},o\text{-}\mathbf{HH}intra)\text{-}N_3]}$). The Rmab samples were buffer exchanged into phosphate buffer (10 mM, pH 7.4) before CD analysis. CD spectra measured between 205 and 260 nm were acquired at 25°C (Figure 5.28).

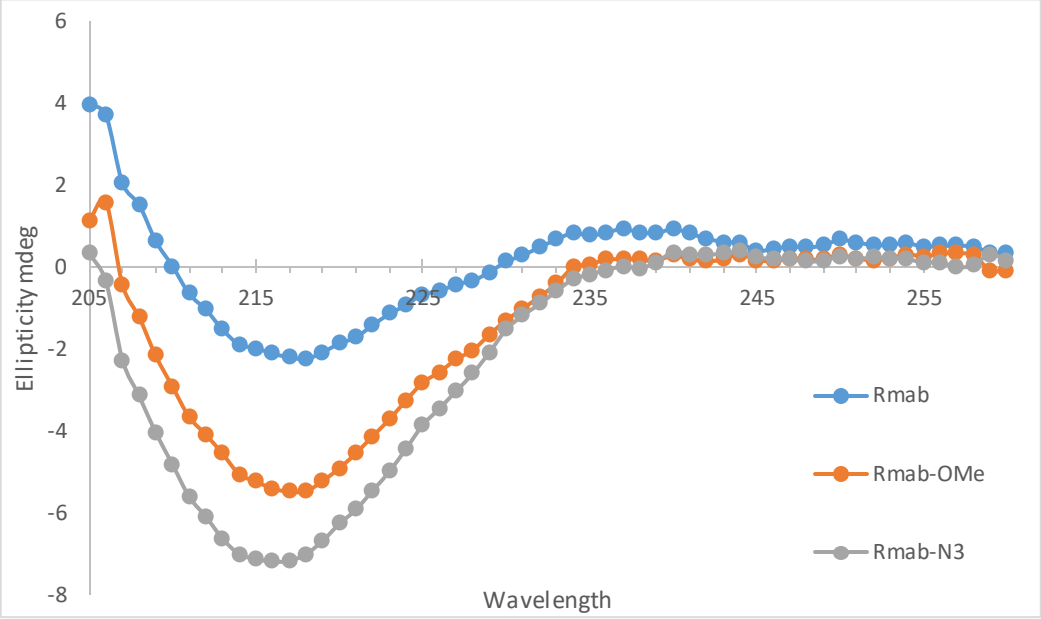

Figure 5.28. CD spectrum of Rmab samples over range of 205-260 nm wavelength at 25 °C showing different spectrum of the cross-linked Rmab comparing to the control Rmab.

CD spectra of the cross-linked Rmab were found to be different from CD spectra of the control Rmab (Figure 5.28). By deconvoluting the representative spectra using CDNN software, the secondary structure composition of α-helix and β-sheet of rebridged Rmab were found to be different from the control Rmab (Table 5.1).

There are various different factors that affects CD spectrum, such as concentration of the sample, presence of excipients (although cross-linked Rmab samples were purified by spinning down in phosphate buffer (3 times)), as well as the molecular weight of the protein which would include the molecular weight of the linkers in the rebridged Rmab samples. As CD spectra are usually normalized to the concentration of proteins and it is

deemed as the largest source of variability in CD measurement.[195] Therefore, we could not draw a clear conclusion from the obtained CD measurements.

Table 5.1. Deconvoluted CD data Rmab samples (acquired at 25°C) over the range of 205-260 nm. Data obtained using CDNN software.

mAb	Rmab	Rmab-OMe	Rmab-N3
wavelength range	205-260 nm	205-260 nm	205-260 nm
Helix	**5.10%**	**9.90%**	**13.90%**
Antiparallel	**42.10%**	**31.70%**	**26.10%**
Parallel	**5.50%**	**5.60%**	**5.70%**
Beta-Turn	17.10%	17.20%	17.60%
Rndm. Coil	35.20%	35.10%	34.90%
Total Sum	105.00%	99.50%	98.10%

Next, thermal stability was also assessed using CD spectrum by following changes in the spectrum with increasing temperature. As such, variable temperature CD was performed over the temperature range of 25-90°C. Variable temperature circular dichroism data for Rmab samples, which shows the changing in the structural abundance of α-helix and β-sheet as a percentage of the total protein with temperature increasing are shown in (Figure 5.29).

Melting temperature (unfolding of proteins) is generally indicative of the thermal stability of the proteins and the tendency of proteins to aggregate and precipitate. One can note that melting temperature of Rmab samples (between 70-75 °C) have not significantly changed among the different Rmab samples, which indicates that the overall thermal stability of the cross-linked Rmab has not been affected and likewise the conformational stability.

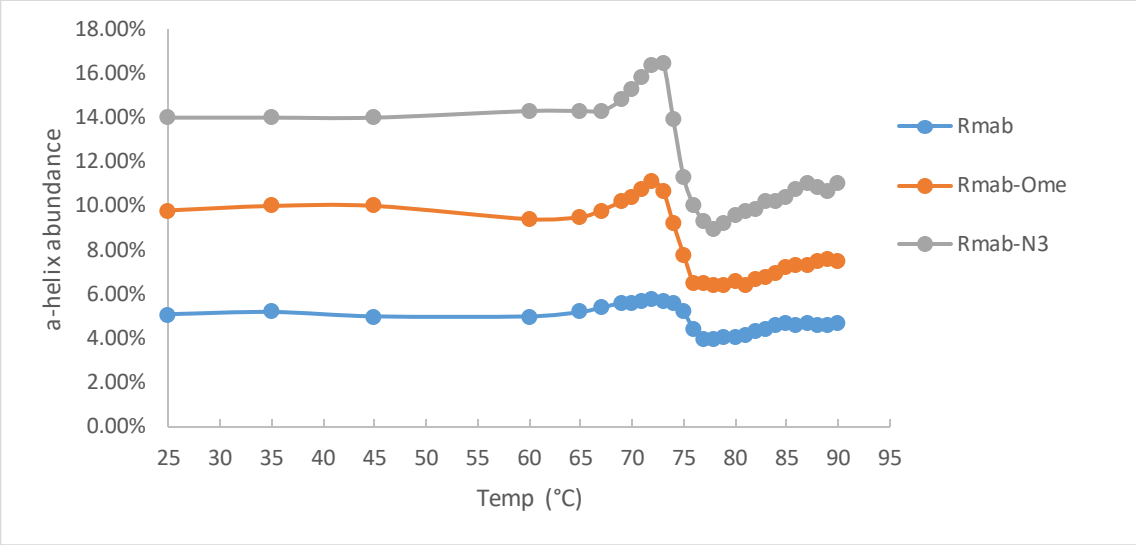

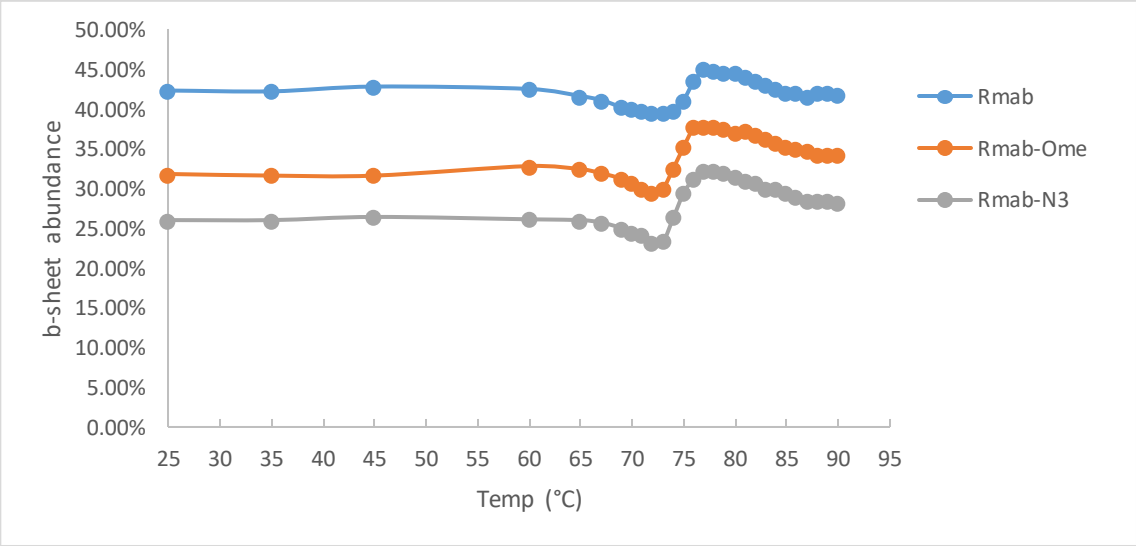

Figure 5.29. Variable temperature CD data for Rmab samples showing structural abundance of α-helix, and β-sheet as a percentage of the total protein. Measured over a temperature range of 25-90°C.

We aimed next to evaluate the tertiary structure of Rmab and compare it to the cross-linked by using DLS technique. DLS (Dynamic light scattering) technique is commonly used to study the tertiary structure of proteins as well as the presence of protein aggregates. DLS analysis was carried out to compare particle size of native Rmab and $Rmab_{bis\text{-}[(o\text{-}\mathbf{HL},o\text{-}\mathbf{HH}intra)\text{-}OMe]}$, which will give us more understanding of the tertiary structure of mAb. As such, the average particle size of the Rmab and cross-linked Rmab were found to be 14.92 and 12.00 nm, respectively (Figure 5.30). Given that, there is no

significant difference between average particle size of control and cross-linked Rmab, we can conclude that the rebridged half-antibodies are associated together in solution and presented as intact antibody. Moreover, no apparent protein aggregates were observed in both samples.

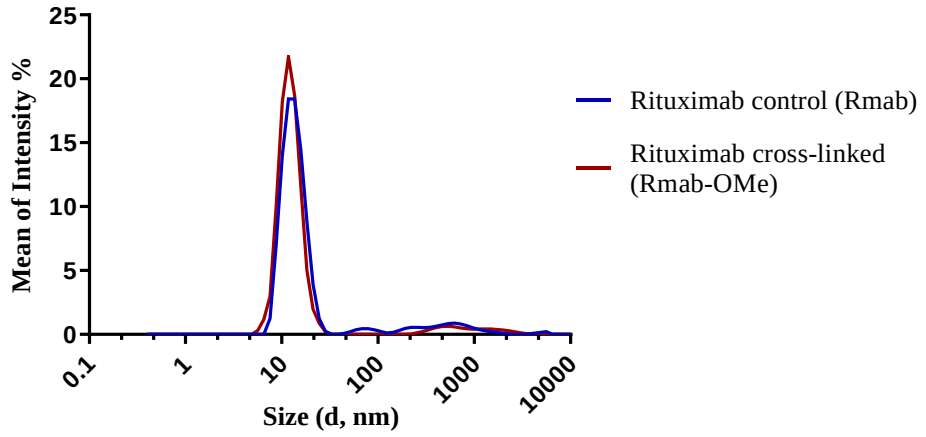

Figure 5.30. Hydrodynamic radius distribution by intensity for Rmab and cross-linked Rmab at 2 mg/mL, indicating that there is a major peak for Rmab and cross-linked Rmab-OMe with methyl 3,4-bis(2-bromoacetamido) benzoate (**4.23**) at 14.92 nm and 12.00 nm, respectively.

5.10 Stability of rebridged Rmab half antibody: $Rmab_{bis\text{-}[(o\text{-}\mathbf{HL},o\text{-}\mathbf{HH}intra)\text{-}OMe]}$ under reducing conditions and after 2 months at 4°C

Stability of the conjugated mAb in plasma is one of the major concerns and obstacles of construction of ADCs, especially maleimide based ADCs. It is widely acknowledged that maleimide−thiol conjugates, are not stable and might slowly undergo retro-Michael addition to reform maleimide. A new thiol conjugate will form in the presence of circulating peptides and proteins in biological environment, particularly albumin and glutathione (see Section 1.4.2.1).[84,196]

To this end, we aimed next to test the stability of the fully rebridged half antibody, previously characterised in Figure 5.27, in plasma mimicking conditions [20 µM glutathione, 600 µM human serum albumin (HSA)]. Fully rebridged half antibody (Figure 5.31, lane 1) has been buffer exchanged to fresh buffer (pH 7.4) by repeated

diafiltration, then glutathione (20 µM final concentration) and HSA (600 µM final concentration) were added.

The sample was incubated at 37°C for 7 days. The stability was monitored by SDS-PAGE analysis, which revealed that the cross-linked Rmab was stable over seven days in plasma mimicking conditions with no new bands corresponding to the formation adducts between HSA or glutathione with heavy or light chains of Rmab (expected masses around 115, 90, 50 and 25 kDa) were observed (Figure 5.31, lane 2-6).

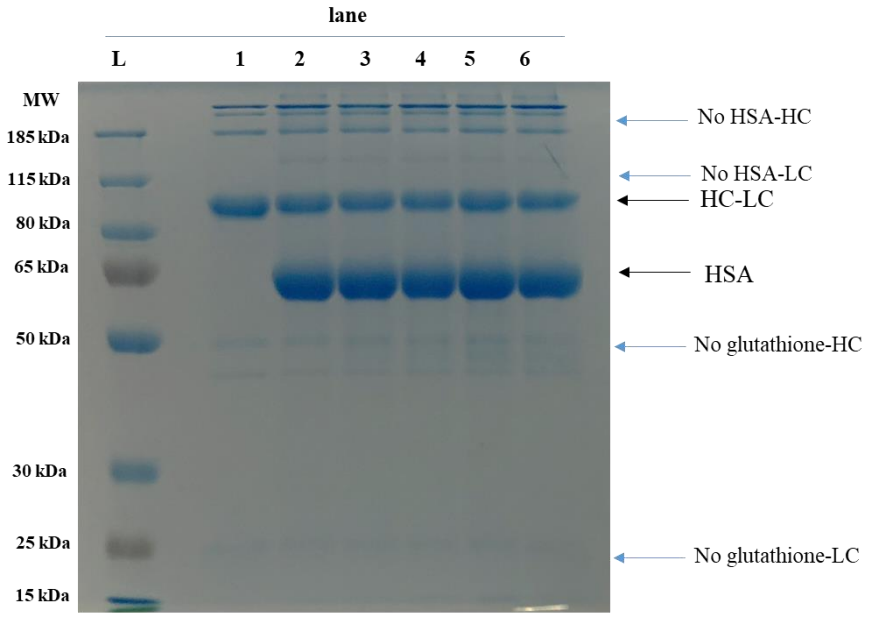

Figure 5.31. Stability of fully rebridged half antibody (Rmab$_{\text{bis-[(o-}\mathbf{HL}\text{,o-}\mathbf{HH}\text{intra)-OMe]}}$) in plasma mimicking condition. SDS–PAGE analysis of cross-linked Rmab following incubation in plasma mimicking conditions for 0, 1, 3, 5 and 7 days (lanes 2-6, respectively). Protein samples were resolved by reducing SDS-PAGE (10% gel).

Next, fully rebridged half antibody, previously characterised in Figure 5.27, was buffer exchanged into fresh buffer (pH 7.4) and held at 4°C for two months. The stability was monitored by SDS-PAGE, which revealed the complete stability of the conjugate after 2 months of storage at 4°C (Figure 5.32).

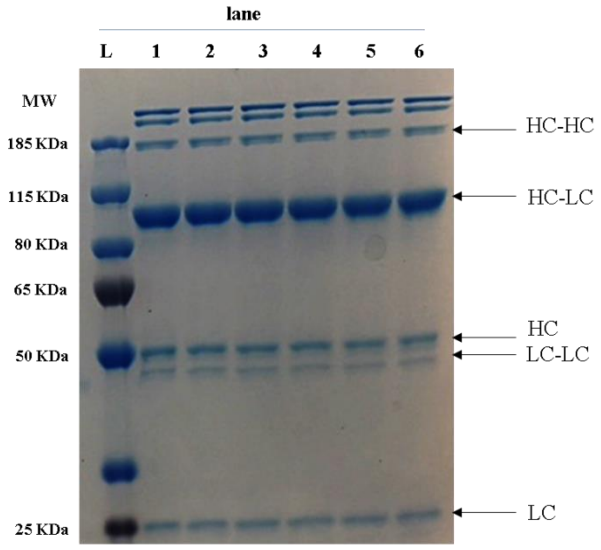

Figure 5.32. Stability of fully rebridged half antibody (Rmab$_{bis\text{-}[(o\text{-}\mathbf{HL},o\text{-}\mathbf{HH}intra)\text{-}OMe]}$) after storage at 4°C. SDS–PAGE analysis of rebridged Rmab following incubation in fresh buffer at 4°C after 0, 1, 2, 4, 6 and 8 weeks (lanes 1-6, respectively). Protein samples were resolved by reducing SDS-PAGE (10% gel).

5.11 Cross-linking of human complement protein C3dg

Having demonstrated the efficiency of bis-haloacetamide linkers in cross-linking disulfide bond of mAbs, we sought to demonstrate the usefulness of these reagents in cross-linking wider range of proteins and studying protein-protein interactions by chemically cross-linking proteins together affording more stable interactions.

Recently, it has been observed by our collaborators that human complement protein C3dg forms homo-dimers in solution through formation of disulfide bridges. In attempt to further elaborate this observation and understand how it is related to the role of this protein in human body, we sought to chemically cross-link C3dg protein using bis-haloacetamide linkers to be further tested by our collaborators.

As such, C3dg protein (wild-type) was incubated with 0.75 equiv. of methyl 3,4-bis(2-haloacetamido) benzoate linkers (**4.22-4.25**) linkers at room temperature overnight, the reaction products were resolved using SDS-PAGE (Figure 5.33, lane 3-6).

A new distinct band around 60 kDa was observed with all the evaluated linkers, which corresponds to the homo-dimer of C3dg protein (Figure 5.33, lane 3-6). However, higher molecular weight protein band were mainly observed with meta-substituted

methyl 3,5-bis(2-bromoacetamido) benzoate (**4.22**) and methyl 3,5-bis(2-iodoacetamido) benzoate (**4.24**) (Figure 5.33, lane 4 and 6).

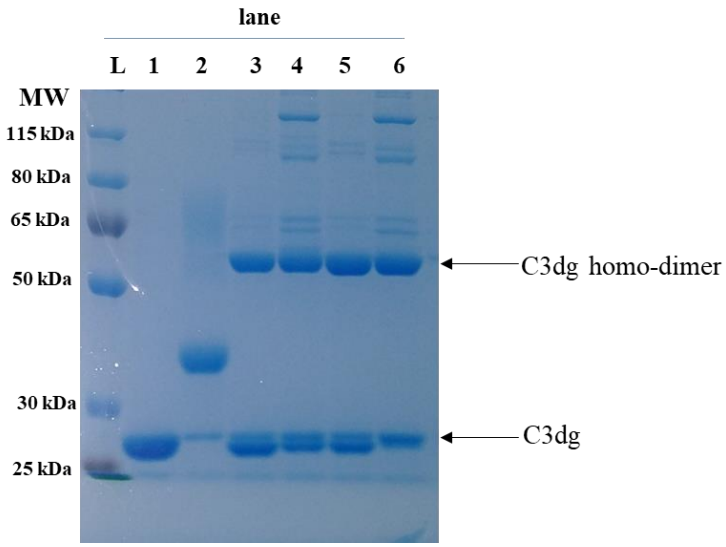

Figure 5.33. Cross-linking of C3dg (2 mg/ml, 5 µM) with linkers bis-haloacetamide linkers (**4.22, 4.23, 4.24, 4.25**). L: protein ladder, lane 1: control (non-reducing dye), lane 2: C3dg incubated with 5 kDa PEG-maleimide (10 equiv.), lanes 3: C3dg incubated with 0.75 equiv. methyl 3,4-bis(2-bromoacetamido) benzoate (**4.23**), lane 4: C3dg incubated with 0.75 equiv. methyl 3,5-bis(2-bromoacetamido) benzoate (**4.22**), lanes 5: C3dg incubated with 0.75 equiv. methyl 3,4-bis(2-iodoacetamido) benzoate (**4.25**), lane 6: C3dg incubated with 0.75 equiv. methyl 3,5-bis(2-iodoacetamido) benzoate (**4.24**) at room temperature overnight. Protein samples were resolved by reducing SDS-Page (10% gel).

Next, we sought to evaluate cross-linking of C3dg using a range of equivalents (0.5, 0.75 and 1.5 equiv.) of methyl 3,4-bis(2-bromoacetamido) benzoate (**4.23**) in order to evaluate their influence on the percentage of conversion to the homo-dimers.

One can note that with incremental increase of the equivalents of methyl 3,4-bis(2-bromoacetamido) benzoate (**4.23**), there is observed increase of newly formed (distinct) band at similar molecular weight of C3dg (Figure 5.34, lane 2-4). This observed pattern raised a couple of question related to this distinct band.

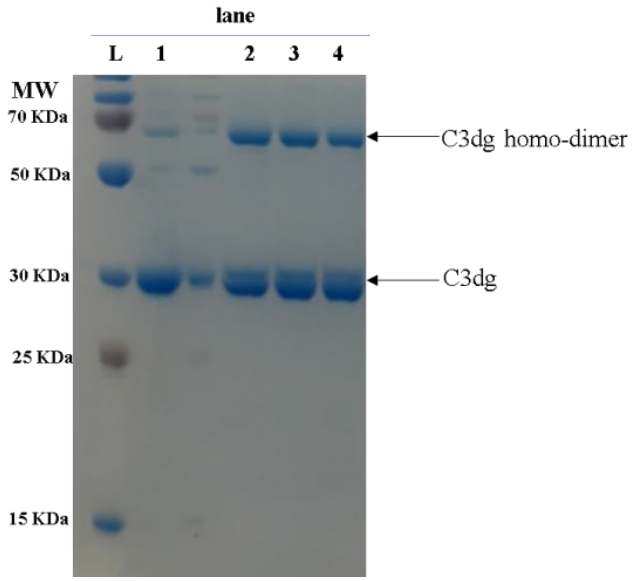

Figure 5.34. Cross-linking of C3dg (2 mg/ml, 5 µM) with methyl 3,4-bis(2-bromoacetamido) benzoate (**4.23**) linker. L: protein ladder, lane 1: control (non-reducing dye), lanes 2: C3dg incubated with 0.5 equiv. methyl 3,4-bis(2-bromoacetamido) benzoate (**4.23**), lane 3: C3dg incubated with 0.75 equiv. methyl 3,4-bis(2-bromoacetamido) benzoate (**4.23**), lane 4: C3dg incubated with 1.5 equiv. methyl 3,4-bis(2-bromoacetamido) benzoate (**4.23**) at room temperature overnight. Protein samples were resolved by reducing SDS-Page (15% gel).

To further characterise the obtained results, protein MS was performed. A native protein showed a single peak at 34,7742.28 Da (Figure 5.35 A). Cross-linked C3dg with 3,4-bis(2-bromoacetamido) benzoate (**4.23**) showed a major peak at 34988.40 Da, which corresponds to C3dg with one cross-linked intra-disulfide bond and a minor peak at 69,730.48 Da, Which correspond to the cross-linked homo-dimer of C3dg (Figure 5.35 B). These results revealed that the lower band seen in lane 2-4 previously is rebridged intra-disulfide bond C3dg (Figure 5.30, lane 2-4).

C3dg homo-dimers were separated from the cross-linked monomer by using SEC to obtain the pure dimer of C3dg to be further tested by our collaborators (purification of C3dg homo-dimers was conducted by our research group colleague).

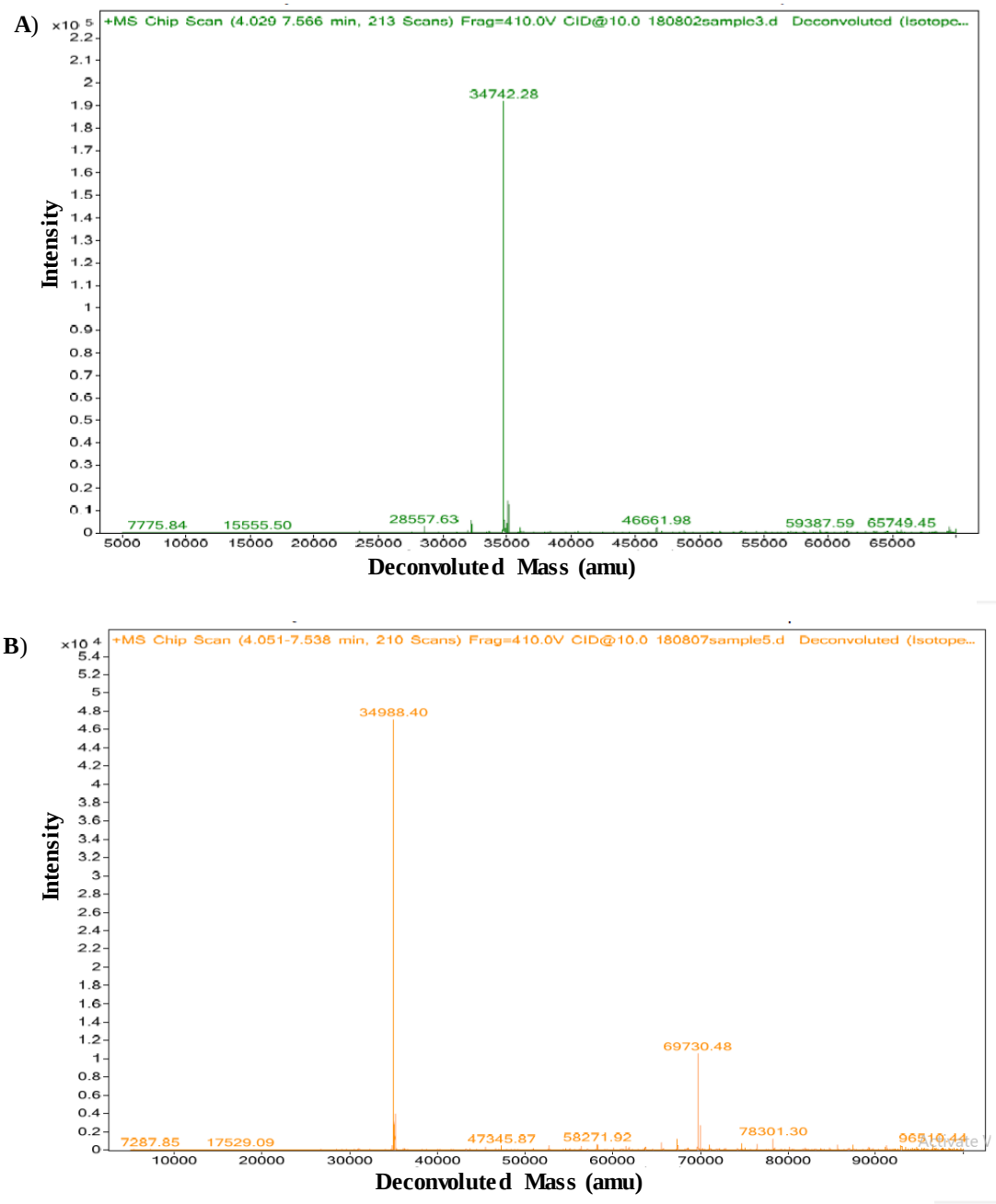

Figure 5.35. Deconvoluted spectrum protein MS of Cross-linking of C3dg with bis-haloacetamide linkers. **A**) Native C3dg showing a peak at 34,742.28. **B**) Cross-linked C3dg with 0.5 equiv. of methyl 3,4-bis(2-bromoacetamido) benzoate (**4.23**) showing a cross-linked monomer peak at 34,988.40 Da and homo-dimer peak at 69,730.48 Da.

5.12 Conclusion

From the detailed and thorough evaluation of the applicability of aryl bis-haloacetamide linkers in rebridging mAbs, such as Tmab and Rmab, we can conclude the following:

1. Reduction conditions of the 4 disulfide bonds of Tmab were optimised to obtain fully and partially reduced Tmab.
2. An interesting rebridged half antibody (rebridging both intra-chain heavy-heavy disulfide bonds and inter-chain heavy-light disulfide bonds) of mAbs was observed as a major product using bis-haloacetamide linkers.
3. It has been demonstrated that well-defined and stable rebridging of half antibodies were obtained with these linkers.
4. Functionalisation of mAbs with clickable handle (azide) was achievable affording a mAbs with clickable handle to be used in azide cyclooctyne cycloaddition reaction.
5. Selectivity of different bis-haloacetamide linkers towards the reduced disulfide bonds of mAbs was studied, which enabled us to better understand the order of the reduction susceptibility of disulfide bonds and to successfully construct hetero bi-functional mAbs.
6. Applicability of aryl bis-haloacetamide linkers in cross-linking of different proteins, affording better understanding of protein-protein interactions, was confirmed.

6 Synthesis of an immunomodulating antibody conjugate: Trastuzumab–Sbi

6.1 Introduction

6.1.1 The human complement system

The human complement system is a large family of related proteins and proteolytic fragments that is deemed to be an essential part of innate immunity and a regulator of adaptive immunity against microbes. In addition to the vital inflammatory resolving role of this system through mediating the clearance of apoptotic cellular debris and antigen-antibody complexes (immune complexes).[197,198] This system comprises more than 30 components, including proteins, receptors and regulators presented on cell surfaces or in plasma. These components play a vital role in innate immune response as well as they mount an effective adaptive immune response. Therefore, any deficiency of the complement components predisposes the patient to bacterial infection and immune complex diseases.[199]

A great amount of research has been undertaken on the complement system and its components. These studies provide immense insights into each component of this system and the essential role of the complement system in inflammatory diseases. It has become apparent that inappropriate or uncontrolled activation of the complement system has a significant impact on various inflammatory diseases. Currently there are two anti-complement drugs are on the market, with many more under development for various infectious, inflammatory, and degenerative diseases.[200,201]

6.1.1.1 Complement activation pathways

Complement activation can be initiated through three distinct pathways, these are the classical (CP), lectin (LP), and alternative pathways (AP) as shown in Figure 6.1.

The classical pathway is initiated by recognition of the C1q molecule of the antigen-antibody complex of IgG or IgM antibodies, which triggers self-activation of C1r to activate the proteolytic C1s (Figure 6.1). C1s cleaves C4 into C4a and C4b, and C2 into

C2a and C2b, to assemble C4bC2a which is known as C3 convertase.[202] In the lectin pathway, mannan-binding lectins (MBLs) which are pattern recognition molecules, bind to mannose or other bacterial carbohydrate motifs. Recognition of bacterial carbohydrates trigger activation of MBL-associated serine proteases (MASPs) which have a similar role to C1r and C1s in assembling C3 convertase.[203]

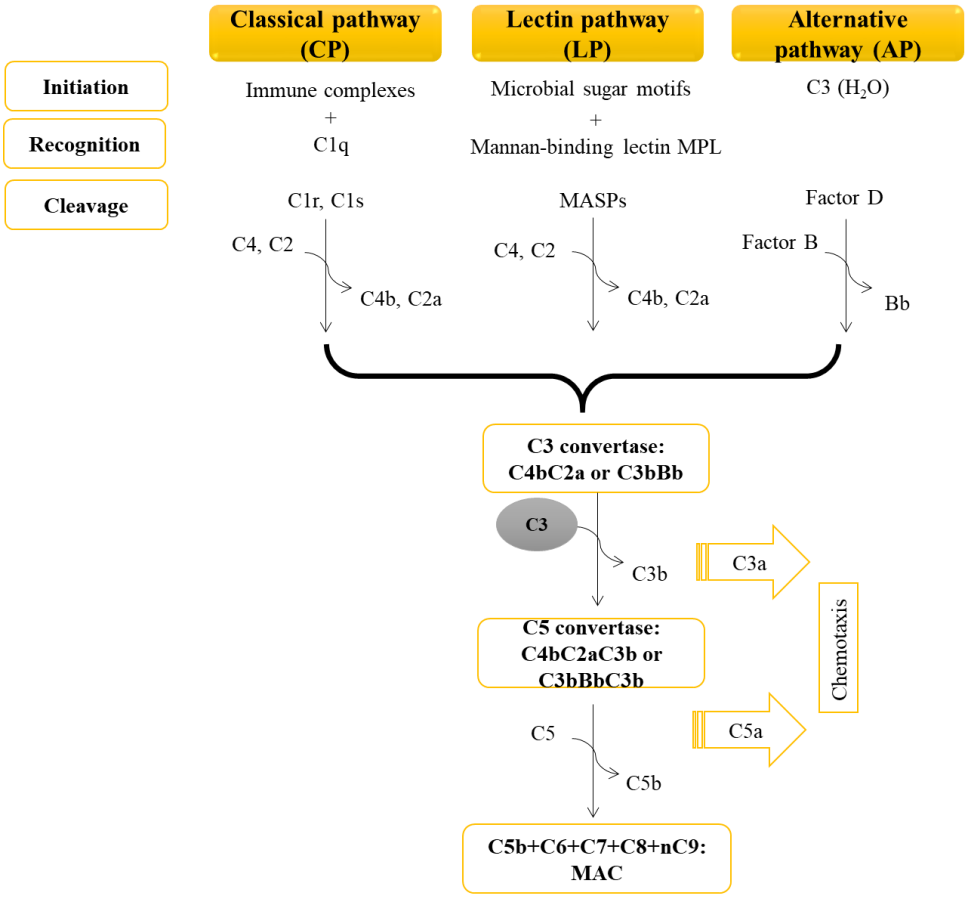

Figure 6.1. Complement activation pathways. Regardless of the initiators of each pathway, all three pathways aim to form C3 convertase which activates the central component of the complement system C3. C5 convertase will then be constructed to cleave C5 and form C5b-C9 membrane attack complex (MAC). C3a and C5a are well-known chemotactic agents.

However, in the alternative pathway, activation occurs spontaneously and continuously at a low rate via C3 associating with a water molecule (hydrolysis) forming C3 (H_2O), which in turn activates factor B (fB) and factor D (fD). Factor D, a serine protease in serum, can enzymatically cleave factor B to Bb affording C3bBb which is an alternative pathway C3 convertase. C3 convertase can be stabilised in plasma via binding to

properdin, which is a positive regulator of the alternative pathway. The alternative pathway functions as an amplification loop for the other pathways.[200,204,205] The spontaneous hydrolysis of the thioester bond of C3 is known as a tick-over mechanism, which ensures and maintains a low level of complement activation in the fluid phase to constantly screen for any pathogenic invasion.[206]

Regardless of the initiation of the three pathways, they will all merge at C3 convertase construction which activates C3, an essential component of the complement system. C3 convertase cleaves C3 into C3a, a chemotactic agent, and C3b which opsonises cell surfaces. The latter will bind C3 convertase to assemble C5 convertase which in turn releases C5b and the proinflammatory C5a. The generated C5b binds to C6 and subsequently C7 and C8 in addition to 10-16 C9 molecules affording the membrane attack complex (MAC) C5b-C9, which leads eventually to cell death through lysis (Figure 6.1).

6.1.1.2 Regulation of the complement system

Given that the complement system does not discriminate between self and non-self cells, it is strictly controlled by a broad range of membrane-bound and fluid-phase inhibitors to prevent damage to self-cells.[201]

The decay accelerating factor (DAF or CD55) is a membrane-bound inhibitor that promotes the degradation of C3 and C5 convertases, thereby interfering with the downstream activation processes, eventually restricting the assembly of the MAC on cells that express DAF.[207] The membrane cofactor protein (MCP or CD46) is another membrane bound regulator which functions as a cofactor for serum factor I (fI). Other complement system membrane-bound regulators include the surfaced-expressed protectin (CD59), which blocks assembly of the MAC, and the surface-expressed CR1, which exhibits fI cofactor activity. fI is a serum factor that cleaves C3b to iC3b, which is further cleaved to C3c and C3dg.[208] Factor H (fH) is the master plasma protein regulator of AP at the C3b level. It competes with fB and prevents it from binding to the C3b protein, in addition to accelerating the decay of the C3 convertase (C3bBb). The C-terminus of factor H can bind to two ligands: C3b and surface-expressed polyanionic

glycosaminoglycans (GAGs), including sialic acid residues. However, the N-terminus domains of fH perform decay accelerating and fI cofactor activities, thereby protecting host self-cells from complement activation. Mutations and SNPs (single nucleotide polymorphisms) in fH have been widely associated with complement-mediated cellular damage which leads to a variety of human inflammatory diseases including age-related macular degeneration (AMD) and atypical hemolytic uremic syndrome (aHUS).[209–211] Factor H-related proteins (FHR1-5) are a group of related proteins which are deemed to be positive regulators of the AP of the complement by competing with fH interaction with C3b and/or GAGs.[212]

The C1 inhibitor is a fluid phase serine protease that irreversibly binds to and cleaves C1r, C1s, MASP-1, and MASP-2, thereby interfering with both classical and MBL pathways.[199]

6.1.1.3 The C3 complement component

The C3 component is the central and most abundant complement protein in serum and body fluids. It is present in a concentration of 1.2–1.5 mg/mL in circulation.[213] C3 is a large protein of 1,400–1,800 amino-acid residues. C3 consists of two chains, a β-chain (residues 1–645, 75 kDa) and an α-chain (residues 650–1,641, 110 kDa) connected together covalently through a disulfide bond and non-covalent forces. The α-chain and β-chain of C3 protein form 13 domains. Perhaps the most important domain of the C3 protein is the thioester-containing domain (TED), where the thioester bond is buried deep between the TED and MG8 domains in order to prevent its access to the hydroxyl nucleophiles.[214]

Upon activation by the C3 convertases, C3 is cleaved between Arg726 and Ser727 to remove the small anaphylatoxin domain (C3a) from the N-terminus of the α-chain to attain C3a and C3b fragments. This cleavage leads to noticeable conformational changes in the structure of C3 to displace the thioester moiety and expose it completely to the surface. Therefore, the solvent accessible thioester will covalently interact with other acceptor sites, such as pathogens and foreign structures. This process, which is known as opsonization, enhances phagocytosis via involvement of CR1, CR3, and CR4

receptors. Active C3b has a short serum half-life and is readily cleaved into iC3b fragments by fI in the presence of fH, CR1, or the membrane cofactor protein and further to C3dg. Lastly, C3dg is cleaved by tryptic enzymes to C3d and C3g.[214,215]

Both iC3b and C3dg, but not C3b, can stimulate B cells via binding to CR2 receptor (also known as CD21) that is expressed on the B-cell to mount effective antibody production and an immune response, by dropping the threshold for B-cell activation by 1000 to 10,000 fold.[216,217]

In conclusion, complement system plays an essential role in both innate and adaptive immunity to protect against pathogenic infections. One of the opportunistic pathogens that causes significant infections in human is *Staphylococcus aureus* (*S. aureus*) which is an abundant bacteria of the skin microbiome of humans. *S. aureus* has developed an arsenal of protective mechanisms against innate and adaptive immunity, in particular against the complement system.

6.1.2 Immune evasion mechanisms of *Staphylococcus aureus*

The human pathogen *S. aureus* chiefly colonizes the moist squamous epithelium of anterior nares, but it can also be found in the gastrointestinal tract and on the skin. Approximately 30% of people carry *S. aureus* continuously, which mainly adheres to nasal mucosa, while around 70% of people host *S. aureus* intermittently.[218]

S. aureus causes various infections ranging from superficial skin infection, such as abscesses and impetigo, to invasive life-threating infections such as septic arthritis, osteomyelitis and endocarditis. *S. aureus* has a tremendous ability to evade the human immune system owing to its ability to express different virulence factors breaching both innate and adaptive immune responses.[219,220]

After breaching skin and squamous epithelium, *S. aureus* begins to confront early innate immune responses mediated by neutrophils. C5a, a proteolytic fragment of the C5 complement protein, and formylated peptides secreted from growing bacterial cells initiate a strong inflammatory response at the site of invasion, which in turn recruits neutrophils from the blood to the site of inflammation. In response, *S. aureus* produces

the staphylococcal superantigen-like protein 7 (SSL-7) which binds to P-selectin glycoprotein ligand (PSGL)-1 on neutrophils and interferes with the binding of P-selectin to neutrophils, ultimately interfering with the migration of neutrophils to the site of infection.[221] About 60% of *S. aureus* strains produce the chemotaxis inhibitory protein of *S. aureus* (CHIPS) which blocks the binding of C5a and formylated peptides on neutrophils to prevent their migration to the site of inflammation.[222]

Following this, *S. aureus* produces a wide range of virulence factors, blocking opsonization of its surface in order to establish successful infection and subvert the phagocytic processes. Of these factors, protein A or Staphylococcal cell wall anchored protein A (SpA) binds to the Fcγ domain of IgGs thereby blocking the phagocytosis process.[223] Clumping factor A (ClfA) is another dominantly expressed protein on the surface of *S. aureus* cells. It prevents opsonization and recognition of opsonins through coating the cell surface with fibrinogen.[224] In addition to the previously mentioned surface proteins, about 90% of *S. aureus* strains express capsular polysaccharides, predominantly capsule types 5 or 8. The presence of the polysaccharide capsule reduces the phagocytosis *S. aureus* by forming a layer which creates a barrier on the bacterial cell surface against opsonins.[225]

Production of coagulases is a hallmark of all the isolated *S. aureus*. These secreted proteins bind to and activate prothrombin to the enzymatically active staphylothrombin. Staphylothrombin activates fibrinogen to fibrin fibrils, generating a protective fibrin meshwork against phagocytes.[226]

S. aureus also produces staphylokinase which is a plasminogen activator that binds in a 1:1 ratio to the cell-bound plasminogen and activates the latter to the potent serine-protease plasmin. Plasmin cleaves cell-bound C3b and IgG and disturbs the opsonization process.[227]

In addition to the above mentioned virulence factors, *S. aureus* secretes cytolytic toxins that destruct the membranes of host leukocytes and kill neutrophils which results in the formation of abscess lesions.[228]

6.1.2.1 *Staphylococcus aureus* complement evasion mechanisms

S. aureus produces an arsenal of complement evasion factors in order to avoid deposition of complement proteins on the bacterial cell surface; therefore, it is considered to be a chief pathogen of complement evasion.[229] Indeed, C3b deposition is the central host defense mechanism against *S. aureus*, with three out of the five complement receptors, namely CR1, CR3 and CRIg found to be the most relevant receptors for successful host defense.[221]

S. aureus produces unique proteins targeting mainly the central complement components, namely C3 and C5. Therefore, it interferes with the downstream signaling and activation pathways. The extracellular fibrinogen-binding protein (Efb) and the recently identified Efb-homologous proteins (Ehp) bind to the C3d domain of C3b, inducing conformational changes and deactivating C3, thereby inhibiting the adaptive immune response, opsonophagocytosis and cellular lysis.[230,231] Staphylococcal complement inhibitors (SCINs) are small proteins that bind to and stabilise C3 convertase in a inactivel state, thereby blocking the downstream signaling and the three activation pathways.[232,233] Unlike Efb and Ehp, SCINs can only bind to the C3 convertase but not to C3 or its fragments.[232]

S. aureus produces two main inhibitors at the C5 level in order to subvert the assembly of MAC and the chemotaxis process. Staphylococcal superantigen-like protein 7 (SSL-7) binds with high affinity to C5, hinders its cleavage by C5 convertase, and consequently inhibits complement-mediated cellular lysis.[234] The chemotaxis inhibitory protein of *S. aureus* (CHIPS) interferes with C5a, the complement inflammatory agent, through binding to C5a receptors on phagocytes. Given that C5a has a vital role in the inflammatory process, several studies have tested the potential employment of the CHIPS protein in the treatment of inflammatory diseases.[222,235]

S. aureus has a cell wall binding protein, namely staphylococcal cell wall anchored protein A (SpA), which interferes at an early stage of complement activation. The SpA protein binds to the Fc domain of IgG protein and blocks C1q binding thereby interfering with the activation of the complement classical pathway.[236]

Interestingly, deep analysis of IgG binding activity of *S. aureus* proteins has revealed a second protein, in addition to SpA, with IgG binding capacity, namely Staphylococcus immunoglobulin-binding protein (Sbi).[237]

6.1.3 The Staphylococcus immunoglobulin-binding (Sbi) protein

Sbi is a 436-residue immune-evasion protein, expressed by several strains of *S. aureus*. From its N-terminus, Sbi consists of an extracellular region, followed by a cell wall spanning region (proline repeat region), and a C-terminus region (tyrosine-rich region, 130-residue). The extracellular region consists of four globular domains (I-IV). Sbi I-II (residues 42-156) binds to the Fc region of IgG, interfering with C1q binding. However, Domains III and IV of Sbi (residues 150-266) are two novel C3-binding domains (Figure 6.2).[238]

In contrast with SpA, Sbi does not have the typical cell wall anchoring sequence (LPXTG).[238] Therefore, Sbi can be found both anchored to the cell envelope by binding to lipoteichoic acid and as a secreted protein, but only the secreted form of Sbi can interact with C3 of complement proteins.[239]

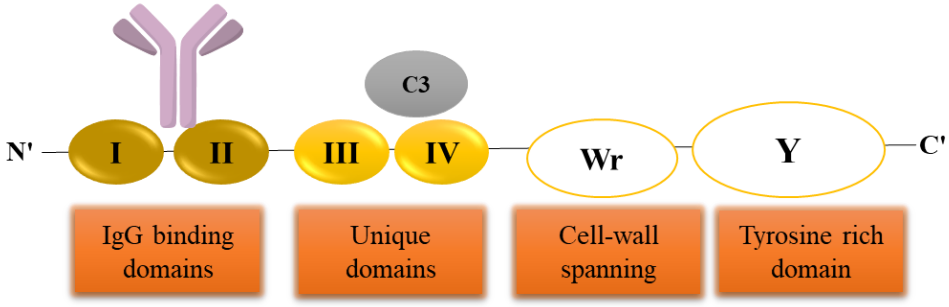

Figure 6.2. Full domains structure of Sbi protein. It comprises four extracellular globular domains (I-IV), the cell wall spanning domain (Wr) and the tyrosine rich region (Y).

Sbi I-II domains bind to the Fcγ domain of IgG, thus interfering with complement fixation and phagocytosis. Both domain I and II exhibit sequence homology with IgG-binding domains of SpA (E, D, A, B and C) with almost identical amino acids to those involved in Fc binding.[240]

Sbi III-IV domains on the other hand, interact with C3 mainly through C3dg sub-domains. By binding to C3, Sbi interferes with all three complement activation pathways which converge at the C3 convertase.[238] It has been shown that the secreted Sbi III-IV has a distinctive complement evasion mechanism through consumptive activation of the AP, which leads to futile cleavage of C3 away from the bacterial surface thereby avoiding C3b-mediated opsonization and C3a-mediated chemotaxis.[238] Sbi I-II are known as IgG binding domains as discussed earlier, and it is known that the C3b fragment has a short half-life and a unique ability to covalently bind to other proteins through the displayed thioester bond. IgGs, on the other hand, are well-known transacylation targets of C3b and therefore, *S. aureus* provides another protective mechanism against the activated C3 protein.[241,242] Moreover, it has been shown that Sbi III-IV binds to the active metastable C3b and thus prevents the normal turnover of the C3b fragment by fH and fI.[243]

The proposed mechanism of Sbi III-IV in the consumption of C3 is via construction of a tripartite complex with C3b and complements regulatory proteins (FHR-1), which competitively antagonize the activity of factor H and stabilize the C3 convertase of AP. Ultimately, Sbi III-IV ensures that C3 is consistently activated and consumed, while stabilizing the nascent C3b fragments.[243]

Taken together, the unique mechanism of Sbi III-IV provides great potential to be utilized as an immunomodulator of the complement AP to attain potential opsinization of a targeted antigen (as a vaccine), or through cellular lysis of cancer cells. As such, we set out to develop novel conjugation method to produce immunoconjugates of Sbi III-IV and the mAbs (Trastuzumab). It was postulated that immunoconjugates of Sbi III-IV and Tmab would activate AP of the complement system, causing selective and targeted opsinization of HER2 positive cancer cells with C3b, ultimately leading to cellular lysis (Figure 6.3).

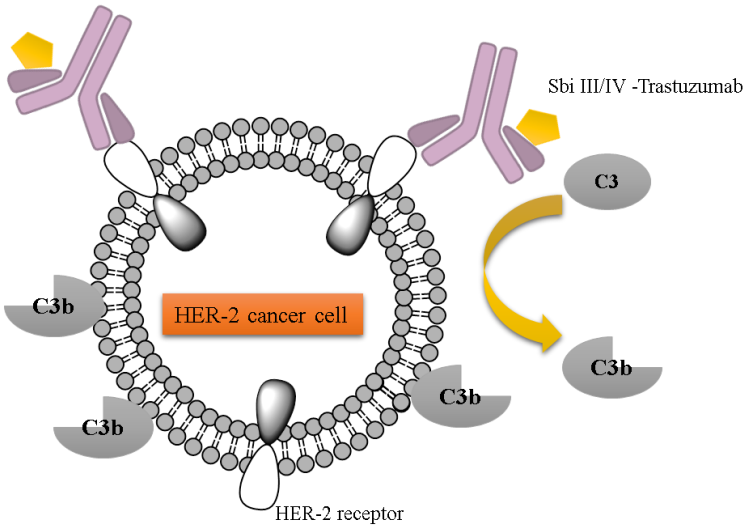

Figure 6.3. Our proposed mechanism of the immunoconjugates of Trastuzumab-Sbi III/IV which activate the C3 component of complement system to selectively opsonize HER-2 positive cancer cells with C3b and ultimately causing cellular lysis.

6.2 Synthesis of bis-dihaloacetamide $(PEG)_3$

The conjugate format of one Sbi III/IV-2xCys bound to Fab region of Tmab is what we are interested to initially develop and test (Figure 6.4). The proposed format will be achieved through binding of one Sbi III/IV-2xCys per Tmab, through specifically linking Sbi III/IV protein to the heavy-light disulfide bond of the Fab region (Figure 6.4). Therefore, we sought to synthesise a tetra-haloacetamide linker, with two rebridging heads (bis-dihaloacetamide $(PEG)_3$ linkers) for dual rebridging of heavy-light chains of Tmab and the 2 cysteine residues (at C-terminus of domain IV) of Sbi III/IV-2xCys to construct immunomodulating conjugates. Bis-dihaloacetamide $(PEG)_3$ linker will afford a simple, one pot approach without the need to use 'Click' chemistry to obtain the immunoconjugates.

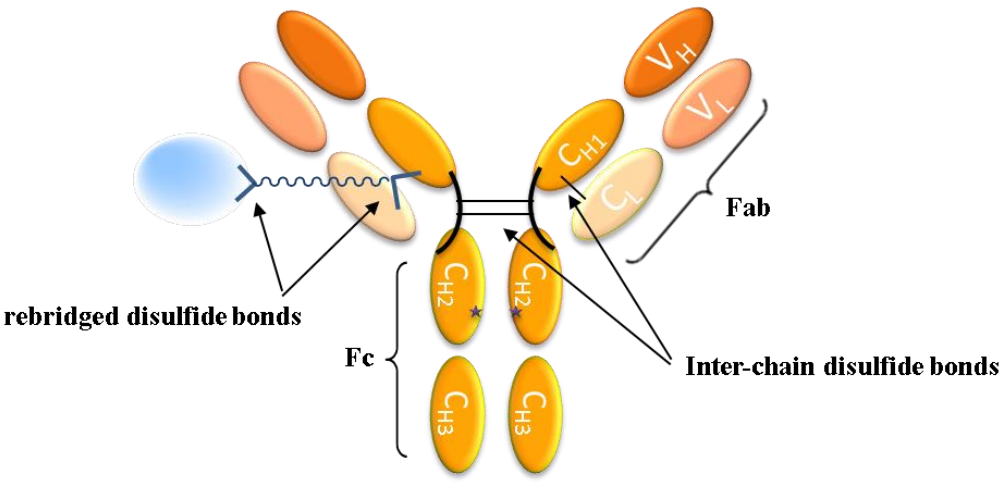

Figure 6.4. Schematic representation of the conjugation format used to attain conjugation of Tmab and Sbi ( ).

Given that ortho-linkers showed higher selectivity towards rebridging the reduced heavy-light disulfide bonds of Tmab as shown previously in Chapter 5, we sought to prepare ortho-bis-dihalooacetamide $(PEG)_3$ **6.1** and **6.2** linkers to bridge the disulfide bond of a certain protein and to attached it to the rebridged heavy-light chain of Tmab (Figure 6.4).

As such, bis-o-dihaloacetamide $(PEG)_3$ linkers **(6.1** and **6.2)** were synthesised over 4 steps shown in Figure 6.5. First, acetylation of 3,4-diaminobenzoic acid using 2-chloroacetyl chloride gave **4.44** in 90% yield, followed by synthesis of activated ester **(4.45)** using *N*-hydroxysuccinimide (45% yield). Next, the activated ester (**4.45**) was reacted with 1,11-Diamino-3,6,9-trioxaundecane (**6.3**) for 1 h (75% yield) to attain bis-dichloroacetamide $(PEG)_3$ (**6.4**), which was then converted to either iodo- or bromo-derivatives using KI or LiBr, respectively (Figure 6.5).

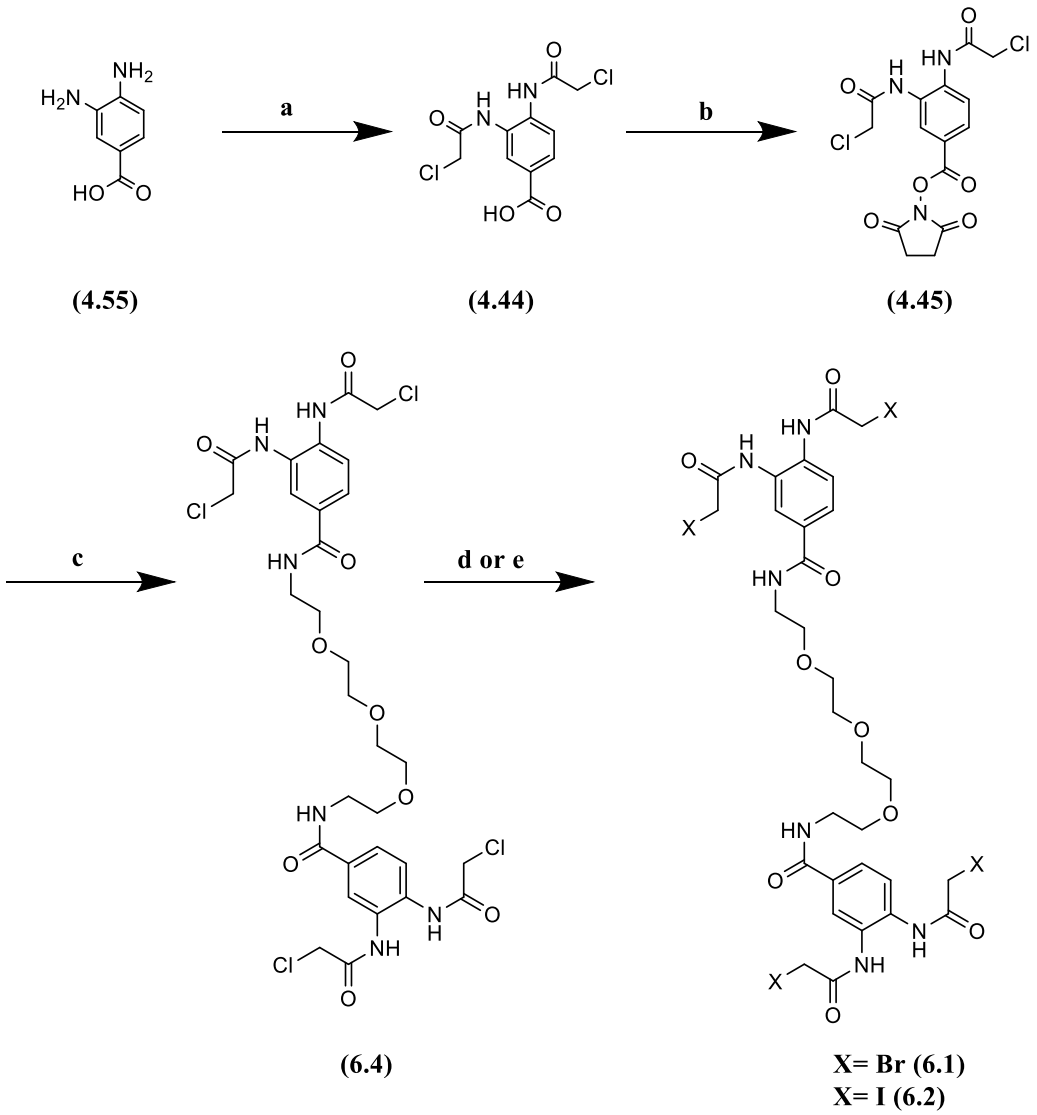

Figure 6.5. Synthesis of bis-dihaloacetamide $(PEG)_3$ **6.1** and **6.2** linkers. **a**) $ClCOCH_2Cl$, THF, **b**) NHS, EDC.HCl, THF, **c**) 1,11-Diamino-3,6,9-trioxaundecane (**6.3**), THF, **d**) LiBr, dry acetone, reflux to give **6.1**, e) KI, dry acetone, reflux to give **6.2**.

6.3 The two employed strategies to produces Tmab-Sbi conjugate

The two strategies that were evaluated to construct Tmab-Sbi conjugate with bis-dihaloacetamide $(PEG)_3$ linkers (**6.1** and **6.2**) are shown in Figure 6.6. Tmab-Sbi conjugate were constructed either through conjugation of functionalised Tmab with pre-reduced Sbi III/IV-2xCys (strategy 1) or through conjugation of functionalised Sbi III/IV-2xCys with partially reduced Tmab (strategy 2).

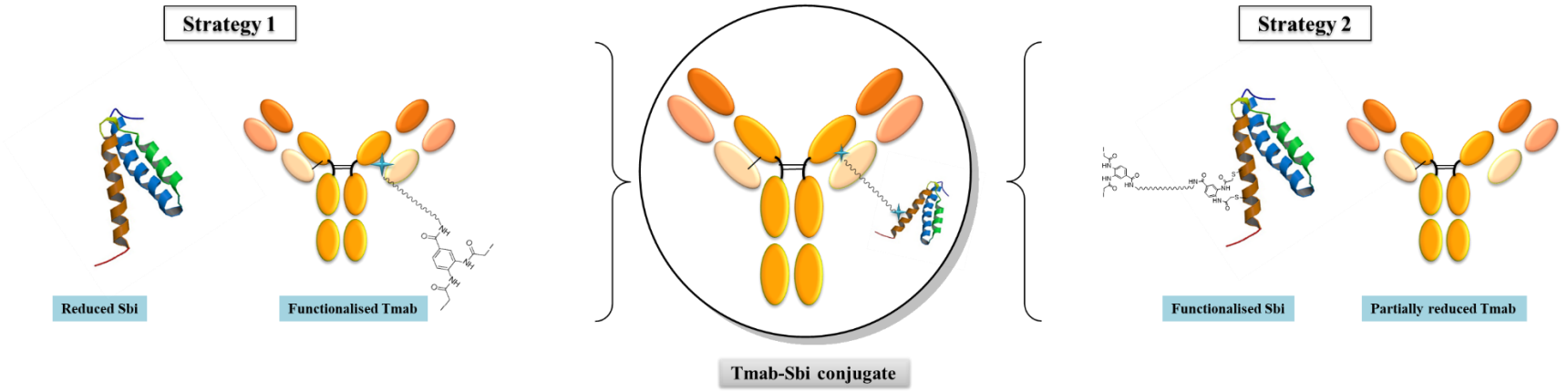

Figure 6.6. Schematic representation of the strategies evaluated to produce Tmab-Sbi conjugate, either by the conjugation of functionalised Tmab with reduced Sbi (strategy 1) or through conjugation of functionalised Sbi with partially reduced Tmab (strategy 2).

6.4 Conjugation of functionalised Tmab with reduced Sbi (Strategy 1)

As described previously in Chapter 5, optimum reaction yield were obtained when 1 equivalent of reducing agent and linkers were employed. Therefore, we sought to initially optimise the reduction step (partially) of Tmab using 1 equivalent of TCEP. The reduction conditions followed by conjugation with bis-bromoacetamides (**4.22**, **4.23**, **4.28** and **4.29**) will be evaluated initially in order to optimise the required conditions for bis-o-dihaloacetamide $(PEG)_3$ **6.1** and **6.2** linkers.

We first set out to determine the optimum concentration of Tmab, as such a set of three concentrations of Tmab were evaluated: 2, 5 and 10 mg/mL. Tmab in conjugation Tris.HCl buffer (100 mM, pH 7.5) and concentrated to (2, 5, or 10 mg/mL). Tmab was first reduced (partially) by incubation with TCEP (1.1 equiv.) for 2 h at 4°C, then incubated with 1.1 equiv. of each bis-bromoacetamide linker (**4.22**, **4.23**, **4.28** and **4.29**) and held at room temperature overnight. Reaction products were resolved using SDS-PAGE.

Attempting only 1.1 equivalent of TCEP followed by 1.1 equivalent of each linker would produce rebridged half-antibody product (75 kDa) of one Fab of Tmab, in addition to the unreacted second Fab (50 kDa, 25 kDa).

By observing the intensity of the HC-LC (75 kDa under reducing conditions) and HC (50 kDa under reducing conditions) bands under reducing conditions, one can note the high yields obtained with most the performed reactions (equal bands intensity), particularly at 5 mg/mL concentration of Tmab (Figure 6.7, lane 9-12). Moreover, adopting a higher concentration (10 mg/mL), did not, however, improve the cross-linking yield (Figure. 6.7, lane 17-20).

Samples of the reactions were run also under non-reducing conditions to evaluate the cross-linking of intra-chain disulfide bonds of heavy chain (50 and 75 kDa bands under non-reducing condition). It can be concluded that the major products obtained is the desired rebridged half-antibody (heavy-light disulfide bonds) with one linker, while

rebridged half-antibody with two linkers (intra-chain heavy-heavy and heavy-light disulfide bonds) was found to be a very minor product.

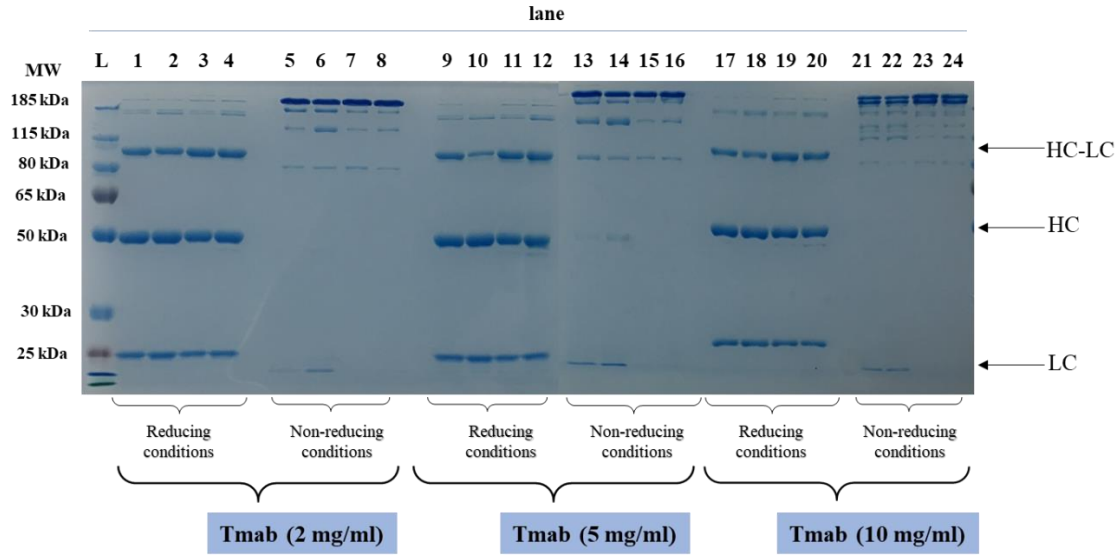

Figure 6.7. SDS-PAGE analysis of cross-linking of partially reduced Tmab in Tris.HCl buffer (100 mM, 150 mM NaCl, 5 mM EDTA, pH 7.5) with bis-bromoacetamide linkers. Tmab was reduced with 1.1 equiv. of TCEP for 2 h at 4°C and incubated with 1.1 equiv. each linker at room temperature overnight. Lane 1, 9 and 17: Tmab incubated with 1.1 equiv. of methyl 3,4-bis(2-bromoacetamido)benzoate (**4.23**), Lane 2, 10 and 18: Tmab incubated with 1.1 equiv. of methyl 3,5-bis(2-bromoacetamido)benzoate (**4.22**), Lane 3, 11 and 19: Tmab incubated with 1.1 equiv. of *N*,*N*'-(1,2-phenylene)bis(2-bromoacetamide) (**4.29**), Lane 4, 12 and 20: Tmab incubated with 1.1 equiv. of *N*,*N*'-(1,3-phenylene)bis(2-bromoacetamide) (**4.28**). Lane 5-8, 13-16, and 21-24 represent the same reactions in the same described order but run under non-reducing conditions (non-reducing dye).

Consistent with what we observed previously, the ortho-substituted linkers (**4.23** and **4.29**) displayed almost 100% observed conversion to the desired product as equal bands of HC-LC and HC were observed under reducing conditions (Figure. 6.7, lane 9 and 11).

Further analysis of Tmab cross-linking reaction with ortho-substituted linkers (**4.23** and **4.29**) at 5 mg/mL was performed with protein MS. Gratifyingly, both ortho-linkers displayed almost equal intensity of the half-antibody peak at 75 kDa (with one linker rebridging heavy-light disulfide bond) and the heavy chain peak at 50 kDa (uncross-linked) (Figure 6.8 A and B).

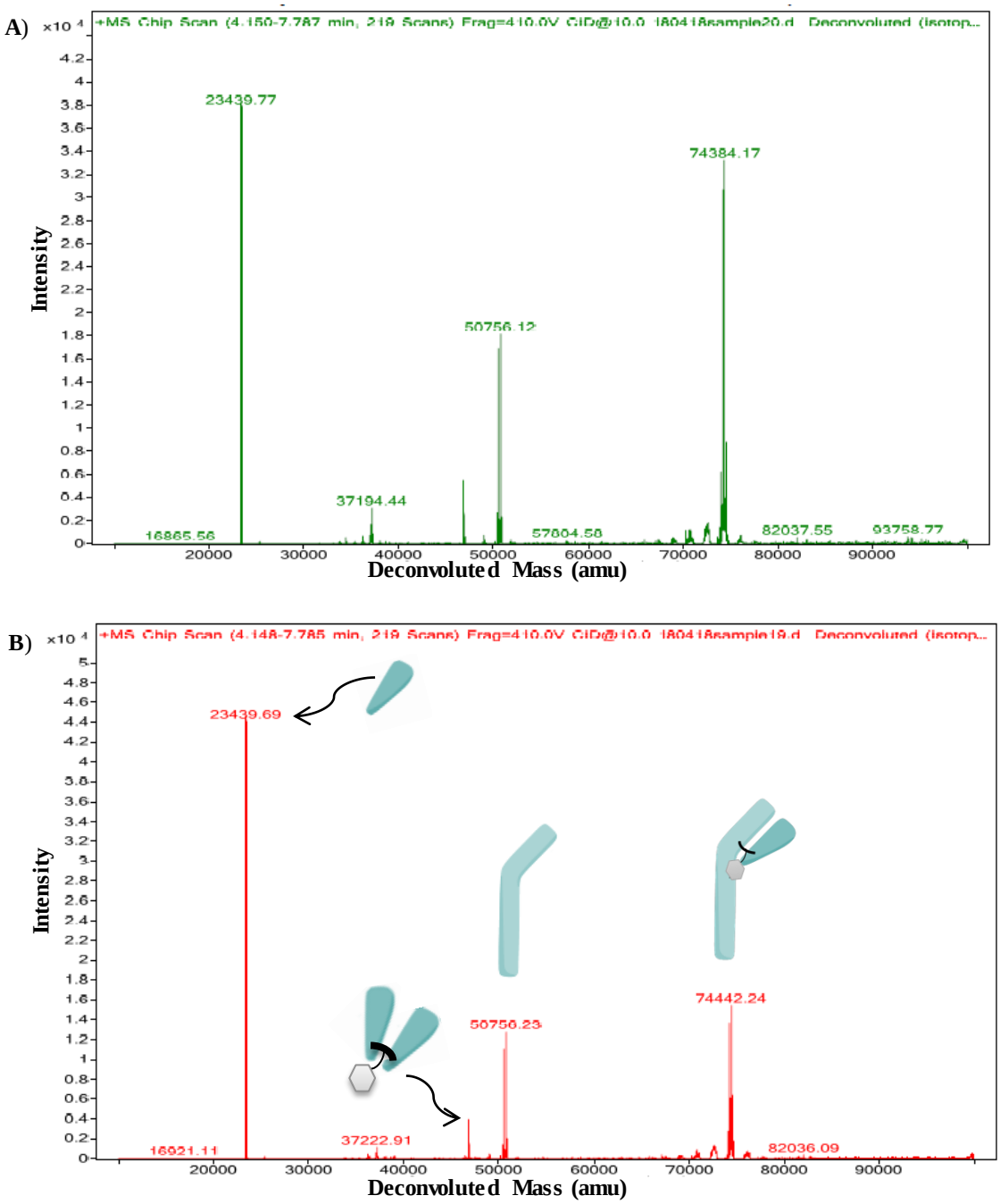

Figure 6.8. A) Deconvoluted protein MS spectrum of cross-linked Tmab with 1.1 equiv. of methyl 3,4-bis(2-bromoacetamido) benzoate (**4.23**) showing major peak at half antibody at 74,384.17 Da and a peak at 50,765.12 Da (unfunctionalised heavy chain). **B**) Deconvoluted protein MS spectrum of cross-linked Tmab with 1.1 equiv. *N*,*N*'-(1,2-phenylene)bis(2-bromoacetamide) (**4.27**) showing two major peaks at 50,756.23 Da (unfunctionalised heavy chain) and half-antibody at 74,442.24 Da. Both spectra showed light chain peak at 23,439.7 Da (unfunctionalised light chain).

With optimum reduction and cross-linking methods in hand, we next sought to evaluate the rebridging of partially reduced Tmab with bis-o-dihaloacetamide $(PEG)_3$ **6.1** and **6.2**.

6.4.1 Rebridging of partially reduced Tmab with bis-dihaloacetamide $(PEG)_3$ linker

Having successfully established the selective reduction conditions, we next tend to evaluate their rebridging ability with partially reduced Tmab. As such, Tmab (5 mg/mL) in conjugation buffer Tris.HCl (100 mM, pH 7.5) was reduced by incubation with TCEP (1.1 equiv.) for 2 h at 4°C. The reduced Tmab was then incubated with 1.1 or 2 equivalents of bis-o-diiodoacetamide $(PEG)_3$ linker (**6.2**) and held at room temperature overnight.

SDS-PAGE analysis of the reaction products displayed inferior rebridging capability of heavy-light chains (75 kDa) with bis-o-diiodoacetamide $(PEG)_3$ linker (**6.2**) (Figure 6.9, lane 1 and 2) compared to methyl 3,4-bis(2-bromoacetamido) benzoate (**4.23**), which was used as a positive control to confirm the optimum reduction condition (Figure 6.9, lane 3). Possibly, the cross-linking of heavy-light was decreased because of the non-selective cross-linking of heavy-heavy chains with the second head of bis-o-diiodoacetamide $(PEG)_3$ linker (**6.2**) as observed by SDS-PAGE analysis of these reactions (higher MW bands around 125 and 150 kDa under reducing conditions) (Figure 6.9, lanes 1 and 2).

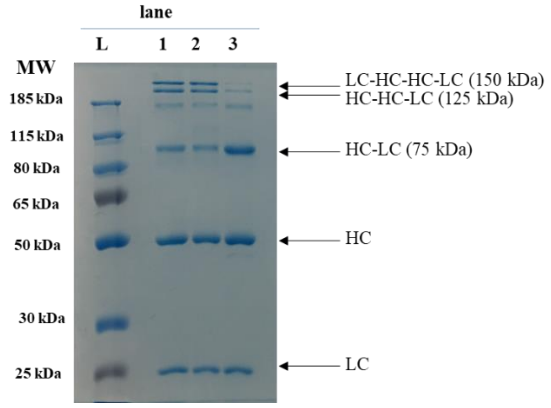

Figure 6.9. SDS-PAGE of cross-linking of partially reduced Tmab (5.0 mg/ml, 34 µM) in Tris.HCl buffer (100 mM, pH 7.5) containing 150 mM NaCl, and 5 mM EDTA, with bis-o-diiodoacetamide $(PEG)_3$ linker (**6.2**). Tmab was reduced with 1.1 equiv. of TCEP (37 µM) for 2 h at 4°C and incubated with the linker at room temperature overnight. Lane 1: Tmab incubated with 1 equiv. of bis-o-diiodoacetamide $(PEG)_3$ linker (**6.2**), Lane 2: Tmab incubated with 2 equiv. of bis-o-diiodoacetamide $(PEG)_3$ linker (**6.2**), Lane 3: Tmab incubated with 1.1 equiv. of methyl 3,4-bis(2-bromoacetamido)benzoate (**4.23**) at room temperature overnight.

We observed previously that bis-iodoacetamide linkers are more selective toward cross-linking of heavy-heavy disulfide bonds, thus we proposed that bis-o-dibromoacetamide $(PEG)_3$ linker (**6.1**) would be more selective toward heavy-light disulfide bonds.

To this end, Tmab (5 mg/mL) in Tris.HCl buffer was reduced by incubation with TCEP (1.1 equiv.) for 2 h at 4℃. The reduced Tmab was incubated with 5 equivalents of bis-dihaloacetamide $(PEG)_3$ linkers and held at room temperature overnight. Both bis-o-dihaloacetamide linkers (**6.1** and **6.2**) displayed similar level of rebridging of heavy-light chains (75 kDa) (Figure 6.10, lanes 4 and 5).

In comparison with methyl 3,4-bis(2-bromoacetamido) benzoate (**4.23**), both bis-dihaloacetamide linkers (**6.1** and **6.2**) showed a lower degree of heavy-light chain rebridging and higher level of high molecular weight bands (at 125 kDa and 150 kDa) as observed by SDS-PAGE of the reaction products (Figure 6.10, lanes 4 and 5).

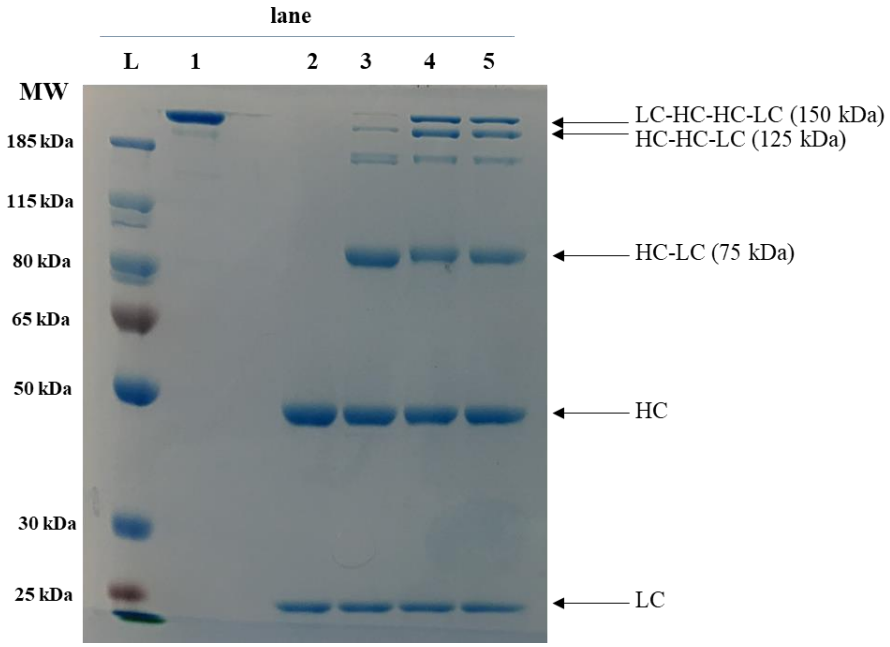

Figure 6.10. SDS-PAGE of cross-linking of partially reduced Tmab (5.0 mg/ml, 34 µM) in Tris.HCl buffer (100 mM, pH 7.5) containing 150 mM NaCl, and 5 mM EDTA, with bis-o-dihaloacetamide $(PEG)_3$ linkers. Tmab was reduced with 1.1 equiv. of TCEP (37 µM) for 2 h at 4 ℃ and incubated with the linkers at room temperature overnight. Lane 1: Tmab control non-reducing dye, lane 2: Tmab control reducing dye, lane 3: Tmab incubated with 1.1 equiv. of methyl 3,4-bis(2-bromoacetamido)benzoate (**4.23**), lane 4: Tmab incubated with 5 equiv. of bis-dibromoacetamide $(PEG)_3$ linker (**6.1**), lane 5: Tmab incubated with 5 equiv. of bis-o-diiodoacetamide $(PEG)_3$ linker (**6.2**).

In summary, despite the reduced level of LC-HC cross-linking, the optimised conditions were considered suitable to attempt the conjugation of Tmab with Sbi III/IV-2xCys.

6.4.2 Tmab-Sbi conjugation

With optimised selective reduction conditions of Tmab in hand, we sought next to attempt conjugation of Tmab and Sbi using the first proposed strategy.

Conjugation of Sbi III/IV-2xCys with Tmab was evaluated by conjugation of reduced Sbi III/IV-2xCys (5 mg/mL) in Tris.HCl buffer with functionalised Tmab (5 mg/mL). Briefly, Tmab was reduced with 1.1 equiv. of TCEP for 2 h at 4°C and reacted with bis-dihaloacetamide $(PEG)_3$ **6.1** and **6.2** (5 equiv.) linkers for 3 h at room temperature. Excess reagent was removed by buffer exchange into conjugation buffer (100 mM, 150 mM NaCl, 5 mM EDTA, pH 7.5). In tandem with this, Sbi III/IV-2xCys was reduced with 2 equiv. of TCEP for 1 h followed by quenching step using penta-PEG azide (**2.13**) for 1 h. Then, reduced Sbi III/IV-Cys (4 equiv.) was then added to functionalized Tmab and left at room temperature overnight. The reaction products were resolved by SDS-PAG analysis. The estimated MW of the product would be around 90 kDa under reducing conditions.

SDS-PAGE analysis of the reaction products revealed that the conjugation using this method did not work (Figure 6.11, lane 7 and 8). One possible explanation is the presence of off-target disulfide bonds of Tmab, which have reduced the yield of the production of half-antibody (75 kDa) as well as interfered with the conjugation step with the reduced Sbi.

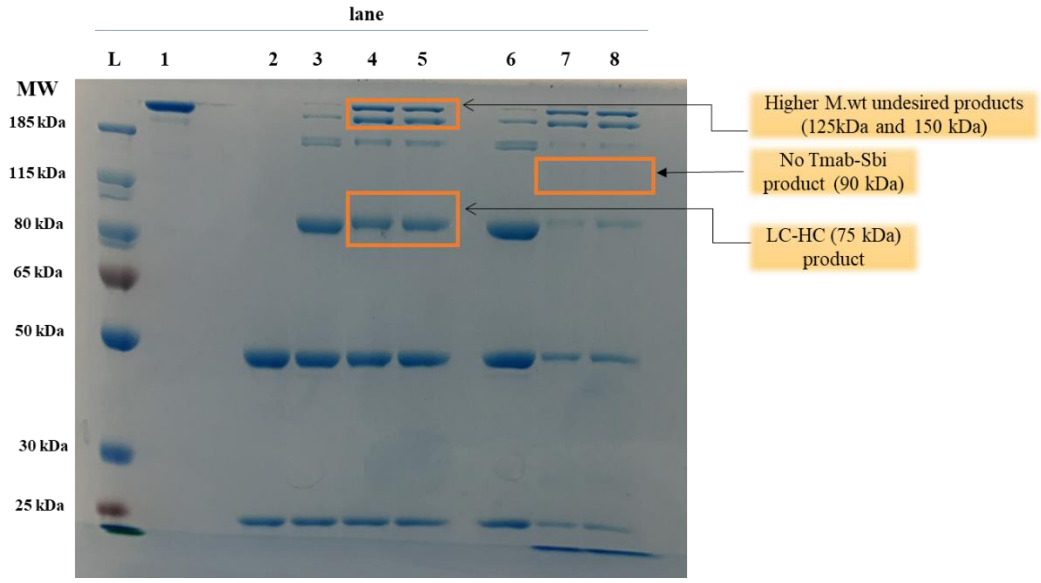

Figure 6.11. SDS-PAGE representing conjugation of partially reduced Tmab and Sbi III/IV-2xCys in Tris.HCl buffer using bis-dihaloacetamide $(PEG)_3$ linkers **6.1** and **6.2**. Tmab was reduced with 1.1 equiv. of TCEP for 2 h at 4°C. Sbi III/IV-2xCys was reduced with 2 equiv. of TCEP for 1 h followed by quenching step with hexa-diazide (10 equiv..) for 1 h. lane 1: Tmab control (non-reducing dye). lane 2: Tmab control (reducing dye), lane 3: Tmab was incubated with 1.1 equiv. of methyl 3,4-bis(2-bromoacetamido)benzoate (**4.23**) linker at room temperature for 3 h, lane 4: Tmab incubated with 5 equiv. of bis-o-diiodoacetamide $(PEG)_3$ linker (**6.2**) at room temperature for 3 h, lane 5: Tmab incubated with 5 equiv. of bis-dibromoacetamide $(PEG)_3$ linker (**6.1**) at room temperature for 3 h, lane 6: Tmab was incubated with 1.1 equiv. of methyl 3,4-bis(2-bromoacetamido)benzoate (**4.23**) at room temperature overnight, lane 7: conjugation reaction of functionalised Tmab-diiodoacetamide with Sbi III/IV-2xCys (4 equiv.) at room temperature overnight, lane 8: conjugation reaction of functionalised Tmab-dibromoacetamide with Sbi III/IV-2xCys (4 equiv.) at room temperature overnight. Protein samples were resolved by reducing SDS-Page (10% gel).

6.5 Conjugation of functionalised Sbi with partially reduced Tmab (Strategy 2)

As we were not able to construct Tmab-Sbi conjugate using the first proposed strategy, we next sought to evaluate the conjugation of Tmab and Sbi protein through using the second strategy where functionalised Sbi will be conjugated to the partially reduced Tmab.

As such, Sbi III/IV-2xCys (5 mg/mL) in Tris.HCl buffer (100 mM, pH 7.5) was reduced with TCEP **2.2** (2 equiv.) for 1 h. Then, quenching step using penta-PEG azide (**2.13**) for 1 h was followed by addition of bis-o-diiodoacetamide $(PEG)_3$ linker **6.2** (5 equiv.) and incubation for 3 h at room temperature. Excess reagent was removed by buffer exchange into the conjugation buffer using Amicon® Ultra-15mL (3 kDa) centrifugal

filters. Meanwhile, Tmab (5 mg/mL) was reduced with TCEP **2.2** (1.1 equiv.) for 2 h at 4°C. Functionalised Sbi III/IV-2xCys (4 equiv.) was then added to the partially reduced Tmab and left at room temperature overnight. The reaction products were resolved using SDS-PAGE (Figure 6.12 B, lane 2).

Immobilized metal affinity chromatography (IMAC) was performed to purify the reaction using Ni^{2+} column (1 mL HisTrap, FF) (Figure 6.12 A). The estimated MW of the product would be around 90 kDa under reducing conditions which matches with the obtained bands of between HC-HC band (100 kDa) and HC-LC band (75 kDa). As Sbi III/IV-2xCys is a his-tagged protein, IMAC purification was performed to separate Tmab-Sbi conjugate from unfunctionalised Tmab. IMAC purification was successful in the separation of unfunctionalised Tmab (Figure 6.12 A, lane 3) from Tmab-Sbi conjugate (Figure 6.12 A, lane 5).

To our delight, we were able to construct Tmab-Sbi through using the second strategy, nevertheless, the obtained quite low overall yield of protein conjugate can be possibly attributed to is the short length of the PEG [$(PEG)_3$] linker and the steric hindrance which make the association of the two large proteins difficult. Thus, a longer chain of the linker would be expected to reduce the steric hindrance when attempting to link Sbi III/IV-2xCys and Tmab and increase the obtained yield of the conjugate. To investigate this theory, we set out the synthesis of the $(PEG)_7$ linker **6.5**

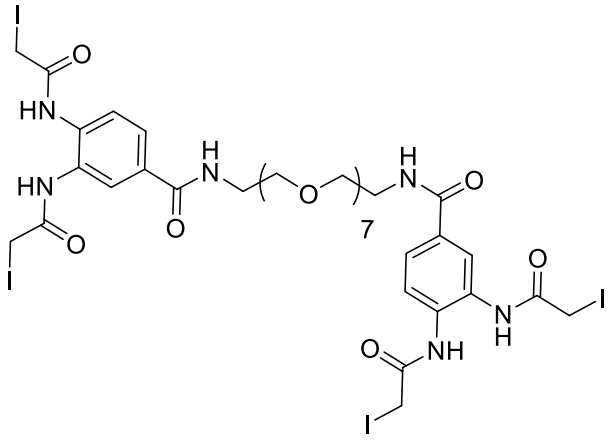

(**6.5**)

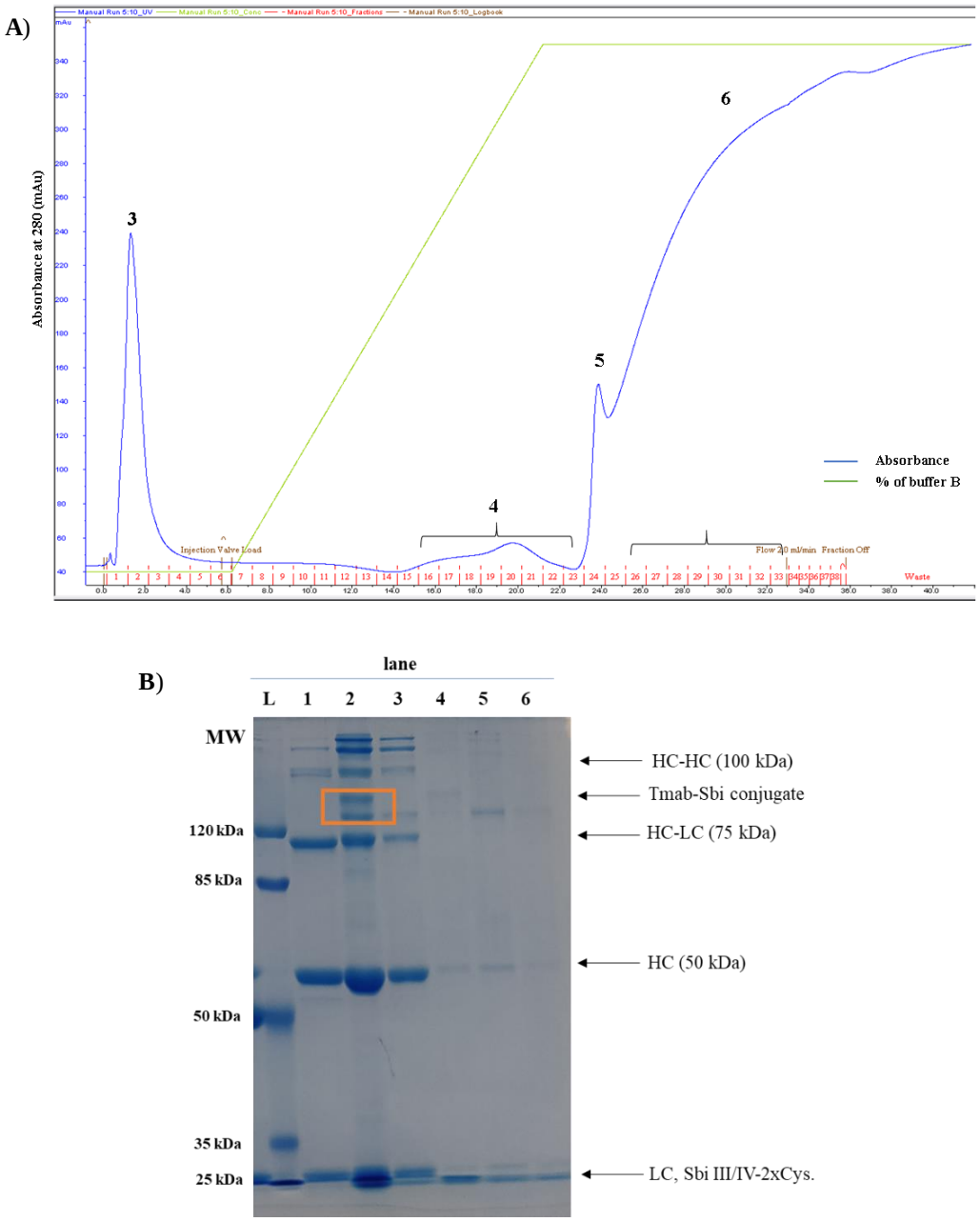

Figure 6.12. A) Affinity chromatography purification of Tmab-Sbi conjugation reaction to separate unfunctionalised Tmab **3** from Tmab-Sbi conjugate **5**. **B**) SDS-PAGE analysis of conjugation of partially reduced Tmab and Sbi III/IV-2xCys in Tris.HCl buffer (100 mM, pH 7.5) using bis-o-diiodoacetamide $(PEG)_3$ linker (**6.2**). Lane 1: Tmab incubated with 1.1 equiv. of methyl 3,4-bis(2-bromoacetamido)benzoate (**4.23**), lane 2: Tmab conjugation with Sbi III/IV-2xCys at room temperature overnight before performing affinity chromatography purification, lane 3: collected early fractions (F1-4) of affinity chromatography purification, lane 4: collected eluted fractions (F16-23), lane 5: collected eluted fractions (F24-25), lane 6: collected eluted fractions (F26-33). Arrow indicates the expected band of Tmab-Sbi conjugate around 90 kDa. Protein samples were resolved by reducing SDS-Page (10% gel).

6.6 Synthesis of bis-o-diiodoacetamide $(PEG)_7$ (6.5)

Bis-diiodoacetamide $(PEG)_7$ linkers **(6.5)** was postulated as a more water soluble than **6.1** and **6.2** linkers with a longer chain length, permitting more amenable protein-protein conjugation. Given that both bromo- **6.1** and iodo-linkers **6.2** and showed comparable rebridging (see Figure 6.11), and as iodo-linker synthesis can be achieved more readily, we set out to synthesise the bis-o-diiodoacetamide $(PEG)_7$ **(6.5)**.

The 1,23-diamino-3,6,9,12,15,18,21-heptaoxatricosane (**6.6**) was first synthesised over 3 steps by tosylation reaction of 3,6,9,12,15,18,21-heptaoxatricosane-1,23-ditol (**6.8**) using 4-toluenesulphonyl chloride overnight (60% yield). Then, 1,23-diazido-3,6,9,12,15,18,21-heptaoxatricosane (**6.10**) was synthsised by refluxing **6.9** with NaN_3 overnight (80.6% yield). Lastly, the azide groups were reduced to amines using triphenylphosphine (Ph_3P) to obtain the di-amino$(PEG)_7$ **(6.6)** (57% yield) (Figure 6.13).

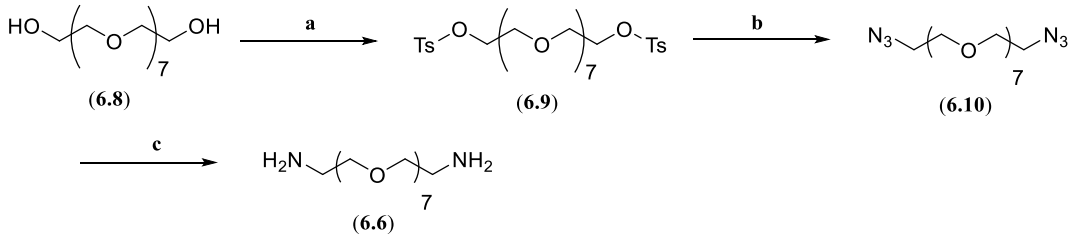

Figure 6.13. Synthesis of di-amino$(PEG)_7$ (**6.6**). **a**) *p*-TsCl, pyridine, DMC, **b**) NaN_3, DMF, 80°C, reflux, **c**) Ph_3P, dry THF overnight, then H_2O overnight.

Then, bis-o-diiodoacetamide $(PEG)_7$ linker **(6.5)** was synthesised by reacting the activated ester (**4.45**) with 1,23-diamino-3,6,9,12,15,18,21-heptaoxatricosane (**6.6**) to generate the bis-dichloroacetamide $(PEG)_7$ (**6.7**) (89% yield), which was then was converted to bis-o-diiodoacetamide $(PEG)_7$ derivative by refluxing with KI for 3 h (93.5% yield) (Figure 6.14).

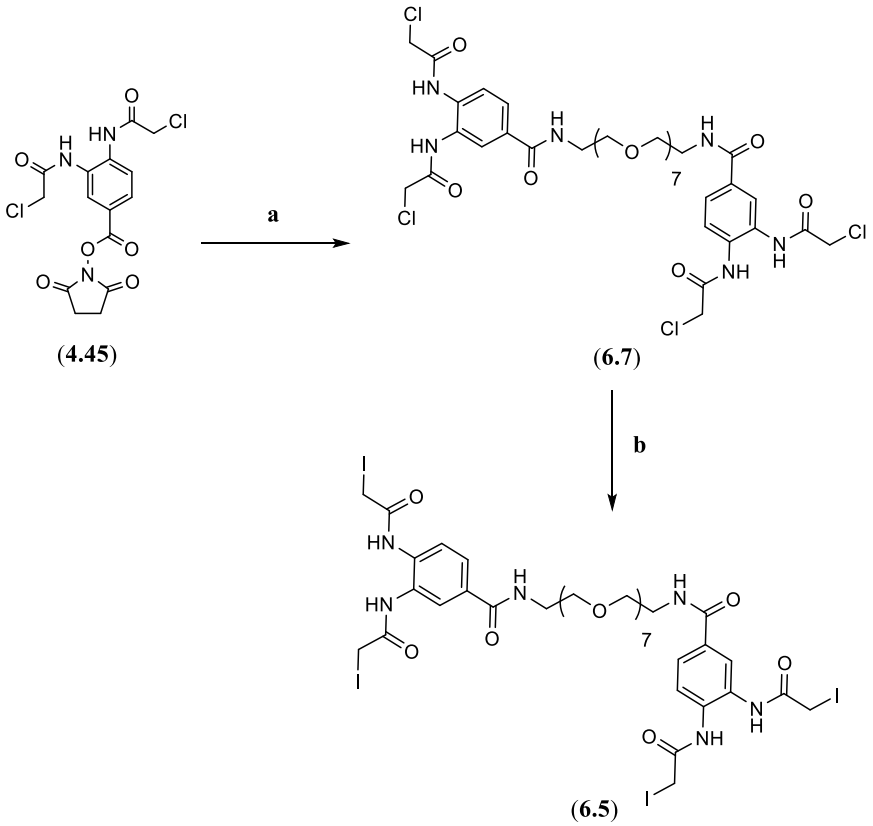

Figure 6.14. Synthesis of bis-o-diiodoacetamide $(PEG)_7$ **(6.5**). **a**) di-amine$(PEG)_7$ (**6.6**) THF, **b**) KI, dry acetone, reflux 3 h.

6.7 Application of bis-o-diiodoacetamide $(PEG)_7$ (6.5) in construction of $Tmab_{o\text{-}HL}$-PEG_7-$Sbi_{o\text{-}bis\text{-}Cys}$ conjugate (6.11)

Having successfully synthesised bis-diodoacetamide $(PEG)_7$ **6.5**, we set out to employ it to construct Tmab-Sbi conjugate using a similar conjugation method (strategy 2) as described in Section 6.5

To this end, Sbi III/IV-2xCys (5 mg/mL) in Tris.HCl buffer was reduced with TCEP **2.2** (2 equiv.) for 1 h, then, quenching step using penta-PEG azide (**2.13**) for 1 h was followed by addition of the bis-o-diiodoacetamide $(PEG)_7$ linker **6.5** (5 equiv.) and incubation for 3 h at room temperature. Excess reagent was removed by buffer exchange (3 times, using Amicon® Ultra-0.5 mL (3 kDa) centrifugal filters) into conjugation buffer.

Meanwhile, Tmab (5 mg/mL) was reduced with TCEP **2.2** (1.1 equiv.) for 2 h at 4°C. The functionalised Sbi III/IV-2xCys (4 equiv.) was then added to the reduced Tmab and left at room temperature overnight.

The reaction products were analysed using SDS-PAGE (reducing conditions) and revealed a band with estimated MW of 90 kDa which matches the expected mass of Tmab-Sbi conjugate (Figure 6.15, lane 6). In line with what was proposed previously regarding the length of the chain of the linker, a significant increase in the yield of the conjugate was obtained with bis-o-diiodoacetamide $(PEG)_7$ **6.5** (Figure 6.15, lane 6) in comparison with bis-o-diiodoacetamide $(PEG)_4$ **6.2** (Figure 6.12, lane 2).

IMAC purification was performed using Ni^{2+} column (1 mL HisTrap, FF) to separate Tmab-Sbi conjugate from unfunctionalised Tmab as Sbi III/IV-2xCys is a his-tagged protein. IMAC purification was successful in the separation of unfunctionalised Tmab (Figure 6.15, lane 7) from Tmab-Sbi conjugate (Figure 6.15, lane 8).

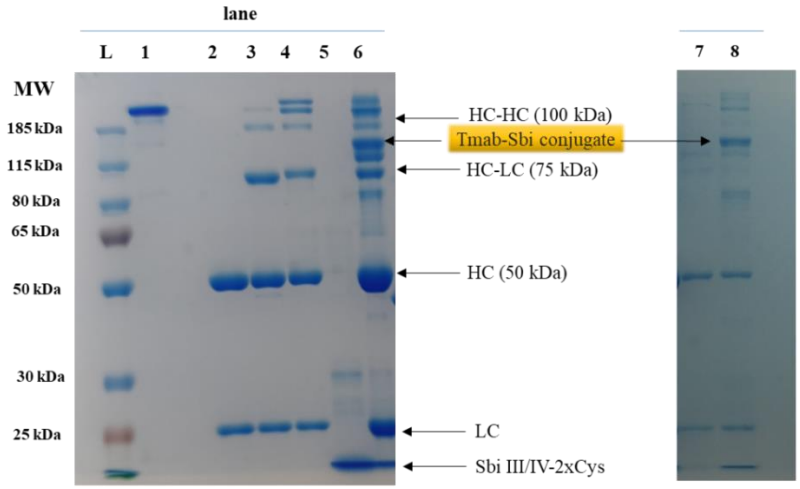

Figure 6.15. SDS-PAGE analysis of conjugation of partially reduced Tmab and Sbi III/IV-2xCys in Tris.HCl buffer (100 mM, pH 7.5) containing 150 mM NaCl, and 5 mM EDTA, using bis-o-diiodoacetamide $(PEG)_7$ linker (**6.5**). Lane 1: Tmab control (non-reducing), lane 2: Tmab control (reduced dye), lane 3: Tmab incubated with 1 equiv. of methyl 3,4-bis(2-bromoacetamido)benzoate (**4.23**), lane 4: Tmab incubated with 3 equiv. of bis-o-diiodoacetamide $(PEG)_7$ linker (**6.5**), lane 5: Sbi III/IV-2xCys Incubated with 5 equiv. of bis-o-diiodoacetamide $(PEG)_7$ linker (**6.5**), lane 6: Tmab conjugation with Sbi III/IV-Cys at room temperature overnight before affinity chromatography purification showing the correct estimated mass of the conjugate around 90 kDa, lane 7: combined early fractions of affinity chromatography purification, lane 8: combined eluted fractions of affinity chromatography with His-B buffer (1 mM imidazole) using Ni^{2+} column (1 mL HisTrap, FF). Protein samples were resolved by reducing SDS-Page (10% gel).

We rationalized that the observed HC-LC band (75 kDa) in the previously performed reaction can be mainly attributed to the incomplete removal of excess linker when spin filters were used (Figure 6.15, lane 6). Therefore, in order to evaluate the proposed hypothesis the same conjugation reaction was performed as mentioned above, but with a quick step of purification using Ni^{+2} column was proposed to remove excess linker from functionalised Sbi III/IV-2xCys solution prior to conjugation with partially reduced Tmab.

The stability of the attached linker after performing IMAC was tested using protein MS to confirm that iodide groups did not hydrolyse during the process of purification. The expected mass of functionalised Sbi III/IV-2xCys. is calculated as 16,726.16 Da, and was observed at 16,727.07 Da (Figure 6.14 B).

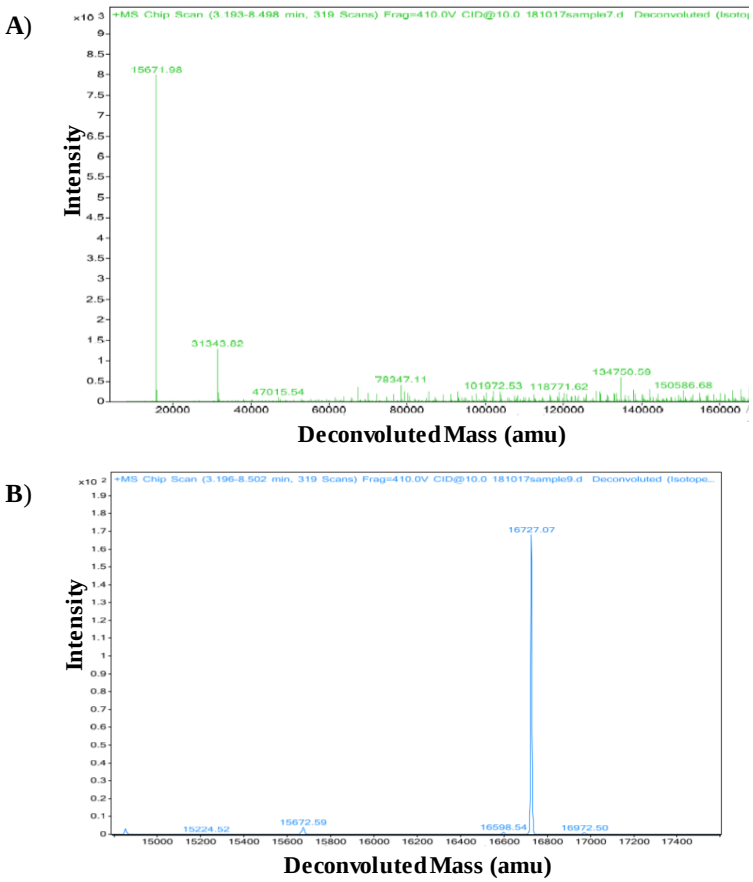

Figure 6.16. A) Deconvoluted protein MS spectrum of Sbi III/IV-2xCys control showing major peak at 15,671.98 Da. **B)** Deconvoluted spectrum protein MS of functionalised Sbi III/IV-2xCys with bis-o-diiodoacetamide $(PEG)_7$ linker (**6.5**) showing major peak at 16,272.07 Da.

A significant reduction in the 75 kDa band (half-antibody) was observed when IMAC was conducted as a quick purification step before performing Tmab-Sbi conjugation (Figure 6.17 A, lane 4 vs. lane 8). The obtained results proved that using spin filters was not sufficient to remove excess linkers from the reaction mixture of Sbi III/IV-2xCys and confirm that quick purification step using Ni^{+2} column was sufficient to get the pure functionalised Sbi III/IV-2xCys.

IMAC purification was further performed to purify the Tmab-Sbi conjugate using Ni^{2+} column (1 mL HisTrap, FF), which was successful in the separation of unfunctionalised Tmab from Tmab-Sbi conjugate (Figure 6.17 A and B, lane 5-7).

It is worth pointing out the significant increase in the yield of Tmab-Sbi conjugate using bis-o-diiodoacetamide $(PEG)_7$ linker (**6.5**) in comparison with bis-o-diiodoacetamide $(PEG)_3$ linker (**6.2**) (Figure 6.17 A, lane 4 vs. lane 9).

Having successfully improved the yield of conjugation and obtained the purified Tmab-Sbi conjugate using Ni^{2+} column, however, unreacted Sbi III/IV-2xCys (Figure 6.17 A, lanes 6 and 7) was eluted with Tmab-Sbi and therefore a further purification step is necessary.

We proposed that purification of Tmab-Sbi conjugate from unreacted Sbi III/IV-2xCys could be achieved through using protein A column (1 mL HiTrap Protein A, FF, GE Healthcare). Protein A column is widely used column for antibodies purification due to the high affinity of protein A (SpA) for human IgGs (see Section 6.1.2.1). We assumed that Tmab-Sbi would bind to protein A column, while un-reacted Sbi would be not bind and therefore separated from the desired product. To our surprise, we were not able to separate the reaction mixture by using protein A column and we could not extract the reaction products from the column. One possible explanation of what we experienced is the possible interaction between both *S. aureus* proteins, protein A (SpA) and Sbi. To the best of our knowledge, this interaction has not been studied before and need to be further evaluated in future studies.

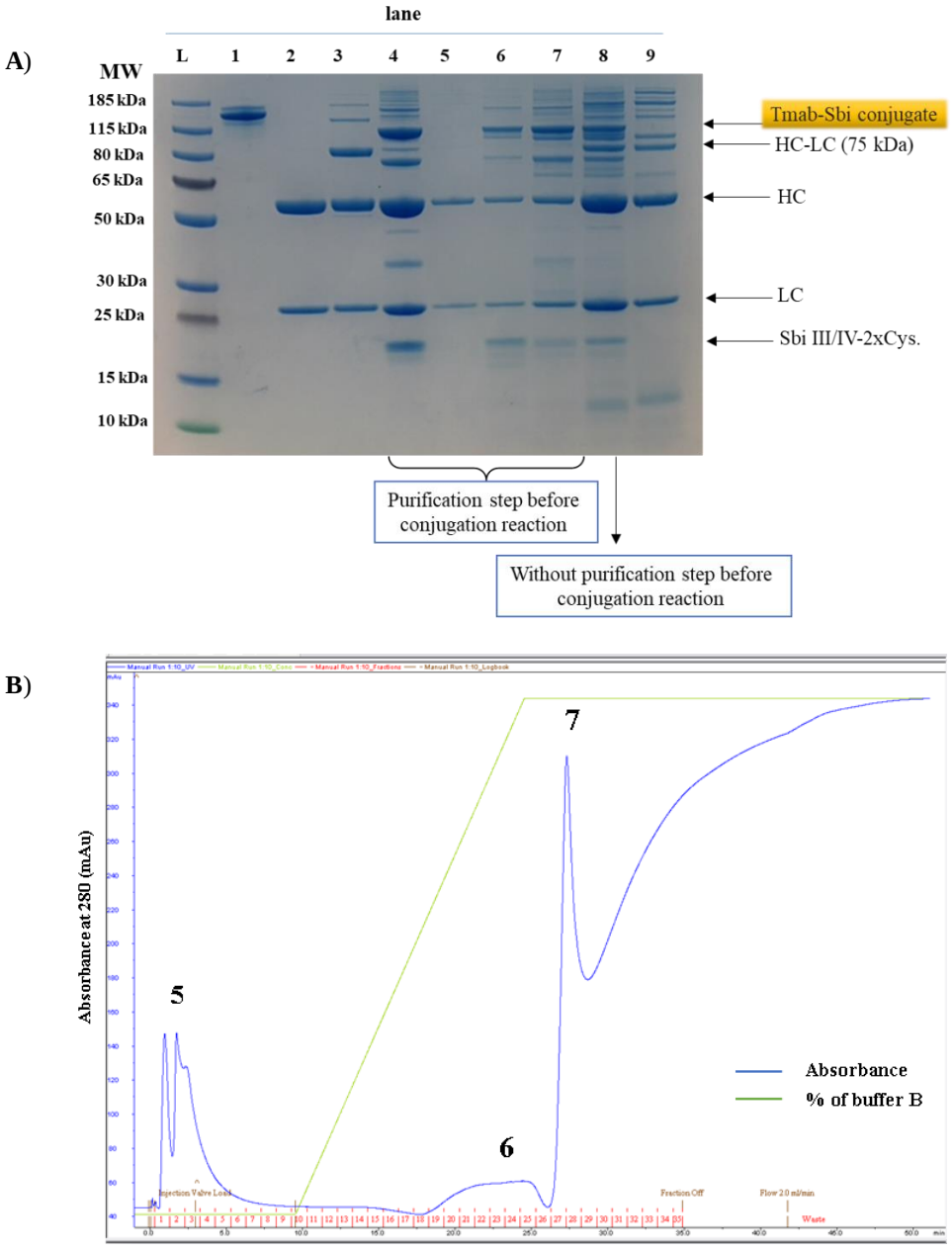

Figure 6.17. A) SDS-PAGE analysis of conjugation of partially reduced Tmab and Sbi III/IV-2xCys in Tris.HCl buffer (100 mM, pH 7.5) containing 150 mM NaCl, and 5 mM EDTA, using bis-o-diiodoacetamide $(PEG)_7$ linker (**6.5**). Lane 1: Tmab control (non-reducing), lane 2: Tmab control (reduced dye), lane 3: Tmab incubated with 1.1 equiv. of methyl 3,4-bis(2-bromoacetamido)benzoate (**4.23**), lane 4: Tmab conjugation with Sbi III/IV-2xCys at room temperature overnight before affinity chromatography purification step showing the correct estimated mass of the conjugate around 90 kDa, lane 5: collected early fractions (F1-5), lane 6: collected eluted fractions (F19-25), lane 7: collected eluted fractions (F27-29). Lane 8: Tmab conjugation reaction with Sbi III/IV-2xCys at room temperature overnight using bis-o-diiodoacetamide $(PEG)_7$ linker (**6.5**) without the quick in between purification step (see Figure 6.15). Lane 9: Tmab conjugation reaction with Sbi III/IV-2xCys at room temperature overnight using bis-o-diiodoacetamide $(PEG)_3$ linker (**6.2**) (see Figure 6.12). Protein samples were resolved by reducing SDS-PAGE (4-12% gel). **B)** Affinity chromatography purification of unconjugated Tmab (lane 5) from Tmab-Sbi conjugate (lane 6 and 7) using Ni^{2+} column (1 mL HisTrap, FF).

Next, in order to separate Tmab-Sbi conjugate from Sbi III/IV-2xCys based on the large mass difference, size exclusion chromatography (SEC) was performed using a superdex column (200 pg, GE Healthcare). To our delight, unconjugated Sbi III/IV-2Cys. has been successfully separated from Tmab-Sbi III/IV-2Cys conjugate by using SEC (Figure 6.18 A and B, lane 5).

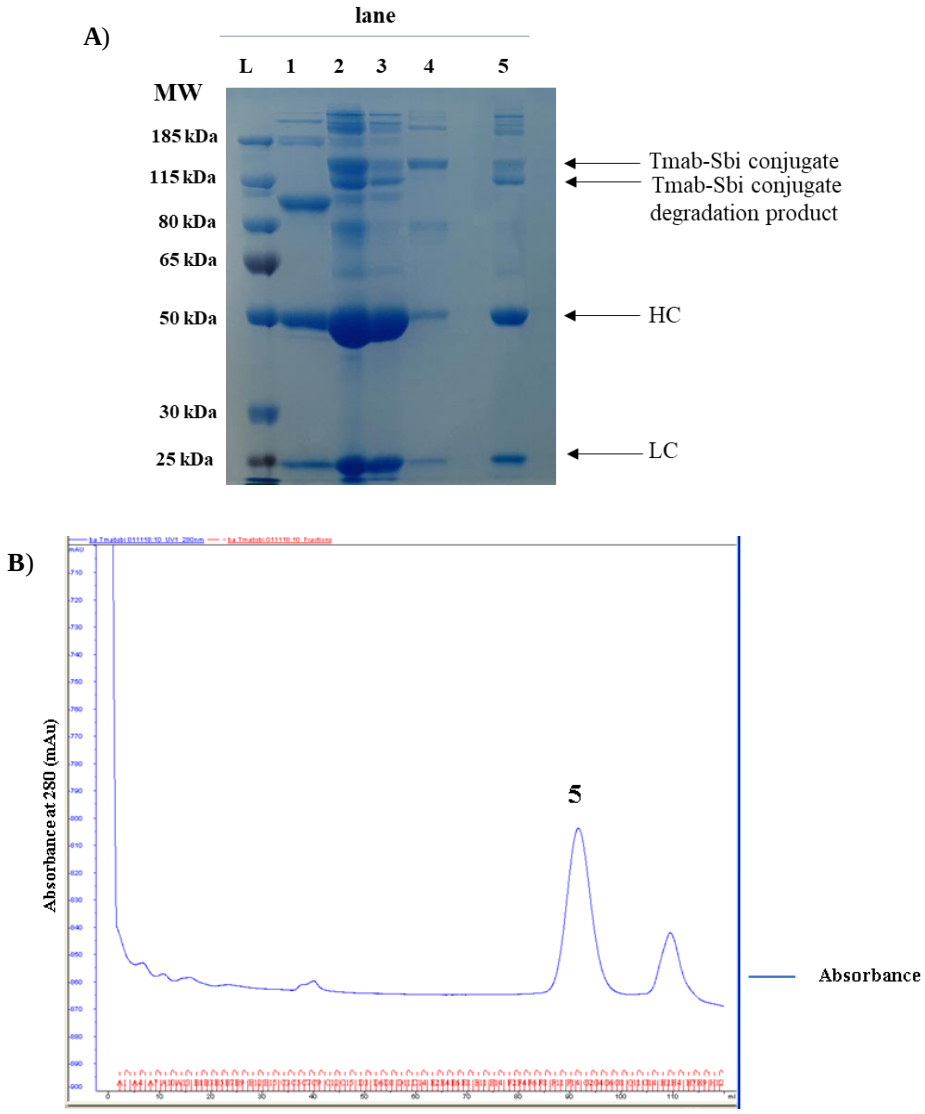

Figure 6.18. A) SDS-PAGE analysis of conjugation of partially reduced Tmab and Sbi III/IV-2xCys in Tris.HCl buffer (100 mM, pH 7.5) containing 150 mM NaCl, and 5 mM EDTA, using bis-o-diiodoacetamide $(PEG)_7$ linker (**6.5**). Lane 1: Tmab incubated with 1.1 equiv. of methyl 3,4-bis(2-bromoacetamido)benzoate (**4.23**), lane 2: Tmab conjugation with Sbi III/IV-2xCys at room temperature overnight before affinity chromatography, lane 4: collected pure fractions (F19-25) before performing SEC, lane 5: size exclusion chromatography purification (F10-G5). **B)** Size exclusion chromatography purification of Sbi-Tmab conjugation reaction to separate unconjugated Sbi III/IV-2xCys from Tmab-Sbi conjugate (lane 5). Protein samples were resolved by reducing SDS-Page (10% gel).

However, the pure conjugate degraded, most probably between domain III and IV of Sbi, affording Tmab-Sbi IV as a final stable product (as indicated by the arrows) (Figure 6.18 A, lane 5). Protein mass spectrum was conducted to confirm the degradation of Tmab-Sbi III/IV to attain Tmab-Sbi IV with an estimated mass of 157033 Da and the found mass was 156990.64 Da (Figure 6.19).

The degradation of Tmab-Sbi III/IV-2Cys conjugate is, most probably, proteases-dependent degradation, which mainly cleaved Sbi between the two domains, domain III and IV. Another possible mechanism of degradation of Sbi III-IV is through mAb-mediated degradation. Both mechanism need to be further evaluated in future.

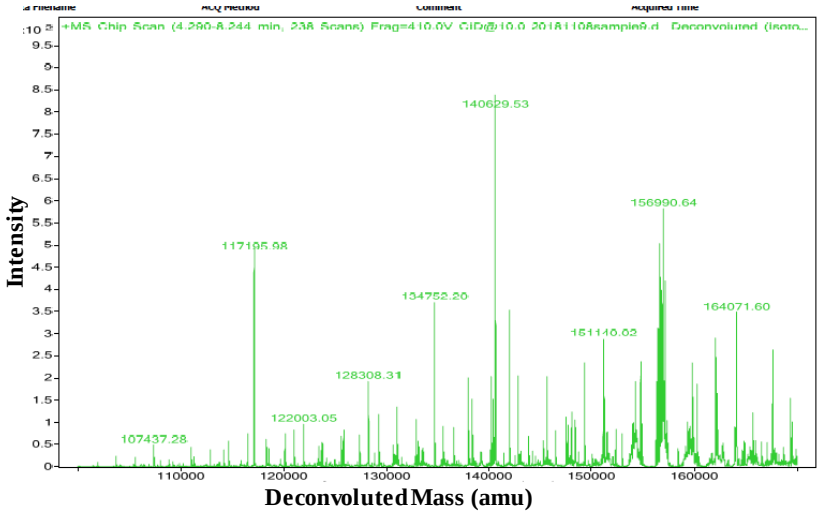

Figure 6.19. Deconvoluted protein MS spectrum of Tmab-Sbi III/IV conjugate, showing a mass around 156,990.64 Da of the degraded product (Tmab-Sbi IV).

6.8 Conclusion and future work

Construction of the immunomodulating Tmab conjugate, in order to improve the limited advantages that have attained from using Tmab as a single therapy, would provide a new and promising conjugates in breast cancer treatment to be further evaluated *in vitro* and *in vivo* against HER2 positive breast cancer. Inspired by the notion of ACDs, we aimed to utilise Tmab as a carrier of Sbi III-IV and the latter will activate the human complement protein C3 against cancer tissue.

In this work we were able to chemically synthesise the re-bridging bis-o-diiodoacetamid $(PEG)_7$ linker **6.5**, which was used to construct the immunomodulating conjugate in feasible and easy to follow procedure without the need to use genetic engineering. Moreover, the purification steps were successful to separate the desired conjugate.

With the unfortunate degradation of Sbi III-IV, in the future work, more effort will put to enhance the stability of Sbi and therefore construct a stable Tmab conjugate which includes the followings:

1- Define the cleavage site and the degraded products.
2- Further evaluate the protease-dependent mechanism and test the possibility of incorporation of different protease inhibitors during the conjugation process.
3- Modify the sequence of Sbi III/IV at the cleavage site (sites) to prevent the degradation without influencing the activity of the protein.
4- Test the possible mechanism of degradation of Sbi that is related to the actual conjugation to mAbs and if this a natural mechanism associated with this protein.

Next, *in vitro* and *in vivo* evaluation of the immunoconjugate of Tmab-Sbi will be conducted against HER2 positive and negative breast cancer. The applicability of this work could be translated to different types of cancer, which provided a novel anti-cancer mechanism to activate complement system against cancer tissue.

7 The chemical synthesis of Fc containing bi-specific antibody using Bis-dihaloacetamide PEG cross-linkers

7.1 Introduction

In general, diseases are not caused by a single defined factor but by the interactions between multiple underlying factors. Therefore, the simultaneous modulation of more than one factor can improve the efficacy of disease treatment with potential to prevent the development of biological resistance. Bi-specific antibodies (bsAbs) are a modified and potentially ground-breaking class of mAb biotherapies. As their name implies, bsAbs simultaneously recognise and engage with two different receptor targets, thus enabling more complex intervention mechanisms. Bi-specific antibodies have gained particular popularity in the field of oncology due to the limited and unconvincing benefits of employing native mAbs in cancer therapy. Recently, this field has gained substantial attention as more than 50 bsAbs are under investigation in clinical trials for various malignancies.[244,245]

BsAbs were primarily constructed to recruit components of the immune system against cancer cells by reorienting effector cells against tumour cells, eliciting mAb Fc receptor function, or by activating T cell receptors (TCR). Amongst the effector cells, both T-cells (usually through the CD3 receptor) and Natural Killer (NK) cells have recently begun to receive considerable attention in immunotherapeutic approaches.[246]

T-cell engagers (BiTE) are a well-recognised subtype of bsAb that recruit the cytotoxic role of T-cells in cancer immunotherapy. BiTE has been shown to have a potential advantage in chemotherapy resistant cancer cells and quiescent stem cells.[247] In addition, bsAbs can be used to target two separate disease receptors or mediators leading to substantial therapeutic effect (increased potency or efficacy), and suppression of biologic resistance and relapse.[248]

Initially, bsAbs were produced by co-expression of two light and heavy chains in a single host cell line, also known as hybrid-hybridoma or quadroma technology. One example of the earliest approved bsAb with the entire IgG format is Catumaxomab,

which was the first approved bsAb. It was approved by the European Union in 2009 for the intraperitoneal therapy of patients with malignant ascites. Catumaxomab targets both Epithelial Cell Adhesion Molecule (EpCAM) antigen and also activates T-cells through binding to the T-cell surface protein CD3.[249] Catumaxomab belongs to Triomab® class of bsAbs. The Triomab® family consists of two half antibodies: a mouse IgG_{2a} and a rat IgG_{2b} (anti-CD3), which are constructed through fusion (hybridization) of different hybridoma cell lines (quadroma technology).[250] One of the major restrictions of the this first generation bsAbs is the difficulty in the production of sufficient quantities of homogenous, clinical-grade species of bsAbs.[251] Other obstacles include the required complex methods of purification to sequester homodimers contaminants,[252] as well as the activation of a human anti-mouse antibody (HAMA) response in the majority of treated patients owing to the murine origin of mAbs. Researchers have therefore investigated alternative recombinant DNA techniques and chemical conjugation methods to overcome these drawbacks.

BsAbs can be classified into different categories according to the resemblance of IgG antibody structure, molecular size, the presence of an Fc region, the construction methods used and the function (Figure 7.1).[245] With more than 100 bsAbs construct, most of them were produced using recombinant technologies, with the most prominent difference being the molecular weight with these formats, which mainly depends on the presence or absence of an Fc region. The presence of an Fc region in bsAb format, usually referred to as 'trifunctioal' antibody, not only exerts essential cytotoxic effector mechanisms, but also extends the plasma half-life of the construct and therefore precludes a multiple dosing regimen.[253] Therefore, bsAbs can be classified into two major categories: bsAbs lacking of the Fc region and Fc containing bsAbs.

7.1.1 Classes of bi-specific antibodies lacking of Fc region

A plethora of different classes for the construction of bsAb has been proposed by using genetic engineering methods (recombinant technologies), in particular variable-fragment based formats. Variable fragment (Fv) with a short peptide chain connecting the VH and VL domains, also known as single-chain variable domain fragments (scFv) (Figure 7.1),

are commonly used as building blocks in creating variable-fragment bsAb, such as tandem single chain variable fragment molecules (taFvs), and diabodies (Dbs).[244]

The taFvs format is constructed by the fusion of two scFv molecules using a flexible linker (Figure 7.1). Dbs, on the other hand, are constructed by expressing two different chains VH_1-VL_2 and VH_2-VL_1 within one cell. The two variable domains of each individual chain are connected via a short five-residue peptide linker to avoid mispairing of variable regions within one chain, therefore allowing the desired crossover pairing of the two chains affording Dbs (Figure 7.1).[254]

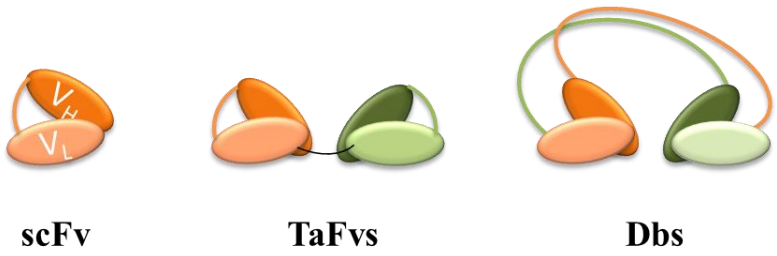

Figure 7.1. Schematic representation of the two well-known bispecific antibody classes lacking of the Fc region. Orange and green indicate different specificities (binds to different antigens). scFv: single-chain variable domain fragment, TaFvs: Tandem single chain variable fragments, Dbs: diabodies.

Blinatumomab is the first clinically effective member of bispecific T engager (BiTE) antibodies (diabodies), which target cancer cells via binding to CD19 receptor on B-cells and recruiting T-cells via CD3 receptor binging. Blinatumomab is used in patients with relapsed/ refractory precursor B-cell acute lymphoid leukemia.[255]

Recently, Hull *et al.* have developed an elegant chemical cross-linking approach without the need to incorporate unnatural amino acid or recombinant technologies. They were able to cross-link the disulfide bonds of mAb using rebridging approach affording a stable and homogenous bsAbs. This approach is based on using bis-(dibromomaleimide) PEG (**7a**) linker in order to construct bsAb of scFv-Fab format.[256]

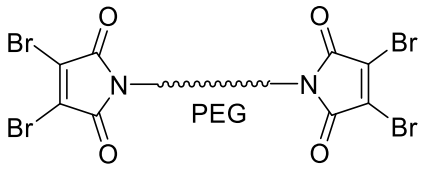

(**7a**)

7.1.2 Entire IgG classes: Fc region containing bi-specific antibodies

BsAbs containing Fc region offer a range of advantages related to effector functions of this region, such as antibody-dependent cell-mediated cytotoxicity (ADCC), complement-dependent cytotoxicity (CDC). In addition, the presence of Fc region facilitates the purification steps and modulates both solubility and stability of the construct and more importantly, increases the plasma half-life mediated through FcRn receptors.

One of the major obstacles to obtain bsAbs with IgG-like structure is the mispairing of heavy and light chains resulting in homodimer formation. Therefore, in order to produce bsAb with IgG-like format with minimal mispairing potential, Knobs-into-holes hetero-dimerization technology has been developed as an elegant protocol for the production of bsAbs with two distinguished and independent Fab regions while maintaining the overall native IgG architecture. This technology is made possible through the introduction of complimentary mutations in the C_{H3} domains to promote the association (hetero-dimerization) between heavy chains of the two different antibodies (one antibody has a 'knob' mutation and the other one has 'hole' mutations) as shown in in Figure 7.2.[257] This concept, however, has been modulated with different approaches, to assure the heterodimerization of heavy chains. These approaches cannot however, prevent the homodimersization of light chains. Thus, in order to maintain the native IgG structure without using unnatural domain junctions in order to stop homodimersization of light chains, one proposed solution is to use common light chain.[258]

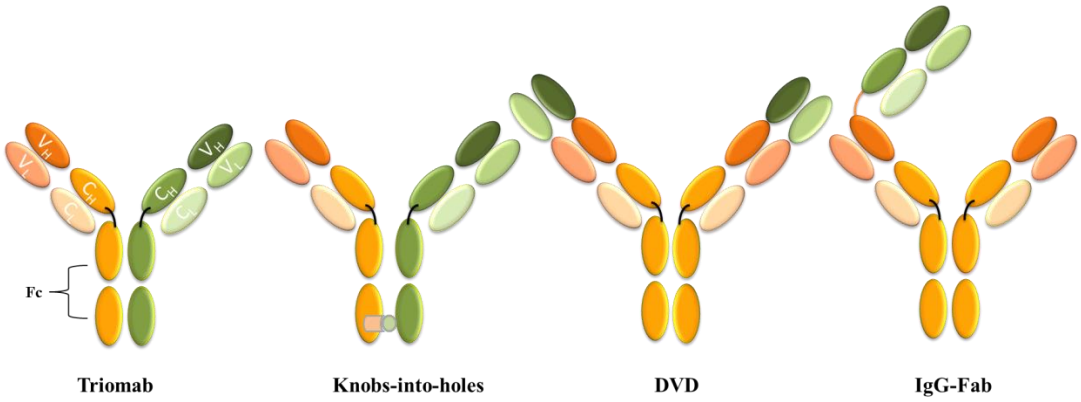

Figure 7.2. Schematic representation of some of the Fc-containing bsAbs classes. Orange and green indicate different specificities (binds to different antigens). DVD: dual variable-domain.

Spiess *et al.* have developed a new approach to prevent the homodimersization of heavy and light chains. They separately have expressed half-antibodies (75 kDa) in two bacterial strains. Then, they combined these halves to generate a bispecific antibody.[259]

In addition to the requirement for complex production and purification methods, accurate and complex quantitative analytical methods are also required. These analytical methods have to be capable of distinguishing between the product of interest and the product-related variants, such as covalently- and noncovalently-linked homodimers.[260,261]

Alternatively, a different approach was developed to ameliorate bsAb mispairing complications through engineering a modified variable region to be able recognise and bind to two unrelated antigens through different binding sites on the antibody variable region. Therefore, a single kind of heavy and light chain is required. For instance, anti-HER2 antibody has been developed by phage display. It can recognise HER2 receptor but also bind to a second and unrelated antigen, such as VEGF while preserving high binding affinity to HER2 receptor. This bsAb is known as "two-in-one" antibody, or Dual Action Fab (DAF).[244]

Differently, various approaches have maintained the normal IgG-structure of the mAb of interest and achieved bi-specificity through the addition of variable region-containing fragments, for example the fusing of a single-chain Fv fragment (scFv) to the C-terminus of the heavy chain of antibodies. Alternatively, bsAb can be constructed

through the combining the variable domains VH_2 and VL_2 domains to the variable domains of the antibody in tandem, generating what is known as a dual variable-domain antibody (DVD) (Figure 7.2).[262]

As shown previously, most of the recombinant technologies-based approaches were focused on using single chain variable building blocks of the Fab region which contain only antigen recognition domains of heavy and light chains, and lack constant regions of heavy and light chains. The natural construction of the Fab fragment affords a stabilising effect for the variable regions, ameliorating solubility characteristics, and preventing aggregation possibilities. For these reasons, Wu *et al.* developed another recent class of bsAbs was achieved through fusing the whole Fab region to the mAb of interest (Figure 7.2).[263] The Fab-based bsAbs were noticeably more thermally stable than scFv-based bsAbs. Moreover, Fab-based bsAbs showed negligible susceptibility to aggregation, whereas the scFv-based bsAbs displayed substantial tendencies to form aggregates.[263]

In general, chemical conjugation methods afford a reliable and facile approach for the construction of multiple formats of bsAb without the need for complex expression and purification technologies.

Yu Cao *et al.* developed a chemical based approach to achieve different formats of the two major bsAbs categories, anti-HER2/anti-CD3 bsAbs lacking of the Fc region and Fc containing anti-HER2/anti-CD3 bsAbs. They incorporate p-acetylphenylalanine (non-canonical amino acid residue) into anti-HER2 and anti-CD3 mAbs. Then the engineered mAbs have been reacted with bifunctional polymer affording oxime linkage and clickable handle (azide or ocyne functionalities).[111] They produced multiple classes of monovalent or divalent bsAbs with and without the Fc region. IgG formats with Fc region have found to display enhanced cytotoxicity against HER2 positive cancer cells compared to Fab-based ones. Moreover, it has been found that anti-HER2/anti-CD3 bsAbs showed enhanced efficacy against the xenograft model with low expression of HER2 cancer cells.[111]

In conclusion, despite the enhanced efficacy of Fc-containing bsAbs over the Fc-deprived bsAbs, to the best of our knowledge there is no current chemical method suitable to construct bsAbs (trifunctional) without the need for mutagenesis, complex expression and purification technologies.

7.2 The rationale for Tmab-IFab bsAb

As discussed previously, provided that IgG-like classes of bsAbs seem to attract considerable attention with a wide range of offered advantages, herein we are devoted to provide an alternative novel approach for the chemical construction of the trifunctional anti-HER2/anti-CTLA-4 bsAb antibody with Tmab-IFab format using our previously established conjugation platform, bis-o-dihaloacetamide PEG linker.

Our approach is based on the conjugation of the rebridged heavy-light chains of Tmab with the rebridged heavy-light chains of Fab of Ipilimumab (IFab) using bis-o-dihaloacetamide PEG approach (Figure 7.3). The construct of Tmab-IFab will interact/block with the following: HER2 receptors on cancer cells (T_1), CTLA-4 receptors on T-cell (T_2). In addition, the Fc region of mAb has the potential to interact with complement proteins and several effectors cells exerting the cytotoxic effector mechanisms of ADCC and CDC (T_3). Given that this construct is expected to exert the three main cytotoxic mechanisms, it is referred to as a trifunctional antibody (Figure 7.3).[264]

Trastuzumab (Tmab), a well-established humanized mAb, binds the HER2 receptor, it is widely used in the treatment of HER2 positive subtype (for more details about Tmab see Section 5.1).

Ipilimumab (Imab), a fully human monoclonal antibody against the CTLA-4 antigen, was licenced by the FDA in 2011 for the treatment of metastatic melanoma. Ipilimumab belongs to a group of drugs known as immune checkpoint inhibitors which are regarded as immunotherapy that regulates and activates the function of T-cells. CTLA-4 antigens are immune checkpoint molecules expressed on T-cells to bring about homeostasis and prevent against autoimmunity.[265,266]

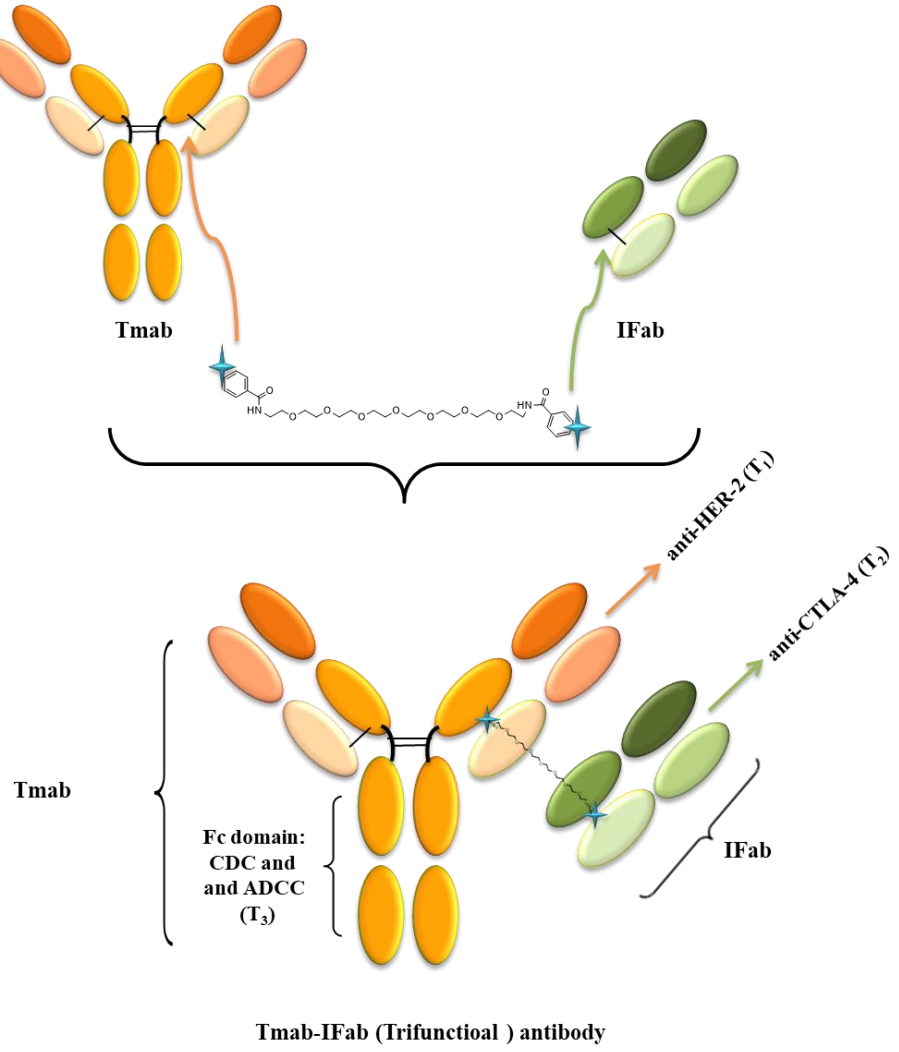

Figure 7.3. Schematic representation of anti-HER2/anti-CTLA-4 bsAb antibody (Trifunctional antibody) with mAb-Fab format that will be further constructed in this work. Orange represents mAb (anti-HER2) and green represents Fab (anti-CTLA-4).

T-cells require two signals in order to be fully activated. The first signal occurs when a specific antigen is recognized by the T-cell receptor, while the second signal is more complex and mainly mediated via the interactions between ligands on antigen-presenting cells, such as B7.1 and B7.2, with the CD28 receptor on T-cells. However, under certain circumstances, T-cells overexpress the negative regulator receptor CTLA-4, which competes with CD28 in binding to B7.1 and B7.2. This ultimately prevents (in certain situations) specific T-cells from being fully activated. The binding and blocking

of CTLA-4 on the cell surface of T-cells using Ipilimumab could interrupt the negative signal of the CTLA-4 molecule, restarting the signalling mechanism through CD28 to restore T-cell activation.[265,267,268]

There is considerable evidence supporting the essential role of the immune cells in the tumor microenvironment in either activation or inhibition of tumor growth in breast cancer and other types of cancer, which can be used as a prognostic indicator for breast cancer.[269] Approximately 70-80% of the immune cells population in the breast cancer microenvironment are composed of T-lymphocytes.[269] In light of the observed success of immunotherapy in treating various types of cancers, a growing amount of research has particularly shown the clinical benefits of immunotherapy in breast cancer.[269,270] For instance, Ertumaxomab is a bsAb targeting against HER2 and CD3 which has shown a phase I clinical trial in HER2 positive metastatic breast cancer patients. Ertumaxomab provides an elegant therapeutic approach in the treatment of patients with low HER2 antigen expression when trastuzumab treatment is insufficient.[271]

Moreover, the combination of checkpoint inhibitors with conventional cancer therapy provides another promising approach in immunotherapy for breast cancer patients. Currently, there is a growing number of clinical trials utilising CTLA-4 inhibitors, such as Tremelimumab or Ipilimumab as a conjunctive therapy of different types for HER2 negative breast cancer (NCT02536794 and NCT02381314).

Altogether, in this work we sought to provide a novel chemical method to construct bsAbs of Tmab-IFab with immunomodulating function through re-activation of T-cells in breast cancer microenvironment. This conjugate has the potential to meet the limitations of using Tmab as a mono therapy or could be used in a wide range breast cancer subtypes.

7.3 Construction of the Tmab-IFab bsAb

The Fab region of Imab was produced using papain enzyme-based digestion method which cleaves mAbs into two Fab fragments and one Fc domain.[272] Then the digested IFab was purified using protein A column (1 mL HiTrap Protein A, FF).

To this end, IFab (5 mg/mL) in Tris.HCl buffer was reduced with TCEP **2.2** (2 equiv.) for 1 h, quenching step using penta-PEG azide (**2.13**) for 1 h was followed by the addition of bis-o-diiodoacetamide $(PEG)_3$ linker **6.2** (5 equiv.) and incubation for 3 h at room temperature. Excess reagent was removed by buffer exchange into conjugation buffer (100 mM Tris.HCl, 150 mM NaCl, 5 mM EDTA, pH 7.5). Meanwhile, Tmab (5 mg/mL) was reduced with TCEP **2.2** (1.1 equiv.) for 2 h at 4°C. Functionalised IFab (4 equiv.) was then added to reduced Tmab and left at room temperature overnight. The reaction was purified using size exclusion chromatography (Superdex 200, GE Healthcare). The reaction products were then resolved separately using SDS-PAGE.

The estimated MW of the desired product would be around 125 kDa under reducing conditions. Figure 7.4 A shows a distinct band around 125 kDa (lane 3). Size exclusion chromatography purification was successful in separation of functionalised IFab (50 kDa) from the conjugate Tmab-IFab (HC-LC(Tmab)-IFab) (Figure 7.4, 5 and 6).

However, the low yield of the protein conjugate can be possibly attributed to steric hindrance which creates difficulty in the conjugation of IFab and Tmab. Therefore, longer chain of linker is expected to improve the conjugation yield and reduce the hindrance when attempting to link Tmab with IFab (as showed previously in Chapter 6, Section 6.7, Figure 6.15). To next sought to investigate the using of **6.5** in the construction of Tmab-IFab conjugate.

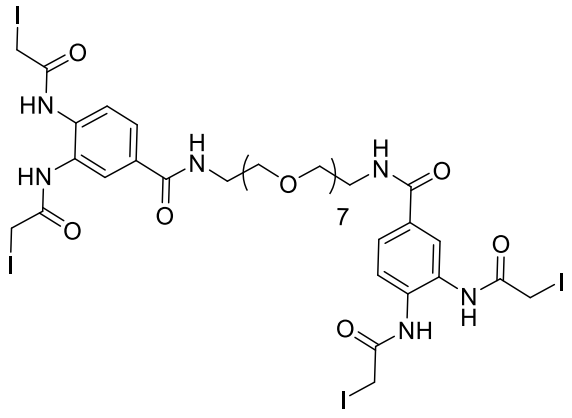

(**6.5**)

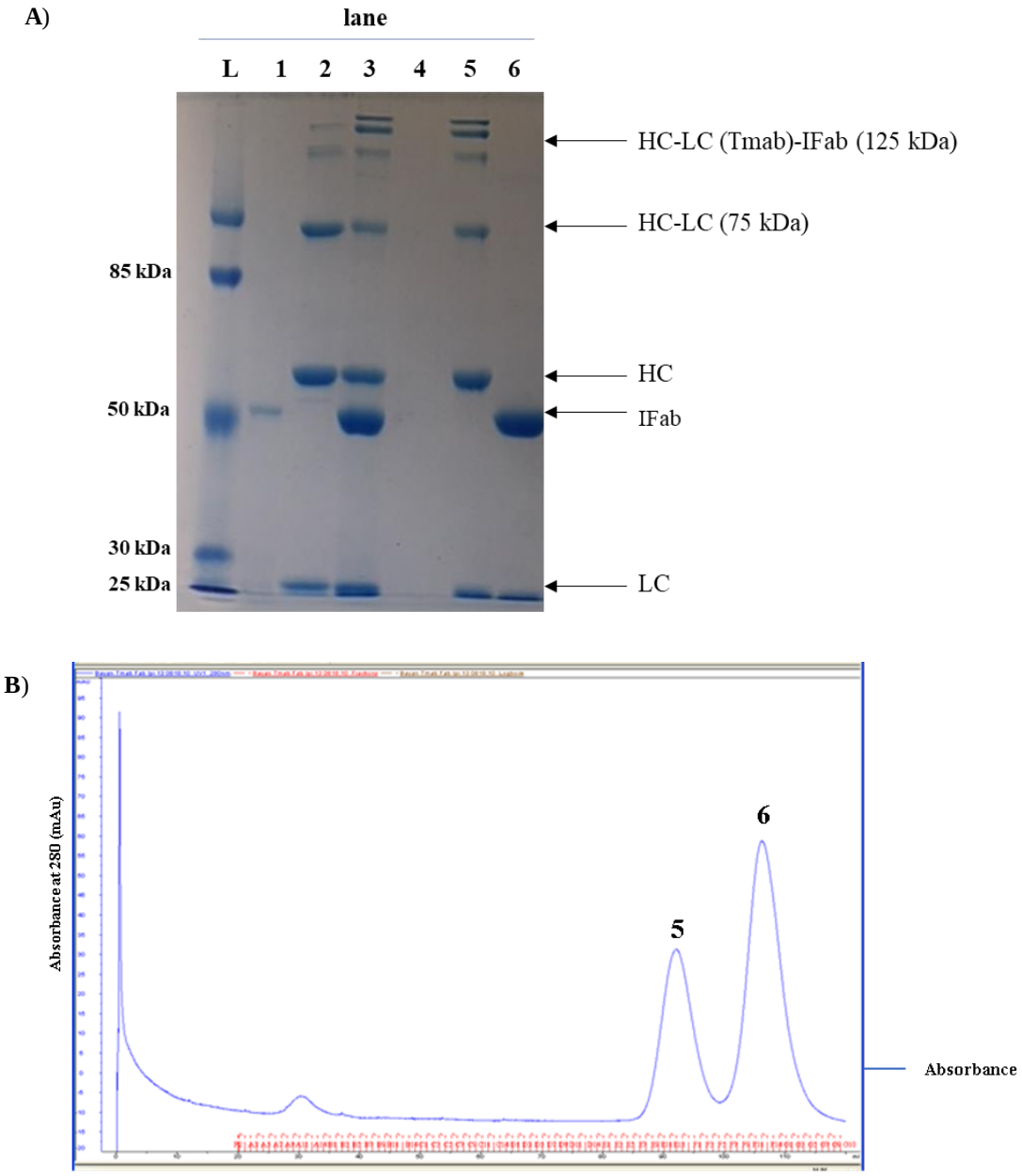

Figure 7.4. A) SDS-PAGE analysis of conjugation of partially reduced Tmab and IFab in Tris.HCl buffer (100 mM, 150 mM NaCl, 5 mM EDTA, pH 7.5) using bis-o-diiodoacetamide $(PEG)_3$ linker (**6.2**). Lane 1: crossed-linked Ipilimumab-fab using bis-o-diiodoacetamide $(PEG)_3$ linker (**6.2,** 4 equiv.), lane 2: Tmab incubated with 1.1 equiv. of methyl 3,4-bis(2-bromoacetamido)benzoate (**4.23**), Lane 3: Tmab conjugation with crossed-linked IFab at room temperature overnight before size exclusion chromatography purification, lane 4: size exclusion column purification collected fractions (FA7-A14), lane 5: size exclusion column purification collected fractions (FE7-F1), lane 6: size exclusion column purification collected fractions (FF9-G1). **B)** Size exclusion chromatography of Tmab-Fab conjugation reaction to separate functionalised IFab (lane 6) from Tmab-IFab conjugate (lane 5).

Therefore, conjugation of Tmab and IFab was attempted by using **6.5** using a similar conjugation method as described previously in Figure 7.4. Briefly, IFab (5 mg/mL) in

Tris.HCl buffer was reduced with TCEP **2.2** (2 equiv.) for 1 h, then, quenching step using penta-PEG azide (**2.13**) for 1 h was followed by addition of bis-o-diiodoacetamide $(PEG)_7$ linker **6.5** (5 equiv.) and incubation for 3 h at room temperature. Excess reagent was removed by buffer exchange into Tris.HCl conjugation buffer. Meanwhile, Tmab (5 mg/mL) was reduced with TCEP **2.2** (1.1 equiv.) for 2 h at 4°C. Functionalised IFab (4 equiv.) was then added to reduced Tmab and left at room temperature overnight.

The conjugation reaction products were evaluated by SDS-PAGE, which revealed a band around the estimated MW of the product ≈ 125 kDa under reducing condition. (Figure 7.5, lane 6). In line with what we observed before, attempting longer chain linkers **6.5** has significantly increased the yield of the conjugate obtained in comparison with **6.2** linker (Figure 7.4, lane 6).

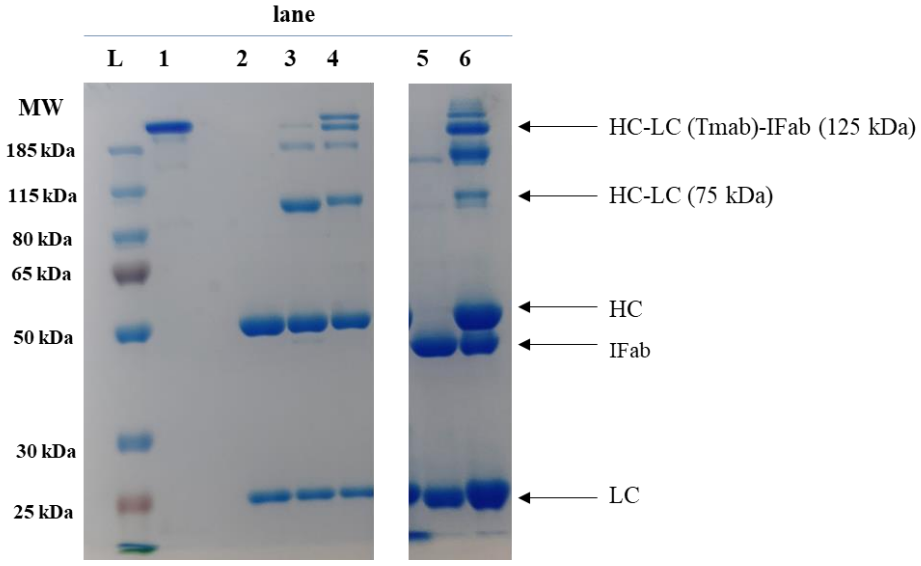

Figure 7.5. SDS-PAGE analysis of conjugation of partially reduced Tmab and IFab in Tris.HCl buffer (100 mM, pH 7.5) containing 150 mM NaCl, and 5 mM EDTA, using bis-o-diiodoacetamide $(PEG)_7$ linker (**6.5**). Lane 1: Tmab control (non-reducing), lane 2: Tmab control (reduced dye), lane 3: Tmab incubated with 1.1 equiv. of methyl 3,4-bis(2-bromoacetamido)benzoate (**4.23**), lane 4: Tmab incubated with 3 equiv. of bis-o-diiodoacetamide $(PEG)_7$ linker (6.5), lane 5: IFab incubated with 5 equiv. of bis-o-diiodoacetamide $(PEG)_7$ linker (6.5), lane 6: Tmab conjugation with IFab at room temperature overnight showing the correct estimated mass of the conjugate around 125 kDa.

7.3.1 Optimisation of the conjugation method

In order to optimise the conjugation yield and evaluate the first functionalisation step of IFab, we sought to evaluate the efficiency of functionalization step by protein MS (Figure 7.4). The MS spectrum showed the correct mass at 48,691.08 Da which represents IFab with linker attached (Figure 7.4 A and C). The performed MS reflected the good stability of the linker, and the good yield of the functionalisation step.

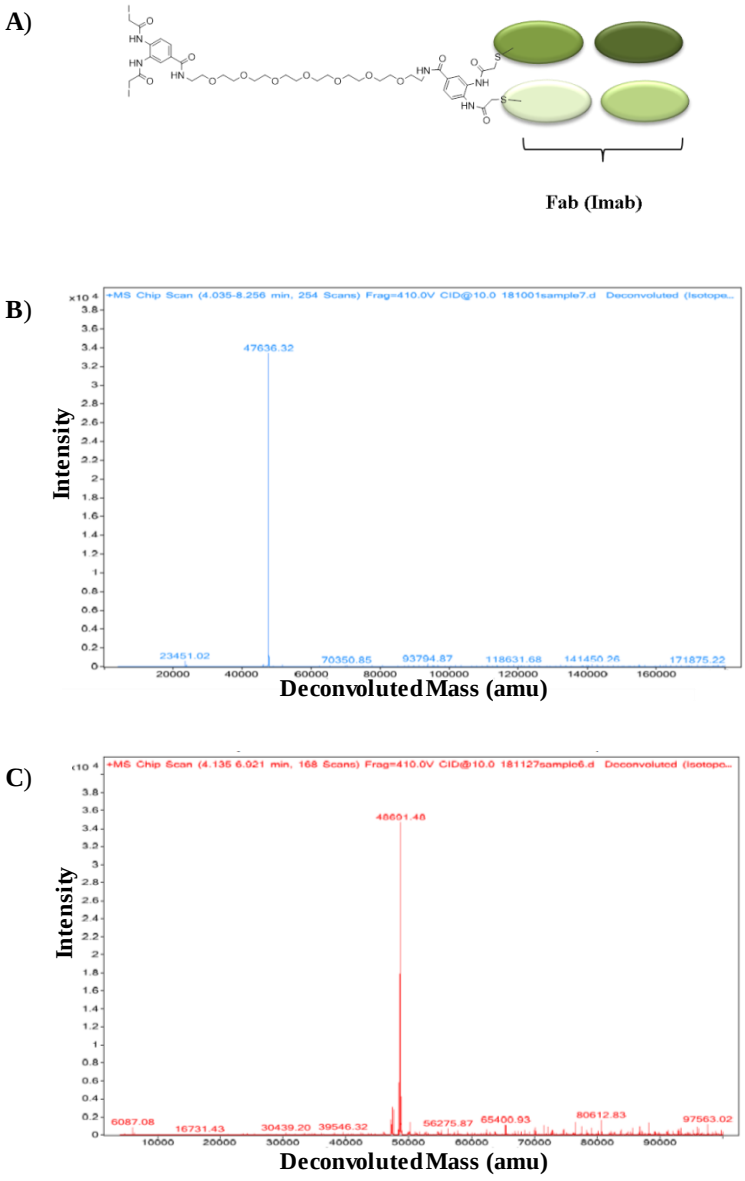

Figure 7.6. A) Schematic representation of functionalisation of IFab with bis-o-diiodoacetamide $(PEG)_7$ (**6.5**) linker. **B**) Deconvoluted protein MS spectrum of IFab control (non-reduced) showing major peaks at 47,636.32 Da. **C**) Deconvoluted protein MS spectrum of functionalised IFab with bis-o-diiodoacetamide $(PEG)_7$ linker (**6.5**) showing major peaks at 48,690.90 Da.

Further optimisation of the conjugation reaction was performed by attempting to reduce the observed band half-antibody (HC-LC, 75 kDa) in Figure 7.5, lane 6.

One possible explanation of the presence of this 75 kDa band is the incomplete removal of the excess linker using the VivaSpin sample concentrators, therefore, a quick step of purification using protein A column (1 mL HisTrap, FF) was performed before start conjugation of IFab with partially reduced Tmab.

As such, another conjugation reaction was attempted using the same previously described procedure in Figure 7.5, but with a quick purification step using protein a column of functionalised IFab instead of using spin filters. A significant reduction in the half-antibody band (HC-LC) was observed when protein A was used as quick purification step before performing Tmab-Fab conjugation (Figure 7.7 A, lane 3). Therefore, buffer exchange using VivaSpin sample concentrators is not sufficient to remove excess linkers and a quick step of purification is not only essential to remove excess linkers but to improve the yield of conjugation.

To our delight, the reaction products were purified using SEC, and the desired product (Tmab-IFab) was isolated with high purity (Figure 7.7 A, lane 4). The desired product fractions were combined together, final concentration was determined and from which the yield of the conjugation reaction was calculated and found to be ~60%.

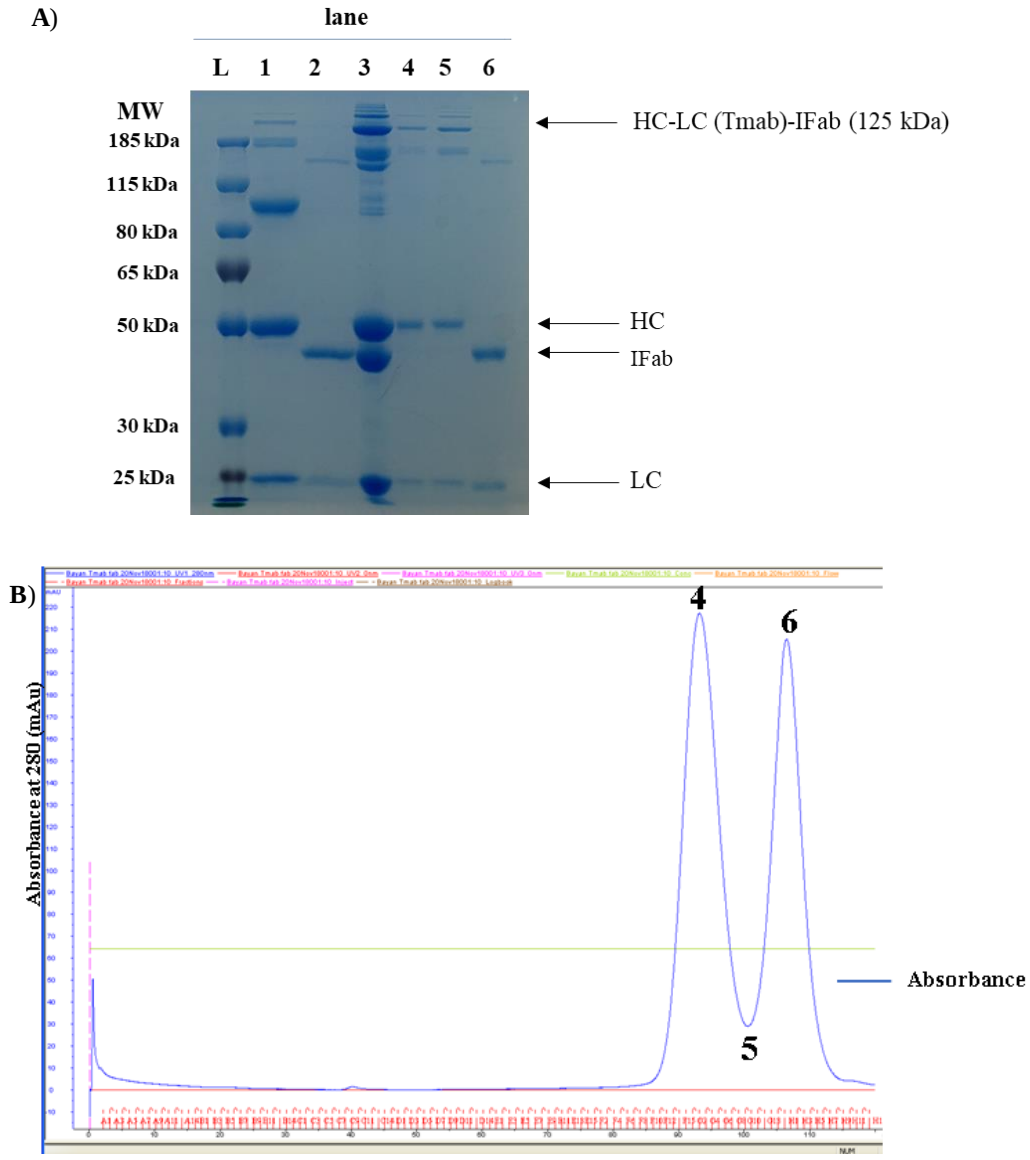

Figure 7.7. A) SDS-PAGE analysis of conjugation of partially reduced Tmab with Ipilimumab-fab in Tris.HCl buffer (100 mM, pH 7.5) containing 150 mM NaCl, and 5 mM EDTA, using bis-o-diiodoacetamide $(PEG)_7$ linker (6.5). Lane 1: Tmab incubated with 1.1 equiv. of methyl 3,4-bis(2-bromoacetamido)benzoate (**4.23**), lane 2: Tmab conjugation with IFab at room temperature overnight showing the correct estimated mass of the conjugate around 125 kDa with significant reduction of the 75 kDa band (half-antibody) before performing size exclusion chromatography, lane 4: size exclusion column purification collected fractions (F6-G2), lane 5: size exclusion column purification collected fractions (G4-G13), lane 6: : size exclusion column purification collected fractions (H1-H7). **B)** Size exclusion chromatography of Tmab-Fab conjugation reaction to separate cross-linked IFab (lane 6) from Tmab-Fab conjugate (lane 4).

7.4 Conclusion and future work

Given that bsAbs are rapidly emerging as a promising future approach in immunooncology, a more an efficient and high yielding method for their production is of significant importance. The currently available methods require mutagenesis of native antibodies, or complex expression and purification procedures. With the lack of chemical-based method to construct bsAbs containing Fc region, herein a chemical conjugation method is described based on bis-diiodoacetamid $(PEG)_7$ linker which was used to efficiently to construct the anti-HER2/anti-CTLA-4 Tmab-IFab trifunctional antibody.

The described methods of conjugation and purification in this Chapter afford promising preliminary foundation for the applicability this conjugation method to produce various classes of rebridged, thus more stable, bsAbs in good yield (~60%) through an easy adaptable procedure.

As this work provides a proof of concept of the applicability of our elegant rebridging linker (**6.5**) in the vast field of bsAb, future work in this approach will be scaled up, the conjugate activity against HER2 positive cancer cell lines will be evaluated *in vitro* and eventually *in vivo* studies will be performed to confirm activity and stability of the immunoconjugate.

8 Experimental

8.1 General reagents

Chemical reagents and solvents were purchased from Sigma-Aldrich, Fisher Scientific and Alfa Aesar unless otherwise stated. Anhydrous solvents were obtained from Sigma-Aldrich. Deuterated solvents for NMR were purchased from Cambridge Isotope Laboratories and Sigma-Aldrich. Preparative reverse phase chromatography (C-18) was performed using Biotage® SNAP cartridge (KP-C18-HS, 30 g).

Reagents that have been used in cell-culture (NaCl, imidazole, Tris base and glycine) were of molecular biology grade. Isopropyl thiogalactoside (IPTG) and Ampicillin sodium salt (BioReagent) were obtained from Fisher. Amicon® Ultra (3 and 10 kDa) centrifugal filters were purchased from Sigma-Aldrich.

Trastuzumab (Herceptin) 150 mg vials and Rituximab (Mabthera) 100 mg vials were kindly provided as gifts from Qualasept ltd. Sbi III/IV-Cys and Sbi IV-2xCys were over-expressed using the general expression procedure in the following Section.

8.2 General methods

8.2.1 Chemical synthesis

All reactions were carried out at atmospheric pressure under argon with stirring at room temperature unless otherwise stated. Thin layer chromatography (TLC) was carried out on aluminium backed TLC plates silica gel 60 (0.25 mm thickness), viewed under UV light (wavelength 254 nm) or stained with potassium permanganate solution [potassium permanganate (3 g) and potassium carbonate (20 g) in 5% aqueous sodium hydroxide (5 mL) and water (200 mL)] for a non-UV active compound. Silica gel column chromatography was performed on silica gel 60 Å (200-400 mesh) (Sigma-Aldrich). All compounds were prepared and purified to ≥ 94% purity as evaluated by HPLC [Chimatzo, detection wavelengths 280 nm and 214 nm, reverse phase (C18) column: HiQ sil C18 HS (150 x 4.60 mm)].

Nuclear magnetic resonance spectra were recorded in deuterated solvents $CDCl_3$, DMF-d_7 or DMSO-d_6 (unless another solvent is mentioned) using Bruker Advance III (400 and 500 MHz) spectrometers operating at ambient 20 °C probe. Data is reported for ^1H as following: chemical shift in ppm (multiplicity, *J* coupling constant in Hz, number of protons); and for ^{13}C: chemical shift in ppm. Multiplicity is presented as follows: s (singlet), d (doublet), t (triplet), q (quartet), m (multiplet), dd (doublet of doublet), dt (doublet of triplets), td (triplet of doublet).

High resolution mass spectrometry was obtained on a BrukerMicrOTOF electrospray ionisation mass spectrometer. Samples were prepared in acetonitrile solvent at a final concentration of 10 µg/mL. Infrared spectra were recorder on a PerkinElmer Spectrum 65 FT-IR spectrometer.

8.2.2 Standard work-up

Standard work-up is usually performed before silica gel column chromatography purification to remove salts. It is performed by diluting the crude reaction in appropriate organic solvent (mentioned), washing with H_2O, followed by washing with brine. The organic phases were then combined and dried over anhydrous $MgSO_4$, filtered and the filtrate concentrated under reduced pressure.

8.2.3 Protein over-expression

8.2.3.1 Primary and secondary culture

The general procedure for the recombinant proteins in this project is as follows. A single colony of *E.coli* BL21 (DE3) strain with an expression vector was picked and grown at 37°C overnight with shaking at 180 rpm in a 100 mL of LB medium with final concentration of ampicillin 100 µg/mL.

The overnight primary culture was then inoculated with 1-liter of LB medium containing ampicillin (100 µg/mL). Cells were grown at 37°C overnight with shaking at 180 rpm. The expression of protein was generally induced during the exponential phase of bacterial growth ($OD_{600}\geq0.7$) by adding isopropyl thiogalactoside (IPTG) to the

culture to final concentration of 1 mM in the culture. The culture held at 37°C with shaking at 180 rpm for 3 h.

8.2.3.2 Lysis and harvesting of cells

Cells from the secondary culture (8.2.3.1) were harvested by centrifugation at 8000 g for 25 minutes and suspended in HisA buffer (50 mM Tris, 300 mM NaCl and 50 mM Imidazole, pH 7.4). Cells were lysed by sonication. Cells were kept cold during the sonication cycles (6 cycles with 10 minutes interval between each sonication to cool down cells) at 80% amplitude for a total of 10 seconds. Then, the insoluble cell debris was removed by centrifugation at 60,000 g for 25 minutes at 4°C.

8.2.3.3 AKTA purification

The supernatant from 8.2.3.2 was collected and purified through immobilized metal affinity chromatography using nickel column (1mL, HisTrap HP, GE healthcare) attached to an AKTA purifier. The loaded column was washed with 15 column volumes of HisA buffer and the bound protein was eluted with a 0-100% gradient of HisB buffer (50 mM Tris, 300 mM NaCl and 1 M Imidazole, pH 7.4).

8.2.3.4 Concentrator and concentration measurement

Protein containing fractions from 8.2.3.3 were collected and appraised initially by SDS-PAGE analysis. Collected fractions containing pure protein were concentrated using Amicon® Ultra-15mL (3 kDa) centrifugal filters and finally buffer exchanged into phosphate buffer saline (PBS) buffer or other conjugation buffer and stored at -20°C.

Protein concentration was determined using BCA assay. Briefly, the concentration of protein was determinated against standard curve of BSA standards (2000, 1500, 1000, 750, 500, 250, 125, 25 and 0 µg/mL) which were prepared according to manufacturing protocol (Pierce™ BCA Protein Assay Kit) (Figure 8.1). Absorbance was measured at 550 nm using plate reader (FLUOstar OPTIMA plate reader, BMG LAB OPTIMA software 2.20R2). The concentration of the protein was calculated using Equation 8.1.

$$\text{Conc } (\mu g/ml) = \frac{(\text{Absorbance}+0.0525)}{0.0013} \qquad \text{(Equation 8.1)}$$

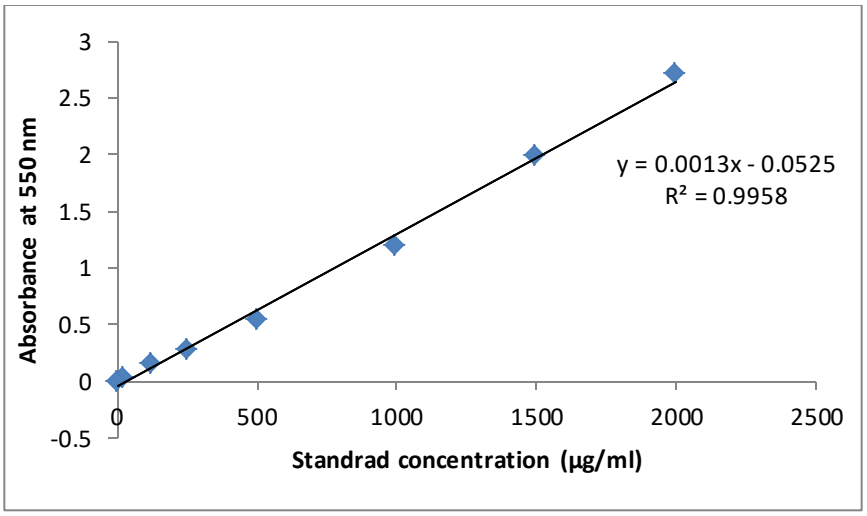

Figure 8.1. Standard curve of BSA standards (2000, 1500, 1000, 750, 500, 250, 125, 25 and 0 µg/mL) used in the BCA protein assay.

8.2.4 SDS-PEGE gel electrophoresis

Sodium dodecyl sulphate polyacrylamide gel electrophoresis (SDS-PAGE) was used to resolve protein samples according to the standard lab procedure using Invitrogen™ Mini Gel system. 4% stacking gel and 10% or 15% acrylamide gel (non-reducing glycine gel) were prepared using Novex gel cassettes (1.0 mm, invitrogen™). Recipes are stated in Table 8.1.

Pre-cased Bis-Tris, 10-well protein gels (4-12%) were also used when required and run using MES SDS running buffer (NuPAGE™).

Protein samples were mixed in 1:1 ratio with either 2x reducing loading dye sample buffer (0.5 M Tris-HCl, pH 6.8, 10% SDS, 50% glycerol, 2-mercaptoethanol, and 0.18% bromophenol blue) or non-reducing loading dye (without 2-mercaptoethanol) and vortexed for 1 minute, then heated at 75°C for 3 minutes.

Table 8.1. Composition of SDS-PAGE gel, stacking and resolving gels, running buffer, Coomassie blue stain and destain solution.

Stacking gel (4%) 2x gels	Tris 0.5 M pH 6.8 (1.625 mL), H_20 (4 mL), 40% v/v Acrylamide/bis-acrylamide (0.625 mL), 10% APS (31.25 µl), TEMED (6.25 µl).
Resolving gel (15%) 2x gels	Tris 1.5 M pH 8.8 (3.125 mL), H_20 (4.625 mL), 40% v/v Acrylamide/bis-acrylamide (4.675 mL), 10% APS (62.5 µl), TEMED (5.625 µl).
Resolving gel (10%) 1x gels	Tris 1.5 M pH 8.8 (1.25 mL), H_20 (2.50 mL), 40% v/v Acrylamide/bis-acrylamide (1.25 mL), 10% APS (50 µl), TEMED (5 µl).
Coomassie blue stain	40% Methanol, 0.1% (w/v) Brilliant blue R250, 10% Acetic acid, 50% H2O
Running buffer 10X /L	Tris Base (30.3 g), Glycine (143.75 g), SDS (10 g)
Destain solution	25% Methanol, 10% Acetic acid, 65% H2O

Protein samples (5-8 µL) were loaded onto each lane of acrylamide gels (4% stacking and 10 or 15% separating gel) and separated by electrophoresis at 80-100 mA using 1x glycine running buffer (Table 8.1). Gels were stained with Coomassie blue dye for 1 h before being destained (Table 8.1). Prestained Ladder (PageRuler™, ThermoFisher) was used to estimate the size (MW) of proteins (Figure 8.2).

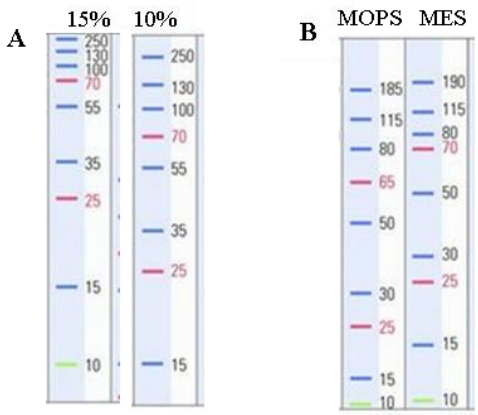

Figure 8.2. Protein band profile of the prestained PageRuler™ ladder. **A**) Images are from 15% and 10% tris-glycine gel, **B**) Images are from a 4-12% Bis-Tris gel (Thermo Scientific).

8.2.5 Protein LC-MS analysis

The appraised protein sample was transferred to Amicon® Ultra-0.5mL (3 or 10 kDa) centrifugal filter which was subsequently spun at 14,000 g for 20 minutes (Eppendorf centrifuge 5415R). The filtrate was discarded and 500 µL of milli-Q water was added and spun at 14000 g for 20 minutes. This step was repeated two times to remove the salt present in the sample. The desalted and concentrated samples (1-10 mg/mL) were then reduced by the addition TCEP (2-3 equiv.).

Mass spectrometric analysis was performed on Agilent 6520 CHIPCube Q-TOF LC/MS coupled to an Agilent 1200 series nanoflow LC (Agilent Technologies, California, USA). The CHIP we used is 43mm x 75um Zorbax 300SB-C8 5um with an enrichment column 4 mm 40 nl. The Time of flight MS scan range was from 100 – 4000 mass-to-charge ratio (m/z) at an acquisition rate of 1 spectrum per second. The injection volume has been between 0.1 to 1 µL. The gradient flow over 12 minutes was done as follows: 0-4 min from 3% B to 50% B, 4-5 min to 100% B, 5-11 min 100% B, 11-12 min from 100% to 3% B. Where mobile phase A: 100% H_2O + 0.1% formic acid and B: Acetonitrile/H_2O (90:10%) + 0.1% formic acid. Acquiring has been done over the mass range m/z 100 - 4000 and using Agilent MassHunter Qualitative Analysis software for data processing and deconvolution (Agilent, California, USA).

8.3 Chapter 2 Experimental

8.3.1 Chemical synthesis

*3,6-dioxaoctane-1,8-ditosylate (**2.14**)*

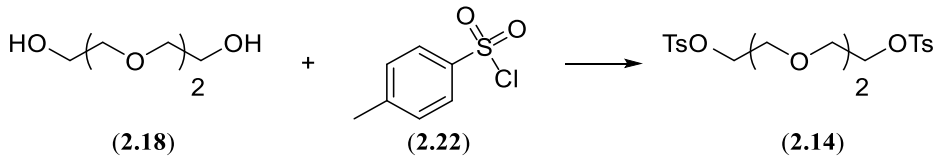

(**2.18**) (**2.22**) (**2.14**)

4-Toluenesulfonyl chloride **2.22** (3.30 g, 17.3 mmol, 2.6 equiv.) was added to a solution of triethylene glycol **2.18** (1.0 g, 6.7 mmol) in a mixture of anhydrous pyridine (1.3 mL) and anhydrous DCM (10 mL). The reaction mixture was left to stir under N_2 overnight at room temperature. The solution was then concentrated under reduced pressure and subjected to standard work-up (EtOAc). The resultant solid powder was then purified by precipitation (DCM/petroleum ether) to give the 3,6-dioxaoctane-1,8-ditosylate (**2.14**) as a white powder (2.8 g, 92%). NMR spectra (^{1}H and ^{13}C) were consistent with those previously reported.[273] ^{1}H NMR (400 MHz, $CDCl_3$): δ 7.78 (d, *J* = 8 Hz, 4H), 7.34–7.31 (m, 4H), 4.14–4.10 (m, 4H), 3.68–3.63 (m, 4H), 3.51 (s, 4H), 2.43 (s, 6H). ^{13}C NMR (100 MHz, $CDCl_3$): δ 144.76, 132.97, 129.76, 127.87, 70.62, 69.12, 68.68, 21.54. HRMS (ESI): Expected for $C_{20}H_{26}O_8S_2Na$ ($M+Na^+$) = *m/z* 481.0967. Found: *m/z* 481.0983.

*1,8-Diazido-3,6-dioxaoctane (**2.10**)*

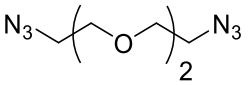

(**2.10**)

Sodium azide (1.14 g, 17.4 mmol, 4 equiv.) was added to a solution of 3,6-dioxaoctane-1,8-ditosylate **2.14** (2.0 g, 4.3 mmol) in acetone/water (3:1, 24 mL), and the mixture was allowed to stir at 37°C overnight. The mixture was then concentrated under reduced pressure to remove the acetone and the product was extracted with ethyl acetate (3 × 20 mL). The organic extract was then washed with saturated brine solution, dried over

$MgSO_4$, concentrated and then purified by silica gel chromatography (10 to 60% EtOAc/petroleum ether) to give the diazide (**2.10**) as a colorless oil (0.70 g, 80%). NMR spectra (^1H and ^{13}C) were consistent with those previously reported.[273] ^1H NMR (400 MHz, $CDCl_3$): δ 3.69–3.67 (m, 8H), 3.37 (t, *J* = 8Hz, 4H). ^{13}C NMR (100 MHz, $CDCl_3$): δ 70.68, 70.06, 50.64. HRMS (ESI): Expected for $C_6H_{12}N_6O_2Na$ ($M+Na^+$) = *m*/*z* 223.0919. Found: *m*/*z* 223.0925.

*3,6,9-trioxaundecane-1,11-ditosylate (**2.15**)*

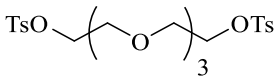

(**2.15**)

4-Toluenesulfonyl chloride **2.22** (2.50 g, 13.4 mmol, 2.6 equiv.) was added to a solution of tetraethylene glycol **2.19** (1.0 g, 5.2 mmol) in mixture of anhydrous pyridine (1 mL) and anhydrous DCM (10 mL). The reaction mixture was left to stir under N_2 overnight at room temperature. The solution was then concentrated under reduced pressure and was subjected to standard work-up (EtOAc). The resultant residue was then purified by silica gel chromatography (10 to 60% EtOAc/petroleum ether) to give 3,6,9-trioxaundecane-1,11-ditosylate (**2.15**) as a colorless oil (2.2 g, 85%). NMR spectra (^1H and ^{13}C) were consistent with those previously reported.[273] ^1H NMR (400 MHz, $CDCl_3$): δ 7.74–7.71 (m, 4H), 7.30–7.72 (m, 4H), 4.11–4.08 (m, 4H), 3.62–3.60 (m, 4H), 3.56–3.43 (m, 8H), 2.38 (s, 6H). ^{13}C NMR (100 MHz, $CDCl_3$): δ 144.77, 132.90, 129.77, 127.81, 70.50, 69.26, 68.54, 21.51. HRMS (ESI): Expected for $C_{22}H_{30}S_2O_9Na$($M+Na^+$) = *m*/*z* 525.1229. Found: *m*/*z* 525.1279.

1,11-Diazido-3,6,9-trioxaundecane ***(2.11)***

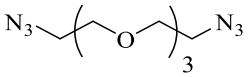

(**2.11**)

Sodium azide (1.04 g, 16.0 mmol, 4 equiv.) was added to a solution of 3,6,9-trioxaundecane-1,11-ditosylate **2.15** (2.0 g, 4.0 mmol) in acetone/water (3:1, 24 mL), the mixture was allowed to stir at 37°C overnight. The mixture was then concentrated under reduced pressure to remove the acetone and the product was extracted using ethyl acetate (3 × 20 mL). The organic extract was then washed with saturated brine solution, dried over $MgSO_4$, concentrated and then purified by silica gel chromatography (10 to 60% EtOAc/petroleum ether) to give the diazide (**2.11**) as a colorless oil (0.80 g, 82%). NMR spectra (^1H and ^{13}C) were consistent with those previously reported.[273] ^1H NMR (400 MHz, $CDCl_3$): δ 3.67–3.62 (m, 12H), 3.35 (t, *J* = 8 Hz, 4H). ^{13}C NMR (100 MHz, $CDCl_3$): δ 70.63, 70.62, 69.94, 50.59. HRMS (ESI): Expected for $C_8H_{16}N_6O_3Na$ ($M+Na^+$) = *m*/*z* 267.118159. Found: *m*/*z* 267.1228.

3,6,9,12-tetraoxatetradecane-1,14-ditosylate ***(2.16)***

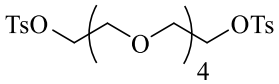

(**2.16**)

4-Toluenesulfonyl chloride **2.22** (2.07 g, 10.9 mmol, 2.6 equiv) was added to a solution of pentaethylene glycol **2.20** (1.0 g, 4.2 mmol) in mixture of anhydrous pyridine (0.8 mL) and anhydrous DCM (10 mL), and the mixture was left to stir under N_2 overnight at room temperature. The solution was then concentrated under reduced pressure and was subjected to standard work-up (EtOAc). The resultant residue was then purified by silica gel chromatography (10 to 60% EtOAc/petroleum ether) to give 3,6,9,12-tetraoxatetradecane-1,14-ditosylate (**2.16**) as a colorless oil (2.0 g, 87%). NMR spectra (^1H and ^{13}C) were consistent with those previously reported.[273] ^1H NMR (400 MHz, $CDCl_3$): δ 7.78 (d, 4H, *J* = 8 Hz), 7.33 (t, 4H, *J* = 8 Hz), 4.14 (t, 4H, *J* = 8 Hz), 3.68–

3.65 (m, 4H), 3.60 (t, 12H, J = 8 Hz), 2.43 (s, 6H). ^{13}C NMR (100 MHz, $CDCl_3$): δ 144.71, 133.00, 129.94, 127.83, 70.68, 70.49, 69.81, 68.61, 21.55. HRMS (ESI): Expected for $C_{24}H_{35}O_{10}S_2$ ($M+H^+$) = m/z 547.1672. Found: m/z 547.1666.

*1,14-Diazido-3,6,9,12-tetraoxatetradecane (**2.12**)*

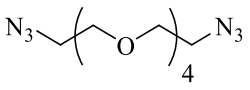

(**2.12**)

Sodium azide (0.95 g, 15 mmol, 4 equiv.) was added to a solution of 3,6,9,12-tetraoxatetradecane-1,14-ditosylate **2.16** (2.0 g, 3.7 mmol) in acetone/water (3:1, 24 mL) and the mixture was allowed to stir at 37°C overnight. The mixture was then concentrated under reduced pressure to remove the acetone and the product was extracted using ethyl acetate (3 × 20 mL). The organic extract was then washed with saturated brine solution, dried over $MgSO_4$, concentrated and then purified by silica gel chromatography (10 to 60% EtOAc/petroleum ether) to give the diazide (**2.12**) as a colorless oil (0.85 g, 81%). NMR spectra (^{1}H and ^{13}C) were consistent with those previously reported.[273] ^{1}H NMR (400 MHz, $CDCl_3$): δ 3.68–3.65 (m, 16H), 3.37 (t, 4H, J = 4.0 Hz). ^{13}C NMR (100 MHz, $CDCl_3$): δ 70.65, 70.62, 70.57, 69.95, 50.64. HRMS (ESI): Expected for $C_{10}H_2N_6O_4Na$ ($M+Na^+$) = m/z 311.1443. Found: m/z 311.1434.

3,6,9,12,15-pentaoxaheptadecane-1,17-ditosylate (***2.17***)

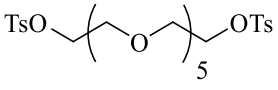

(**2.17**)

4-Toluenesulfonyl chloride **2.22 (**1.73 g, 9.10 mmol, 2.6 equiv.) was added to a solution of anhydrous pyridine (0.76 mL) and hexaethylene glycol **2.21** (1.0 g, 3.5 mmol) in anhydrous DCM (10 mL), and the mixture was left to stir under N_2 overnight at room temperature. The solution was then concentrated under reduced pressure and was

subjected to standard work-up (EtOAc). The resultant residue was then purified by silica gel chromatography (10 to 60% EtOAc/petroleum ether) to give 3,6,9,12,15-pentaoxaheptadecane-1,17-ditosylate (**2.17**) as a colorless oil (1.70 g, 82%). NMR spectra (^{1}H and ^{13}C) were consistent with those previously reported.[274] ^{1}H NMR (400 MHz, $CDCl_3$): δ 7.77 (d, 4H, *J* = 8 Hz), 7.32 (d, 4H, *J* = 8 Hz), 4.15–4.12 (m, 4H), 3.68–3.55 (m, 20H), 2.42 (s, 6H, Me). ^{13}C NMR (100 MHz, $CDCl_3$): δ 144.70, 133.00, 129.74, 127.89, 70.67, 70.54, 70.49, 70.44, 69.18, 68.60, 21.55. HRMS (ESI): Expected for $C_{26}H_{39}O_{11}S_2$ ($M+H^+$) = *m*/*z* 591.1934. Found: *m*/*z* 591.1928.

*1,17-Diazido-3,6,9,12,15-pentaoxaheptadecane (**2.13**)*

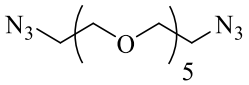

(**2.13**)

Sodium azide (0.91 g, 14 mmol, 4 equiv.) was added to a solution of 3,6,9,12,15-pentaoxaheptadecane-1,17-ditosylate **2.17** (2.0 g, 3.4 mmol) in acetone/water (3:1, 24 mL), and the mixture was allowed to stir at 37°C overnight. The mixture was then concentrated under reduced pressure to remove the acetone and the product was extracted using ethyl acetate (3 × 20 mL). The organic extract was then washed with saturated brine solution, dried over $MgSO_4$, concentrated and then purified by silica gel chromatography (10 to 60% EtOAc/petroleum ether) to give the diazide (**2.13**) as a colorless oil (0.89 g, 79%). NMR spectra (^{1}H and ^{13}C) were consistent with those previously reported.[275] ^{1}H NMR (400 MHz, $CDCl_3$): δ 3.67–3.64 (m, 20H), 3.36 (t, *J* = 4 Hz, 4H). ^{13}C NMR (100 MHz, $CDCl_3$): δ 70.48, 70.44, 69.87, 50.54. HRMS (ESI): Expected for $C_{12}H_{24}N_6O_5$ Na ($M+Na^+$) = *m*/*z* 355.1706. Found: *m*/*z* 355.1728.

8.3.2 Determination of the mass and molar solubilities of PEG-azide 2.10-2.13 and 4-ABA 2.7

Mass solubility of each PEG-azide **2.10-2.13** was determined by gradual addition (100 µl) of water or buffer until 500 mg of each PEG-azide was completely dissolved, the mixture was vortexed for about 30 second in between. The solubilities of each azide were reported as the minimum required volume of the solvent (water or buffer) to completely dissolve 500 mg of each PEG-azide.

Mass solubility of 4-ABA **2.7** was determined by gradual addition (1000 µl) of water or buffer until 100 mg of 4-ABA **2.7** was completely dissolved, the mixture was vortexed for about 30 second in between. The solubility of 4-ABA **2.7** were reported as the minimum required volume of the solvent (water or buffer) to completely dissolve 100 mg of 4-ABA **2.7**.

8.3.3 Determination of the rate of consumption of TCEP using ^{31}P NMR spectroscopy

For determination of rates of oxidation of TCEP in the presence of PEG-azide **2.10-2.13**, a solution of TCEP.HCl **2.2** (14.4 mg, 50.2 µmol, 50.2 mM, 1 mL) in Tris.HCl buffer (100 mM, pH 7) was mixed with a solution of each PEG-azide (0.5 mmol, 10 equiv., 1 mL) in the same buffer, the held at 37℃ and analysed by ^{31}P NMR spectroscopy after 3, 13, 23, 33, 43, 53 and 63 minutes.

For determination of rates of oxidation of TCEP in the presence of 4-ABA **2.7**, a solution of TCEP **2.2** (5.0 mg, 17 µmol, 17 mM, 1 mL) in Tris.HCl buffer (100 mM, pH 8) was mixed with a solution of 4-ABA (52 mM, 3 equiv., 1 mL) in the same buffer, then held at 37℃ and analysed by ^{31}P NMR spectroscopy after 3, 13, 23, 33, 43, 53 and 63 minutes.

The determination of the percentage of remaining of TCEP was performed using Equation 2.1.

8.4 Chapter 3 Experimental

8.4.1 Chemical synthesis

*2-(2-Methoxyethoxy)ethyl 4-methylbenzenesulfonate (**3.1**)*

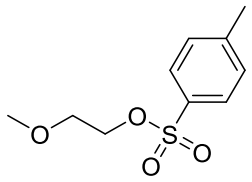

(**3.1**)

4-Toluenesulphonyl chloride **2.22** (3.25 g, 17.1 mmol, 1.3 equiv.) was added to a solution of 2-methoxyethan-1-ol **3.11** (1.0 g, 13 mmol) in a mixture of anhydrous pyridine (1.25 mL, 15.8 mmol, 1.2 equiv.) and anhydrous DCM (10 mL). The mixture left to stir under N_2 overnight at room temperature. The solution was then concentrated under reduced pressure and subjected to standard work-up (EtOAc). The resultant residue was then purified by silica gel chromatography (10 to 60% EtOAc/petroleum ether) to give the 2-methoxyethyl 4-methylbenzenesulfonate (**3.1**) as a colorless oil (2.7 g, 90%). NMR spectra (^{1}H and ^{13}C) were consistent with those previously reported.[276] ^{1}H NMR ($CDCl_3$, 400 MHz): δ 7.73 (d, *J* = 8.3 Hz, 2H), 7.28 (dt, *J* = 7.9, 0.7 Hz, 2H), 4.14 – 4.04 (m, 2H), 3.56 – 3.45 (m, 2H), 3.24 (s, 3H), 2.38 (s, 3H). ^{13}C NMR ($CDCl_3$, 101 MHz): δ 144.73, 133.00, 129.72, 127.86, 69.85, 68.99, 58.88, 21.52. ESI-HRMS: Expected for $C_{10}H_{15}O_4S$ ($M+H^+$) = m/z 231.0686. Found: m/z 231.069500. HPLC: column: HiQ sil C18 HS (150 x 4.60 mm). Mobile phase: isocratic: (0.75 mL/minutes) 35% MeCN: 65% water. Detection at 280 nm. Retention time: 23.154 minutes, purity: 96%.

*2-(2-Methoxyethoxy)ethyl 4-fluorobenzenesulfonate (**3.2**)*

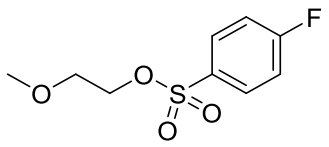

(**3.2**)

4-fluorobenzenesulphonyl chloride **3.13** (3.30 g, 17.1 mmol, 1.3 equiv.) was added to a solution of 2-methoxyethan-1-ol **3.11** (1.0 g, 13 mmol) in a mixture of anhydrous pyridine (1.25 mL, 15.8 mmol, 1.2 equiv.) and anhydrous DCM (10 mL). The mixture left to stir under N_2 overnight at room temperature. The solution was then concentrated under reduced pressure and subjected to standard work-up (EtOAc). The resultant residue was then purified by silica gel chromatography (10 to 60% EtOAc/ petroleum ether) to give the 2-methoxyethyl 4-fluorobenzenesulfonate (**3.2**) as a colorless oil (2.8 g, 91%). ^{1}H NMR ($CDCl_3$, 400 MHz): δ 7.92 – 7.88 (m, 2H), 7.21 – 7.15 (m, 2H), 4.16 – 4.14 (m, 2H), 3.55 – 3.51 (m, 2H), 3.25 (d, *J* = 1.5 Hz, 3H). ^{13}C NMR ($CDCl_3$, 100 MHz): δ 166.96, 164.41, 130.74, 130.64, 116.54, 116.32, 69.80, 69.30, 58.91. ESI-HRMS: Expected for $C_9H_{11}O_4SFNa$ ($M+Na^+$) = m/z 257.0254. Found: m/z 257.0266.

*2-(2-Methoxyethoxy)ethyl 3-bromobenzenesulfonate (**3.3**)*

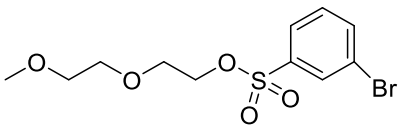

(**3.3**)

3-bromobenzenesulphonyl chloride **3.15** (2.74 g, 10.8 mmol, 1.3 equiv.) was added to a solution of 2-(2-methoxyethoxy)ethan-1-ol **3.14** (1.0 g, 8.3 mmol) in a mixture of anhydrous pyridine (1.25 mL, 15.8 mmol, 1.2 equiv.) and anhydrous DCM (10 mL). The reaction left to stir under N_2 overnight at room temperature. The solution was then concentrated under reduced pressure and subjected to standard work-up (EtOAc). The resultant residue was then purified by silica gel chromatography (10 to 60% EtOAc/petroleum ether) to give the 2-(2-Methoxyethoxy)ethyl 3-Bromobenzenesulfonate (**3.3**) as a colorless oil (2 g, 70.92%). ^{1}H NMR ($CDCl_3$, 400

MHz): 8.02 (t, 1H, *J* = 2 Hz), 7.83 (d, 2H, *J* = 8 Hz), 7.65 (d, 2H, *J* =8 Hz), 7.40 (t, 2H, *J* = 8 Hz), 4.21 (t, 2H, *J*=4.8 Hz), 3.67 (t, 2H, *J*=5.2 Hz), 3.54 (t, 2H, *J*=4 Hz), 3.45 (m, 2H, *J* = 4 Hz), 3.31 (S, 3H). ^{13}C NMR ($CDCl_3$, 100 MHz): δ 137.89, 136.72, 130.68, 130.65, 126.40, 123.01, 71.73, 70.60, 69.89, 68.52, 58.94. ESI-HRMS: Expected for $C_{11}H_{15}O_5SBrNa$ ($M+Na^+$) = m/z 360.9721. Found: m/z 360.9743.

*2-methoxyethyl 3-chlorobenzenesulfonate (**3.4**)*

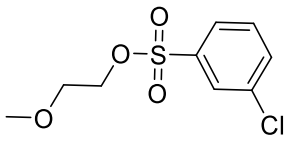

(**3.4**)

3-Chlorobenzenesulphonyl chloride **3.16** (3.57 g, 17.1 mmol, 1.3 equiv.) was added to a solution of 2-methoxyethan-1-ol **3.11** (1.0 g, 13 mmol) in a mixture of anhydrous pyridine (1.25 mL, 15.8 mmol, 1.2 equiv.) and anhydrous DCM (10 mL). The reaction was left to stir under N_2 overnight at room temperature. The solution was then concentrated under reduced pressure and subjected to standard work-up (EtOAc). The resultant residue was then purified by silica gel chromatography (10 to 60% EtOAc/petroleum ether) to give the 2-methoxyethyl 3-chlorobenzenesulfonate (**3.4**) as a colorless oil (3 g, 91%). ^{1}H NMR ($CDCl_3$, 400 MHz): δ 7.86 (t, 1H, *J* =1.6), 7.75 (dt, *J* = 8, 1.6 Hz, 1H), 7.57 (dt, *J* = 8.0, 1.6 Hz, 1H), 7.44 (t, 1H, *J* = 8.4), 4.17 (t, *J* = 4.8 Hz, 2H), 3.53 (t, *J* = 4.8 Hz, 2H), 3.25 (s, 3H). ^{13}C NMR ($CDCl_3$, 100 MHz): δ 137.77, 135.32, 133.80, 130.40, 127.93, 125.92, 69.76, 69.72, 58.90. ESI-HRMS: Expected for $C_9H_{11}O_4SClNa$ ($M+Na^+$) = 272.9959 m/z. Found: 272.9992 m/z. HPLC: column: HiQ sil C18 HS (150 x 4.60 mm), Mobile phase: isocratic: (0.75 mL/minutes) 35% MeCN: 65% water. Detection at 280 nm. Retention time: 12.57 minutes, purity: 99.9%.

*2-(2-Methoxyethoxy)ethyl 4-nitrobenzenesulfonate (**3.5**)*

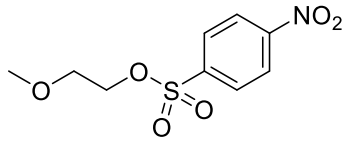

(**3.5**)

4-nitrobenzenesulphonyl chloride **3.17** (3.57 g, 17.1 mmol, 1.3 equiv.) was added to a solution of 2-methoxyethan-1-ol **3.11** (1.0 g, 13 mmol) in a mixture of anhydrous pyridine (1.25 mL, 15.8 mmol, 1.2 equiv.) and anhydrous DCM (10 mL). The reaction left to stir under N_2 overnight at room temperature. The solution was then concentrated under reduced pressure and subjected to standard work-up (EtOAc). The resultant residue was then purified by silica gel chromatography (10 to 60% EtOAc/petroleum ether) to give the 2-methoxyethyl 4-nitrobenzenesulfonate (**3.5**) as a yellow solid (2 g, 59%). ^{1}H NMR ($CDCl_3$, 400 MHz): δ 8.34 (d, *J* = 9.1 Hz, 2H), 8.07 (d, *J* = 9.0 Hz, 2H), 4.5 (t, *J* = 4.4 Hz, 2H), 3.54 (t, *J* = 4.8 Hz, 2H), 3.22 (s, 3H). ^{13}C NMR ($CDCl_3$, 100 MHz): δ 150.67, 141.96, 129.20, 124.23, 70.28, 69.69, 58.88. ESI-HRMS: Expected for $C_9H_{11}O_6SNNa$ ($M+Na^+$) = m/z 284.0199. Found: m/z 284.0196. HPLC: column: HiQ sil C18 HS (150 x 4.60 mm). Mobile phase: isocratic: (0.75 mL/minutes) 35% MeCN: 65% water. Detection at 280 nm. Retention time: 15.178 minutes, purity: 97.9%.

*3-methoxypropyl 4-methylbenzenesulfonate (**3.6**)*

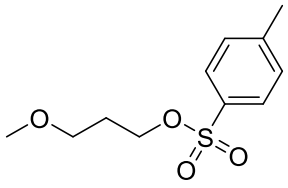

(**3.6**)

4-Toluenesulphonyl chloride **2.22** (2.87 g, 14.4 mmol, 1.3 equiv.) was added to a solution of 3-methoxypropan-1-ol **3.18** (1.0 g, 11 mmol) in a mixture of anhydrous pyridine (1.05 mL, 13.3 mmol, 1.2 equiv.) and anhydrous DCM (10 mL). The reaction left to stir under N_2 overnight at room temperature. The solution was then concentrated

under reduced pressure and subjected to standard work-up (EtOAc). The resultant residue was then purified by silica gel chromatography (10 to 60% EtOAc/petroleum ether) to give the 3-methoxypropyl 4-methylbenzenesulfonate (**3.6**) as colorless oil (2.6 g, 96%). NMR spectra (^{1}H and ^{13}C) were consistent with those previously reported.[277] ^{1}H NMR ($CDCl_3$, 500 MHz): δ 7.72 (d, *J* = 8.0 Hz, 2H), 7.28 (d, *J* = 8.0 Hz, 2H), 4.05 (t, *J* = 6.3 Hz, 2H), 3.31 (t, *J* = 6.0 Hz, 2H), 3.17 (s, 3H), 2.38 (s, 3H), 1.82 (p, *J* = 6.1 Hz, 2H).^{13}C NMR ($CDCl_3$, 126 MHz): δ 144.72, 133.05, 129.82, 127.90, 67.98, 67.71, 58.66, 29.26, 21.63. ESI-HRMS: Expected for $C_{11}H_{16}O_4SNa$ ($M+Na^+$) = m/z 267.0662. Found: m/z 267.0692. HPLC: column HiQ sil C18 HS (150 x 4.60 mm). Mobile phase: isocratic: (0.75 mL/minutes) 35% MeCN: 65% water. Detection at 280 nm. Retention time: 16.30 minutes, purity: 96.7%.

*3-methoxypropyl 3-chlorobenzenesulfonate (**3.7**)*

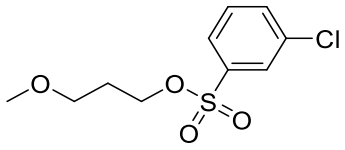

(**3.7**)

3-Chlorobenzenesulphonyl chloride **3.16** (3.02 g, 14.4 mmol, 1.3 equiv.) was added to a solution of 3-methoxypropan-1-ol **3.18** (1.0 g, 11 mmol) in a mixture of anhydrous pyridine (1.05 mL, 13.3 mmol, 1.2 equiv.) and anhydrous DCM (10 mL). The reaction was left to stir under N_2 overnight at room temperature. The solution was then concentrated under reduced pressure and subjected to standard work-up (EtOAc). The resultant residue was purified by silica gel chromatography (10 to 60% EtOAc/petroleum ether) to give the 3-methoxypropyl 3-chlorobenzenesulfonate (**3.7**) as colorless oil (2.7 g, 93%). ^{1}H NMR ($CDCl_3$, 400 MHz): δ 7.85 – 7.84 (m, 1H), 7.76-7.74 (m, 1H), 7.58- 7.56 (m, 1H), 7.45 (t, 1H, *J* = 8 Hz), 4.14 (t, *J* = 6.4 Hz, 2H), 3.35 (t, *J* = 5.6 Hz, 2H), 3.20 (s, 3H), 1.96 – 1.84 (m, 2H). ^{13}C NMR ($CDCl_3$, 100 MHz): δ 137.84, 135.41, 133.73, 130.40, 127.84, 125.87, 68.32, 67.73, 58.59, 29.19. ESI-HRMS: Expected for $C_{10}H_{13}O_4SClNa$ ($M+Na^+$) = m/z 278.0115. Found: m/z 287.0171. Infrared

(NaCl disc): 1584, 1364, 1185, 1127, 929, 674 cm^{-1}. HPLC: column HiQ sil C18 HS (150 x 4.60 mm). Mobile phase: isocratic: (0.75 mL/minutes), 35% MeCN: 65% water. Detection at 280 nm. Retention time: 20 minutes, purity: 99.7%.

*3-methoxypropyl 4-Nitrobenzenesulfonate (**3.8**)*

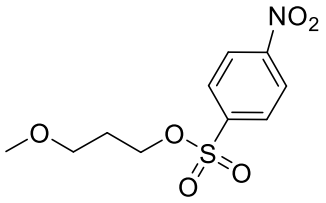

(**3.8**)

4-nitrobenzenesulphonyl chloride **3.17** (3.19 g, 14.4 mmol, 1.3 equiv.) was added to a solution of 3-methoxypropan-1-ol **3.18** (1.0 g, 11 mmol) in a mixture of anhydrous pyridine (1.05 mL, 13.3 mmol, 1.2 equiv.) and anhydrous DCM (10 mL). The reaction was left to stir under N_2 for 2 h at room temperature. The solution was concentrated under reduced pressure and subjected to standard work-up (EtOAc). The resultant residue was purified by silica gel chromatography (10 to 60% EtOAc/petroleum ether) to give the 3-methoxypropyl 4-nitrobenzenesulfonate (**3.8**) as yellow solid (2.5 g, 82%). ^{1}H NMR ($CDCl_3$, 400 MHz): δ 8.51 – 8.20 (m, 2H), 8.19 – 7.89 (m, 2H), 4.19 (t, 2H, *J* = 6.4 Hz), 3.35 (t, 2H, *J* = 5.9 Hz,), 3.19 (s, 3H), 1.89 (p, 2H, *J* = 6.1 Hz). ^{13}C NMR ($CDCl_3$, 100 MHz): δ 150.69, 141.89, 129.13, 124.33, 68.92, 67.58, 58.59, 29.17. ESI-HRMS: Expected for $C_{10}H_{13}O_6SNNa$ ($M+Na^+$) = m/z 298.0361. Found: m/z 298.0349. HPLC: column HiQ sil C18 HS (150 x 4.60 mm), isocratic: (0.75 mL/minutes) 35% MeCN: 65% water. Detection at 280 nm. Retention time: 12.05 minutes, purity: 96.12 %.

*2-hydroxy-N-(2-methoxyethyl)acetamide (**3.21**)*

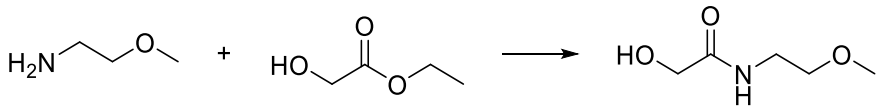

(**3.19**) (**3.20**) (**3.21**)

2-methoxyethan-1-amine **3.19** (2.88 g, 38.5 mmol, 4 equiv.) was added to a stirring solution of ethyl glycolate **3.20** (1.0 g, 9.6 mmol) in ethanol and refluxed for two days. Excess 2-methoxyethan-1-amine was removed under reduced pressure to afford 2-hydroxy-N-(2-methoxyethyl)acetamide (**3.21**) as yellow liquid (1.1 g, 86%). ^{1}H NMR ($CDCl_3$, 400 MHz): δ 7.15 (s, 1H), 4.86 (s, 1H), 3.90 (s, 2H), 3.36 – 3.21 (m, 4H), 3.21 (s, 3H). ^{13}C NMR ($CDCl_3$, 100 MHz): δ 172.28, 70.94, 66.00, 58.85, 38.61. ESI-HRMS: Expected for $C_5H_{12}O_3N$ ($M+H^+$) = m/z 134.0812. Found: m/z 134.0826.

*2-((2-methoxyethyl)amino)-2-oxoethyl 4-methylbenzenesulfonate (**3.9**)*

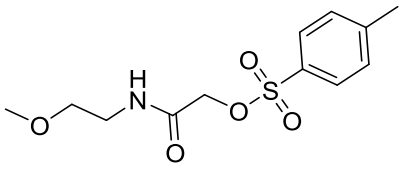

(**3.9**)

4-methylbenzenesulphonyl chloride **2.22** (1.86 g, 9.77 mmol, 1.3 equiv.) was added to a solution of 2-hydroxy-N-(2-methoxyethyl)acetamide **3.21** (1.0 g, 7.5 mmol) in a mixture of anhydrous pyridine (0.710 mL, 9.02 mmol, 1.2 equiv.) and anhydrous DCM (10 mL). The reaction was left to stir under N_2 for 2 h at room temperature. The solution was then concentrated under reduced pressure and subjected to standard work-up (EtOAc). The resultant residue was then purified by silica gel chromatography (10 to 60% EtOAc/petroleum ether) to give the 2-((2-methoxyethyl)amino)-2-oxoethyl 4-methylbenzenesulfonate (**3.9**) as white solid (1.5 g, 69%). ^{1}H NMR ($CDCl_3$, 400 MHz): δ 7.76 (d, *J* = 8.2 Hz, 2H), 7.33 (d, *J* = 8.0 Hz, 2H), 6.55 (s, 1H), 4.37 (s, 2H), 3.39 (s,

4H), 3.31 (s, 3H), 2.42 (s, 3H). ^{13}C NMR ($CDCl_3$, 101 MHz): δ 165.07, 145.71, 131.72, 130.10, 128.06, 70.56, 66.86, 58.77, 38.95, 21.62. ESI-HRMS: Expected for $C_{12}H_{17}O_5SNNa$ ($M+Na^+$) = m/z 310.0725. Found: m/z 310.0743. HPLC: column HiQ sil C18 HS (150 x 4.60 mm). Mobile phase: isocratic: (0.75 mL/minutes), 35% MeCN: 65% water. Detection at 280 nm. Retention time: 8.179 minutes, purity: 94.4%.

*2-((2-methoxyethyl)amino)-2-oxoethyl 4-methylbenzenesulfonate (**3.10**)*

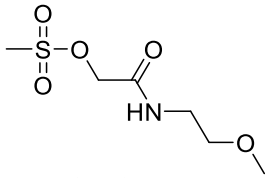

(**3.10**)

Methansulphonyl chloride **3.22** (1.11 g, 9.77 mmol, 1.3 equiv.) was added to a solution of 2-hydroxy-N-(2-methoxyethyl)acetamide **3.21** (1.0 g, 7.5 mmol) in a mixture of anhydrous pyridine (0.710 mL, 9.02 mmol, 1.2 equiv.) and anhydrous DCM (10 mL). The reaction was left to stir under N_2 for 2 h at room temperature. The solution was concentrated under reduced pressure and subjected to standard work-up (EtOAc). The resultant residue was then purified by silica gel chromatography (10 to 60% EtOAc/petroleum ether) to give the 2-((2-methoxyethyl)amino)-2-oxoethyl methansulfonate (**3.10**) as white solid (1 g, 63%). ^{1}H NMR ($CDCl_3$, 400 MHz): δ 6.60 (s, 1H), 4.59 (s, 2H), 3.52 – 3.36 (m, 4H), 3.30 (s, 3H), 3.07 (s, 3H). ^{13}C NMR ($CDCl_3$, 101 MHz): δ 165.16, 70.57, 66.51, 58.73, 39.04, 37.83.ESI-HRMS: Expected for $C_6H_{13}O_5SNNa$ ($M+Na^+$) = m/z 234.0407. Found: m/z 234.0395.

8.4.2 Determination of aqueous stability of sulfonate derivatives using ^{1}H NMR (solvent suppression method)

8.4.2.1 ^{1}H NMR solvent suppression method

NMR spectra were recorded using a Bruker Avance III NMR spectrometer operating at 500.13 MHz for ^{1}H. Solvent suppression for samples analysed in proteo-solvents was achieved using a pre-saturation pulse sequence (noesygppr1d). Typical parameters used

were; TD 65536 points, 64 transients, spectral width 20.66 ppm and acquisition time 3.17 s, D1 2.

8.4.2.2 Sample preparation and determination of stability

Stability of sulfonate derivatives (1 mg/mL) was determined in 100 mM phosphate buffer, pH 7, 8 or 8.5 containing 10% deuterated solvent using solvent suppression method (solvent suppression experiment at 4.7 ppm).

A stock solution of each sulfonate (10 mg) was prepared in deuterated solvent and 100 µL of which was added to 900 µL of aqueous phosphate buffer just before analysing by ^{1}H NMR experiment (less than 3 minutes after sulfonate reactant was added to buffer). ^{1}H-NMR spectra were acquired at 3, 6, 24, 48 and 96 h.

^{1}H-NMR (solvent suppression experiment) was acquired over 4 days to evaluate the stability and to calculate the hydrolysis rates. The percentage (%) of remaining sulfonate derivatives was calculated using Equation 3.1.

8.4.3 Determination of glutathione reactivity of sulfonates using ^{1}H NMR (solvent suppression method)

For determination of rates of reactivity of sulfonates with GSH, the sulfonate reactant (1 mg, 1 equiv.) was incubated at room temperature with glutathione (3 equiv.) in 100 mM potassium phosphate buffer, pH 7.5 containing 10% DMF-d_7 or acetone-d_6. A stock solution of each sulfonate (10 mg) was prepared in deuterated solvent and 100 µL of which was added to 900 µL of glutathione solution in aqueous phosphate buffer just prior to analysis by ^{1}H NMR (less than 3 minutes after sulfonate reactant was added to buffer). In a parallel experiment, the sulfonate derivatives **3.4**, **3.7** and **3.8** were held in phosphate buffer (100 mM, pH 7.5) without glutathione.

To calculate the rates of reactivity of sulfonates **3.4**, **3.7** and **3.8**, aliquots were taken at specific time intervals with and without glutathione and the percent of remaining for each sulfonate was calculated using Equation 3.1. To exclude the hydrolysis factor, the percent of remaining of sulfonate derivatives in presence of glutathione (reactivity rate)

was calculated by subtraction from the percentage remaining of sulfonate derivatives in the absence of glutathione.

For sulfonate derivative **3.9** the reaction rate was calculated using equation 3.1 assuming the rate of hydrolysis is negligible. For sulfonate derivative **3.10,** the reaction rate was calculated using Equation 3.3 assuming the rate of hydrolysis is negligible.

8.4.4 Conjugation buffer

In this study, conjugation buffer refers to 100 mM Tris.HCl (pH 7.5), containing 150 mM NaCl, and 5 mM EDTA. The pH of the buffer was adjusted directly before commencing conjugation reaction by using pH meter (Hanna instrument HI2210). Calibration of pH meter was performed on a regular basis.

8.4.5 Expression of Sbi IV-Cys

The expression of Sbi IV-Cys was performed according to the general method of protein over-expression (see Section 8.2.3). Briefly, a single colony *Escherichia coli* strain BL21 (DE3) with transformed Sbi IV-Cys construct (pET-15b) was inoculated in primary LB media and held at 37°C with shaking at 180 rpm overnight which was inoculated with 1 L of LB medium containing ampicillin (100 μg/mL) and held under the same conditions. The expression of Sbi IV-Cys protein was induced during the exponential phase of bacterial growth by adding IPTG and held at 37°C with shaking at 180 rpm for 3 h. Cells from the secondary culture were harvested, suspended in HisA buffer and lysed by sonication. Then, the insoluble cell debris was removed and the supernatant was collected (15 mL) and purified using immobilized metal affinity chromatography using nickel column attached to an AKTA purifier (Figure 8.3 A).

Sbi IV-Cys containing fractions (F6-13) were collected and appraised by 15% SDS-PAGE analysis (Figure 8.3 B). Then, the collected fractions were concentrated and finally buffer exchanged into PBS buffer and stored at -20°C. Protein concentration was determined used BCA assay. The concentration of Sbi IV-Cys was calculated using Equation 8.1 and found 1.7 mg/mL and total of 5 mg protein was obtained from 1-liter culture.

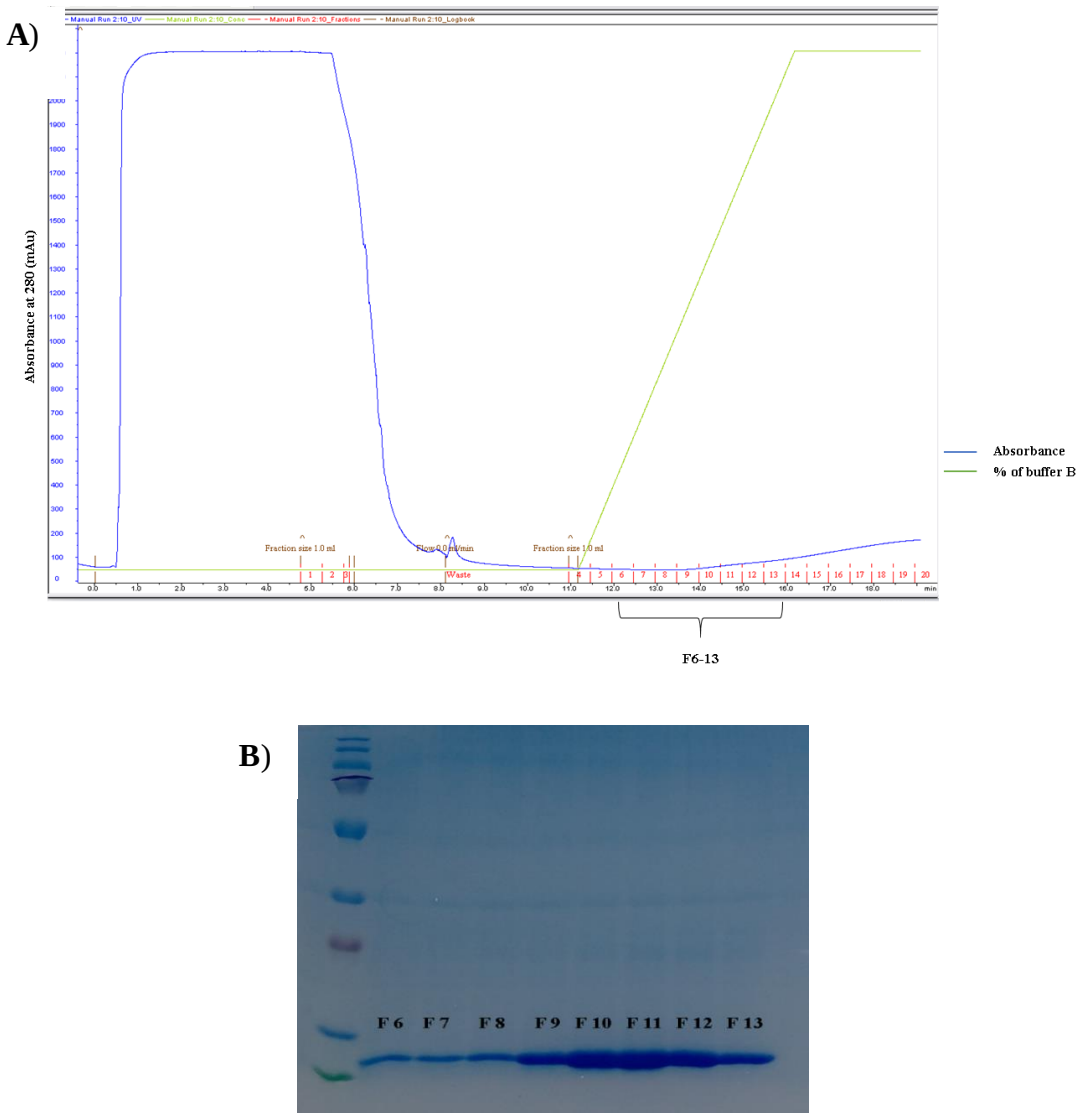

Figure 8.3. A) Chromatogram of immobilized metal affinity purification of the lysate containing Sbi IV-Cys protein using nickel column. **B**) SDS-PAGE (15%) analysis of the eluted F6-13.

8.4.6 Sbi IV-Cys reactivity with sulfonate derivatives

Sbi IV-Cys was buffer exchanged to 100 mM Tris.HCl buffer (pH 7.5), containing 150 mM NaCl, and 5 mM EDTA at and concentrated to (2 mg/mL, 0.187 µmol, 0.187 mM) using Amicon® Ultra-0.5 mL (3 kDa) centrifugal filter. Stock solution of TCEP **2.2** (4.0 mg/mL, 0.042 mmol, 14 mM) was prepared in Tris.HCl (100 mM, 150 mM NaCl, 5 mM EDTA, pH 7.5). The protein was first reduced by incubation with TCEP **2.2** (2 equiv.) for 1 h at room temperature. The reduced protein was aliquoted into 200 µL

samples for each reaction (4 reactions). The reduced control protein sample was held at room temperature overnight. A stock solution of each sulfonate was prepared in DMF to a final concentration of 10 mg/mL, with working solutions of sulfonate derivatives then prepared by serial dilution with DMF. Sulfonate derivatives **3.6**, **3.8**, **3.9** and **3.10** (10 equiv.) were mixed with the protein (up to 10% DMF final concentration) and held at room temperature overnight.

The reactions were then desalted, concentrated down using the previously mentioned method and analysed by protein MS according to the general method for protein MS analysis (see Section 8.2.5).

8.5 Chapter 4 Experimental

8.5.1 Chemical synthesis

*2-chloro-N-(2-methoxyethyl)acetamide (**4.3**)*

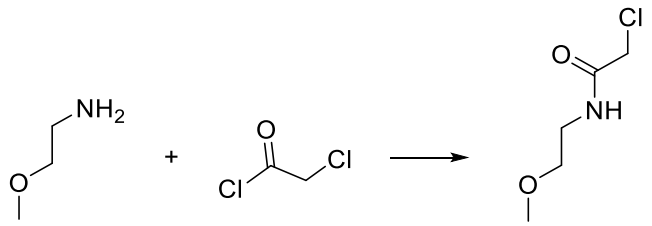

(**4.47**) (**4.4**) (**4.3**)

Sodium hydride (NaH, 67 mg, 28 mmol, 2.1 equiv.) was added to a solution 2-methoxyethan-1-amine **4.47** (1.0 g, 13 mmol) in THF. Subsequently, 2-chloroacetyl chloride **4.4** (2.9 g, 26 mmol, 2 equiv.) was added dropwise, and the resulting mixture was stirred at room temperature for 24 h. THF was evaporated under reduced pressure, ice-cooled water was added, the resulted aqueous mixture was extracted with DCM, dried over $MgSO_4$ and the solvent was evaporated under reduced pressure to give 2-chloro-N-(2-methoxyethyl)acetamide (**4.3**) as a white solid. (1.8 g, 90%). ^{1}H NMR spectrum was consistent with that previously reported.[278] ^{1}H NMR ($CDCl_3$, 400 MHz): δ 6.84 (s, 1H, NH), 4.00 (s, 2H), 3.44 (s, 4H), 3.32 (s, 3H). ^{13}C NMR ($CDCl_3$, 100 MHz):

δ 165.93, 70.65, 58.75, 42.51, 39.50. ESI-HRMS: Expected for $C_5H_{10}ClNO_2Na$ ($M+Na^+$) = m/z 174.0298. Found: m/z 174.0294.

*Attempted synthesis of 2-chloro-N-(2-chloroacetyl)-N-(2-methoxyethyl)acetamide (**4.1**)*

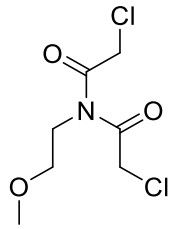

(**4.1**)

Attempt using pyridine as base

Pyridine (1.30 g, 16.4 mmol, 2.5 equiv.) was added to a cooled solution of 2-chloro-N-(2-methoxyethyl)acetamide **4.3** (1.0 g, 6.6 mmol) in DCM. 2-chloroacetyl chloride **4.12 (**1.48 g, 13.1 mmol, 2 equiv.) was added dropwise, and the resulting mixture was stirred at room temperature for 24 h. The reaction was then concentrated under reduced pressure and subjected to standard work-up (DCM). Purification of the crude product attempted by silica gel chromatography: (5% to 10% MeOH/DCM). A mixture of products was obtained and no product could be isolated for characterisation.

Attempt using TEA as base

TEA (2.5 equiv.) was added to a solution of 2-chloro-N-(2-methoxyethyl)acetamide **4.3** (1.0 g, 6.6 mmol) in DCM. 2-chloroacetyl chloride **4.4 (**1.48 g, 13.2 mmol, 2 equiv.) was added dropwise, and the resulting mixture was refluxed for 4 h. The reaction was then concentrated under reduced pressure and subjected to standard work-up (DCM). The crude product was further purified by silica gel chromatography: (5% to 10% MeOH/DCM). A mixture of undefined products was obtained though the desired product could not be confirmed by ^{1}H NMR and MS.

Base free attempt

2-chloroacetyl chloride **4.4** (1.48 g, 13.2 mmol) was added dropwise to a solution of 2-chloro-N-(2-methoxyethyl)acetamide **4.3** (1.0 g, 6.6 mmol) in dry toluene (10 mL) and refluxed for 24 hr. After 24 h of reflux, the reaction was then concentrated under reduced pressure, subjected to standard work-up (DCM) and analysed by MS. Analysis of MS identified only the starting material (**4.3**) and a product of elimination of the methoxy group. Expected mass for C_4H_7OClN ($M+H^+$) = m/z 120.0216 and found: m/z 120.0228

*2-Chloro-N-phenylacetamide (**4.5**)*

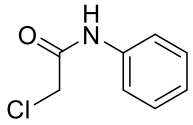

(**4.5**)

2-chloroacetylchloride **4.4** (2.41 g, 21.5 mmol, 2 equiv.) was added dropwise to a cooled solution of aniline **4.48** (1.0 g, 11 mmol) in DCM. The mixture was allowed to warm and stirred at room temperature for 2 h. The obtained solution was washed with water, saturated ammonium chloride solution, dried over $MgSO_4$ and the solvent was evaporated under reduced pressure to give the acetamide **4.5** as a white solid (1.64 g, 90%). NMR spectra (^1H and ^{13}C) were consistent with those previously reported.[279] ^1H NMR ($CDCl_3$, 400 MHz): δ 8.16 (s, 1H, NH), 7.50 (d, *J* = 8 Hz, 2H, Ar), 7.31 (t, *J* = 8 Hz, 2H, Ar), 7.13 (t, *J* = 8 Hz, 1H, Ar), 4.14 (s, 2H). ^{13}C NMR ($CDCl_3$, 100 MHz): δ 163.63, 136.60, 129.07, 125.17, 120.03, 42.79. ESI-HRMS: Expected for C_8H_8OClN Na ($M+Na^+$) = m/z 192.0192. Found: m/z 192.0180.

*2-chloro-N-(2-chloroacetyl)-N-phenylacetamide **(4.2)***

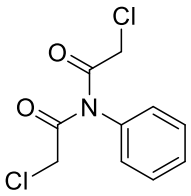

(**4.2**)

2-chloro-N-phenylacetamide **4.5** (1.0 g, 5.9 mmol) was refluxed with 2-chloroacetylchloride **4.4** (6.6 g, 59 mmol, 10 equiv.) to boiling in toluene for 48 h. The solution was then concentrated under reduced pressure and subjected to standard work-up (DCM). The crude was further purified by silica gel chromatography: (5% to 10% MeOH/DCM) to give the acetamide **4.2** as a white solid (1.08 g, 75%). ^{1}H NMR ($CDCl_3$, 400 MHz): δ 7.50-7.46 (m, 3H, Ar), 7.18-7.15 (m, 2H, Ar), 4.33 (s, 4H, CH_2). ^{13}C NMR ($CDCl_3$, 100 MHz): δ 168.65, 136.14, 130.26, 130.10, 128.66, 45.28. ESI-HRMS: Expected for $C_{10}H_9O_2Cl_2NNa$ ($M+Na^+$) = m/z 267.9908. Found: m/z 267.9883.

Reaction of thiophenol with 2-chloro-N-phenylacetamide

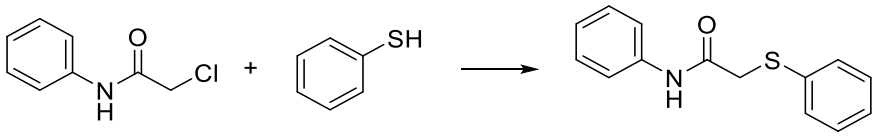

(**4.5**) (**4.6**) (**4.7**)

Thiophenol **4.6** (19.53 mg, 177.5 µmol, 3 equiv.) was added to a solution of 2-chloro-N-phenylacetamide **4.5** (10.0 mg, 59.2 µmol) in aqueous Tris.HCl buffer (100 mM, pH 7.5, 1 mL) and MeCN (1 mL). The reaction was monitored by HRMS after 6 h. The product was confirmed as **4.7** by HRMS (*m/z* 266.0583 ($M+Na^+$)).

Reaction of thiophenol with 2-chloro-N-(2-chloroacetyl)-N-phenylacetamide

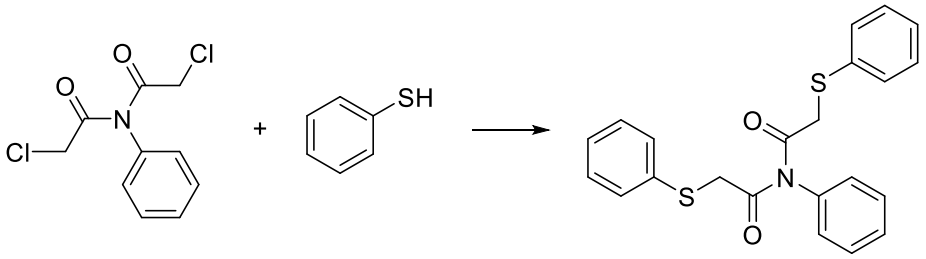

(**4.4**) (**4.6**) (**4.8**)

Thiophenol **4.6** (26.94 mg, 244.9 µmol, 6 equiv.) was added to a solution of 2-chloro-N-(2-chloroacetyl)-N-phenylacetamide **4.4** (10.0 mg, 40.8 µmol) in aqueous Tris.HCl buffer (100 mM, pH 7.5, 1 mL) and MeCN (1 mL). The reaction was monitored by HRMS after 6 h. The product was confirmed as **4.8** by HRMS (*m/z* 416.0756 ($M+Na^+$)).

Reaction of thiophenol with 2-chloro-N-(2-chloroacetyl)-N-(3,4,5-trimethoxyphenyl)acetamide

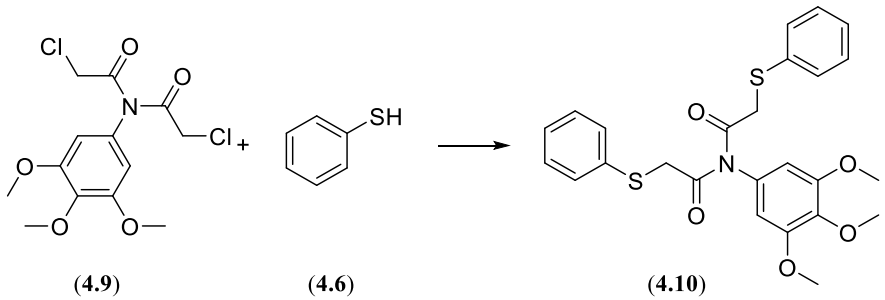

(**4.9**) (**4.6**) (**4.10**)

Thiophenol **4.6** (19.7 mg, 180 µmol, 6 equiv.) was added to a solution of 2-chloro-N-(2-chloroacetyl)-N-(3,4,5-trimethoxyphenyl)acetamide **4.9** (10 mg, 30 µmol, purchased from Enamine EN300-31080) in aqueous Tris.HCl buffer (100 mM, pH 7.5, 1 mL) and MeCN (1 mL). The reaction was monitored by HRMS after 6 h. The product was confirmed as **4.10** by HRMS (m/z 506.1078 ($M+Na^+$)).

Ethyl 4-(2-chloroacetamido)benzoate ***(4.12)***

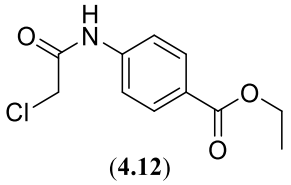

(**4.12**)

2-Chloroacetyl chloride **4.4** (0.90 g, 7.9 mmol, 1.3 equiv.) was added dropwise to a cooled solution of benzocaine **4.49** (1.0 g, 6.1 mmol) in DCM. The mixture was allowed to warm and stirred at room temperature for 2 h. The obtained solution was washed with water and saturated ammonium chloride solution, dried over $MgSO_4$ and the solvent was evaporated under reduced pressure to give the acetamide **4.12** as a white solid (1.4 g, 96%). NMR spectra (^1H and ^{13}C) were consistent with those previously reported.[280] ^1H NMR ($CDCl_3$, 400 MHz): δ 8.32 (s, 1H, NH), 8.00 (d, *J* = 8.8 Hz, 2H, Ar), 7.60 (d, *J* = 8.8 Hz, 2H, Ar), 4.35-4.29 (q, *J* = 7.2 Hz, 2H, CH_2), 4.16 (s, 2H, CH_2), 1.43 (t, *J* =7.2 Hz, 3H, Me). ^{13}C NMR ($CDCl_3$, 100 MHz): δ 165.85, 163.87, 140.55, 130.78, 126.93, 119.04, 60.94, 42.80, 14.27. ESI-HRMS: Expected for $C_{11}H_{12}ClNO_3Na$ ($M+Na^+$) = m/z 264.0398. Found: m/z 264.0439.

Ethyl 4-(2-chloro-N-(2-chloroacetyl)acetamido)benzoate ***(4.11)***

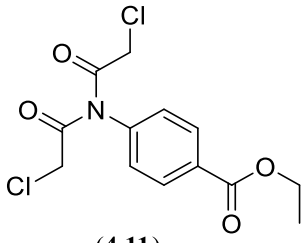

(**4.11**)

Ethyl 4-(2-chloroacetamido)benzoate **4.12** (1.0 g, 4.2 mmol) was refluxed with 2-chloroacetyl chloride **4.4** (4.6 g, 42 mmol, 10 equiv.) to boiling in toluene for 48 h. The product was extracted with DCM and dried over $MgSO_4$, filtered and concentrated under reduced pressure. The crude was further purified by silica gel chromatography: (10% to 30% EtOAc/petroleum ether) to give the acetamide **4.11** as a white solid (1g, 76%). ^1H NMR ($CDCl_3$, 400 MHz): δ 8.16 (d, *J* = 8 Hz, 2H), 7.26 (d, *J* = 8 Hz, 2H),

4.37 (q, *J* = 8 Hz, 2H), 4.32 (s, 4H), 1.37 (t, *J* = 8 Hz, 3H). ^{13}C NMR, ($CDCl_3$, 100 MHz): δ 168.36, 165.08, 139.91, 132.28, 131.49, 128.88, 61.57, 45.14, 14.23. ESI-HRMS: Expected for $C_{13}H_{13}Cl_2NO_4Na$ ($M+Na^+$) = m/z 340.0114. Found: m/z 340.0104.

Ethyl 4-(2-chloro-N-(2-chloroacetyl)acetamido)benzoate reaction with glutathione

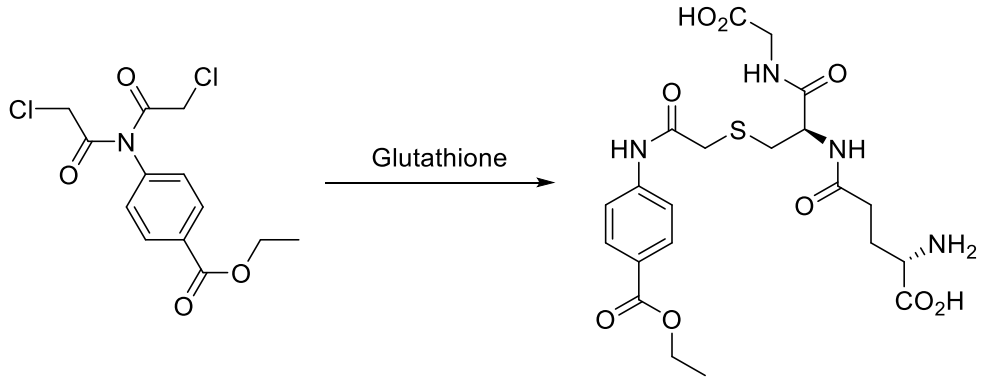

(**4.11**) (**4.13**)

Ethyl 4-(2-chloro-N-(2-chloroacetyl)acetamido)benzoate **4.11** (100 mg, 0.315 mmol) was dissolved in a solution of THF (2 mL) and added gradually to the aqueous solution of glutathione **3.23** (0.58 g, 1.9 mmol, 6 equiv.) in aqueous sodium phosphate (500 mM, pH = 7.5, 8 mL). The reaction was stirred at room temperature overnight. The reaction was subsequently purified by C-18 chromatography (100% H_2O to 40% MeCN/H_2O) to give the compound **4.13** as a sticky solid (100 mg, 63%). ^{1}H NMR (D_2O, 500 MHz): δ 7.89 (d, J = 9 Hz, 2H), 7.49 (d, J = 9 Hz, 2H), 4.58 – 4.47 (m, 1H), 4.26 (q, J = 7 Hz, 2H), 3.71- 3.62 (m, 3H), 3.41 (s, 2H), 3.12 – 2.85 (m, 2H), 2.41 (t, J = 7.5 Hz, 2H), 2.03- 1.97 (m, 2H), 1.28 (t, J = 7 Hz, 3H). ^{13}C NMR (D_2O, 126 MHz): δ 176.17, 174.86, 174.06, 171.66, 170.91, 168.30, 141.57, 130.54, 125.92, 120.29, 62.13, 54.11, 52.91, 43.36, 36.22, 33.65, 31.40, 26.22, 13.39. HRMS: Expected for $C_{21}H_{28}O_9SN_4Na$ ($M+Na^+$) = m/z 535.1469. Found: m/z 535.1462.

Methyl 3,5-bis(2-chloroacetamido)benzoate ***(4.15)***

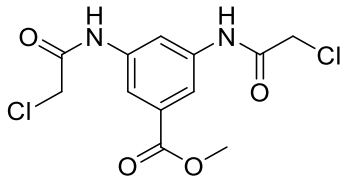

(**4.15**)

2-Chloroacetyl chloride **4.4** (1.4 g, 12 mmol, 2 equiv.) was added dropwise to a cooled solution of methyl 3,5-diaminobenzoate **4.50** (1.0 g, 6.0 mmol) in DCM. The mixture was allowed to warm and stirred at room temperature for 2 h. The obtained precipitate was filtered, washed with water 5-6 times, and completely dried under high vacuum to give the acetamide **4.15** as a white solid (1.7 g, 89%). ^{1}H NMR ($CDCl_3$, 400 MHz): δ 8.31 (s, 2H, NH), 8.20 (s, 1H, Ar), 7.93 (s, 2H, Ar), 4.16 (s, 2H, 2x CH_2), 3.88 (s, 3H, Me). ^{13}C NMR ($CDCl_3$, 100 MHz): δ 165.82, 164.10, 137.58, 131.88, 117.45, 115.56, 52.45, 42.71. ESI-HRMS: Expected for $C_{12}H_{12}Cl_2N_2O_4Na$ ($M+Na^+$) = m/z 341.0066. Found: m/z 341.0077. HPLC: column: HiQ Sil HS (150 x 4.60 mm). Mobile phase: isocratic: (0.75 mL/min), 35% MeCN: 65% water. Detection at 280 nm. Retention time: 8.26 minutes, purity: 99.1%.

Methyl 3,4-bis(2-chloroacetamido)benzoate ***(4.16)***

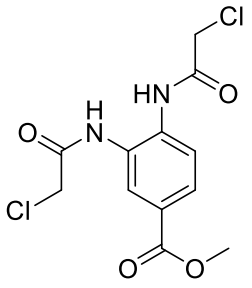

(**4.16**)

2-Chloroacetyl chloride **4.4** (1.4 g, 12 mmol, 2 equiv.) was added dropwise to a cooled solution of methyl 3,4-diaminobenzoate **4.51** (1.0 g, 6.0 mmol) in DCM. The mixture was allowed to warm and stirred at room temperature for 2 h. The obtained precipitate was filtered, washed with water 5-6 times and completely dried under high vacuum to

give the acetamide **4.16** as a white solid (1.5 g, 79%). ^{1}H NMR ($CDCl_3$, 400 MHz): δ 8.84 (s, 1H, NH), 8.54 (s,1H, NH), 8.04 (d, *J* = 2 Hz, 1H, Ar), 7.94 (dd, *J* = 8.4, 2 Hz, 1H, Ar), 7.75 (d, *J* = 8.4 Hz, 1H, Ar), 4.19 (d, *J* = 12 Hz, 4H, 2 x CH_2), 3.88 (s, 3H, Me). ^{13}C NMR ($CDCl_3$, 100 MHz): δ 165.82, 164.10, 137.58, 131.88, 117.45, 115.56, 52.45, 42.71. ESI-HRMS: Expected for $C_{12}H_{12}Cl_2N_2O_4Na$ ($M+Na^+$) = m/z 341.0066. Found: m/z 341.0086. HPLC: column: HiQ Sil HS (150 x 4.60 mm), isocratic: (0.75 mL/minutes) 35% MeCN: 65% water. Detection at 280 nm. Retention time: 9.03 minutes, purity: 98.1%.

N,N'-(1,3-phenylene)bis(2-bromoacetamide) ***(4.38)***

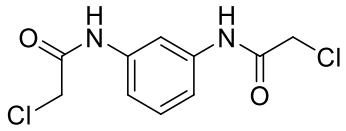

(**4.38**)

2-Chloroacetyl chloride **4.4** (9.3 g, 84 mmol, 6 equiv.) was added dropwise to a cooled aqueous NaOH (0.55 M) solution of benzene-1,3-diamine **4.52** (1.5 g, 14 mmol). The mixture was allowed to warm and stirred at room temperature overnight. The obtained precipitate was filtered, washed with water 5-6 times and completely dried under high vacuum to give the acetamide **4.38** as a white solid (0.97 g, 27%). NMR spectra (^{1}H and ^{13}C) were consistent with those previously reported.[281] ^{1}H NMR (DMSO-d_6, 400 MHz): δ 10.34 (s, 2H, NH), 7.96 (t, *J* = 2.0 Hz, 1H, Ar), 7.37- 7.25 (m, 3H, Ar), 4.25 (s, 4H, 2 x CH_2). ^{13}C NMR (DMSO-d_6, 100 MHz): δ 164.61, 138.82, 129.14, 114.81, 110.36, 45.53. ESI-HRMS: Expected for $C_{10}H_{10}Cl_2N_2O_2Na$ ($M+Na^+$) = m/z 283.0012. Found: m/z 283.0049.

*N,N'-(1,2-phenylene)bis(2-bromoacetamide) (**4.39**)*

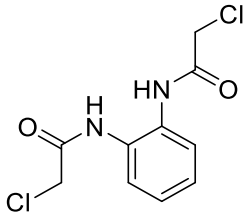

(**4.39**)

2-Chloroacetyl chloride **4.4** (9.3 g, 84 mmol, 6 equiv.) was added dropwise to a cooled aqueous NaOH (0.55 M) solution of benzene-1,2-diamine **4.53** (1.5 g, 14 mmol). The mixture was allowed to warm and stirred at room temperature overnight. The obtained precipitate was filtered, washed with water 5-6 times and the obtained solid compound obtained was completely dried under high vacuum to give the acetamide **4.39** as a white solid (1.8 g, 51%). NMR spectra (^{1}H and ^{13}C) were consistent with those previously reported.[282] ^{1}H NMR (DMSO-d_6, 400 MHz): δ 9.69 (s, 2H, NH), 7.55 (dd, *J* = 7.4, 3.7 Hz, 2H, Ar), 7.23 (dd, *J* = 6.1, 3.5, 2 Hz, 2H, Ar), 4.34 (s, 4H, 2 x CH_2). ^{13}C NMR ($CDCl_3$, 100 MHz): δ 165.12, 130.17, 125.61, 125.08, 43.19. ESI-HRMS: Expected for $C_{10}H_{10}Cl_2N_2O_2Na$ ($M+Na^+$) = m/z 283.0012. Found: m/z 283.0010.

*Ethyl 4-(2-bromoacetamido)benzoate (**4.20**)*

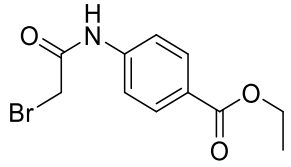

(**4.20**)

2-bromoacetyl bromide (1.6 g, 7.9 mmol, 1.3 equiv.) was added dropwise to a cooled solution of benzocaine **4.49** (1.0 g, 6.1 mmol) and TEA (1.35 g, 13.3 mmol, 2.2 equiv.) in DCM. The mixture was allowed to warm and stirred at room temperature for 2 h. The obtained precipitate was filtered and washed with water 5-6 times before washing with ether. The solid compound was dried under high vacuum to give the acetamide **4.20** as a white solid (1.2 g, 69.2%). ^{1}H NMR ($CDCl_3$, 500 MHz): δ 8.30 (s, 1H, NH), 8.26 – 8.03 (m, 2H, Ar), 8.03 – 7.54 (m, 2H, Ar), 4.40 (q, *J* = 7.1 Hz, 2H, CH_2), 4.06 (s, 2H,

$COCH_2Br$), 1.42 (t, *J* = 7.1 Hz, 3H, OMe). ^{13}C NMR ($CDCl_3$, 126 MHz): δ 165.94, 163.49, 140.87, 130.83, 126.94, 119.01, 61.02, 29.36, 14.35. ESI-HRMS: Expected for $C_{11}H_{11}ClNO_3$ ($M\text{-}H^+$) = m/z 283.9920. Found: m/z 283.9928. The general procedure to synthesise bromo-derivtives was done according to previously mentioned method by Tripathi *et al.*[283]

Methyl 3,5-bis(2-bromoacetamido)benzoate ***(4.22)***

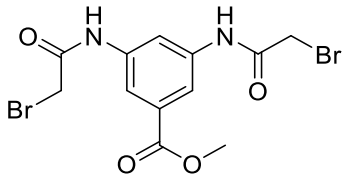

(**4.22**)

2-bromoacetyl bromide (2.65 g, 13.2 mmol, 2.2 equiv.) was added dropwise to a cooled solution of methyl 3,4-diaminobenzoate **4.50** (1.0 g, 6.0 mmol) and TEA (1.35 g, 13.2 mmol, 2.2 equiv.) in DCM. The obtained precipitate was filtered and washed with water 5-6 times before washing with ether. The solid compound was dried under vacuum to give the acetamide **4.22** as a white solid (1.83 g, 75%). ^1H NMR (DMSO-d_6, 500 MHz): δ 10.68 (s, 2H, NH), 8.20 (s, 1H, Ar), 7.98 (s, 2H, Ar), 4.06 (s, 4H, 2 X CH_2), 3.87 (s, 3H, OMe). ^{13}C NMR (DMSO-d_6, 126 MHz): δ 165.66, 165.17, 139.35, 130.58, 115.02, 113.88, 52.34, 30.24. ESI-HRMS: Expected for $C_{12}H_{13}Br_2N_2O_4Na$ ($M+Na^+$) = m/z 406.9261. Found: m/z 406.9237. HPLC: column: HiQ Sil HS (150 x 4.60 mm). Mobile phase: isocratic: (0.75 mL/min), 35% MeCN: 65% water. Detection at 280 nm. Retention time: 9.63 minutes, purity: 98.9%.

Methyl 3,4-bis(2-bromoacetamido)benzoate ***(4.23)***

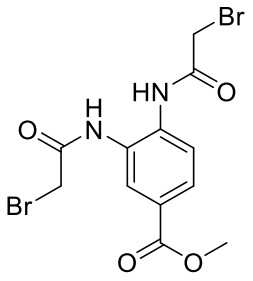

(**4.23**)

2-bromoacetyl bromide (2.65 g, 13.2 mmol, 2.2 equiv.) was added dropwise to a cooled solution of methyl 3,4-diaminobenzoate **4.51** (1.0 g, 6.0 mmol) and TEA (1.35 g, 13.3 mmol, 2.2 equiv.) in DCM. The obtained precipitate was filtered and washed with water 5-6 times before washing with ether. The solid compound was dried under high vacuum to give the acetamide **4.23** as a white solid (1.59 g, 65%). ^{1}H NMR (DMSO-d_6, 500 MHz): δ 9.92 (d, *J* = 5.3 Hz, 2H, NH), 8.10 (s, 1H, Ar), 7.82 (d, *J* = 2.8 Hz, 2H, Ar), 4.15 (d, *J* = 13.2 Hz, 4H, 2 X CH_2), 3.85 (s, 3H, OMe). ^{13}C NMR (DMSO-d_6, 126 MHz): δ 165.39, 134.98, 129.32, 126.55, 126.13, 123.94, 52.19, 30.17. ESI-HRMS: Expected for $C_{12}H_{11}Br_2N_2O_4$ ($M\text{-}H^+$) = m/z 404.9130. Found: m/z 404.9091. HPLC: column: HiQ Sil HS (150 x 4.60 mm). Mobile phase: isocratic: (0.75 mL/min), 35% MeCN: 65% water. Detection at 280 nm. Retention time: 8.77 minutes, purity: 96.57%.

N,N'-(1,3-phenylene)bis(2-bromoacetamide) ***(4.28)***

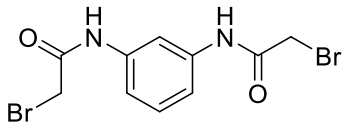

(**4.28**)

2-bromoacetyl bromide (2.05 g, 10.2 mmol, 2.2 equiv.) was added dropwise to a cooled solution of benzene-1,3-diamine **4.52** (0.5 g, 4.6 mmol) and TEA (1.35 g, 13.3 mmol, 2.2 equiv.) in DCM. The obtained precipitate was filtered and washed with water 5-6 times before washing with ether. The solid compound was dried under high vacuum to give the acetamide **4.28** as a pale yellow solid (2.48 g, 77%). NMR spectra (^{1}H and ^{13}C)

were consistent with those previously reported.[163] ^{1}H NMR (DMSO-d_6, 500 MHz): δ 10.42 (s, 2H, 2 X NH), 7.96 (t, *J* = 2.0 1H, Ar), 7.37-7.24 (m 3H, Ar), 4.04 (s, 4H, 2 X CH_2). ^{13}C NMR (DMSO-d_6, 126 MHz): δ 164.79, 138.95, 129.14, 114.72, 110.17, 30.36. ESI-HRMS: Expected for $C_{10}H_{10}Br_2N_2O_2Na$ ($M+Na^+$) = m/z 370.9001. Found: m/z 370.9039.

N,N'-(1,2-phenylene)bis(2-bromoacetamide) ***(4.29)***

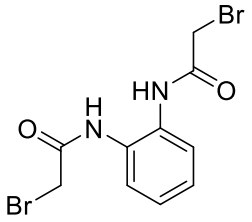

(**4.29**)

2-bromoacetyl bromide (2.05g, 10.2 mmol, 2.2 equiv.) was added dropwise to a cooled solution of benzene-1,2-diamine **4.53** (0.50 g, 4.6 mmol) and TEA (1.03 g, 10.2 mmol, 2.2 equiv.) in DCM. The obtained precipitate was filtered and washed with water 5-6 times before washing with ether. The solid compound was dried under vacuum to give the acetamide **4.29** as a yellow solid (1.87 g, 58%). NMR spectra (^{1}H and ^{13}C) were consistent with those previously reported.[163] ^{1}H NMR (DMSO-d_6, 500 MHz): δ 9.71 (s, 2H, NH), 753 (dd, *J* = 7.5, 3.7 Hz, 2H, Ar), 7.23 (dd, *J* = 6.0, 3.5 Hz 2H, Ar), 4.13 (s, 4H, 2 X CH_2). ^{13}C NMR (DMSO-d_6, 126 MHz): δ 165.14, 130.27, 125.56, 124.93, 30.14. ESI-HRMS: Expected for $C_{10}H_{10}Br_2N_2O_2Na$ ($M+Na^+$) = m/z 370.9001. Found: m/z 370.9012.

Ethyl 4-(2-Iodoacetamido)benzoate ***(4.21)***

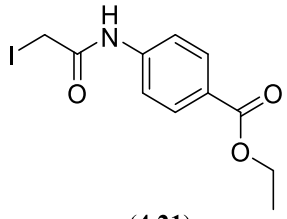

(**4.21**)

KI (1.38 g, 8.30 mmol, 2 equiv.) was added to a solution of Ethyl 4-(2-chloroacetamido) benzoate **4.12** (1.0 g, 4.2 mmol) in dry acetone (20 mL). The mixture was refluxed for 3 h. The obtained mixture was filtrated and the solvent was evaporated under reduced pressure to give the acetamide **4.21** as a yellow solid (1.25 g, 90%). NMR spectra (^{1}H and ^{13}C) were consistent with those previously reported.[284] ^{1}H NMR ($CDCl_3$, 400 MHz): δ 7.98 (d, *J* = 8.4, 2H, Ar), 7.81 (s, 1H, NH), 7.54 (d, *J* = 8.4, 2H, Ar), 4.34- 4.29 (q, *J* = 7.2 Hz, 2H, CH_2), 3.82 (s, 2H, CH_2), 1.34 (t, *J* = 6.8 Hz, 3H, Me). ^{13}C NMR ($CDCl_3$, 100 MHz): δ 165.90, 165.04, 141.24, 130.73, 118.82, 60.92, 14.26, -0.57. ESI-HRMS: Expected for $C_{11}H_{12}INO_3Na$ ($M+Na^+$) = m/z 355.9754. Found: m/z 355.9773. The followed procedure to synthesise iodo-derivatives was done according to previously mentioned method by Lalit *et al.*[285]

Methyl 3,5-bis(2-iodoacetamido)benzoate ***(4.24)***

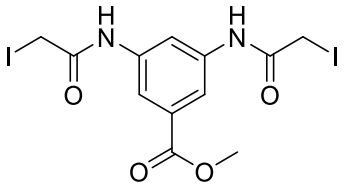

(**4.24**)

KI (1.6 g, 9.4 mmol, 3 equiv.) was added to a solution of Methyl 3,4-bis(2-chloroacetamido) benzoate **4.15** (1.0 g, 3.1 mmol) in dry acetone (20 mL). The mixture was refluxed for 3 h. The obtained mixture was filtrated and the solvent was evaporated under reduced pressure to give the acetamide **4.24** as a yellow solid (1 g, 63%). ^{1}H NMR (CD_3COCD_3, 500 MHz): δ 9.91 (s, 2H, NH), 8.20 (s, 1H, Ar), 8.16 (s, 2H, Ar), 4

(s, 4H, 2 X CH_2), 3.89 (s, 3H, OMe). ^{13}C NMR (CD_3COCD_3, 126 MHz): δ 166.82, 166.09, 140.01, 127.53, 131.52, 115.56, 114.00, 51.85, -0.00. HRMS: Expected for $C_{12}H_{13}I_2N_2O_4$ ($M+H^+$) = m/z 502.8969, Found: m/z 502.8959. HPLC: column: HiQ Sil HS (150 x 4.60 mm). Mobile phase: isocratic: (0.75 mL/min), 35% MeCN: 65% water. Detection at 280 nm. Retention time: 12.35 minutes, purity, 97.9%.

Methyl 3,4-bis(2-iodoacetamido)benzoate ***(4.25)***

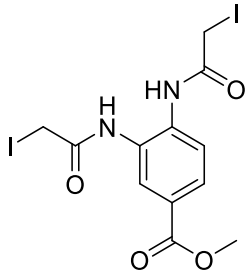

(**4.25**)

KI (1.6 g, 9.4 mmol, 3 equiv.) was added to a solution of methyl 3,4-bis(2-chloroacetamido) benzoate **4.16** (1.0 g, 3.1 mmol) in dry acetone (20 mL). The mixture was refluxed for 3 h. The obtained mixture was filtrated and the solvent was evaporated under reduced pressure to give the acetamide **4.25** as a yellow solid (1 g, 63%). ^1H NMR ($CDCl_3$, 500 MHz): δ 9.73 (s, 1H, NH), 9.61 (s, 1H, NH), 8.02 (s, 1H, Ar), 7.80 (d, *J* = 8.5 Hz, 1H, Ar), 7.65 (d, *J* = 8.5 Hz, 1H, Ar), 3.86 (s, 3H, OMe), 3.86 (s, 4H, 2 X CH_2). ^{13}C NMR ($CDCl_3$, 126 MHz): 167.79, 167.15, 165.94, 127.53, 127.36, 126.65, 124.22, 52.11, -0.74, -1.0. HRMS: Expected for $C_{12}H_{13}I_2N_2O_4$ ($M+H^+$) = m/z 502.8969. Found: m/z 502.8959. HPLC: column: HiQ Sil HS (150 x 4.60 mm). Mobile phase: isocratic: (0.75 mL/min), 35% MeCN: 65% water. Detection at 280 nm. Retention time: 10.85 minutes, purity: 95.9%.

N,N'-(1,3-phenylene)bis(2-iodoacetamide) ***(4.30)***

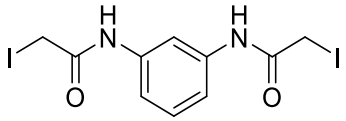

(**4.30**)

KI (1.3 g, 7.7 mmol, 4 equiv.) was added to a solution of N,N'-(1,3-phenylene)bis(2-chloroacetamide) **4.38** (0.50 g, 1.9 mmol) in dry acetone (20 mL). The mixture was refluxed for 3 h. The obtained mixture was filtrated and the solvent was evaporated under reduced pressure to give the acetamide **4.30** as a yellow solid (0.63 g, 74%). ^{1}H NMR (DMSO-d_6, 500 MHz): δ 10.36 (s, 2H, NH), 7.92 (t, J = 2.0 Hz, 1H, Ar), 7.33-7.22 (m, 3H, Ar), 3.83 (s, 4H, 2 X CH_2). ^{13}C NMR (DMSO-d_6, 126 MHz): δ 166.56, 139.18, 129.10, 114.36, 109.86, 1.58. HRMS: Expected for $C_{10}H_{10}I_2N_2O_2Na$ ($M+Na^+$) = m/z 466.8724, Found: m/z 466.8758. HPLC: column: HiQ Sil HS (150 x 4.60 mm). Mobile phase: isocratic: (0.75 mL/min), 35% MeCN: 65% water. Detection at 280 nm. Retention time, 8.89 minutes, purity, 93.4%.

N,N'-(1,2-phenylene)bis(2-iodoacetamide) ***(4.31)***

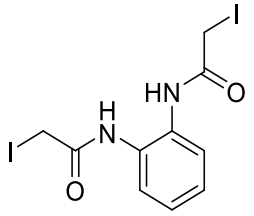

(**4.31**)

KI (1.3 g, 7.7 mmol, 4 equiv.) was added to a solution of N,N'-(1,3-phenylene)bis(2-chloroacetamide) **4.39** (0.50 g, 1.9 mmol) in dry acetone (20 mL). The mixture was refluxed for 3 h. The obtained mixture was filtrated and the solvent was evaporated under reduced pressure to give the acetamide **4.31** as a yellow solid (0.63 g, 45%). ^{1}H NMR (DMSO-d_6, 500 MHz): δ 9.63 (s, 2H, NH), 7.49 (dd, J = 7.4, 3.7 Hz, 2H, Ar), 7.20 (dd, J = 6.1, 3.5 Hz, 2H, Ar), 3.90 (s, 4H, 2 X CH_2). ^{13}C NMR (DMSO-d_6, 126 MHz): δ 166.92, 130.42, 125.35, 124.70, 1.49. HRMS: Expected for $C_{10}H_{10}I_2N_2O_2Na$ ($M+Na^+$) = m/z 466.8724. Found: m/z 466.8770.

Reaction of TCEP with methyl 3,5-bis(2-chloroacetamido)benzoate

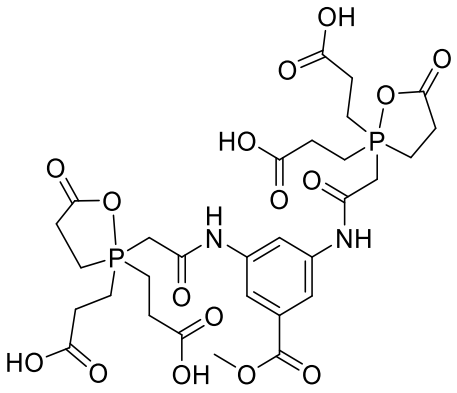

(**4.40**)

TCEP (0.25 g, 0.92 mmol, 3 equiv.) was dissolved in a solution of aqueous sodium phosphate buffer (500 mM, pH 7.5, 10 mL). Methyl 3,5-bis(2-chloroacetamido)benzoate **4.15** (100 mg, 0.310 mmol) was dissolved in THF (2 mL) and added gradually to TCEP aqueous solution and held overnight at room temperature. The reaction was subsequently concentrated down under reduced pressure and purified by C-18 chromatography (100% H_2O to 20% MeCN/H_2O) to give compound **4.40** as a transparent sticky solid (0.1 g, 50%). ^{1}H NMR (500 MHz, D_2O): δ 7.84 (d, J = 2.0 Hz, 2H, Ar), 7.67 (t, J = 2.0 Hz, 1H, Ar), 3.81 (s, 4H, OMe), 2.60 – 2.37 (m, 28H, 6x CH_2CH_2OH, 2x CH_2). ^{13}C NMR (D_2O, 126 MHz): δ 178.03, 119.09, 99.98, 52.92, 28.68, 16.81, 16.41. ^{31}P NMR (202 MHz, D_2O): δ 34.92. ESI-HRMS: Expected for $C_{30}H_{40}N_2O_{16}$ (M-H^+) = m/z 745.1780. Found: m/z 745.1804. IR cm^{-1}: 3396.42, 2527.16, 2096.42, 1646.87, 1445.89, 1239.27, 1081.18.

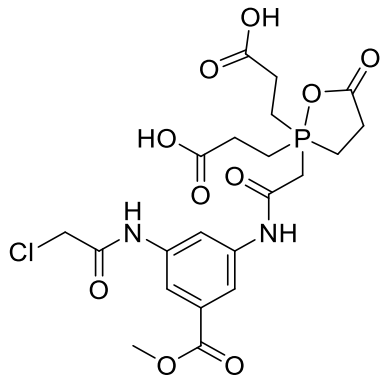

(**4.41**)

The compound **4.41** was also isolated as a transparent solid (0.1g, 40%). ^{1}H NMR (500 MHz, D_2O): δ 7.81 – 7.53 (m, 3H, Ar), 4.17 (s, 2H, $COCH_2Cl$), 3.78 (s, 3H, OMe), 2.55-2.43 (m, 14H, 3x CH_2CH_2OH, $COCH_2P$). ^{13}C NMR (D_2O, 126 MHz): δ 178.07, 167.87, 167.70, 137.51, 130.78, 118.47, 117.72, 52.90, 43.01, 28.69, 16.81, 16.41. ^{31}P NMR (202 MHz, D_2O): δ 34.91. ESI-HRMS: Expected for $C_{12}H_{26}N_2O_{10}ClP$ ($M\text{-}H^+$) = m/z 531.0930. Found: m/z 531.0907.

γ-L-glutamyl-S-((5-(methoxycarbonyl)-1,3-phenylene)bis(azanediyl))bis(2-oxoethane-2,1-diyl))-L-cysteinylglycine ***(4.17)***

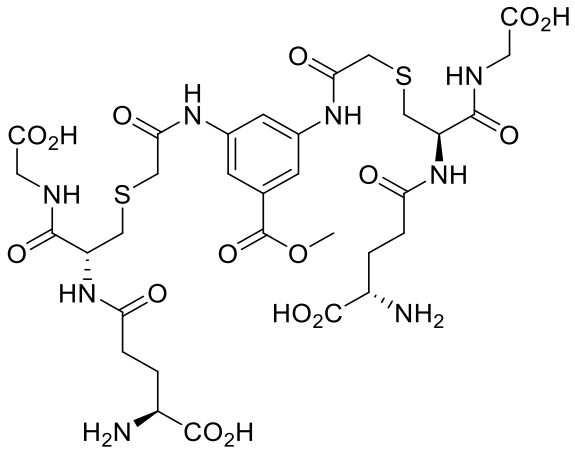

(**4.17**)

Glutathione **3.23** (290 mg, 0.943 mmol, 3 equiv.) was dissolved in a solution of aqueous sodium phosphate buffer (100 mM, pH 7.5, 8 mL). Methyl 3,5-bis(2-chloroacetamido)benzoate **4.15** (100 mg, 0.314 mmol) was dissolved in THF (2 mL),

added gradually to glutathione aqueous solution and held overnight at room temperature. The reaction was subsequently concentrated down under reduced pressure and purified by C-18 chromatography (100% H_2O to 20% MeCN/H_2O) to give the product **4.17** as a sticky solid (0.20 mg, 74%). ^{1}H NMR (D_2O, 500 MHz): δ 7.73 (s, 1H, Ar), 7.56 (s, 2H, Ar), 4.57-4.54 (m, 2H, 2 x NHC<u>H</u>CO), 3.79 (s, 3H, OMe), 3.73 – 3.63 (m, 6H, 2 x NHC<u>H</u>$_2$COOH, CH2<u>C</u>HNH$_2$), 3.40 (s, 4H, 2 x SC<u>H</u>$_2$CO), 3.13-2.89 (m, 4H, 2 x SC<u>H</u>$_2$CH), 2.43 (t, *J* = 8 Hz, 4H, 2 x CH$_2$C<u>H</u>$_2$CO), 2.06-2.01 (m, 4H, 2 x C<u>H</u>$_2$CH$_2$CO). ^{13}C NMR (126 MHz, D_2O): δ 176.17, 174.81, 174.00, 171.69, 170.39, 167.65, 137.89, 130.43, 117.32, 54.11, 52.92, 52.89, 43.42, 36.24, 33.77, 31.37, 26.19. HRMS: Expected for $C_{32}H_{44}O_{16}S_2N_8Na$ (M+Na+) = m/z 883.2209 Found: m/z 883.2187. HPLC: column: HiQ Sil HS (150 x 4.60 mm). Mobile phase: isocratic: (1 mL/min), 10% MeCN: 90% water: 0.1% TFA. Detection at 214 nm. Retention time: 36.39 minutes, purity: 99%.

*γ-L-glutamyl-S-((5-(methoxycarbonyl)-1,2-phenylene)bis(azanediyl))bis(2-oxoethane-2,1-diyl))-L-cysteinylglycine (**4.18**)*

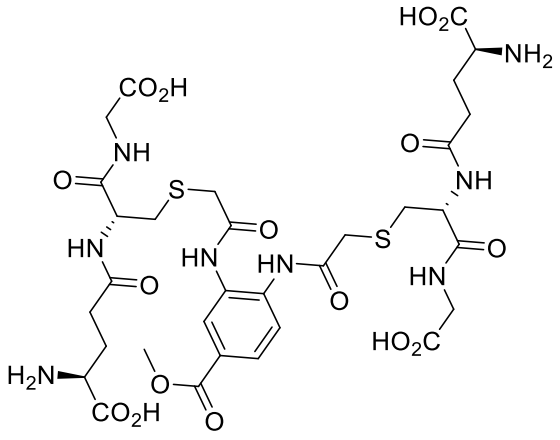

(**4.18**)

Glutathione **3.23** (290 mg, 0.943 mmol, 3 equiv.) was dissolved in a solution of aqueous sodium phosphate buffer (100 mM, pH 7.5, 8 mL). Methyl 3,4-bis(2-chloroacetamido)benzoate **4.16** (100 mg, 0.314 mmol) was dissolved in THF (2 mL), added gradually to glutathione aqueous solution and held overnight at room temperature. The reaction was subsequently concentrated down under reduced pressure

and purified by C-18 chromatography (100 % H_2O to 20 % MeCN/H_2O) to give the product **4.18** as a sticky solid (0.17 mg, 63%). ^{1}H NMR (500 MHz, D_2O): δ 8.00 (s, 1H, Ar), 7.93 (dd, *J* = 8.5, 2 Hz, 1H, Ar), 7.63 (d, *J* = 8.5 Hz, 1H, Ar), 4.70-4.56 (m, 2H, 2 x NHC<u>H</u>CO), 3.86 (s, 3H, OMe), 3.76–3.65 (m, 6H, 2 x NHC<u>H$_2$</u>COOH, CH2<u>C</u>HNH$_2$), 3.52-3.45 (m, 4H, 2 x SC<u>H$_2$</u>CO), 3.15–2.90 (m, 4H, 2 x SC<u>H$_2$</u>CH), 2.47-2.43 (m, 4H, 2 x CH$_2$C<u>H$_2$</u>CO), 2.07 -2.02 (m, 4H, 2 x C<u>H$_2$</u>CH$_2$CO). ^{13}C NMR (126 MHz, D_2O): δ 176.11, 174.88, 173.88, 171.63, 171.22, 167.95, 135.56, 128.79, 128.22, 128.04, 125.81, 54.08, 52.90, 52.81, 43.35, 35.72, 35.52, 33.85, 33.79, 31.36, 26.09. HRMS: Expected for $C_{32}H_{44}O_{16}S_2N_8Na$ ($M+Na^+$) = m/z 883.2209. Found: m/z 883.2187. HPLC: column: HiQ Sil HS (150 x 4.60 mm). Mobile phase: isocratic: (1 mL/min), 10% MeCN: 90% water: 0.1% TFA. Detection at 214 nm. Retention time: 14.25 minutes, purity: 99%.

L-γ-Glutamyl-S-(1-ethyl-2,5-dioxo-3-pyrrolidinyl)-L-cysteinylglycine ***(4.19)***

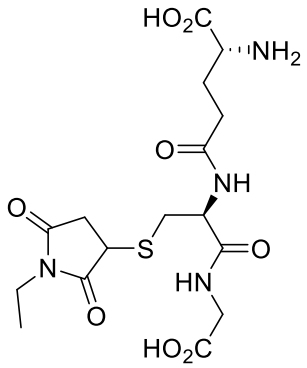

(**4.19**)

Glutathione **3.23** (419 mg, 1.60 mmol, 2 equiv.) was dissolved in a solution of aqueous sodium phosphate buffer (100 mM, pH 7.5, 8 mL). N-ethylmaleimide **2.4** (0.1 g, 0.8 mmol) was dissolved in THF (2 mL), added gradually to glutathione aqueous solution and held overnight at room temperature. The reaction was subsequently concentrated down under reduced pressure and purified by C-18 chromatography (100% H_2O to 20% MeCN/H_2O) to give the product **4.19** as a sticky solid (0.23 mg, 66%). ^{1}H NMR (500 MHz, D_2O): δ 4.58 (dd, *J* = 8.5, 5.0 Hz, 1H, SCH$_2$C<u>H</u>NH), 3.98 – 3.95 (m, 1H, CH$_2$C<u>H</u>NH$_2$), 3.88 (s, 2H, NHC<u>H$_2$</u>COOH), 3.73 (t, *J* = 6.5 Hz, 1H, S<u>CH</u>CH$_2$CO), 3.46 (q, *J* = 7.5 Hz, 2H, NH<u>CH$_2$</u>CH$_3$), 3.29 – 3.05 (m, 2H, SCH<u>CH$_2$</u>CO), 2.94 (dd, *J* = 14.5,

5.5 Hz, 1H, S$\underline{CH_2}$CHNH), 2.64 – 2.57 (m, 1H, SC$\underline{H_2}$CHNH), 2.52-2.41 (m, 2H, $CH_2C\underline{H_2}CO$), 2.09 (q, *J* = 7.5 Hz, 2H, $C\underline{H_2}CH_2CO$), 1.04 (t, *J* = 7.5 Hz, 3H, $CH_2C\underline{H_3}$). ^{13}C NMR (126 MHz, D_2O): δ 179.39, 178.23, 174.78, 173.68, 173.59, 172.15, 53.79, 52.77, 41.65, 39.94, 35.79, 34.29, 32.49, 31.19, 26.02, 11.74. Expected for $C_{16}H_{24}O_8SN_4Na$ ($M+Na^+$) = m/z 455.1207. Found: m/z 455.1204.

*Synthesis of 3,5-bis(2-chloroacetamido)benzoic acid (**4.42**)*

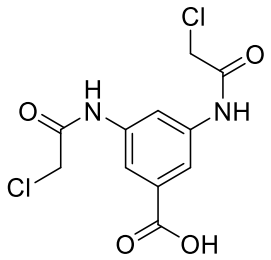

(**4.42**)

2-Chloroacetyl chloride **4.12** (1.62 g, 14.5 mmol, 2.2 equiv.) was added dropwise to a cooled solution of methyl 3,4-diaminobenzoate **4.54** (1.0 g, 6.6 mmol) in THF. The mixture was allowed to warm and stirred at room temperature for 2 h. The obtained precipitate was filtered, washed with water 5-6 times and then completely dried under high vacuum to give the acetamide **4.42** as a bale yellow solid (1.8 g, 90%). NMR spectra (^1H and ^{13}C) were consistent with those previously reported.[286] ^1H NMR (CD_3COCD_3, 400 MHz): δ 9.64 (s, 2H, NH), 8.24 (d, *J* = 78.3 Hz, 3H, Ar), 4.30 (s, 4H, CH_2). ^{13}C NMR (CD_3COCD_3, 101 MHz) δ 166.91, 140.07, 132.58, 117.11, 115.48, 44.07. ESI-HRMS: Expected for $C_{11}H_9Cl_2N_2O_4$ ($M-H^+$) = m/z 302.9939. Found: m/z 302.9956.

*Synthesis of 2,5-dioxopyrrolidin-1-yl 3,5-bis(2-chloroacetamido)benzoate (**4.43**)*

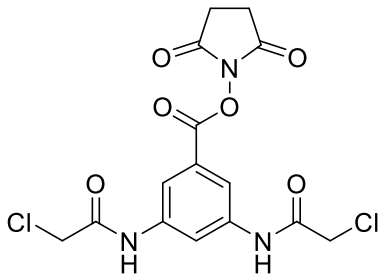

(**4.43**)

A solution of EDC.HCl (0.63 g, 3.3 mmol, 1.1 equiv.) in DMF (5 mL) was added to a stirred solution of acid **4.42** (1 g, 3 mmol) and N-hydroxysuccinimide (0.38 g, 3.3 mmol, 1.1 equiv.) in THF at room temperature. The reaction was then stirred at room temperature for 2 h before being concentrated under reduced pressure. The obtained residue was dissolved in EtOAc and washed with water, dried over $MgSO_4$ and the solvent was evaporated under reduced pressure giving a foamy solid. The crude was further purified by precipitation (EtOAc/petroleum ether) to give acetamide the **4.43** a yellow solid (0.75 g, 57%). ^{1}H NMR (CD_3COCD_3, 400 MHz,): δ 9.78 (s, 2H, NH), 8.34 (d, *J* = 64.1 Hz, 3H, Ar), 4.32 (s, 4H, 2 x ClC<u>H</u>$_2$CO), 2.99 (s, 4H, COC<u>H</u>2C<u>H</u>2CO). ^{13}C NMR (CD_3COCD_3, 101 MHz): δ 170.86, 170.43, 170.37, 165.95, 162.44, 140.81, 127.32, 117.21, 117.15, 44.06, 26.40. ESI-HRMS: Expected for $C_{15}H_{13}Cl_2N_3O_6Na$ ($M+Na^+$) = m/z 424.0074. Found: m/z 424.0106.

*2-(2-(2-(2-azidoethoxy)ethoxy)ethoxy)ethan-1-amine (**4.46**)*

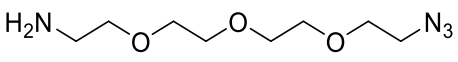

(**4.46**)

A solution of Ph_3P (0.54 g, 2.1 mol, 1 equiv.) in ether (5 mL) was added dropwise to aqueous HCl (5%, 5 mL) solution of tri-PEG azide **2.11** (0.50 g, 2.1 mmol), the mixture was left stirring for 24 h. Then, the ether was removed under reduced pressure, and the aqueous layer was extracted with DCM until Ph_3P oxide was not detected in the aqueous layer. The aqueous layer was adjusted to pH = 12, and azide-linked amine was extracted

from the aqueous layer with DCM. The combined DCM solution was evaporated under reduced pressure to give the azide-linked amine **4.46** as a light yellow liquid (0.25 g, 56%). NMR spectra (^{1}H and ^{13}C) were consistent with those previously reported.[287] ^{1}H NMR ($CDCl_3$, 400 MHz): δ 3.65 – 3.53 (m, 11H), 3.44 (td, *J* = 5.2, 1.3 Hz, 2H), 3.41 – 3.22 (m, 3H), 2.79 (td, *J* = 5.3, 1.4 Hz, 2H). ^{13}C NMR ($CDCl_3$, 101 MHz): δ 73.41, 70.65, 70.60, 70.58, 70.23, 69.95, 50.63, 41.75. ESI-HRMS: Expected for $C_8H_{19}N_4O_3$ ($M+H^+$) = m/z 219.1452. Found: m/z 219.1464. The followed procedure to synthesise **4.46** was done according to previously mentioned method by Lalit *et al.*[285]

*N,N'-(4-((2-(2-(2-(2-azidoethoxy)ethoxy)ethoxy)ethyl)carbamoyl)-1,3-phenylene)bis(2-chloroacetamide) (**4.36**)*

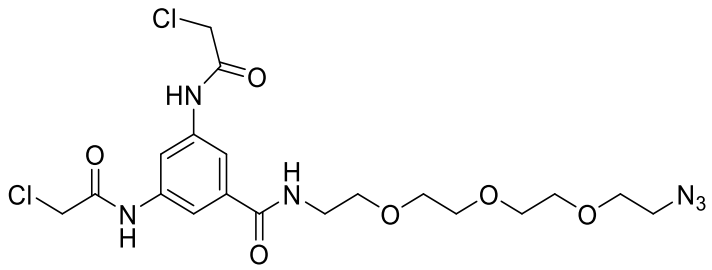

(**4.36**)

2-(2-azidoethoxy)ethan-1-amine **4.46** (0.34 g, 1.6 mmol, 1.3 equiv.) was added to an anhydrous solution of activated ester **4.43** (0.50 g, 1.2 mmol) in THF. The reaction mixture was then stirred at room temperature for 1 h before being concentrated under reduced pressure. The obtained residue was dissolved in DCM and washed with water, dried over $MgSO_4$ and the solvent was evaporated under reduced pressure. The crude was further purified by silica gel chromatography: (5% to 20% MeOH/DCM) to give azide-linked acetamide **4.36** as a white solid (0.39 g, 62%). ^{1}H NMR ($CDCl_3$, 400 MHz,): δ 8.78 (s, 2H, N<u>H</u>CH), 8.02 (s, 1H, Ar), 7.68 (s, 2H, Ar), 7.20 (d, *J* = 8.8 Hz, 1H, CON<u>H</u>CH2), 4.13 (s, 4H, 2 x ClC<u>H</u>$_2$CO), 3.75 – 3.41 (m, 14H), 3.27 (t, *J* = 5.0 Hz, 2H, CH_2<u>C</u>H_2N_3). ^{13}C NMR ($CDCl_3$, 101 MHz): δ 166.77, 164.69, 137.88, 135.96, 115.04, 114.31, 70.57, 70.51, 70.47, 70.24, 69.84, 69.55, 50.57, 42.96, 40.08. ESI-HRMS: Expected for $C_{15}H_{13}Cl_2N_3O_6Na$ ($M+Na^+$) = m/z 424.0074. Found: m/z 424.0106. HPLC: column: HiQ Sil HS (150 x 4.60 mm). Mobile phase: isocratic: (0.75

mL/min), 35% MeCN: 65% water. Detection at 280 nm. Retention time: 6.54 minutes, purity: 99.3%.

*N,N'-(4-((2-(2-(2-(2-azidoethoxy)ethoxy)ethoxy)ethyl)carbamoyl)-1,3-phenylene)bis(2-iodoacetamide) (**4.33**)*

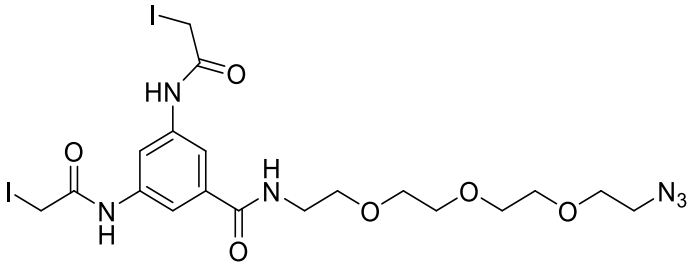

(**4.33**)

KI (1.0 g, 8.0 mmol, 4 equiv.) was added to a solution of N,N'-(4-((2-(2-(2-(2-azidoethoxy)ethoxy)ethoxy)ethyl)carbamoyl)-1,3-phenylene)bis(2-chloroacetamide) **4.36** (1.0 g, 2.0 mmol) in dry acetone (20 mL). The mixture was refluxed for 3 h. The obtained mixture was filtrated and the solvent was evaporated under reduced pressure. The crude was further purified by silica gel chromatography: (50 % to 70 % acetone/chloroform) to give azide-linked acetamide **4.33** as a yellow solid (1.19 g, 88%). ^{1}H NMR (CD_3COCD_3, 500 MHz): δ 9.98 (s, 2H, 2 x NHCH), 7.93 (d, *J* = 3.7 Hz, 3H, Ar), 7.69 (d, *J* = 5.3 Hz, 1H, CONHCH2), 3.95 (s, 4H, ICH_2CO), 3.60 – 3.11 (m, 16H). ^{13}C NMR (CD_3COCD_3, 126 MHz): δ 170.49, 167.51, 140.48, 137.24, 114.46, 113.41, 71.14, 70.58, 51.42, 40.42, 1.34. ESI-HRMS: Expected for $C_{19}H_{27}Cl_2N_6O_6$ ($M+H^+$) = m/z 505.1364. Found: m/z 505.141600. HPLC: column: HiQ Sil HS (150 x 4.60 mm). Mobile phase: isocratic: (0.75 mL/min), 35% MeCN: 65% water. Detection at 280 nm. Retention time: 10.31 minutes, purity: 97.8%.

*3,4-bis(2-chloroacetamido)benzoic acid (**4.44**)*

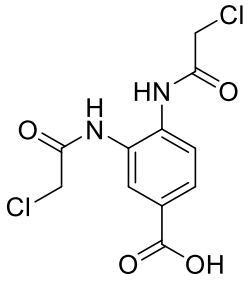

(**4.44**)

2-chloroacetyl chloride **4.4** (1.62 g, 14.5 mmol, 2.2 equiv.) was added dropwise to a cooled solution of methyl 3,4-diaminobenzoate **4.55** (1.0 g, 6.6 mmol) in THF. The mixture was allowed to warm and stirred at room temperature for 2 h. The obtained precipitate was filtered, washed with water 5-6 times and the obtained solid compound was completely dried under high vacuum to give the acetamide **4.44** as a white solid (1.8 g, 90%). ^{1}H NMR (DMF-d_7, 500 MHz): δ 10.09 (d, J = 20.4 Hz, 2H, NH), 8.30 (d, J = 1.9 Hz, 1H, Ar), 8.00 – 7.83 (m, 2H, Ar), 4.45 (d, J = 7.7 Hz, 4H, CH_2). ^{13}C NMR (126 MHz, DMF-d_7): δ 166.86, 166.02, 165.84, 135.31, 129.94, 128.03, 127.15, 127.00, 124.12, 43.64, 43.56. ESI-HRMS: Expected for $C_{11}H_{11}Cl_2N_2O_4Na$ ($M+Na^+$) = m/z 305.0090. Found: m/z 305.0092. HPLC: column: HiQ Sil HS (150 x 4.60 mm). Mobile phase: isocratic: (0.75 mL/min), 35% MeCN: 65% water. Detection at 280 nm. Retention time: 4.38 minutes, purity: 93%.

*2,5-dioxopyrrolidin-1-yl 3,4-bis(2-chloroacetamido)benzoate (**4.45**)*

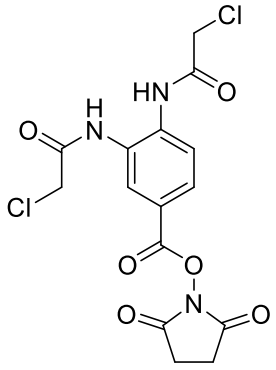

(**4.45**)

A solution of EDC.HCl (0.63 g, 3.3 mmol, 1.1 equiv.) in DMF (5 mL) was added to a stirred solution of acid **4.44** (1 g, 3 mmol) and N-hydroxysuccinimide (0.38 g, 3.3 mmol, 1.1 equiv.) in THF at room temperature. The reaction mixture was then stirred at room temperature for 2 h before being concentrated under reduced pressure. The obtained residue was dissolved in EtOAc and washed with water, dried over $MgSO_4$ and the solvent was evaporated under reduced pressure giving foamy solid. The crude was further purified by precipitation (EtOAc /petroleum ether) to give the acetamide **4.45** as a yellow solid (0.6 g, 45%). ^{1}H NMR (CD_3COCD_3, 400 MHz): δ 9.51 (d, *J* = 16.2 Hz, 2H, NH), 8.34 (s, 1H, Ar), 8.18 – 7.89 (m, 2H, Ar), 4.38 (s, 4H, 2 x ClC<u>H</u>$_2$CO), 2.98 (s, 4H, COC<u>H</u>2C<u>H</u>2CO). ^{13}C NMR (CD_3COCD_3, 100 MHz): δ 170.48, 166.85, 166.31, 161.95, 138.26, 130.66, 129.04, 128.65, 125.21, 122.83, 43.88, 26.39. ESI-HRMS: Expected for $C_{15}H_{13}Cl_2N_3O_6Na$ ($M+Na^+$) = m/z 424.0074. Found: m/z 424.0094.

*N,N'-(4-((2-(2-(2-(2-azidoethoxy)ethoxy)ethoxy)ethyl)carbamoyl)-1,2-phenylene)bis(2-chloroacetamide) (**4.37**)*

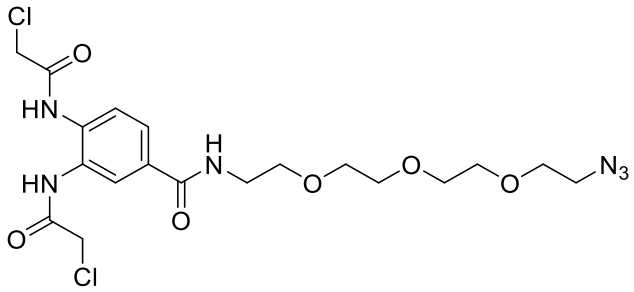

(**4.37**)

2-(2-azidoethoxy)ethan-1-amine **4.46** (0.34 g, 1.6 mmol, 1.3 equiv.) was added to an anhydrous solution of activated ester **4.45** (0.50 g, 1.2 mmol) in THF. The reaction mixture was then stirred at room temperature for 1 h before being concentrated under reduced pressure. The obtained residue was dissolved in DCM and washed with water, dried over $MgSO_4$ and the solvent was evaporated under reduced pressure. The crude was further purified by silica gel chromatography: (5% to 20% MeOH/DCM) to give the azide-linked acetamide **4.37** as a white solid (0.25 g, 40%). ^{1}H NMR ($CDCl_3$, 500 MHz): δ 9.05 (s, 2H, 2 x NHCH), 7.66 (s, 1H, Ar), 7.58 – 7.40 (m, 2H, Ar), 7.14 (t, *J* = 5.4 Hz, 1H, CONHCH2), 4.15 (d, *J* = 10.6 Hz, 4H, 2 x $ClCH_2CO$), 3.69 – 3.46 (m, 14H), 3.26 (t, *J* = 5.0 Hz, 2H, $CH_2CH_2N_3$). ^{13}C NMR ($CDCl_3$, 126 MHz): δ 166.29, 166.09, 165.49, 132.96, 132.74, 129.15, 125.57, 125.10, 124.86, 70.63, 70.60, 70.51, 70.24, 69.94, 69.65, 50.63, 42.91, 42.68, 40.01. ESI-HRMS: Expected for $C_{19}H_{27}Cl_2N_6O_6$ ($M+H^+$) = m/z 505.1364. Found: m/z 505.1365. HPLC: column: HiQ Sil HS (150 x 4.60 mm). Mobile phase: isocratic: (0.75 mL/min), 35% MeCN: 65% water. Detection at 280 nm. Retention time: 6.76 minutes, purity: 99.8%.

*N,N'-(4-((2-(2-(2-(2-azidoethoxy)ethoxy)ethoxy)ethyl)carbamoyl)-1,2-phenylene)bis(2-iodoacetamide)(**4.35**)*

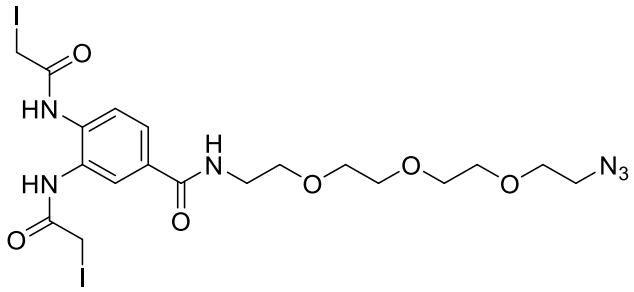

(**4.35**)

KI (1.0 g, 8.0 mmol, 4 equiv.) was added to a solution of N,N'-(4-((2-(2-(2-(2-azidoethoxy)ethoxy)ethoxy)ethyl)carbamoyl)-1,2-phenylene)bis(2-chloroacetamide) **4.37** (1.0 g, 2.0 mmol) in dry acetone (20 mL). The mixture was refluxed for 3 h. The obtained mixture was filtrated and the solvent was evaporated under reduced pressure. The crude was further purified by silica gel chromatography: (50 % to 70 % acetone/chloroform) to give the azide-linked acetamide **4.35** as a yellow solid (1 g, 73%). ^{1}H NMR ($CDCl_3$, 500 MHz): δ 9.30 (s, 1H, 2 x NHCH), 9.17 (s, 1H, NH), 7.61 (s, 1H, Ar), 7.41 (s, 1H, CONHCH2), 7.27 (s, 2H, Ar), 3.93 (d, *J* = 10.8 Hz, 4H, 2 x ICH_2CO), 3.75 – 3.48 (m, 14H), 3.36 (t, *J* = 5.0 Hz, 2H, $CH_2CH_2N_3$). ^{13}C NMR ($CDCl_3$, 126 MHz): δ 170.97, 168.13, 166.49, 129.71, 125.31, 125.01, 70.48, 70.31, 70.24, 69.73, 50.60, 40.09, -0.33, -0.53. ESI-HRMS: Expected for $C_{19}H_{27}I_2N_6O_6$ ($M+H^+$) = m/z 689.0076. Found: m/z 689.0108. HPLC: column: HiQ Sil HS (150 x 4.60 mm). Mobile phase: isocratic: (0.75 mL/min), 35% MeCN: 65% water. Detection at 280 nm. Retention time: 9.10 minutes, purity: 96.2%.

*N,N'-(4-((2-(2-(2-(2-azidoethoxy)ethoxy)ethoxy)ethyl)carbamoyl)-1,2-phenylene)bis(2-bromoacetamide)(**4.34**)*

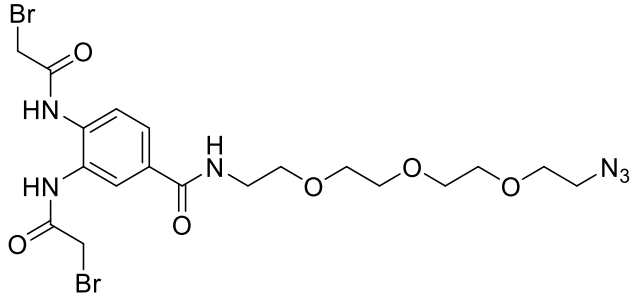

(**4.34**)

KBr (1.4 g, 12 mmol, 6 equiv.) was added to a solution of N,N'-(4-((2-(2-(2-(2-azidoethoxy)ethoxy)ethoxy)ethyl)carbamoyl)-1,2-phenylene)bis(2-chloroacetamide) **4.37** (1.0 g, 2.0 mmol) in dry acetone (20 mL). The mixture was refluxed for 4 days. The obtained mixture was filtrated and the solvent was evaporated under reduced pressure. The crude was further purified by silica gel chromatography: (50 % to 70 % acetone/chloroform) to give the azide-linked acetamide **4.34** as a white solid (0.5 g, 43%). ^{1}H NMR ($CDCl_3$, 500 MHz,): δ 9.02 (s, 1H, NHCH), 8.96 (s, 1H, NHCH), 7.79 (d, *J* = 2.0 Hz, 1H, Ar), 7.70 – 7.60 (m, 2H, Ar), 7.15 (s, 1H, CONHCH2), 4.09 (d, *J* = 12.2 Hz, 4H, $BrCH_2CO$), 3.78 – 3.50 (m, 14H), 3.37 (t, *J* = 5.0 Hz, 2H, $CHCH_2N_3$). ^{13}C NMR ($CDCl_3$,126 MHz): δ 166.31, 165.79, 165.13, 133.28, 132.55, 132.28, 125.68, 125.14, 124.79, 70.64, 70.62, 70.52, 70.26, 69.96, 69.63, 50.65, 40.10, 29.71, 29.09, 28.71. ESI-HRMS: Expected for $C_{19}H_{27}Br_2N_6O_6$ ($M+H^+$) = m/z 593.0353. Found: m/z 593.0344. HPLC: column: HiQ Sil HS (150 x 4.60 mm). Mobile phase: isocratic: (0.75 mL/min), 35% MeCN: 65% water. Detection at 280 nm. Retention time: 7.62 minutes, purity: 99.1%.

*N,N'-(5-((2-(2-(2-(2-azidoethoxy)ethoxy)ethoxy)ethyl)carbamoyl)-1,3-phenylene)bis(2-bromoacetamide) (**4.32**)*

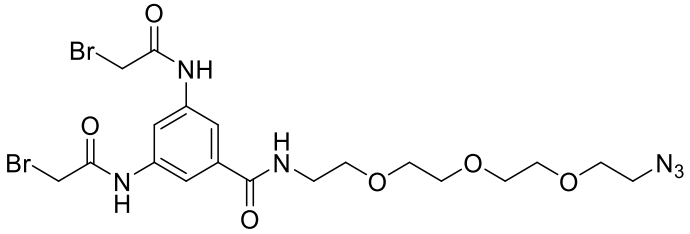

(**4.32**)

KBr (1.4 g, 12 mmol, 6 equiv.) was added to a solution of N,N'-(4-((2-(2-(2-(2-azidoethoxy)ethoxy)ethoxy)ethyl)carbamoyl)-1,3-phenylene)bis(2-chloroacetamide) **4.36** (1.0 g, 2.0 mmol) in dry acetone (20 mL). The mixture was refluxed for 4 days. The obtained mixture was filtrated and the solvent was evaporated under reduced pressure. The crude was further purified by silica gel chromatography: (50 % to 70 % acetone/chloroform) to give the azide-linked acetamide **4.32** as a yellow solid (0.6 g, 51%). ^{1}H NMR ($CDCl_3$, 500 MHz,): δ 8.79 (s, 2H, 2 x NHCH), 7.96 (s, 1H, Ar), 7.67 (s, 2H, Ar), 7.10 (s, 1H, NHCH), 3.95 (s, 4H, $BrCH_2CO$), 3.84 – 3.44 (m, 14H), 3.27 (t, *J* = 5.0 Hz, 2H, $CHCH_2N_3$). ^{13}C NMR ($CDCl_3$,126 MHz): δ 167.04, 164.62, 138.22, 135.84, 114.87, 114.14, 70.67, 70.59, 70.55, 70.36, 69.94, 69.59, 50.64, 40.24, 29.42. ESI-HRMS: Expected for $C_{19}H_{27}Br_2N_6O_6$ ($M+H^+$) = m/z 593.0353. Found: m/z 593.0344. HPLC: column: HiQ Sil HS (150 x 4.60 mm). Mobile phase: isocratic: (0.75 mL/min), 40% MeCN: 60% water. Detection at 280 nm. Retention time: 6.52 minutes, purity: 99.4%.

8.5.2 Evaluation of the aqueous stability of bis-haloacetamides using ^{1}H NMR (solvent suppression method)

Bis-haloacetamide (1 mg/mL) stability was determined in 100 mM phosphate buffer at pH 7.5 containing30% deuterated acetone-d_6 or DMF-d_7 using the general ^{1}H-NMR solvent suppression method (see Section 8.4.2.1). ^{1}H-NMR spectra were acquired at zero time (within 3 minutes of addition of aqueous buffer), 24 h, 48 h and 96 h.

Percentage remaining of bis-haloacetamide derivative was determined by following the change in the integration of the α-methylene protons ($XC\underline{H_2}CONH$) over time.

For bis-chloroacetamide derivatives, the change in the integration of α-methylene protons at δ 4.32 ppm ($ClC\underline{H_2}CONH$) was followed over time. For bis-bromoacetamide derivatives, the change in the integration of integration of α-methylene protons at δ 4.17 ppm ($BrC\underline{H_2}CONH$) was followed over time and for iodo-acetamide derivatives integration of α-methylene protons at δ 3.85 ppm ($IC\underline{H_2}CONH$) was followed over time (see appendix 10.5).

8.5.3 Determination of bis-haloacetamides reactivity with glutathione of using ^{1}H NMR (solvent suppression method)

For determination of rates of reaction of bis-haloacetamides with glutathione, each bis-haloacetamide reagent (1 mg) was incubated at room temperature with glutathione (2.2 or 6 equiv.) in 100 mM potassium phosphate buffer, pH 7.5 containing 10% DMF-d_7 or acetone-d_6. A stock solution of each bis-haloacetamide (10 mg/mL) was prepared in deuterated solvent. 100 µL of stock acetamide solution was added to 900 µL of glutathione solution in aqueous phosphate buffer just before analysis by ^{1}H NMR (less than 3 min after bis-haloacetamide reagent was dosed into buffer). Spectra were acquired at specific time points using ^{1}H NMR the general solvent suppression method (see Section 8.4.21).

The reaction rates were calculated based on the disappearance of the signal feom acetamide protons ($XC\underline{H_2}CONH$) and appearance of a peak at δ 3.43 ppm corresponding to the acetamide-glutathione adduct. The percentage remaining of each linker was determined using the ratio of integral of the acetamide peak to the sum of integrals of acetamide signal and the acetamide-glutathione adduct signal at 3.8 ppm (Equation 8.2).

$$\%\ \boldsymbol{of\ remaining\ of\ bishaloacetmide} = \frac{I_a}{(I_a + I_{ag})} * \mathbf{100} \qquad \textbf{(Equation 8.2)}$$

Where;

I_a= Integration of the α-methylene protons ($XC\underline{H_2}CONH$).
I_{ag}= Integration of the acetamide-glutathione adduct signal at δ 3.8 ppm which corresponds to (2 x $CH_2SC\underline{H_2}CONH$) protons.

8.5.4 Determination of the aqueous stability of glutathione conjugates (4.17-4.19) using HPLC

Each glutathione conjugate (1 mg) was dissolved in phosphate buffer (100 M, pH 7) with or without DTT (50 mM), samples were evaluated weekly over 4 weeks. Peak areas were acquired at zero time and percentage remaining was calculated by comparison with peak area obtained at zero time.

The following HPLC method was used to evaluate the stability of each glutathione conjugate: A mobile phase consisting of water: acetonitrile (90:10, v/v) contain 0.1 % TFA (pH 1.98) was passed through a reversed column (HiQ sil C18 HS) with particle size of 4.4 µm and dimensions of (150 x 4.60 mm). The flow rate was 0.7 mL/minutes for glutathione-Mal conjugate (**4.19**) and 1 mL/min for bis-glutathione conjugates (**4.17** and **4.18**) with injection volume of 5 µL. Absorption was measured at 214 nm wavelength.

The retention times for glutathione-Mal conjugate (**4.19**), 3,5-bis-glutathione conjugate (**4.17**) and 3,4-bis-glutathione conjugate (**4.18**) were approximately 9.60 and 10.85, 36.93, and 14.25 minutes, respectively.

Linearity of the methods used was determined by calibration of five concentrations of each analyte (0.1 mg/mL to 1 mg/mL). Peak areas of the calibration standards were plotted in the Y-axis against the nominal standard concentration, and the linearity of the plotted curve was evaluated through the value of the correlation coefficient (R^2) which was greater than 0.98 for all the analytes **4.17**-**4.19**.

8.6 Chapter 5 Experimental

8.6.1 TCEP quantification using 5,5'-Dithiobis(2-nitrobenzoic acid) (DNTP) reagent

In order to quantify TCEP, DNTP reagent was used as described by Han & Han in 1994.[124] Briefly, TCEP stiochiometrically reduces DNTP forming two equivalent of 2-nitro-5-thio-benzoic acid. The latter has a molar extension coefficient of 14,150 M^{-1} cm^{-1} at 412 nm. Stock solution of TCEP (20 mM) was prepared in water which was diluted 40 times in water to get 0.5 mM working solution. 10 µL was taking of the working solution and added to 990 µL of DNTP solution (100 µM). The absorbance was measured at 412 nm and found 0.1413 + 0.00153 (n=3). With back calculation of the concentration of 2-nitro-5-thio-benzoic acid, TCEP concentration was found 4.98 µM.

8.6.2 Procedure for TCEP reduction of Tmab

Tmab was buffer exchanged to conjugation 100 mM Tris.HCl buffer (pH 7.5) containing 150 mM NaCl and 5mM EDTA and diluted to (5 mg/mL, 0.033 µmol) using Amicon® Ultra-0.5 mL (3 kDa) centrifugal filters. Stock solution of TCEP.HCl was prepared in the same buffer (4 mg/mL, 0.042 mmol, 14 mM). Calculated volume of TCEP solution was added to Tmab solution and incubated at room temperature for 2 h unless other conditions are stated.

8.6.3 Tmab bioconjugates 1-4

The following acronyms are used in this project to describe antibody fragments: Heavy chain (HC), light chain (LC), heavy-heavy (HC-HC), light-light (LC-LC), heavy-light (HC-LC, half antibody).

The following table 8.2 summarises the prepared bioconjugates of Tmab in this project.

Table 8.2. Tmab-bioconjugates prepared in this project.

Tmab bioconjugate	Description	Acronyms
Tmab bioconjugate 1 (**5.1**) 	Fully rebridging inter HC-LC and intra HC-HC disulfide bonds with by the same linker	$Tmab_{bis\text{-}[(o\text{-}\mathbf{HL},o\text{-}\mathbf{HH}intra)\text{-}OMe]}$ 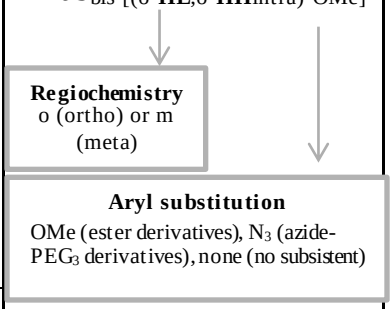
Tmab bioconjugate 2 (**5.2**) 	Rebridging of both intra HC-LC disulfide bonds to produce partially cross-linked Tmab by the same linker	$Tmab_{bis\text{-}(o\text{-}\mathbf{HL}\text{-}OMe)}$
Tmab bioconjugate 3 (**5.3**) 	Rebridging of one inter HC-LC disulfide bond	$Tmab_{o\text{-}\mathbf{HL}\text{-}OMe}$
Tmab bioconjugate 4 (**5.4**) 	Rebridging inter HC-LC and intra HC-HC disulfide bonds with different linkers to produce bifunctional mAb.	$Tmab_{bis(o\text{-}\mathbf{HL}\text{-}OMe,m\text{-}\mathbf{HH}intra\text{-}N_3)}$

8.6.3.1 Construction of Tmab bioconjugate 1 (5.1) with methyl 3,4-bis(2-bromoacetamido) benzoate linker (4.23)

Tmab was buffer exchanged to conjugation Tris.HCl buffer (pH 7.5) and diluted to (5.0 mg/mL, 0.034 µmol, 1 ml) using Amicon® Ultra-0.5 mL (10 kDa) centrifugal filters. A stock solution of TCEP (4.0 mg/mL, 0.042 mmol, 14 mM) was prepared in the same conjugation buffer. Tmab was reduced by incubation with TCEP (5 equiv. relative to Tmab) for 2 h at room temperature. The reduced protein was aliquoted into 100 µL aliquots for each reaction.

A stock solution of methyl 3,4-bis(2-bromoacetamido) benzoate (**4.23**) was prepared in DMF at final concentration (1.0 mg/mL, 2.5 µmol, 2.5 mM). 5 equiv. of methyl 3,4-bis(2-bromoacetamido) benzoate **4.23** (7 µL, 5 equiv. relative to Tmab aliquot) was added to reduced protein and held at room temperature overnight.

For other linkers, just refer to this method.

8.6.3.2 Construction of Tmab bioconjugate 2 (5.2) using a portion-wise reduction method

Tmab was buffer exchanged to conjugation Tris.HCl buffer (pH 7.5) and diluted to (5.0 mg/mL, 0.034 µmol, 1 ml) using Amicon® Ultra-0.5 mL (10 kDa) centrifugal filters. Tmab was reduced by incubation with TCEP (1 equiv. relative to Tmab) for 2 h at 4°C. The reduced protein was aliquoted into 100 µL samples for each reaction.

A stock solution of methyl 3,4-bis(2-bromoacetamido) benzoate (**4.23**) was prepared in DMF at final concentration (1.0 mg/mL, 2.5 µmol, 2.5 mM). Working solution of **4.23** (0.2 mg/mL) was prepared by serial dilution with DMF. 1 equiv. of working solution of methyl 3,4-bis(2-bromoacetamido) benzoate **4.23** (7 µL, 1 equiv. relative to Tmab aliquot) was added to the reduced protein and held at room temperature overnight. Another reduction step (1 equiv.) for 2 h at 4°C was followed by incubation with the same linker (1 equiv.) overnight.

For other linkers, just refer to this method.

8.6.3.3 Construction of Tmab bioconjugate 2 (5.2) using Direct *in-situ* method

Tmab was buffer exchanged to conjugation Tris.HCl buffer (pH 7.5) and diluted to (5.0 mg/mL, 0.034 µmol, 1 ml) using Amicon® Ultra-0.5 mL (10 kDa) centrifugal filters. Tmab was reduced by incubation with TCEP (2.2 equiv. relative to Tmab) for 2 h at 4°C. The reduced protein was aliquoted into 100 µL samples for each reaction.

A stock solution of methyl 3,4-bis(2-bromoacetamido) benzoate (**4.23**) was prepared in DMF at final concentration (1.0 mg/mL, 2.5 µmol, 2.5 mM). Working solution of **4.23** (0.44 mg/mL) was prepared by serial dilution with DMF. 2.2 equiv. of working solution of methyl 3,4-bis(2-bromoacetamido) benzoate **4.23** (7 µL, 2.2 equiv. relative to Tmab aliquot) was added to the reduced protein and held at room temperature overnight.

For other linkers, just refer to this method.

8.6.3.4 Construction Tmab bioconjugate 3 (5.3)

Tmab was buffer exchanged to conjugation Tris.HCl buffer (pH 7.5) and diluted to (5.0 mg/mL, 0.034 µmol, 1 ml). Tmab was reduced by incubation with TCEP **2.2** (1.1 equiv. relative to Tmab) for 2 h at 4°C. The reduced protein was aliquoted into 100 µL samples for each reaction.

A stock solution of methyl 3,4-bis(2-bromoacetamido) benzoate (**4.23**) was prepared in DMF at final concentration (1.0 mg/mL, 2.5 µmol, 2.5 mM). Working solution of **4.23** (0.2 mg/mL) was prepared by serial dilution with DMF. 1.1 equiv. of working solution of methyl 3,4-bis(2-bromoacetamido) benzoate **4.23** (7.7 µL, 1.1 equiv. relative to Tmab aliquot) was added to the reduced protein and held at room temperature overnight.

For other linkers, just refer to this method.

8.6.3.5 Construction of Tmab bioconjugate 4 (5.4)

Tmab was buffer exchanged to conjugation Tris.HCl buffer (pH 7.5) and diluted to (5.0 mg/mL, 0.034 µmol, 1 ml). Tmab was reduced by incubation with TCEP (2.2 equiv. relative to Tmab) for 2 h at 4°C.

A stock solution of methyl 3,4-bis(2-bromoacetamido) benzoate (**4.23**) was prepared in DMF at final concentration (1.0 mg/mL, 2.5 µmol, 2.5 mM). Working solution of **4.23** (0.44 mg/mL) was prepared by serial dilution with DMF. 2.2 equiv. of working solution of methyl 3,4-bis(2-bromoacetamido) benzoate **4.23** (7 µL, 2.2 equiv. relative to Tmab aliquot) was added to the reduced protein and held at room temperature overnight.

Mono-functionalised Tmab ($Tmab_{bis\text{-}(o\text{-}\mathbf{HL}\text{-}OMe)}$) was buffer exchanged to the same conjugation buffer. Second reduction step using 2.2 equiv. of TCEP for 2 h at 4°C was followed. A stock solution of **4.33** was prepared in DMF at final concentration (1.0 mg/mL, 1.5 µmol, 1.5 mM). 4 equiv. of **4.33** (10 µL, 2.2 equiv. relative to Tmab aliquot) was added to the reduced protein and held at room temperature overnight.

8.6.4 Rmab bioconjugate 1

$Rmab_{bis\text{-}[(o\text{-}\mathbf{HL},o\text{-}\mathbf{HH}intra)\text{-}OMe]}$ was synthesised using the same previously described method to construct Tmab bioconjugate 1 (**5.1**).

8.6.5 CD spectrum analysis of $Rmab_{bis\text{-}[(o\text{-}HL,o\text{-}HHintra)\text{-}OMe]}$

The secondary structure compositions of Rmab was analysed by circular dichroism (CD) using a Chirascan spectrometer (Applied Photophysics). For CD measurement, Rmab (0.1 mg/mL) was buffer exchanged to phosphate buffer (10 mM, pH 7.4). The CD experiments were carried out using a using a Quartz Suprasil Cuvette (Hellma Analytics, Essex, UK) of pathlength 0.1 cm. The same buffer was used to blank before CD spectrum acquiring. CD spectrum measured far-UV region (205–260 nm) over a temperature range of 25–90°C in steps of +1 °C/minutes. CD data were averaged, smoothed, and the buffer signal was subtracted. Finally, the measurements were converted to mean residual ellipticity (θ). The averaged CD spectra of Rmab were deconvoluted using CDNN software. CDNN software compares the acquired CD spectrum with a range of reference spectra of known protein structure, to get estimation of the secondary structure composition of the required protein.

8.6.6 DLS analysis of Rmab bioconjugate 1 ($Rmab_{bis\text{-}[(o\text{-}\mathbf{HL},o\text{-}\mathbf{HH}intra)\text{-}OMe]}$)

Before commencing the DLS analysis, samples were centrifuged at 20,000 g for 10 minutes to remove any aggregates. Then, around 150 µL of 2 mg/mL was exposed to laser light in optical microcuvette (ZEN0040, Malvern) using Zetasizer NanoSeries Nano S. (Malvern).

8.6.7 Stability of Rmab bioconjugate 1 ($Rmab_{bis\text{-}[(o\text{-}\mathbf{HL},o\text{-}\mathbf{HH}intra)\text{-}OMe]}$) in plasma mimicking condition and at 4°C for 2 months

$Rmab_{bis\text{-}[(o\text{-}\mathbf{HL},o\text{-}\mathbf{HH}intra)\text{-}OMe]}$ (5.0 mg/mL, 0.035 µmol) was buffer exchanged into a fresh buffer (pH 7.4) by spinning into fresh buffer using Amicon® Ultra-0.5 mL (10 kDa) centrifugal filters several times then, human serum albumin (HSA) (final concentration 600 µM) and glutathione (GSH) (final concentration 20 µM) were added. The solution was incubated at 37°C for 7 days. The reaction was monitored by SDS-PAGE (10 %).

$Rmab_{bis\text{-}[(o\text{-}\mathbf{HL},o\text{-}\mathbf{HH}intra)\text{-}OMe]}$ (5.0 mg/mL, 0.035 µmol) was buffer exchanged into a fresh buffer (pH 7.4) by spinning into fresh buffer using Amicon® Ultra-0.5 mL (10 kDa) centrifugal filters several times then, the reaction was held at 4°C and samples were monitored by SDS-PAGE (10 %).

8.7 Chapter 6 Experimental

8.7.1 Chemical synthesis

*N,N',N'',N'''-((5,8,11-trioxa-2,14-diazapentadecanedioyl)bis(benzene-4,1,2-triyl))tetrakis(2-chloroacetamide) (**6.4**)*

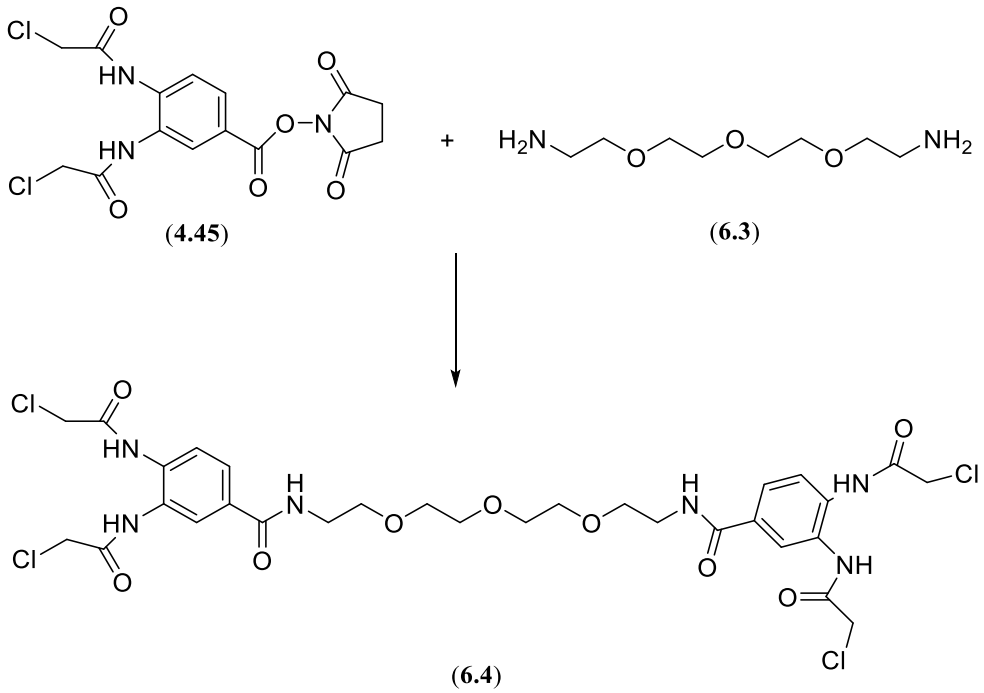

1,11-Diamino-3,6,9-trioxaundecane **6.3** (100 mg, 0.520 mmol) was added to an anhydrous solution of activated ester **4.45** (0.52 g, 1.3 mmol, 2.5 equiv.) in THF. The reaction mixture was then stirred at room temperature for 1 h before being concentrated under reduced pressure. The crude was purified by silica gel chromatography: (5 % to 20 % MeOH/DCM) to give the acetamide **6.4** as a white solid (300 mg, 75%). ^{1}H NMR (DMSO-d_6, 500 MHz,): δ 9.80 (d, *J* = 24.1 Hz, 4H, N<u>H</u>CH), 8.54 (s, 2H, CON<u>H</u>CH2), 7.98 (s, 2H, Ar), 7.73 (s, 4H, Ar), 4.35 (d, *J* = 9.0 Hz, 8H, 2 x ClC<u>H</u>$_2$CO), 3.66 – 3.42 (m, 12H), 3.40 (q, *J* = 5.9 Hz, 4H).^{13}C NMR (DMSO-d_6, 126 MHz): δ 172.72, 165.39, 165.19, 133.26, 131.12, 129.15, 124.99, 124.60, 123.81, 69.68, 69.55, 68.82, 43.28, 43.21. ESI-HRMS: Expected for $C_{30}H_{36}Cl_4N_6O_9Na$ ($M+Na^+$) = m/z 787.1190. Found: m/z 787.1231. HPLC: column: HiQ Sil HS (150 x 4.60 mm). Mobile phase: isocratic: (0.75 mL/minutes), 35% MeCN: 65% water. Detection at 280 nm. Retention time: 6.18 minutes, purity: 96.7%.

N,N',N'',N'''-((5,8,11-trioxa-2,14-diazapentadecanedioyl)bis(benzene-4,1,2-triyl))tetrakis(2-iodoacetamide) ***(6.2)***

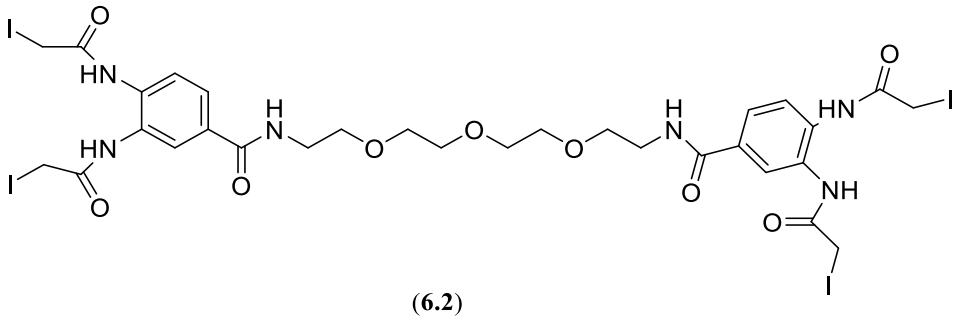

(**6.2**)

KI (435 mg, 2.62 mmol, 10 equiv.) was added to a solution of N,N',N'',N'''-((5,8,11-trioxa-2,14-diazapentadecanedioyl)bis(benzene-4,1,2-triyl))tetrakis(2-chloroacetamide) **6.4** (200 mg, 0.262 mmol) in mixture of dry acetone and DMF (400 mL). The mixture was refluxed for 3 h. The resultant mixture was filtrated and the solvent was evaporated under reduced pressure. The obtained solid was washed with water 5-6 times and completely dried under high vacuum to give the acetamide **6.2** as a white solid (200 mg, 67.6%). ^{1}H NMR (DMSO-d_6, 500 MHz,): δ 9.76 (d, *J* = 19.4 Hz, 4H, N<u>H</u>CH), 8.54 (t, *J* = 5.6 Hz, 2H, CON<u>H</u>CH2), 7.92 (s, 2H, Ar), 7.69 (d, *J* = 2.1 Hz, 4H, Ar), 3.91 (d, *J* = 10.9 Hz, 8H, 2 x ClC<u>H</u>$_2$CO), 3.66 – 3.42 (m, 12H), 3.40 (q, *J* = 5.9 Hz, 4H).^{13}C NMR (DMSO-d_6, 126 MHz): δ 165.72, 165.60, 163.84, 132.11, 129.38, 127.89, 123.16, 122.88, 121.94, 68.25, 68.13, 67.40, 0.07, -0.00. ESI-HRMS: Expected for $C_{30}H_{36}I_4N_6O_9Na_1$ ($M+Na^+$) = m/z 1154.8615. Found: m/z 1154.8667. HPLC: column: HiQ Sil HS (150 x 4.60 mm). Mobile phase: isocratic: (0.75 mL/minutes), 35% MeCN: 65% water. Detection at 280 nm. Retention time: 9.03 minutes, purity: 97%.

*N,N',N'',N'''-((5,8,11-trioxa-2,14-diazapentadecanedioyl)bis(benzene-4,1,2-triyl))tetrakis(2-bromoacetamide) (**6.1**)*

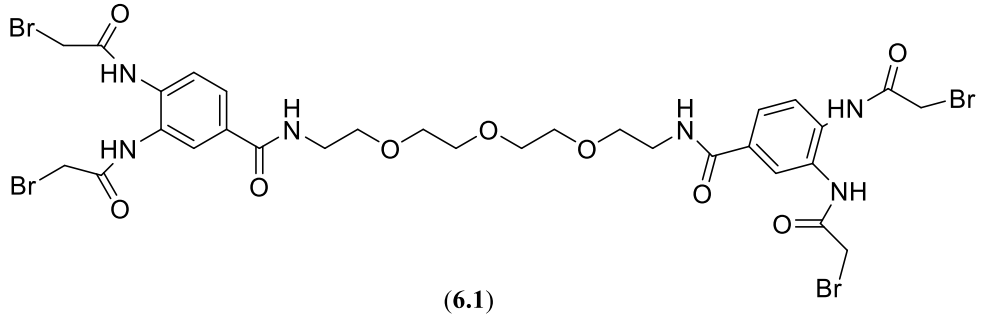

(**6.1**)

LiBr (450 mg, 5.23 mmol, 20 equiv.) was added to a solution of N,N',N'',N'''-((5,8,11-trioxa-2,14-diazapentadecanedioyl)bis(benzene-4,1,2-triyl))tetrakis(2-chloroacetamide) **6.4** (200 mg, 0.262 mmol) in mixture of dry TFF. The mixture was refluxed for 24 h. The resultant mixture was filtrated and the solvent was evaporated under reduced pressure. The obtained solid was washed with water 5-6 times and completely dried under high vacuum to give the acetamide **6.1** as a white solid (120 mg, 48.8 %). ^{1}H NMR (DMSO-d_6, 500 MHz,): δ 9.87 (d, *J* = 17.3 Hz, 4H, N<u>H</u>CH), 8.57 (d, *J* = 6.4 Hz, 2H, CON<u>H</u>CH2), 7.96 (s, 2H, Ar), 7.73 (s, 4H, Ar), 4.15 (d, *J* = 9.1 Hz, 8H, 2 x Cl<u>C</u>H_2CO), 3.52 (s, 12H), 3.44-3.38 (m, 4H).^{13}C NMR (DMSO-d_6, 126 MHz): δ 165.41, 165.20, 133.37, 131.06, 131.06, 124.83, 124.57, 123.64, 69.68, 69.55, 68.82, 30.18, 30.12. ESI-HRMS: Expected for $C_{30}H_{36}Br_4N_6O_9Na$ ($M+Na^+$) = m/z 962.9169. Found: m/z 962.9150. HPLC: column: HiQ Sil HS (150 x 4.60 mm). Mobile phase: isocratic: (0.75 mL/minutes), 35% MeCN: 65% water. Detection at 280 nm. Retention time: 6.63 minutes, purity: 97%.

*3,6,9,12,15,18,21-heptaoxatricosane-1,23-ditosylate (**6.9**)*

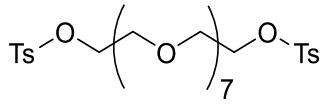

(**6.9**)

4-Toluenesulphonyl chloride **2.22** (1.33 g, 7.02 mmol, 2.6 equiv.) was added to a solution of anhydrous pyridine (0.51 g, 6.5 mmol, 2.4 equiv.) and 3,6,9,12,15,18,21-

heptaoxatricosane-1,23-ditol **6.8** (1.0 g, 2.7 mmol) in anhydrous DCM (10 mL) and the mixture left to stir under N_2 overnight at room temperature. The solution was then concentrated under reduced pressure and subject to standard work-up (EtOAc). The resultant residue was then purified by silica gel chromatography (40 to 80% EtOAc/petroleum ether) to give 3,6,9,12,15,18,21-heptaoxatricosane-1,23-ditosylate (**6.9**) as a colourless oil (1.1 g, 60%). NMR spectra (^{1}H and ^{13}C) were consistent with those previously reported.[288] ^{1}H NMR ($CDCl_3$, 400 MHz): δ 7.81 – 7.68 (m, 4H, Ar), 7.34 – 7.26 (m, 4H, Ar), 4.23 – 4.01 (m, 4H, 2x SO2OC$\underline{H}_2$), 3.70 – 3.48 (m, 28H), 2.39 (d, *J* = 1.5 Hz, 6H, CHCC$\underline{H}_3$). ^{13}C NMR ($CDCl_3$, 101 MHz): δ 144.74, 132.87, 129.77, 127.92, 70.67, 70.54, 70.49, 70.44, 69.20, 68.60, 21.60. ESI-HRMS: Expected for $C_{30}H_{47}O_{13}S_2$ ($M+H^+$) = m/z 679.2453. Found: m/z 679.2448.

*1,23-diazido-3,6,9,12,15,18,21-heptaoxatricosane (**6.10**)*

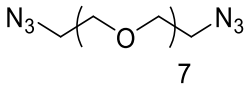

(**6.10**)

Sodium azide (2 g, 30 mmol, 10 equiv.) was added to a solution of the ditosylate **6.9** (2.0 g, 3.0 mmol) in DMF and the mixture allowed to stir at 80°C overnight. The mixture was then concentrated under reduced pressure to remove DMF and the product extracted using ethyl acetate (3 x 20 mL). The organic extract was then washed with saturated brine solution, dried over $MgSO_4$, concentrated to give diazide **6.10** as a colourless oil (1 g, 80.6 %). NMR spectra (^{1}H and ^{13}C) were consistent with those previously reported.[285] ^{1}H NMR ($CDCl_3$, 400 MHz): δ 3.66 – 3.54 (m, 28H), 3.36 – 3.28 (m, 4H, 2x N_3CH_2). ^{13}C NMR ($CDCl_3$, 101 MHz): δ ^{13}C NMR δ 70.62, 69.96, 50.60. ESI-HRMS: Expected for $C_{16}H_{33}O_7N_6$ ($M+H^+$) = m/z 421.2405. Found: m/z 421.2466. Synthesis procedure of **6.12** was carried out according to the reported procedure by Dreaden *et al.*[288]

*1,23-diamino-3,6,9,12,15,18,21-heptaoxatricosane (**6.6**)*

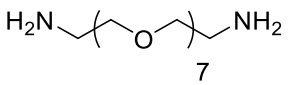

(**6.6**)

Triphenylphosphine (1.87 g, 7.14 mmol, 3 equiv.) was added portion-wise to a stirred solution of diazide **6.10** (1.0 g, 2.4 mmol) in dry THF. The reaction was stirred at room temperature overnight. Water (50 mL) was added and the reaction was left stirring at room temperature overnight. The THF was evaporated under reduced pressure and the reaction was filtrated and the filtrate was then washed with DCM (3 x 100 mL) to remove phosphine oxide. The filtrate was evaporated under reduced pressure to yield diamino-PEG (**6.6**) as yellow oil (0.50 g, 57 %). NMR spectra (^{1}H and ^{13}C) were consistent with those previously reported.[289] ^{1}H NMR ($CDCl_3$, 400 MHz,) δ: δ 3.58 (dd, *J* = 2.4, 1.1 Hz, 24H), 3.44 (t, *J* = 5.2 Hz, 4H, 2x $NH_2CH_2C\underline{H}_2O$), 2.80 (t, *J* = 5.2 Hz, 4H, 2x $NH_2C\underline{H}_2CH_2O$), 1.67 (s, 4H, 2x $N\underline{H}_2$). ^{13}C NMR ($CDCl_3$,101 MHz,) δ: δ 73.27, 70.48, 70.18, 41.68. ESI-HRMS: Expected for $C_{16}H_{37}O_7N_2$ ($M+H^+$) = m/z 369.2600. Found: m/z 369.2850. Synthesis procedure of **6.6** was carried out according to the reported procedure by Gu *et al.*[19]

*N,N',N'',N'''-((5,8,11,14,17,20,23-heptaoxa-2,26-diazaheptacosanedioyl)bis(benzene-4,1,2-triyl))tetrakis(2-chloroacetamide) (**6.7**)*

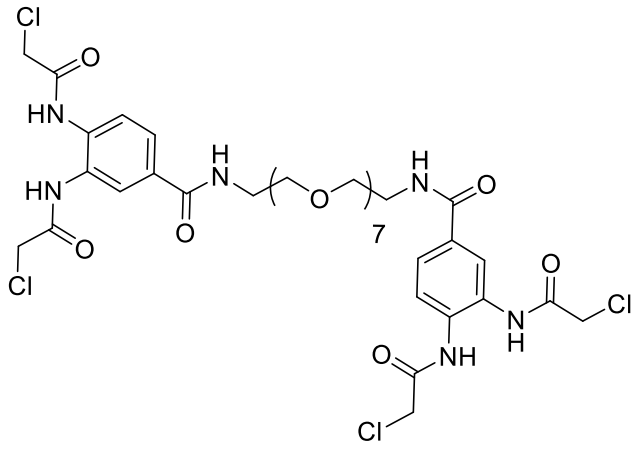

(**6.7**)

1,23-diamino-3,6,9,12,15,18,21-heptaoxatricosane **6.6** (150 mg, 0.407 mmol) was added to an anhydrous solution of activated ester **4.45** (409 mg, 1.02 mmol, 2.5 equiv.) in anhydrous THF. The reaction mixture was then stirred at room temperature for 2 h before being concentrated under reduced pressure. The crude was purified by silica gel chromatography: (5 % to 20 % MeOH/DCM) to give the acetamide **6.7** as a white solid (340 mg, 89%). ^{1}H NMR (DMSO-d_6, 500 MHz,): δ 9.81 (d, *J* = 25.2 Hz, 4H), 8.54 (t, *J* = 5.6 Hz, 2H), 7.98 (s, 2H), 7.73 (d, *J* = 1.4 Hz, 4H), 4.35 (d, *J* = 9.3 Hz, 8H), 3.64 – 3.45 (m, 28H), 3.41 (q, *J* = 5.9 Hz, 4H).^{13}C NMR (DMSO-d_6, 126 MHz): δ 172.72, 165.38, 165.20, 165.17, 133.26, 131.12, 129.13, 124.98, 124.59, 123.79, 69.71, 69.56, 68.83, 43.28, 43.21. ESI-HRMS: Expected for $C_{38}H_{53}Cl_4N_6O_{13}$ ($M+H^+$) = m/z 941.2419. Found: m/z 941.2451. HPLC: column: HiQ Sil HS (150 x 4.60 mm). Mobile phase: isocratic: (0.75 mL/min), 35% MeCN: 65% water. Detection at 280 nm. Retention time: 5.83 minutes, purity: 98%.

N,N',N'',N'''-((5,8,11,14,17,20,23-heptaoxa-2,26-diazaheptacosanedioyl)bis(benzene-4,1,2-triyl))tetrakis(2-Iodoacetamide) ***(6.5)***

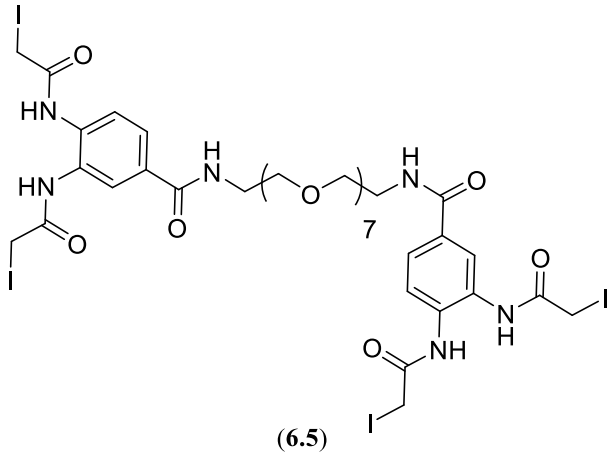

(**6.5**)

KI (176 mg, 1.06 mmol, 10 equiv.) was added to a solution of N,N',N'',N'''-((5,8,11,14,17,20,23-heptaoxa-2,26-diazaheptacosanedioyl)bis(benzene-4,1,2-triyl))tetrakis(2-chloroacetamide) **6.7** (100 mg, 0.106 mmol) in mixture of dry acetone (400 mL). The mixture was refluxed for 3 h. The resultant mixture was filtrated and the solvent was evaporated under reduced pressure. The crude was purified by silica gel chromatography: (50 % to 70 % Acetone/Chloroform) to give acetamide **6.5** as a white solid (130 mg, 93.5%). ^{1}H NMR (DMSO-d_6, 500 MHz,): δ 9.62 (d, *J* = 16.8 Hz, 4H), 8.31 (d, *J* = 4.9 Hz, 3H), 7.98 (s, 2H), 7.84 – 7.59 (m, 4H), 3.98 (d, *J* = 7.0 Hz, 8H), 3.75 – 3.30 (m, 32H). ^{13}C NMR (DMSO-d_6, 126 MHz): δ 167.18, 167.09, 165.31, 133.53, 130.78, 129.30, 124.57, 124.29, 123.34, 69.64, 68.87, 1.67, 1.59. ESI-HRMS: Expected for $C_{38}H_{52}I_4N_6O_{13}Na_1$ ($M+Na^+$) = m/z 1330.9669. Found: m/z 1330.9765. HPLC: column: HiQ Sil HS (150 x 4.60 mm). Mobile phase: isocratic: (0.75 mL/minu), 35% MeCN: 65% water. Detection at 280 nm. Retention time: 9.55 minutes, purity: 98%.

8.7.2 Expression of Sbi III/IV-2xCys

The expression procedure was done according to the general procedure provided in Section 8.2.3. The differences in expression of Sbi III/IV-2xCys are highlighted next.

Primary LB media (100 mL with final concentration of ampicillin 100 µg/mL) was inoculated with a single colony of SHuffle® T7 *E. coli* with transformed Sbi III/IV-2xCys construct (pET-15b) and held at 30°C with shaking at 180 rpm overnight. The overnight primary culture was then inoculated with 1-liter of LB medium containing ampicillin (100 µg/mL). The secondary culture was held at 30°C with shaking at 180 rpm until the OD_{600} value reached 0.7.

Then, the expression of Sbi III/IV-2xCys protein was induced by adding IPTG to final concentration of 1 mM in the culture. The culture held at 22°C with shaking at 180 rpm for overnight.

Cells from the secondary culture were harvested, suspended in HisA buffer contains protease inhibitor cocktail mini tablets (EDTA free, Roche) and lysed by sonication. Cells were kept cold during the sonication cycles (4 cycles with 10 minutes interval between each sonication to cool down cells) at 80% amplitude.

Then, the insoluble cell debris was removed by centrifugation and the supernatant was collected and purified through immobilized metal affinity chromatography using nickel column (1mL, HisTrap HP) attached to an AKTA purifier. The loaded column was washed with 15 column volumes of HisA buffer and the bound protein was eluted with a 0-100% gradient of HisB buffer.

Sbi III/IV-2xCys. containing fractions (F14-21) were collected and appraised by 15% SDS-PAGE analysis (Figure 8.4). Collected fractions were concentrated and finally buffer exchanged into conjugation buffer and stored at -20°C.

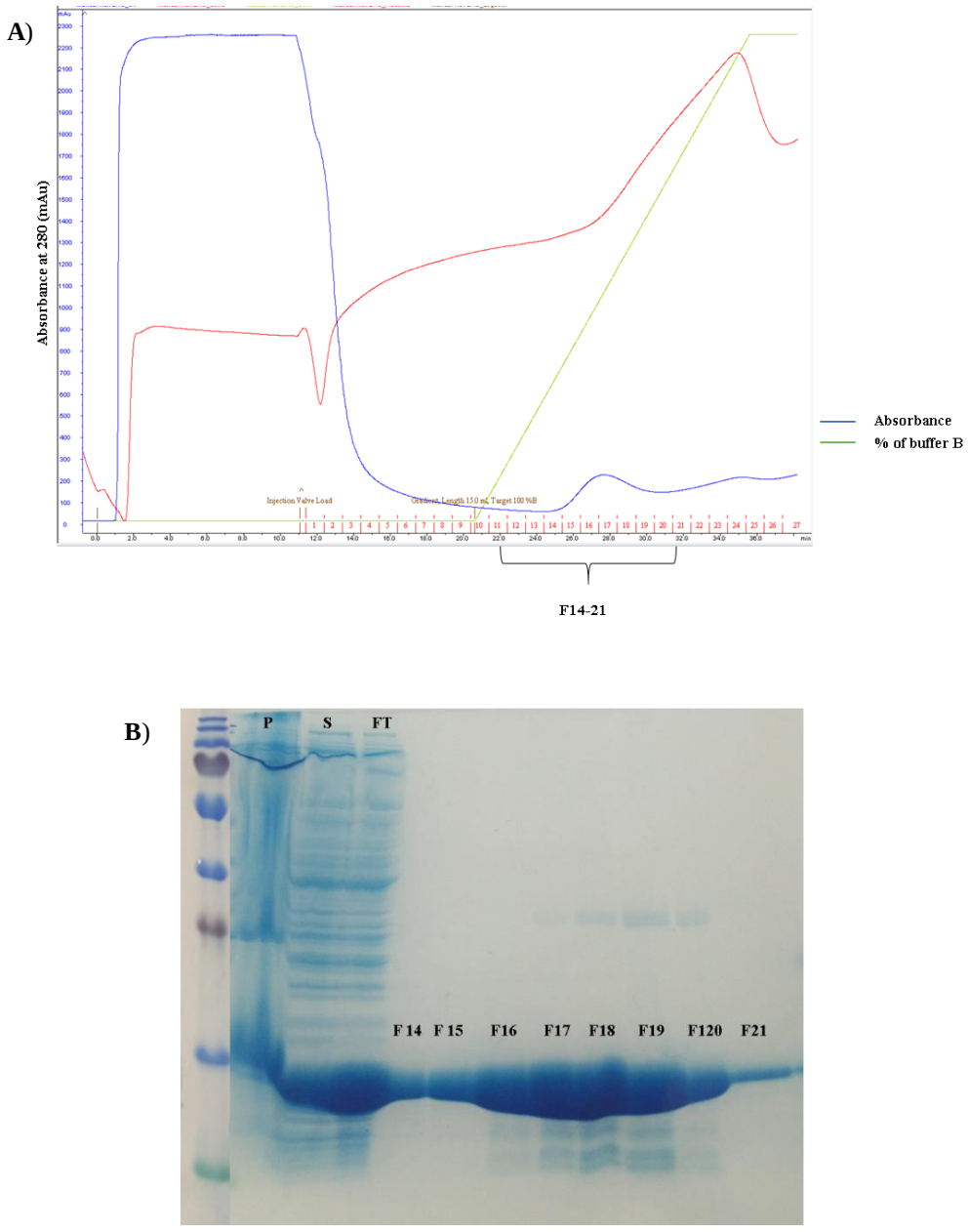

Figure 8.4. A) AKTA purification of the lysate using HisTrap column. **B**) SDS-PAGE gel 15%. P (Pellet), S (supernatant), FT (flow through).

The concentration of Sbi III/IV-2xCys was calculated by measuring the absorbance reading at 280 nm and found 5 mg/mL with total of 15 mg protein was obtained from 1-liter culture.

8.7.3 Construction of $Tmab_{o\text{-}HL}$-PEG_7-$Sbi_{o\text{-}bis\text{-}Cys}$ conjugate (6.11) with bis-o-diiodoacetamide $(PEG)_7$ 6.5

1- Sbi III/IV-2xCys was buffer exchanged to conjugation Tris.HCl buffer (pH 7.5) and diluted to (5.0 mg/mL, 0.32 µmol) using Amicon® Ultra-0.5 mL (3 kDa) centrifugal filters. Stock solution of TCEP (4.0 mg/mL, 0.042 mmol, 14 mM) was prepared in the same conjugation buffer. Sbi III/IV-2xCys was reduced by incubation with TCEP (2 equiv. relative to Sbi III/IV-2xCys) for 1 h at room temperature. Then quenching step using penta-PEG azide (**2.13**) for 1 h was followed.

2- The reduced Sbi III/IV-Cys. with bis-o-diiodoacetamide $(PEG)_7$ linker **6.5** (10 µL of 20 mg/mL stock solution, 5 equiv. relative to Sbi III/IV-2xCys) for 3 h at room temperature.

3- Excess reagent was removed by using quick step of purification using Ni^{+2} column to remove excess linkers from functionalized Sbi III/IV-2xCys solution prior to conjugation with partially reduced Tmab

4- Meanwhile Tmab was buffer exchanged to Tris.HCl (100 mM, 150 mM NaCl, 5mM EDTA, pH 7.5) and diluted to (5.0 mg/mL, 0.034 µmol) using Amicon® Ultra-0.5 mL (10 kDa) centrifugal filters. Tmab was reduced by incubation with TCEP (1.1 equiv. relative to Tmab) for 2 h at 4°C.

5- Functionalised Sbi III/IV-Cys. (4 equiv. relative to Tmab) was then added to the reduced Tmab and left at room temperature overnight.

8.7.4 Sequential purification of $Tmab_{o\text{-}HL}$-PEG_7-$Sbi_{ortho\text{-}bis\text{-}Cys}$ conjugate (6.11) using IMAC followed by size exclusion chromatography (SEC).

IMAC purification was performed using Ni^{2+} column (1 mL HisTrap, FF) to separate Tmab-Sbi conjugate from unfunctionalised Tmab as Sbi III/IV-2xCys is a his-tagged protein. Before performing the purification the reaction was buffer exchanged sample into His-A buffer to remove EDTA by using using Amicon® Ultra-0.5 mL (3 kDa) centrifugal filters.

The column was loaded with the reaction mixture. The loaded column washed with 4-10 mLs of HisA buffer and the bound his-tagged proteins were eluted with a 0-100% gradient of HisB buffer (around 20 column volume).

The collected protein samples were concentrated using Amicon® Ultra-15mL (3 kDa) centrifugal filters and finally buffer exchanged into phosphate buffer saline (PBS) buffer stored at -20°C. Samples from each combined fraction were analysed by SDS-PAGE (10%)

The pure concentrated fractions were further purified using SEC, which was performed using superdex column (HiLoad 16/600, Superdex 200 pg, GE Healthcare). Before loading into the column, samples were centrifuged at 20,000 g for 10 minutes to remove any aggregates. The used buffer and the details regarding the run are summarised in Table 8.3. The collected fraction containing the conjugate were buffer exchanged into conjugation buffer, sterilised using 0.45 µm membrane filters and stored at -20°C.

Table 8.3. The details regarding the buffer used in SEC and the run specifications.

Buffer	Tris.HCl buffer (20 mM, 150 mM NaCl, pH 7.4)
Flow rate	1 mL/min
Total run time	2 h
Collected fraction size	1 mL

8.8 Chapter 7 Experimental

8.8.1 Construction and purification of the trifunctionalTmab: $Tmab_{o\text{-}HL}$-PEG_7-$IFab_{o\text{-}HL}$ conjugate (7.1) with bis-o-diiodoacetamide $(PEG)_7$ 6.5 linker

1. IFab was buffer exchanged to conjugation Tris.HCl buffer (pH 7.5) and diluted to (5 mg/mL, 0.1 µmol) using Amicon® Ultra-0.5 mL (3 kDa) centrifugal filters.

Stock solution of TCEP (4.0 mg/mL, 0.042 mmol, 14 mM) was prepared in the same conjugation buffer. IFab was reduced by incubation with TCEP (2 equiv. relative to IFab) for 1 h at room temperature. Then quenching step using penta-PEG azide (**2.13**) for 1 h was followed.

2. The reduced IFab was incubated with bis-o-diiodoacetamide $(PEG)_7$ linker **6.5** (10 µL of stock solution (7 mg/mL), 5 equiv.) for 3 h at room temperature.
3. Excess reagent was removed by using quick step of purification using protein A column (1 mL HisTrap, FF) to remove excess linkers from functionalized IFab solution prior to conjugation with partially reduced Tmab. The binding buffer Tris.HCl (20 mM, 500 mM NaCl, pH 7.4) was used to collect Fab fractions, then the collected faction were concentrated using were concentrated using Amicon® Ultra-15 mL (3 kDa) centrifugal filters and finally buffer exchanged into conjugation buffer.
4. Meanwhile Tmab was buffer exchanged to Tris.HCl (100 mM, 150 mM NaCl, 5 mM EDTA, pH 7.5) and diluted to (5.0 mg/mL, 0.03 µmol) using Amicon® Ultra-0.5 mL (10 kDa) centrifugal filters. Tmab was reduced by incubation with TCEP (1.1 equiv. relative to Tmab) for 2 h at 4°C.
5. Functionalised IFab (4 equiv. relative to Tmab) was then added to the reduced Tmab and left at room temperature overnight.
6. SEC was performed using superdex column (HiLoad 16/600, Superdex 200 pg, GE Healthcare). Before loading into the column, samples were centrifuged at 20,000 g for 10 minutes. The used buffer and the details regarding the run are summarised in Table 8.3. The collected fraction containing the conjugate were buffer exchanged into conjugation buffer and sterilised using 0.45 µm membrane filters.

9 General discussion, conclusion and future implications

Bioconjugation chemistry is a wide range set of techniques that covalently links a biomolecule with an exogenous moiety to provide it with desirable properties. This novel construct shares the combined properties of its individual components. This field has received a huge attention as it has revolutionised the therapeutic perspective of cancer disease. It has provided means to formulate more stable and efficient therapeutics, facilitated *in vivo* dynamic studying of proteins in the biological systems and contributed widely in diseases diagnostic approaches. Although it has received huge attention, the effectiveness of bioconjugation techniques are still inadequate and limited to certain applications. The work herein aimed to tackle a couple of substantial limitations and explore possible new applications, which was divided into two main subsequent themes, optimizing pre-labelling conditions of proteins and developing a novel conjugation chemistry to construct various anti-cancer antibody-protein immunoconjugates.

Starting with the first aim of this project, we have developed a one-pot approach to optimise and facilitate protein reduction protocol and activate thiolate side chains of cysteine residues toward conjugation reactions. Protein labelling procedure through their reactive cysteine residues offers a number of advantages, including its good nucleophilicity and low availability, which have put cysteine-targeted approaches in the spotlight. Provided that most of the cysteine amino acids are paired together in disulfide bonds, therefore a pre-reduction step is essential to attain free reactive thiolate group. Removing excess reducing agents before thiol alkylation is essential to obtain optimum labelling and reduce off-target reactions.

A series of water-soluble PEG-azides were employed to quench excess phosphine reductants though Staudinger reaction. In Chapter 2, we provided the synthesis of a series of water-soluble PEG azides, determination of their aqueous solubility and the rates of oxidation of phosphine reductants. Combining both the desired aqueous solubility characteristics of these quenchers with the improved yield of protein labelling, we can conclude that the newly developed *in situ* method can be widely applied in

protein conjugation reactions facilitating the labelling of cysteine residues and avoid the requirements of purification methods after commencing the reduction step.

Therefore, in this work we have provided an efficient method to remove excess reducing agents, which will eventually improve the level of protein labelling. The importance of this work centered at its wide possible applicability in protein conjugation reactions. Throughout this thesis, we have found it very efficient to apply this quenching method prior to protein labelling using different thiol alkylating approaches, such as our developed sulfonate-based method (Chapter 3) and bis-haloacetmide linkers (Chapter 4).

In the following Chapters of this project, we aimed to provide a new conjugation approach that can be applied in the construction of novel immunoconjugates. We deeply looked at different parameters affecting the electrophilic characteristics of various sulfonate esters derivatives in Chapter 3. Generally, one conclusion that can be drawn is the poor aqueous stability of these linkers which was directly correlated with the pK_a values of their corresponding sulfonic acids.

The nature of the α-substituent groups was the most relevant parameter, which has enabled us to identify the lead sulfonate-based linker. The α-amide group was identified as a very good acceptor group through significantly increasing the reactivity rate of tosylate groups toward glutathione with excellent observed aqueous stability. The provided results in Chapter 3 were in line with the previously published work regarding the reactivity of electrophiles bearing α-amide acceptor with thiolate anion of cysteine.

The reactivity of tosyl-acetamide with proteins has been evaluated using model protein with one cysteine residue, which confirmed our drawn conclusions and proved that tosyl acetamide was the optimum identified sulfonate linker amongst the evaluate derivatives.

The provided linkers in Chapter 3 could be considered as an alternative approach to the well-known maleimide-based approach with the advantage of constructing a more stable conjugate consistent with what has been shown before regarding iodoacetamide linkers. We based this conclusion on the same constructed conjugate with both approaches

(sulfonyl acetamide and halo acetamide). One of the offered advantages of using tosyl acetamide linker over maleimide is the significant higher aqueous stability of the former linker, especially at basic conditions where the half-life of *N*-ethylmaleimide drops dramatically to 1.7 h and it is advised that the solution of maleimide linker should be prepared fresh for each labelling reaction.[290]

However, with the slow reaction kinetics of the proposed sulfonate ester derivatives, on this occasion, we could not apply them to develop our devoted new chemistry in order to construct the novel immunoconjugates. Nevertheless, the interesting findings regarding tosyl acetamide linker (**3.9**) could find another implication where the slow kinetics and size of our sulfonate linker is favorable in certain conjugation reactions. One example could be developing bifunctional linkers with two different electrophiles, such as sulfonate acetamide and other well-known electrophiles to specifically label certain reactive sites on proteins through a very reactive electrophile, which leaves our sulfonate acetamide to be activated with tracking probe, PEG or cytotoxic drug when required. Alternatively, PEGylation of proteins using sulfonates, such as PEG tresylate[6,291] is one of the early developed approaches to enhance the solubility and stability of therapeutic proteins, our current work provides a more reactive and stable sulfonate derivative that can be employed to prepare PEGs functionalised with tosyl-acetamide group.

To our delight, we have developed stable and reactive bis-haloacetamide linkers that have been applied in the rebridging of the reduced disulfide bonds of antibodies as described in Chapter 4 and 5. The novel scaffold of these linkers was developed based on preliminary findings regarding the stability of mono-haloacetamide derivatives and the previously published work related to DNA cross-linking.

Detailed synthesis, aqueous stability and glutathione reactivity of various aryl bis-haloacetamide derivatives have been described in Chapter 4. Generally, the provided results reflect the inherent reactivity of iodo- and bromo-derviavtives in comparison to chloro-derivatives. Different factors were evaluated, including the regiochemistry of the haloacetamide groups relative to each other, and the impact of aryl substituent.

Regardless of the aryl substituent, meta-derivatives were more stable and less reactive toward thiol alkylation of glutathione in comparison to ortho-derivatives. Aryl substitution did not influence the reactivity of the bis-haloacetamide derivatives, which have enabled us to prepare bis-haloacetamide derivatised with bioorthogonal group, which is suitable for Click reactions.

Given that the plasma stability [84,196] of the constructed protein conjugates is one of the most essential challenges that needed to be considered when a new conjugation chemistry is proposed, in Chapter 4 we studied the stability of bis-glutathione conjugates in aqueous buffer and in the presence of DTT over 4 weeks in comparison to maleimide-glutathione conjugate. With very stable conjugates in the presence and the absence of DTT, we can conclude that the provided scaffold of aryl bis-haloacetamide holds more advantages over the current available chemistries.

Having established a full stability and reactivity study of aryl bis-haloacetamide linkers, we evaluated the rebridging of the reduced disulfide bonds of model antibodies, namely Trastuzumab and Rituximab (Chapter 5). With interesting rebridged half antibody (rebridging both intra-chain heavy-heavy disulfide bonds and inter-chain heavy-light disulfide bonds), our bis-haloacetamide linkers interacted differently to the currently available rebridging approaches.[156,185] The developed half-antibody was confirmed as a major product by using protein MS analysis, which was observed with all the developed aryl bis-haloacetamide linkers.

The obtained rebridged half antibody could find interesting applications in anti-cancer and chronic diseases treatments. With significantly smaller size, the obtained rebridged half antibody could have good tissue penetration potential without the need to misplace the effector function of the Fc region, which could be used in the treatment of solid tumors. In addition, half-antibody (monovalent antibody) represents a class of therapeutic antibodies that have received considerable attention particularly when bivalency of antibodies can produce dimerisation of receptors and agonistic effect.[292] One example of the currently approved half-antibodies is onartuzumab (MetMAb), which blocks interaction between hepatocyte growth factor receptor (MET) receptors

and its hepatocyte growth factor (HGF) ligand and interferes with this signalling pathway. It consists of a single antigen-binding fragment (Fab) fused to a complete constant domain fragment (Fc).[293] Moreover, recently, ADCs of IgG4 subclass have been constructed showing a favorable safety profile in comparison to IgG1 subclass.[294] One of the attractive characteristics of IgG4 subclass is its tendency to form half antibodies and half antibody exchange forming bispecific antibodies.[295] In this work, we have provided a solid method to form well-defined half antibodies, which might afford attractive approach to form bispecific antibodies of IgG4 subclass.

Herein, it was demonstrated that well-defined and stable rebridged half antibodies were obtained with aryl bis-haloacetamide linkers under plasma mimicking conditions, which as described earlier is one of the essential desired characteristic of the immunoconjugate of antibodies, particularly ADCs.

The construction of ADCs is considered as a revolutionary milestone and one of the recent cutting-edge approaches in the field of oncology, which are capable of specific targeting of highly potent cytotoxic drugs toward tumour site. However, with the long list of encountered drawbacks ranging from heterogeneity of ADCs species to poor plasma stability of the antibodies construct, different approaches were developed to overcome the drawbacks experienced with the first generation ADCs, including genetic and enzymatic-based approaches, and the recently introduced disulfide re-bridging approaches. Both of the disulfide re-bridging approaches ThioBridge® (form 3-carbon bridges) and bis-reactive maleimide (form 2-carbon bridges) were established to obtain a well-defined fully cross-linked mAb of 150 kDa mass. Employing of the aryl bis-haloacetamide linkers to attach a cytotoxic payload, while maintaining the post-reduction structure of antibodies, could be one of the most promising application of this novel linkers in the oncology field.

Moreover, functionalisation of mAbs with a clickable handle (azide) was achievable affording mAbs that could be used in azide cyclooctyne cycloaddition reaction (Click reaction). There is a wide range of applications of the provided stable, well-defined rebridged half-antibodies functionalised with azide bio-orthogonal chemistry.

Click reaction especially SPAAC has been widely garnered substantial attention in the broad field of biomedical sciences due to the outstanding selectivity, favourable reaction rates and biocompatibility. It has been chiefly used in specific tumor cell imaging for diagnostic purposes and for dynamic intracellular tracking strategies. Recently, Click chemistry has been widely used in the development of nanoparticles modified with biological ligands, such as antibodies for targeted imaging or drug delivery.[296,297]

The rebridged half-antibodies functionalised with azide group (for example the constructed $Tmab_{bis\text{-}[(o\text{-}\mathbf{HL},o\text{-}\mathbf{HH}intra)\text{-}N_3]}$) can be widely employed in a huge number of applications, including medical therapeutics and diagnostics areas. It could be used to construct ADCs through cycloaddition reaction of derivatised cytotoxic drugs, or it can be linked to radiolabel or fluorescein confirming the utility of our promising applications of this conjugation method.

Alternatively, this approach could be used to construct protein-protein conjugates of mAbs or antibody fragments with other proteins to achieve bi-specificity. In a similar approach to Yu Cao *et al.* where they employ Click chemistry to develop various formats of Anti-HER2/AntiCD3 bsAbs,[111] herein we provided a chemical method to construct bsAbs without the need to genetically incorporate non-canonical amino acids.

Moreover, in most cases, antibody fragments are modified to modulate their characteristics, such as their short plasma half-life which widely tackled through attachment of human serum Albumin[298] to the native proteins. Therefore, the developed azide-functionalised bis-haloacetamides can be utilised to tackle the shortcoming of employing antibody fragments through utilising Click chemistry to construct the well-accepted albumin protein approach.

One of the most interesting findings regarding aryl bis-haloacetamide derivatives is their pattern of selectivity towards the four reduced disulfide bonds of mAbs (heavy-light and heavy-heavy disulfide bonds) which, to the best of our knowledge, has not been shown before. We found that the regiochemistry of haloacetamide groups relative to each other was the most relevant parameter. Meta-linkers were more selective toward cross-linking intra-heavy-heavy disulfide bonds. These results have enabled us to understand the order of the reduction susceptibility of disulfide bonds and more importantly to

construct hetero-bifunctional mAbs. With versatile applications of these conjugates, the provided constructs with site-selective conjugation provided a facile method to manipulate the quantity and functionalities attached to mAbs. For example, combining unique anti-cancer properties of cytotoxic payload with fluorescence emission or radiolabelling.

One of the possible advantages of site-selective conjugation at heavy-heavy disulfide bonds is to manipulate the effector function of mAbs. This could be achieved through the attachment of a bulky group that hinders the binding sites for FcγR or C1q. Such method could provide a ground-breaking technique where the effector function of the mAbs could be selectivity modified without the need to genetically modify the antibody or use antibody fragments.[299]

Lastly, we can conclude from the last conducted experiment in Chapter 5 to produce homodimers of C3dg, the utility of employing aryl bis-haloacetamide linkers to not only produce homodimers of proteins, but possibly heterodimers. These results are particularly important to study and understand protein-protein interactions.[300]

As described before, bioconjugation chemistry has revolutionised the targeted therapeutic prospects and delivery approaches. Beyond the context of this thesis, aryl bis-haloacetamide could found a huge number of promising applications in other areas, for instance in the construction of bioconjugated oligonucleotides, which recently have started to be successfully interpreted to the clinical practice with the potential to treat long list of diseases. Bioconjugation has provided oligonucleotides with a wide range of features to modulate their physical properties, enhance tissue penetration, promote target specificity and develop resistance to nucleases. These properties have been achieved through different adopted conjugation approaches, including binding to antibodies, fatty acids, cell penetrating peptides, and α-tocopherol.[301] Given that aryl bis-haloacetamides were used before in cross-linking of oligonucleotides,[163] therefore our developed azide-bearing linkers could found interesting applications to construct various bioconjugated oligonucleotides.

In the last 2 Chapters of this work, we provided a novel cross-coupling approach to efficiently construct antibody-protein conjugates. In general, this platform affords a stable, well-defined and facile chemical method to construct bsAbs and trispecific antibodies, which could be widely applied in the construction of various formats of bsAbs in good yield and feasible procedure. We provided the construction of two different immunoconjugates of Tmab using bis-o-diiodoacetamide $(PEG)_7$ linker (**6.5):** Tmab-Sbi (Chapter 6) and Tmab-IFab (Chapter 7).

In Chapter 6, we inspired by the basic concept behind ACDs where Tmab was utilised as a carrier of Sbi III-IV protein, which activates the human complement protein C3 against cancer tissue.

S. aureus produces an arsenal of immune evasion proteins to particularly, interfere with the function of the human complement system. These immune evasion proteins have different modes of action, ultimately to block convertase proteins, to interfere with opsonization and to counteract the action of the chemotactic molecules, mainly C5a. Rather than direct inhibition, Sbi III-IV is *Staphylococcal* protein that uniquely activates the C3 component of complement system through AP thus, Sbi III-IV ensures that C3 is consistently activated and consumed, while stabilizing the nascent C3b fragments.[302] Taking advantage of the unique mode of action of Sbi III-IV as C3 activator, it has been shown that utilizing Sbi as a vaccine adjuvant with mycobacterium tuberculosis antigen Ag85b, has significantly enhanced the immune response through efficient opsonisation of Ag85b with C3 fragments.[302]

In this work, we aimed to exploit Sbi protein as AP activator of the complement system in cancer treatment. Given that antibody-based therapy has transformed the landscape of cancer treatment, we speculated that by conjugating the Sbi together with mAbs, targeted immunotherapy approach would be achieved along with the significantly enhancing the antibody-mediated killing of cancerous cell. The constructed immunomodulating conjugate could be a ground-breaking strategy in the treatment of various types of cancers by conjugating different antibodies or antibody fragments to Sbi protein.

The constructed immunoconjugates of Tmab-Sbi will be further evaluated *in vitro* against cancer cell lines and possibly *in vivo* against xenograft cancer model. Appropriate drug delivery approach, possibly through the previously described nanoparticles, could be further developed to achieve higher stability of the construct.

Bi-specific antibodies are a present-day trend of cancer treatment, which has gained particular to achieve multiple intervention mechanisms in order to overcome the limited benefits of employing mAbs in cancer therapy. This field has received extensive consideration with more than 50 bsAbs are under investigation in clinical trials for various malignancies.[244,245] In Chapter 7, we have described the conjugation and purification methods to construct trispecific antibody of Tmab with one of the checkpoint inhibitors, namely Ipilimumab. The obtained good yield provide a promising preliminary foundation to produce various classes of rebridged bsAbs in good yield and through an easily adaptable procedure. In this work, we were able to provide a proof of concept for our trispecific immunomodulating platform, the obtained results could be further implemented into other mAbs or antibody fragments to achieve bi-specificity and possibly tri-specificity.

It has been widely acknowledged the direct association between cancer growth and progression with the developed immune suppression by cancer cells. Cancer cells are able to modulate various immune checkpoint pathways in order to interfere with immunosuppressive mechanisms. Recently, mAbs that inhibit immune checkpoints have been considered as a massive breakthrough in cancer therapeutics. Amongst the approved immune checkpoints inhibitors, PD-1/PD-L1 and CTLA-4 inhibitors have shown encouraging therapeutic outcomes with various types of malignancies.[303] Nevertheless, with the relatively limited response and the observed immune-mediated adverse effects in some cancer patients, we speculated that construction of bsAbs of these immune checkpoint inhibitors could enhance the observed benefits amongst cancer patients. Future studies, possibly pre-clinical studies, will be conducted to evaluate treatment outcomes of Tmab-IFab construct in HER2 positive and negative breast cancer model.

10 References

(1) Knorre, D. G., Kudryashova, N. V, and Godovikova, T. S. (2009) Chemical and functional aspects of posttranslational modification of proteins. *Acta Naturae 1*, 29–51.

(2) Spoel, S. H. (2018) Orchestrating the proteome with post-translational modifications. *J. Exp. Bot. 69*, 4499–4503.

(3) Walsh, C. T., Garneau-Tsodikova, S., and Gatto, G. J. (2005) Protein Posttranslational Modifications: The Chemistry of Proteome Diversifications. *Angew. Chemie Int. Ed. 44*, 7342–7372.

(4) Mann, M., and Jensen, O. N. (2003) Proteomic analysis of post-translational modifications. *Nat. Biotechnol. 21*, 255–261.

(5) Krall, N., Da Cruz, F. P., Boutureira, O., and Bernardes, G. J. L. (2016) Site-selective protein-modification chemistry for basic biology and drug development. *Nat. Chem. 8*, 103–113.

(6) Koniev, O., and Wagner, A. (2015) Developments and recent advancements in the field of endogenous amino acid selective bond forming reactions for bioconjugation. *Chem. Soc. Rev. 44*, 5495–5551.

(7) Hermanson, G. T. (2013) Introduction to Bioconjugation, in *Bioconjugate Techniques*, pp 1–125. Elsevier.

(8) Means, G. E., and Feeney, R. E. (1990) Chemical modifications of proteins: history and applications. *Bioconjug. Chem. 1*, 2–12.

(9) Lequin, R. M. (2005) Enzyme immunoassay (EIA)/enzyme-linked immunosorbent assay (ELISA). *Clin. Chem. 51*, 2415–8.

(10) Mahmood, T., and Yang, P.-C. (2012) Western blot: technique, theory, and trouble shooting. *N. Am. J. Med. Sci. 4*, 429–34.

(11) Alauddin, M. M. (2012) Positron emission tomography (PET) imaging with (18)F-based radiotracers. *Am. J. Nucl. Med. Mol. Imaging 2*, 55–76.

(12) Treglia, G., and Salsano, M. (2013) PET imaging using radiolabelled antibodies: future direction in tumor diagnosis and correlate applications. *Res. Reports Nucl. Med.* 9.

(13) Kalia, J., and Raines, R. T. (2010) Advances in Bioconjugation. *Curr. Org. Chem. 14*, 138–147.

(14) Zeglis, B. M., Sevak, K. K., Reiner, T., Mohindra, P., Carlin, S. D., Zanzonico, P., Weissleder, R., and Lewis, J. S. (2013) A Pretargeted PET Imaging Strategy Based on Bioorthogonal Diels-Alder Click Chemistry. *J. Nucl. Med. 54*, 1389–1396.

(15) Rashidian, M., Keliher, E. J., Dougan, M., Juras, P. K., Cavallari, M., Wojtkiewicz, G. R., Jacobsen, J. T., Edens, J. G., Tas, J. M. J., Victora, G., Weissleder, R., and Ploegh, H. (2015) Use of ^{18} F-2-Fluorodeoxyglucose to Label Antibody Fragments for Immuno-Positron Emission Tomography of Pancreatic Cancer. *ACS Cent. Sci. 1*, 142–147.

(16) Dimitrov, D. S. (2012) Therapeutic Proteins, in *Methods in molecular biology (Clifton, N.J.)*, pp 1–26.

(17) Pasut, G., and Veronese, F. M. (2009) PEG conjugates in clinical development or use as anticancer agents: An overview. *Adv. Drug Deliv. Rev. 61*, 1177–1188.

(18) Rosa, J., Sabelli, M., and Soriano, E. R. (2010) Prefilled certolizumab pegol (Cimzia(®)) syringes for self-use in the treatment of rheumatoid arthritis. *Med. Devices (Auckl). 3*, 25–31.

(19) Goldblatt, D. (2000) Conjugate vaccines. *Clin. Exp. Immunol. 119*, 1–3.

(20) Kelly, D. F., Moxon, E. R., and Pollard, A. J. (2004) Haemophilus influenzae type b conjugate vaccines. *Immunology 113*, 163–74.

(21) Peltola, H., Kilpi, T., Anttila, M., Peltola, H., and Kilpi, T. (1992) Rapid disappearance of Haemophilus influenzae type b meningitis after routine childhood immunisation with conjugate vaccines. *Lancet 340*, 592–594.

(22) Chalouni, C., and Doll, S. (2018) Fate of Antibody-Drug Conjugates in Cancer Cells. *J. Exp. Clin. Cancer Res. 37*, 1–12.

(23) Pento, J. T. (2017) Monoclonal Antibodies for the Treatment of Cancer. *Anticancer Res. 37*, 5935–5939.

(24) DeVita, V. T., and Chu, E. (2008) A history of cancer chemotherapy. *Cancer Res. 68*, 8643–8653.

(25) HITCHINGS, G. H., and ELION, G. B. (1954) The chemistry and biochemistry of purine analogs. *Ann. N. Y. Acad. Sci. 60*, 195–9.

(26) Moudi, M., Go, R., Yien, C. Y. S., and Nazre, M. (2013) Vinca alkaloids. *Int. J. Prev. Med. 4*, 1231–5.

(27) Kondo, N., Takahashi, A., Ono, K., and Ohnishi, T. (2010) DNA damage induced by alkylating agents and repair pathways. *J. Nucleic Acids 2010*, 543531.

(28) WARWICK, G. P. (1963) The Mechanism of Action of Alkylating Agents. *Cancer Res. 23*, 1315–33.

(29) Iqbal, N., and Iqbal, N. (2014) Imatinib: a breakthrough of targeted therapy in cancer. *Chemother. Res. Pract. 2014*, 357027.

(30) Scott, A. M., Allison, J. P., and Wolchok, J. D. (2012) Monoclonal antibodies in cancer therapy. *Cancer Immun. 12*, 14.

(31) Dos Santos, M. L., Quintilio, W., Manieri, T. M., Tsuruta, L. R., and Moro, A. M. (2018) Advances and challenges in therapeutic monoclonal antibodies drug development. *Brazilian J. Pharm. Sci. 54*, 1–15.

(32) Harpaz, Y., and Chothia, C. (1994) Many of the Immunoglobulin Superfamily

Domains in Cell Adhesion Molecules and Surface Receptors Belong to a New Structural Set Which is close to That Containing Variable Domains. *J. Mol. Biol. 238*, 528–539.

(33) Vidarsson, G., Dekkers, G., and Rispens, T. (2014) IgG subclasses and allotypes: From structure to effector functions. *Front. Immunol. 5*, 1–17.

(34) Schroeder, H. W., and Cavacini, L. (2010) Structure and Function of Immunoglobulins. *J. Allergy Clin. Immunol. 125*, S41–S52.

(35) Liu, H., and May, K. (2012) Disulfide bond structures of IgG molecules: Structural variations, chemical modifications and possible impacts to stability and biological function. *MAbs 4*, 17–23.

(36) Wang, W., Erbe, A. K., Hank, J. A., Morris, Z. S., and Sondel, P. M. (2015) NK Cell-Mediated Antibody-Dependent Cellular Cytotoxicity in Cancer Immunotherapy. *Front. Immunol. 6*, 368.

(37) Tatake, R. J., Maniar, H. S., Chiplunkar, S. V, Somasundaram, R., Amin, M. K., Saikia, T., and Gangal, S. G. (1990) Antibody dependent cellular cytotoxicity and complement mediated cytotoxicity on leukemic cells mediated by anti K562 monoclonal antibodies. *J. Clin. Lab. Immunol. 31*, 87–91.

(38) Adams, G. P., and Weiner, L. M. (2005) Monoclonal antibody therapy of cancer. *Nat. Biotechnol. 23*, 1147–1157.

(39) Khazaeli, M. B., Conry, R. M., and LoBuglio, A. F. (1994) Human immune response to monoclonal antibodies. *J. Immunother. Emphasis Tumor Immunol. 15*, 42–52.

(40) Reff, M. E., Hariharan, K., and Braslawsky, G. (2002) Future of Monoclonal Antibodies in the Treatment of Hematologic Malignancies. *Cancer Control 9*.

(41) Harding, F. A., Stickler, M. M., Razo, J., and DuBridge, R. B. (2010) The immunogenicity of humanized and fully human antibodies: residual immunogenicity resides in the CDR regions. *MAbs 2*, 256–65.

(42) Oldham, R. K., and Dillman, R. O. (2008) Monoclonal antibodies in cancer therapy: 25 Years of progress. *J. Clin. Oncol. 26*, 1774–1777.

(43) Sievers, E. L., and Senter, P. D. (2013) Antibody-Drug Conjugates in Cancer Therapy. *Annu. Rev. Med. 64*, 15–29.

(44) Ritchie, M., Tchistiakova, L., and Scott, N. (2013) Implications of receptor-mediated endocytosis and intracellular trafficking dynamics in the development of antibody drug conjugates. *MAbs 5*, 13–21.

(45) Beck, A., Goetsch, L., Dumontet, C., and Corvaïa, N. (2017) Strategies and challenges for the next generation of antibody–drug conjugates. *Nat. Rev. Drug Discov. 16*.

(46) Chari, R. V. J. (2008) Targeted Cancer Therapy: Conferring Specificity to Cytotoxic Drugs. *Acc. Chem. Res. 41*, 98–107.

(47) Frigerio, M., and Kyle, A. F. (2017) The Chemical Design and Synthesis of Linkers Used in ADCs 3393–3424.

(48) Carter, P. J., and Senter, P. D. (2008) Antibody-Drug Conjugates for Cancer Therapy. *Cancer J. 14*, 154–169.

(49) McCombs, J. R., and Owen, S. C. (2015) Antibody drug conjugates: design and selection of linker, payload and conjugation chemistry. *AAPS J. 17*, 339–51.

(50) Bouchard, H., Viskov, C., and Garcia-Echeverria, C. (2014) Antibody-drug conjugates—a new wave of cancer drugs. *Bioorg. Med. Chem. Lett. 24*, 5357–63.

(51) FDA. (2017) Press Announcements - FDA approves Mylotarg for treatment of acute myeloid leukemia. *https://www.fda.gov/NewsEvents/Newsroom/PressAnnouncements/ucm574507.htm*. Office of the Commissioner.

(52) Beck, A., Haeuw, J.-F., Wurch, T., Goetsch, L., Bailly, C., and Corvaïa, N. (2010)

The next generation of antibody-drug conjugates comes of age. *Discov*. *Med*. *10*, 329–39.

(53) Perez, H. L., Cardarelli, P. M., Deshpande, S., Gangwar, S., Schroeder, G. M., Vite, G. D., and Borzilleri, R. M. (2014) Antibody–drug conjugates: current status and future directions. *Drug Discov*. *Today 19*, 869–881.

(54) Deng, C., Pan, B., and O'Connor, O. A. (2013) Brentuximab vedotin. *Clin*. *Cancer Res*. *19*, 22–7.

(55) Francisco, J. A., Cerveny, C. G., Meyer, D. L., Mixan, B. J., Klussman, K., Chace, D. F., Rejniak, S. X., Gordon, K. A., DeBlanc, R., Toki, B. E., Law, C.-L., Doronina, S. O., Siegall, C. B., Senter, P. D., and Wahl, A. F. (2003) cAC10-vcMMAE, an anti-CD30-monomethyl auristatin E conjugate with potent and selective antitumor activity. *Blood 102*, 1458–65.

(56) Frigerio, M., and Kyle, A. F. (2018) The Chemical Design and Synthesis of Linkers Used in Antibody Drug Conjugates. *Curr*. *Top*. *Med*. *Chem*. *17*, 3393–3424.

(57) Owens, M. A., Horten, B. C., and Da Silva, M. M. (2004) HER2 amplification ratios by fluorescence in situ hybridization and correlation with immunohistochemistry in a cohort of 6556 breast cancer tissues. *Clin*. *Breast Cancer 5*, 63–9.

(58) Amiri-Kordestani, L., Blumenthal, G. M., Xu, Q. C., Zhang, L., Tang, S. W., Ha, L., Weinberg, W. C., Chi, B., Candau-Chacon, R., Hughes, P., Russell, A. M., Miksinski, S. P., Chen, X. H., McGuinn, W. D., Palmby, T., Schrieber, S. J., Liu, Q., Wang, J., Song, P., Mehrotra, N., Skarupa, L., Clouse, K., Al-Hakim, A., Sridhara, R., Ibrahim, A., Justice, R., Pazdur, R., and Cortazar, P. (2014) FDA approval: ado-trastuzumab emtansine for the treatment of patients with HER2-positive metastatic breast cancer. *Clin*. *Cancer Res*. *20*, 4436–41.

(59) Brinkley, M. (1992) A brief survey of methods for preparing protein conjugates with dyes, haptens and crosslinking reagents. *Bioconjug*. *Chem*. *3*, 2–13.

(60) Anderson, G. W., Zimmerman, J. E., and Callahan, F. M. (1964) The Use of Esters

of N-Hydroxysuccinimide in Peptide Synthesis. *J. Am. Chem. Soc. 86*, 1839–1842.

(61) Riggs, J. L., Seiwald, R. J., Burckhalter, J. H., Downs, C. M., and Metcalf, T. G. (1991) Isothiocyanate compounds as fluorescent labeling agents for immune serum. *Am. J. Pathol. 34*, 1081–97.

(62) Denora, N., Laquintana, V., Lopalco, A., Iacobazzi, R. M., Lopedota, A., Cutrignelli, A., Iacobellis, G., Annese, C., Cascione, M., Leporatti, S., and Franco, M. (2013) In vitro targeting and imaging the translocator protein TSPO 18-kDa through G(4)-PAMAM–FITC labeled dendrimer. *J. Control. Release 172*, 1111–1125.

(63) Kingshott, P., McArthur, S., Thissen, H., Castner, D. G., and Griesser, H. J. (2002) Ultrasensitive probing of the protein resistance of PEG surfaces by secondary ion mass spectrometry. *Biomaterials 23*, 4775–4785.

(64) Mori, Y., Goto, M., and Kamiya, N. (2011) Transglutaminase-mediated internal protein labeling with a designed peptide loop. *Biochem. Biophys. Res. Commun. 410*, 829–833.

(65) Nanda, J. S., and Lorsch, J. R. (2014) Labeling a Protein with Fluorophores Using NHS Ester Derivitization, in *Methods in enzymology*, pp 87–94.

(66) Banks, P. R., and Paquette, D. M. Comparison of three common amine reactive fluorescent probes used for conjugation to biomolecules by capillary zone electrophoresis. *Bioconjug. Chem. 6*, 447–58.

(67) Patil, U. S., Osorno, L., Ellender, A., Grimm, C., and Tarr, M. A. (2015) Cleavable ester linked magnetic nanoparticles for labeling of solvent exposed primary amine groups of peptides/proteins. *Data Br. 4*, 302–307.

(68) Bjerneld, E. J., Johansson, J. D., Laurin, Y., Hagner-McWhirter, Å., Rönn, O., and Karlsson, R. (2015) Pre-labeling of diverse protein samples with a fixed amount of Cy5 for sodium dodecyl sulfate–polyacrylamide gel electrophoresis analysis. *Anal. Biochem. 484*, 51–57.

(69) Smith, G. P. (2006) Kinetics of Amine Modification of Proteins. *Bioconjugate Chem*. *17*, 501−506.

(70) Stephanopoulos, N., and Francis, M. B. (2011) Choosing an effective protein bioconjugation strategy. *Nat*. *Chem*. *Biol*. *7*, 876–884.

(71) Chen, Y., Kim, M. T., Zheng, L., Deperalta, G., and Jacobson, F. (2016) Structural Characterization of Cross-Linked Species in Trastuzumab Emtansine (Kadcyla). *Bioconjug*. *Chem*. *27*, 2037–2047.

(72) Adamo, R., Nilo, A., Castagner, B., Boutureira, O., Berti, F., and Bernardes, G. J. L. Synthetically defined glycoprotein vaccines: current status and future directions.

(73) Möginger, U., Resemann, A., Martin, C. E., Parameswarappa, S., Govindan, S., Wamhoff, E. C., Broecker, F., Suckau, D., Pereira, C. L., Anish, C., Seeberger, P. H., and Kolarich, D. (2016) Cross Reactive Material 197 glycoconjugate vaccines contain privileged conjugation sites. *Sci*. *Rep*. *6*, 1–13.

(74) Seeberger, P. H., and Werz, D. B. (2007) Synthesis and medical applications of oligosaccharides. *Nature 446*, 1046–1051.

(75) Hoyle, C. E., and Bowman, C. N. (2010) Thiol-Ene Click Chemistry. *Angew*. *Chemie Int*. *Ed*. *49*, 1540–1573.

(76) Gunnoo, S. B., and Madder, A. (2016) Chemical Protein Modification through Cysteine. *ChemBioChem 17*, 529–553.

(77) Thornton, J. M. (1981) Disulphide bridges in globular proteins. *J*. *Mol*. *Biol*. *151*, 261–87.

(78) Tallec, G., Loh, C., Liberelle, B., Garcia-Ac, A., Duy, S. V., Sauvé, S., Banquy, X., Murschel, F., and De Crescenzo, G. (2018) Adequate Reducing Conditions Enable Conjugation of Oxidized Peptides to Polymers by One-Pot Thiol Click Chemistry. *Bioconjug*. *Chem*. acs.bioconjchem.8b00684.

(79) Hermanson, G. T. (2013) Chapter 3 – The Reactions of Bioconjugation, in *Bioconjugate Techniques*, pp 229–258.

(80) King, H. D., Dubowchik, G. M., and Walker, M. A. (2002) Facile synthesis of maleimide bifunctional linkers. *Tetrahedron Lett. 43*, 1987–1990.

(81) Sochaj, A. M., Świderska, K. W., and Otlewski, J. (2015) Current methods for the synthesis of homogeneous antibody–drug conjugates. *Biotechnol. Adv. 33*, 775–784.

(82) Boutureira, O., and Bernardes, G. J. L. (2015) Advances in Chemical Protein Modification. *Chem. Rev. 115*, 2174–2195.

(83) Fontaine, S. D., Reid, R., Robinson, L., Ashley, G. W., and Santi, D. V. (2015) Long-Term Stabilization of Maleimide–Thiol Conjugates. *Bioconjug. Chem. 26*, 145–152.

(84) Akkapeddi, P., Azizi, S.-A., Freedy, A. M., Cal, P. M. S. D., Gois, P. M. P., and Bernardes, G. J. L. (2016) Construction of homogeneous antibody–drug conjugates using site-selective protein chemistry. *Chem. Sci. 7*, 2954–2963.

(85) Shen, B.-Q., Xu, K., Liu, L., Raab, H., Bhakta, S., Kenrick, M., Parsons-Reponte, K. L., Tien, J., Yu, S.-F., Mai, E., Li, D., Tibbitts, J., Baudys, J., Saad, O. M., Scales, S. J., McDonald, P. J., Hass, P. E., Eigenbrot, C., Nguyen, T., Solis, W. A., Fuji, R. N., Flagella, K. M., Patel, D., Spencer, S. D., Khawli, L. A., Ebens, A., Wong, W. L., Vandlen, R., Kaur, S., Sliwkowski, M. X., Scheller, R. H., Polakis, P., and Junutula, J. R. (2012) Conjugation site modulates the in vivo stability and therapeutic activity of antibody-drug conjugates. *Nat. Biotechnol. 30*, 184–9.

(86) Lyon, R. P., Setter, J. R., Bovee, T. D., Doronina, S. O., Hunter, J. H., Anderson, M. E., Balasubramanian, C. L., Duniho, S. M., Leiske, C. I., Li, F., and Senter, P. D. (2014) Self-hydrolyzing maleimides improve the stability and pharmacological properties of antibody-drug conjugates. *Nat. Biotechnol. 32*, 1059–1062.

(87) Goddard, D. R., and Michaelis, L. (1935) Derivatives of Keratin. *J. Biol. Chem. 112*, 361–371.

(88) Lundell, N., and Schreitmüller, T. (1999) Sample Preparation for Peptide Mapping— A Pharmaceutical Quality-Control Perspective. *Anal. Biochem. 266*, 31–47.

(89) Nielsen, M. L., Vermeulen, M., Bonaldi, T., Cox, J., Moroder, L., and Mann, M. (2008) Iodoacetamide-induced artifact mimics ubiquitination in mass spectrometry. *Nat. Methods 5*, 459–460.

(90) Lopez-Jaramillo, F. J., Ortega-Muñoz, M., Megia-Fernandez, A., Hernandez-Mateo, F., and Santoyo-Gonzalez, F. (2012) Vinyl Sulfone Functionalization: A Feasible Approach for the Study of the Lectin–Carbohydrate Interactions. *Bioconjug. Chem. 23*, 846–855.

(91) Masri, M. S., and Friedman, M. (1988) Protein reactions with methyl and ethyl vinyl sulfones. *J. Protein Chem. 7*, 49–54.

(92) Roberts, M. J., Bentley, M. D., and Harris, J. M. (2002) Chemistry for peptide and protein PEGylation. *Adv. Drug Deliv. Rev. 54*, 459–76.

(93) Morpurgo, M., Veronese, F. M., Kachensky, D., and Harris, J. M. (1996) Preparation and Characterization of Poly(ethylene glycol) Vinyl Sulfone. *Bioconjug. Chem. 7*, 363–368.

(94) Agarwal, P., and Bertozzi, C. R. (2015) Site-specific antibody-drug conjugates: The nexus of bioorthogonal chemistry, protein engineering, and drug development. *Bioconjug. Chem.*

(95) Junutula, J. R., Raab, H., Clark, S., Bhakta, S., Leipold, D. D., Weir, S., Chen, Y., Simpson, M., Tsai, S. P., Dennis, M. S., Lu, Y., Meng, Y. G., Ng, C., Yang, J., Lee, C. C., Duenas, E., Gorrell, J., Katta, V., Kim, A., McDorman, K., Flagella, K., Venook, R., Ross, S., Spencer, S. D., Lee Wong, W., Lowman, H. B., Vandlen, R., Sliwkowski, M. X., Scheller, R. H., Polakis, P., and Mallet, W. (2008) Site-specific conjugation of a cytotoxic drug to an antibody improves the therapeutic index. *Nat. Biotechnol. 26*, 925–932.

(96) Li, X., Nelson, C. G., Nair, R. R., Hazlehurst, L., Moroni, T., Martinez-Acedo, P.,

Nanna, A. R., Hymel, D., Burke, T. R., and Rader, C. (2017) Stable and Potent Selenomab-Drug Conjugates. *Cell Chem. Biol. 24*, 433–442.e6.

(97) Alley, S. C., and Anderson, K. E. (2013) Analytical and bioanalytical technologies for characterizing antibody-drug conjugates. *Curr. Opin. Chem. Biol. 17*, 406–411.

(98) Junutula, J. R., Flagella, K. M., Graham, R. A., Parsons, K. L., Ha, E., Raab, H., Bhakta, S., Nguyen, T., Dugger, D. L., Li, G., Mai, E., Phillips, G. D. L., Hiraragi, H., Fuji, R. N., Tibbitts, J., Vandlen, R., Spencer, S. D., Scheller, R. H., Polakis, P., and Sliwkowski, M. X. (2010) Engineered thio-trastuzumab-DM1 conjugate with an improved therapeutic index to target human epidermal growth factor receptor 2-positive breast cancer. *Clin. Cancer Res. 16*, 4769–4778.

(99) Hofer, T., Skeffington, L. R., Chapman, C. M., and Rader, C. (2009) Molecularly defined antibody conjugation through a selenocysteine interface. *Biochemistry 48*, 12047–12057.

(100) Axup, J. Y., Bajjuri, K. M., Ritland, M., Hutchins, B. M., Kim, C. H., Kazane, S. A., Halder, R., Forsyth, J. S., Santidrian, A. F., Stafin, K., Lu, Y., Tran, H., Seller, A. J., Biroc, S. L., Szydlik, A., Pinkstaff, J. K., Tian, F., Sinha, S. C., Felding-Habermann, B., Smider, V. V, and Schultz, P. G. (2012) Synthesis of site-specific antibody-drug conjugates using unnatural amino acids. *Proc. Natl. Acad. Sci. U. S. A. 109*, 16101–6.

(101) Zimmerman, E. S., Heibeck, T. H., Gill, A., Li, X., Murray, C. J., Madlansacay, M. R., Tran, C., Uter, N. T., Yin, G., Rivers, P. J., Yam, A. Y., Wang, W. D., Steiner, A. R., Bajad, S. U., Penta, K., Yang, W., Hallam, T. J., Thanos, C. D., and Sato, A. K. (2014) Production of site-specific antibody-drug conjugates using optimized non-natural amino acids in a cell-free expression system. *Bioconjug. Chem. 25*, 351–361.

(102) Panowski, S., Bhakta, S., Raab, H., Polakis, P., and Junutula, J. R. (2014) Site-specific antibody drug conjugates for cancer therapy. *MAbs 6*, 34–45.

(103) Boeggeman, E., Ramakrishnan, B., Pasek, M., Manzoni, M., Puri, A., Loomis, K. H., Waybright, T. J., and Qasba, P. K. (2009) Site specific conjugation of fluoroprobes

to the remodeled Fc N-glycans of monoclonal antibodies using mutant glycosyltransferases: Application for cell surface antigen detection. *Bioconjug. Chem. 20*, 1228–1236.

(104) Strop, P., Liu, S. H., Dorywalska, M., Delaria, K., Dushin, R. G., Tran, T. T., Ho, W. H., Farias, S., Casas, M. G., Abdiche, Y., Zhou, D., Chandrasekaran, R., Samain, C., Loo, C., Rossi, A., Rickert, M., Krimm, S., Wong, T., Chin, S. M., Yu, J., Dilley, J., Chaparro-Riggers, J., Filzen, G. F., O'Donnell, C. J., Wang, F., Myers, J. S., Pons, J., Shelton, D. L., and Rajpal, A. (2013) Location matters: Site of conjugation modulates stability and pharmacokinetics of antibody drug conjugates. *Chem. Biol. 20*, 161–167.

(105) Beerli, R. R., Hell, T., Merkel, A. S., and Grawunder, U. (2015) Sortase Enzyme-Mediated Generation of Site-Specifically Conjugated Antibody Drug Conjugates with High In Vitro and In Vivo Potency. *PLoS One 10*, e0131177.

(106) Petersen, M. T., Jonson, P. H., and Petersen, S. B. (1999) Amino acid neighbours and detailed conformational analysis of cysteines in proteins. *Protein Eng. 12*, 535–48.

(107) Leung, H. J., Xu, G., Narayan, M., and Scheraga, H. A. (2008) Impact of an easily reducible disulfide bond on the oxidative folding rate of multi-disulfide-containing proteins. *J. Pept. Res. 65*, 47–54.

(108) Bhattacharyya, R., Pal, D., and Chakrabarti, P. (2004) Disulfide bonds, their stereospecific environment and conservation in protein structures. *Protein Eng. Des. Sel. 17*, 795–808.

(109) Hu, Q. Y., Berti, F., and Adamo, R. (2016) Towards the next generation of biomedicines by site-selective conjugation. *Chem. Soc. Rev. 45*, 1691–1719.

(110) Singh, S., Dubinsky-Davidchik, I. S., and Kluger, R. (2016) Strain-promoted azide–alkyne cycloaddition for protein–protein coupling in the formation of a bis-hemoglobin as a copper-free oxygen carrier. *Org. Biomol. Chem. 14*, 10011–10017.

(111) Cao, Y., Axup, J. Y., Ma, J. S. Y., Wang, R. E., Choi, S., Tardif, V., Lim, R. K. V, Pugh, H. M., Lawson, B. R., Welzel, G., Kazane, S. A., Sun, Y., Tian, F., Srinagesh, S.,

Javahishvili, T., Schultz, P. G., and Kim, C. H. (2015) Multiformat T-cell-engaging bispecific antibodies targeting human breast cancers. *Angew. Chem. Int. Ed. Engl. 54*, 7022–7.

(112) Jewett, J. C., and Bertozzi, C. R. (2010) Cu-free click cycloaddition reactions in chemical biology. *Chem. Soc. Rev. 39*, 1272–9.

(113) Sletten, E. M., and Bertozzi, C. R. (2009) Bioorthogonal chemistry: fishing for selectivity in a sea of functionality. *Angew. Chem. Int. Ed. Engl. 48*, 6974–98.

(114) Sletten, E. M., and Bertozzi, C. R. (2011) From mechanism to mouse: a tale of two bioorthogonal reactions. *Acc. Chem. Res. 44*, 666–676.

(115) Saxon, E., and Bertozzi, C. R. (2000) Cell Surface Engineering by a Modified Staudinger Reaction. *Science (80-.). 287*, 2007–2010.

(116) Saxon, E., Armstrong, J. I., and Bertozzi, C. R. (2000) A "Traceless" Staudinger Ligation for the Chemoselective Synthesis of Amide Bonds. *Org. Lett. 2*, 2141–2143.

(117) Huisgen, R. (1963) Kinetics and Mechanism of 1,3-Dipolr Cycloadditions. *Angew. Chemie Int. Ed. English 2*, 633–645.

(118) Rostovtsev, V. V., Green, L. G., Fokin, V. V., and Sharpless, K. B. (2002) A Stepwise Huisgen Cycloaddition Process: Copper(I)-Catalyzed Regioselective "Ligation" of Azides and Terminal Alkynes. *Angew. Chemie Int. Ed. 41*, 2596–2599.

(119) Cline, D. J., Redding, S. E., Brohawn, S. G., Psathas, J. N., Schneider, J. P., and Thorpe, C. (2004) New Water-Soluble Phosphines as Reductants of Peptide and Protein Disulfide Bonds: Reactivity and Membrane Permeability. *Biochemistry 43*, 15195–15203.

(120) Getz, E. B., Xiao, M., Chakrabarty, T., Cooke, R., and Selvin, P. R. (1999) A Comparison between the Sulfhydryl Reductants Tris(2-carboxyethyl)phosphine and Dithiothreitol for Use in Protein Biochemistry. *Anal. Biochem. 273*, 73–80.

(121) Burns, J. A., Butler, J. C., Moran, J., and Whitesides, G. M. (1991) Selective reduction of disulfides by tris(2-carboxyethyl)phosphine. *J. Org. Chem. 56*, 2648–2650.

(122) Cherkaoui, S., Bettinger, T., Hauwel, M., Navetat, S., Allémann, E., and Schneider, M. (2010) Tracking of antibody reduction fragments by capillary gel electrophoresis during the coupling to microparticles surface. *J. Pharm. Biomed. Anal. 53*, 172–178.

(123) Krężel, A., Latajka, R., Bujacz, G. D., and Bal, W. (2003) Coordination properties of tris(2-carboxyethyl)phosphine, a newly introduced thiol reductant, and its oxide. *Inorg. Chem. 42*, 1994–2003.

(124) Han, J. C., and Han, G. Y. (1994) A procedure for quantitative determination of tris(2- carboxyethyl)phosphine, an odorless reducing agent more stable and effective than dithiothreitol. *Anal. Biochem*.

(125) Švagera, Z., Hanzlíková, D., Šimek, P., and Hušek, P. (2012) Study of disulfide reduction and alkyl chloroformate derivatization of plasma sulfur amino acids using gas chromatography–mass spectrometry. *Anal. Bioanal. Chem. 402*, 2953–2963.

(126) ThermoFisher. Pierce TCEP-HCl - Thermo Fisher Scientific. *https://www.thermofisher.com/order/catalog/product/20490#/legacy=www.piercenet.com*.

(127) Cumnock, K., Tully, T., Cornell, C., Hutchinson, M., Gorrell, J., Skidmore, K., Chen, Y., and Jacobson, F. (2013) Trisulfide Modification Impacts the Reduction Step in Antibody–Drug Conjugation Process. *Bioconjug. Chem. 24*, 1154–1160.

(128) Visser, C. C., Voorwinden, L. H., Harders, L. R., Eloualid, M., Van Bloois, L., Crommelin, D. J. A., Danhof, M., and De Boer, A. G. (2004) Coupling of metal containing homing devices to liposomes via a maleimide linker: Use of TCEP to stabilize thiol-groups without scavenging metals. *J. Drug Target. 12*, 569–573.

(129) Kantner, T., and Watts, A. G. (2016) Characterization of Reactions between Water-Soluble Trialkylphosphines and Thiol Alkylating Reagents: Implications for

Protein-Conjugation Reactions. *Bioconjug. Chem. 27*, 2400–2406.

(130) Shafer, D. E., Inman, J. K., and Lees, A. (2000) Reaction of tris(2-carboxyethyl)phosphine (TCEP) with maleimide and α- haloacyl groups: Anomalous elution of TCEP by gel filtration. *Anal. Biochem. 282*, 161–164.

(131) Shriver-Lake, L. C., North, S. H., and Rowe Taitt, C. (2013) Loss of cationic peptides with agarose gel-immobilized tris[2-carboxyethyl]phosphine (TCEP). *Biotechniques 55*, 292–4.

(132) Henkel, M., Röckendorf, N., and Frey, A. (2016) Selective and Efficient Cysteine Conjugation by Maleimides in the Presence of Phosphine Reductants. *Bioconjug. Chem. 27*, 2260–2265.

(133) Lin, F. L., Hoyt, H. M., van Halbeek, H., Bergman, R. G., and Bertozzi, C. R. (2005) Mechanistic Investigation of the Staudinger Ligation. *J. Am. Chem. Soc. 127*, 2686–2695.

(134) Kantner, T., Alkhawaja, B., and Watts, A. G. (2017) In Situ Quenching of Trialkylphosphine Reducing Agents Using Water-Soluble PEG-Azides Improves Maleimide Conjugation to Proteins. *ACS Omega 2*, 5785–5791.

(135) Kantner, T. (2015) Bioconjugation Strategies Through Thiol-Alkylation of Peptides and Proteins. University of Bath.

(136) Mahou, R., and Wandrey, C. (2012) Versatile Route to Synthesize Heterobifunctional Poly(ethylene glycol) of Variable Functionality for Subsequent Pegylation. *Polymers (Basel). 4*, 561–589.

(137) Smith, M. B. (2010) Organic Chemistry: An Acid—Base Approach. CRC Press.

(138) Raamat, E., Kaupmees, K., Ovsjannikov, G., Trummal, A., Kütt, A., Saame, J., Koppel, I., Kaljurand, I., Lipping, L., Rodima, T., Pihl, V., Koppel, I. A., and Leito, I. (2013) Acidities of strong neutral Brønsted acids in different media. *J. Phys. Org. Chem. 26*, 162–170.

(139) Jaffé, H. H. (1953) A reëxamination of the hammett equation. *Chem. Rev. 53*, 191–261.

(140) Cee, V. J., Volak, L. P., Chen, Y., Bartberger, M. D., Tegley, C., Arvedson, T., McCarter, J., Tasker, A. S., and Fotsch, C. (2015) Systematic study of the glutathione (GSH) reactivity of N-arylacrylamides: 1. Effects of aryl substitution. *J. Med. Chem. 58*, 9171–9178.

(141) McDaniel, D. H., and Brown, H. C. (1958) An Extended Table of Hammett Substituent Constants Based on the Ionization of Substituted Benzoic Acids. *J. Org. Chem. 23*, 420–427.

(142) Schreck, J. O. (1971) Nonlinear Hammett relationships. *J. Chem. Educ. 48*, 103.

(143) Chalker, J. M., Bernardes, G. J. L., Lin, Y. A., and Davis, B. G. (2009) Chemical modification of proteins at cysteine: opportunities in chemistry and biology. *Chem. Asian J. 4*, 630–40.

(144) Dahl, K. H., and McKinley-McKee, J. S. (1981) The reactivity of affinity labels: A kinetic study of the reaction of alkyl halides with thiolate anions-a model reaction for protein alkylation. *Bioorg. Chem. 10*, 329–341.

(145) Mayr, H., Breugst, M., and Ofial, A. R. (2011) Farewell to the HSAB treatment of ambident reactivity. *Angew. Chemie - Int. Ed. 50*, 6470–6505.

(146) Baldwin, A. D., and Kiick, K. L. (2011) Tunable degradation of maleimide-thiol adducts in reducing environments. *Bioconjug. Chem. 22*, 1946–53.

(147) Davey, S. (2015) All about that rate. *Nat. Chem. Biol. 11*, 241–241.

(148) Liu, H., Chumsae, C., Gaza-Bulseco, G., Hurkmans, K., and Radziejewski, C. H. (2010) Ranking the susceptibility of disulfide bonds in human IgG1 antibodies by reduction, differential alkylation, and LC-MS analysis. *Anal. Chem. 82*, 5219–5226.

(149) Press, E. M. (1975) Fixation of the first component of complement by immune

complexes: effect of reduction and fragmentation of antibody. *Biochem. J. 149*, 285–8.

(150) Wright, J. K. (1978) Reduced immunoglobulin G activates complement system with decreased cooperativity. *Biochem. Biophys. Res. Commun. 83*, 1284–1290.

(151) Shen, Y., Zeng, L., Zhu, A., Blanc, T., Patel, D., Pennello, A., Bari, A., Ng, S., Persaud, K., Kang, Y. K., Balderes, P., Surguladze, D., Hindi, S., Zhou, Q., Ludwig, D. L., and Snavely, M. (2013) Removal of a C-terminal serine residue proximal to the inter-chain disulfide bond of a human IgG1 lambda light chain mediates enhanced antibody stability and antibody dependent cell-mediated cytotoxicity. *MAbs 5*, 418–31.

(152) Badescu, G., Bryant, P., Bird, M., Henseleit, K., Swierkosz, J., Parekh, V., Tommasi, R., Pawlisz, E., Jurlewicz, K., Farys, M., Camper, N., Sheng, X., Fisher, M., Grygorash, R., Kyle, A., Abhilash, A., Frigerio, M., Edwards, J., and Godwin, A. (2014) Bridging disulfides for stable and defined antibody drug conjugates. *Bioconjug. Chem. 25*, 1124–1136.

(153) Maruani, A., Smith, M. E. B., Miranda, E., Chester, K. A., Chudasama, V., and Caddick, S. (2015) A plug-and-play approach to antibody-based therapeutics via a chemoselective dual click strategy. *Nat. Commun. 6*, 6645.

(154) Schumacher, F. F., Nobles, M., Ryan, C. P., Smith, M. E. B., Tinker, A., Caddick, S., and Baker, J. R. (2011) In situ maleimide bridging of disulfides and a new approach to protein PEGylation. *Bioconjug. Chem. 22*, 132–136.

(155) Smith, M. E. B., Schumacher, F. F., Ryan, C. P., Tedaldi, L. M., Papaioannou, D., Waksman, G., Caddick, S., and Baker, J. R. (2010) Protein modification, bioconjugation, and disulfide bridging using bromomaleimides. *J. Am. Chem. Soc. 132*, 1960–5.

(156) Lee, M. T. W., Maruani, A., Baker, J. R., Caddick, S., and Chudasama, V. (2016) Next-generation disulfide stapling: reduction and functional re-bridging all in one. *Chem. Sci. 7*, 799–802.

(157) Singh, R. K., Kumar, S., Prasad, D. N., and Bhardwaj, T. R. (2018) Therapeutic

journery of nitrogen mustard as alkylating anticancer agents: Historic to future perspectives. *Eur. J. Med. Chem. 151*, 401–433.

(158) Shatsauskas, A. L., Abramov, A. A., Saibulina, E. R., Palamarchuk, I. V., Kulakov, I. V., and Fisyuk, A. S. (2017) Synthesis of 3-amino-6-methyl-4-phenylpyridin-2(1H)-one and its derivatives. *Chem. Heterocycl. Compd. 53*, 186–191.

(159) Khraiwesh, M. H., Lee, C. M., Brandy, Y., Akinboye, E. S., Berhe, S., Gittens, G., Abbas, M. M., Ampy, F. R., Ashraf, M., and Bakare, O. (2012) Antitrypanosomal activities and cytotoxicity of some novel imido-substituted 1,4-naphthoquinone derivatives. *Arch. Pharm. Res. 35*, 27–33.

(160) Chan, S., and Braish, T. F. (1994) The tandem Michael-SN2 reaction for the construction of the 3-azabicyclo[3.1.0]hexane ring system. *Tetrahedron 50*, 9943–9950.

(161) Donskikh, A. I., Tseitlin, G. M., Tomina, O. I., Saikina, Z. F., and Doroshenko, J. E. (1989) Hydrolytic Stability of Imides of Different Structures. *Period. Polytech. Chem. Eng. 33*, 61–67.

(162) Tabone, J. C., Stamm, M. R., Gamper, H. B., and Meyer, R. B. (1994) Factors Influencing the Extent and Regiospecificity of Cross-Link Formation between Single-Stranded DNA and Reactive Complementary Oligodeoxynucleotides. *Biochemistry 33*, 375–383.

(163) Coleman, R. S., and Pires, R. M. (1997) Covalent cross-linking of duplex DNA using 4-thio-2'-deoxyuridine as a readily modifiable platform for introduction of reactive functionality into oligonucleotides. *Nucleic Acids Res. 25*, 4771–4777.

(164) Jöst, C., Nitsche, C., Scholz, T., Roux, L., and Klein, C. D. (2014) Promiscuity and selectivity in covalent enzyme inhibition: A systematic study of electrophilic fragments. *J. Med. Chem. 57*, 7590–7599.

(165) Agarwal, P., and Bertozzi, C. R. (2015) Site-specific antibody-drug conjugates: The nexus of bioorthogonal chemistry, protein engineering, and drug development. *Bioconjug. Chem. 26*, 176–192.

(166) Zhou, Q. (2017) Site-Specific Antibody Conjugation for ADC and Beyond. *Biomedicines 5*, 64.

(167) Nature Milestones Antibodies. Herceptin (anti-HER2) receives FDA approval for metastatic breast cancer. *http://www.nature.com/milestones/mileantibodies/full/mileantibodies41_supp.html*.

(168) McKeage, K., and Perry, C. M. (2002) Trastuzumab: a review of its use in the treatment of metastatic breast cancer overexpressing HER2. *Drugs 62*, 209–43.

(169) Slamon, D. J., Leyland-Jones, B., Shak, S., Fuchs, H., Paton, V., Bajamonde, A., Fleming, T., Eiermann, W., Wolter, J., Pegram, M., Baselga, J., and Norton, L. (2001) Use of chemotherapy plus a monoclonal antibody against HER2 for metastatic breast cancer that overexpresses HER2. *N. Engl. J. Med. 344*, 783–92.

(170) Loibl, S., and Gianni, L. (2017) HER2-positive breast cancer. *Lancet (London, England) 389*, 2415–2429.

(171) Engel, R. H., and Kaklamani, V. G. (2007) HER2-Positive Breast Cancer. *Drugs 67*, 1329–1341.

(172) Köstler, W. J., and Yarden, Y. (2011) The EGFR/ErbB Family in Breast Cancer: From Signalling to Therapy, in *Drugs for HER-2-positive Breast Cancer*, pp 1–32. Springer Basel, Basel.

(173) Lewis Phillips, G. D., Li, G., Dugger, D. L., Crocker, L. M., Parsons, K. L., Mai, E., Blättler, W. A., Lambert, J. M., Chari, R. V. J., Lutz, R. J., Wong, W. L. T., Jacobson, F. S., Koeppen, H., Schwall, R. H., Kenkare-Mitra, S. R., Spencer, S. D., and Sliwkowski, M. X. (2008) Targeting HER2-positive breast cancer with trastuzumab-DM1, an antibody-cytotoxic drug conjugate. *Cancer Res. 68*, 9280–90.

(174) Ahmad, A., and Sarkar, F. H. (2013) Current Understanding of Drug Resistance Mechanisms and Therapeutic Targets in HER2 Overexpressing Breast Cancers, in *Breast Cancer Metastasis and Drug Resistance*, pp 261–274. Springer New York, New York, NY.

(175) Spector, N., Xia, W., El-Hariry, I., Yarden, Y., and Bacus, S. (2007) HER2 therapy. Small molecule HER-2 tyrosine kinase inhibitors. *Breast Cancer Res. 9*, 205.

(176) Capelan, M., Pugliano, L., De Azambuja, E., Bozovic, I., Saini, K. S., Sotiriou, C., Loi, S., and Piccart-Gebhart, M. J. (2013) Pertuzumab: new hope for patients with HER2-positive breast cancer. *Ann. Oncol. 24*, 273–282.

(177) Valabrega, G., Montemurro, F., and Aglietta, M. (2007) Trastuzumab: Mechanism of action, resistance and future perspectives in HER2-overexpressing breast cancer. *Ann. Oncol. 18*, 977–984.

(178) Hudis, C. A. (2007) Trastuzumab — Mechanism of Action and Use in Clinical Practice. *N. Engl. J. Med. 357*, 39–51.

(179) Bartsch, R., and Steger, G. G. (2011) Trastuzumab as Adjuvant Treatment for Early Stage HER-2-positive Breast Cancer, in *Drugs for HER-2-positive Breast Cancer*, pp 33–49. Springer Basel, Basel.

(180) Maximiano, S., Magalhães, P., Guerreiro, M. P., and Morgado, M. (2016) Trastuzumab in the Treatment of Breast Cancer. *BioDrugs 30*, 75–86.

(181) Nahta, R., Yuan, L. X. H., Zhang, B., Kobayashi, R., and Esteva, F. J. (2005) Insulin-like Growth Factor-I Receptor/Human Epidermal Growth Factor Receptor 2 Heterodimerization Contributes to Trastuzumab Resistance of Breast Cancer Cells. *Cancer Res. 65*, 11118–11128.

(182) Nagy, P., Friedländer, E., Tanner, M., Kapanen, A. I., Carraway, K. L., Isola, J., and Jovin, T. M. (2005) Decreased accessibility and lack of activation of ErbB2 in JIMT-1, a herceptin-resistant, MUC4-expressing breast cancer cell line. *Cancer Res. 65*, 473–82.

(183) Morgillo, F., Orditura, M., Troiani, T., Martinelli, E., De Vita, F., and Ciardiello, F. (2011) Trastuzumab Resistance in Breast Cancer, in *Drugs for HER-2-positive Breast Cancer*, pp 51–60. Springer Basel, Basel.

(184) Sanchez-De Melo, I., Grassi, P., Ochoa, F., Bolivar, J., García-Cózar, F. J., and Durán-Ruiz, M. C. (2015) N-glycosylation profile analysis of Trastuzumab biosimilar candidates by Normal Phase Liquid Chromatography and MALDI-TOF MS approaches. *J. Proteomics 127*, 225–233.

(185) Schumacher, F. F., Nunes, J. P. M., Maruani, A., Chudasama, V., Smith, M. E. B., Chester, K. A., Baker, J. R., and Caddick, S. (2014) Next generation maleimides enable the controlled assembly of antibody–drug conjugates *via* native disulfide bond bridging. *Org. Biomol. Chem*. *12*, 7261–7269.

(186) Awoonor-Williams, E., and Rowley, C. N. (2016) Evaluation of Methods for the Calculation of the p K_a of Cysteine Residues in Proteins. *J. Chem. Theory Comput. 12*, 4662–4673.

(187) Roos, G., Foloppe, N., and Messens, J. (2012) Understanding the p K a of Redox Cysteines: The Key Role of Hydrogen Bonding . *Antioxid. Redox Signal. 18*, 94–127.

(188) Grillo-López, A. J., White, C. A., Dallaire, B. K., Varns, C. L., Shen, C. D., Wei, A., Leonard, J. E., McClure, A., Weaver, R., Cairelli, S., and Rosenberg, J. (2000) Rituximab: the first monoclonal antibody approved for the treatment of lymphoma. *Curr. Pharm. Biotechnol. 1*, 1–9.

(189) Genetech. (2006) FDA Approves Rituxan - The First Targeted B-Cell Therapy for Treatment of Moderate-to-Severe Rheumatoid Arthritis. *https://www.gene.com/media/press-releases/9407/2006-02-28/fda-approves-rituxan-the-first-targeted-*.

(190) Reff, M., Carner, K., Chambers, K., Chinn, P., Leonard, J., Raab, R., Newman, R., Hanna, N., and Anderson, D. (1994) Depletion of B cells in vivo by a chimeric mouse human monoclonal antibody to CD20. *Blood 83*.

(191) Dotan, E., Aggarwal, C., and Smith, M. R. (2010) Impact of Rituximab (Rituxan) on the Treatment of B-Cell Non-Hodgkin's Lymphoma. *P T 35*, 148–57.

(192) Kosmas, C., Stamatopoulos, K., Stavroyianni, N., Tsavaris, N., and Papadaki, T.

(2002) Anti-CD20-based therapy of B cell lymphoma: State of the art. *Leukemia 16*, 2004–2015.

(193) Cragg, M. S., Walshe, C. A., Ivanov, A. O., and Glennie, M. J. (2005) The biology of CD20 and its potential as a target for mAb therapy. *Curr. Dir. Autoimmun. 8*, 140–74.

(194) Naeim, F., Rao, P. N., Grody, W. W., and Naeim, F. (2008) Principles of Immunophenotyping, in *Hematopathology*, pp 27–55. Elsevier.

(195) Barnett, G. V., Balakrishnan, G., Chennamsetty, N., Meengs, B., Meyer, J., Bongers, J., Ludwig, R., Tao, L., Das, T. K., Leone, A., and Kar, S. R. (2018) Enhanced Precision of Circular Dichroism Spectral Measurements Permits Detection of Subtle Higher Order Structural Changes in Therapeutic Proteins. *J. Pharm. Sci. 107*, 2559–2569.

(196) Shen, B.-Q., Xu, K., Liu, L., Raab, H., Bhakta, S., Kenrick, M., Parsons-Reponte, K. L., Tien, J., Yu, S.-F., Mai, E., Li, D., Tibbitts, J., Baudys, J., Saad, O. M., Scales, S. J., McDonald, P. J., Hass, P. E., Eigenbrot, C., Nguyen, T., Solis, W. A., Fuji, R. N., Flagella, K. M., Patel, D., Spencer, S. D., Khawli, L. A., Ebens, A., Wong, W. L., Vandlen, R., Kaur, S., Sliwkowski, M. X., Scheller, R. H., Polakis, P., and Junutula, J. R. (2012) Conjugation site modulates the in vivo stability and therapeutic activity of antibody-drug conjugates. *Nat. Biotechnol. 30*, 184–9.

(197) Walport, M. J. (2001) Complement. *N. Engl. J. Med.* (Mackay, I. R., and Rosen, F. S., Eds.) *344*, 1058–1066.

(198) Ricklin, D., Hajishengallis, G., Yang, K., and Lambris, J. D. (2010) Complement: a key system for immune surveillance and homeostasis. *Nat. Immunol. 11*, 785–97.

(199) Mathern, D. R., and Heeger, P. S. (2015) Molecules great and small: The complement system. *Clin. J. Am. Soc. Nephrol. 10*, 1636–1650.

(200) Morgan, B. P., and Harris, C. L. (2015) Complement, a target for therapy in inflammatory and degenerative diseases. *Nat. Rev. Drug Discov. 14*, 857–877.

(201) Mollnes, T. E., Song, W. C., and Lambris, J. D. (2002) Complement in inflammatory tissue damage and disease. *Trends Immunol. 23*, 61–64.

(202) Cooper, N. R. (1985) The classical complement pathway: activation and regulation of the first complement component. *Adv. Immunol. 37*, 151–216.

(203) Thiel, S., Jensen, L., Degn, S. E., Nielsen, H. J., Gál, P., Dobó, J., and Jensenius, J. C. (2012) Mannan-binding lectin (MBL)-associated serine protease-1 (MASP-1), a serine protease associated with humoral pattern-recognition molecules: normal and acute-phase levels in serum and stoichiometry of lectin pathway components. *Clin. Exp. Immunol. 169*, 38–48.

(204) Kim, D. D., and Song, W.-C. (2006) Membrane complement regulatory proteins. *Clin. Immunol. 118*, 127–136.

(205) Medicus, R. G., Götze, O., and Müller-Eberhard, H. J. (1976) Alternative pathway of complement: recruitment of precursor properdin by the labile C3/C5 convertase and the potentiation of the pathway. *J. Exp. Med. 144*, 1076–93.

(206) Merle, N. S., Church, S. E., Fremeaux-Bacchi, V., and Roumenina, L. T. (2015) Complement System Part I - Molecular Mechanisms of Activation and Regulation. *Front. Immunol. 6*, 262.

(207) Medof, M. E., Kinoshita, T., and Nussenzweig, V. (1984) Inhibition of complement activation on the surface of cells after incorporation of decay-accelerating factor (DAF) into their membranes. *J. Exp. Med. 160*, 1558–78.

(208) Kim, Y. U., Kinoshita, T., Molina, H., Hourcade, D., Seya, T., Wagner, L. M., and Holers, V. M. (1995) Mouse complement regulatory protein Crry/p65 uses the specific mechanisms of both human decay-accelerating factor and membrane cofactor protein. *J. Exp. Med. 181*, 151–9.

(209) Makou, E., Herbert, A. P., and Barlow, P. N. (2013) Functional Anatomy of Complement Factor H. *Biochemistry 52*, 3949–3962.

(210) Donoso, L. A., Vrabec, T., and Kuivaniemi, H. (2010) The Role of Complement Factor H in Age-related Macular Degeneration: A Review. *Surv. Ophthalmol. 55*, 227–246.

(211) Ferreira, V. P., Pangburn, M. K., and Cortés, C. (2010) Complement control protein factor H: The good, the bad, and the inadequate. *Mol. Immunol. 47*, 2187–2197.

(212) Clark, S., and Bishop, P. (2014) Role of Factor H and Related Proteins in Regulating Complement Activation in the Macula, and Relevance to Age-Related Macular Degeneration. *J. Clin. Med. 4*, 18–31.

(213) Sahu, A., and Lambris, J. D. (2001) Structure and biology of complement protein C3, a connecting link between innate and acquired immunity. *Immunol. Rev. 180*, 35–48.

(214) Gros, P., Milder, F. J., and Janssen, B. J. C. (2008) Complement driven by conformational changes. *Nat. Rev. Immunol. 8*, 48–58.

(215) Erdei, A., Sándor, N., Mácsik-Valent, B., Lukácsi, S., Kremlitzka, M., and Bajtay, Z. (2016) The versatile functions of complement C3-derived ligands. *Immunol. Rev. 274*, 127–140.

(216) Hannan, J. P., Young, K. A., Guthridge, J. M., Asokan, R., Szakonyi, G., Chen, X. S., and Holers, V. M. (2005) Mutational analysis of the complement receptor type 2 (CR2/CD21)-C3d interaction reveals a putative charged SCR1 binding site for C3d. *J. Mol. Biol. 346*, 845–858.

(217) Dempsey, P. W., Allison, M. E., Akkaraju, S., Goodnow, C. C., and Fearon, D. T. (1996) C3d of complement as a molecular adjuvant: bridging innate and acquired immunity. *Science 271*, 348–50.

(218) Somerville, G. A., and Proctor, R. A. The Biology of Staphylococci, in *Staphylococci in Human Disease*, pp 1–18. Wiley-Blackwell, Oxford, UK.

(219) Lowy, F. (1998) Staphylococcus aureus infections. *N. Engl. J. Med. 339*, 520–

532.

(220) Stryjewski, M. E., Nannini, E. C., and Corey, G. R. Skin and Soft Tissue Infections, in *Staphylococci in Human Disease*, pp 378–394. Wiley-Blackwell, Oxford, UK.

(221) Gresham, H. D., and Foster, T. J. Host Defense against Staphylococcal Infection, in *Staphylococci in Human Disease*, pp 147–169. Wiley-Blackwell, Oxford, UK.

(222) de Haas, C. J. C., Veldkamp, K. E., Peschel, A., Weerkamp, F., Van Wamel, W. J. B., Heezius, E. C. J. M., Poppelier, M. J. J. G., Van Kessel, K. P. M., and van Strijp, J. A. G. (2004) Chemotaxis inhibitory protein of Staphylococcus aureus, a bacterial antiinflammatory agent. *J. Exp. Med. 199*, 687–95.

(223) Foster, T. J., Geoghegan, J. A., Ganesh, V. K., and Höök, M. (2014) Adhesion, invasion and evasion: the many functions of the surface proteins of Staphylococcus aureus. *Nat. Rev. Microbiol. 12*, 49–62.

(224) Foster, T. J. (2005) Immune evasion by staphylococci. *Nat. Rev. Microbiol. 3*, 948–58.

(225) Thakker, M., Park, J. S., Carey, V., and Lee, J. C. (1998) Staphylococcus aureus serotype 5 capsular polysaccharide is antiphagocytic and enhances bacterial virulence in a murine bacteremia model. *Infect. Immun. 66*, 5183–5189.

(226) Thammavongsa, V., Kim, H. K., Missiakas, D., and Schneewind, O. (2015) Staphylococcal manipulation of host immune responses. *Nat. Rev. Microbiol. 13*, 529–43.

(227) Rooijakkers, S. H. M., Van Wamel, W. J. B., Ruyken, M., Van Kessel, K. P. M., and Van Strijp, J. A. G. (2005) Anti-opsonic properties of staphylokinase. *Microbes Infect. 7*, 476–484.

(228) Menestrina, G., Dalla Serra, M., Comai, M., Coraiola, M., Viero, G., Werner, S., Colin, D. A., Monteil, H., and Prévost, G. (2003) Ion channels and bacterial infection:

The case of β-barrel pore-forming protein toxins of Staphylococcus aureus. *FEBS Lett. 552*, 54–60.

(229) Lambris, J. D., Ricklin, D., and Geisbrecht, B. V. (2008) Complement evasion by human pathogens. *Nat. Rev. Microbiol. 6*, 132–142.

(230) Hammel, M., Sfyroera, G., Ricklin, D., Magotti, P., Lambris, J. D., and Geisbrecht, B. V. (2007) A structural basis for complement inhibition by Staphylococcus aureus. *Nat. Immunol. 8*, 430–437.

(231) Lee, L. Y. L., Liang, X., Höök, M., and Brown, E. L. (2004) Identification and characterization of the C3 binding domain of the Staphylococcus aureus extracellular fibrinogen-binding protein (Efb). *J. Biol. Chem. 279*, 50710–50716.

(232) Jongerius, I., Köhl, J., Pandey, M. K., Ruyken, M., van Kessel, K. P. M., van Strijp, J. A. G., and Rooijakkers, S. H. M. (2007) Staphylococcal complement evasion by various convertase-blocking molecules. *J. Exp. Med. 204*, 2461–71.

(233) Rooijakkers, S. H. M., Ruyken, M., Roos, A., Daha, M. R., Presanis, J. S., Sim, R. B., van Wamel, W. J. B., van Kessel, K. P. M., and van Strijp, J. A. G. (2005) Immune evasion by a staphylococcal complement inhibitor that acts on C3 convertases. *Nat. Immunol. 6*, 920–927.

(234) Langley, R., Wines, B., Willoughby, N., Basu, I., Proft, T., and Fraser, J. D. (2005) The Staphylococcal Superantigen-Like Protein 7 Binds IgA and Complement C5 and Inhibits IgA-Fc RI Binding and Serum Killing of Bacteria. *J. Immunol. 174*, 2926–2933.

(235) Bunschoten, A., Ippel, J. H., Kruijtzer, J. A. W., Feitsma, L., De Haas, C. J. C., Liskamp, R. M. J., and Kemmink, J. (2011) A peptide mimic of the chemotaxis inhibitory protein of Staphylococcus aureus: Towards the development of novel anti-inflammatory compounds. *Amino Acids 40*, 731–740.

(236) Cedergren, L., Andersson, R., Jansson, B., Uhlén, M., and Nilsson, B. (1993) Mutational analysis of the interaction between staphylococcal protein A and human

IgG1. *Protein Eng. 6*, 441–8.

(237) Zhang, L., Jacobson, K., Vasi, J., Lindberg, M., and Frykberg, L. (2015) second IgG-binding protein in *408*, 985–991.

(238) Burman, J. D., Leung, E., Atkins, K. L., Seaghdha, M. N. O., Bernadó, P., Bagby, S., Svergun, D. I., Foster, T. J., David, E., and Elsen, J. M. H. Van Den. (2009) Interaction of Human Complement with Sbi , a Staphylococcal Immunoglobulin-binding Protein : *J. Biol. Chem*. *283*, 17579–17593.

(239) Smith, E. J., Corrigan, R. M., van der Sluis, T., Gründling, A., Speziale, P., Geoghegan, J. A., and Foster, T. J. (2012) The immune evasion protein Sbi of Staphylococcus aureus occurs both extracellularly and anchored to the cell envelope by binding lipoteichoic acid. *Mol. Microbiol. 83*, 789–804.

(240) Atkins, K. L., Burman, J. D., Chamberlain, E. S., Cooper, J. E., Poutrel, B., Bagby, S., Jenkins, A. T. A., Feil, E. J., and van den Elsen, J. M. H. (2008) S. aureus IgG-binding proteins SpA and Sbi: Host specificity and mechanisms of immune complex formation. *Mol. Immunol. 45*, 1600–1611.

(241) Fries, L. F., Gaither, T. a, Hammer, C. H., and Frank, M. M. (1984) C3b covalently bound to IgG demonstrates a reduced rate of inactivation by factors H and I. *J. Exp. Med. 160*, 1640–1655.

(242) Sim, R. B., Twose, T. M., Paterson, D. S., and Sim, E. (1981) The covalent-binding reaction of complement component C3. *Biochem. J. 193*, 115–27.

(243) Yang, Y., Back, C., Graewert, M., Wahid, A., Denton, H., Kildani, R., Paulin, J., Woerner, K., Kaiser, W., Svergun, D. I., Sartbaeva, A., Watts, A., Marchbank, K., and Elsen, J. M. van den. (2018) Utilisation of staphylococcal immune evasion protein Sbi as a novel vaccine adjuvant. *bioRxiv* 413294.

(244) Spiess, C., Zhai, Q., and Carter, P. J. (2015) Alternative molecular formats and therapeutic applications for bispecific antibodies. *Mol. Immunol. 67*, 95–106.

(245) Krishnamurthy, A., and Jimeno, A. (2018) Bispecific antibodies for cancer therapy: A review. *Pharmacol. Ther. 185*, 122–134.

(246) Stein, C., Schubert, I., and Fey, G. H. (2012) Natural Killer (NK)- and T-Cell Engaging Antibody-Derived Therapeutics. *Antibodies*.

(247) Huehls, A. M., Coupet, T. A., and Sentman, C. L. (2015) Bispecific T-cell engagers for cancer immunotherapy. *Immunol. Cell Biol. 93*, 290–296.

(248) Lu, D., Jimenez, X., Zhang, H., Wu, Y., Bohlen, P., Witte, L., and Zhu, Z. (2001) Complete inhibition of vascular endothelial growth factor (VEGF) activities with a bifunctional diabody directed against both VEGF kinase receptors, fms-like tyrosine kinase receptor and kinase insert domain-containing receptor. *Cancer Res. 61*, 7002–8.

(249) Linke, R., Klein, A., and Seimetz, D. (2010) Catumaxomab: clinical development and future directions. *MAbs 2*, 129–136.

(250) Lindhofer, H., Mocikat, R., Steipe, B., and Thierfelder, S. (1995) Preferential species-restricted heavy light-chain pairing in rat mouse quadromas - implications for a single-step purification of bispecific antibodies. *J. Immunol. 155*, 219–225.

(251) Byrne, H., Conroy, P. J., Whisstock, J. C., and O'Kennedy, R. J. (2013) A tale of two specificities: Bispecific antibodies for therapeutic and diagnostic applications. *Trends Biotechnol. 31*, 621–632.

(252) Suresh, M. R., Cuello, A. C., and Milstein, C. (1986) Advantages of bispecific hybridomas in one-step immunocytochemistry and immunoassays. *Proc. Natl. Acad. Sci. U. S. A. 83*, 7989–93.

(253) Viardot, A., and Bargou, R. (2018) Bispecific antibodies in haematological malignancies. *Cancer Treat. Rev. 65*, 87–95.

(254) Kontermann, R. E. (2005) Recombinant bispecific antibodies for cancer therapy. *Acta Pharmacol. Sin. 26*, 1–9.

(255) Wu, J., Fu, J., Zhang, M., and Liu, D. (2015) Blinatumomab: a bispecific T cell engager (BiTE) antibody against CD19/CD3 for refractory acute lymphoid leukemia. *J. Hematol. Oncol. 8*, 1–7.

(256) Hull, E. A., Livanos, M., Miranda, E., Smith, M. E. B., Chester, K. A., and Baker, J. R. (2014) Homogeneous bispecifics by disulfide bridging. *Bioconjug. Chem. 25*, 1395–1401.

(257) Ridgway, J. B., Presta, L. G., and Carter, P. (1996) "Knobs-into-holes" engineering of antibody CH3 domains for heavy chain heterodimerization. *Protein Eng. 9*, 617–21.

(258) Schaefer, W., Regula, J. T., Bahner, M., Schanzer, J., Croasdale, R., Durr, H., Gassner, C., Georges, G., Kettenberger, H., Imhof-Jung, S., Schwaiger, M., Stubenrauch, K. G., Sustmann, C., Thomas, M., Scheuer, W., and Klein, C. (2011) Immunoglobulin domain crossover as a generic approach for the production of bispecific IgG antibodies. *Proc. Natl. Acad. Sci. 108*, 11187–11192.

(259) Spiess, C., Merchant, M., Huang, A., Zheng, Z., Yang, N. Y., Peng, J., Ellerman, D., Shatz, W., Reilly, D., Yansura, D. G., and Scheer, J. M. (2013) Bispecific antibodies with natural architecture produced by co-culture of bacteria expressing two distinct half-antibodies. *Nat. Biotechnol. 31*, 753–758.

(260) MacChi, F. D., Yang, F., Li, C., Wang, C., Dang, A. N., Marhoul, J. C., Zhang, H. M., Tully, T., Liu, H., Yu, X. C., and Michels, D. A. (2015) Absolute Quantitation of Intact Recombinant Antibody Product Variants Using Mass Spectrometry. *Anal. Chem. 87*, 10475–10482.

(261) Giese, G., Williams, A., Rodriguez, M., and Persson, J. (2018) Bispecific antibody process development: Assembly and purification of knob and hole bispecific antibodies. *Biotechnol. Prog. 34*, 397–404.

(262) Müller, D., and Kontermann, R. E. (2010) Bispecific Antibodies for Cancer Immunotherapy. *BioDrugs 24*, 89–98.

(263) Wu, X., Sereno, A. J., Huang, F., Lewis, S. M., Lieu, R. L., Weldon, C., Torres, C., Fine, C., Batt, M. A., Fitchett, J. R., Glasebrook, A. L., Kuhlman, B., and Demarest, S. J. (2015) Fab-based bispecific antibody formats with robust biophysical properties and biological activity. *MAbs 7*, 470–482.

(264) Fournier, P., and Schirrmacher, V. (2013) Bispecific antibodies and trispecific immunocytokines for targeting the immune system against cancer: Preparing for the future. *BioDrugs 27*, 35–53.

(265) Ramagopal, U. A., Liu, W., Garrett-Thomson, S. C., Bonanno, J. B., Yan, Q., Srinivasan, M., Wong, S. C., Bell, A., Mankikar, S., Rangan, V. S., Deshpande, S., Korman, A. J., and Almo, S. C. (2017) Structural basis for cancer immunotherapy by the first-in-class checkpoint inhibitor ipilimumab. *Proc. Natl. Acad. Sci. 114*, E4223–E4232.

(266) Lipson, E. J., and Drake, C. G. (2011) Ipilimumab: an anti-CTLA-4 antibody for metastatic melanoma. *Clin. Cancer Res. 17*, 6958–62.

(267) Syn, N. L., Teng, M. W. L., Mok, T. S. K., and Soo, R. A. (2017) De-novo and acquired resistance to immune checkpoint targeting. *Lancet Oncol. 18*, e731–e741.

(268) Mansh, M. (2011) Ipilimumab and cancer immunotherapy: a new hope for advanced stage melanoma. *Yale J. Biol. Med. 84*, 381–9.

(269) Yu, L. Y., Li, M. P., Kuang, D. Bin, Zhang, C. M., and Chen, X. P. (2016) New immunotherapy strategies in breast cancer. *Chinese Pharmacol. Bull. 32*, 1037–1040.

(270) Sears, A. K., Perez, S. A., Clifton, G. T., Benavides, L. C., Gates, J. D., Clive, K. S., Holmes, J. P., Shumway, N. M., Van Echo, D. C., Carmichael, M. G., Ponniah, S., Baxevanis, C. N., Mittendorf, E. A., Papamichail, M., and Peoples, G. E. (2011) AE37: a novel T-cell-eliciting vaccine for breast cancer. *Expert Opin. Biol. Ther. 11*, 1543–1550.

(271) Kiewe, P., Hasmüller, S., Kahlert, S., Heinrigs, M., Rack, B., Marmé, A., Korfel, A., Jäger, M., Lindhofer, H., Sommer, H., Thiel, E., and Untch, M. (2006) Phase I Trial

of the Trifunctional Anti-HER2 x Anti-CD3 Antibody Ertumaxomab in Metastatic Breast Cancer. *Clin. Cancer Res. 12*, 3085–3091.

(272) ThermoFisher. Antibody Fragmentation - UK. *https://www.thermofisher.com/uk/en/home/life-science/antibodies/antibodies-learning-center/antibodies-resource-library/antibody-methods/antibody-fragmentation.html*.

(273) Bonger, K. M., van den Berg, R. J. B. H. N., Heitman, L. H., IJzerman, A. P., Oosterom, J., Timmers, C. M., Overkleeft, H. S., and van der Marel, G. A. (2007) Synthesis and evaluation of homo-bivalent GnRHR ligands. *Bioorg. Med. Chem. 15*, 4841–4856.

(274) Fujino, T., Naitoh, H., Miyagawa, S., Kimura, M., Kawasaki, T., Yoshida, K., Inoue, H., Takagawa, H., and Tokunaga, Y. (2018) Formation of [2]- and [3]Rotaxanes through Bridging under Kinetic and Thermodynamic Control. *Org. Lett. 20*, 369–372.

(275) Kimura, Y., Miyabara, Y., Terashima, T., and Sawamoto, M. (2016) Polyacrylamide pseudo crown ethers via hydrogen bond-assisted cyclopolymerization. *J. Polym. Sci. Part A Polym. Chem. 54*, 3294–3302.

(276) Gichinga, M. G., and Striegler, S. (2009) Regioselective alkylation of hydroxysalicylaldehydes. *Tetrahedron 65*, 4917–4922.

(277) Sastraruji, K., Sastraruji, T., Pyne, S. G., Ung, A. T., Jatisatienr, A., and Lie, W. (2010) Semisynthesis and Acetylcholinesterase Inhibitory Activity of Stemofoline Alkaloids and Analogues. *J. Nat. Prod. 73*, 935–941.

(278) HIRATA, T., WATANABE, M., MIURA, S., IJICHI, K., FUKASAWA, M., and SAKAKIBARA, R. (2000) Inhibition of Tumor Cell Growth by A Specific 6-Phosphofructo-2-kinase Inhibitor, *N* -Bromoacetylethanolamine Phosphate, and Its Analogues. *Biosci. Biotechnol. Biochem. 64*, 2047–2052.

(279) Yong, S. R., Ung, A. T., Pyne, S. G., Skelton, B. W., and White, A. H. (2007) Syntheses of spiro[cyclopropane-1,3′-oxindole]-2-carboxylic acid and cyclopropa[c]quinoline-7b-carboxylic acid and their derivatives. *Tetrahedron 63*, 1191–

1199.

(280) Abou-Seri, S. M., Eldehna, W. M., Ali, M. M., and Abou El Ella, D. A. (2016) 1-Piperazinylphthalazines as potential VEGFR-2 inhibitors and anticancer agents: Synthesis and in vitro biological evaluation. *Eur. J. Med. Chem. 107*, 165–179.

(281) Fyles, T. M., James, T. D., Pryhitka, A., and Zojaji, M. (1993) Assembly of Ion Channel Mimics from a Modular Construction Set. *J. Org. Chem. 58*, 7456–7468.

(282) Ramkumar, K., Samanta, S., Kyani, A., Yang, S., Tamura, S., Ziemke, E., Stuckey, J. A., Li, S., Chinnaswamy, K., Otake, H., Debnath, B., Yarovenko, V., Sebolt-Leopold, J. S., Ljungman, M., and Neamati, N. (2016) Mechanistic evaluation and transcriptional signature of a glutathione S-transferase omega 1 inhibitor. *Nat. Commun. 7*, 13084.

(283) Tripathi, A., and Pandey, P. S. (2011) Hydrogen sulfate-induced organogelation of a bile acid based anion-receptor. *Tetrahedron Lett. 52*, 3558–3560.

(284) Corrie, J. E. T., Craik, J. S., and Munasinghe, V. R. N. (1998) A homobifunctional rhodamine for labeling proteins with defined orientations of a fluorophore. *Bioconjug. Chem. 9*, 160–167.

(285) Goswami, L. N., Houston, Z. H., Sarma, S. J., Jalisatgi, S. S., and Hawthorne, M. F. (2013) Efficient synthesis of diverse heterobifunctionalized clickable oligo(ethylene glycol) linkers: potential applications in bioconjugation and targeted drug delivery. *Org. Biomol. Chem. 11*, 1116.

(286) Heng, S., Stieglitz, K. A., Eldo, J., Xia, J., Cardia, J. P., and Kantrowitz, E. R. (2006) T-state Inhibitors of E. coli Aspartate Transcarbamoylase that Prevent the Allosteric Transition. *Biochemistry 45*, 10062–10071.

(287) Hynes, M. J., and Maurer, J. A. (2012) Unmasking Photolithography: A Versatile Way to Site-Selectively Pattern Gold Substrates. *Angew. Chemie Int. Ed. 51*, 2151–2154.

(288) Dreaden, E. C., Gryder, B. E., Austin, L. A., Tene Defo, B. A., Hayden, S. C., Pi, M., Quarles, L. D., Oyelere, A. K., and El-Sayed, M. A. (2012) Antiandrogen gold nanoparticles dual-target and overcome treatment resistance in hormone-insensitive prostate cancer cells. *Bioconjug. Chem. 23*, 1507–12.

(289) Anderson, J. P., Reynolds, B. L., Baum, K., and Williams, J. G. (2010) Fluorescent Structural DNA Nanoballs Functionalized with Phosphate-Linked Nucleotide Triphosphates. *Nano Lett. 10*, 788–792.

(290) Nishiyama, J., and Kuninori, T. (1992) Assay of thiols and disulfides based on the reversibility of N-ethylmaleimide alkylation of thiols combined with electrolysis. *Anal. Biochem. 200*, 230–234.

(291) Roberts, M. J., Bentley, M. D., and Harris, J. M. (2012) Chemistry for peptide and protein PEGylation. *Adv. Drug Deliv. Rev. 64*, 116–127.

(292) Wilkinson, I. C., Fowler, S. B., Machiesky, L. A., Miller, K., Hayes, D. B., Adib, M., Her, C., Borrok, M. J., Tsui, P., Burrell, M., Corkill, D. J., Witt, S., Lowe, D. C., and Webster, C. I. (2013) Monovalent IgG4 molecules: Immunoglobulin Fc mutations that result in a monomeric structure. *MAbs 5*, 406–417.

(293) Merchant, M., Ma, X., Maun, H. R., Zheng, Z., Peng, J., Romero, M., Huang, A., Yang, N. -y., Nishimura, M., Greve, J., Santell, L., Zhang, Y.-W., Su, Y., Kaufman, D. W., Billeci, K. L., Mai, E., Moffat, B., Lim, A., Duenas, E. T., Phillips, H. S., Xiang, H., Young, J. C., Vande Woude, G. F., Dennis, M. S., Reilly, D. E., Schwall, R. H., Starovasnik, M. A., Lazarus, R. A., and Yansura, D. G. (2013) Monovalent antibody design and mechanism of action of onartuzumab, a MET antagonist with anti-tumor activity as a therapeutic agent. *Proc. Natl. Acad. Sci. 110*, E2987–E2996.

(294) Herbener, P., Schönfeld, K., König, M., Germer, M., Przyborski, J. M., Bernöster, K., and Schüttrumpf, J. (2018) Functional relevance of in vivo half antibody exchange of an IgG4 therapeutic antibody-drug conjugate. *PLoS One 13*, 1–22.

(295) Schuurman, J., Van Ree, R., Perdok, G. J., Van Doorn, H. R., Tan, K. Y., and

Aalberse, R. C. (1999) Normal human immunoglobulin G4 is bispecific: it has two different antigen-combining sites. *Immunology 97*, 693–8.

(296) Colombo, M., Sommaruga, S., Mazzucchelli, S., Polito, L., Verderio, P., Galeffi, P., Corsi, F., Tortora, P., and Prosperi, D. (2012) Site-Specific Conjugation of ScFvs Antibodies to Nanoparticles by Bioorthogonal Strain-Promoted Alkyne – Nitrone Cycloaddition. *Angew Chem Int Ed Engl. 51*, 496–499.

(297) Yi, G., Son, J., Yoo, J., Park, C., and Koo, H. (2018) Application of click chemistry in nanoparticle modification and its targeted delivery 1–8.

(298) Sleep, D., Cameron, J., and Evans, L. R. (2013) Albumin as a versatile platform for drug half-life extension. *Biochim. Biophys. Acta - Gen. Subj. 1830*, 5526–5534.

(299) Kellner, C., Otte, A., Cappuzzello, E., Klausz, K., and Peipp, M. (2017) Modulating Cytotoxic Effector Functions by Fc Engineering to Improve Cancer Therapy. *Transfus. Med. Hemother. 44*, 327–336.

(300) Tang, X., and Bruce, J. E. (2009) Chemical Cross-Linking for Protein–Protein Interaction Studies, pp 283–293. Humana Press.

(301) Martin, A., Gissot, A., Barthélémy, P., Benizri, S., Vialet, B., and Grinstaff, M. W. (2019) Bioconjugated Oligonucleotides: Recent Developments and Therapeutic Applications. *Bioconjug. Chem.*

(302) Yang, Y., Back, C. R., Gräwert, M. A., Wahid, A. A., Denton, H., Kildani, R., Paulin, J., Wörner, K., Kaiser, W., Svergun, D. I., Sartbaeva, A., Watts, A. G., Marchbank, K. J., and van den Elsen, J. M. H. (2018) Utilization of Staphylococcal Immune Evasion Protein Sbi as a Novel Vaccine Adjuvant. *Front. Immunol. 9*, 3139.

(303) Darvin, P., Toor, S. M., Sasidharan Nair, V., and Elkord, E. (2018) Immune checkpoint inhibitors: recent progress and potential biomarkers. *Exp. Mol. Med. 50*, 165.

(304) Xing, L., Hung, M., Bonfiglio, T., Hicks, D. G., and Tang, P. (2010) The expression patterns of eR, pR, HeR2, cK5/6, eGFR, Ki-67 and AR by

Immunohistochemical Analysis in Breast cancer cell Lines 1–7.

11 Appendices

11.1 Cloning vector

pET-15b sequence landmarks	
T7 promoter	463-479
T7 transcription start	452
His•Tag coding sequence	362-380
Multiple cloning sites	
(*Nde* I - *Bam* H I)	319-335
T7 terminator	213-259
lacI coding sequence	(866-1945)
pBR322 origin	3882
bla coding sequence	4643-5500

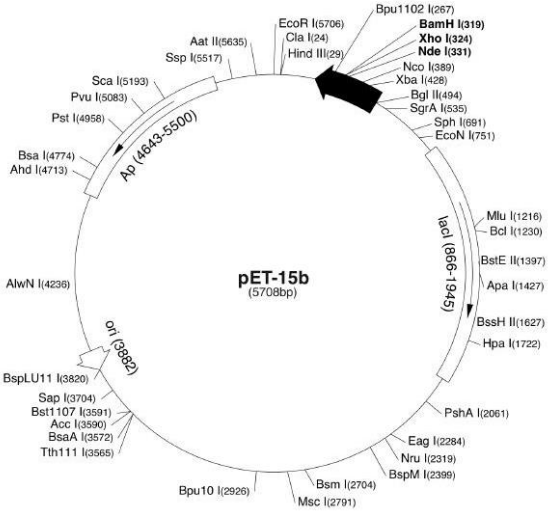

11.2 HPLC standard curves of glutathione conjugates

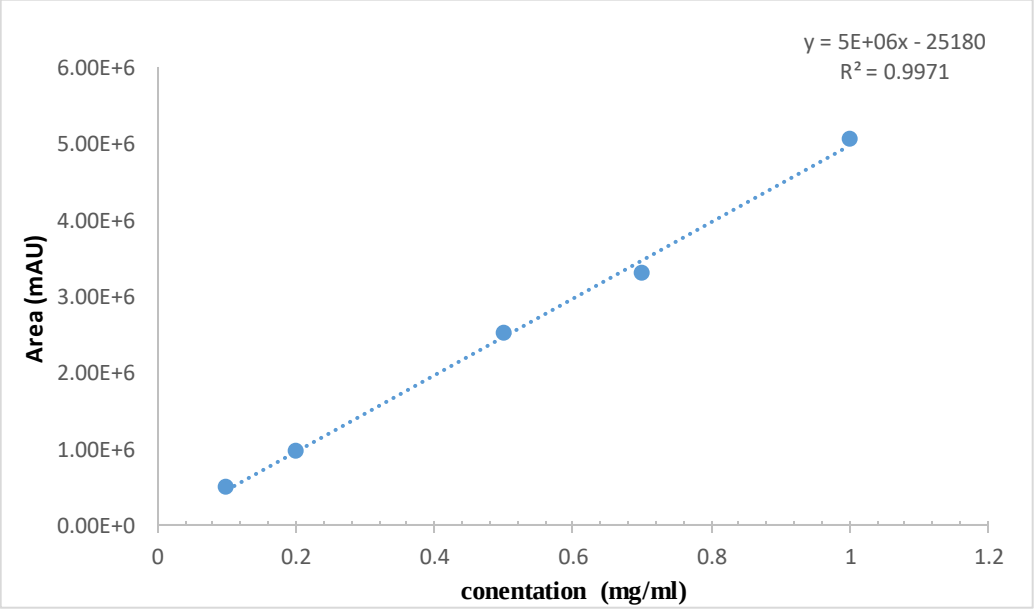

Figure 11.1. Standard curve of Mal-glutathione conjugate (4.19)

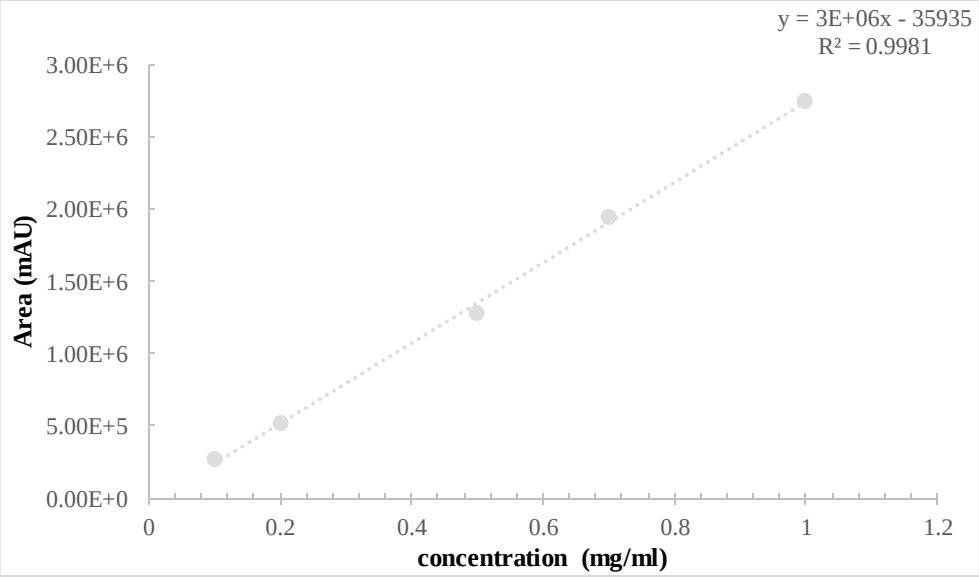

Figure 11.2. Standard curve of 3.5 DAB-glutathione conjugate (**4.17**)

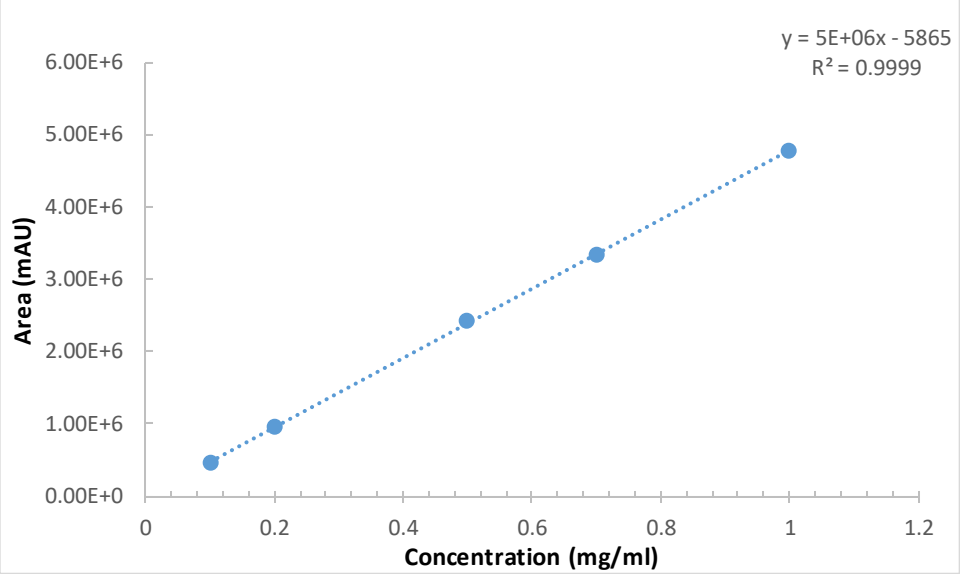

Figure 11.3. Standard curve of 3.4 DAB-glutathione conjugate (**4.18**)

11.3 Cell line and toxicity assay

11.3.1 Materials and methods

The breast cancer cell lines BT474 were purchased from ATCC. BT474 cells were

maintained in at 37℃, 5% CO_2 in RPMI 1640, HyClone™ medium supplemented with 10% foetal calf serum and 1% of antibiotic mixture: cell culture grade streptomycin 10mg/ml and cell culture grade penicillin 10,000 units/ml (named as complete medium). Medium renewed three times weekly, and 1:3 subcultivation ratio was conducted on weekly basis.

BT474 Cells (ATCC® HTB-20™) were plated in 96-well plates at 10,000 cells/well and allowed to attach for 24 h. Cells were counted using haemocytometer counting device. Briefly, cells in T-75 flask (10 mls) were harvested using 2 mls TrypLE™ express enzyme (Trypsin Replacement) and incubated for 5 minutes at 37 ℃, 5% CO_2. Then, cells were suspended in complete medium (8 mls), centrifuged for 3 minutes at 1000 rpm, and re-suspended in complete medium. Cells were counted in the 4 corner large squares (1 mm^2) of the haemocytometer and averaged.

Serial dilution of Tmab, Tmab-Sbi conjugates were incubated with the cells at concentrations ranging from 100 to 0 mg/ml in complete growth medium in presence of 2% HCS. After 96 h cell viability was measured using the LIVE/DEAD® Viability/Cytotoxicity Kit. The assay was followed according to the manufacture protocol, calcein AM was prepared in sterile PBS with final concentration of 0.5 μM. 100 μL of the reagents solution was added to each well which pre-incubated with 100 μL of PBS and held in dark place for 30 minutes at 37℃.

The fluorescence measurements were analysed using plate reader (SPECRTOstar OMEGA plate reader, BMG-LAB TECH, MARS data analysis software 3.00R2). Green Fluorescence of live cells was measured at ex/em ~495 nm/~515 nm.

11.3.2 *In vitro* cytotoxicity assay

With the pure Tmab-Sbi conjugate in hand, we set out to evaluate their activity *in vitro*. BT-474 cancer cell lines belong to Luminal B subtype of cancer, which was shown to be ER negative, PR positive, HER-2 positive.[304] These cells were cultivated according to the product specifications (ATCC® HTB-20™).

Cell survival percent was measured using LIVE/DEAD® Viability/Cytotoxicity Kit to

construct dose response curve for Tmab and Tmab-Sbi IV conjugate.

This assay is based on using two reagents: the nonfluorescent, cell-permeant calcein AM which activated upon internalisation in live cells via the activity of the intracellular ubiquitous esterase enzyme to the intensely fluorescent calcein (green fluorescence in live cells) and EthD-1 which enters damaged cells and undergoes a 40-fold enhancement of fluorescence upon binding to nucleic acids (bright red fluorescence in dead cells). We tend to mainly focus on using calcein AM to test cellular viability.

In order to evaluate the optimum and compatible concentration of calcein AM reagents with BT-474 cells, optimization tests of the working concentration of the reagents were conducted according to the manufacturer's instructions. The best working concentration of was chosen as the lowest reagent concentration that gives sufficient signal as observed under fluorescence microscope. As such a range between 0.1-10 µM concentrations of calcein AM were evaluated and 0.5 µM calcein AM concentration was found the optimum concentration to work with.

Cellular density was appraised at 5,000, 10,000 and 25,000 cells/well. Both 5,000 and 25,000 cells/well were not optimum to attain reflective fluorescence measurements. As 5,000 cells/well was very low density and 25,000 cells/well was very dense and cells have died because of lack of sufficient nutrients. Therefore, BT474 Cells (ATCC® HTB-20™) were plated in 96-well plates at 10,000 cells/well and allowed to attach for 24 h. *In vitro* cytotoxicity of Tmab and Tmab-Sbi conjugate were compared over the concentration range between 0.001 µg/ml to 100 µg/ml.

Tmab and Tmab-Sbi conjugates were incubated with the cells in complete growth medium in presence of 2% human serum complement (HSC). After 96 h cell viability was measured using the LIVE/DEAD® Viability/Cytotoxicity Kit. The assay was followed according to the manufacture protocol. The fluorescence measurements at (ex/em ~495 nm/~515 nm) were analysed using plate reader.

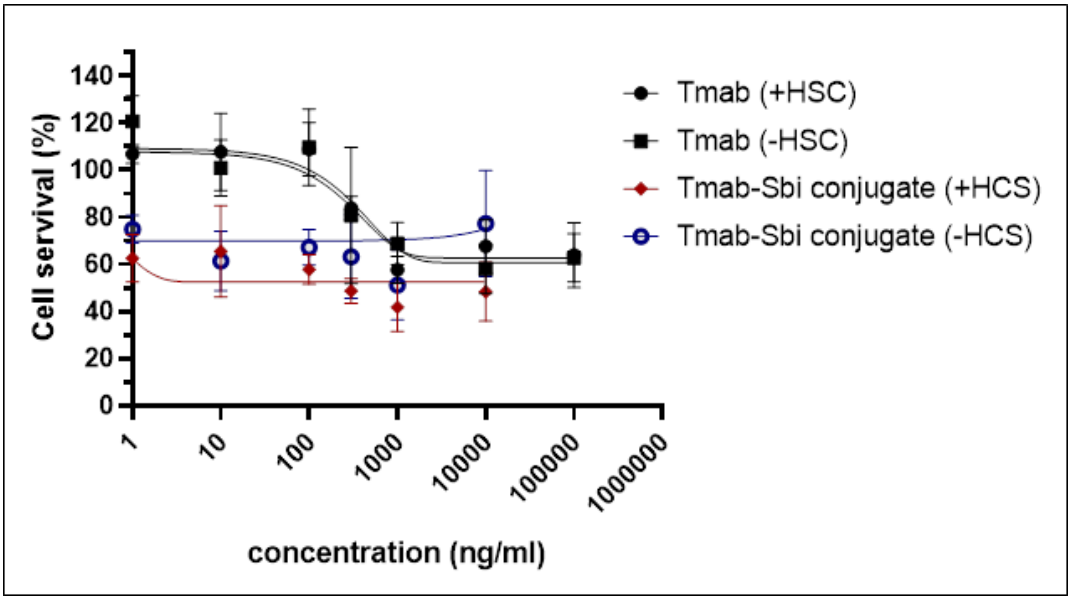

Figure 11.4. Inhibition of the survival in BT 474-cancer cell line by using different concentration levels of Tmab and Tmab-Sbi. HCS: human complement serum.

From the obtained preliminary tests we can conclude that there is no significant cellular death observed with 2% HSC. Moreover, Tmab-Sbi conjugate significantly ($P < 0.05$) reduced the percent of survival of cancer cells at all the tested doses (Figure 11.4).

It worthwhile mentioning that the preliminary obtained results do not represent the actual anti-cancer activity of Tmab-Sbi conjugate because of the earlier explained instability issues. These assays were conducted directly after preparation and purification of the Tmab-Sbi conjugates. The current limitations of the conducted test are as follows: The test should be conducted again with shorter incubation time (48 h) to be able to compare the activity of Tmab-Sbi conjugate with Tmab. In addition, we observed that BT-474 cells tend to adhere to the walls of the well and nor speared all over it and that explain the high variability of some of the measurements. Therefore, it is suggested to harvest the cells using TrypLE^{TM} express enzyme (Trypsin Replacement) before conducting the measurements. Lastly, the fluorescence measurements using plate reader needed to be further optimised regarding the scan dimer and the gain.

11.4 Publications and posters

The following article and poster have been published as a result of the work reported in this thesis:

Kantner, T., Alkhawaja, B., and Watts, A. G. (2017) In Situ Quenching of Trialkylphosphine Reducing Agents Using Water-Soluble PEG-Azides Improves Maleimide Conjugation to Proteins. *ACS Omega 2*, 5785–5791

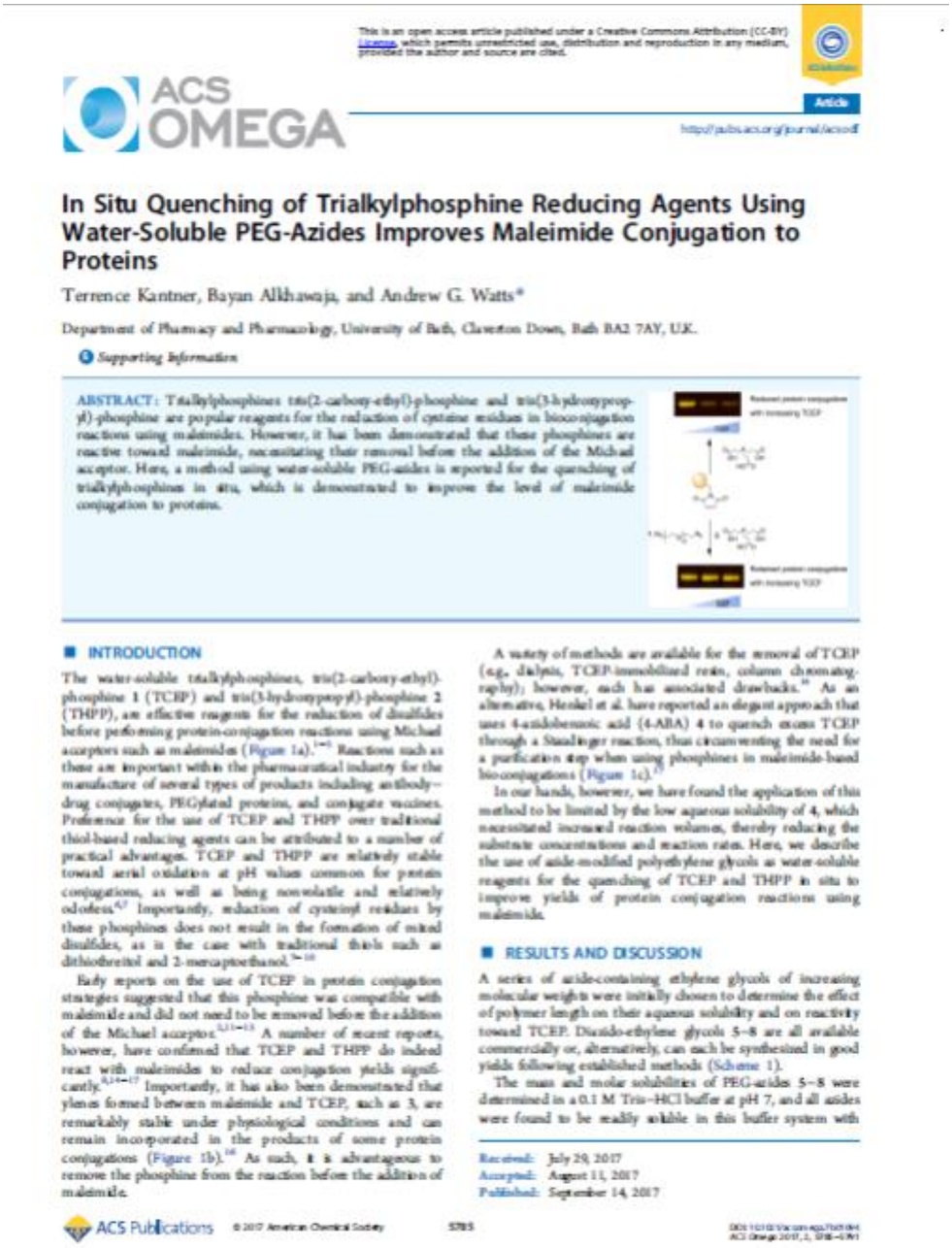

ACS OMEGA

Article

http://pubs.acs.org/journal/acsodf

In Situ Quenching of Trialkylphosphine Reducing Agents Using Water-Soluble PEG-Azides Improves Maleimide Conjugation to Proteins

Terrence Kantner, Bayan Alkhawaja, and Andrew G. Watts*

Department of Pharmacy and Pharmacology, University of Bath, Claverton Down, Bath BA2 7AY, U.K.

Supporting Information

ABSTRACT: Trialkylphosphines tris(2-carboxy-ethyl)-phosphine and tris(3-hydroxypropyl)-phosphine are popular reagents for the reduction of cysteine residues in bioconjugation reactions using maleimides. However, it has been demonstrated that these phosphines are reactive toward maleimide, necessitating their removal before the addition of the Michael acceptor. Here, a method using water-soluble PEG-azides is reported for the quenching of trialkylphosphines in situ, which is demonstrated to improve the level of maleimide conjugation to proteins.

INTRODUCTION

The water-soluble trialkylphosphines, tris(2-carboxy-ethyl)-phosphine **1** (TCEP) and tris(3-hydroxypropyl)-phosphine **2** (THPP), are effective reagents for the reduction of disulfides before performing protein-conjugation reactions using Michael acceptors such as maleimides (Figure 1a).[1−3] Reactions such as these are important within the pharmaceutical industry for the manufacture of several types of products including antibody−drug conjugates, PEGylated proteins, and conjugate vaccines. Preference for the use of TCEP and THPP over traditional thiol-based reducing agents can be attributed to a number of practical advantages. TCEP and THPP are relatively stable toward aerial oxidation at pH values common for protein conjugations, as well as being nonvolatile and relatively odorless.[4,7] Importantly, reduction of cysteinyl residues by these phosphines does not result in the formation of mixed disulfides, as is the case with traditional thiols such as dithiothreitol and 2-mercaptoethanol.[8−10]

Early reports on the use of TCEP in protein conjugation strategies suggested that this phosphine was compatible with maleimide and did not need to be removed before the addition of the Michael acceptor.[2,11−13] A number of recent reports, however, have confirmed that TCEP and THPP do indeed react with maleimides to reduce conjugation yields significantly.[8,14−17] Importantly, it has also been demonstrated that ylenes formed between maleimide and TCEP, such as **3**, are remarkably stable under physiological conditions and can remain incorporated in the products of some protein conjugations (Figure 1b).[16] As such, it is advantageous to remove the phosphine from the reaction before the addition of maleimide.

A variety of methods are available for the removal of TCEP (e.g., dialysis, TCEP-immobilized resin, column chromatography); however, each has associated drawbacks.[18] As an alternative, Henkel et al. have reported an elegant approach that uses 4-azidobenzoic acid (4-ABA) **4** to quench excess TCEP through a Staudinger reaction, thus circumventing the need for a purification step when using phosphines in maleimide-based bioconjugations (Figure 1c).[7]

In our hands, however, we have found the application of this method to be limited by the low aqueous solubility of **4**, which necessitated increased reaction volumes, thereby reducing the substrate concentrations and reaction rates. Here, we describe the use of azide-modified polyethylene glycols as water-soluble reagents for the quenching of TCEP and THPP in situ to improve yields of protein conjugation reactions using maleimide.

RESULTS AND DISCUSSION

A series of azide-containing ethylene glycols of increasing molecular weights were initially chosen to determine the effect of polymer length on their aqueous solubility and on reactivity toward TCEP. Diazido-ethylene glycols **5**−**8** are all available commercially or, alternatively, can each be synthesized in good yields following established methods (Scheme 1).

The mass and molar solubilities of PEG-azides **5**−**8** were determined in a 0.1 M Tris−HCl buffer at pH 7, and all azides were found to be readily soluble in this buffer system with

Received: July 29, 2017
Accepted: August 11, 2017
Published: September 14, 2017

Presented at **GP2A 2017** – 25th Annual GP2A Medicinal Chemistry Conference – Liverpool UK 31 August -1 September 2017

The *in situ* quenching of tri-alkylphosphine reducing agents using water soluble PEG-azides improves maleimide conjugation to proteins

Bayan Alkhawaja, Terrence Kantner and Andrew G. Watts
Department of Pharmacy and Pharmacology, University of Bath, Claverton Down, Bath BA2 7AY, United Kingdom

UNIVERSITY OF BATH

SUMMERY

The tri-alkylphosphines TCEP and THPP are popular reagents for the reduction of cysteine residues in bioconjugation reactions utilizing maleimides. It has been demonstrated that these phosphines are reactive towards maleimide, necessitating their removal prior to addition of the Michael acceptor, such as maleimides.
Here, we developed a method using water-soluble PEG-azides for the quenching of tri-alkylphosphines *in situ*, which is demonstrated to improve the level of maleimide conjugation to proteins.

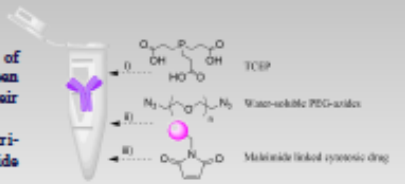

INTRODUCTION

ADCs, or antibody drug conjugates, are cutting-edge drugs which are capable of selectively targeting highly potent cytotoxic drugs toward cancerous cells. ADCs comprise a mAb which acts as a vehicle to target a specific receptor on the cancer cell and a cytotoxic drug which performs the cell killing function. One of the most widely-applied approaches to construct ADC's such as Brentuximab vardotin (Adcetris®) involves thiolate alkylation of the partially reduced mAb with a maleimide-linked cytotoxic drug.[1-3]

Water soluble trialkylphosphines, such as tris (2-carboxyethyl)-phosphine **1**, are effective reagents for the reduction of disulfides prior to performing protein-conjugation reactions using Michael acceptors such as maleimides.[3]
Recently, it has been confirmed that TCEP reacts with maleimides such as N-ethyl maleimide **2** and reduce conjugation yields significantly. Importantly, it has also been demonstrated that ylenes such as **3** are formed between maleimide and TCEP.[4]

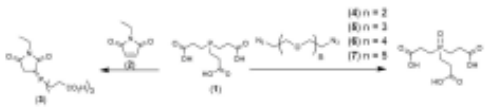

RESULTS AND DISCUSSION

A series of azide containing ethylene glycols of increasing molecular weights were synthesised to determine the effect of polymer length on their aqueous solubility and on reactivity towards TCEP. All azides were found to be readily soluble in Tris-HCl buffer system with values ranging from 25 mg/mL for the di-PEG 4, up to 130 mg/mL for the penta-PEG 7.
The ability of azides 4-7 to quench TCEP by promoting oxidation of phosphines was evaluated using ^{31}P NMR spectroscopy to quantify the rate of consumption of phosphine. The azides 4-7 were found to have similar reactivities, with complete consumption of TCEP occurring after 50-60 min.

An important application of maleimide for conjugation to proteins involves the attachment of large PEG polymers (kDa's), a technique used widely within the pharmaceutical industry to improve the pharmacokinetic properties of protein therapeutics.
Here, it was considered that investigating the use of azides 4-7 *in situ* in protein PEGylation reactions. Denatured yeast enolase protein was reduced with varying amounts of TCEP (1, 5 and 10 equiv.), then incubated with 2kDa PEG-maleimide. In parallel, samples of the TCEP-reduced enolase were treated with azide **6** for one hour, prior to incubation with 2kDa PEG-maleimide under similar conditions.
The extent of protein PEGylation decreases significantly with increasing amounts of TCEP when treated with 2 kDa PEG-maleimide directly following reduction (Lanes 3 – 5). In contrast, for enolase incubated with azide **6** prior to incubation with 2 kDa PEG-maleimide, increased levels of PEGylation were observed for all samples, regardless of the TCEP concentration used (Lanes 6-8).

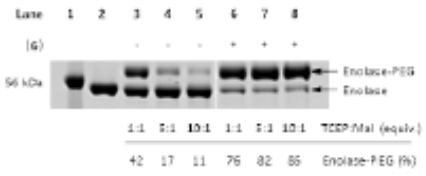

CONCLUSIONS

In summary, we have shown here that the PEG-azides 4–7 have suitable aqueous solubilities to enable their use in bioconjugation strategies employing maleimide.
Furthermore, it has been demonstrated that the treatment of phosphine-reduced protein with PEG-azides such as **6** *in situ*, prior to the addition of maleimide, leads to higher levels of protein conjugations.

REFERENCES

1. Francisco, J. A.; Cerveny, C. G.; Meyer, D. L.; et. al. *Blood* 2003, *102*, 1458–65.
2. Shen, B.-Q.; Xu, K.; Liu, L.; Raab, H.; et. al. *Nat. Biotechnol.* 2012, *30*, 184–9.
3. Burns, J. A.; Butler, J. C.; Moran, J.; Whitesides, G. M. Selective reduction of disulfides by tris(2-carboxyethyl)phosphine. *J. Org. Chem.* 1991, *56*, 2648–2650.
4. Kantner, T.; Watts, A. G. *Bioconjug. Chem.* 2016, *27*, 2400–2406.